39th Benelux Meeting

on

Systems and Control

March 10 − 12, 2020

Elspeet, The Netherlands

Book of Abstracts

The 39th Benelux Meeting on Systems and Control is sponsored by

Raffaella Carloni, Bayu Jayawardhana, and Erjen Lefeber (Eds.)
Book of Abstracts - 39th Benelux Meeting on Systems and Control

Part 1

Programmatic Table of Contents

Tuesday, March 10, 2020

Plenary: P0   **De Grote Zael**
Welcome and Opening

Chair: Raffaella Carloni   **11.25–11.30**

Mini Course: P1   **De Grote Zael**
Learning nonlinear dynamics - Part I
Thomas Schön
Chair: Raffaella Carloni   **11.30–12.30**

T. Schön

Mini Course: P2   **De Grote Zael**
Learning nonlinear dynamics - Part II
Thomas Schön
Chair: Bayu Jayawardhana   **13.40–14.40**

T. Schön

TuA01   **Lucasgat A**
Drones, Autonomous Vehicle & Logistics I
Chair: Nima Monshizadeh   **15.00-17.30**

TuA01-1   **15.00-15.25**
Carrier-vehicle Routing Problem in City Environments 19
N. Bono Rossello   Université Libre de Bruxelles
E. Garone   Université Libre de Bruxelles

TuA01-2   **15.25-15.50**
Routing Strategy for Large-Scale Dense AGVs Systems 20
V. Mazulina   Eindhoven University of Technology
A. Pogromsky   Eindhoven University of Technology
H. Nijmeijer   Eindhoven University of Technology

TuA01-3   **15.50-16.15**
Energy Optimal Coordination of Fully Autonomous Vehicles in Urban Intersections 21
C. Pelosi   Eindhoven University of Technology
P. Padilla   Eindhoven University of Technology
T. Donkers   Eindhoven University of Technology

TuA01-4   **16.15-16.40**
Communication Strategies for Synchronized Merging of Cooperative Vehicles 22
D. Liu   University of Groningen
H. Trentelman   University of Groningen
B. Besselink   University of Groningen

TuA01-5   **16.40-17.05**
Learning-Based Risk-Averse Model Predictive Control for Adaptive Cruise Control With Stochastic Driver Models 23
M. Schuurmans   Katholieke Universiteit Leuven
A. Katriniok, H. Eric Tseng   Ford
P. Patrinos   Katholieke Universiteit Leuven

TuA01-6   **17.05-17.30**
Design of a Highway On-ramp Merging Maneuver for Cooperative Platoons 24
W. Scholte   Eindhoven University of Technology
P. Zegelaar   Eindhoven University of Technology
H. Nijmeijer   Eindhoven University of Technology

TuA02   **Lucasgat B**
Mobile Robots & Robotics I
Chair: Julien Hendrickx   **15.00-17.05**

TuA02-1   **15.00-15.25**
Mobile Robot Path Following Control: Singularity Elimination 25
W. Yao   University of Groningen
M. Cao   University of Groningen

TuA02-2   **15.25-15.50**
Model Predictive Control Toolchain for Constraint-based Task Specification of Robot Motions 26
A. Suresha Sathya   Katholieke Universiteit Leuven
J. Gillis, G. Pipeleers   Katholieke Universiteit Leuven
W. Decre, J. Swevers   Katholieke Universiteit Leuven

TuA02-3   **15.50-16.15**
A Predictive Model for Nafion-based IPMC Soft Actuators 27
R. Langius   University of Groningen
R. D'Anniballe   University of Groningen
R. Carloni   University of Groningen

TuA02-4   **16.15-16.40**
Towards a Toolchain for Fast MPC Deployment on Serial Robots 28
A. Astudillo   Katholieke Universiteit Leuven
J. Gillis, W. Decré   Katholieke Universiteit Leuven
G. Pipeleers, J. Swevers   Katholieke Universiteit Leuven

TuA02-5   **16.40-17.05**
Forward Dynamics of Hyper-elastic Soft Robots . 29
B. Caasenbrood   Eindhoven University of Technology
A. Pogromsky   Eindhoven University of Technology
H. Nijmeijer   Eindhoven University of Technology

TuA03   **Lucasgat C**
Nonlinear & Hybrid Control Systems I
Chair: Erik Steur   **15.00-17.30**

TuA03-1   **15.00-15.25**
Frequency-Domain Stability Tools for Hybrid Integrator-Gain Systems 30
S. v/d Eijnden   Eindhoven University of Technology
M. Heertjes   Eindhoven University of Technology
H. Nijmeijer   Eindhoven University of Technology

TuA03-2   **15.25-15.50**
On Geometric and Differentiation Index of Nonlinear Differential Algebraic Equations 31
Y. Chen   University of Groningen
S. Trenn   University of Groningen

TuA03-3   **15.50-16.15**

Pattern and Bifurcation Analysis of Delay-coupled
Luré Systems 32

K. Rogov   Eindhoven University of Technology
A. Pogromsky   Eindhoven University of Technology
E. Steur   Eindhoven University of Technology
W. Michiels, H. Nijmeijer

TuA03-4   **16.15-16.40**

Extended Projected Dynamical Systems:A Frame-
work for Analysis of Hybrid Integrator-Gain Sys-
tems 33

B. Sharif   Eindhoven University of Technology
M. Heertjes   Eindhoven University of Technology
M. Heemels   Eindhoven University of Technology

TuA03-5   **16.40-17.05**

Set Stability of Luré Systems With Preisach But-
terfly Operator 34

M. Vasquez-Beltran   University of Groningen
B. Jayawardhana   University of Groningen
R. Peletier   University of Groningen

TuA03-6   **17.05-17.30**

Benefiting From Linear Behaviour of a Nonlinear
Reset-based Element at Certain Frequencies . . . 35

N. Karbasizadeh   Delft University of Technology
A. Ahmadi Dastjerdi   Delft University of Technology
N. Saikumar   Delft University of Technology
S. Hassan HosseinNia

TuA04	**Lucasgat D**
Distributed Parameter Systems I	
Chair: Joseph Winkin	**15.00-17.05**

TuA04-1   **15.00-15.25**

Local Exponential Stability of Nonlinear Dis-
tributed Parameter Systems: Application to a
Nonisothermal Tubular Reactor 36

A. Hastir   University of Namur
J. Winkin   University of Namur
D. Dochain   Université Libre de Bruxelles

TuA04-2   **15.25-15.50**

Observer Design for Linear Parabolic PDE Systems 37

I. Francisco Yupanqui Tello   Mons University
A. Vande Wouwer   Mons University
D. Coutinho   Federal University of Santa Catarina

TuA04-3   **15.50-16.15**

Complex Gaussian Process Regression for Esti-
mating Spatially Varying Coefficients in Thermal
Transport 38

R. van Kampen   DIFFER
A. Das   Eindhoven University of Technology
S. Weiland   Eindhoven University of Technology
M. van Berkel

TuA04-4   **16.15-16.40**

Rational Approximation of Positive-real Functions 39

M. Mamunuzzaman   University of Twente
H. Zwart   University of Twente

TuA04-5   **16.40-17.05**

A Non-linear Model for the Water Hammer Prob-
lem 40

T. Xu   University of Groningen
A. Waters   University of Groningen

TuA05	**Lucasgat E**
Energy Systems I	
Chair: Michele Cucuzzella	**15.00-17.05**

TuA05-1   **15.00-15.25**

Empirical Battery Modelling for High Currents:
The Effect of Nonlinear Overpotential and In-
evitable Self-Heating 41

F. Hoekstra   Eindhoven University of Technology
H. Jan Bergveld   Eindhoven University of Technology
T. Donkers   Eindhoven University of Technology
Y. Heuts

TuA05-2   **15.25-15.50**

Passivity Properties for Regulation of DC Net-
works With Stochastic Load Demand 42

A. Silani   University of Groningen
M. Cucuzzella, J. Scherpen University of Groningen
M. Javad Yazdanpanah   University of Groningen

TuA05-3   **15.50-16.15**

Towards Characterizing DC Power Flow With
Sign-indefinite Constant-power Loads 43

M. Jeeninga   University of Groningen
C. De Persis   University of Groningen
A. van der Schaft   University of Groningen

TuA05-4   **16.15-16.40**

A Sub-optimal PWM-like Ratio-based Algorithm
for the Charge and Balance of a String of Battery
Cells 44

A. Goldar Davila   Université Libre de Bruxelles
M. Kinnaert   Université Libre de Bruxelles
E. Garone   Université Libre de Bruxelles

TuA05-5   **16.40-17.05**

Fault Diagnosis and Maintenance Decision Mak-
ing for Energy Systems 45

J. Fu   Delft University of Technology

TuA06	**Solsegat**
Optimal Control I	
Chair: Ömür Arslan	**15.00-17.05**

TuA06-1   **15.00-15.25**

Analytic Optimal Ellipsoidal Trajectory Bounds
for Second-Order Dynamical Systems 46

Ö. Arslan   Eindhoven University of Technology

TuA06-2   **15.25-15.50**

Model Predictive Control for Integrated Synchro-
modal Transport 47

R. Brammer Larsen   Delft University of Technology
B. Atasoy   Delft University of Technology
R. Negenborn   Delft University of Technology

TuA06-3 15.50-16.15

Nonlinear MPC for Tracking for Star-shaped Admissible Output Sets 48

A. Cotorruelo — Université Libre de Bruxelles
D. Limon — Universidad de Sevilla
E. Garone — Université Libre de Bruxelles

TuA06-4 16.15-16.40

Conditions for Obtaining Robustness and Stability in Data-driven Predictive Control 49

J. Declercq — Université Libre de Bruxelles
M. Versteyhe — Université Libre de Bruxelles

TuA06-5 16.40-17.05

Explicit Reference Governor for a Boom Crane System 50

M. Ambrosino — Université Libre de Bruxelles
E. Garone — Université Libre de Bruxelles
A. Dawans — Entreprises Jacques Delens

TuA07 Hooge Duvel
Systems Identification I
Chair: Xiaodong Cheng 15.00-17.30

TuA07-1 15.00-15.25

Identifiability in Dynamic Networks Through Switching Modules 51

M. Dreef — Eindhoven University of Technology
T. Donkers — Eindhoven University of Technology
P. Van den Hof — Eindhoven University of Technology

TuA07-2 15.25-15.50

Excitation Allocation for Generic Identifiability of a Single Module in Dynamic Networks 52

S. Shi — Eindhoven University of Technology
X. Cheng — Eindhoven University of Technology
P. Van den Hof — Eindhoven University of Technology

TuA07-3 15.50-16.15

Linear Time-Varying System Identification in the Presence of Nonlinear Distortions 53

N. Hallemans — Vrije Universiteit Brussel
R. Pintelon — Vrije Universiteit Brussel
J. Lataire — Vrije Universiteit Brussel

TuA07-4 16.15-16.40

Local Dynamics Identification Via a Graph-theoretical Approach 54

A. Legat — Université Libre de Bruxelles
J. Hendrickx — Université Libre de Bruxelles

TuA07-5 16.40-17.05

Non-Parametric Kernelized Identification of Closed Loop Nonlinear Systems 55

F. Shakib — Eindhoven University of Technology
R. Toth — Eindhoven University of Technology
A. Pogromsky — Eindhoven University of Technology
A. Pavlov, N. van de Wouw

TuA07-6 17.05-17.30

Structural Identifiability of Linear State Space Models: A State and Output Sensitivity Controllability Perspective 56

C. Mendez-Blanco — Eindhoven University of Technology
L. Ozkan — Eindhoven University of Technology

TuA08 Groenendal
State Observer, Fault Detection & Isolation
Chair: Alessandro Saccon 15.00-17.30

TuA08-1 15.00-15.25

Fault Detection and Isolation for Linear Structured Systems 57

J. Jia — University of Groningen
H. Trentelman — University of Groningen
K. Camlibel — University of Groningen

TuA08-2 15.25-15.50

Robust Reference Model-based Fault Detection and Isolation for Discrete-time Systems 58

S. de Melo Schons — Université Libre de Bruxelles
M. Kinnaert — Université Libre de Bruxelles
D. Coutinho — Universidade Federal de Santa Catarina

TuA08-3 15.50-16.15

Fault-compensation Controller for LPV Systems 59

T. Rosa — University of Groningen
L. Carvalho — University of Groningen
B. Jayawardhana — University of Groningen
O. Costa

TuA08-4 16.15-16.40

A Data-Rate Constrained Observer for Unicycle-type Robots 60

Q. Voortman — Eindhoven University of Technology
A. Pogromsky — Eindhoven University of Technology
H. Nijmeijer — Eindhoven University of Technology
D. Efimov, J. Richard

TuA08-5 16.40-17.05

Detection of Cyber Attacks on Collaborative Systems Using a Sliding Mode Observer Based Approach 61

T. Keijzer — Delft University of Technology
R. Ferrari — Delft University of Technology

TuA08-6 17.05-17.30

Health Monitoring of an Electromechanical Actuator for Aircraft Primary Flight Surface Control 62

B. Wauthion — Université Libre de Bruxelles
M. Kinnaert — Université Libre de Bruxelles
E. Garone — Université Libre de Bruxelles

Wednesday, March 11, 2020

Mini Course: P3   **De Grote Zael**
Learning nonlinear dynamics - Part III
Thomas Schön
Chair: Bayu Jayawardhana   **8.30–9.30**

WeM01   **Lucasgat A**
Drones, Autonomous Vehicle & Logistics II
Chair: Roland Toth   **09.45-12.15**

WeM01-1   **09.45-10.10**
Interactive Demo on the Indoor Localization, Control and Navigation of Drones 63
M. Bos   Katholieke Universiteit Leuven
R. Beck   Flanders Make
J. Swevers, G. Pipeleers Katholieke Universiteit Leuven

WeM01-2   **10.10-10.35**
Decision Making for Autonomous Vehicles: Combining Safety and Optimality 64
J. Verbakel   Eindhoven University of Technology
M. Fusco, D. Willemsen   TNO
A. van de Mortel   Eindhoven University of Technology
M. Heemels

WeM01-3   **10.35-11.00**
Experimental Results of Distributed Multi UAV Search Optimization 65
J. Fransman   Delft University of Technology
B. De Schutter   Delft University of Technology

WeM01-4   **11.00-11.25**
Modeling and Control of a Quad-tiltrotor Aimed for Interaction Tasks 66
J. Cezar Vendrichoski   Vrije Universiteit Brussel
B. Vanderborght   Vrije Universiteit Brussel
E. Garone   Université Libre de Bruxelles

WeM01-5   **11.25-11.50**
Extended Kalman Filter for Accurate Distance Estimation Using RSSI and GPS Measurements in Quadcopter Formation Flights 67
B. Njinwoua   Mons University
A. Vande Wouwer   Mons University

WeM01-6   **11.50-12.15**
Gaussian Processes Based Learning Control for Quadcopters 68
Y. Liu   Eindhoven University of Technology
R. Toth   Eindhoven University of Technology

WeM02   **Lucasgat B**
Mobile Robots & Robotics II
Chair: Zhiyong Sun   **09.45-12.15**

WeM02-1   **09.45-10.10**
Towards Prescribed Performance Control of Persistent Formations With Signed Area Constraints   69
F. Mehdifar   Université Catholique de Louvain
C. Bechlioulis   National Technical University of Athens
J. Hendrickx   Université Catholique de Louvain

WeM02-2   **10.10-10.35**
Formation Control for Circular Robots 70
N. Chan   University of Groningen
B. Jayawardhana   University of Groningen

WeM02-3   **10.35-11.00**
Simultaneous Distributed Localization, Mapping and Formation Control of Mobile Robots Based Local Relative Measurement 71
M. Guo   University of Groningen
B. Jayawardhana   University of Groningen
J. Gyu Lee   University of Cambridge
H. Shim

WeM02-4   **11.00-11.25**
Cooperative Passivity-Based Control for End-Effector Synchronisation 72
O. de Groot   Delft University of Technology
L. Valk   Delft University of Technology
T. Kevickzy   Delft University of Technology

WeM02-5   **11.25-11.50**
Passivity Based Velocity Tracking and Formation Control Without Velocity Measurements 73
N. Li   University of Groningen
J. Scherpen   University of Groningen
A. van der Schaft   University of Groningen

WeM02-6   **11.50-12.15**
A Directed Spanning Tree Adaptive Control Framework for Time-Varying Formations 74
D. Yue   Delft University of Technology
S. Baldi, B. De Schutter Delft University of Technology
Q. Li, J. Cao   Delft University of Technology

WeM03   **Lucasgat C**
Nonlinear & Hybrid Control Systems II
Chair: Luis Pablo Borja Rosales   **09.45-12.15**

WeM03-1   **09.45-10.10**
Incremental Dissipativity Analysis of Nonlinear Systems Using the Linear Parameter-Varying Framework 75
C. Verhoek   Eindhoven University of Technology
P. Koelewijn   Eindhoven University of Technology
R. Toth   Eindhoven University of Technology

WeM03-2   **10.10-10.35**
Trajectory Convergence From Coordinate-wise Decrease of Energy Functions 76
J. Hendrickx   Université Catholique de Louvain
B. Gerencser   Institute of Mathematics, Hungary

WeM03-3   **10.35-11.00**
Incremental Stability Based Analysis and Control of Nonlinear Systems Using the LPV Framework   77
P. Koelewijn   Eindhoven University of Technology
R. Toth   Eindhoven University of Technology
S. Weiland   Eindhoven University of Technology

WeM03-4   **11.00-11.25**
Tuning Rules for Gradient Systems   78
C. Chan-Zheng   University of Groningen
P. Borja   University of Groningen
J. Scherpen   University of Groningen

WeM03-5   **11.25-11.50**
Linear Parameter-Varying Embedding of Nonlinear Models Based on Polynomial Approximation   79
A. Sadeghzadeh   Eindhoven University of Technology
R. Toth   Eindhoven University of Technology

WeM03-6   **11.50-12.15**
Nearest Neighbor Control For Incrementally Passive Nonlinear Systems With Known Constant Input   80
M. Zaki Almuzakki   University of Groningen
B. Jayawardhana   University of Groningen
A. Tanwani   Université de Toulouse

WeM04   **Lucasgat D**
Discrete-event & Embedded Control Systems
Chair: Erjen Lefeber   **09.45-11.50**

WeM04-1   **09.45-10.10**
Graphical Modeling for Supervisor Synthesis . . .   81
F. Reijnen   Eindhoven University of Technology
J. van de Mortel   Eindhoven University of Technology
M. Reniers   Eindhoven University of Technology
J. Rooda

WeM04-2   **10.10-10.35**
Model Reduction for Supervisor Synthesis   82
L. Moormann   Eindhoven University of Technology
J. van de Mortel   Eindhoven University of Technology
W. Fokkink   Vrije Universiteit Amsterdam
J. Rooda

WeM04-3   **10.35-11.00**
Supervisory Control for Product Lines With Dynamic Feature Configuration   83
S. Thuijsman   Eindhoven University of Technology
M. Reniers   Eindhoven University of Technology

WeM04-4   **11.00-11.25**
Correct-by-design Control Synthesis for Stochastic Systems   84
B. van Huijgevoort   Eindhoven University of Technology
S. Haesaert   Eindhoven University of Technology

WeM04-5   **11.25-11.50**
Synthesis of Efficient Failure-recovering Supervisors   85
N. Paape   Eindhoven University of Technology
A. van de Mortel   Eindhoven University of Technology
L. Swartjes   Vanderlande
M. Reniers

WeM05   **Lucasgat E**
Medicine and systems biology
Chair: Steffen Waldherr   **09.45-12.15**

WeM05-1   **09.45-10.10**
Strategies of Drug Dosing Based on Pharmacokinetic Models   86
P. Thémans   University of Namur
F. Musuamba Agency for medicines & health, Belgium
J. Winkin   University of Namur

WeM05-2   **10.10-10.35**
Dynamical Analysis of an Age-dependent SIR Epidemic Model   87
C. Sonveaux   University of Namur
J. Winkin   University of Namur

WeM05-3   **10.35-11.00**
Luenberger Observer Design for a Dynamic Biotechnological Model With Embedded Linear Program   88
K. De Becker   Katholieke Universiteit Leuven
K. Bernaerts   Katholieke Universiteit Leuven
S. Waldherr   Katholieke Universiteit Leuven

WeM05-4   **11.00-11.25**
Particle Filter Design for an Agent-based Crop Model   89
J. Lopez-Jimenez   Mons University
N. Quijano   Universidad de los Andes
A. Vande Wouwer   Mons University

WeM05-5   **11.25-11.50**
Surrogate Modelling of Activated Sludge Wastewater Treatment Plant   90
M. Agung Prawira Negara   University of Groningen

WeM05-6   **11.50-12.15**
Mathematical Modelling of Malaria Transmission Considering the Influence of Current Prevention and Treatment   91
O. Diao   Université Catholique de Louvain

WeM06   **Solsegat**
Optimal Control II
Chair: Bram de Jager   **09.45-12.15**

WeM06-1   **09.45-10.10**
Distributed Model Predictive Control for Linear Systems Under Time-varying Communication . .   92
B. Jin   University of Groningen
M. Cao   University of Groningen

WeM06-2   **10.10-10.35**
Real Time Iterations for Mixed-Integer MPC . .   93
M. De Mauri   Katholieke Universiteit Leuven
W. Van Roy   Katholieke Universiteit Leuven
G. Pipeleers, J. Swevers Katholieke Universiteit Leuven

WeM06-3 10.35-11.00

Imprecise Probabilistic MPC (iMPC) for Systems With Non-deterministic Uncertainty 94

F. Debrouwere	Katholieke Universiteit Leuven
K. Shariatmadar	Katholieke Universiteit Leuven
M. Versteyhe	Katholieke Universiteit Leuven
F. Debrouwere	

WeM06-4 11.00-11.25

Short-Horizon MPC of Large-scale Thermal Systems 95

T. Meijer	Eindhoven University of Technology
V. Dolk	ASML
B. de Jager	Eindhoven University of Technology
M. Heemels	

WeM06-5 11.25-11.50

Optimal Control of Hybrid Systems: Dual Dynamic Programming Approach 96

B. Legat	Université Catholique de Louvain
J. Bouchat	Université Catholique de Louvain
R. Jungers	Université Catholique de Louvain

WeM06-6 11.50-12.15

Optimal Irrigation Management for Large-scale Precision Farming Using Model Predictive Control 97

R. Cobbenhagen	Eindhoven University of Technology
D. Antunes	Eindhoven University of Technology
R. v/d Molengraft	Eindhoven University of Technology
M. Heemels	

WeM07	**Hooge Duvel**
Systems Identification II	
Chair: John Lataire	**09.45-12.15**

WeM07-1 09.45-10.10

Optimal Experiment Design for a Wafer Stage: A Sequential Relaxation Approach 98

N. Dirkx	Eindhoven University of Technology
J. van de Wijdeven	ASML
T. Oomen	Eindhoven University of Technology

WeM07-2 10.10-10.35

A Novel LPV/LTV Method for Nonlinear System Identification 99

M. Ghasem Sharabiany	Vrije Universiteit Brussel
J. Lataire	Vrije Universiteit Brussel
R. Pintelon	Vrije Universiteit Brussel

WeM07-3 10.35-11.00

Nonlinear Data-driven Identification of a Thermoelectric System 100

J. Noël	Eindhoven University of Technology
E. Evers	Eindhoven University of Technology
T. Oomen	Eindhoven University of Technology

WeM07-4 11.00-11.25

Consistent Identification of Dynamic Networks Subjected to White Noise Using Weighted Null-Space Fitting 101

S. Fonken	Eindhoven University of Technology
M. Ferizbegovic	KTH Royal Institute of Technology
H. Hjalmarsson	KTH Royal Institute of Technology

WeM07-5 11.25-11.50

Identification and Identifiability of Physical Networks 102

| L. Kivits | Eindhoven University of Technology |
| P. Van den Hof | Eindhoven University of Technology |

WeM07-6 11.50-12.15

Representing Music Using MIMO Models for Genre Clustering 103

| B. Geelen | Katholieke Universiteit Leuven |
| B. De Moor | Katholieke Universiteit Leuven |

WeM08	**Groenendal**
Learning in Control I	
Chair: Tom Oomen	**09.45-12.15**

WeM08-1 09.45-10.10

Repetitive Control to Improve Pressure Tracking Performance in Mechanical Ventilation of Sedated Patients 104

J. Reinders	Eindhoven University of Technology
R. Verkade	DEMCON
B. Hunnekens	DEMCON
N. van de Wouw, T. Oomen	

WeM08-2 10.10-10.35

Generic Signal Parametrizations for Low-Dimensional Learning Control 105

J. Willems	Flanders Make
E. Kikken	Flanders Make
B. Depraetere, S. Bengea	Flanders Make

WeM08-3 10.35-11.00

Gaussian Process Repetitive Control for Suppressing Spatial Disturbances: With Application to a Substrate Carrier System 106

N. Mooren	Eindhoven University of Technology
G. Witvoet	Eindhoven University of Technology
T. Oomen	Eindhoven University of Technology

WeM08-4 11.00-11.25

Balancing On-sample and Intersample Behavior in Sampled-data System Inversion 107

| W. Ohnishi | Eindhoven University of Technology |
| J. van Zundert | Eindhoven University of Technology |

WeM08-5 11.25-11.50

Multi-System Iterative Learning Control: Extending ILC Towards Interconnected Systems. 108

D. Ronzani	Katholieke Universiteit Leuven
A. Steinhauser	Katholieke Universiteit Leuven
J. Swevers	Katholieke Universiteit Leuven

WeM08-6 11.50-12.15

Intermittent Sampling in Iterative Learning Control: a Monotonically-Convergent Gradient-Descent Approach With Application to Time Stamping 109

| N. Strijbosch | Eindhoven University of Technology |
| T. Oomen | Eindhoven University of Technology |

Plenary: P4 De Grote Zael
Data-driven model learning
Paul Van den Hof
Chair: Erjen Lefeber **13:30–14.30**

Data-driven model learning in linear dynamic networks 219
P. Van den Hof

WeA01 **Lucasgat A**
Games and Multi-Agent Systems I
Chair: Ming Cao **14.45-17.15**

WeA01-1 **14.45-15.10**
Charging Plug-in Electric Vehicles: a Game Theoretic Approach 110
C. Cenedese University of Groningen
F. Fabiani University of Oxford
M. Cucuzzella University of Groningen
J. Scherpen, M. Cao, S. Grammatico

WeA01-2 **15.10-15.35**
Lower Bound Performance for Averaging Algorithms in Open Multi-Agent Systems 111
C. de Galland Université Catholique de Louvain
J. Hendrickx Université Catholique de Louvain

WeA01-3 **15.35-16.00**
On the Inclusion of Cognitive Mechanisms in Social Diffusion Models 112
L. Zino University of Groningen
M. Ye University of Groningen
M. Cao University of Groningen

WeA01-4 **16.00-16.25**
Nash Equilibrium Seeking Under Partial-decision Information 113
M. Bianchi Delft University of Technology
G. Belgioioso Delft University of Technology
S. Grammatico Delft University of Technology

WeA01-5 **16.25-16.50**
Distributed H2 Suboptimal Filter Design for Linear Systems 114
J. Jiao University of Groningen
H. Trentelman University of Groningen
K. Camlibel University of Groningen

WeA01-6 **16.50-17.15**
Autocratic Strategies for Infinitely Repeated N-player Games With Arbitrary Actions Spaces . . 115
E. Martirosyan University of Groningen
A. Govaert University of Groningen
M. Cao University of Groningen

WeA02 **Lucasgat B**
Systems Theory I
Chair: Stephan Trenn **14.45-17.15**

WeA02-1 **14.45-15.10**
Memristors as Building Blocks for Neuromorphic Computing 116
A. Huijzer University of Groningen
B. Besselink University of Groningen

WeA02-2 **15.10-15.35**
A Forward Approach to Controllability of Switched DAEs 117
P. Wijnbergen University of Groningen
S. Trenn University of Groningen

WeA02-3 **15.35-16.00**
A New Framework for Control of Multi-agent Systems Over Wireless 118
M. Pezzutto University of Padova
E. Garone Université Libre de Bruxelles

WeA02-4 **16.00-16.25**
Robust H-infinity Controller Design for Uncertain Time-delay Systems 119
P. Appeltans Katholieke Universiteit Leuven
W. Michiels Katholieke Universiteit Leuven

WeA02-5 **16.25-16.50**
Strong Structural Properties of Structured Linear Systems 120
B. Shali University of Groningen
H. van Waarde University of Groningen
K. Camlibel, H. Trentelman University of Groningen

WeA02-6 **16.50-17.15**
Model Reduction of Switched Systems in Time-varying Approach 121
M. Sumon Hossain University of Groningen
S. Trenn University of Groningen
S. Hossain University of Groningen

WeA03 **Lucasgat C**
Electromechanical & High-Precision Systems I
Chair: Siep Weiland **14.45-17.15**

WeA03-1 **14.45-15.10**
On Co-designing Active Seismic Control of a Tall Building With Actuator Selection 122
T. Singh Katholieke Universiteit Leuven
J. Swevers Katholieke Universiteit Leuven
G. Pipeleers Katholieke Universiteit Leuven

WeA03-2 **15.10-15.35**
High Pixel Number Deformable Mirror Concept Utilizing Piezoelectric Hysteresis for Stable Shape Configurations 123
A. Schmerbauch University of Groningen
M. Augusto Vasquez Beltran University of Groningen
A. Vakis University of Groningen
B. Jayawardhana, R. Huisman

WeA03-3 **15.35-16.00**
Ageing-Aware Charging of Lithium-ion Batteries Using an Electrochemistry-Based Model With Capacity-Loss Side Reactions 124
Z. Khalik Eindhoven University of Technology
H. Jan Bergveld Eindhoven University of Technology
T. Donkers Eindhoven University of Technology

WeA03-4   **16.00-16.25**

Motion Control of Piezo-electric Actuators for Nanopositioning 125
C. Bosman Barros Eindhoven University of Technology

WeA03-5   **16.25-16.50**

Effects of Laser Surface Texturing on the Non-Steady Friction Behaviour 126
K. Driesen   Katholieke Universiteit Leuven
F. Debrouwere   Katholieke Universiteit Leuven
S. Debruyne   Katholieke Universiteit Leuven
M. Versteyhe

WeA03-6   **16.50-17.15**

Quadratic Tracking Control of Photopolymerization for Additive Manufacturing 127
K. Classens   Eindhoven University of Technology
T. Hafkamp   Eindhoven University of Technology
S. Westbeek   Eindhoven University of Technology
J. Remmers, S. Weiland

WeA04	**Lucasgat D**
Koopman Operator & Gaussian Process	
Chair: Alexandre Mauroy	**14.45-17.15**

WeA04-1   **14.45-15.10**

Linear Predictors for Interconnected Systems: a Koopman Operator Approach. 128
C. Garcia-Tenorio   Mons University
E. Mojica-Nava   Universidad Nacional de Colombia
A. Vande Wouwer   Mons University

WeA04-2   **15.10-15.35**

Two Methods to Approximate the Koopman Operator With a Reservoir Computer 129
M. Gulina   University of Namur
A. Mauroy   University of Namur

WeA04-3   **15.35-16.00**

Koopman Operator Approach Applied to Switched Nonlinear Systems 130
C. Mugisho Zagabe   University of Namur
A. Mauroy   University of Namur

WeA04-4   **16.00-16.25**

Numerical Gaussian Process Kalman Filtering . 131
A. Küper   Katholieke Universiteit Leuven
S. Waldherr   Katholieke Universiteit Leuven

WeA04-5   **16.25-16.50**

Gaussian Process Regression for Time-series Estimation 132
G. Birpoutsoukis   Université Catholique de Louvain
J. Hendrickx   Université Catholique de Louvain

WeA04-6   **16.50-17.15**

LPV Modeling Using the Koopman Operator . . 133
L. Cristian Iacob   Eindhoven University of Technology
R. Toth   Eindhoven University of Technology
M. Schoukens   Eindhoven University of Technology

WeA05	**Lucasgat E**
Optimization	
Chair: Jan Swevers	**14.45-17.15**

WeA05-1   **14.45-15.10**

Exact Gradient Methods With Memory 134
M. Florea   Université Catholique de Louvain

WeA05-2   **15.10-15.35**

The Proximal Augmented Lagrangian Method for Nonconvex Quadratic Programs 135
B. Hermans   Katholieke Universiteit Leuven
A. Themelis   Katholieke Universiteit Leuven
P. Patrinos   Katholieke Universiteit Leuven

WeA05-3   **15.35-16.00**

Co-design of a Continuous Variable Transmission Using a Sequential Quadratic Programming Based Control Optimization 136
C. Fahdzyana   Eindhoven University of Technology
T. Donkers   Eindhoven University of Technology
T. Hofman   Eindhoven University of Technology

WeA05-4   **16.00-16.25**

Transition-time Optimization for Multi-actor Dynamical Systems 137
W. Van Roy   Katholieke Universiteit Leuven
J. Gillis   Katholieke Universiteit Leuven
G. Pipeleers   Katholieke Universiteit Leuven
J. Swevers

WeA05-5   **16.25-16.50**

Effortless Modeling of Optimal Control Problems With Rockit 138
J. Gillis   Katholieke Universiteit Leuven
B. Vandewal   Katholieke Universiteit Leuven
G. Pipeleers   Katholieke Universiteit Leuven
J. Swevers

WeA05-6   **16.50-17.15**

Local Spline Relaxation for Multiple Shooting . . 139
B. Vandewal   Katholieke Universiteit Leuven
J. Gillis   Katholieke Universiteit Leuven
J. Swevers   Katholieke Universiteit Leuven

WeA06	**Solsegat**
Data-driven in Control I	
Chair: Bayu Jayawardhana	**14.45-17.15**

WeA06-1   **14.45-15.10**

Data-driven Distributionally Robust LQR With Multiplicative Noise 140
P. Coppens   Katholieke Universiteit Leuven
M. Schuurmans   Katholieke Universiteit Leuven
P. Patrinos   Katholieke Universiteit Leuven

WeA06-2   **15.10-15.35**

Data Informativity for System Analysis and Control Part 1: Analysis 141
J. Eising   University of Groningen
H. van Waarde   University of Groningen
H. Trentelman, K. Camlibel   University of Groningen

WeA06-3   **15.35-16.00**

Data Informativity for System Analysis and Control Part 2: Design 142
H. van Waarde   University of Groningen
J. Eising   University of Groningen
H. Trentelman, K. Camlibel   University of Groningen

WeA06-4   **16.00-16.25**
Informativity for Data-driven Moment Matching   143
A. Burohman   University of Groningen
B. Besselink   University of Groningen
K. Camlibel, J. Scherpen   University of Groningen

WeA06-5   **16.25-16.50**
Data-Driven Rational LPV Controller Synthesis
for Unstable Systems Using Frequency Response
Functions   144
T. Bloemers   Eindhoven University of Technology
R. Toth   Eindhoven University of Technology
T. Oomen   Eindhoven University of Technology

WeA06-6   **16.50-17.15**
A Data-driven Approach to Distributed Control .   145
T. Steentjes   Eindhoven University of Technology
M. Lazar   Eindhoven University of Technology
P. Van den Hof   Eindhoven University of Technology

WeA07	**Hooge Duvel**
Systems Identification III	
Chair: Paul Van den Hof	**14.45-17.15**

WeA07-1   **14.45-15.10**
Generalized Sensing and Actuation Schemes for
Consistent Local Module Identification in Dy-
namic Networks   146
K. Ramaswamy   Eindhoven University of Technology
P. Van den Hof   Eindhoven University of Technology
A. Dankers   University of Calgary

WeA07-2   **15.10-15.35**
Allocation of Excitation Signals for Generic Iden-
tifiability of Dynamic Networks   147
X. Cheng   Eindhoven University of Technology
S. Shi   Eindhoven University of Technology
P. Van den Hof   Eindhoven University of Technology

WeA07-3   **15.35-16.00**
Model Order Selection for Robust-control-relevant
Identification   148
P. Tacx   Eindhoven University of Technology
R. de Rozario   Eindhoven University of Technology
T. Oomen   Eindhoven University of Technology

WeA07-4   **16.00-16.25**
Time-Varying Ankle Joint Stiffness Identification
During Cyclic Movement   149
R. van 't Veld   University of Twente
A. Moya Esteban   University of Twente
A. Schouten   University of Twente

WeA07-5   **16.25-16.50**
A Column Space Based Approach to Solve Multi-
parameter Eigenvalue Problems   150
C. Vermeersch   Katholieke Universiteit Leuven
B. De Moor   Katholieke Universiteit Leuven

WeA07-6   **16.50-17.15**
Unsupervised Wind Turbine Anomaly Detection:
A Weighted Cepstral Distance Application   151
O. Lauwers   Katholieke Universiteit Leuven
B. De Moor   Katholieke Universiteit Leuven

WeA08	**Groenendal**
Learning in Control II	
Chair: Tom Oomen	**14.45-17.15**

WeA08-1   **14.45-15.10**
Commutation-angle Iterative Learning Control for
Walking Piezo-stepper Actuators   152
L. Aarnoudse   Eindhoven University of Technology
N. Strijbosch   Eindhoven University of Technology
E. Verschueren   Thermo Fisher Scientific
T. Oomen

WeA08-2   **15.10-15.35**
Model-based Similarity Assessment for Nonlinear
Systems   153
A. Steinhauser   Katholieke Universiteit Leuven
J. Swevers   Katholieke Universiteit Leuven

WeA08-3   **15.35-16.00**
Similarity Assessment for Efficient Initialization
of New Controllers   154
R. Beck, J. Willems   Flanders Make
E. Kikken, S. Bengea   Flanders Make
B. Depraetere   Flanders Make

WeA08-4   **16.00-16.25**
On the Role of Models in Learning Control: Actor-
Critic Iterative Learning Control   155
M. Poot   Eindhoven University of Technology
J. Portegies   Eindhoven University of Technology
T. Oomen   Eindhoven University of Technology

WeA08-5   **16.25-16.50**
From Reward Function to Cost Function: Modi-
fied Stage Cost in MPC Inspired by Reinforcement
Learning   156
D. Sun   Delft University of Technology
A. Jamshidnejad   Delft University of Technology
B. De Schutter   Delft University of Technology

WeA08-6   **16.50-17.15**
Comparison of Deep Learning Methods for System
Identification   157
G. Beintema   Eindhoven University of Technology
R. Toth   Eindhoven University of Technology
M. Schouken   Eindhoven University of Technology

Plenary: P5	**De Grote Zael**
Cooperative and/or Autonomous driving	
Henk Nijmeijer	
Chair: Erjen Lefeber	**17:30–18.30**

Cooperative and/or Autonomous driving: where
are we going?   238
H. Nijmeijer

Event: E1	**De Grote Zael**
Best Thesis Award Ceremony	
Chair: Henk Nijmeijer	**18.30–18.45**

13

Thursday, March 12, 2020

Plenary: P6   **De Grote Zael**
Autonomous agents
Ming Cao
Chair: Raffaella Carloni   **8.30–9.30**

Strategic decision-making and learning for autonomous agents 244
M. Cao

Plenary: P7   **De Grote Zael**
Hybrid integrator-gain systems
Marcel Heertjes
Chair: Erjen Lefeber   **9.45–10.45**

Hybrid integrator-gain systems: How to use them in motion control of wafer scanners? 256
M. Heertjes

ThM01   **Lucasgat A**
Games & Multi-Agent Systems II
Chair: Sergio Grammatico   **10.45-12.25**

ThM01-1   **10.45-11.10**
Analysis and Control of Interconnected Systems: Definition of Agents 158
A. Ben Ayed   Université Libre de Bruxelles
D. Dochain   Université Libre de Bruxelles
I. Prodan   Eindhoven University of Technology
C. Robles Rodriguez

ThM01-2   **11.10-11.35**
On Path-Complete Lyapunov Functions : Comparison Between a Graph and Its Expansion 159
V. Debauche   Université Libre de Bruxelles
R. Jungers   Université Libre de Bruxelles

ThM01-3   **11.35-12.00**
Limit Cycles in Replicator-Mutator Dynamics With Game-Environment Feedback 160
L. Gong   University of Groningen
M. Cao   University of Groningen

ThM01-4   **12.00-12.25**
Energy Efficiency of Flow-mediated Flocking . . 161
M. Shi   Université Libre de Bruxelles
J. Hendrickx   Université Libre de Bruxelles

ThM02   **Lucasgat B**
Systems Theory II
Chair: Bart Besselink   **10.45-12.25**

ThM02-1   **10.45-11.10**
Bringing Intuitive Weighting Filters Into $\mathcal{H}_\infty$ Control Design Practice 162
L. Jacobs   Katholieke Universiteit Leuven
J. Swevers   Katholieke Universiteit Leuven
G. Pipeleers   Katholieke Universiteit Leuven

ThM02-2   **11.10-11.35**
Extended Model Order Reduction for Linear Time Delay Systems 163
S. Naderi Lordejani   Eindhoven University of Technology
B. Besselink   University of Groningen
N. van de Wouw   Eindhoven University of Technology

ThM02-3   **11.35-12.00**
A Discussion on the Canonical Decomposition of Two Dimensional Descriptor Systems 164
B. Vergauwen   Katholieke Universiteit Leuven
B. De Moor   Katholieke Universiteit Leuven

ThM03   **Lucasgat C**
Electromechanical & High-Precision Systems II
Chair: Hassan HosseinNia   **10.45-12.25**

ThM03-1   **10.45-11.10**
Sliding Mode Observer Based Hysteresis Compensation Control for Piezoelectric Stacks 165
J. Hu   University of Groningen
S. Trenn   University of Groningen

ThM03-2   **11.10-11.35**
Impulsive Control of Precision Motion System . 166
R. Behinfaraz   Delft University of Technology
H. HosseinNia   Delft University of Technology

ThM03-3   **11.35-12.00**
Cylinder-individual Charge Mass Estimation by Time-frequency Analysis of In-cylinder Pressure Measurements 167
P. Garg   Eindhoven University of Technology
P. Mentink   TNO
X. Seykens   Eindhoven University of Technology
F. Willems

ThM03-4   **12.00-12.25**
User-friendly Nonparametric Framework for Vibro-acoustic Industrial Measurements With Multiple Inputs 168
P. Zoltan Csurcsia   Vrije Universiteit Brussel
B. Peeters   Siemens

ThM04   **Lucasgat D**
Distributed Parameter Systems II
Chair: Hans Zwart   **10.45-12.00**

ThM04-1   **10.45-11.10**
Extending the Method of Images to Thermomechanical Systems 169
D. Veldman   Eindhoven University of Technology
R. Fey   Eindhoven University of Technology
H. Zwart   Eindhoven University of Technology
M. van de Wal, J. van den Boom, H. Nijmeijer

ThM04-2   **11.10-11.35**
Boundary Control of Counter-current Heat Exchanger 170
J. Kadima Kazaku   Université Libre de Bruxelles
D. Dochain   Université Libre de Bruxelles
J. Winkin   University of Namur
M. Mukepe Kahilu, J. Kalenga Kaunde

ThM04-3   **11.35-12.00**
Optimal Control and Approximations 171
H. Zwart   University of Twente
K. Morris   University of Waterloo
O. Iftime   University of Groningen

ThM05	**Lucasgat E**
Energy Systems II	
Chair: Raffaella Carloni	**10.45-12.25**

ThM05-1   **10.45-11.10**
A Convex Formulation of a Bilevel Optimization Problem for Energy Markets 172
K. Shomalzadeh   University of Groningen

ThM05-2   **11.10-11.35**
A Microscopic Energy Consumption Prediction Tool 173
C. Beckers   Eindhoven University of Technology
I. Besselink   Eindhoven University of Technology
H. Nijmeijer   Eindhoven University of Technology

ThM05-3   **11.35-12.00**
Local Voltage Control of an Inverter-based Power Distribution Network With a Class of Slope-restricted Droop Controllers 174
M. Chong   Eindhoven University of Technology
D. Umsonst   KTH Royal Institute of Techonology
H. Sandberg   KTH Royal Institute of Technology

ThM05-4   **12.00-12.25**
Active Damping of a DC Network: An Adaptive Scheme 175
J. Machado   University of Groningen
R. Ortega   CNRS-SUPELEC
A. Astolfi   Imperial College of London

ThM06	**Solsegat**
Data-driven in Control II	
Chair: Manon Kok	**10.45-12.25**

ThM06-1   **10.45-11.10**
Real-Time Inverse Dynamics Learning for Feed-forward Control Using Gaussian Process Regression 176
W. van Dijk   University of Twente
W. Hakvoort   University of Twente
B. Rosic   University of Twente

ThM06-2   **11.10-11.35**
Data-driven Set Invariance Verification for Black-box Nonlinear Systems 177
Z. Wang   Université Libre de Bruxelles
R. Jungers   Université Libre de Bruxelles

ThM06-3   **11.35-12.00**
Tensor-based Methods for Sensor Fusion and Gaussian Process Regression 178
C. Menzen   Delft University of Technology
M. Kok   Delft University of Technology
K. Batselier   Delft University of Technology

ThM06-4   **12.00-12.25**
Imitation Learning for Autonomous Vehicle Driving Using Constrained Policy Networks and B-Spline Parametrization 179
F. Acerbo   Siemens
H. Van der Auweraer   Siemens
S. Tong Duy   Siemens

Event: E2	**De Grote Zael**
DISC Certificates & Best Presentation Award	
Chair: Award Committee	**12.30–12.50**

Plenary: P8	**De Grote Zael**
Closure	
Chair: Organizing Committee	**12.50–13.00**

Part 2

Contributed Lectures

Carrier-vehicle Routing Problem in City Environments

Nicolás Bono Rosselló, Emanuele Garone
Department of Control Engineering and System Analysis
Université libre de Bruxelles
50, av. F.D. Roosevelt, CP 165/55
1050 Bruxelles, Belgique
nbonoros@ulb.ac.be, egarone@ulb.ac.be

1 Introduction

The use of autonomous vehicles is incessantly gaining ground in daily life activities. Their technological advancements in terms of performance and reliability have been gathering the attention of several fields. In this context, delivery and transportation tasks have raised as one of their main areas of application, where the capabilities of these systems are highly appreciated and demanded [1].

Transportation and delivery problems have been widely studied by the scientific literature. How to combine a fleet of vehicles and to compute their optimal routes has been established as one of the well known combinatorial optimization problems in the literature.
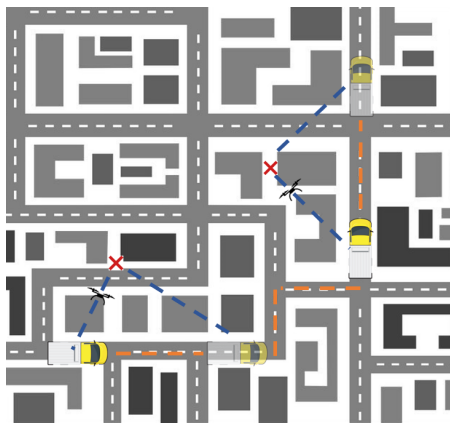
Figure 1: Schematic of the carrier-vehicle system.

In this contribution we present an extension of the carrier-vehicle problem [2] for the case of delivery in an urban environment. The small vehicle, namely a drone, performs the delivery of goods at the customer address while the large vehicle is in charge of transporting, launching, recovering and servicing the drone. In this work it is assumed that the take-off and landing points are not at the location of the customer but fixed spots predefined by the city. The selection of these spots is restricted by the autonomy of the drone and the velocity of both vehicles.

2 Problem Statement

This contribution deals with the problem of transport and delivery of packages by employing a two vehicles system in an urban environment. The aim of the mission is to deliver n packages to a set $P = \{p_1, \ldots, p_n\} \in \mathbb{R}^2$ of assigned delivery locations in the shortest time possible.

The system considered for such a task is composed by a big and slow vehicle carrier and a small and fast carried vehicle. The carrier is assumed to be a terrestrial vehicle which must follow the predefined routes given by the city distribution, e.g. a truck. On the other hand, the carried vehicle is assumed to be an aerial vehicle, namely a drone, which can move freely in the space.

This system, in the case of n customers, presents two kind of time intervals. The time when the vehicle is on board of the truck, denoted by $t_i^{l,to}, i = 1, \ldots, n+1$ and when the vehicle is airborne denoted by $t_i^{to,l}$, $i = 1, \ldots, n$. Knowing that the drone flight time is limited by the endurance a, the following constraints must be satisfied:

$$0 \le t_i^{to,l} \le a \quad i = 1, \ldots, n, \tag{1}$$

$$0 \le t_i^{l,to} \quad i = 1, \ldots, n+1. \tag{2}$$

The optimal route for both vehicles is the route which minimizes the sum of all these time intervals. In this framework, based on [2], this route can be defined and computed by selecting the launch and recovery spots for the drone and the shortest path between these points.

References

[1] S. A. Bagloee, M. Tavana, M. Asadi, and T. Oliver, "Autonomous vehicles: challenges, opportunities, and future implications for transportation policies," *J. Mod. Transport.*, vol. 24, pp. 284–303, Dec. 2016.

[2] E. Garone, R. Naldi, and A. Casavola, "Traveling Salesman Problem for a Class of Carrier-Vehicle Systems," *Journal of Guidance, Control, and Dynamics*, vol. 34, pp. 1272–1276, July 2011.

Routing Strategy for Large-Scale Dense AGVs Systems

Veronika Mazulina, Alexander Pogromskiy, Henk Nijmeijer
Dynamics and Control Group, Department of Mechanical Engineering
Eindhoven University of Technology
Email: v.mazulina@tue.nl, a.pogromski@tue.nl, h.nijmeijer@tue.nl

1 Introduction

Over the past decade, the volumes of goods purchased online has grown tremendously. Along with this, e-commerce companies must meet the growing demands of clients in order to remain competitive in the market. Private customers usually make small orders consisting of several items. Also, they want to choose among a wide range of products and expect that the order will be delivered in a short time without any fails.

The above challenges led to the necessity to increase the performance of the order picking process. The first step was to move from a conventional warehouse, where orders were collected manually by humans, to the automated ones, where sorting process is executed by automated guided vehicles (AGVs). However, this was not enough since the number of online orders is continuing to grow.

To provide the required level of performance, online retailers are increasing the area of the distribution centers and the number of sorting AGVs. New large-scale dense repositories require new routing strategies that speed up the sorting process while ensuring the absence of deadlocks and congestions in the AGVs system.

Therefore, the goal of this project is to develop a routing strategy that provides the best performance for the large (the size of the workspace is 10,000 m^2) and dense (AGVs occupy 20% of the workspace zones) AGVs systems.

2 Case Study

The parcel sorting system has been chosen as a case study. Its work is organized as follows: when a new parcel arrives at the pick-up station, an idle vehicle is sent to pick it up. Upon arrival at the pick-up station, the parcel is loaded on the AGV. Following this, the vehicle drives to the predefined drop-off station to dump a parcel. After that, the AGV can be sent to a new job or sent to the depot if all parcels are sorted.

A workspace layout of the parcel sorting system is shown in Figure 1. The surface on which AGVs move could be represented as a square grid. The elements of the grid are called zones. There are four types of zones: pick-up stations (purple diamonds), drop-off stations (black square), drop-off points (yellow diamonds), intersections (the remaining zones). Pick-up stations, drop-off points and
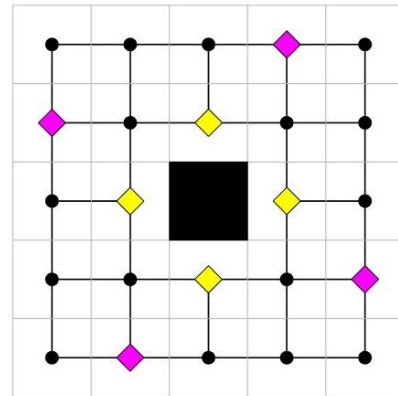
Figure 1: Workspace layout of the parcel sorting system

intersections are connected by bidirected path segments. The drop-off stations are consist of four drop-off points. Drop-off points are located on each side of the drop-off station to which they relate and have the same ID.

3 Routing Strategy

According to the literature review [1,2], the time-windows method looks the most promising for the achievement of the project goal. In this method, the AGVs reserve not only the zones on the way to the target, but also the time interval in which they are going to occupy each zone. Computation of AGVs routes is carried out in prioritized order.

In the presentation, the detailed explanation of the time-windows algorithm, its extensions for the parcel sorting system, the results of the numeric simulations and comparison with heuristic algorithm will be presented.

References

[1] Smolic-Rocak, Nenad, et al. "Time windows based dynamic routing in multi-AGV systems." IEEE Transactions on Automation Science and Engineering 7.1 (2009): 151-155.

[2] ter Mors, Adriaan, Jonne Zutt, and Cees Witteveen. "Context-Aware Logistic Routing and Scheduling." In ICAPS, pp. 328-335. 2007.

Energy Optimal Coordination of Fully Autonomous Vehicles in Urban Intersections

C. Pelosi, G.P. Padilla, M.C.F. Donkers
Control Systems Group, Dep. of Electrical Engineering, Eindhoven University of Technology
c.pelosi@student.tue.nl, {g.p.padilla.cazar, m.c.f.donkers}@tue.nl

1 Introduction

A major challenge in modern transportation is to achieve zero accidents while at the same time emit as little greenhouse gasses and harmful pollutants. One of the main causes can be attributed to traffic congestion and idling time of vehicles at signalized intersections [1, 2].

The topic of coordination of vehicles along an intersection has been addressed in the literature from different researchers. The proposed solutions focus on safety and often considers heuristic approaches to define the intersection crossing priority, which might lead to an energy sub-optimal solution [3]. On the other hand, energy optimality of trajectories for vehicles have been analyzed in the context of eco-driving [4], where the coordination problem in intersections is not addressed.

This paper proposes an approach which aims to fill the gap noticed in the literature by proposing an optimal control problem formulation able to solve any kind of intersection conflict scenarios between autonomous vehicles aiming to cross an intersection with the objective to minimize the global energy consumption of the vehicles. Moreover, an alternative modelling framework is propose in order to simplify the formulation of the problem and finally, a Sequential Quadratic Programming (SQP) formulation is adopted in order to solve the problem.

2 Coordination of Urban Intersections

The coordination of an urban intersection scenario of N_v Autonomous Vehicles (AVs) is proposed. Each vehicle follows a pre-defined route such that a collision might occur if no control action is applied. The desired route of each AV is considered to be a priori given, i.e., by using a high-level path planning algorithm, which is outside the scope of this study. Hence, the objective is to control the velocity of each vehicle along its trajectory such that the energy consumption is minimized and the position of each vehicle is mutually exclusive, i.e, a control agent will modify the desired velocity profiles of the vehicles in order to let them cross safely while minimizing energy losses.

Specifically, a four-way perpendicular crossroad is considered (see Fig. 1) in this analysis, since first it represent a typical urban crossroad and secondly because it allows to perform analysis on complex intersection scenarios. Finally, all vehicles are considered to be equipped with V2V, V2I
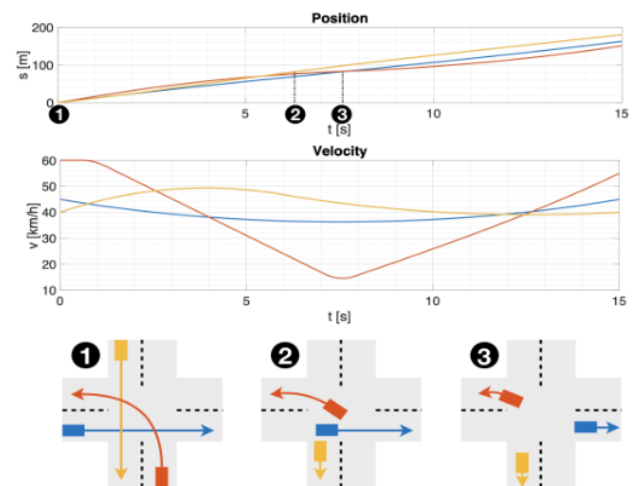
Figure 1: Position, velocity profiles and order resolution of a three vehicles intersection scenario.

communication systems and at most one vehicle per lane is approaching the intersection.

3 Optimal Control Problem

The conflict resolution problem is formulated as an optimal control problem, where the objective is to minimize energy consumption of all the vehicles, while avoiding collisions. The presence of non linear dynamics and integer decision variables in the problem formulation is a clear indicator of its complexity. In this paper, we proposed a SQP approach to fins local solutions to this problem. Simulation results point out how relying on AVs instead of human-driven can reduce the overall energy consumption, up to 16.2%.

References

[1]   Schrank D. and Lomax T. and Eisele B., "Urban Mobility Report", 2019.

[2]   Kural E., Parrilla A.F., and Grauers A., " Traffic light assistant system for optimized energy consumption in an electric vehicle," in Proc. Int. Conf. Connected Vehicles, 2014.

[3]   Campos G.R., Falcone P. and Sjoberg J., "Traffic safety at intersections: a priority based approach for cooperative collision avoidance," in Proc. Int. Symp. Future Active Safety Technology, 2015.

[4]   Han J., Vahidi A. and Sciarretta A., "Fundamentals of energy efficient driving for combustion engine and electric vehicles: An optimal control perspective," in Automatica, 2016.

Communication Strategies for Synchronized Merging of Cooperative Vehicles

Di Liu, Harry L. Trentelman, and Bart Besselink
Bernoulli Institute for Mathematics, Computer Science and Artificial Intelligence,
University of Groningen, The Netherlands
di.liu@rug.nl, h.l.trentelman@rug.nl, b.besselink@rug.nl

Abstract

Strategies for cooperative control of autonomous vehicles that have been proposed in the past suffer from the drawback of dealing only with acyclic graphs, for example the look-ahead topology. However, more complex maneuvers, such as synchronized merging/splitting, are likely to require cyclic communication strategies, on this note, we describe the problem formulation and further introduce the problem of vehicle parametric uncertainty.

Problem Statement and Idea

Consider the longitudinal dynamics of an automated vehicle:

$$\begin{pmatrix} \dot{s}_i \\ \dot{v}_i \\ \dot{a}_i \end{pmatrix} = \begin{pmatrix} 0 & 1 & 0 \\ 0 & 0 & 1 \\ 0 & 0 & -\frac{1}{\tau_i} \end{pmatrix} \begin{pmatrix} s_i \\ v_i \\ a_i \end{pmatrix} + \begin{pmatrix} 0 \\ 0 \\ \frac{1}{\tau_i} \end{pmatrix} u_i, \qquad (1)$$

where s_i, v_i, a_i and u_i are respectively the position, velocity, acceleration (m/s^2) and external input (m/s^2) of the ith vehicle, and τ_i (s) represents each vehicle's driveline time constant. While in most existing literatures the driveline time constant is considered to be known, a relevant problem is having uncertain τ_i. Consider the merging maneuver in Fig. 1 where one vehicle must merge in the gap between two other vehicles, and consider the communication graphs in Fig. 2. we consider a constant time headway (CTH) spacing policy, which defines the desired distance as:

$$d_{j,i}(t) = r_{j,i}(t) + h v_i(t) , \qquad (2)$$

where $d_{j,i}(t)$ is the distance (m) between vehicles i and j, $r_{j,i}$ is the standstill distance (m) between the same vehicles and h the time headway (s). Let us now define the state error (spacing distance, relative velocity, and relative acceleration) between the jth and the ith vehicle as:

$$e_{j,i}(t) = \begin{pmatrix} s_j(t) \\ v_j(t) \\ a_j(t) \end{pmatrix} - \begin{pmatrix} s_i(t) \\ v_i(t) \\ a_i(t) \end{pmatrix} + \begin{pmatrix} d_{j,i}(t) \\ 0 \\ 0 \end{pmatrix} \qquad (3)$$

which is defined for any two adjacent vehicles between which a communication link exists.

Problem: With reference to the benchmark of Fig. 1, given the vehicle dynamics (1) with unknown driveline constants,
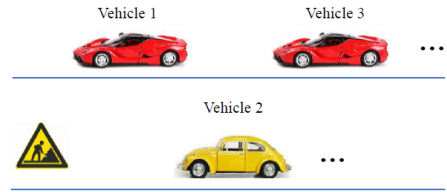
Figure 1: Merging maneuver under consideration: the yellow vehicle must merge with the red vehicles due to traffic roadworks.

find a cyclic communication strategy such that merging can be achieved.

(a) During merging
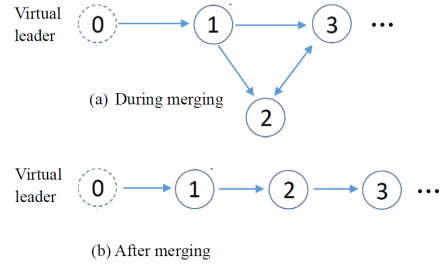
(b) After merging

Figure 2: Spacing policy during and after merging.

Idea: The idea for solving the problem is to consider it as an adaptive synchronization problem:

Reference dynamics for the platoon are defined by

$$\begin{aligned} \begin{pmatrix} \dot{s}_0 \\ \dot{v}_0 \\ \dot{a}_0 \end{pmatrix} &= \begin{pmatrix} 0 & 1 & 0 \\ 0 & 0 & 1 \\ 0 & 0 & -\frac{1}{\tau_0} \end{pmatrix} \begin{pmatrix} s_0 \\ v_0 \\ a_0 \end{pmatrix} + \begin{pmatrix} 0 \\ 0 \\ \frac{1}{\tau_0} \end{pmatrix} u_0 \\ \begin{pmatrix} \dot{s}_0 \\ \dot{v}_0 \\ \dot{a}_0 \end{pmatrix} &= \begin{pmatrix} 0 & 1 & 0 \\ 0 & 0 & 1 \\ a_{01} & a_{02} & a_{03} \end{pmatrix} \begin{pmatrix} s_0 \\ v_0 \\ a_0 \end{pmatrix} + \begin{pmatrix} 0 \\ 0 \\ b_{00} \end{pmatrix} w \end{aligned} \qquad (4)$$

Where w is desired acceleration of the leading vehicle, a_{01}, a_{02}, a_{03} are design parameters selected such that the matrix is Hurwitz. Merging will be achieved by designing u_i such that $e_{j,i}$ in (3) is regulated to zero for all links that exist during all phases of the merging.

Learning-Based Risk-Averse Model Predictive Control for Adaptive Cruise Control with Stochastic Driver Models

Mathijs Schuurmans[1],   Alexander Katriniok[2],   Hongtei Eric Tseng[3],   Panagiotis Patrinos[1]

[1] ESAT-STADIUS, KU Leuven   [2,3] Ford Research & Innovation Center
Kasteelpark Arenberg 10   [2]52072, Aachen, Germany
3001, Leuven, Belgium   [3]Dearborn MI 48123, USA

1 Background and motivation

In recent decades, the usage of adaptive cruise control (ACC) systems has become widespread in the automotive research and industry, as they have demonstrated numerous benefits in terms of safety, fuel efficiency, passenger comfort, etc. The term ACC generally refers to longitudinal control systems that are aimed at maintaining a user-specified velocity, while avoiding collisions with preceding vehicles (see Figure 1).

Due to the inherent uncertainty about the future behavior of the preceding vehicle, stochastic model predictive control (MPC) has been a particularly popular strategy towards this application [1, 3]. Here, the lead vehicle behavior is commonly modelled by a combination of continuous physics-based dynamics with a discrete, stochastic decision model for the driver (e.g., [2, 1]). We follow this line of reasoning and model the preceding vehicle using double integrator dynamics, where the driver's inputs are generated by a Markov chain. The vehicle pair is thus described by a discrete-time Markov jump linear system with dynamics of the form

$$x_{t+1} = A(w_{t+1})x_t + B(w_{t+1})u_t + p(w_{t+1}),$$

where $x_t \in \mathbb{R}^{n_x}$ is the state vector $u_t \in \mathbb{R}^{n_u}$ is the input and $(w_t)_{t \in \mathbb{N}}$ is a Markov chain with transition matrix $P \in \mathbb{R}^{M \times M}$, with elements $P_{i,j} = \mathbb{P}[w_t = j \mid w_{t-1} = i]$.

A major shortcoming of stochastic MPC approaches, however, is their reliance on accurate knowledge of P, as in practice, only a data-driven estimate $\hat{P}$ is available. This results in uncertainty on the probability distributions governing the stochastic process, often referred to as *ambiguity*. Due to this ambiguity, stochastic controllers may perform unreliably with respect to the true distributions.

2 Risk-averse model predictive control formulation

We generalize the stochastic MPC methodology for ACC systems by adopting a distributionally robust approach which accounts for data-driven ambiguity. We define an *ambiguity set* $\mathscr{A}_i$ for each row $\hat{P}_i \in \mathbb{R}^M$ of the estimated transition matrix $\hat{P}$ as

$$\mathscr{A}_i := \left\{ \mu \in \mathbb{R}^M \; \middle| \; \begin{array}{l} \|\mu - \hat{P}_i\|_1 \leq r_i, \\ \sum_{j=1}^{M} \mu_j = 1, \mu \geq 0 \end{array} \right\}, \qquad (1)$$
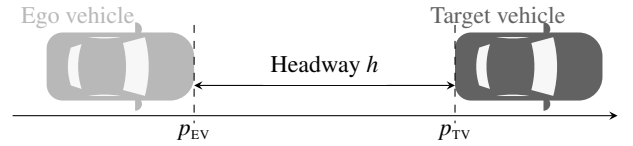
Figure 1: Illustration of the ACC problem.

where r_i is computed such that $\mathbb{P}[P_i \in \mathscr{A}_i] \geq 1 - \beta$, with $\beta \in (0,1)$ an arbitrary confidence level using result from [4].

By minimizing the expected cost subject to chance constraints with respect to the worst-case distributions in these ambiguity sets, we obtain a so-called multi-stage risk-averse risk-constrained optimal control problem (OCP). By virtue of the polytopic structure of (1), this can be cast to a convex conic optimization problem [5], which can be efficiently solved. When $\mathscr{A}_i = \{P_i\}, \forall i \in \mathbb{N}_{[1,M]}$, the problem reduces to the original stochastic OCP.

The closed-loop MPC controller is obtained by resolving the risk-averse OCP in every time step, where for all visited modes i, the radii r_i of the ambiguity sets $\mathscr{A}_i$ are decreased over time as more data is gathered. As a result, the obtained controller gradually becomes less conservative during closed-loop operation. Finally, we derive an inner approximation of the maximal robust control invariant set, which we use as a terminal constraint set for all realizations of the stochastic system. This allows us to establish recursive feasibility of the MPC scheme, and thus guarantee safe operation while using observed data to improve performance.

References
[1]   M. Bichi, G. Ripaccioli, S. D. Cairano, D. Bernardini, A. Bemporad, and I. V. Kolmanovsky. Stochastic model predictive control with driver behavior learning for improved powertrain control. In *49th IEEE Conference on Decision and Control (CDC)*, pages 6077–6082, Dec. 2010.
[2]   U. Kiencke, R. Majjad, and S. Kramer. Modeling and performance analysis of a hybrid driver model. *Control Engineering Practice*, 7(8):985–991, 1999.
[3]   D. Moser, R. Schmied, H. Waschl, and L. d. Re. Flexible Spacing Adaptive Cruise Control Using Stochastic Model Predictive Control. *IEEE Transactions on Control Systems Technology*, 26(1):114–127, Jan. 2018.
[4]   M. Schuurmans, P. Sopasakis, and P. Patrinos. Safe learning-based control of stochastic jump linear systems: a distributionally robust approach. *arXiv preprint arXiv:1903.10040*, 2019.
[5]   P. Sopasakis, M. Schuurmans, and P. Patrinos. Risk-averse risk-constrained optimal control. In *2019 18th European Control Conference (ECC)*, pages 375–380, June 2019.

Design of a Highway On-ramp Merging Maneuver for Cooperative Platoons

W.J. Scholte, P.W.A. Zegelaar, H. Nijmeijer
Eindhoven University of Technology, P.O. Box 513, 5612 AP Eindhoven, The Netherlands
Email corresponding author: w.j.scholte@tue.nl

Introduction

Cooperative platooning is a technology that allows vehicles to drive closely together in a string using wireless communication. It has the potential to reduce traffic congestion, fuel consumption and emissions [3]. Cooperative adaptive cruise control (CACC) is often used for cooperative platooning. For practical applications, automated merges in a highway environment of such a string are desirable. Research on automated merges often does not often focus on platoons [3]. However, in the grand cooperative driving challenge the merging of two cooperative platoons was investigated. During this event two platoons merged into one large platoon. The platoons were driving alongside each other at the start of the maneuver [1]. In this paper the merge of a single vehicle in a highway on-ramp scenario is considered. For such a situation the new vehicle typically does not drive alongside the existing platoon at the start. Therefore, a different control approach is designed.

Merging Control Strategy

The merge maneuver has been visualized in Figure 1. In essence, we consider a single vehicle that joins a cooperative platoon at a highway on-ramp. The platoon is driven using the CACC algorithm as described in Ploeg et al. [2]. Due to the highway on-ramp there are spatial constraints for the new vehicle. Furthermore, there may be a velocity difference between the platoon and the new vehicle when it arrives at the on-ramp. Therefore, the new vehicle is not necessarily aligned with its desired location in the platoon at the start of the maneuver. When a suitable position is selected the gap can be opened in the platoon while the new vehicle simultaneously aligns with the gap. This ensures that the platoon can accommodate the new vehicle when it arrives at the desired position.

A control strategy for highway on-ramp merge maneuvers was designed. The main focus of the current work was the gap creation in the platoon and a longitudinal and lateral trajectory of the new vehicle. The selection of the new vehicle's position in the platoon (platoon sequence management) was done using an elementary algorithm. The new vehicle selects the gap closest to itself. The switching of the preceding vehicle was performed
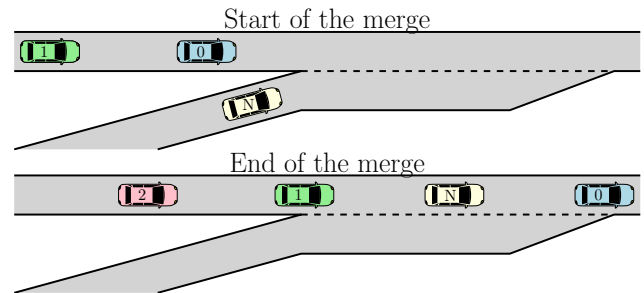
Figure 1: A highway on-ramp merge of a new vehicle into an existing CACC platoon.

by a hard switch in the CACC controller.

Conclusions and Future Work

A control strategy for highway on-ramp merge maneuvers was designed and experimentally validated using small robots. Improvements of the platoon sequence management and the preceding vehicle switching strategy of the current strategy are subject to future research.

Acknowledgments

References

[1]   HULT, Robert, et al. Design and experimental validation of a cooperative driving control architecture for the grand cooperative driving challenge 2016. IEEE Transactions on Intelligent Transportation Systems, 2018, 19.4: 1290-1301.

[2]   PLOEG, Jeroen; VAN DE WOUW, Nathan; NIJMEIJER, Henk. Lp string stability of cascaded systems: Application to vehicle platooning. IEEE Transactions on Control Systems Technology, 2013, 22.2: 786-793.

[3]   RIOS-TORRES, Jackeline; MALIKOPOULOS, Andreas A. A survey on the coordination of connected and automated vehicles at intersections and merging at highway on-ramps. IEEE Transactions on Intelligent Transportation Systems, 2016, 18.5: 1066-1077.

Mobile Robot Path Following Control: Singularity Elimination

Weijia Yao, Ming Cao

ENTEG, University of Groningen

Email: {w.yao, m.cao}@rug.nl

In vector-field-based path following (VF-PF), a vector field is designed and utilized to guide a robot to follow a desired path. VF-PF algorithms have been shown to achieve high path-following precision under small control effort compared with many other path following algorithms. However, due to the existence of singular points where the vector field vanishes, the global convergence of VF-PF algorithms to the desired path cannot be guaranteed. Moreover, as holds for most of the existing path following algorithms, VF-PF algorithms may fail to enable following a self-intersected desired path. Therefore, we propose a method to assist generic VF-PF algorithms in their global convergence. In particular, our method creates vector fields free of singular points in a higher-dimensional space containing the lower-dimensional desired path. Subsequently, the projection of our vector fields on the lower-dimensional space of the desired path can be exploited to guarantee the global convergence of the robot to the desired path, including those self-intersected.

1 Motivation

In the VF-PF problem, the desired path to follow is usually described by the zero-level set of a sufficiently smooth function. In particular, a planar desired path is described by the following set:

$$\overline{\mathcal{P}} = \{(x,y) \in \mathbb{R}^2 : \overline{\phi}(x,y) = 0\}, \qquad (1)$$

where $\overline{\phi} : \mathbb{R}^2 \to \mathbb{R}$ is twice continuously differentiable. The solutions to the differential equation $\dot{\xi}(t) = \overline{\chi}(\xi(t))$ are the *integral curves* of the vector field $\overline{\chi}$. Therefore, one aims to find a suitable vector field $\overline{\chi}$ such that the integral curves will approach the desired path eventually, and will stay on the desired path once it starts from it. One example of such a vector field is given in (Kapitanyuk et al, 2017):

$$\overline{\chi}(x,y) = E\nabla\overline{\phi}(x,y) - k\psi(\overline{\phi}(x,y))\nabla\overline{\phi}(x,y), \quad (2)$$

where $E = \begin{bmatrix} 0 & -1 \\ 1 & 0 \end{bmatrix}$ is the 90° rotation matrix, k is a positive constant, $\psi : \mathbb{R} \to \mathbb{R}$ is a strictly increasing function with $\psi(0) = 0$, and $\nabla(\cdot)$ denotes the gradient of a scalar function.

Proposition 1. *Denote a crossing point of the desired path $\overline{\mathcal{P}}$ in (1) by $c \in \overline{\mathcal{P}}$. Then c is a singular point of the vector field in (2); that is, $\overline{\chi}(c) = \mathbf{0}$.*

2 Problem Formulation

We propose to add an extra dimension to the original 2D guiding vector field to eliminate possible singular points. The spatial desired path $\mathcal{P}$ in $\mathbb{R}^3$ is naturally characterized by adding an additional constraint in $\mathbb{R}^3$ as follows:

$$\mathcal{P} = \{\xi \in \mathbb{R}^3 : \phi_1(\xi) = 0, \ \phi_2(\xi) = 0\}, \qquad (3)$$
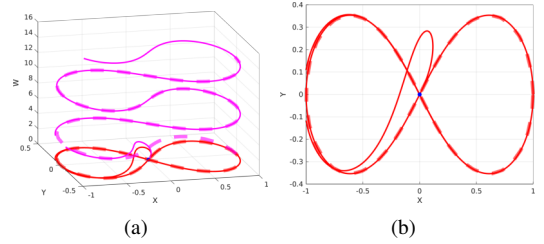
Figure 1: (a) The magenta and red dashed lines are the spatial desired path $\mathcal{P}$ and the projected desired path $\overline{\mathcal{P}}$ respectively. The magenta solid line is the 3D trajectory $\xi(t)$ of $\dot{\xi} = \chi(\xi)$, and the red solid line is the projected "2D trajectory". (b) The "2D trajectory" $\xi_2'(t)$ in the XY-plane, where the blue point is the starting position $(0,0)$.

where $\phi_1, \phi_2 \in C^2$, $\xi = (x,y,w) \in \mathbb{R}^3$ and w is the extra dimension of the vector field. The corresponding 3D guiding vector field $\chi : \mathbb{R}^3 \to \mathbb{R}^3$ that solves the path following problem and the corresponding singular set $\mathcal{C}$ are respectively (Yao et al, 2018):

$$\chi(\xi) = \nabla\phi_1(\xi) \times \nabla\phi_2(\xi) - \sum_{i=1}^{2} k_i\phi_i(\xi)\nabla\phi_i(\xi). \qquad (4)$$

$$\mathcal{C} = \{c \in \mathbb{R}^3 : \chi(c) = \mathbf{0}\}. \qquad (5)$$

A linear projection operator $P_a : \mathbb{R}^3 \to \mathbb{R}^3$ is defined by
$$P_a = I - \hat{a}\hat{a}^\top, \qquad (6)$$

where I is the identity matrix of suitable dimensions and $\hat{a} := a/\|a\|$. Now we can define the *projected desired path* as follows:

$$\mathcal{P}' = \{\xi' \in \mathbb{R}^3 : \xi' = P_a\xi, \ \xi \in \mathcal{P}\}. \qquad (7)$$

Problem. *Given a (possibly self-intersected) planar desired path $\overline{\mathcal{P}} \subset \mathbb{R}^2$, one aims to find a spatial desired path $\mathcal{P} \subset \mathbb{R}^3$, which satisfies the following conditions: a) There exist functions $\phi_i(\cdot) \in C^2$ such that $\mathcal{P}$ is described by (3). b) There exists a projection operator P_a in (6) such that the projected desired path $\mathcal{P}'$ in (7) satisfies $\mathcal{P}' = \{(x,y,0) \in \mathbb{R}^3 : (x,y) \in \overline{\mathcal{P}}\}$. c) The singular set $\mathcal{C}$ of the corresponding higher-dimensional vector field $\chi : \mathbb{R}^3 \to \mathbb{R}^3$ in (4) is empty.*

We propose a new idea to seek such a spatial desired path $\mathcal{P} \subset \mathbb{R}^3$. Once such a spatial desired path is obtained, the 3D vector field will be automatically generated by (4). An example is illustrated in Fig. 1.

References

[1] W. Yao, H. G. de Marina, and M. Cao, "Mobile robot path following control in 2d using a 3d guiding vector field: Singularity elimination and global convergence," 2019, under review.

Model predictive control toolchain for constraint-based task specification of robot motions

Ajay Suresha Sathya, Joris Gillis, Goele Pipeleers, Wilm Decre, Jan Swevers
Department of Mechanical Engineering, Division PMA
KU Leuven, BE-3001, Heverlee, Belgium
DMMS lab, Flanders Make, Leuven, Belgium
firstname.secondname@kuleuven.be

1 Introduction

Several frameworks such as [1] have been proposed to specify continous motion tasks of a robot. Such a task specification approach achieves separation-of-concerns where the problem of task programming is separated from robot programming, therefore making it easier to program the same task for different robot platforms. [1] also follows a constraint-based approach which allows for straightforward composition of different tasks (for example: transporting a glass of water can be specified as a point-to-point motion constraint composed with a constraint on orientation).

But to the best of our knowledge, these frameworks provide interface to an instantaneous robot controller without a prediction horizon. An important drawback of an instantaneous controller is that the prediction horizon is too short (equal to the sample time) to adjust the control action to prevent infeasibilities in the near future. This forces the programmer to use conservative bounds on joint velocity/torques, which can affect performance, or to come up with adhoc solutions that modify the behaviour near infeasibilities, which is very time-consuming and does not generalize to different tasks easily. In this work we aim to retain the advantages of constraint-based robot task specification and also deal with the aforementioned issues by using model predictive control (MPC) to control the robot motions.

2 MPC toolchain

Figure 1 shows the modular structure of the MPC toolchain that we are currently working towards. Expressions relevant to task specification, such as end effector pose, are automatically generated as CasADi expressions by evaluating the robot kinematics and dynamics using Pinocchio library. Task specifications on these expressions and MPC options are supplied by the user to formulate MPC problem as a nonlinear program (NLP). Utilizing the interfaces provided to external NLP solvers and the task specification, code generation is employed to obtain an MPC program. This program could be deployed in the real world and/or visualized in virtual environments such as RViz.
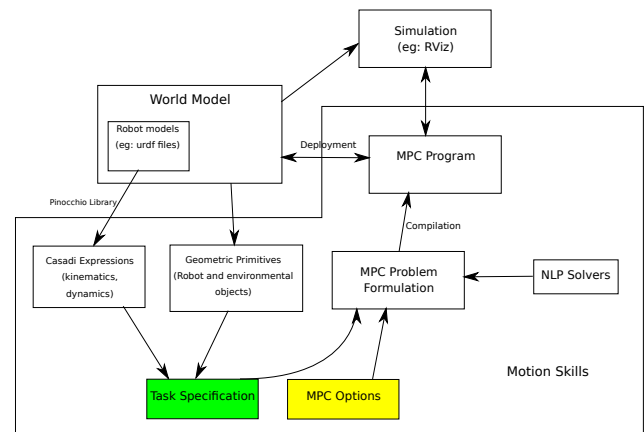
Figure 1: Structure of the MPC toolchain

3 Conclusions and Future work

The modular structure of the proposed framework allows for re-usability of individual components. It also provides an important benefit of abstracting away details such as NLP solvers, computation of kinematics and dynamics. The programmer only needs to focus on the task specification and MPC options box therefore simplifying the development of robot motion skills with MPC.

As future work, we aim to validate and benchmark our toolchain on complex multirobot tasks such as laser contour tracing and a force control task involving wiping a surface.

References

[1] Erwin Aertbeliën and Joris De Schutter. etasl/etc: A constraint-based task specification language and robot controller using expression graphs. In *Intelligent Robots and Systems (IROS 2014), 2014 IEEE/RSJ International Conference on*, pages 1540–1546. IEEE, 2014.

A Predictive Model for Nafion-based IPMC Soft Actuators

Ruben Langius
University of Groningen
Nijenborgh 9, 9747 AG
langiusruben@gmail.com

Riccardo D'Anniballe
University of Groningen
Nijenborgh 9, 9747 AG
r.danniballe@rug.nl

Raffaella Carloni
University of Groningen
Nijenborgh 9, 9747 AG
r.carloni@rug.nl

1 Introduction

Ionic polymer-metal composites (IPMCs) are electro-active polymers that, when stimulated by an electric field, convert electrical energy into mechanical energy. Characteristics such as low actuation voltage, softness, and self-sensing make IPMCs interesting materials in soft actuation and, more in general, in the broad field of soft robotics [1].

2 Fabrication and Electromechanical Characterization

Three IPMC soft actuators have been fabricated by means of Nafion^{TM} 117. The chemical process proposed in [2] has been used, which consists of four main steps: (i) treating the surface of the Nafion^{TM} 117; (ii) submersing the Nafion^{TM} 117 in a salt solution that contains metal ions; (iii) reducing the absorbed metal ions to a metallic state nanoparticle; (iiii) creating a secondary plating.

The realized IPMC soft actuators have been electromechanically characterized. Specifically, the collected data are the actuators' tip forces over time in relation to the voltage supplied to the actuators.

The measurements have been performed with the Instron® Electropulse E1000 test machine (https://www.instron.us/), equipped with the Instron® static load cell 2530-5N.

Each actuator has been stimulated by different voltages (2, 3, and 4 V), generated by the RIGOL DG1022 waveform generator (https://www.rigolna.com), combined with the TREK 10/10B-HS high-voltage amplifier (https://www.trekinc.com). The measurements set-up is sketched in Figure 1.

3 Neural Network Model

The soft actuators have been modeled by means of a feedforward neural network, implemented with a multilayer perceptron architecture. The neural network has been designed in the Pytorch framework, and the Adam algorithm has been chosen as optimization algorithm for the network.

The neural network has been trained and validated on two out of three fabricated IPMC soft actuators. Specifically, the two actuators have been fabricated by following the same procedure, but they differ in dimensions. The data collected
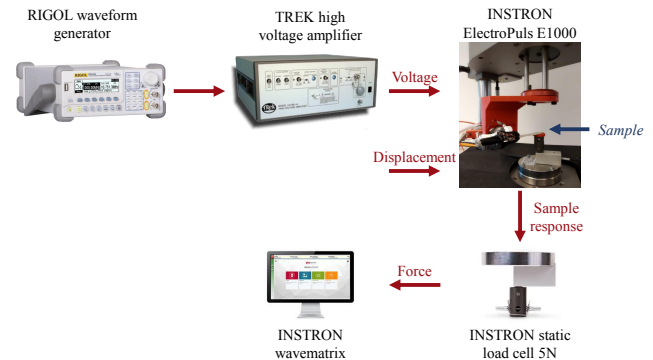
Figure 1: Measurements set-up for the electromechanical characterization.

on the two actuators have been split into a training and a validation set. The training set consists of 80% of the data and has been trained for 25 epochs. The validation set consists of the rest 20%. The performance of the neural network has been evaluated by using the root mean square error (RMSE), i.e., by comparing the measured forces in the validation data set with the predicted forces from the neural network. After training, a RMSE of 0.042 has been achieved on the validation set.

The resulting neural network has been tested on the third actuator, fabricated with the same dimensions as one of the two actuators used for the training and validation. The RMSE on the third actuator is 0.034.

4 Conclusions

The neural network can predict the tip force of the Nafion^{TM} 117 IPMC soft actuators within 120 s and with a good accuracy. The predicted model can be used for testing and comparing performances of different fabrication methods and control methods.

References

[1]   M. Shahinpoor and K.J. Kim, "Ionic polymer-metal composites: IV. Industrial and medical applications", Smart Materials and Structures, vol. 14, no. 1, pp. 197-214, 2 2005.

[2]   V. De Luca, *et al.*, "Ionic electroactive polymer metal composites: Fabricating, modeling, and applications of postsilicon smart devices", Journal of Polymer Science Part B: Polymer Physics, vol. 51, no. 9, pp. 699-734, 5 2013.

Towards a toolchain for fast MPC deployment on serial robots

Alejandro Astudillo[1*], Joris Gillis[1], Wilm Decré[1], Goele Pipeleers[1], Jan Swevers[1]

[1]MECO Research Team, Dept. of Mechanical Engineering, KU Leuven, Leuven, Belgium.

[1]DMMS Lab, Flanders Make, Leuven, Belgium.

[*]Email: `alejandro.astudillovigoya@kuleuven.be`

1 Abstract

Competitiveness and quality within modern industry requires serial robots to be easily configured, safe to work with, and to autonomously perform tasks in a precise manner. This creates demand for software tools that ease the workflow of robot-based solution deployment. Model predictive control (MPC) has been widely studied throughout the past decades. This control methodology allows for actively controlling a system while minimizing a performance cost and accounting for its dynamics, actuation limits, and safety constraints. This work proposes a toolchain for MPC of serial robots based on modules for rigid body dynamics, numerical optimization, and robot control. The proposed toolchain is evaluated with a numerical study regarding a path-following task for a serial robot.

2 Methodology

The objective of this toolchain is to define a workflow from problem definition to solution deployment in the framework of MPC for serial robots.
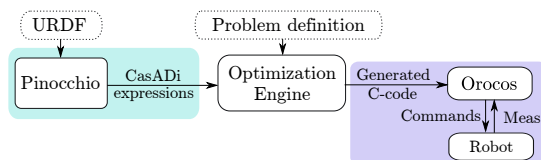
Figure 1: Overview of the toolchain for MPC on serial robots.

The toolchain, which overview is shown in Fig. 1, is based on the open-source software CasADi, Pinocchio, Optimization Engine, and Orocos. CasADi [1] is a framework for numerical optimization and algorithmic differentiation and is used as a back-end for expressions handling and code-generation. The workflow of the toolchain is defined as follows. The toolchain requires two user inputs: a problem definition, and a Unified robot description format (URDF) file. The problem definition is a Python script which sets the optimization problem on which the MPC controller is based by using CasADi expressions. On the other hand, a URDF is a file describing parametric and geometric features of a robot. The URDF file is used by the rigid body dynamics library Pinocchio to generate CasADi expressions for robot's forward dynamics, forward kinematics, and actuation limits. Afterwards, Optimization

Engine, a framework aimed for embedded nonconvex optimization, uses the CasADi expressions coming from Pinocchio and from the problem definition to set the optimization problem to be solved using PANOC [2], a first order algorithm for solving nonlinear programs, and the Augmented Lagrangian method. Optimization Engine then code-generates a solution for the defined optimization problem. This code-generated solution is then deployed into Orocos, a robotics control framework with hard real-time capabilities. Orocos executes the control action while sending commands to and receiving measurements from a (real or simulated) robot.

3 Results

We evaluate the proposed toolchain considering a path-following task for a 7-degrees-of-freedom Kinova Gen3 robot. The result achieved with the toolchain is compared with that using the SQP method with the QRQP QP-solver [3] performing just one SQP iteration, while using N_c cores to parallelize the evaluation of the dynamics constraints within the code-generated solution. Thus, the runtime speed-up using the proposed toolchain, with respect to the SQP method, with $N_c = 1, 2, 4$, and 8 is $1.02x$, $1.37x$, $1.83x$, and $2.25x$, respectively, with the toolchain's solution having a runtime of 1.501 ms with $N_c = 8$. The cooperation of the tools in the toolchain is efficient in terms of both computation and engineering time.

References

[1] J. Andersson, J. Gillis, G. Horn, J.B. Rawlings, and M. Diehl, "CasADi: a software framework for nonlinear optimization and optimal control," Mathematical Programming Computation, 2019.

[2] L. Stella, A. Themelis, P. Sopasakis, and P. Patrinos, "A simple and efficient algorithm for nonlinear model predictive control," 2017 IEEE 56th Annual Conference on Decision and Control (CDC), 2017.

[3] J. Andersson, and J.B. Rawlings, "Sensitivity Analysis for Nonlinear Programming in CasADi," IFAC-PapersOnLine 51(20), 2018.

Forward dynamics of hyper-elastic soft robots

Brandon Caasenbrood
Eindhoven University of Technology
`b.j.caasenbrood@tue.nl`

Alexander Progromsky
Eindhoven University of Technology
`a.y.pogromskiy@tue.nl`

Henk Nijmeijer
Eindhoven University of Technology
`h.nijmeijer@tue.nl`

1 Introduction

Unlike rigid robots, soft robots are composed of flexible material that enable complex and continuum-body motions. Due to their low compliance, soft robots can achieve incredible features with relative ease, such as grasping or locomotion, that can be relatively challenging for rigid robots. However, due to their inherent flexibility, modeling the dynamics can be challenging. In this work, we described an approach to model the nonlinear dynamics of a soft robot (see Fig. 1). Here, we use Lie group notations similar to [1].

2 Dynamic modeling

To describe the hyper-flexibility, we regard the body of the soft robot as a differentiable spatial curve that is subjected to finite displacements and small strains. This spatial curve is parameterized given a coordinate $\sigma \in X$ with $X \in [0,1]$, which may be viewed as an infinitesimal cross-section along the centerline of the soft robot. Each material point can be described by a position in $\mathbb{R}^3$ and a orientation matrix $R \in \mathbb{SO}(3)$. Given this context, we can write the configuration of a material point as an rigid body transformation $g : X \mapsto \mathbb{SE}(3)$ expressed in the Lie group $\mathbb{SE}(3)$. Then, the entire configuration space can be described by

$$C := \{g : \sigma \in [0,l] \mapsto g(\sigma) \in \mathbb{SE}(3)\}. \qquad (1)$$

Since the rigid body transformation depends on σ and t, its space-time variations can be described by two unique vector fields η and ξ belonging to the Lie algebra $\mathfrak{se}(3)$, that is,

$$\eta = (g^{-1}\dot{g})^{\vee}, \qquad (2)$$

$$\xi = (g^{-1}g')^{\vee}, \qquad (3)$$

where $\hat{\eta} \in \mathfrak{se}(3)$ and $\hat{\xi} \in \mathfrak{se}(3)$ are respectively the vector field for twist and strain, and $(\hat{\cdot})$ the isomorphism of $\mathbb{R}^6 \mapsto \mathfrak{se}(3)$. By applying Hamilton's variational principle, we obtain a PDE of the robot with an external wrench $\bar{\tau}$ acting along the elastic body of the soft robot:

$$\dot{\Sigma} - \mathrm{ad}_{\eta}^{\top}\Sigma = \Lambda' - \mathrm{ad}_{\xi}^{\top}\Lambda + \bar{\tau}, \qquad (4)$$

where $\Sigma = M\eta$ and $\Lambda = C(\xi - \xi_0)$ are the kinetic momenta and elastic internal stress along the soft robot, respectively.
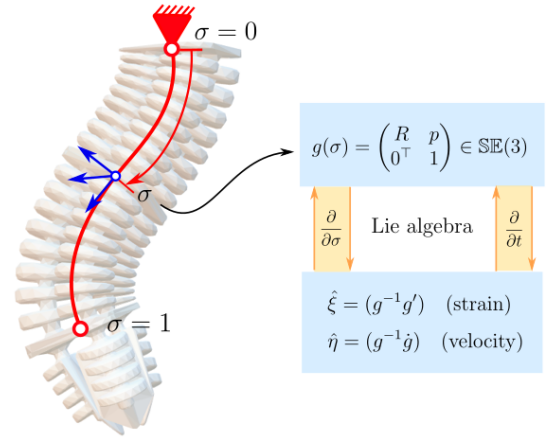
Figure 1: Schematic representation of the soft robot and its configuration space expressed in the Lie group $\mathbb{SE}(3)$.

3 Parametrization of the strain

In our analysis, we describe the dynamics of our robotic system through the parameterization of strain. For the numerical purposes, the strain vector field is discretized as follow

$$\xi = \xi_0(\sigma) + \Phi(\sigma)q(t), \qquad (5)$$

where $\xi_o = (g_o^{-1}g_o')^{\vee}$ is a vector field of zero strains, $\Phi = \mathrm{diag}\left(\Phi_1^{\top}, ..., \Phi_n^{\top}\right)$ is a block diagonal matrix composed of unique shape functions of the form $\Phi_i : \mathbb{R} \mapsto \mathbb{R}^n$, and $q(t) \in \mathbb{R}^n$ is a vector of generalized coordinates. From this notation and the previous relation in (4), we can obtain the equation of motion in the generic form:

$$M(q)\ddot{q} + C(q,\dot{q}) + D\dot{q} + Kq = \tau(t). \qquad (6)$$

The model is numerically implemented in MATLAB through the ODE45 solver. Furthermore, the approach is suitable for various soft robots, e.g., grippers and crawlers.

References

[1] S. Murray, Richard M, Zexiang Li, *A Mathematical Introduction to Robotic Manipulation*, vol. 53, no. 9. 1994.

[2] F. Renda, M. Giorelli, M. Calisti, M. Cianchetti, and C. Laschi, *Dynamic model of a multibending soft robot arm driven by cables*, IEEE Transactions on Robotics, vol. 30 (5), pp. 1109- 1122, 2014.

Frequency-Domain Stability Tools for Hybrid Integrator-Gain Systems

S.J.A.M. van den Eijnden, M.F. Heertjes, and H. Nijmeijer

Department of Mechanical Engineering, Eindhoven University of Technology, The Netherlands

s.j.a.m.v.d.eijnden@tue.nl

1 Introduction

Due to the inherent switching behaviour, stability analysis of hybrid integrator-gain systems (HIGS) is a challenging task. The vast majority of available tools rely on finding suitable (quadratic) Lyapunov functions, for example by solving a set of linear matrix inequalities (LMIs) [1] or using circle-criterion-like arguments [2]. Although LMI-based methods can be extremely useful, these rely on accurate parametric plant models, which are hard to obtain for complex industrial systems. Contrarily, the circle-criterion provides conditions that are graphically verifiable on the basis of measured frequency response data, and therefore is often considered favourable in practice. However, this approach may render a rather conservative estimate on closed-loop stability.

For reset control systems, the H_β-condition has been proposed in [3] as a frequency-domain tool for stability analysis. Inspired by this result, new frequency-domain stability conditions for HIGS-controlled systems are presented.

2 Main Results

Consider the feedback configuration depicted in Figure 1. Here, $G(s) \in \mathbb{C}$ is a linear time-invariant system with input $u \in \mathbb{R}$ and output $y \in \mathbb{R}$, and $\mathscr{H}(\cdot)$ denotes the hybrid integrator-gain system.

$$\mathscr{H} : \begin{cases} \dot{x}_h = \omega_h z & \text{if } q \in \mathscr{F}_1, \\ x_h = k_h z & \text{if } q \in \mathscr{F}_2, \\ u = x_h. \end{cases}$$
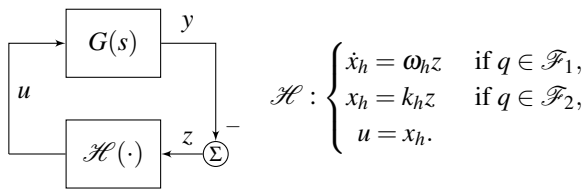
Figure 1: System configuration (left) and HIGS description (right) with $q = (z, u, \dot{z})$, and where $\omega_h, k_h \in \mathbb{R}$ denote the integrator frequency and gain, respectively. Here $\mathscr{F}_1, \mathscr{F}_2$ are the integrator and gain mode regions.

Definition 1 *The HIGS-controlled system in Figure 1 is said to satisfy the $H_{\beta,k}$-condition if there exist $\beta, k \geq 0$ such that the transfer function*

$$H_{\beta,k}(s) := (C(s) + \beta)S(s) - \beta, \qquad (1)$$

with $C(s) = \frac{\omega_h + kk_h}{s+k}$, $S(s) = \frac{1}{1+C(s)G(s)}$, is strictly positive real (SPR).

Theorem 1 *The HIGS-controlled system in Figure 1 is exponentially stable if it satisfies the $H_{\beta,k}$-condition.*

3 Example

Consider the following mass-spring-damper system

$$G(s) = \frac{k_p}{ms^2 + bs + c}, \qquad (2)$$

with $m = 1$ kg, $b = 0.2$ Ns/m, $c = 100$ N/m and $k_p = 1.5$. From the circle criterion, it is concluded that this system is stable for $k_h \in (0, 2.69)$ and $\omega_h \in (0, \infty)$. Next, stability is verified on the basis of Theorem 1 by conducting a search for finding β, k that render $H_{\beta,k}(s)$ in (1) SPR. The result for different pairs (k_h, ω_h) are shown in Figure 2. Clearly for this example, the $H_{\beta,k}$-condition provides less conservative results as compared to the circle-criterion.
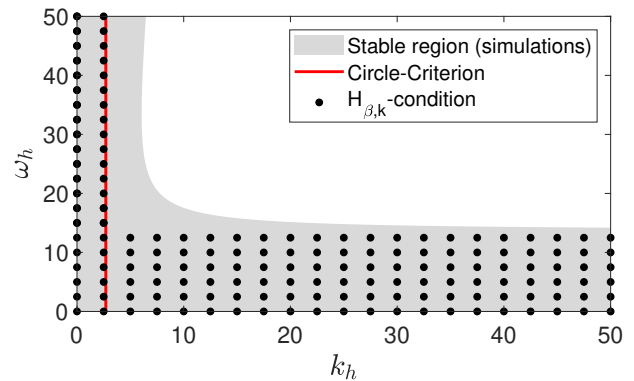
Figure 2: Stability evaluated using the circle-criterion (red), $H_{\beta,k}$-condition (black dots), and simulations (grey area).

4 Conclusion

New frequency-domain stability conditions for hybrid integrator-gain systems are presented, and the potential is demonstrated by means of example.

References

[1]   S. van den Eijnden, M. Heertjes, and H. Nijmeijer (2019). Robust stability and nonlinear loop-shaping design for hybrid integrator-gain-based control systems. *Proc of the ACC*, Philadelphia, USA, 3063-3068.

[2]   D. Deenen, M. Heertjes, M. Heemels, and H. Nijmeijer (2017). Hybrid integrator design for enhanced tracking in motion control, *Proc of the ACC*, Seattle, USA, 2863-2868.

[3]   O. Beker, C. Hollot, Y. Chait, H. Han (2004). Fundamental properties of reset control systems. Automatica, 40(6), 905-915.

On geometric and differentiation index of nonlinear differential algebraic equations

Yahao Chen
Bernoulli Institute, RUG
yahao.chen@rug.nl

Stephan Trenn
Bernoulli Institute, RUG
s.trenn@rug.nl

1 Introduction

We consider differential-algebraic equations DAEs of the following form

$$\Xi: \ E(x)\dot{x} = F(x), \qquad (1)$$

where $x \in X$ is called the generalized state and X is an open subset of $\mathbb{R}^n$, and where $E : X \to \mathbb{R}^{l \times n}$ and $F : X \to \mathbb{R}^l$ are $\mathcal{C}^\infty$-smooth maps. A DAE of form (1) will be denoted by $\Xi_{l,n} = (E,F)$ or, simply, Ξ. A solution of Ξ is a $\mathcal{C}^1$-curve $\gamma : I \to X$ with an open interval I such that for all $t \in I$, $\gamma(t)$ solves (1). To characterize different properties of nonlinear DAEs, various notions of index are proposed, see the survey or survey-like papers on index of DAEs: [1],[2],[3]. The most commonly used notions of index in DAEs theory seem to be the geometric index (see e.g., [4]) and the differentiation index (see [2] and [1]).

The main idea of geometric analysis of DAEs is to view the DAE as a vector field on a submanifold M^*, the later is called the maximal invariant submanifold, it is where the solutions of DAEs exist. The following locally maximal invariant submanifold algorithm is a recursive way to construct M^* [5]:
For a DAE $\Xi_{l,n} = (E,F)$, set $M_0 = X$, assume that a point $x_0 \in M_0$ satisfies $F(x_0) \in \operatorname{Im} E(x_0)$. Step 1: set

$$M_1 = \{x \in X : F(x) \in \operatorname{Im} E(x)\};$$

Step k: assume that $M_{k-1} \subsetneq \cdots \subsetneq M_0$, for a certain $k \geq 1$, have been constructed and for some open neighborhood $U_{k-1} \subseteq X$ of x_0 that the intersection $M_{k-1} \cap U_{k-1}$ is a smooth submanifold and denote by M_{k-1}^c the connected component of $M_{k-1} \cap U_{k-1}$ satisfying $x_0 \in M_{k-1}^c$. Set

$$M_k = \left\{x \in M_{k-1}^c \mid F(x) \in E(x)T_x M_{k-1}^c\right\}.$$

Definition 1. (Geometric index) The geometric index of $\nu_g \in \mathbb{N}$ of a DAE Ξ is defined by

$$\nu_d := \min\left\{k \geq 0 \mid (M_k = M_{k+1}) \wedge (M_k \neq \emptyset)\right\}.$$

The differentiation index of DAEs is defined via the differential array shown in equation (2) below. Consider a nonlinear DAE $\Xi_{l,n} = (E,F)$, let $H(x,\zeta_1) = E(x)\zeta_1 - F(x)$, denote $(\frac{\mathrm{d}^k}{\mathrm{d}t^k}H) = H^{(k)}$ and define

$$H_k(x,\bar{\zeta}_{k+1}) = \begin{bmatrix} H^{(0)}(x,\zeta_1) \\ H^{(1)}(x,\zeta_1,\zeta_2) \\ \vdots \\ H^{(k)}(x,\bar{\zeta}_{k+1}) \end{bmatrix} = 0, \qquad (2)$$

where $\bar{\zeta}_{k+1} = (\zeta_1,\ldots,\zeta_{k+1})$, set $\mathcal{M}_0 = X$, assume that for $k > 0$,

$$\begin{aligned}
\mathcal{M}_k &= \left\{x \in X \mid H_{k-1}(x,\bar{\zeta}_k) = 0\right\} \quad \text{and} \\
\mathcal{Z}_1^k &= \left\{\zeta_1 \in \mathbb{R}^n \mid H_{k-1}(x,\bar{\zeta}_k) = 0, \ x \in \mathcal{M}_k\right\}
\end{aligned}$$

are smooth submanifolds of X and $\mathbb{R}^n$, respectively.
Definition 2. (Differentiation index) For a DAE $\Xi_{l,n} = (E,F)$, the differentiation index ν_d is defined by $\nu_d := 0$ if $(l = n) \wedge (E : X \to Gl(l,\mathbb{R}))$; otherwise, ν_d is the smallest integer such that $(\mathcal{M}_k \neq \emptyset) \wedge (\mathcal{Z}_1^k = \mathcal{Z}_1^k(x)$ is a singleton$) \wedge (\mathcal{Z}_1^k(x) \in T_x \mathcal{M}_k, \forall x \in \mathcal{M}_k)$.

The aim of the present work is to have a comprehensive understanding of the two notions of DAE index. Both of the two indices serve as a measure of the difficulties of solving DAEs, but we show that they are actually related to the existence and uniqueness of solutions in a different manner. We also show that the two DAE indices have close relations with each other when some assumptions of smoothness and constant rankness are satisfied.

References

[1] Griepentrog, E., Hanke, M., and März, R. (1992). *Toward a better understanding of differential algebraic equations (Introductory survey)*. Humboldt-Universität zu Berlin, Mathematisch-Naturwissenschaftliche Fakultät II.

[2] Campbell, S.L. and Gear, C.W. (1995). The index of general nonlinear DAEs. *Numerische Mathematik*, 72(2), 173–196.

[3] Mehrmann, V. (2015). Index concepts for differential-algebraic equations. *Encyclopedia of Applied and Computational Mathematics*, 676–681.

[4] Rabier, P.J. and Rheinboldt, W.C. (2002). *Theoretical and Numerical Analysis of Differential-Algebraic Equations*. Elsevier.

[5] Chen, Y. and Respondek, W. (2019). Geometric analysis of nonlinear differential-algebraic equations by nonlinear control theory. Preprint.

Pattern and Bifurcation analysis of delay-coupled Lur'e systems

K.Rogov[1,2], A.Pogromsky[1], E.Steur[1], W. Michiels[2] and H.Nijmeijer[1]

[1] Dynamics and Control, Dept. of Mechanical Engineering, TU Eindhoven, The Netherlands

[2] NUMA, Department of Computer Science, KU Leuven, Belgium

E-mail:k.rogov@tue.nl

1 Introduction

In recent years, the investigation of behavior of complex networks, formed by coupled nonlinear dynamical systems, has been a significant subject in mathematical biology, control theory, applied physics, and interdisciplinary fields. Substantial number of natural phenomena can be described by complex networks (e.g. neuronal systems, heart cells synchronization, social networks, flocks of birds and other kinds of collective behavior). The problem of emergence of oscillations in coupled inert systems started with Turing's work on morphogenesis. Results for different synchronous regimes and pattern formation, such as synchronization, partial synchronization, and pattern formation, are presented in many studies in different fields. These studies considered diffusive coupling, which is (usually) symmetric and delay-free. We consider networks of Lur'e systems interconnected via time-delayed coupling functions. Such time-delay coupling functions appear, among others, in network of neurons, electrical circuits, and networked control systems. In this work, we extend results of previous work [1] and develop a method for determining an oscillatory profile (e.g. offset components, amplitudes, phases and a frequency) of oscillatory patterns emerged in the networks of nonlinear systems of Lur'e form interconnected via time-delayed coupling functions. We consider the case where a Hopf bifurcation causes the instability of the network dynamics. The coupling strength and time-delay term take the role of bifurcation parameters. It is shown, that the Multivariable Harmonic Balance method for delay-coupled systems (DMHB) can be used for analysis of oscillations even if they are of a nonharmonic (relaxation) type. In addition our approach deals with multistability and can predict both stable and unstable periodic solutions.

2 Problem formulation and Methodology

The goal of our work is to develop a method which is able to compute oscillatory patterns that appear in delay-coupled nonlinear systems. We focus on networks of a particular class of Lur'e systems, which exhibit oscillatory behavior when a Hopf Bifurcation occurs. Since there are two bifurcation parameters (coupling strength and time-delay), the bifurcation analysis must be performed before the DMHB analysis. Since the number of eigenvalues crossing the imaginary axis is finite, the Hopf bifurcation theorem holds

and nonlinearities can be replaced by its linear approximation by means of the describing function method. Subsequently the problem of determining the oscillatory profile is transposed into an easily solvable eigenvalue problem called the MHB equation. A numerical optimization routine has been developed which determines optimal solutions to the MHB equation for delay-coupled system and therewith predicts all possible stable and unstable patterns of oscillations.

3 Results

The MHB method is applied to the network of Lur'e systems which exhibits oscillatory behavior the (subcritical or supercritical) Hopf bifurcation occurs. In Table 1, we show the accuracy of the DMHB method comparing to DDE simulations for an example of 3-nodes network by providing the residual norm of the MHB equation and comparing offset components, amplitudes and frequency with the ones that are extracted from DDE simulation. Note that phases are always accurately computed. The DMHB method ac-

Residual	γ	τ	$\Delta\omega$ in %	$\Delta\alpha_0$ in %	$\Delta\alpha$ in %
2.87e-8	0.71	1.53	0.02	100*	0.94

Table 1: Comparison of the DMHB method with the DDE simulation for 3-node network

curately computes the approximation of the oscillatory pattern with arbitrary (equal, in this case) amplitudes, occurring in networks of delay-coupled identical Lur'e systems. The method finds all stable and unstable patterns that occur in such networks. *Note that this difference is a numerical issue and does affect the accuracy of the predicated pattern.

Acknowledgements

References

[1] K. Rogov, A. Pogromsky, E. Steur, W. Michiels and H. Neijmeijer, "Pattern Analysis in Networks of Diffusively Coupled Lure Systems", *Internation Journal of Bifurcation and Chaos*, **29**, 2019.

Extended Projected Dynamical Systems:
A Framework for Analysis of Hybrid Integrator-Gain Systems

Bardia Sharif, Marcel Heertjes, Maurice Heemels
Mechanical Engineering Department, Eindhoven University of Technology, The Netherlands.
Email: b.sharif@tue.nl

1 Introduction

Hybrid integrator-gain systems (HIGS), are sector bounded integrators recently proposed in the literature, aiming at overcoming fundamental limitations of linear time-invariant feedback control. In this work we present a mathematical framework to formally describe HIGS-controlled systems based on extensions of the class of projected dynamical systems (PDS). Using this formalized description, HIGS-controlled systems are shown to be well-posed, in the sense of global existence of solutions.

2 Projected Dynamical Systems

Let us first start by introducing the "classical" PDS [1]. To this end, consider a differential equation

$$\dot{x}(t) = f(x(t)), \tag{1}$$

in which $x(t) \in \mathbb{R}^n$ denotes the state at time $t \in \mathbb{R}_{\geq 0}$. There is a restriction on the state of the system in the sense that $x(t)$ has to remain inside a set $S \subseteq \mathbb{R}^n$. In PDS this is ensured by redirecting the vector field at the boundary of S in case the state tends to leave S by following (1). Formally, a PDS is given by

$$\dot{x}(t) = \Pi_S(x(t), f(x(t))), \tag{2}$$

with $\Pi_S(x, v) = \operatorname{argmin}_{w \in T_S(x)} \|w - v\|$ for $x \in S$ and $v \in \mathbb{R}^n$. Here, $T_S(x)$ is the tangent cone to the set S at point x and defines the set of permissible velocities, i.e., all the directions in which the dynamics can evolve such that the state remains inside S. Based on this formulation, $\Pi_S(x, v)$ can be interpreted as an operator that selects the vector closest to v, which lies in the set of admissible velocities at x. In PDS (2), the constraint $x(t) \in S$ is satisfied by projecting the complete vector field $f(x(t))$. As a result, the projection results in modifications of velocities of *all* the states x. Consequently, PDS fall short in modeling phenomena in which only part of the dynamics can be projected. Moreover, (2) is well-defined for constraint sets S, which satisfy certain regularity conditions. Motivated by these restrictions of PDS a new class of discontinuous dynamical systems is introduced in Section 3 that are well-defined for a wider variety of constraint sets as well as *partial* projection of dynamics. In fact, HIGS-controlled systems motivate this extension (see Section 4).

3 Extended Projected Dynamical Systems

In this section, we present the new class of discontinuous dynamical systems, for which we coin the term *extended Projected Dynamical Systems* (ePDS). To do so, consider agian the differential equation (1) and a non-empty closed constraint set $S \subseteq \mathbb{R}^n$. Formally, an ePDS is given by

$$\dot{x}(t) = \Pi_{S,E}(x(t), f(x(t))) \tag{3}$$

with $\Pi_{S,E}(x, v) = \operatorname{argmin}_{w \in T_S(x), w-v \in \operatorname{im} E} \|w - v\|$ for $x \in S$ and $v \in \mathbb{R}^n$. Here, $E \in \mathbb{R}^{n \times n_E}$ is used to specify the direction in which dynamics are projected, thereby facilitating partial projection of dynamics. In [2], (3) is shown to be well-defined for constraint sets of the form

$$S = \mathscr{K} \cup -\mathscr{K}, \tag{4}$$

where $\mathscr{K}$ is a convex polyhedral cone. The sets of the form (4), do not necessarily satisfy the regularity conditions required in the PDS literature, see, e.g. [1].

4 Formal Description of HIGS-Controlled Systems

Consider the closed-loop interconnection of a HIGS element $\mathscr{H}$ with a linear time-invariant (LTI) system G as in Fig. 1. As explained in [2], $\mathscr{H}$ primarily acts as a linear integrator
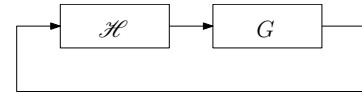
Figure 1: Closed-loop interconnection of a HIGS element $\mathscr{H}$ with an LTI plant G.

leading to the closed-loop dynamics

$$\dot{x}(t) = A_i x(t), \tag{5}$$

where $x = \begin{bmatrix} x_h^\top & x_g^\top \end{bmatrix}^\top$ with $x_h \in \mathbb{R}$ the state of $\mathscr{H}$ and $x_g \in \mathbb{R}^{n_g}$ the state of G. When (5) results in trajectories that leave HIGS's sector $S_h \subseteq \mathbb{R}^{n_g+1}$, $\mathscr{H}$ switches to a so-called gain mode (only changing the dynamics of $\mathscr{H}$ and not of G) such that the trajectories remain on the boundary of S_h (see [2]). This operation can be formalized in the ePDS framework as

$$\dot{x}(t) = \Pi_{S_h, E}(x(t), A_i x(t)) \tag{6}$$

with $E = \begin{bmatrix} 1 & 0_{n_g}^\top \end{bmatrix}^\top$ and S_h the sector of the HIGS (see [2] equation (27)) which has the form as in (4). As S_h is of the form (4), (6) is well-defined. In [2], the ePDS (6) is shown to be well-posed in the sense of global existence of solutions.

5 Conclusions

A mathematical framework for formal description of HIGS-controlled systems is presented and used to prove their well-posedness, thereby laying down a proper basis for formal studies of HIGS-based controllers.

References

[1] A. Nagurney and D. Zhang. *Projected dynamical systems and variational inequalities with applications*, volume 2. Springer Science & Business Media, 2012.

[2] B. Sharif, M.F. Heertjes, and W.P.M.H. Heemels. Extended projected dynamical systems with applications to hybrid integrator-gain systems. In *58th IEEE Conference on Decision and Control 2019, Nice, France.*, 2019.

Set stability of Lur'e Systems with Preisach butterfly operator

M. A. Vasquez-Beltran, B. Jayawardhana, R. Peletier

University of Groningen, 9747AG Groningen, The Netherlands

m.a.vasquez.beltran [b.jayawardhana; r.f.peletier] @rug.nl

1 Introduction

In this paper we study the asymptotic stability of the feedback interconnection of a linear system and a Preisach butterfly operator, as introduced in [1], with respect to a set of equilibrium points. We follow a differential approach as in [3] where a time-varying relation between the input and output rates of a given Preisach operator that satisfies a sector boundary condition (under mild assumptions over the weighting function of the Preisach operator) is established. In this way, we can analyze the interconnection as a Lur'e type system so that circle criterion [2, 4] can directly be applicable.

2 The Preisach operator and its input-output rate relation

The Preisach hysteresis operator Φ is defined by

$$\big(\Phi(u,L_0)\big)(t) := \iint\limits_{(\alpha,\beta)\in P} \mu(\alpha,\beta)\left(\mathscr{R}^{\circlearrowleft}_{\alpha,\beta}\big(u,\hat{r}_{\alpha,\beta}(L_0)\big)\right)(t)\,\mathrm{d}\alpha\mathrm{d}\beta \tag{1}$$

where P is the Preisach plane, μ is a weighting function that takes value from the Preisach plane, $\mathscr{R}_{\alpha,\beta}$ are relay operators parameterized by $\alpha > \beta$, L_0 is the initial interface and $\hat{r}_{\alpha,\beta}$ is an auxiliary function that determines the initial condition r_0 of every relay accordingly.

We introduce a differential formulation of the Preisach operator that allows us to express explicitly the time-varying relation between the output rate and the input rate in the form $\dot{\Phi}(t) = \psi(t)\dot{u}(t)$ with $\psi(t)$ given by

$$\psi(t) = \begin{cases} 2\displaystyle\int_{m_t}^{u(t)} \mu(u(t),\beta)\mathrm{d}\beta & \text{if } \dot{u}(t) > 0, \\[3mm] 2\displaystyle\int_{u(t)}^{M_t} \mu(\alpha,u(t))\mathrm{d}\alpha & \text{if } \dot{u}(t) < 0, \\[3mm] 0 & \text{otherwise}, \end{cases} \tag{2}$$

and where m_t and M_t correspond to the last maximum and last minimum of the truncated input $u_t = \{u(\tau)\,|\,0 \le \tau \le t\}$ that are stored in the Preisach memory. It can be shown that when μ has a compact support, it is possible to find a sector bound for (2).

3 Lur'e system with Preisach butterfly operator

We consider a feedback interconnection of a linear system Σ_1 and a Preisach butterfly operator Σ_2 which is described by

$$\Sigma_1 : \begin{aligned} \dot{x}(t) &= Ax(t) + Bv(t), & x(0) &= x_0, \\ z(t) &= Cx(t) \end{aligned}$$

$$\Sigma_2 : y(t) = \big(\Phi(u,L_0)\big)(t), \qquad L_0 \in \mathscr{I},$$
$$\text{with } v(t) = -y(t),\ u(t) = z(t), \tag{3}$$

where $x \in \mathbb{R}^n$ and A, B and C are matrices with appropriate dimensions, and whose set of equilibria is given by

$$\mathscr{E} = \{(x_{ss}, L_{ss}) \in \mathbb{R}^n \times \mathscr{I} \mid Ax_{ss} - B\Phi(Cx_{ss}, L_{ss}) = 0\}$$

where $\mathscr{I}$ is the set of all possible initial interfaces of the Preisach operator. Based on the differential formulation obtained by the relation (2) and under mild assumptions over the observability and controllability of the pairs (A,C) and (A,B) and the positive realness of the transfer function given by

$$\overline{G}(j\omega) := (1 + \lambda_M G(j\omega))(1 + \lambda_m G(j\omega))^{-1},$$

where λ_M and λ_m are the upper and lower sector bounds of ψ in (2), and $G(j\omega) = C(sI - A)^{-1}B$ is the transfer function corresponding to the linear system Σ_1 in (3), it can be proven that $(x(t), L_t) \to \mathscr{E}$ as $t \to \infty$.

References

[1]   B. Jayawardhana, M. A. Vasquez-Beltran, W. J. van de Beek, C. de Jonge, M. Acuautla, S. Damerio, R. Peletier, B. Noheda, and R. Huisman, "Modeling and analysis of butterfly loops via Preisach operators and its application in a piezoelectric material" in Proc. IEEE Conf. Decision and Control (CDC), Dec. 2018, pp. 6894–6899.

[2]   B. Jayawardhana, H. Logemann, and E. P. Ryan, "The circle criterion and input-to-state stability," IEEE Control Systems Magazine, vol. 31, no. 4, pp. 32–67, Aug 2011.

[3]   H. Logemann and E. Ryan, "Systems with hysteresis in the feedback loop: existence, regularity and asymptotic behavior of solutions," ESAIM: Control, Optimisation and Calculus of Variations, vol. 9, pp. 169–196, 2003.

[4]   H. Khalil, Nonlinear Systems, ser. Pearson Education. Prentice Hall, 2002.

Benefiting from Linear Behaviour of a Nonlinear Reset-based Element at Certain Frequencies

Nima Karbasizadeh, Ali Ahmadi Dastjerdi, Niranjan Saikumar and S. Hassan HosseinNia
Department of Precision and Microsystem Engineering, Delft University of Technology, Delft, The Netherlands
{N.KarbasizadehEsfahani; A.AhmadiDastjerdi; N.Saikumar; S.H.HosseinNiaKani}@tudelft.nl

1 Introduction

This abstract addresses a phenomenon caused by resetting only one of the two states of a so-called second order "Constant in gain Lead in phase" (CgLp) element [1]. CgLp is a newly introduced reset-based nonlinear element, bound to circumvent the well-known linear control limitation – the waterbed effect. The ideal behaviour of such a filter in the frequency domain is unity gain while providing a phase lead for a broad range of frequencies. However, CgLp's ideal behaviour is based on a describing function, which is a first order approximation that neglects the effects of higher order harmonics in the output of the filter. Consequently, achieving the ideal behaviour is challenging when higher order harmonics are relatively large. It is shown in this paper that by resetting only one of the two states of a second order CgLp, the nonlinear filter will act as a linear one at a certain frequency, provided that some conditions are met. This phenomenon can be used to the benefit of reducing higher order harmonics of CgLp's output and achieving the ideal behaviour and thus better performance of the filter in terms of precision.

2 Second Order Single State Reset Element (SOSRE)

Figure 1 shows the block diagram of a CgLp element which uses a Second Order Reset Element (SORE) in a particular configuration, in which the first integrator does not reset.

Remark. Assuming a sinusoidal input to a reset element, if the phase shift between the output of its base linear system and its input is zero, the reset action will be of no effect in steady state response, and thus the reset element can be regarded as a linear system in terms of steady state response at that certain frequency.

According to the above Remark, in the case of a SOSRE, if $e(t) = \sin(\omega t)$, the reset action of the first integrator will be of no effect if:

$$\angle \frac{X_1(j\omega)}{E(j\omega)} = \frac{\pi}{2} - \tan^{-1}\left(\frac{2\beta_r \omega_{r\alpha}\omega}{-\omega^2 + \omega_{r\alpha}}\right) = 0 \quad (1)$$

$$\Rightarrow \omega = \omega_{r\alpha}.$$

Resetting action creates nonlinearity in the system whose one of the drawbacks is the higher order harmonics in the response of the controller. Higher order harmonics can create problems in tracking for mass-spring-damper systems in
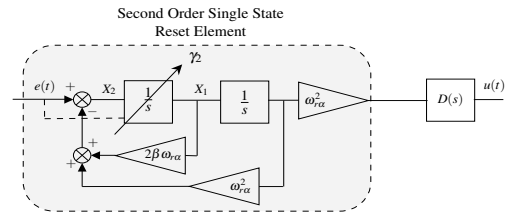
Figure 1: Block diagram of a SOSRE CgLp. The second integrator is not reset. $D(s)$ is the linear part of the CgLp.
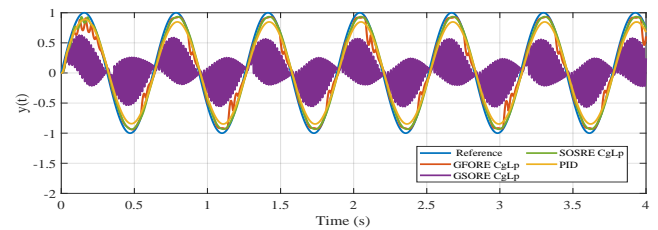
Figure 2: Simulation results of output, $y(t)$. Reference is $r(t) = \sin(10t)$.

which resonance peak of the higher order harmonic happens in frequencies below bandwidth. This can cause the system to behave unexpectedly, since the nonlinear controllers are usually designed based on their first order describing function in frequency domain. Tuning the linear behaviour of SOSRE to cancel the third order harmonic peak, the tracking performance can be improved significantly in problematic frequency of ordinary SORE CgLp.

3 Results

Figure 2, shows the simulation result for a mass-spring-damper system controlled by CgLp elements based on FORE, SORE and SOSRE. Comparison is also done with PID, in the absence of noise and disturbance. Input frequency is at the third order harmonic resonance peak. CgLps based on FORE and SORE has the worst performance in this frequency. The figure shows the better performance of CgLp based on SOSRE and also proves the concept pf the remark.

References

[1]   SAIKUMAR, N., SINHA, R., AND HOSEINNIA, S. H. 'constant in gain lead in phase'element-application in precision motion control. *IEEE/ASME Transactions on Mechatronics* (2019).

Local exponential stability of nonlinear distributed parameter systems: Application to a nonisothermal tubular reactor

Anthony Hastir[*], Joseph J. Winkin[*] and Denis Dochain[†]

[*] Namur Institute for Complex Systems (naXys) and Department of Mathematics,University of Namur, Rempart de la vierge 8, B-5000 Namur, Belgium

[†] Institute of Information and Communication Technologies, Electronics and Applied Mathematics (ICTEAM),

Université Catholique de Louvain, Avenue Georges Lemaitre 4-6, B-1348 Louvain-La-Neuve, Belgium

anthony.hastir@unamur.be, joseph.winkin@unamur.be, denis.dochain@uclouvain.be

Deducing exponential stability of an equilibrium of a nonlinear distributed parameter, i.e. infinite-dimensional, system on the basis of the stability of a linear approximation of it is in general quite challenging. Some of the existing theories, see e.g. [4, 1], rely on the Fréchet differentiability of the nonlinear semigroup generated by the nonlinear operator dynamics. However, checking Fréchet differentiability for nonlinear operators defined on an infinite-dimensional space is difficult or even impossible if these are unbounded. In many cases, the general theory cannot be applied and a case-by-case study has to be performed by working directly on the semigroup instead of its generator.

The approach that is proposed here is based on an adapted concept of Fréchet differentiability which takes different spaces and norms into account. This is called the $(Y,X)-$Fréchet differentiability, where X is the state (Hilbert) space and Y is an auxiliary space chosen to handle more easily norm-inequalities when working in infinite-dimensions (typically L^∞ or Sobolev spaces ($H^p, p \in \mathbb{N}_0$), which are all multiplicative algebras). The systems that are considered here are governed by the following abstract ODE:

$$\dot{x}(t) = Ax(t) + N(x(t)),\ x(0) = x_0, \qquad (1)$$

where $A : D(A) \subset X \to X$ and $N : D(N) \subset X \to X$ are linear and nonlinear operators, respectively. Let $x^e \in D(A) \cap D(N)$ be an equilibrium of (1).

Definition : Let $(Y, \|\cdot\|_Y)$ be an infinite-dimensional (possibly Banach) space such that $D(A) \cap D(N) \subset Y \subseteq X$. The operator N is called $(Y,X)-$Fréchet differentiable at x^e if there exists a bounded linear operator $dN(x^e) : X \to X$ such that for all $h \in D(A) \cap D(N), N(x^e + h) - N(x^e) = dN(x^e)h + R(x^e, h)$ where $\lim_{\|h\|_Y \to 0} \|R(x^e, h)\|_X / \|h\|_X = 0$.

This allows more easily checkable adapted Fréchet differentiability conditions, provided that local exponential stability of the equilibrium of (1) holds in a weaker sense, see [3]. Based on this new concept, our approach to deduce exponential stability of the equilibrium of (1) can be summarazied as in Figure 1. Let $(S(t))_{t\geq0}$ be the nonlinear semigroup generated by the operator $A+N$ on X. The standard concept of Fréchet differentiability is needed for $(S(t))_{t\geq0}$ on Y, with $(T_{x^e}(t))_{t\geq0}$ as Fréchet derivative, the linear semigroup generated by the Gâteaux derivative $A + dN(x^e)$ of $A+N$. After showing that $(T_{x^e}(t))_{t\geq0}$ satisfies some Lyapunov-type stability condition and that it is exponentially stable on X, the new concept of $(Y,X)-$Fréchet differentiability pops up to make the connection between Y and X, in order to deduce
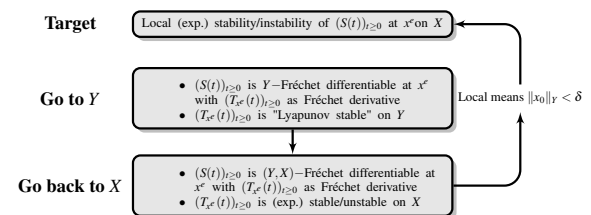
Figure 1: Illustration of the new theoretical framework.

local exponential stability of the equilibrium of (1) on X, see [3]. Local means here that the $Y-$norm of the initial condition has to be small instead of its $X-$norm.

Our theoretical approach is illustrated on a nonisothermal axial dispersion tubular reactor which exhibits different numbers of equilibria depending on the diffusion coefficients: see [2] for the existence and multiplicity of the equilibria. Our main result states that, in the case of only one equilibrium profile, the latter is locally exponentially stable for the nonlinear system governing the dynamics. Moreover, in the case where the reactor exhibits three equilibria, local exponential bistability is established, that is, the pattern "stable – unstable – stable" is highlighted, see [3].

References

[1]   R. Al Jamal and K. Morris, 2018. "Linearized stability of partial differential equations with application to stabilization of the kuramotosivashinsky equation", SIAM Journal on Control and Optimization 56 (1), 120 – 147

[2]   A. Hastir, F. Lamoline, J.J. Winkin and D. Dochain, 2019. "Analysis of the existence of equilibrium profiles in nonisothermal axial dispersion tubular reactors", IEEE Transactions on Automatic Control, to appear

[3]   A. Hastir, J.J. Winkin and D. Dochain, 2019. "Exponential stability of nonlinear infinite-dimensional systems: application to nonisothermal axial dispersion tubular reactors", submitted

[4]   N. Kato, 1995. "A principle of linearized stability for nonlinear evolution equations", Transactions of the American Mathematical Society 347 (8), 2851 – 2868.

Observer Design for Linear Parabolic PDE Systems

Ivan Yupanqui Tello and Alain Vande Wouwer
Department of Automatic Control
University of Mons
31, Boulevard Dolez, 7000 Mons
Belgium
Email: ivan.yupanquitello@umons.ac.be
Email: alain.vandewouwer@umons.ac.be

Daniel Coutinho
Department of Automation and Systems
Federal University of Santa Catarina
R. Delfino Conti, 88040-900 Florianópolis
Brazil
Email: daniel.coutinho@ufsc.br

1 Introduction

The state estimation problem of parabolic PDE systems from its input and measured outputs over some finite time interval has been an active field of research over the last years (see e.g. [1], and the references therein). This work aims at designing observers for systems described by certain class of parabolic PDEs. The state estimation problem is transformed into a well-posed stabilization problem for the dynamics of the state estimation error which is formulated in terms of Linear matrix Inequalities (LMIs).

2 System Description and Formulation

Consider the following class of parabolic PDE systems:

$$x_t(z,t) = \gamma x_{zz}(z,t) - \upsilon x_z(z,t) + k(z)x(z,t) \tag{1}$$

$$\begin{aligned} \gamma x_z(0,t) &= \upsilon(x(0,t) - x_{in}(t)) \\ x_z(l,t) &= 0. \end{aligned} \tag{2}$$

The associated state estimation problem for the system (1)-(2) consists in designing a dynamical observer on the basis of its mathematical model, the measurement

$$y(t) = \int_0^l \mathbf{c}^T(z)x(z,t)dz \tag{3}$$

and the input signal $x_{in}(t)$ which produces a convergent state estimate $\hat{x}(z,t)$ such that $\lim_{t\to\infty} \|x(\cdot,t) - \hat{x}(\cdot,t)\|_2 = 0$.

2.1 Measurement sensors

The vector $\mathbf{c}(z) = \begin{bmatrix} c_1(z) & c_2(z) & \cdots & c_{n_y}(z) \end{bmatrix}$ in (3) will lead to different forms of local measurement. For example, the choice

$$c_j(z) = \begin{cases} \frac{1}{2\varepsilon_j} & z \in [z_j - \varepsilon_j, z_j + \varepsilon_j] \\ 0 & \text{elsewhere} \end{cases}, \ j \in \mathbb{N}_y = \{1, 2, ..., n_y\}. \tag{4}$$

corresponds to piecewise measurement that produces n_y zones of piecewise uniform sensing in the interval $[z_j - \varepsilon_j, z_j + \varepsilon_j]$, where $0 < z_1 < z_2 < ... < z_{n_y} < l$. This case is ilustrated in Figure 1.
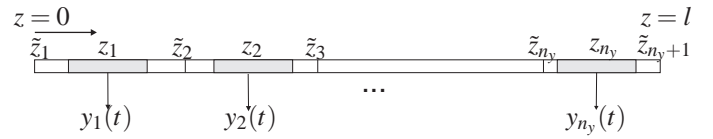
Figure 1: Distributed measurement

3 Observer design

The proposed Luenberger-type PDE observer for (1)-(2) is given by

$$\begin{aligned} \hat{x}_t(z,t) &= \gamma \hat{x}_{zz}(z,t) - \upsilon \hat{x}_z(z,t) + k_0(z)\hat{x}(z,t) \\ &\quad + \mathbf{c}(z)l_M \int_0^l \mathbf{c}^T(z)(\hat{x}(z,t) - x(z,t))dz \end{aligned} \tag{5}$$

$$\begin{aligned} \gamma \hat{x}_z(0,t) &= \upsilon(\hat{x}(0,t) - x_{in}(t)) \\ \hat{x}_z(l,t) &= 0 \quad \text{where } l_M = diag\{l_1,...,l_{n_y}\}. \end{aligned} \tag{6}$$

Using Lyapunov's approach, the following theorem provides a solution to the state estimation problem.

Theorem 3.1 *Considering the PDE system (1)-(2) with a given positive constants γ, υ and the measurement output $y(t)$ of the form (3). If there exist constants l_j, $j \in \mathbb{N}_y$ satisfying the following LMIs:*

$$\begin{bmatrix} k(z) - \frac{1}{4}\pi^2\gamma\varphi_j^{-2} & \frac{1}{4}\pi^2\gamma\varphi_j^{-2} \\ \frac{1}{4}\pi^2\gamma\varphi_j^{-2} & -\frac{l_j^2}{\tilde{z}_{j+1}-\tilde{z}_j} - \frac{1}{4}\pi^2\gamma\varphi_j^{-2} \end{bmatrix} < 0 \ \forall j \in \mathbb{N}_y \tag{7}$$

with $\varphi_j^2 = max\{(z_j + \varepsilon_j - \tilde{z}_j)^2, (\tilde{z}_{j+1} - z_j + \varepsilon_j)^2\}$, $j \in \mathbb{N}_y$, then the Luenberger-type PDE observer of the form (5)-(6) ensures the exponential convergence of $\|x(\cdot,t) - \hat{x}(\cdot,t)\|_2$.

References

[1] Z. Hidayat, R. Babuska, B. De Schutter, and A. Nunez, "Observers for linear distributed-parameter systems: A survey," Proceedings of the 2011 IEEE International Symposium on Robotic and Sensors Environments (ROSE), 2011.

Complex Gaussian Process Regression for Estimating Spatially Varying Coefficients in Thermal Transport

Ricky van Kampen[1,2], Amritam Das[3], Siep Weiland[3], Matthijs van Berkel[1,2]

[1] Energy Systems and Control Group, DIFFER, Eindhoven, the Netherlands

[2] Control Systems Technology Group, Eindhoven University of Technology, Eindhoven, the Netherlands

[3] Control Systems Group, Eindhoven University of Technology, Eindhoven, the Netherlands

R.J.R.vanKampen@differ.nl

1 Introduction

Thermal transport determines the efficiency of future fusion reactors. To understand how, transport is often studied by means of perturbative experiments. This thermal transport is typically modeled by a one dimensional parabolic partial differential equation (PDE), where the coefficients can vary over space. The most commonly used estimators only estimate the diffusion under the assumption that the heat deposition is known. However, recent results showed that the heat deposition did not match with the assumptions, affecting the estimate of the diffusion coefficient [1]. Hence, a method which simultaneously estimates all spatial varying coefficients is required.

2 Problem formulation

In this work, we consider the following 1D linear parabolic partial differential equation

$$\frac{\partial z}{\partial t} = D(x)\frac{\partial^2 z}{\partial x^2} + U(x)\frac{\partial z}{\partial x} + K(x)z + P(x)p(t), \quad (1)$$

with temperature $z(x,t)$, spatial coordinate $x \in \mathbb{X} := [0,L]$ and time t. The physical parameters $D(x)$, $U(x)$ and $K(x)$ are the diffusion, advection, and reaction coefficients, respectively. The input consists of the spatial deposition profile $P(x)$ and the time signal $p(t)$. Furthermore, the *boundary* and *initial* conditions are considered to be unknown.

The goal is to simultaneously estimate $D(x)$, $U(x)$, $K(x)$ and $P(x)$ based on $p(t)$ and the measurements of z on a limited number of locations $y(t) = \mathrm{col}(z(x^1,t),\ldots,z(x^M,t))$.

3 Methodology

In [2] a frequency domain approach is proposed, but due to the limited number of sensors and spatially varying coefficients, the optimization problem is often undetermined, resulting in overfitting (figure 1, blue line). By extending the proposed approach with Complex Gaussian Process Regression (CGPR), a (weak) form of regularization is applied.

The discrete measurement data is first continuated over space, for a fixed frequency applying CGPR. One of the advantages is that CGPR not only provides a smooth profile, but a complete probability density function. The mean function can be considered as a state estimate (without assuming any dynamics), while the variance is used for weighting in the cost-function and determining the confidence bounds on the estimated parameters.

Having a state-estimate also allows the problem to be written as a linear least squares problem, instead of the non-linear cost-function necessary to be solved in [2].

4 First results

The first results of the simultaneous estimation of $D(x)$ and $P(x)$ with CGPR are promising. The estimate of $D(x)$ is shown in figure 1, where it can be seen that the newly developed method does not suffer from overfitting.
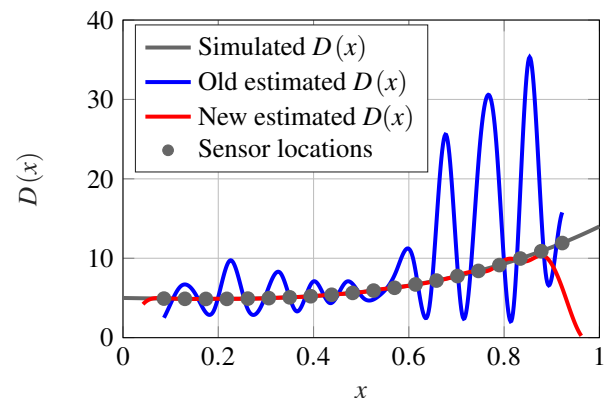
Figure 1: Estimate of $D(x)$ based on measurements (blue) and with the state estimate obtained from CGPR (red).

References

[1] M. van Berkel *et al.*, "Simultaneous estimation of transport and power deposition profiles and its consequences for transport," in *46th European Physical Society Conference on Plasma Physics (EPS 2019), July 8-12, 2019, Milan, Italie (invited semi-plenary)*, 2019.

[2] A. Das, S. Weiland, and M. van Berkel, "Frequency Domain Estimation of Spatially Varying Parameters in Heat and Mass Transport," *2019 American Control Conference (ACC)*, pp. 600–605, 2019.

Rational approximation of Positive-real functions

Mir Mamunuzzaman
Hybrid Systems, EEMCS
University of Twente
P.O. Box 217, 7500 AE Enschede
The Netherlands
Email: m.mamunuzzaman@utwente.nl

Hans Zwart
Hybrid Systems, EEMCS
University of Twente
P.O. Box 217, 7500 AE Enschede
The Netherlands
Email: h.j.zwart@utwente.nl

1 Abstract

Transfer function of systems described by PDE's are irrational functions and the corresponding states lies in an infinite dimensional space (see e.g., [1]). Since almost all available controller design techniques require a low-order finite-dimensional state space representation, it is desirable to have system description whose corresponding transfer function is rational. In this study, we preform such model approximation by using data-driven approaches. In particular, we are interested in implementing an interpolation approach namely Löwner based framework [3]. This has the advantage that it only needs the evaluation of the transfer function in a few frequency points.

As a test case, we consider a vibrating string. Some damping is considered to include dissipation of energy. We select the force at the right boundary as input, and the position at the same end as output. We assume that the string held stationary at the other end. For simplicity the length of the string is normalised i.e., $L = 1$. The frequency-domain input-output data for such a setup are collected from its frequency response at 200 frequency points in the range $[10^0, 10^4]$ and this data set is used to construct Löwner matrices which are key to our system approximation.

Passivity is an important property for many physical systems. Preserving the passivity in the model approximation is crucial since otherwise the approximate model might not be used in time domain simulation. For finite dimensional LTI systems, passivity corresponds to positive realness of its transfer function. A rational transfer function with real coefficients is called positive real if it is stable and it maps the open right half plane into the closed right half plane. The transfer function of the considered system in this work is positive real, hence, it is desired to preserve the propertiy in the approximate model.

The Löwner framework, nonetheless, does not preserve stabilty of the original system for many cases, nor the positive realness. One approach to preserve the passivity is to expand the data set. In Löwner framework if the given data set and the mirror image data set are used as interpolation points then the constructed Löwner matrix is similar to the Pick matrix. Since the transfer function is a real rational function, the function value at a conjugate node must be equal to the conjugate of the function value at the original node. The necessary and sufficient condition for the existence of a positive real interpolant is that the Pick matrix (Löwner matrix) is positive definite or semi-definite. However, since the original data set are the frequency responses, considering both the original and the mirror image data set as interpolation points make the diagonal entries of the Pick matrix infinity, hence, both these data set can not be used in the Löwner framework.

Reference [2] proposed a new approach of the positive real interpolation problem within Löwner framework for a particular choice of interpolation points namely spectral zeros. Spectral zeros of a LTI system is defined as the zeros of $H(s) + H^*(-s)$, where $H(s)$ is the transfer function of the system. However, it is almost impossible to know the spectral zeros a priori. Hence, an estimation of the spectral zeros is necessary. In which at first a minimal state space realization is obtained by using the Löwner framework based on the data on the imaginary axis. Next the spectral zeros and the transfer function evaluation at those spectral zeros are computed. Finally, the new data set interpolating on spectral zeros is used to construct the passive realization of the linear system using the Löwner framework further.

2 Acknowledgement

References

[1]   R. Curtain and H. Zwart, "An Introduction to Infinite-Dimensional Linear Systems Theory," volume 21, Springer, 2012.

[2]   A.C. Antoulas, "A new result on passivity preserving model reduction," Systems Control Lett., 54(4): 361-374, 2005.

[3]   A.J. Mayo and A.C. Antoulas, "A framework for the solution of the generalized realization problem," Linear Algebra and Its Applications, 425:634-662, 2007.

A non-linear model for the water hammer problem

Teke Xu, Alden Waters

Systems, Control and Applied Analysis, Bernoulli Institute, University of Groningen
PO Box 407, 9700AK Groningen, The Netherlands
Email: T.xu@rug.nl, A.M.S.waters@rug.nl

1 Introduction

Water hammer in a water distribution network is inevitable, due to the sudden close of valves inside the network, which can introduce pressure jumps or impulses in the water pipes, causing unexpected damage. Classically, Euler equations are partial differential equations (PDEs) for modelling the gas or water flow in 1D rigid cylindrical pipes. These have gained popularity in modelling water hammer networks [1]. The difficulty in new models is including the non-linear friction term. The results of [2] show that under some suitable assumptions the PDEs can be simplified to differential algebraic equations (DAEs), however they only show numerical results of PDE solutions eventually converge to the solutions of DAEs. In particular, the sudden change in DAEs (Switched-DAEs) may cause a Dirac impulse, c.f., [3]. We aim to find precise rates of convergence to various equilibria using the PDE. Our results represent the first time a fully nonlinear model for the PDE has been analysed with changing boundary conditions- e.g. the opening and closing of the valves.

2 Problem

A variant of the classical Euler equation with a friction term for water flow without the dynamics of the energy balance is given as

$$\begin{cases} \partial_t \rho + \partial_x q = 0 \\ \partial_t q + \partial_x \left(\frac{q^2}{\rho} + P(\rho) \right) = -\frac{c_f q |q|}{2D\rho}, \end{cases} \tag{1}$$

where $\rho(x,t)$ is the water density with $x \in [0,L]$, $q(x,t)$ is the flux, c_f is the friction constant and D is the diameter of the pipe. In addition, the pressure law $P(\rho)$ is given by

$$P(\rho) = P_a + K \frac{\rho - \rho_a}{\rho_a}, \tag{2}$$

where $K > 0$ is the *bulk modulus*, $P_a > 0$ is atmospheric pressure, and ρ_a is the density at atmospheric pressure.
According to [2], we assume that $\frac{\partial \rho}{\partial t} = 0$, and let $Q = qA$ (A is the area of cross section) be mass flow in the pipe. Then the PDE can be reduced to an ODE as

$$\frac{dQ}{dt} + \frac{A}{L}(P_L(t) - P_0(t)) + \frac{c_f}{2D\rho_a A} Q|Q| = 0, \tag{3}$$

where $P_L(t)$ is the pressure at $x = L$ and $P_0(t)$ is the pressure at $x = 0$. Obtaining a precise analytical solution of (1) is quite difficult. While there are many known results on the classical Euler's equation, these models are not robust in including the presence of the nonlinear friction term. As of present in the literature, there is only one work on the solution of the related ODE (3) which shows a purely numerical convergence for the water hammer network.

3 Result

Our main result is the analytical convergence of the solution of (1) for various initial data and dynamical valve moments. These scenarios include not only initial data which start in equilibria, unlike previous works, but also dynamical initial data. We can precisely quantify the pressure term and the errors in the model in the sense of distributions. We use a combination of linearization and numerical convergence results. As a result, we can compare the error between the solutions of linearized PDE and ODE model with one valve opening and closing.

4 Future work

Equations (1) and (3) are both modelling for only one pipe in 1d, however, we aim to model a system of water pipes (2d and higher), where different pipes may intersect with each other. Water flows in different pipes are coupled which for sure increases the complexity of the analysis. In the case of multiple pipelines, Dirac impulses may also interact with each other, and our analysis allows for the water hammer problem to be analyzed for more than one pipe.

References

[1]   G. Bertaglia, M. Ioriatti, A. Valiani, M. Dumbser, V. Caleffi. "Numerical methods for hydraulic transients in visco-elastic pipes" in *Journal of Fluids and Structures* Vol. 81, 2018 pp 230-254.

[2]   R. Kausar, "Analysis and modeling of water distribution network in the framework of switched DAEs," PhD thesis, Technische Universität Kaiserslautern, 2019.

[3]   S. Trenn, "Switched differential algebraic equations," in *Dynamics and Control of Switched Electronic Systems- Advanced Perspectives for Modeling, Simulation and Control of Power Converters*, Springer, London, 2012.

Empirical Battery Modelling for High Currents: The Effect of Nonlinear Overpotential and Inevitable Self-Heating

F.S.J. Hoekstra, Y.J.J. Heuts, H.J. Bergveld, M.C.F. Donkers
Control Systems Group - Eindhoven University, The Netherlands
Email: {f.s.j.hoekstra,h.j.bergveld,m.c.f.donkers}@tue.nl
and y.j.j.heuts@student.tue.nl.

1 Introduction

Electric race cars are a challenging application for battery management. The main issue is that the use of extremely high currents leads to additional nonlinear behaviour in the battery. The source of this nonlinear behaviour can be found in the nonlinear Butler-Volmer relation between currents and overpotentials, as well as self-heating that occurs when large currents are drawn through the electrical resistance of the battery. As a result, nonlinearities in the input-output behaviour are caused by both factors. To accurately model the nonlinear overpotential behaviour using empirical battery models, it is necessary to be able to distinguish between the contribution of both sources of nonlinearities.

2 Available Data and Motivating Example

Available to us is a data set of an electric race car, containing the pack current and voltage, and cooling fluid temperature measured during 4 different races. The experiments have been reproduced on a single high-power cell, which can withstand peak currents of up to 50C, in a dedicated battery test setup to obtain reliable measurements. The significant self-heating is seen in Fig. 1. To demonstrate the significant nonlinearity that is present in the overpotential, a Linear Time-Invariant (LTI) overpotential model has been fitted in a Least-Squares (LS) fashion on a low current cycle (100 to 250 seconds in Fig. 2). Its poor predictive abilities for high currents are shown between 300 and 450 seconds.
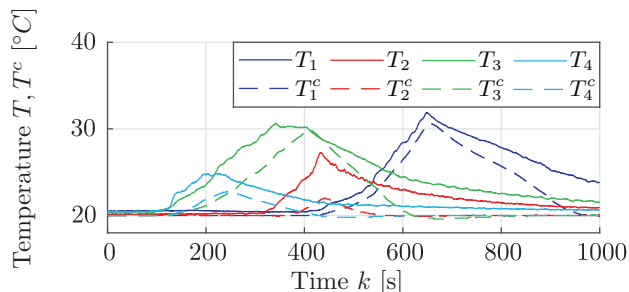
Figure 1: Surface temperature (T) and test-chamber temperature (T^c) of 4 different cycles.

3 Modelling approach

To capture the effect of the nonlinearity induced by the current and to simultaneously deal with the dynamic temperature encountered in racing profiles, a global Linear
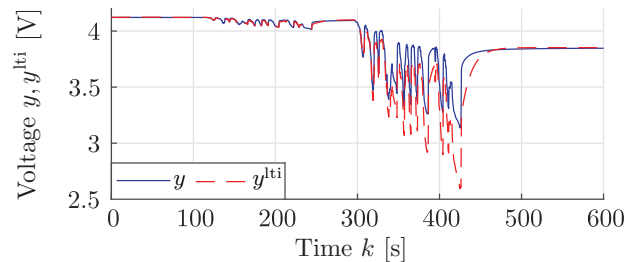
Figure 2: Comparison of simulated (y^{lti}) and measured voltage.

Parameter-Varying (LPV) state-space identification procedure has been applied. The global procedure minimises the prediction error using a gradient-based algorithm, which uses a Gauss-Newton scheme, as described in [1]. The nonlinearity of the current is modelled by combining multiple nonlinearly scaled inputs. The resulting model will be referred to as a temperature-dependent nonlinear parameter-varying model (Tnlpv).

4 Results

The proposed model's performance is compared to a Linear Parameter-Varying model that only depends on the temperature (Tlpv). The results are shown in Fig. 3, for which the corresponding root-mean-square errors in mV are 174, 86.2 and 12.6, respectively, for LTI, Tlpv and Tnlpv [2].
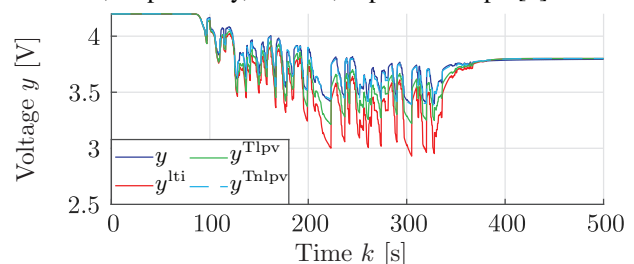
Figure 3: Model performance.

References

[1]   P. Cox, "Towards Efficient Identification of Linear Parameter-Varying State-Space Models." Ph.D. dissertation, Eindhoven University of Technology, 2018.

[2]   F. S. J. Hoekstra, Y. J. J. Heuts, H. J. Bergveld, and M. C. F. Donkers, "Empirical Battery Modelling for High Currents: The Effect of Nonlinear Overpotential and Inevitable Self-Heating," *submitted to IFAC*, 2020.

Passivity properties for regulation of DC networks with stochastic load demand

Amirreza Silani*, Michele Cucuzzella, Jacquelien M. A. Scherpen and Mohammad Javad Yazdanpanah

Jan C. Wilems Center for Systems and Control, ENTEG, Faculty of Science and Engineering,
University of Groningen, Nijenborgh 4, 9747 AG Groningen, the Netherlands
* Email: a.silani@rug.nl

Abstract

We present new (stochastic) passivity properties for Direct Current (DC) power networks, where the unknown and unpredictable load demand is modelled by a stochastic process. More precisely, the considered power network consists of distributed generation units supplying ZIP loads, i.e., nonlinear loads comprised of impedance (Z), current (I) and power (P) components. Differently from the majority of the results in the literature, where each of these components is assumed to be constant, we consider time-varying loads whose dynamics are described by a class of stochastic differential equations. Finally, we prove that an existing distributed control scheme achieving current sharing and (average) voltage regulation ensures the asymptotic stochastic stability of the controlled network.

Motivation and Contributions

In recent works, the load components have been assumed to be constant [1, 2]. However, it is well known that electric loads are in practice time-varying and, due to the random and unpredictable diversity of usage patterns, it is more realistic to consider unknown time-varying loads described for instance by stochastic processes. In our work, (i) each component of the ZIP load is modeled as the sum of an unknown constant and the solution to a Stochastic Differential Equation (SDE) describing the load dynamics; (ii) sufficient conditions for the stochastic passivity of the open-loop system are presented, facilitating the interconnection with passive control systems; (iii) the asymptotic stochastic stability of the considered network controlled by the distributed controller in [1] is proved.

Problem formulation

Let $\mathcal{G} = (\mathcal{V}, \mathcal{E})$ be a connected and undirected graph that describes the considered DC network. The nodes and the edges are denoted by $\mathcal{V} = \{1, \ldots, n\}$ and $\mathcal{E} = \{1, \ldots, m\}$, respectively. Fig. 1 illustrates the structure of the considered DC microgrid. The models of the network components are the following:

DGU model: The dynamic model of DGU $i \in \mathcal{V}$ is described by

$$L_{gi}\dot{I}_{gi} = -V_i + u_i$$
$$C_{gi}\dot{V}_i = I_{gi} - I_{li}(V_i) - \sum_{k \in \mathcal{E}_i} I_k. \qquad (1)$$
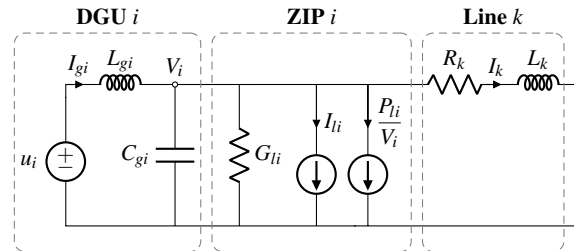
Figure 1: Electrical scheme of DGU i, ZIP load i and transmission line k.

Load model: In this work, we consider a general *nonlinear* and *stochastic* load model including the parallel combination of the following *unknown* load components:

(1) impedance component (Z): $G_{li}^* + \hat{G}_{li}$,

(2) current component (I): $I_{li}^* + \hat{I}_{li}$,

(3) power component (P): $P_{li}^* + \hat{P}_{li}$,

where $G_{li}^*, I_{li}^*, P_{li}^*$ are unknown constants and $\hat{G}_{li}, \hat{I}_{li}, \hat{P}_{li}$ are stochastic processes [3]. Thus, $I_{li}(V_i)$ is given by

$$I_{li}(V_i) = (G_{li}^* + \hat{G}_{li})V_i + I_{li}^* + \hat{I}_{li} + V_i^{-1}(P_{li}^* + \hat{P}_{li}). \qquad (2)$$

Line model: The dynamics of the current I_k exchanged between nodes i and j are described by

$$L_k\dot{I}_k = (V_i - V_j) - R_k I_k, \qquad (3)$$

The main control goals of this work are:

Goal 1 (Current sharing).
$$\lim_{t \to \infty} I_g(t) = \bar{I}_g = Q^{-1}\mathbb{1}i_g^*, \qquad (4)$$

Goal 2 (Average voltage regulation).
$$\lim_{t \to \infty} \mathbb{1}^\top Q^{-1}V(t) = \mathbb{1}^\top Q^{-1}\bar{V} = \mathbb{1}^\top Q^{-1}V^*, \qquad (5)$$

References

[1] S. Trip, M. Cucuzzella, X. Cheng, and J. M. A. Scherpen, "Distributed Averaging Control for Voltage Regulation and Current Sharing in DC Microgrids. IEEE Control Systems Letters", IEEE Control Systems Letters, vol. 3, no. 1, pp. 174-179, 2019.

[2] M. Cucuzzella, S. Trip, C. De Persis, X. Cheng, A. Ferrara, and A. J. van der Schaft, "A Robust Consensus Algorithm for Current Sharing and Voltage Regulation in DC Microgrids. IEEE Transactions on Control Systems Technology", IEEE Transactions on Control Systems Technology, vol. 27, no. 4, pp. 1583-1595, 2019.

[3] K. J. Astrom, E. R. Weitenberg, and F. Dorfler, "Introduction to stochastic control theory", Academic press New York and London, 1970.

Towards characterizing DC power flow
with sign-indefinite constant-power loads

Mark Jeeninga
ENTEG / Bernoulli Institute
University of Groningen
Email: m.jeeninga@rug.nl

Claudio De Persis
ENTEG
University of Groningen
Email: c.de.persis@rug.nl

Arjan J. van der Schaft
Bernoulli Institute
University of Groningen
Email: a.j.van.der.schaft@rug.nl

1 Abstract

In this work we analyze DC power grids with sign-indefinite constant-power loads. We deduce the DC power flow equations, which arise from balancing supply and demand in a power grid, and aim to characterize when they are solvable.

2 Introduction

To control a DC power grid, various control schemes are employed to converge to a desirable equilibrium (operating point) and ensure long term (voltage) stability. In the analysis of such schemes it is common to assume the existence of an equilibrium [3], or to adopt simpifying assumptions to guarantee existence of an equilibrium [4]. However, before considering a control scheme, a fundamental question arises: Under which condition(s) do equilibria exist, and when is the control objective feasible?

3 Constant-power loads

In this work we consider DC power grids. A power grid contains sources, which supply the grid with power by means of fixed voltage at generators. Other nodes in the power grid are assumed to be constant-power loads, which have fixed power injection. The power injection is sign-indefinite. That is, a load can drain power, but might also generate it. We refer to such nodes as prosumers.

Every prosumer is modeled by a ZIP node: a node with a constant impedance, constant current and constant power component. Classically, the constant power component is chosen to be negative, and thus the nodes always drain power from the system. We extend this notion by introducing a sign-indefinite constant-power component, with which we may model a power grid containing prosumers.

4 DC power flow

The DC Power flow equations are obtained by balancing the power supply and demand in the network. For simplicity we only consider the constant power component. They are given by

$$\mathrm{diag}(V_L)(Y_{LL}V_L + Y_{LS}V_S) = P_c,$$

where $\begin{pmatrix} V_L^\top & V_S^\top \end{pmatrix}^\top$ is the voltage potential of nodes, $\begin{pmatrix} Y_{LL} & Y_{LS} \end{pmatrix}$ describes the interconnection of lines from any node to a load node, and P_c is the constant power injection of the loads.

We define $A := \mathrm{diag}(Y_{LL}^{-1}Y_{LS}V_s)^{-1}Y_{LL}^{-1}\mathrm{diag}(Y_{LL}^{-1}Y_{LS}V_s)^{-1}$. We can show that the power flow equations have a solution if and only if

$$\mathrm{diag}(z)Az - z = P_c$$

has a solution satisfying $(Az)_i < 1$ for all i. In this research we focus on the map $z \mapsto z - \mathrm{diag}(z)Az$ and aim to characterize its image.

References

[1] J.W. Simpson-Porco, F. Dörfler, F. Bullo. *Voltage Collapse in Complex Power Grids.* Nature Communications, 7(10790), 2016.

[2] A. Dymarsky. *On the Convexity of Image of a Multidimensional Quadratic Map.* arXiv: 1410.2254, 2014.

[3] C. De Persis, E.R.A. Weitenberg, F. Dörfler. *A power consensus algorithm for DC microgrids.* Automatica, Vol. 89, 2018, pp. 364-375.

[4] J. Zhao, F. Dörfler. *Distributed control and optimization in DC microgrids.* Automatica, Vol. 61, 2015, pp. 18-26.

[5] A.S. Matveev, J.E. Machado, R. Ortega, J. Schiffer, A. Pyrkin. *On the Existence and Long-Term Stability of Voltage Equilibria in Power Systems with Constant Power Loads.* arXiv: 1809.08127, 2018.

A sub-optimal PWM-like ratio-based algorithm for the charge and balance of a string of battery cells

Alejandro Goldar, Michel Kinnaert, Emanuele Garone
Service d'Automatique et d'Analyse des Systèmes - Université libre de Bruxelles
agoldard@ulb.ac.be, michel.kinnaert@ulb.ac.be, egarone@ulb.ac.be

Battery packs are built with hundreds, and even thousands, of battery cells in series-parallel arrangements to deliver a required power and to have a specific capacity. Although all the cells have, theoretically speaking, identical characteristics; in practice we can observe voltage and State of Charge (SOC) variations between them.

During the charge, these variations must be equalized to take advantage of the full capacity of the pack. Current charging protocols implement voltage equalization either by dissipating the excess of energy in over-charged cells (passive balancing) or by redistributing the energy (active balancing) from the over-charged cells to the non-charged ones. Although widely implemented, most of the existing balancing techniques do not explicitly account for the interplay between the charging current and the equalization. However, quite recently, Pozzi et al (2019) introduced a non-linear constrained policy, within the framework of Model Predictive Control (MPC) that maximizes the charging current of a string of Li-ion cells while reducing SOC imbalances between the cells accounting for degradation mechanisms that can accelerate ageing. This contribution considers an active balancing grid where an over-charged or risky cell is completely shunted from the grid (Fig. 1).

Theoretically, one should consider ideal switches within this shunting grid to represent the scenarios where a j-th cell is completely connected or shunted from the grid. However, the scenarios description through auxiliary binary variables $\lambda_j \in \{0, 1\} \subset \mathbf{Z}^+$ ($\lambda_j = 0$ -cell shunted- and $\lambda_j = 1$ -cell being charged-) within the MPC formulation yields a mixed-integer non-linear constrained policy, which is most likely to be non-solvable in polynomial times (NP-hard).

To avoid the complexity of a mixed-integer non-linear optimization problem, instead of considering ideal switches, we can assume that a j-th cell is connected to or shunted from the string during a fraction of a time interval and not for the whole time interval (like in the ideal case). Thus, the fractions of the time interval can be defined as the duty cycles ($d_j \in [0, 1] \subset \mathbb{R}$) of the switches (in a Pulse-Width Modulation approach, PWM) connected to the j-th cell. By doing so, the cell connections can be represented as: $\lambda_j = 0$ when $k < t < k + d_j T_s$ (cell by-passed); or $\lambda_j = 1$, when $k + d_j T_s <$ $t < k+1$, (cell being charged). Although the inclusion of the duty cycles avoids binary variables, the resulting optimization problem is still non-linear due to product of the string charging current and the duty cycles, that represents the individual current of the each cell (i.e., $I_j(k) = d_j(k) I_{string}(k)$).

To further reduce the computational complexity of the optimization problem, we can describe each duty cycle as a fraction of the string charging current passing through a cell ($d_j = \frac{I_j}{I_{string}}$), which allows us to consider each cell as an independent subsystem, if and only if we assume that the duty cycles are time-invariant during the prediction and control horizons of the MPC. Therefore, we can solve an individual optimization problem for each cell within the pack and we can select the charging current of the string as the maximal charging current among the charging currents of N_{cells} within the pack $I_{string} = \arg \max_{I} |I_j| \ \ \forall j \in 1, \cdots, N_{cells}$ and calculate the duty cycles for each cell as the ratio between the individual charging current and the current of the string ($d_j = \frac{I_j}{I_{string}}$).

Simulation results on a serially-connected 4-cell strings show how the ratio-based approach outperforms a non-linear MPC policy in terms of computational burden, dramatically reducing the maximal computational time from 2.027s (in the non-linear MPC case) to 0.324s, while maintaining the charging time of the string of cells in 12.72min.
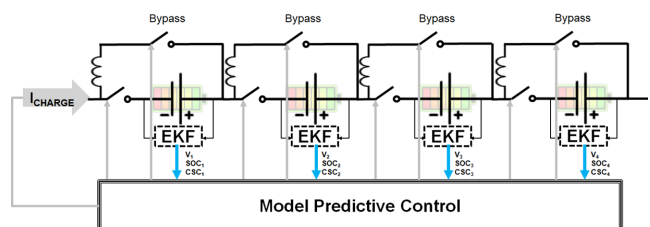
Figure 1: String of Batteries with a shunting balancing grid

Pozzi, A., Zambelli, M., Ferrara, A., and Raimondo, D.M. (2019). Balancing-aware charging strategy for seriesconnected lithium-ion cells: A nonlinear model predictive control approach. arXiv preprint arXiv:1902.02122.

Fault diagnosis and maintenance decision making for energy systems

Jianfeng Fu, Alfredo Nunez, Bart De Schutter
Delft Center for Systems and Control & Department of Engineering Structures
Delft University of Technology
Mekelweg 5, 2628 CD Delft, The Netherlands
Email: {j.fu-1,a.a.nunezvicencio,b.deschutter}@tudelft.nl

1 Introduction

Since in the last years a series of large-area outages has occurred in power systems worldwide, power system reliability is becoming a popular topic both in the field of the academic research as well as for power system companies. The reliability enhancement topic stretches over several sub-topics, e.g. reliability planning when the power systems are designed, maintenance and defense strategies to avoid vital faults, protection strategies to isolate a fault after it has occurred, and outage management to rapidly recover from the fault. This presentation focuses on the maintenance strategies in smart power grids in view of the large costs spent on maintenance and the difficulties to diagnose a fault especially when the complex power electronics devices are installed in large-scale power systems. More specifically, we consider maintenance scheduling for distribution network with micro-grids, and distributed maintenance scheduling considering uncertainties.

2 Maintenance scheduling for distribution network with micro-grids

The utilization of micro-grids increases the flexibility to operate distribution networks. More specifically, the micro-grids can be used to support power to nearby loads when the loads are cut off due to maintenance actions in upstream components. This paper proposes a day-ahead maintenance planning method that utilizes the power supporting potential of micro-grids to avoid load loss due to performance of maintenance actions. The method is embedded in a multi-level decision making structure. At the high level, monthly maintenance actions are decided. At the low level, day-ahead maintenance planning is proposed and formulated as a mixed integer linear programming problem. In addition, to guarantee the power balance during maintenance in the optimization, a switch connection path model is proposed. A case study based on the northwest China distribution network is presented. Results show that the proposed method can reduce load loss during maintenance effectively.

3 Distributed maintenance scheduling considering uncertainties

The day-ahead maintenance decision making for distribution network with micro-grids utilizes micro-grids to sup-
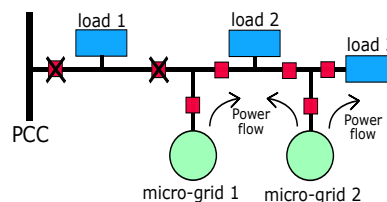
Figure 1: Illustration for supporting potential of micro-grids
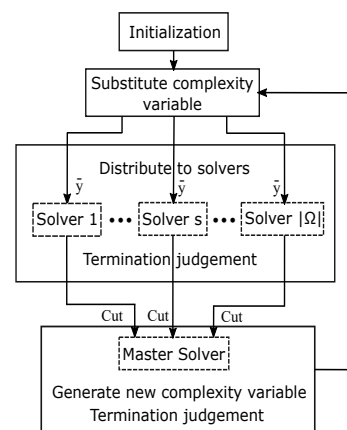
Figure 2: Parallel Benders decomposition

port power to nearby loads when the loads are cut off due to maintenance actions in upstream components. This can efficiently reduce the power loss while the maintenance actions are being performed. However, when considering the uncertainties in wind and solar power generation profiless as well as load profiless, the day-ahead maintenance decision making process becomes more complex and computationally costly compared to the situation without considering uncertainties. Therefore, we propose a hybrid approach based on robust optimization and scenario-based optimization to address the uncertainties in decision making. This hybrid approach avoids the conservatism. In addition, to reduce the computational burden, we apply the parallel Benders decomposition to solve the hybrid problem by a master solver and sub-solvers. The simulation results show the effectiveness of our proposed approach as well as the efficiency of the modified parallel Benders decomposition solver after comparisons to the Branch-and-cut solver.

Analytic Optimal Ellipsoidal Trajectory Bounds for Second-Order Dynamical Systems

Ömür Arslan

Department of Mechanical Engineering
Eindhoven University of Technology
P.O. Box 513, 5600 MB Eindhoven, The Netherlands
Email: O.Arslan@tue.nl

1 Introduction

Fast accurate motion prediction is fundamental for real-time safety verification and constraint satisfaction of autonomous dynamical systems. In this short note, we introduce novel minimum volume energy ellipsoids for motion range prediction of stable second-order dynamical systems. In particular, we show that the system's energy matrix explicitly defines an optimal ellipsoidal bound on the system's trajectory.

2 Second-Order Systems with Quadratic Total Energy

Consider a second-order dynamical system moving in $\mathbb{R}^n$

$$\ddot{x} = u(x, \dot{x}) \tag{1}$$

according to a control policy $u : \mathbb{R}^n \times \mathbb{R}^n \to \mathbb{R}^n$ that is a (Lipschitz continuous) function of system position $x \in \mathbb{R}^n$ and system velocity $\dot{x} \in \mathbb{R}^n$, and its quadratic total energy $E(x, \dot{x})$, with respect to the origin, is defined as

$$E(x, \dot{x}) := x^\mathsf{T} P x + \dot{x}^\mathsf{T} Q \dot{x} \tag{2}$$

where $P, Q \in S^n_{++}$ are $n \times n$ positive definite matrices.

2.1 Motion Control using Total Energy

To asymptotically bring our system to a stop at the origin, an energy dissipating control policy in the form of a proportional-derivative (PD) controller can be designed as [1]:

Proposition 1 *For any positive definite $P, Q \in S^n_{++}$, the dynamical system in (1) is globally asymptotically stable at the origin under the energy dissipating control policy*

$$u(x, \dot{x}) = -Q^{-1} P x - Q^{-1} D \dot{x} \tag{3}$$

where $D \in S^n_{++}$ is a positive definite damping matrix that determines the time rate of energy dissipation as

$$\dot{E}(x, \dot{x}) = -2\dot{x}^\mathsf{T} D \dot{x} \leq 0. \tag{4}$$

2.2 Motion Prediction using Total Energy

A standard geometric model for bounding dynamical system trajectories is an (origin-centered) ellipsoid,

$$\mathcal{E}(\Sigma, \rho^2) := \left\{ \rho \Sigma^{\frac{1}{2}} y \;\middle|\; y \in \mathbb{R}^n, \|y\| \leq 1 \right\} \tag{5}$$

parametrized by a positive semi-definite matrix $\Sigma \in S^n_+$ and a nonnegative scale factor $\rho \in \mathbb{R}_{\geq 0}$, whose volume satisfies

$$\operatorname{vol}(\mathcal{E}(\Sigma, \rho^2)) \propto \det(\rho^2 \Sigma)^{\frac{1}{2}}. \tag{6}$$

For example, the system's total energy can be leveraged for motion prediction as:

Proposition 2 *For any $P, Q, D \in S^n_{++}$, the motion trajectory $x(t)$ of the dynamical system (1), under the energy dissipating control policy in (3), is contained in the projected ellipsoidal energy sublevel set $\mathcal{E}(P^{-1}, E(x(0), \dot{x}(0)))$ for all $t \geq 0$.*

Remark 1 If $P = \kappa_P Q$ and $D = \kappa_D Q$ for some positive scalars $\kappa_P, \kappa_D \in \mathbb{R}_{>0}$, then the control policy in (3) and the total energy in (2) simplify to

$$u(x, \dot{x}) = -\kappa_P x - \kappa_D \dot{x}, \tag{7}$$

$$E(x, \dot{x}) = \kappa_P x^\mathsf{T} Q x + \dot{x}^\mathsf{T} Q \dot{x} = \operatorname{tr}(Q(\kappa_P x x^\mathsf{T} + \dot{x} \dot{x}^\mathsf{T})) \tag{8}$$

and the volume of the projected energy ellipsoid satisfies

$$\operatorname{vol}(\mathcal{E}((\kappa_P Q)^{-1}, E(x, \dot{x})))^2 \propto \det(Q^{-1}) \operatorname{tr}(Q(\kappa_P x x^\mathsf{T} + \dot{x} \dot{x}^\mathsf{T}))^n. \tag{9}$$

Note that for any κ_P and κ_D our system accepts a family of energy functions parameterized by Q. We below present an optimal selection for minimum volume energy ellipsoids.

3 Analytic Minimum Volume Energy Ellipsoids

Lemma 1 *For any positive definite $\Lambda \in S^n_{++}$, the minimum volume ellipsoid of the form $\mathcal{E}(\Sigma, \operatorname{tr}(\Sigma^{-1}\Lambda))$ is $\mathcal{E}(\Lambda, n)$, i.e.,*

$$c\Lambda = \underset{\Sigma \in S^n_{++}}{\arg\min} \operatorname{vol}(\mathcal{E}(\Sigma, \operatorname{tr}(\Sigma^{-1}\Lambda))) \quad \forall c > 0. \tag{10}$$

Theorem 1 *For any initial state $(x, \dot{x}) \in \mathbb{R}^n \times \mathbb{R}^n$, the minimum volume energy ellipsoid containing the future trajectory of the dynamical system, under the control policy in (7), is $\mathcal{E}^*(x, \dot{x}) := \mathcal{E}(\kappa_P^{-1}\Sigma(x, \dot{x}), \operatorname{rank}(\Sigma(x, \dot{x})))$, where $\Sigma(x, \dot{x})$ is the system's energy matrix defined as $\Sigma(x, \dot{x}) := \kappa_P x x^\mathsf{T} + \dot{x} \dot{x}^\mathsf{T}$.*

Proposition 3 *Under the control policy in (7), the minimum volume energy ellipsoid $\mathcal{E}^*(x(t), \dot{x}(t))$ shrinks (i.e., positively inclusive) along the system trajectory $x(t)$,*

$$\mathcal{E}^*(x(t_1), \dot{x}(t_1)) \supseteq \mathcal{E}^*(x(t_2), \dot{x}(t_2)) \quad \forall t_1 \leq t_2. \tag{11}$$

4 Conclusions

We present an analytic optimal ellipsoidal trajectory bound for stable second-order dynamical systems. Our ongoing work generalizes these results to higher-order systems and focuses on their applications in robot motion planning [2].

References

[1] D. E. Koditschek, "The application of total energy as a Lyapunov function for mechanical control systems," *Contemporary Mathematics*, vol. 97, pp. 131–158, 1989.

[2] Ö. Arslan and D. E. Koditschek, "Smooth extensions of feedback motion planners via reference governors," in *IEEE Int. Conf. on Robotics and Automation*, 2017, pp. 4414–4421.

Model Predictive Control for Integrated Synchromodal Transport[1]

Rie B. Larsen, Bilge Atasoy and Rudy R. Negenborn

Dept. of Maritime and Transport Technology, Delft University of Technology, The Netherlands.

Email: `R.B.Larsen|B.Atasoy|R.R.negenborn@tudelft.nl`

1 Background

To decrease the environmental impact of the transport sectors, new approaches are needed. One such approach is synchromodal transport, where all decisions regarding a transport are taken by the transport providers. The only fixed parameters of a transport are thus origin, destination, release time and due date. When the transport providers have the opportunity to change routes in accordance to the status of the transport network, new possibilities for increasing the utilization rate of equipment arise, improving the profit and the environmental impact. New ways of planning, which can ensure both the due delivery of the freight and a reasonable utilization of vehicles are needed as the current methods typically consider one or the other [2]. Our research explores the use of control methods to address this challenge [1].

2 Controller design

Controlling the movements of both containers and vehicles in a synchromodal transport network only yields improvements if the control methods can foresee the cost of the actions, ensure constraint satisfaction and update sufficiently fast. Model predictive control (MPC) was chosen as it fulfils the first two requirements and has a computation time which is highly dependent on the model formulation. Our controller design is thus closely linked to the choice of system model.

To obtain sufficient speed, the controller aggregates the transport orders into commodity flows like in [3]. Two parallel commodity flow models for, respectively, the containers and the trucks are linked by the constraint that containers can only flow on an arch if a sufficient number of trucks flow on the arch. Barges and trains travel according to pre-defined schedules and are modelled as nodes with time-dependent constraints on their in and out flows. With this model formulation, the MPC only has linear constraints. Based on the results in [4] all variables are assumed continuous, which in combination with a quadratic cost makes the MPC optimization problem convex and thus fast to solve. Terminal constraints and costs are omitted as the system is inherently marginally stable and the time-varying constraints on (un)loading the barge and train makes them very complex to compute compared to using a longer prediction horizon.

Earlier methods assume instantaneously availability of trucks. In reality, however, it takes between 2 hours and 2 days to get an unscheduled truck, leading earlier methods to create infeasible plans if used in real time. We investigate in this work the impact of considering that trucks are not instantaneously available.

3 Simulation experiments and results

The impact of using MPC to integrate container and vehicle control has been shown on a simulated synchromodal network. The results show that when movements of containers and vehicles are both considered by the controller, the fluctuation in the number of vehicles needed is smaller than when the controller only optimizes for the container movements and assumes trucks available instantaneously. This implies improved vehicle utilization. Integrated planning also enables planning with a pre-specified finite number of trucks. The results furthermore confirm that MPC is fast on the small simulated network, and thus likely to be a suitable control strategy for realistic network sizes.
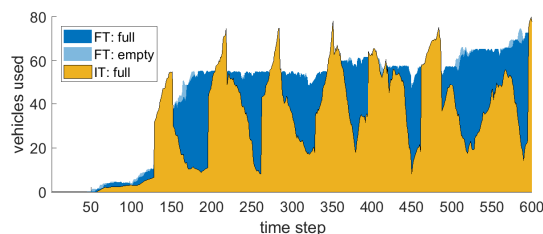
Figure 1: Number of trucks needed when planning is integrated (FT) or with instantaneously availability (IT)

References

[1]   R. B. Larsen et al., "Simultaneous Planning of Container and Vehicle-Routes Using Model Predictive Control," Proc. European Control Conf., 2019

[2]   B. van Riessen et al., "Synchromodal container transportation: an overview of current topics and research opportunities," Proc. Int. Conf. on Computational Logistics, 2015

[3]   J. L. Nabais et al., "Model predictive control for a sustainable transport modal split at intermodal container hubs," Proc. Int. Conf. on Networking, Sensing and Control, 2013.

[4]   S. Sager et al., "The integer approximation error in mixed-integer optimal control," Mathematical Programming, 2012.

Nonlinear MPC for Tracking for Star-shaped Admissible Output Sets

Andres Cotorruelo
Université Libre de Bruxelles
acotorru@ulb.ac.be

Daniel Limon
Universidad de Sevilla
dlm@us.es

Emanuele Garone
Université Libre de Bruxelles
egarone@ulb.ac.be

1 Introduction

Model Predictive Control (MPC) is currently one of the most ubiquitous constrained control schemes in the industry. Due to the fact that MPC arose as a solution for the control of industrial processes, most MPCs deal with the regulation problem (*i.e.* steering the system state to the origin), since most processes have one or more optimal set-points on which to operate.

Nevertheless, the tracking problem (*i.e.* following a time varying reference) is also of relevance, not only to some industrial processes (*e.g.* chemical batch processes), but also, for example, in robot navigation. Since the regular MPC scheme may lose feasibility under sudden set-point changes, an extension of the MPC scheme was presented in [1] that maintains feasibility under piece-wise constant references and guarantees convergence under a few assumptions.

Originally, the MPC for Tracking scheme was limited to convex sets of feasible outputs, but it was extended to be able to with non-convexity in [2] , but required a closed form mapping between the original non-convex set and a convex one. In this publication, we present a further extension, which no longer requires the knowledge of the mapping in closed form.

2 Problem statement

Consider a discrete time LTI system in the form

$$
\begin{aligned}
x^+ &= f(x,u) \\
y &= g(x,u),
\end{aligned}
\tag{1}
$$

where $x^+ \in \mathbb{R}^n$ is the successor state, $x \in \mathbb{R}^n$ is the current state, $u \in \mathbb{R}^m$ is the input, and $y \in \mathbb{R}^p$ is the controlled output of the system. The system is subject to constraints in the form

$$
(x,u) \in \mathscr{Z},
$$

where $\mathscr{Z} \subset \mathbb{R}^n \times \mathbb{R}^m$ is a closed set with a nonempty interior. Accordingly, the set of admissible steady state outputs is defined as follows:

$$
\mathscr{Z}_s = \{(x,u) \in \mathscr{Z} : x = f(x,u)\},
\tag{2}
$$

$$
\mathscr{Y}_s = \{y = h(x,u) : (x,u) \in \mathscr{Z}_s\}.
\tag{3}
$$

The control objective is to steer the system output y towards the target setpoint y_t.
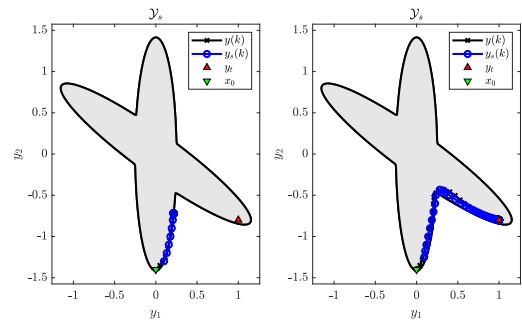
Figure 1: On the left, an example of the evolution of a system with a star-shaped $\mathscr{Y}_s$ controlled with the original MPC for Tracking. On the right, the evolution of the same system controlled with the proposed extension.

A possible solution for this problem is the MPC for Tracking [1], which introduces an artificial set-point y_s that is as close to y_t as possible so that feasibility of the MPC optimization problem is maintained. The convergence of this artificial set-point y_s towards y_t is guaranteed by adding a penalty in the cost function of the deviation between y_s and y_t.

As previously mentioned, this scheme may present convergence issues when $\mathscr{Y}_s$ is non-convex (see Figure 1). To tackle this, in [2] the authors present an extension of the original MPC for Tracking by mapping the non-convex $\mathscr{Y}_t$ to a convex set. However, the mapping is assumed to be known in closed form, which can be unrealistic in some cases.

We now present a further extension of this scheme, which no longer requires the knowledge of the mapping in closed form for a relevant class of non-convex sets: the star-shaped sets. This is done by embedding the mapping in the MPC optimization problem so that it is computed at the same time as the control action.

References

[1] Limon, D., Ferramosca, A., Alvarado, I. and Alamo, T., 2018. *Nonlinear MPC for tracking piece-wise constant reference signals*. IEEE Transactions on Automatic Control, 63(11), pp.3735-3750.

[2] Cotorruelo, A., Limon, D., Garone, E. and Ramirez, D.R., 2018. *Tracking MPC with non-convex steady state admissible sets*. IFAC-PapersOnLine, 51(20), pp.153-156.

Conditions for obtaining robustness and stability in data-driven predictive control

Jens Declercq
Bruges Belgium
jens.declercq@kuleuven.be

Mark Versteyhe
Bruges Belgium
mark.versteyhe@kuleuven.be

1 Introduction

An ever growing number of data-driven techniques being published to understand and control complex systems. The way of handling large amounts of data is crucial if we want to monetize the knowledge that hides in (historical) datasets. The latest well documented control strategies like model predictive control (MPC) use a mathematical formulated model of the process in order to optimize the control system [1].

Figure 1: MPC diagram [1]
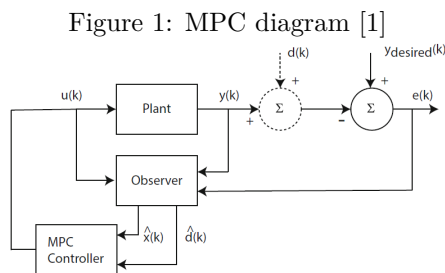
With good results in controlling non-linear constrained systems this method matured as researchers started to analyse the conditions in which the integration of MPC results in stability. The complexity of model-based predictive control lies in the construction of a mathematical model. Accurate models of complex systems, like climate control of large buildings, are build by experts with extensive knowledge of the related first principals [2]. An alternative approach for building these models by hand comes from the field of data analysis. More specifically machine learning algorithms. By using (historical) datasets accurate models are generated that is able to describe the systems dynamics. This approach is known as Data-driven Predictive Control (DPC) or Machine Learning Control (MLC).

2 Problem

Robustness, stability and recursive feasibility are well understood for MPC design. The same can not be said for DPC. This constrains the theoretical and practical capabilities of MLC. Experiments with DPC algorithms already exist and report an increase in performance compared to PID and even MPC strategies. Very few articles, books and papers talk about proving stability for DPC. The effect of parameter variation will be analysed to ensure asymptotic stability.

3 Approach

Random Forest, Weiner Regression, Support Vector Machine and Regression Trees are just a few examples of machine learning algorithms that show potential [3][4]. Ensuring stability is still a concern. Especially in situations where constraints are important. Concepts like Gerschgorin disks, Gerschgorin domains and the Lyapunov theorem are used to guarantee closed-loop stability and convergence for MPC [5]. The main goal of the proposed research is to formulate a similar framework to develop MLC that guarantees asymptotic stability.

Figure 2: DPC concept diagram
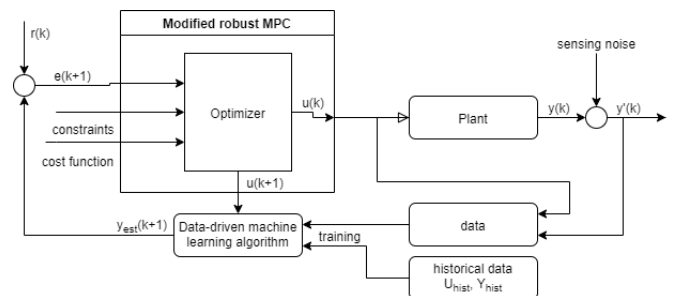
References

[1]   Saša V. Rakovic, William S. Levine Handbook of Model Predictive Control

[2]   Francesco Smarraa, Achin Jainb, Tullio de Rubeisc, Dario Ambrosinic, Alessandro D'Innocenzoa, Rahul Mangharamb Data-driven MPC using random forests for building energy optimization and climate control

[3]   Achin Jain, Francesco Smarra, and Rahul Mangharam DPC using Regression Trees and Ensemble Learning

[4]   Van-Vuong Trinh, M. Alamir, P. Bonnay Data-driven Explicit Nonlinear MPC via Wiener Regression and Reduced-Set Support Vector Machines

[5]   Yuan Guo, Zhongsheng Hou, Shida Liu, and Shangtai Jin Data-Driven Model-Free Adaptive Predictive Control for a Class of MIMO Nonlinear Discrete-Time Systems With Stability Analysis

Explicit Reference Governor for a Boom Crane System

Michele Ambrosino[1], Emanuele Garone[1], and Arnaud Dawans[2]

[1]Department of Control Engineering and System Analysis , Université Libre de Bruxelles (ULB) ,
Michele.Ambrosino@ulb.ac.be, egarone@ulb.ac.be,
[2] Entreprises Jacques Delens S.A. , adawans@jacquesdelens.be

1 Introduction
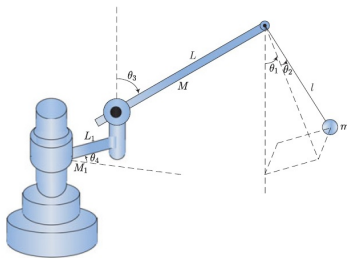
Figure 1: Model of an underactuated boom crane system [1]

Boom cranes (see Fig.1), due to benefits such as high maneuverability, are among the most used cranes for the lift of heavy loads. Currently this kind of crane is driven by a mason, the crane lifts the block from a pallet and brings it closer to its final position. Later on, another mason uses his hands to finish the positioning. This kind of activity is potentially dangerous for the masons, therefore it is essential to design efficient control methods to improve the control performance of the boom crane system and restrict the payload swing amplitudes as much as possible. From the control viewpoint, the boom crane is a nonlinear underactuated system, having fewer independent actuators than the system degrees of freedom (DoFs). Due to this underactuated characteristic, it becomes fairly challenging to control boom crane systems effectively.

The aim of this work is to design a novel control framework, the ERG [2], for boom crane subject to limited joint ranges and static obstacle avoidance constraints. The control law will be able to stabilize the system around each desired point of equilibrium ensuring good dynamic performances.

2 Control design

The dynamic model of an underactuated 3-D boom crane system can be described by the equations presented in [1].

The control objective is to move the boom to the desired position and dampen the load swing at the same time, which can be described mathematically as follows:

$$\lim_{t \to \infty} \theta_1(t) = 0, \quad \lim_{t \to \infty} \theta_2(t) = 0$$
$$\lim_{t \to \infty} \theta_3(t) = \theta_{3d}, \quad \lim_{t \to \infty} \theta_4(t) = \theta_{4d}$$
(1)

where $\theta_1(t)$ is the payload radial swing angle, $\theta_2(t)$ is the payload tangential swing angle, $\theta_3(t)$ is the boom pitch angle, $\theta_4(t)$ is the boom yaw angle, and θ_{3d} and θ_{4d} are the boom's desired angles.

Typically three main types of constraints are considered in this kind of application: constraints concerning the maximum range of the joints, safety constraints related to the suspended load, and constraints modelling the collision avoidance with objects and structure. In particular in this work we consider a simplified model of the wall that must be avoided by the payload.

The control architecture proposed in this paper consists of two cascade control loops. A Linear Quadratic Regulator is used in the inner loop to pre-stabilizes the system and ensure fast dynamics. The external loop consists of an Explicit Reference Governor [2] to ensure constraint satisfaction and reference tracking.

As shown in Fig. 2 the system follows the desired reference and the control low is able to avoid collisions with the wall.
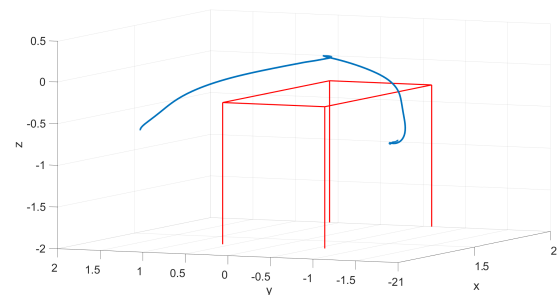
Figure 2: Blue line: Payload Trajectory. Red line: Wall constrain

References

[1]   N. Sun, T. Yang, Y. Fang, B. Lu and Y. Qian, "Nonlinear Motion Control of Underactuated Three-Dimensional Boom Cranes With Hardware Experiments," in IEEE Transactions on Industrial Informatics, vol. 14, no. 3, pp. 887-897, March 2018.

[2]   E. Garone and M. M. Nicotra, "Explicit Reference Governor for Constrained Nonlinear Systems," in IEEE Transactions on Automatic Control, vol. 61, no. 5, pp. 1379-1384, May 2016.

Identifiability in dynamic networks through switching modules [1]

H.J. Dreef   M.C.F. Donkers   P.M.J. Van den Hof

Control Systems, Department of Electrical Engineering, Eindhoven University of Technology

P.O. Box 513 5600 MB Eindhoven

{h.j.dreef,m.c.f.donkers,p.m.j.vandenhof}@tue.nl

1 Introduction

Besides interconnections of systems in dynamic networks, the combination of digital and physical components poses technological challenges in the near future. An attractive approach to achieve safe and efficient operation of these networks is by using model-based techniques. Data-driven modelling of dynamic networks has been studied in recent years to get satisfactory models for this purpose.

An important topic is identifiability, which states whether individual systems or modules can be distinguished from the network structure, see e.g., [1]. Although, switching modules have not been studied in dynamic networks, it has been found that a switching controller in a feedback loop provides additional excitation, see e.g., [2]. This raises the questions whether switching modules in dynamic networks affect identifiability and in what way.

In this work, the conditions are studied under which switching modules provide additional excitation, such that invariant (non-switching) modules become identifiable. This is approached by combining the reasoning on network identifiability in [1] and on switching controllers in [2].

2 Network identifiability

Whether individual parametrized modules can be distinguished from the network structure depends on the transfer matrix from external excitation and noise signals to measured nodes. Information on the network structure, existence and locations of excitation signals is contained in this matrix. Based on this information, the analysis on network identifiability boils down to independent excitation of every input node of a parametrized module, see e.g., [1].

Let us take the network in Figure 1 as an example, where only one excitation signal is present and G_{31} and G_{32} are parametrized. This network is not network identifiable, since w_1 and w_2 are correlated. This can be interpreted as having one equation for two unknowns. Therefore, one way to make this network identifiable is by adding an excitation signal to node w_2, but when this is not possible or desirable other options can be considered.
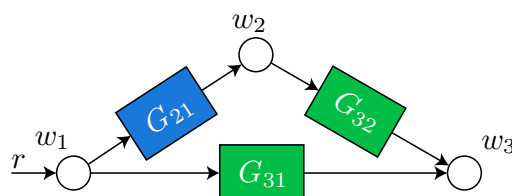
Figure 1: A network example with multiple parametrized modules(green) and a non-parametrized module (blue).
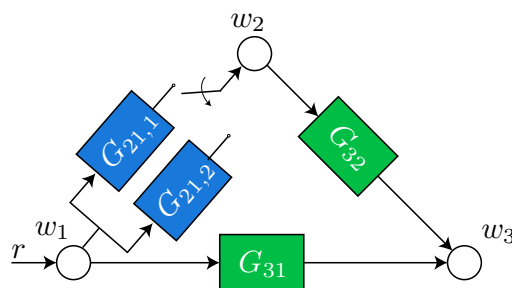
Figure 2: A network example with multiple parametrized modules (green) and a switching module (blue).

3 Identifiability of invariant modules

In addition to external signals that provide excitation, switching modules affect identifiability of the remaining invariant modules. The reasoning, based on [2], is that multiple transfer matrices can be used to recover the invariant parametrized modules uniquely.

Take the network in Figure 2 as an example, where in contrary to Figure 1, module G_{21} is switching between two modes. This yields two different transfer matrices with two invariant parametrized modules, i.e., there are two equations for two unknowns, making these modules identifiable. Thus, switching modules can be used to provide excitation as an alternative to adding external signals. We will present results that show how this principle can be utilized in dynamic networks with a general topology.

References

[1]   H. H. M. Weerts, P. M. J. Van den Hof, and A. G. Dankers, "Identifiability of linear dynamic networks," *Automatica*, 2018.

[2]   T. Söderström, L. Ljung, and I. Gustavsson, "Identifiability conditions for linear multivariable systems operating under feedback," *IEEE Trans. on Automatic Control*, 1976.

Excitation allocation for generic identifiability of a single module in dynamic networks [1]

S. Shi, X. Cheng, P. M. J. Van den Hof
Eindhoven University of Technology, The Netherlands
Email: {s.shi, x.cheng, p.m.j.vandenhof}@tue.nl

Problem formulation

For identifiability of a single module in a dynamic network, excitation signals need to be allocated in the network. Current results hardly address the synthesis question: where to allocate the excitation signals for generic identifiability.

Models in a network model set encompass the relationship among scalar-valued *internal signals* w_j, excitation signals r_k, and unmeasured disturbances e_l. The interconnection among the signals is modeled in a matrix form [1] as

$$w(t) = G(q)w(t) + R(q)r(t) + H(q)e(t), \qquad (1)$$

where q is the delay operator, i.e. $q^{-1}w_j(t) = w_j(t-1)$, and G, R and H are transfer matrices while G is hollow. The locations of zero entries in G, R and H are typically fixed by the user and their structure is encoded by a graph as in Fig. 1, where vertices represent signals and an directed edge from w_i to w_j denotes a transfer function G_{ji}.

A network model set is parameterized (1) with a vector $\theta \subseteq \mathbb{R}^d$. $T \triangleq (I - G)^{-1} \begin{bmatrix} R & H \end{bmatrix}$, the mapping from external signals to internal signals, can typically be identified from data. Generic identifiability of a single module G_{ji} in the model set concerns the uniqueness of G_{ji} given T, and G_{ji} is said generically identifiable if $T(q,\theta_1) = T(q,\theta_2) \implies G_{ji}(q,\theta_1) = G_{ji}(q,\theta_2)$ for almost all θ_1 and θ_2.

The considered problem is: given a parameterized network model and its graph, how to allocate excitation signals r_k such that G_{ji} becomes generically identifiable.

Analysis and synthesis based on disconnecting sets

A new graphic condition is derived using the concept of disconnecting sets [2]. A set of vertices $\mathcal{D}$ is called a $\mathcal{V}_1 - \mathcal{V}_2$ disconnecting set if all directed paths from vertices in $\mathcal{V}_1$ to vertices in $\mathcal{V}_2$ intersect with $\mathcal{D}$. We then demonstrate the theory in Fig. 1 where generic identifiability of G_{21} is of interest. It states that, G_{21} is generically identifiable if and only if w_1 and all vertices in a disconnecting set from w_1 to the other in-neighbors of w_2 through parameterized modules, indicated by the red circle of Fig. 1, receive independent excitation.
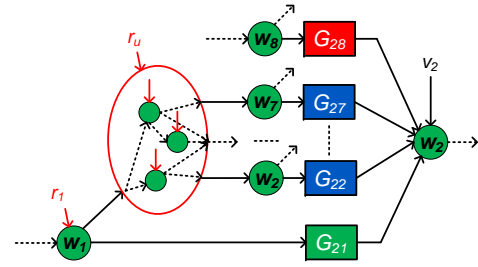
Figure 1: A dynamic network with target module G_{21}, parameterized modules (blue) and a known module G_{28}.
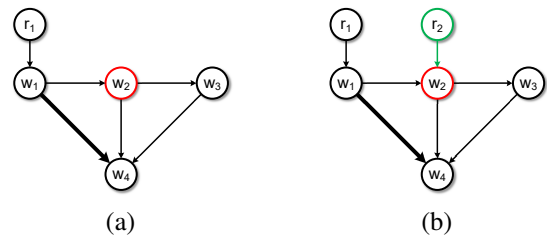
Figure 2: Allocating signals to achieve generic identifiability of G_{41} (thick line).

Following the theory, a synthesis approach is developed to allocate excitation signals, demonstrated in Fig.2(a) where the target is to achieve generic identifiability of G_{41}. Because $\{w_2\}$ is a disconnecting set from w_1 to the other in-neighbors $\{w_2, w_3\}$ of w_4 while it does not receive excitation, G_{41} is not generically identifiable. The synthesis approach then allocates another signal r_2 at the disconnecting set $\{w_2\}$ as in Fig.2(b), where G_{41} is now generically identifiable. This approach can be applied to general model sets and the minimum number of allocated signals can be achieved by constructing the *minimum* disconnecting sets.

References

[1] P. M. J. Van den Hof, A. Dankers, P. S. C. Heuberger, and X. Bombois. Identification of dynamic models in complex networks with prediction error methods-Basic methods for consistent module estimates. *Automatica*, 2013.

[2] S. Shi, X. Cheng, and P. M. J. Van den Hof. Excitation allocation for generic identifiability of a single module in dynamic networks: A graphic approach. *21st IFAC World Congress*. Submitted.

Linear Time-Varying System Identification in the Presence of Nonlinear Distortions

Noël Hallemans, Rik Pintelon, and John Lataire

Vrije Universiteit Brussel, Pleinlaan 2, 1050 Elsene, Belgium. e-mail: `noel.hallemans@vub.be`

1 Motivation and problem formulation

In various measurements of real life systems, for instance corrosion processes, one stumbles upon linear time-varying (LTV) behaviour which is corrupted by both noise and nonlinear distortions. The corruption by noise is well known in the literature. However, the corruption by nonlinear distortions is a new problem in the context of time-varying systems. Mathematically, the corrupted output signal $y(t)$ of an LTV system G can be written as

$$y(t) = \mathscr{L}^{-1}\{G(s,t)U(s)\} + v_{\mathrm{n}}(t) + v_{\mathrm{nl}}(t)$$

where $G(s,t)$ is the time-varying transfer function, $U(s)$ is the Laplace transform of the input signal $u(t)$, $v_{\mathrm{n}}(t)$ represents the noise signal and $v_{\mathrm{nl}}(t)$ the nonlinear distortions. In this research we restrict ourselves to the case where $v_{\mathrm{nl}}(t)$ is the output of a nonlinear time-invariant (NLTI) system. These nonlinear distortions and noise are regarded as disturbances, they could for instance origin from the measurement equipment or unwanted behaviour of the system. The problem consists of extracting $G(s,t)$, which is a linear time-varying model for the system G, from the measurements of $u(t)$ and $y(t)$. Since the noise and the nonlinearities are disturbances, we can compute the associated uncertainty on the model. More specifically, one would like to distinguish between the uncertainty caused by, on the one hand, the noise and on the other hand the nonlinear distortions.

2 Proposed solution

A very useful tool for this problem is the multisine excitation. It permits to make a distinction between time-variation, noise and nonlinear distortions in the output spectrum. When exciting a time-varying system with a multisine, skirts appear around the excited frequencies [1]. Note that these skirts are present at all frequencies and are correlated over frequency. Noise can be present on all frequencies too, but is uncorrelated over frequency. However, due to the particular properties of the multisine, nonlinear distortions can only be present on a well-defined set of bins, i.e. on the integer multiples of the fundamental frequency, which is the inverse of the period of the multisine [2].

An illustration is shown in **Figure 1**. Here the input —•— and output —•— spectra are shown for an LTV system corrupted by both noise and nonlinear distortions. The
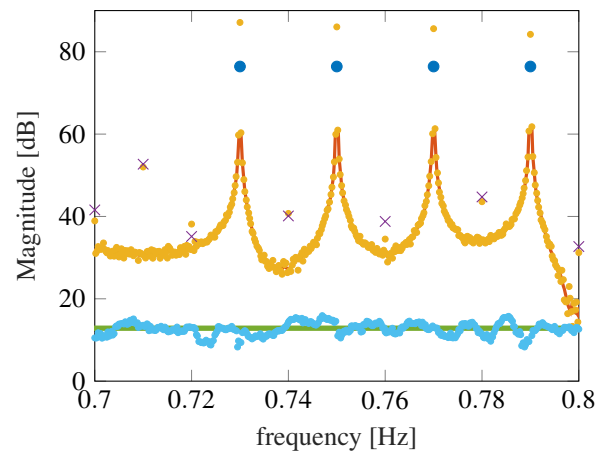
Figure 1: Input —•— spectrum, output spectrum —•—, estimated output spectum ——, estimation of nonlinear distortions —×—, true noise level (std) —— and estimate of noise level —•—.

latter is the output of an NLTI system, excited by the same multisine. From this figure, it is obvious that nonlinear distortions are present, as some output spectrum points do not follow the smooth spectrum of the skirts, i.e. at integer multiples of 0.01 Hz, the fundamental frequency of the multisine.

The main idea is to discard the output spectrum points at which nonlinear distortions could be present. Then, in local frequency bands, one can fit the output spectrum with both hyperbolas and polynomials. From the difference between the spectral model —— and the data —•— one can estimate the noise standard deviations —•— and the nonlinear distortions —×—.

As a result, a model for the LTV system is estimated in the form of a time-varying transfer function $G(s,t)$ together with uncertainty bounds due to separately the noise and the nonlinear distortions.

References

[1]   John Lataire, Rik Pintelon, and Ebrahim Louarroudi. Non-parametric estimate of the system function of a time-varying system. *Automatica*, 48(4):666–672, 2012.

[2]   J. Schoukens, R. Pintelon, T. Dobrowiecki, and Y. Rolain. Identification of linear systems with nonlinear distortions. *Automatica*, 41(3):491 – 504, 2005.

Local dynamics identification via a graph-theoretical approach

Antoine Legat and Julien M. Hendrickx
ICTEAM Institute, UCLouvain, B-1348 Louvain-la-Neuve, Belgium.
Email: { `antoine.legat,` `julien.hendrickx` } @uclouvain.be

1 Introduction

The goal of this work is to recover the local dynamics from the global input-output behavior of a networked system and the knowledge of the network topology.

We consider the identification of a network matrix $G(z)$, where the network is made up of n nodes, with node signals $\{w_1(t), \ldots, w_n(t)\}$, and external excitation signals $\{r_1(t), \ldots, r_n(t)\}$, related to each other by:

$$
\begin{aligned}
w(t) &= G(z)w(t) + Br(t) + v(t) \\
y(t) &= Cw(t),
\end{aligned} \quad (1)
$$

where matrices B and C are binary selections defining which nodes are excited and measured, forming the sets $\mathscr{B}$ and $\mathscr{C}$ respectively. The vector $y(t)$ contains the measured nodes, while $v(t)$ is a noise vector. The nonzero entries of the network matrix $G(z)$ define the topology of the network, and are assumed to be proper and rational.

We assume that the global relation between the excitations r and measures y has been identified, and that the structure of $G(z)$ is known. From this knowledge, we aim at recovering the nonzero entries of $G(z)$.

A first line of work extends the classical closed-loop identification techniques to identify a single module, see e.g. [1]. A recent approach employs graph-theoretical tools to derive identifiability conditions on the graph of the network. Using this approach, [2] address the particular case where all nodes are excited. In the general case of partial measurement *and* excitation, [3] study particular topologies of graphs and provide necessary conditions for identifiability. In this work, we consider partial measurement and excitation for all topologies. We introduce the notion of local generic identifiability, for which we derive conditions and develop an algorithm.

2 Problem reformulation

Starting from the definition of a network system in (1), we first define $T(z) \triangleq (I - G(z))^{-1}$, which is assumed to be proper and stable. The input-output model of network model (1) is then given by

$$
y(t) = CT(z)Br(t) + \tilde{v}(t),
$$

where $\tilde{v}(t) \triangleq CT(z)v(t)$. We assume that $r(t)$ is sufficiently rich so that, for any B and C, $CT(z)B$ can be consistently

estimated from $\{y(t), r(t)\}$ data. From the knowledge of $CT(z)B$, the aim is to re-identify $G(z)$. This motivates the following definition, which restricts the usual generic identifiability from [2] to non-discrete sets of solutions.

Definition 1. *The network matrix $G(z)$ is locally generically identifiable from $\mathscr{B}$ and $\mathscr{C}$ if, for any parametrization $G(P,z)$ consistent with the graph, there exists $\tilde{G}(z)$ consistent with the graph, $\varepsilon > 0$ such that $||\tilde{G}(z) - G(P,z)|| < \varepsilon$ for a suitable notion of norm, and there holds*

$$
C(I - G(P,z))^{-1}B = C(I - \tilde{G}(z))^{-1}B \Rightarrow G(P,z) = \tilde{G}(z) \quad (2)
$$

for all P except possibly those lying on a zero measure set.

In this definition, a network matrix $G(z)$ is said *consistent with the graph* if $G_{ij}(z)$ is zero when there is no edge (i, j).

3 Results

One can linearize (2) to obtain the following criterion

$$
CT(z)\Delta T(z)B = 0 \Rightarrow \Delta = 0, \quad (3)
$$

where Δ is consistent with the graph. Through algebraic computations, we can then re-express (3) as a rank condition on a matrix K constructed from C, B and $T(z)$, which incorporates all the global information available under measurements C and excitations B. This generalizes results in [2] that were derived for the full-excitation case.

Following a similar reasoning, we derive a condition on the identifiability of a specific transfer function $G_{ij}(z)$ by inspecting the kernel of that same matrix K. Building on those results, we then develop an algorithm that, provided the measured and excited nodes, computes which edges are identifiable and which are not. It can be run either symbolically, or stochastically *via* Monte Carlo experiments.

References

[1]   Van den Hof, P. M., Dankers, A., Heuberger, P. S., Bombois, X. "Identification of dynamic models in complex networks with prediction error methods—Basic methods for consistent module estimates," in *Automatica*, 2013.

[2]   Hendrickx, J. M., Gevers, M., and Bazanella, A. S. "Identifiability of dynamical networks with partial node measurements," in *IEEE Trans. on Automatic Control*, 2018.

[3]   Bazanella, A. S., Gevers, M., Hendrickx, J. M. "Network identification with partial excitation and measurement," in *Proceedings of the IEEE CDC*, 2019.

Non-Parametric Kernelized Identification of Closed Loop Nonlinear Systems

Fahim Shakib[1], Roland Tóth[2], Sacha Pogromsky[1], Alexey Pavlov[3], Nathan van de Wouw[1,4]

[1] Dept. of Mechanical Engineering, Eindhoven, Univ. of Tech., The Netherlands

[2] Dept. of Electrical Engineering, Eindhoven, Univ. of Tech., The Netherlands

[3] Dept. of Geoscience and Petroleum, NTNU, Trondheim, Norway

[4] Dept. of Civil, Environmental, and Geo- Engineering, Univ. of Minnesota, USA

Email: m.f.shakib@tue.nl

Introduction

We propose a novel three-step approach to consistent non-parametric state-space identification of nonlinear systems operating under open and closed loop conditions. Our approach uses the core idea of the methodology presented in [1], where no statistical properties were guaranteed. We show that each step of our proposed approach is consistent in the statistical sense. In fact, the overall method we present can be seen as an extension of the SS-ARX subspace identification method [4] for Linear Time-Invariant (LTI) systems to nonlinear systems.

Problem Setting

Discrete-time multi-input, multi-output (MIMO) nonlinear systems that can be represented by the following set of difference (state-space) equations are considered:

$$x_{k+1} = f(x_k, u_k, e_k), \quad y_k = h(x_k) + e_k.$$

Here, $x_k \in \mathbb{R}^n$ denotes the state, $u_k \in \mathbb{R}^m$ denotes the applied input, $y_k \in \mathbb{R}^l$ denotes the measured output and $e_k \in \mathbb{R}^l$ is Gaussian white noise. The data set consists of N samples: $\{u_k, y_k\}_{k=1}^N$. The problem is to identify the mappings f and h non-parametrically and to give an estimate for the noise variance Σ_e.

Three-Step Identification Approach

Step 1: Consistent subspace identification algorithms for LTI systems operating in open or closed loop commonly identify an Auto-Regressive Model with eXogenous inputs (ARX) in the first step to find the noise model or noise sequence. Here, we identify a Nonlinear ARX model using a Least-Squares Support Vector Machine (LS-SVM) approach to yield a consistent estimate $\hat{e}$ for the noise sequence [3] and the empirical estimate $\hat{\Sigma}_e$ for the noise variance.

Step 2: In the scope of LTI systems, the SS-ARX subspace identification technique, reportedly found to be one of the best performing LTI subspace identification techniques [4], performs Canonical Correlation Analysis (CCA) to infer the state from past and future (closed loop) data. Here, we use a kernelized version, namely Kernel CCA (KCCA) [1], to estimate a compatible state sequence of the underlying nonlinear state-space model from past and future input u, output y and noise $\hat{e}$ data. This estimate is consistent in the so-called regularized $\mathscr{F}$-correlation sense [2].

Step 3: Having input u, output y, estimated noise $\hat{e}$ and estimate state $\hat{x}$ at hand, in the final step, we identify the mappings f and h non-parametrically. To this extent, we again use the function estimator based on the LS-SVM approach,

which is consistent. The identified state-space model is defined by the non-parametric mappings $\hat{f}$ and $\hat{h}$.

Simulation Example

Consider the nonlinear system

$$x_{k+1} = \frac{1}{2}x_k(1-x_k) + u_k + e_k, \quad y_k = x_k + e_k,$$

and the feedback law $u_k = r_k - y_k$, where r_k is a reference signal. Applying the three-step identification approach yields a non-parametric identified nonlinear system. The estimated noise sequence is depicted in the top figure of Figure 1. In the bottom figure, the response y of the true system and the response $\hat{y}$ predicted by the identified model are shown. For comparison, also the response of an LTI model $\hat{y}_{\text{LTI}}$ (identified by subspace identification) is shown. It can be seen that the nonlinear model predicts the response accurately while the LTI model does not capture the nonlinear nature of the system.
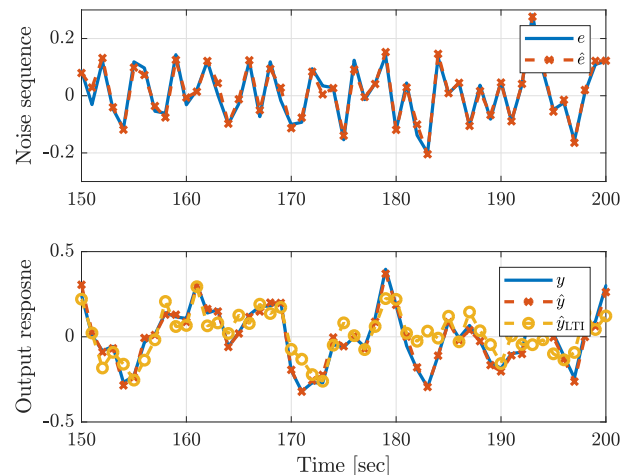
Figure 1: Top: Estimated and true noise sequence. Bottom: Output response of the true system and identified model.

References

[1] Verdult, V., Suykens, J.A., Boets, J., Goethals, I., and De Moor, B. (2004). Least squares support vector machines for kernel CCA in nonlinear state-space identification. In *Proc. of the 16th int. symposium on Mathematical Theory of Networks and Systems (MTNS2004), Leuven, Belgium*.

[2] Bach, F.R. and Jordan, M.I. (2002). Kernel independent component analysis. *Journal of machine learning research*, 3(7), 1–48

[3] De Nicolao, G. and Trecate, G.F. (1999). Consistent identification of NARX models via regularization networks. *IEEE Transactions on Automatic Control*, 44(11), 2045–2049.

[4] Qin, S. J. (2006). An overview of subspace identification. *Computers & Chemical Engineering*, 30(10-12), 1502–1513

Structural Identifiability of Linear State Space Models: A State and Output Sensitivity Controllability Perspective

C.S. Méndez-Blanco, L. Özkan
Control Systems Group, Eindhoven University
email: {c.s.mendez.blanco, l.ozkan}@tue.nl

1 Introduction

Structural identifiability is a theoretical setting that allows for the analysis on model parameters identifiability. This property of nonlineary parametrized state space models is assessed using analyzing the controllability of the output sensitivities. Sensitivity analysis provides a mathematical setting to analyze parameter identifiability from a physically intuitive perspective. The sensitivity representation is vectorized in order to compute the output sensitivity matrix. Both SISO and MIMO case are treated; in the former case the output controllability matrix rank directly allows to draw conclusions on the model structural identifiability.

2 Structural identifiability

Let $\mathcal{S}$ be a dynamical system, and $\mathcal{M}(\cdot)$ be a model structure. Furthermore, $\mathbf{p} \in \mathbb{P} \subseteq \mathbb{R}^p$ be a vector of parameters, where $\mathbb{P} \subseteq \mathbb{R}^p$ is the feasible parameter space, and $\mathcal{M}(\mathbf{p})$ be the specific model obtained when the parameters take the values $\mathbf{p}$. In this sense, structural identifiability tests if the functional or structural form of a particular model allows for the determination of a unique admissible parameter set from noise-free measurements [1]. In this work we restrict our attention to ODE linear models of the form

$$\mathcal{M}(\mathbf{p}): \begin{cases} \dot{x}(t,\mathbf{p}) = A(\mathbf{p})x(t,\mathbf{p}) + B(\mathbf{p})u(t), \ \ x(t=0) = x_0 \\ y(t,\mathbf{p}) = C(\mathbf{p})x(t,\mathbf{p}) \\ \quad \dot{\mathbf{p}} = \mathbf{0} \end{cases}$$

where $x(t,\mathbf{p}) \in \mathbb{R}^n$ is the vector of states, $u(t) \in \mathbb{R}^q$ is the known input vector, $y(t,\mathbf{p}) \in \mathbb{R}^m$ is the measurement or the output vector, and x_0 is the initial state and assumed parameter-independent.

3 Sensitivity representation

Let the model structure $\mathcal{M}(\mathbf{p})$ be a minimal linear state space model given as in (2). Assume that the state x and output are continuous functions of t and $\mathbf{p}$. The state and output parameter sensitivity equations can be written in vectorized form as:

$$\dot{x}_{\mathbf{p}}^{\mathrm{v}} = \mathcal{A}x + \mathbf{A}x_{\mathbf{p}}^{\mathrm{v}} + \mathcal{B}u + \mathbf{B}u_{\mathbf{p}}^{\mathrm{v}}$$
$$y_{\mathbf{p}}^{\mathrm{v}} = \mathcal{C}x + \mathbf{C}x_{\mathbf{p}}^{\mathrm{v}}$$

where $x_{\mathbf{p}}^{\mathrm{v}} = \mathrm{vec}(x_{\mathbf{p}}) \in \mathbb{R}^{np}$, $u_{\mathbf{p}}^{\mathrm{v}} = \mathrm{vec}(u_{\mathbf{p}}) \in \mathbb{R}^{qp}$. In the open-loop case, the input function u rarely depends on the model parameters $\mathbf{p}$, thus without loss of generality $\frac{\partial u}{\partial \mathbf{p}} \equiv 0$. Moreover, since the state and output sensitivities depend explicitly on the state, we can define a joint representation as

$$\begin{bmatrix} \dot{x} \\ \dot{x}_{\mathbf{p}}^{\mathrm{v}} \end{bmatrix} = \underbrace{\begin{bmatrix} A & \mathbf{0}_{n \times np} \\ \mathcal{A} & \mathbf{A} \end{bmatrix}}_{\bar{A}} \begin{bmatrix} x \\ x_{\mathbf{p}}^{\mathrm{v}} \end{bmatrix} + \underbrace{\begin{bmatrix} B \\ \mathcal{B} \end{bmatrix}}_{\bar{B}} u, \qquad \begin{bmatrix} x(0) \\ x_{\mathbf{p}}^{\mathrm{v}}(0) \end{bmatrix} = \begin{bmatrix} x_0 \\ 0 \end{bmatrix}$$

$$\begin{bmatrix} y \\ y_p^{\mathrm{v}} \end{bmatrix} = \underbrace{\begin{bmatrix} C & \mathbf{0}_{m \times np} \\ \mathcal{C} & \mathbf{C} \end{bmatrix}}_{\bar{C}} \begin{bmatrix} x \\ x_{\mathbf{p}}^{\mathrm{v}} \end{bmatrix}$$

4 Testing structural identifiability

In the context of sensitivity analysis, structural identifiability can be interpreted as an output sensitivity controllability problem ([2]). Constructing the output sensitivity controllability matrix $\mathcal{P}$ as

$$\mathcal{P} = \bar{C}\mathcal{K} = \begin{bmatrix} \mathcal{P}_x \\ \mathcal{P}_{x_{\mathbf{p}}^{\mathrm{v}}} \end{bmatrix}$$

where $\mathcal{K} = \begin{bmatrix} \bar{B} & \bar{A}\bar{B} & \cdots & \bar{A}^{n(p+1)-1}\bar{B} \end{bmatrix}$ is the state sensitivity controllability matrix. The model is said to be structurally identifiable if the sensitivity model is output controllable, i.e. $\mathrm{rank}(\mathcal{P}_{x_{\mathbf{p}}^{\mathrm{v}}}) = p$, and the parameter-unidentifiable space is given by the left-null space of $\mathcal{P}_{x_{\mathbf{p}}^{\mathrm{v}}}$

5 Conclusions

In this paper, we established the connection between sensitivity analysis and structural identifiability exploiting the structure of the state and output sensitivity representation. The representation allows us to tackle the problem from an output controllability perspective, that can be helpful when dealing with models with many inputs and outputs. The information is completely encoded in the output sensitivity matrix associated to the sensitivity representation.

References

[1]   E. Walter and L. Pronzato "Identifiabilities and non-linearities" Nonlinear Systems: Modeling and Estimation, ch. 3, vol. pp. 111–143, 1995

[2]   J. Stigter. and R. Peeters "On a geometric approach to the structural identifiability problem and its application in a water quality case study" European Control Conference (ECC), pp. 3450–3456, 2007.

Fault Detection and Isolation for Linear Structured Systems

Jiajia Jia, Harry L. Trentelman, and M. Kanat Camlibel

Bernoulli Institute for Mathematics, Computer Science and Artificial Intelligence,

University of Groningen

`(j.jia, h.l.trentelman, m.k.camlibel)@rug.nl`

1 Introduction

In the past decades, the problem of fault detection and isolation (FDI) has received considerable attention within the control community. In [1] and [2], FDI for linear time-invariant (LTI) systems is performed using unknown input observers that enable so-called output separability of fault subspaces. If such an observer exists, then we say that for the given system the FDI problem is *solvable*. In this work, we consider FDI for a family of LTI systems that share a so-called zero/nonzero/arbitrary structure, called *linear structured systems*. Our aim is to establish conditions under which for a given linear structured system the FDI problem is solvable.

2 Background and Problem Formulation

2.1 FDI Solvability of LTI Systems

Consider the LTI system

$$\begin{aligned} \dot{x} &= Ax + Lf \\ y &= Cx \end{aligned} \tag{1}$$

where $x \in \mathbb{R}^n$, $f \in \mathbb{R}^q$ and $y \in \mathbb{R}^p$ are the state, fault and output, respectively, and A, L and C are matrices of appropriate dimensions. Denote the system (1) by (A, L, C). We say that the ith fault occurs if $f_i \neq 0$ (i.e., not identically equal to 0), where f_i is the ith component of f. To detect and isolate which fault f_i occurs, consider the state observer

$$\dot{\hat{x}} = (A + GC)\hat{x} - Gy, \tag{2}$$

where $\hat{x}$ is the observer state, and $G \in \mathbb{R}^{n \times p}$ is the observer gain to be designed. Define the *innovation* as $r := C\hat{x} - y$ and the *state error* as $e := \hat{x} - x$. By interconnecting (1) and (2), we obtain

$$\begin{aligned} \dot{e} &= (A + GC)e - Lf \\ r &= Ce. \end{aligned} \tag{3}$$

Note that in this work, we do not consider any stability requirement on the observer, which means that we do not require $e(t) \to 0$, and we assume that $e(0) = 0$. Under this assumption, for any fault f, the resulting error trajectory $e(t)$ lies in the reachable subspace of $(A + GC, L)$. Let $\mathcal{V}_i$ be the smallest $(A + GC)$-invariant subspace containing $\operatorname{im} L_i$, where L_i is the ith column of L. It is clear that that the reachable subspace of $(A + GC, L)$ is equal to $\mathcal{V}_1 + \cdots + \mathcal{V}_q$. For

the corresponding innovation trajectory $r(t)$ we then have $r(t) \in C\mathcal{V}_1 + \cdots + C\mathcal{V}_q$. If the subspaces $C\mathcal{V}_1, \cdots, C\mathcal{V}_q$ are independent, then this is a direct sum, and $r(t)$ can be written uniquely as

$$r(t) = r_1(t) + \cdots + r_q(t) \tag{4}$$

with $r_i(t) \in C\mathcal{V}_i$ for all t. We can use the unique representation (4) to determine whether the ith fault occurs. Furthermore, we say that for (A, L, C) the FDI problem is *solvable* if there exists a $G \in \mathbb{R}^{n \times p}$ such that the family of subspaces $\{C\mathcal{V}_i\}_{i=1}^q$ is independent.

2.2 Pattern Matrices and Linear Structured Systems

A pattern matrix is a matrix with entries in the set of symbols $\{0, *, ?\}$. The set of all $r \times s$ pattern matrices will be denoted by $\{0, *, ?\}^{r \times s}$. For a given $r \times s$ pattern matrix $\mathcal{M}$, we define the *pattern class* of $\mathcal{M}$ as

$$\begin{aligned} \mathscr{P}(\mathcal{M}) := \{ M \in \mathbb{R}^{r \times s} \mid &M_{ij} = 0 \text{ if } \mathcal{M}_{ij} = 0, \\ &M_{ij} \neq 0 \text{ if } \mathcal{M}_{ij} = * \}. \end{aligned}$$

This means that for a matrix $M \in \mathscr{P}(\mathcal{M})$, the entry M_{ij} is either (i) *zero* if $\mathcal{M}_{ij} = 0$, (ii) *nonzero* if $\mathcal{M}_{ij} = *$, or (iii) *arbitrary* (zero or nonzero) if $\mathcal{M}_{ij} = ?$. Let $\mathscr{A} \in \{0, *, ?\}^{n \times n}$, $\mathscr{L} \in \{0, *, ?\}^{n \times q}$ and $\mathscr{C} \in \{0, *, ?\}^{n \times p}$. The family of systems (A, L, C) with $A \in \mathscr{P}(\mathscr{A})$, $L \in \mathscr{P}(\mathscr{L})$ and $C \in \mathscr{P}(\mathscr{C})$ is called a *linear structured system*. In the sequel, we use $(\mathscr{A}, \mathscr{L}, \mathscr{C})$ to represent this structured system, and we write $(A, L, C) \in (\mathscr{A}, \mathscr{L}, \mathscr{C})$ if $A \in \mathscr{P}(\mathscr{A})$, $L \in \mathscr{P}(\mathscr{L})$ and $C \in \mathscr{P}(\mathscr{C})$.

2.3 Problem Statement

In this work, we say that for $(\mathscr{A}, \mathscr{L}, \mathscr{C})$ the FDI problem is *solvable* if the FDI problem is solvable for every $(A, L, C) \in (\mathscr{A}, \mathscr{L}, \mathscr{C})$. The research problem is then formally stated as follows.

Problem 1 *Given* $(\mathscr{A}, \mathscr{L}, \mathscr{C})$*, find conditions under which the FDI problem is solvable for* $(\mathscr{A}, \mathscr{L}, \mathscr{C})$*.*

References

[1] M. -A. Massoumnia, "A geometric approach to the synthesis of failure detection filters," IEEE Transactions on Automatic Control, 1980.

[2] P. Rapisarda, A. R. F. Everts, and M. K. Camlibel, "Fault detection and isolation for systems defined over graphs", Proc. of the IEEE Conference on Decision and Control, 2015.

Robust Reference Model-based Fault Detection and Isolation for Discrete-time Systems

Silvane C. M. Schons, Michel Kinnaert
SAAS
Université Libre de Bruxelles (ULB)
Brussels, Belgium
Email: silvane@outlook.com,
michel.kinnaert@ulb.ac.be

Daniel Coutinho
DAS – PPGEAS
Universidade Federal de Santa Catarina (UFSC)
Florianópolis, Brazil
Email: daniel.coutinho@ufsc.br

1 Introduction

During the last decades, robust model-based fault detection and isolation (FDI) has received increasing interest in the literature, [1] [2]. In this work, the design of H_-/H_∞ filters is studied in order to achieve fault detection and isolation for linear discrete-time systems subject to faults and disturbances. The main goal is to generate residuals such that the transfer matrix from faults to residual approximates a given reference model. In order to obtain a numerical and tractable solution, the design conditions are cast in terms of a convex optimization problem subject to Linear Matrix Inequality (LMI) constraints.

2 Problem Statement

Consider the following discrete-time system:

$$\begin{cases} x^+ & = Ax + B_u u + B_w w + B_f f, \\ y & = Cx + D_u u + D_w w + D_f f, \end{cases} \tag{1}$$

where $x \in \mathbb{R}^{n_x}$ is the state vector, $u \in \mathbb{R}^{n_u}$ is a measured input, $w \in \ell_2^{n_w}$ is an exogenous input, $y \in \mathbb{R}^{n_y}$ is the measured output, and $A, B_u, B_w, B_f, C, D_u, D_w, D_f$ are given real matrices with appropriate dimensions. The fault input $f \in \ell_2^m$ can be actuator faults or sensor faults. The following residual generator is proposed:

$$\begin{cases} \tilde{x}^+ & = (A - LC)\hat{x} + (B_w - LD_w)w + (B_f - LD_f)f, \\ r & = Q\,C_r(y - \hat{y}), \end{cases} \tag{2}$$

where $\tilde{x} = x - \hat{x}$, with $\hat{x}$ being the estimation of x, and $\hat{y} \in \mathbb{R}^{n_y}$ is the estimation output vector. The observer matrix gain $L \in \mathbb{R}^{n_x \times n_y}$ as well as $Q \in \mathbb{R}^{m \times m}$ and $C_r \in \mathbb{R}^{m \times n}$ are to be designed. Furthermore, to enforce sensitivity to faults, consider the following reference model:

$$\begin{cases} \check{x}^+ & = \check{A}\check{x} + \check{B}f, \\ \check{r} & = Q(\check{C}\check{x} + \check{D}f), \end{cases} \tag{3}$$

where $\check{x} \in \mathbb{R}^q$ and $\check{r} \in \mathbb{R}^m$ represent the reference state and reference residual, respectively, and $\check{A}$, $\check{B}$, $\check{C}$ and $\check{D}$ are given matrices with appropriate dimensions. Fig. 1 represents the structure proposed in this work for the residual design and generation.

3 Main Result

The problem of concern in this paper is to design the matrices L, Q and C_r such that:
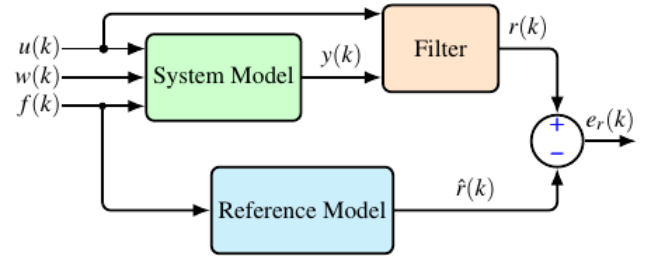
Figure 1: Block diagram representation for FDI purposes.

I $\|\mathscr{G}_{wr}\|_\infty^2 \le \gamma_w$, where $\mathscr{G}_{wr}$ represents the transfer function from disturbance to residual.

II $\|\mathscr{G}_{fr} - \mathscr{G}_{f\check{r}}\|_\infty^2 \le \gamma_f$, where $\mathscr{G}_{fr}$ and $\mathscr{G}_{f\check{r}}$ are the transfer functions from fault to residual and from fault to reference residual, respectively.

III $\|\mathscr{G}_{f\check{r}}\|_-^2 \ge \gamma_c$, where $\mathscr{G}_{f\check{r}}$ is the transfer function from fault to the reference residual.

In this paper, we consider that γ_f and γ_w are to be determined. Besides, the resulting filter meets the following properties: i) the estimation error is bounded and ii) fault detection and isolation is guaranteed provided a solution exists for sufficiently small values of γ_w and γ_f and for a sufficiently large γ_c. Finally, the filter design conditions are numerically determined via a convex optimization problem.

4 Acknowledgement

References

[1] M. Mattei, G. Paviglianiti, V. Scordamaglia, "Nonlinear observers with H_∞ performance for sensor fault detection and isolation: a linear matrix inequality design procedure", Control Engineering Practice, 2005.

[2] P. M. Frank, S. X. Ding, "Survey of robust residual generation and evaluation methods in observer based fault detection systems", Journal of Process Controll, 1997.

Fault-compensation controller for LPV systems

Tábitha E. Rosa*†, Leonardo P. Carvalho*†, Bayu Jayawardhana*, Oswaldo L.V. Costa†,

* University of Groningen, 9747 AG, Groningen, The Netherlands

† Escola Politécnica da Universidade de São Paulo, 05508-010 São Paulo, SP, Brazil

Email: t.esteves.rosa@rug.nl

We propose in this work a fault-compensation controller (FCC) for discrete-time systems affected by time-varying parameters, which also contains the information of the fault occurrence. Let us consider the following system

$$
\begin{aligned}
x(k+1) &= A_{\alpha(k)}x(k) + J_{\alpha(k)}d(k) + F_{\alpha(k)}f(k) \\
y(k) &= C_{\alpha(k)}x(k) + D_{\alpha(k)}d(k)
\end{aligned}
\tag{1}
$$

where $x(k) \in \mathbb{R}^n$ represents the state vector, $d(k) \in \mathbb{R}^p$, $(p \leq n)$, is the exogenous input, $f(k) \in \mathbb{R}^p$ is the fault signal, and $y(k) \in \mathbb{R}^s$ is the measured output. The state-space matrices in system (1) depend on an affine parameter and can be expressed as $M_{\alpha(k)} = M_0 + \sum_{i=1}^m \alpha_i(k)M_i$, where matrices $M_0, \ldots, M_m$ are given matrices and $\alpha(k) = (\alpha_1(k), \ldots, \alpha_m(k))$ are time-varying parameter bounded as $\forall k \geq 0$, $|\alpha_i(k)| \leq t_i$, $t_i \in \mathbb{R}^+$, $i = 1, \ldots, m$.

One of the major premises of the present work is that the parameter $\alpha(k)$ is not instantly accessible, instead it is estimated, which is an approach that has been explored in [2]. This estimation is denoted by $\hat{\alpha}(k)$, and is described as $\hat{\alpha}(k) = \alpha(k) + \sigma(k)$, $i = 1, \ldots, m$. This system can be controlled neglecting the presence of the faults using a state-feedback control law such as $u(k) = Kx(k)$, where K can be obtained using several techniques, for instance, by minimizing the $\mathcal{H}_2$ or $\mathcal{H}_\infty$ norm of system (1) (with $F_{\alpha(k)} = 0$) using linear matrix inequality (LMI) conditions given in [1]. In this work we to design a fault-compensation controller that is able to compensate the fault signal $f(k)$. This controller is described by

$$
\begin{aligned}
\eta(k+1) &= A_{\eta\hat{\alpha}(k)}\eta(k) + M_{\eta\hat{\alpha}(k)}u(k) + B_{\eta\hat{\alpha}(k)}y(k), \\
h(k) &= C_{\eta\hat{\alpha}(k)}\eta(k), \\
\eta(0) &= \eta_0, \ \hat{\alpha}(0) = \alpha_0.
\end{aligned}
\tag{2}
$$

where $\eta \in \mathbb{K}^q$ represents the FCC, $u(k)$ and $y(k)$, are respectively, the control signal from the regular controller and the measured signal from the system, and $\hat{\alpha}(k)$ is the time-varying parameter estimation.

The main goal of this work is to design a FCC as presented in (2) where the difference $o(k) = F_i f(k) - B_i h(k)$ is close to zero. Therefore, the optimization problem is described as

$$
\|\mathcal{G}_{\mathrm{cl}}\|_\infty = \sup_{\|\bar{w}\|_2 \neq 0, \bar{w} \in \mathcal{L}_2} \frac{\|o\|_2}{\|\bar{w}\|_2} < \gamma_c, \ \ \gamma_c > 0.
\tag{3}
$$

The main contribution of this work is stated in the following theorem.

Theorem 1 *If there exist symmetric positive definite matrices* $W_{11_{\alpha(k)}}$, $W_{22_{\alpha(k)}}$ *and matrices* $W_{12_{\alpha(k)}}$, $\check{K}_{\hat{\alpha}(k)}$, $\bar{K}_{\hat{\alpha}(k)}$, $\Omega_{\hat{\alpha}(k)}$, $\nabla_{\hat{\alpha}(k)}$, $\Gamma_{\hat{\alpha}(k)}$, $\Theta_{\hat{\alpha}(k)}$ *with compatible dimensions, and a given scalar parameter* ξ *such that the following inequality holds for all* $\alpha(k)$ *and* $\hat{\alpha}(k)$

$$
\begin{bmatrix}
\Pi^{1,1} & \Pi^{1,2} & \Pi^{1,3} & \Pi^{1,4} & \xi(\check{K}J + \Omega D) & \xi\check{K}F & 0 \\
\bullet & \Pi^{2,2} & \Pi^{2,3} & \Pi^{2,4} & \xi(\check{K}J + \Omega D) & \xi\check{K}F & \Theta_{\hat{\alpha}(k)} \\
\bullet & \bullet & W_{11}^+ - \check{K} - \check{K}' & W_{12}^+ - \bar{K} - \check{K}' & \check{K}J + \Omega D & \check{K}F & 0 \\
\bullet & \bullet & \bullet & W_{22}^+ - \bar{K} - \bar{K}' & \check{K}J + \Omega D & \check{K}F & 0 \\
\bullet & \bullet & \bullet & \bullet & -\delta^2 I & 0 & 0 \\
\bullet & \bullet & \bullet & \bullet & \bullet & -\delta^2 I & 0 \\
\bullet & \bullet & \bullet & \bullet & \bullet & \bullet & -\check{K} - \check{K}' + I
\end{bmatrix} < 0,
$$

with

$$
\begin{aligned}
\Pi^{1,1} ={}& -W_{11} + \xi(\check{K}A - \check{K}BK + \Omega_{\hat{\alpha}(k)}C - \Gamma_{\hat{\alpha}(k)}K \\
& + A'\check{K}' - K'B'\check{K}' + C'\Omega'_{\hat{\alpha}(k)} - K'\Gamma'_{\hat{\alpha}(k)}), \\
\Pi^{1,2} ={}& -W_{12} + \xi(\Theta'_{\hat{\alpha}(k)} + \nabla_{\hat{\alpha}(k)} + \check{K}'(A' - K'B') \\
& + C'\Omega'_{\hat{\alpha}(k)} - K'\Gamma'_{\hat{\alpha}(k)}), \\
\Pi^{1,3} ={}& A'\check{K}' - K'B'\check{K} + C'\Omega'_{\hat{\alpha}(k)} - K'\Gamma'_{\hat{\alpha}(k)} - \xi\check{K}, \\
\Pi^{1,4} ={}& A'\check{K}' - K'B'\check{K}' + C'\Omega'_{\hat{\alpha}(k)} - K'\Gamma'_{\hat{\alpha}(k)} - \xi\bar{K} \\
\Pi^{2,2} ={}& -W_{22} + \xi(\Theta_{\hat{\alpha}(k)} + \nabla_{\hat{\alpha}(k)} + \Theta'_{\hat{\alpha}(k)} + \nabla'_{\hat{\alpha}(k)}), \\
\Pi^{2,3} ={}& \Theta'_{\hat{\alpha}(k)} + \Gamma'_{\hat{\alpha}(k)} - \xi\check{K}, \\
\Pi^{2,4} ={}& \Theta'_{\hat{\alpha}(k)} + \Gamma'_{\hat{\alpha}(k)} - \xi\bar{K},
\end{aligned}
$$

then a suitable linear parameter-varying FCC, as (2), is given by $A_\eta = \bar{K}^{-1}\nabla$, $B_\eta = \bar{K}^{-1}\Omega$, $M_\eta = \bar{K}^{-1}\Gamma$, $C_\eta = \check{K}^{-1}B^{-1}\Theta$, *satisfying the optimization problem (3), considering that the dependency on the time-varying parameters* $\alpha(k)$ *and* $\hat{\alpha}(k)$ *is omitted the for the sake of simplicity in all the aforementioned equations and that* W_{11}^+, W_{12}^+ *and* W_{22}^+ *depend on* $\alpha(k+1)$.

References

[1] Jan De Caigny, Juan F Camino, Ricardo CLF Oliveira, Pedro LD Peres, and Jan Swevers. Gain-scheduled dynamic output feedback control for discrete-time LPV systems. *International Journal of Robust and Nonlinear Control*, 22(5):535–558, 2012.

[2] Jonathan M Palma, Cecília F Morais, and Ricardo CLF Oliveira. H_2 gain-scheduled filtering for discrete-time LPV systems using estimated time-varying parameters. In *2018 Annual American Control Conference*, pages 4367–4372. IEEE, 2018.

A Data-Rate Constrained Observer for Unicycle-type Robots

Quentin Voortman[1,2], Denis Efimov[1], Alexander Pogromsky[2],
Jean-Pierre Richard[1], Henk Nijmeijer[2]

(1) : Team VALSE, Inria Lille Nord-Europe, 40 Avenue Halley, 59650 Villeneuve dAscq, FRANCE,
(2) : Dep. of Mech. Eng., Eindhoven University of Technology, PO Box 513, 5600MB Eindhoven,
Email: {q.j.t.voortman,a.pogromski,h.nijemijer}@tue.nl
{denis.efimov,jean-pierre.richard}@inria.fr

Introduction

We present a data-rate constrained observer for a unicycle-type robot. The robot is equipped with a smart sensor, capable of measuring the position and orientation of the robot and performing computations. It is connected to a remote location via a wireless communication channel. The smart sensor can send messages over this communication channel to the remote location with the objective of providing an estimate of the robot state at the remote location. The particularity of the communication channel is that it is restricted in terms of data-rates that it can transmit. The objective of the communication protocol is that it can reconstruct estimates of the state of the system at a remote location whilst using limited data-rates.

Problem statement

We consider a unicycle-type robot which has the following dynamics:

$$\begin{bmatrix} \dot{z}_1(t) \\ \dot{z}_2(t) \\ \dot{z}_3(t) \end{bmatrix} = \begin{bmatrix} (u_1(t) + d_1(t))\cos(z_1(t)) \\ (u_1(t) + d_1(t))\sin(z_2(t)) \\ (u_2(t) + d_2(t)) \end{bmatrix}, \qquad (1)$$

where $z_1 \in \mathbb{R}$ and $z_2 \in \mathbb{R}$ are the coordinates of the robot, $z_3 \in [0, 2\pi]$ is the orientation angle of the robot, $u_1 \in \mathbb{R}$ and $u_2 \in \mathbb{R}$ are inputs, and $d_1 \in \mathbb{R}$ and $d_2 \in \mathbb{R}$ are time-varying input perturbations. We assume that the input perturbations are continuous signals that verify $|d_i(t)| \leq \delta_i$, $\forall i \in \{1,2\}, \forall t \geq 0$, where δ_i are the maximum input perturbations which are known constants. Moreover, we consider the constant input case, i.e. $u_i(t) = \bar{u}_i$ where $\bar{u}_i$ are known constants A communication protocol consists of

- A sampler which determines the communication instants t_j,

- An alphabet which is a list of symbols that each represent a different messages which can be sent at the communication instants

- A coder which generates the messages $m(t_j)$ to be sent over the communication channel,

- A decoder which generates estimates $\hat{z}(t)$ of the state.

Figure 1 depicts how the different elements interact.
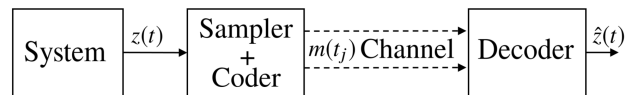
Figure 1: Block diagram of the problem setup

Solution and simulations

We developed a communication protocol that uses limited data-rates and guarantees that the observation error $\|z(t) - \hat{z}(t)\|$ remains below a prescribed maximum error. The main mechanism of the communication protocol can be described as follows: at the sensor side, the state $z(t)$ of the system is continuously measured. A copy of the decoder is simulated by the computational capacity of the sensor such that it is known what estimate $\hat{z}(t)$ the decoder currently has. This copy of the remote estimate which is provided by the smart sensor is denoted $\hat{z}_c(t)$. Starting at the estimate stemming from the last message $\hat{z}(t_j)$ and in the absence of messages, the decoder simply updates the estimate by computing the solution of (1) with $\hat{z}(t_j)$ as an initial condition and $d_i(t) = 0$. When the distance between $z(t)$ and $\hat{z}_c(t) = \hat{z}(t)$ becomes larger than a prescribed maximum error, the sampler decides to communicate and the coder sends a message to the decoder to provide a new estimate $\hat{z}(t_j)$.

The communication protocol was tested both via simulations of Turtlebots in the Gazebo environment as well as via experiments on physical Turtlebots. The designed scheme was proven to be very efficient in terms of required data-rates. A video of the simulations and experiments can be found at `https://youtu.be/zx3Mckyj4EM`

Acknowledgment

Detection of Cyber Attacks on Collaborative Systems using a Sliding Mode Observer based Approach

Twan Keijzer
Delft Center for Systems and Control
Delft University of Technology
The Netherlands
Email: T.Keijzer@tudelft.nl

Riccardo M.G. Ferrari
Delft Center for Systems and Control
Delft University of Technology
The Netherlands
Email: R.Ferrari@tudelft.nl

Distributed systems for collaborative control of vehicles has been pursued by many researchers, due its wide applications. One of these applications is the formation of collaborative autonomous platoons of cars (or trucks) on highways, as depicted schematically in figure 1. This reduces the required distance between cars, and therefore improves road utilisation and reduces emissions. Furthermore the driver workload is alleviated, or potentially completely eliminated.
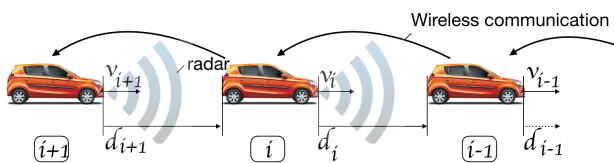
Figure 1: Sensing and communication structure of platooning cars [1]

For these systems, however it is of great importance that they are safe and secure. The cars in such platoons will use a combination of sensor measurements and Vehicle-to-Vehicle (V2V) communication as an input to the controller. The signals received through V2V communication are sensitive to cyber-attacks, and can compromise the security of the overall system. Therefore, the estimation and detection of cyber-attacks on these communicated signals has been the topic of research. [1]

In literature, these cyber-attacks are considered to be crafted with malicious objectives. This means that the attackers aim to effectively use the knowledge and resources available to them, to drive the system to an unsafe state without being detected. In general, therefore, the attacks are classified based on the knowledge and resources they have available. Some of the attacks that have been considered in literature are bias injection, replay, zero dynamics, and covert attacks. [2]

In previous work ([1]) the authors of this abstract have designed a method for detecting and estimating constant data injection attacks for a platoon in which each car uses the Collaborative Adaptive Cruise Control (CACC) law designed and tested by Ploeg et al. [3]. This estimation and detection method was based on a sliding mode observer (SMO) combined with a specifically designed threshold.
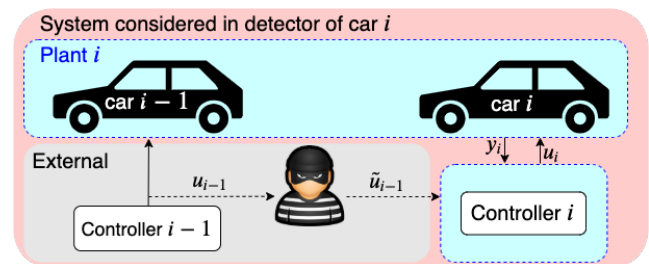
Figure 2: Diagram showing definition of plant, controller, and communicated/attacked signal for an observer in car i of the collaborating platoon. $\tilde{u}$ is the attacked signal.

In this work we present a revised detection threshold where the robustness against false detections is improved. Furthermore, we generalise the estimation and detection method to be applicable, firstly, without any restrictions on the used control law. And secondly, for more general collaborating systems. Figure 2 illustrates what such a generalised system would look like for a car in an autonomous platoon.

References

[1] Twan Keijzer and Riccardo M. G. Ferrari. A sliding mode observer approach for attack detection and estimation in autonomous vehicle platoons using event triggered communication. In *Conference on Desicion and Control*, 2019.

[2] André Teixeira, Iman Shames, Henrik Sandberg, and Karl Henrik Johansson. A secure control framework for resource-limited adversaries. *Automatica*, 51:135–148, 2015.

[3] J. Ploeg, B.T.M. Scheepers, E. van Nunen, N. van de Wouw, and H. Nijmeijer. Design and experimental evaluation of cooperative adaptive cruise control. In *14th International IEEE Conference on Intelligent Transportation Systems (ITSC)*, pages 260–265, October 2011.

Health monitoring of an electromechanical actuator for aircraft primary flight surface control

Benjamin Wauthion, Michel Kinnaert, Emanuele Garone
Department of Control Engineering and System Analysis
Université Libre de Bruxelles, 1050 Bruxelles, Belgique
Email: bewauthi@ulb.ac.be, michel.kinnaert@ulb.ac.be, egarone@ulb.ac.be

1 Introduction

In order to lighten aircraft and thus reduce their fuel consumption, the trend is to replace the hydraulic actuators by electromechanical actuators (EMAs) [1]. This structural change would allow cancelling the overall hydraulic circuit aboard and thus decrease the maintenance needs, the energy consumption and the aircraft weight [2]. To keep an identical level of safety and availability for the EMAs as for hydraulic actuators, their status must be followed. Therefore we aim at designing, implementing and validating a monitoring system for EMAs used in aircraft flight surface control. Such a system should be able to detect in a premature way the most frequent and dangerous fault occurrences on the EMAs (namely the mechanical faults, e.g. jamming, backlash, and preload) and follow their temporal evolution. In that way maintenance operations can be performed in due time to avoid that the degradation leads to functional failures of the actuator.
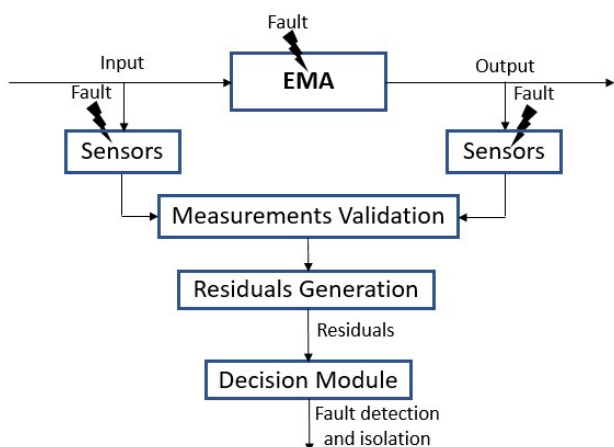
Figure 1: EMA model-based monitoring architecture

In order to account for the physical knowledge of the system, a model-based monitoring approach will be used. It consists of the combination of two steps: the generation of fault indicators (residuals) and the residual evaluation (carried out by the decision module). The residuals come out from an analysis of the consistency between the data collected on the EMA and a mathematical model of its behaviour. The model, built on physical insight and prior knowledge concerning the environment, emulates the EMA healthy behaviour by taking into account the applied inputs and the measured outputs on the EMA. A well designed residual always has a zero value in the absence of fault. In practice, deviations from zero occur due to modelling uncertainties and measurement noise. However, when a fault occurs the residual significantly deviates from zero. Using statistical tools the decision module determines from the pattern of zero and non zero residuals which is the most likely faulty component. The decision system contains thresholds that allow adjusting performance criteria such as false alarm and non detection rates. Figure 1 illustrates the foreseen concept.

2 Challenges

Several research actions are necessary for the development of a reliable, workable and efficient monitoring system. Some of the challenges include,

- Automatic tuning of the monitoring system to fulfil requirements w.r.t. the false alarm and the missed detection probabilities,
- Systematisation of the model parameter tuning using relevant data selection from typical flight data,
- Consideration of the operational constraints and of the model non linearities,
- Validation with data from experimental test benches and numerical simulations.

This project is realised in partnership with the SABCA which ensure to fill the important remaining gap between industrial needs and theoretical developments.

3 Acknowledgement

References

[1]   A. Garcia and al., "Reliable electro-mechanical actuators in aircraft," IEEE Xplore, 2008.

[2]   J-C. Mare., "Les actionneurs aéronautiques Volume 3," IEEE Xplore, 2018.

Interactive Demo on the Indoor Localization, Control and Navigation of Drones

Mathias Bos[† ‡], Rian Beck[*], Jan Swevers[† ‡], Goele Pipeleers[† ‡]

[†]MECO Research Team, Dept. of Mechanical Engineering, KU Leuven, BE-3001 Heverlee
Email: firstname.lastname@kuleuven.be
[‡]DMMS lab, Flanders Make, BE-3001 Heverlee
[*]Flanders Make, BE-3001 Heverlee
Email: rian.beck@flandersmake.be

1 Introduction

Unmanned aerial vehicles (UAV's) are a subject of great interest in the world of research, industry and commerce. This Master's thesis contributes to the practical aspects of automating drone flight. Through the development of a live demo setup it also offers an interactive view on both recent developments in mechatronics such as Model Predictive Control (MPC) for motion planning purposes and more established basic control principles. As such it aims for a broad range of audiences, addressing uninformed enthusiasts up to experienced researchers.

The study makes contributions to the domains of localization, control and navigation, and develops a structure to combine these aspects in a framework that is both robust and flexible regarding demo execution.

2 Indoor drone localization, control and navigation

Firstly an asynchronous Kalman filter for position and velocity state estimation is developed and implemented with accurate timing handling. Meticulous tracking of timing is crucial in an operating system that is prone to communication delay and imperfect controller and measurement rates, such as the commonly used Robot Operating System (ROS). Position measurements are retrieved through an infrared tracker from the HTC Vive virtual reality gaming system mounted on the drone.

Secondly the design and implementation of a model inversion-based feedforward controller with zero phase filtering for trajectory tracking is established. Non-causal low pass filtering through a combination of a forward and reverse sweep of a given reference trajectory enables the superposition of feedback and feedforward control without a phase shift between the two resulting control efforts.

Thirdly this project integrates the OMG-tools motion planning software developed in [1] and provides an experimental validation of both static and dynamic obstacle avoidance. OMG-tools is a Python toolbox incorporating spline-based motion planning methods, applying optimal control in an MPC fashion.

Finally to allow for flexibility in the execution of the demo and to provide a high level decision taking authority, a Finite State Machine (FSM) is developed. The FSM yields situation specific behavior of the mechatronic system with integrated monitoring for detection and safe handling of non-nominal events, such as loss of position measurements or infeasible solutions returned by the motion planning algorithm.

3 Interactive demo

The result of the study is an operational demo setup with a set of visually impressive and interactive tasks, that provides the freedom to execute tasks in any arbitrary order. The default scenario is one where the available tasks are executed in an order of increasing difficulty. Starting from position and velocity setpoint tracking, it proceeds with trajectory tracking with feedforward control, and builds up to optimal autonomous navigation through an obstructed environment. Finally collision avoidance with a dynamic obstacle is touched upon. Figure 1 illustrates one of the autonomous navigation tasks: a slalom between poles.
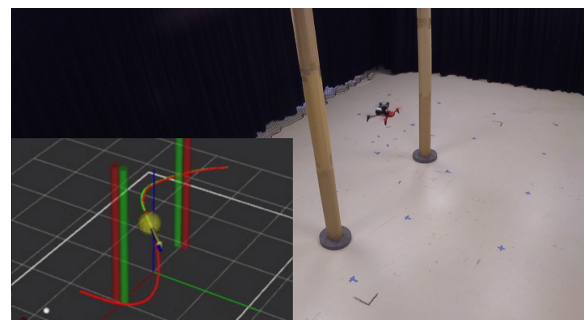
Figure 1: Autonomous navigation example: slalom. This figure shows the real world execution together with the virtual twin represented in ROS' visualization tool *rviz*.

The demo is available as an open-source software package, which together with a modular design encourages further contributions to the current setup [2].

References

[1] R. Van Parys, "Fast and Distributed Model Predictive Control: Tailored solutions for mechatronic systems". PhD thesis, KU Leuven, October 2018

[2] R. Beck and M. Bos, "Interactive autonomous drone demo" https://github.com/RianBeck/DroneDemo, 2019

Decision making for autonomous vehicles: Combining safety and optimality

J.J. Verbakel[1], M. Fusco[2], D.M.C. Willemsen[2], J.M. van de Mortel[1], W.P.M.H. Heemels[1]

[1] Eindhoven University of Technology, P.O.Box 513 5600 MB Eindhoven, The Netherlands.

[2] Integrated Vehicle Safety Department, TNO, 5708 JZ Helmond, The Netherlands.

1 Introduction

Controllers of automated vehicles (AVs) need to make many decisions on how to drive. One of the possible control architectures arranging the necessary tasks is sequential planning [1]. In sequential planning perception, decision making and path planning are separated in three steps. A decision maker (DM) uses perception outputs to select a discrete action from a set of possible actions, such as 'lane change to the left and accelerate'. This action is then used to generate a path.

In this paper, a DM for highway scenarios is presented, combining rule-based safety checks with a Markov decision process (MDP) solved through a tree search algorithm. The methods are chosen such that they will still be computationally tractable for large systems.

2 Problem formulation

Based on the state information provided to the DM by the perception module, e.g., location and speed of other vehicles, an action is chosen. The problem that is addressed can be stated as follows. Given a multi-vehicle state at a discrete time, find an action that guarantees a lower bound on *safety*, maximizes *safety* and *liveness*, and minimizes *activity*. Note that, besides having a lower bound, safety is still included in the optimization, because otherwise it might be beneficial to keep safety as low as possible, which is not desired.

3 Decision Maker architecture

The DM selects an action in two stages (see Fig. 1). First, safe actions are selected (shown in red), second, the best safe action, according to the given criteria, is selected (shown in blue). The orange component creates a quantized state, see, e.g., [4]. The arrows show the flow of information between the components, the transferred information is given in rounded rectangles.

Safety is measured here by taking the time to collision (TTC). Because TTC uses a constant heading, some actions which are clearly unsafe still meet the threshold, these are removed as well. The remaining (safe) actions are used in the MDP to find the optimal action.

The optimal action from the set of safe actions is found using an MDP, see, e.g., [2]. In an MDP, each action incurs a
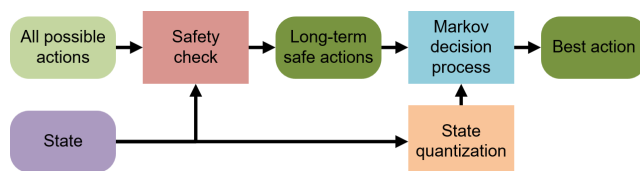
Figure 1: Decision Maker architecture.

reward; the goal is to maximize the reward over future actions. This closely resembles the driving process, where, e.g., a lane change reduces comfort, but speeds up the journey by overtaking slow vehicles. Here, the reward is given by a weighted combination of chosen functions that capture a desirable trait, such as maintaining speed or safety. Hence, by proper selection of the weights, appropriate tradeoffs can be made. The action with the highest expected reward, is found through Anytime AO* [3]. The state is quantized to maintain computational tractability, even for large systems.

4 Results

The behavior of the DM is validated through simulation in 8 important scenarios of highway driving. In which a high fidelity model is used, which is more realistic than the model used for the controller design. The performance of the two-stage DM is compared to the performance of a manually programmed rule-based controller. From this comparison it is concluded that the design successfully implements a scalable DM for AVs in a highway setting.

References

[1]   W. Schwarting, J. Alonso-Mora, and D. Rus, "Planning and decision-making for autonomous vehicles," *Annual Review of Control, Robotics, and Autonomous Systems*, vol. 1, pp. 187–210, 2018.

[2]   R. Sutton and A. Barto, *Introduction to reinforcement learning*. MIT press Cambridge, 1998.

[3]   B. Bonet and H. Geffner, "Action selection for MDPs: Anytime AO* versus UCT," in *Proc. 26th AAAI Conf. AI*, 2012.

[4]   J. Lunze, "Qualitative modelling of linear dynamical systems with quantized state measurements," *Automatica*, vol. 30, no. 3, pp. 417–431, 1994.

Experimental results of distributed multi UAV search optimization

Jeroen Fransman and Bart De Schutter
Delft Center for Systems and Control, Delft University of Technology
Email: `J.E.Fransman@tudelft.nl`

1 Introduction

In cooperative search, several agents need to survey a predefined region as fast as possible in search for particular objects or victims. Typically, these search operations are performed by mobile robots equipped with one or more cameras. In this work, the experimental results for an autonomous search use case with multiple small Unmanned Aerial Vehicles (UAVs) are presented.

2 Problem definition

The (rectangular) search region is defined by its width and height as $R = (R_\mathrm{w}, R_\mathrm{h})$, where $R_\mathrm{w} \geq R_\mathrm{h}$. It is assumed that there are no obstacles and the region is known by all agents. The autonomous search task for UAVs is modeled within Distributed Constraint Optimization Problem (DCOP) as a segmentation problem, where the variables are related to the size of their individual segments $R_i = (R_{i,\mathrm{w}}, R_\mathrm{h})$ and $R_\mathrm{w} = \sum_{i=1}^{N} R_i$. The altitude for all UAVs is kept constant during the search. In addition to the time spent searching, the travel times towards the start of their segments ($p_{i,\mathrm{s}}$) and the travel times from the end of the segment ($p_{i,\mathrm{f}}$) back to their initial positions is taken into account. The UAVs will traverse lawnmower patterns within their search segments, where a *leg* indicates a straight line during which scanning is performed. The lawnmower pattern is optimal for a rectangular search area and UAVs of which the sweep width is larger than the turn radius [1]. The sweep width is based on the size of the camera image (l_w) on the ground. The distance between the legs is based on the sweep width such that consecutive tracks interleave. An additional distance (l_t) is added before the start of the leg to ensure all oscillations (causes by the cornering) are eliminated. An overview of the search segment of a single agent can be seen in Figure 1.

3 Hardware overview

Quad-rotor UAVs (3DR-X4) are equipped with a downward facing camera (GoPro Hero 5 Session). The camera is connected to an onboard computer (Raspberry Pi 3B+), which also runs the Distributed Bayesian (D-Bay) optimization algorithm [2] and handles the communication between the agents. Communication between the agents is done over WiFi and low-power Zigbee (XBee Pro). During flight the UAV is controlled by an autopilot (Pixhawk). An overview of the UAV and its components is given in Figure 2.
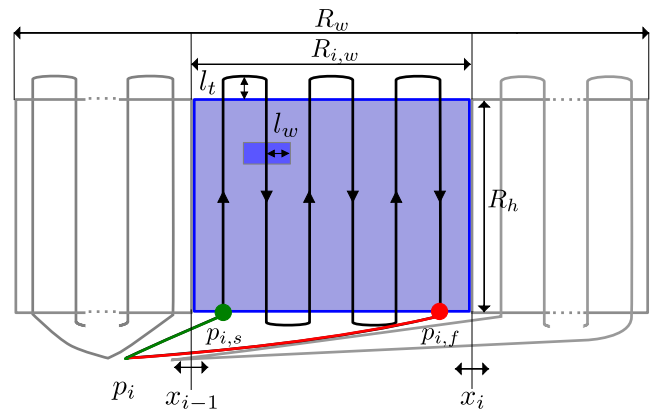
Figure 1: Overview of the search segment of a single agent.
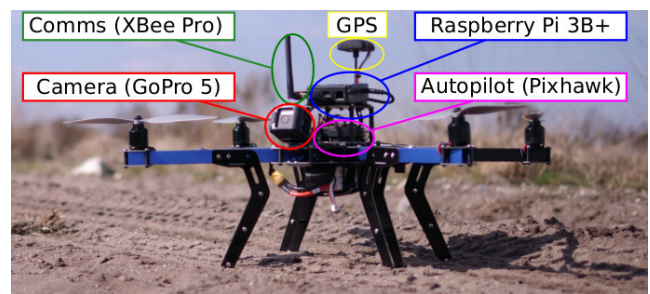
Figure 2: Overview of the equipped 3DR-X4 UAV.

4 Experimental results

Preliminary experiments and simulations have been used to define the parameters of the UAVs, such as scan width of the camera and turn length. For the experiments a group of five UAVs were used. The results are compared to equal segmentation $R_{i,\mathrm{w}} = R_\mathrm{w}/5$. The D-Bay algorithm was able to optimally solve the DCOP, which decreased the total required time by more than $12\,\%$.

References

[1] V Ablavsky and M Snorrason. "Optimal search for a moving target: A geometric approach". In: *AIAA Guidance, Navigation and Control Conference*. 2000.

[2] Jeroen Fransman et al. *Distributed Bayesian: a continuous Distributed Constraint Optimization Problem solver*. 2020. arXiv: `2002.03252`.

Modeling and control of a quad-tiltrotor aimed for interaction tasks

Julio C. Vendrichoski, Bram Vanderborght
BruBotics
Vrije Universiteit Brussel (VUB)
Pleinlaan 2, Building Z, 2nd floor
Brussels, Belgium
Email: juliocv@outlook.com,
bram.vanderborght@vub.ac.be

Emanuele Garone
SAAS
Université Libre de Bruxelles (ULB)
50, av. F.D. Roosevelt, CP 165/55
Brussels, Belgium
Email: egarone@ulb.ac.be

1 Introduction

Quadrotors have attracted recurring interest in recent years to the point of becoming one of the most popular models of unmanned aerial vehicle (UAV). Its standard construction with four fixed rotors, although limited, has proved been enough to robustly perform tasks related to image capture, small loads transportation, among others. However, standard quadrotors are underactuated, i.e., their fixed rotors provide only four actuation variables in order to drive the vehicle's six degrees of freedom. This intrinsic characteristic makes the longitudinal and lateral movements to be dependent, respectively, on the pitch and roll angles. As a consequence, standard quadrotors have limited dexterity to pass through narrow openings and cannot hover in an inclined orientation or instantaneously apply arbitrary forces and torques to interact with the surrounding environment. These limitations of the standard quadrotors justifies the growing search for constructive configurations of UAVs with more degrees of freedom and with an increased wrench capability.

The quad-tiltrotor aerial vehicle presented in this work consists essentially in an adaptation of the a standard quadrotor with its four rotors laying out in a H-shape configuration. However, different from a standard quadrotor, this vehicle has servomotors that actuate tilting the rotors in the longitudinal direction, Fig. 1 [2]. In this configuration, when the rotors are tilted, the generated thrust has a component in the longitudinal direction. The modification does not result in an omnidirectional vehicle (a lateral movement still depends on the roll angle). However, such vehicle can provide a high amount of thrust in the longitudinal direction due to the contribution of all the four rotors, increasing the performance in some particular environment interaction tasks, such as push an object.

2 Methodology and Results

The mathematical model of the entire system is obtained by employing the Euler-Lagrange formalism and a multi-body approach. In order to better observe the flight behavior of the quad-tiltrotor, a simple control strategy is designed, and consists in a linear control law based on a simplified version of the nonlinear model at an operating point that corresponds to the nominal hover state [1]. The control structure is com-
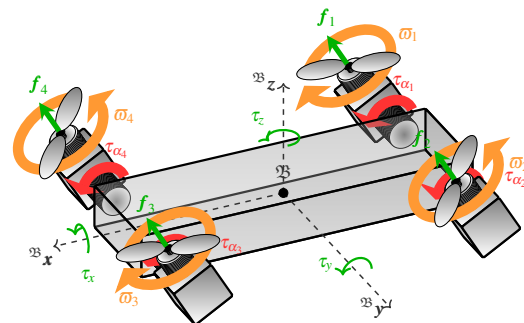
Figure 1: Quad-tiltrotor

posed by three nested feedback loops and a mapping relation to deal with the control allocation problem. The most external loop is the position control. Due to the characteristics of this vehicle, we cannot actuate directly and independently in all the position coordinates, thus the reference of the roll angle is used as a virtual control input. Additionally, this control block generates references of the necessary forces in the quad-tiltrotor body that lead to the desired position. Next, the attitude control computes the necessary body torques given the desired Euler angles. The control allocation maps the desired forces and torques in the body to a necessary combination of thrust in the rotors and the tilting angles in order to reach it. The most inner loop is the tilting angle control and drives the servomotors to reach the desired tilting angles.

3 Acknowledgement

References

[1]　N. Michael, D. Mellinger, Q. Lindsey, V. Kumar,"The GRASP multiple micro-UAV Test Bed", IEEE Robotics and Automation Magazine, vol. 17, no. 3, pp. 56–65, 2010.

[2]　J. C. Vendrichoski, T. L. Costa, E. S. El'Youssef, E. R. Pieri, "Mathematical modeling and control of a quadrotor aerial vehicle with tiltrotors aimed for interaction tasks", 19th International Conference on Advanced Robotics (ICAR), 2019.

Extended Kalman Filter for accurate distance estimation using RSSI and GPS measurements in quadcopter formation flights

Brice Njinwoua
Control Department
Mons University
Boulevard Dolez 31, 7000 Mons
Belgium
Email: Brice.Njinwoua@umons.ac.be

Alain Vande Wouwer
Control Departement
Mons University
Boulevard Dolez 31, 7000 Mons
Belgium
Email: Alain.Vandewouwer@umons.ac.be

1 Introduction

Unmanned Aerial Vehicles, known as UAVs, have known a growing interest in the last decade. This increasing popularity is due to their low cost, agility, simple construction, manoeuvrability and stability [1]. They are used in a vast array of applications, including military applications (rescue, border surveillance), industry and agriculture applications (pipe maintenance, field monitoring), movie production, logistics, and leisure.

Coordinating a flock of UAVs to achieve common tasks can be more efficient rather than using a single UAV. Cooperative control algorithms often require accurate measurements [2]. In the literature, the main issue of cooperative control is relative localisation. Classical GPS measurements leads to an accuracy of around 2 *meters*. This problem has been solved for indoor flight trough the *VICON* system which has a precision of centimetres [4] and for outdoor flights using RTK (Real Time Kinematic) GPS. Some researchers use spectral and IR cameras, laser and mapping algorithm to improve the precision of localisation [3]. However, all this methods require huge investment and resources. In this paper, we propose methods based on fusion of the classic GPS measurements and the Received Signal Strength Indicator RSSI provided by *XBee* devices mounted on the copters.

2 Sensors fusion with EKF

To estimate the relative distance between the two copters in 3 dimension, a dynamical model of the i^{ith} copter is use with the (measured) velocities on each axis as inputs as shown on equation 1 :

$$
\begin{array}{rcl}
\dot{x}_i & = & v_{x_i} + w_{v_{xi}} \\
\dot{y}_i & = & v_{y_i} + w_{v_{yi}} \\
\dot{z}_i & = & v_{z_i} + w_{z_{yi}}
\end{array}
\tag{1}
$$

where v_{x_i}, v_{y_i} and v_{z_i} are the velocities and $w_{v_{xi}}$, $w_{v_{yi}}$ and $w_{v_{zi}}$ are the variance on the velocity measurements respectively on x, y and z axis.

The relative distance d_{ij} between i and j can be calculated trough a non-linear function. An extended Kalman filter based on sensor fusion techniques can be use to get a more accurate estimation of the relative distance. Difference between GPS coordinates with a certain uncertainty (GPS error) ω_{GPS} and the distance compute from the *RSSI* (fig. 1) signal with an error ω_{RSSI} are used as the uncertain measurements, respectively called z_1 and z_2.

As GPS satellite signals are quite weak and thus require line-of-sight from the receiver to the satellite, they do not work as well indoors or in urban environment. By combining the two measurements, we can expect to reduce the global uncertainties for positioning. The RSSI accuracy is about 2 meters in long range (up to 25 meters) in a free inerference environment versus 2 meters under very good conditions for the GPS.
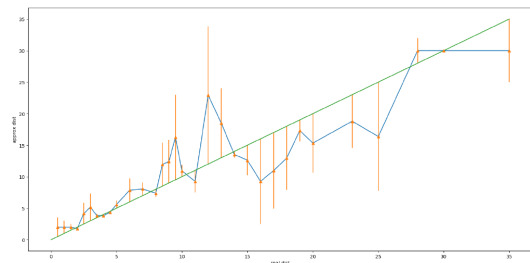
Figure 1: Estimated distance through RSSI vs reality

References

[1]   Abas, Norafizah and Legowo, "Modeling and system identification using extended kalman filter for a quadrotor system," Applied Mechanics and Materials, 2013.

[2]   N. Limbu, H. Ahuja, "Outdoor co-operative control of multiple quadcopters using decentralized GPS localisation," RoMoCo, 2015.

[3]   M. Nagain, T. Chen, "UAV-Borne 3-D Mapping System by Multisensor Integration," IEEE Transactions, 2009.

[4]   R. Thien, K. Yoonsoo, "Decentralized Formation Flight via PID and Integral Sliding Mode Control," IFAC, 2018.

Gaussian Processes Based Learning Control for Quadcopters

Yuhan Liu[1,2] and Roland Tóth[1]

[1]Control Systems Group, Electrical Engineering, Eindhoven University of Technology
P.O. Box 513, 5600 MB Eindhoven, The Netherlands
[2]Department of Control Science and Engineering, Harbin Institute of Technology
150001, Harbin, China
Email: {y.liu11, r.toth}@tue.nl

1 Introduction

Over the past decades, quadcopters have attracted great attention of many research studies due to their wide application. Flight control design for a quadcopter is not a simple task due to the quadcopter having six degrees of freedom with only four inputs to control the vehicle, which also leads to the strong couplings in the dynamics. On the other hand, the time-varying uncertainties and unmodeled dynamics, such as external wind, complex interactions of rotor and wing airflows with the ground and wall, frictions and flapping dynamics of the rotor blades, make the control design problem quite complex [1]. However, at current stage, a comprehensive and precise model of a quadcopter is still costly to obtain. Therefore, the quadcopter requires robust and effective control against various disturbances and unmodeled dynamics.

Recently, machine learning-based control has shown potential to save effort of understanding unmodeled dynamics and achieving superior performance in compensation control over increasing robustness of physical model-based control. Wherein, Gaussian process (GP) regression [2], which is a typical Bayesian nonparametric data-driven modeling method, is promising to automatically extract the important features of the unknown dynamics from system input and output data. In this paper, we present a data-driven approach based on GP that learns the additional dynamics that are not captured by an a priori ideal quadcopter model and is used for feed-forward compensation of the unknown part of the system dynamics.

2 Problem Formulation

The dominant quadcopter dynamics can be viewed as the motion dynamics of a 6 degree-of-freedom rigid body. However, as mentioned in the introduction, there exist unmodeled dynamics that cannot be captured by such an idealistic model nor there is reliable first principle knowledge to characterize them. Hence, we assume that the system dynamics include two parts: *a priori* part and unknown part:

$$\dot{\boldsymbol{x}} = \underbrace{\boldsymbol{f}(\boldsymbol{x},\boldsymbol{u})}_{\text{priori model}} + \underbrace{\boldsymbol{\Delta}(\boldsymbol{x},\boldsymbol{u})}_{\text{unknown model}} \qquad (1)$$

where $\boldsymbol{x}(t) \in \mathbb{R}^{12}$ denotes the quadcopter states and $\boldsymbol{u}(t) \in \mathbb{R}^4$ represents the control inputs. The goal of this paper is to find an estimate of the unknown function $\boldsymbol{\Delta}(\boldsymbol{x},\boldsymbol{u})$ using the measurement data from the system obtained under a priori designed feedback control of $\boldsymbol{f}(\boldsymbol{x},\boldsymbol{u})$. As the estimate of $\boldsymbol{\Delta}(\boldsymbol{x},\boldsymbol{u})$ becomes more accurate, the control performance will improve obviously. We model the unknown part $\boldsymbol{\Delta}(\boldsymbol{x},\boldsymbol{u})$ as a GP. Compared to other learning approaches, such as ANN and SVM, GP provides the predictive variance that can serve as a quantitative evaluation of model uncertainty. Furthermore, GP is capable of making a robust estimation where only a limited set of data points is available.

3 Proposed Approach

In this paper, we propose a GP-based learning control approach to handle with the trajectory tracking problem of quadcopters. The GP learns the unknown dynamic model with the system input and output measurement data, and then provides the mean prediction of the uncertainties at new data points, which is used to feed-forward compensate the unknown part of the system. The illustration of the proposed control approach is shown in Fig.1.
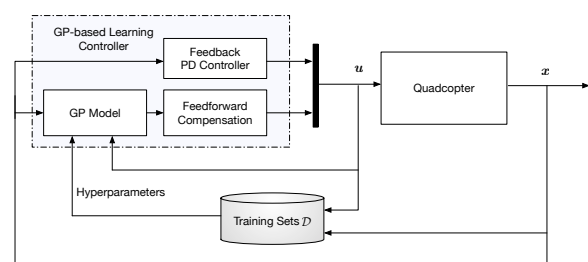
Figure 1: GP-based learning control for the quadcopter

References

[1] R. Mahony, V. Kumar, and P. Corke, "Multirotor aerial vehicles: Modeling, estimation, and control of quadrotor" IEEE robotics & automation magazine, 2012, 19.3:20-32.

[2] C. Rasmussen, "Gaussian Processes in Machine Learning," Summer School on Machine Learning, 2003.

Towards Prescribed Performance Control of Persistent Formations with Signed Area Constraints

Farhad Mehdifar[*], Charalampos P. Bechlioulis[†], and Julien M. Hendrickx[*]

We will take the first steps towards developing a distance-based formation control law with directed inter-agent sensing and signed area constraints using the prescribed performance control method. In distance-based formation control, agents measure the relative positions of their neighbors and actively control their inter-agent distances in order to reach a desired pre-defined shape so that the designed control laws are coordinate-free [1]. Directed sensing is of more practical interest w.r.t. its undirected counterpart because: (i) it introduces robustness to measurement mismatches, and (ii) it can be enforced by heterogeneous limited sensing capabilities among neighboring agents (Fig.1a).

In general, constraining a fomation merely by inter-agent distances may not lead to a uniquely defined shape since shape flipping or reflection ambiguity remains for the whole formation (Fig.1b) leading to only local guarantees for convergence to the correct shape [1, 4]. Recently, this problem has been tackled for undirected and directed distance constrained formations by introducing signed area constraints ($\pm Z_{ijk}^*$ in Fig.1b) to distinguish ambiguities and designing control laws with almost global shape convergence [2, 3].

In our previous work for undirected distance-based formations [4], we have shown that the Prescribed Performance Control (PPC) method not only can be used for designing robust distance-based formation control laws but also for ensuring connectivity maintenance (which is a crucial problem due to limited sensing ranges of agents) and collision avoidance among neighboring agents.

In particular, we will consider 2-D acyclic minimally persistent (directed) formations [1, 3] such that agent 1 is the leader, agent 2 only senses agent 1, and agent $i \geq 3$ has exactly two neighbors (or leaders) j and k such that $i > j$ and $i > k$. Let e_{ij} be the distance error between neighboring agents i and j, and $\widetilde{Z}_{ijk} = Z_{ijk} - Z_{ijk}^*$ be the signed area error, where Z_{ijk}^* is the desired signed area assigned to agent $i \geq 3$. The objective is to design a decentralized robust control protocol to ensure $e_{ij} \to 0$ and $\tilde{Z}_{ijk} \to 0$ as $t \to \infty$ such that (when $Z_{ijk}^* > 0$):

$$
\begin{aligned}
-\underline{e}_{ij}(t) < e_{ij}(t) < \overline{e}_{ij}(t), \quad &\forall t \geq 0, \\
-\underline{Z}_{ijk}(t) < \widetilde{Z}_{ijk}(t), \quad &\forall t \geq 0.
\end{aligned}
\tag{1}
$$

where $\underline{e}_{ij}(t) > 0$, $\overline{e}_{ij}(t) > 0$, and $\underline{Z}_{ijk}(t) > 0$ are proper
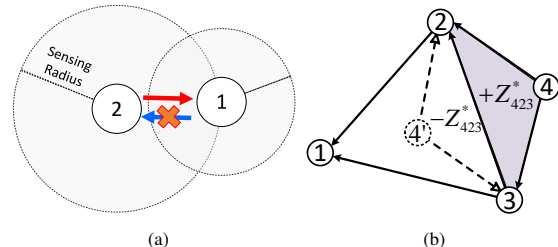
Fig. 1: (a) heterogeneous sensing can lead to directed interactions. (b) Acyclic minimally persistent formation with a sample flip ambiguity. Signed area constraints can distinguish the flip ambiguities and reflections.

decreasing prescribed performance bounds (PPBs) with a nonzero sufficiently small positive limit as $t \to \infty$. Clearly, by a proper design of the PPBs for distance errors $e_{ij}(t)$, connectivity maintenance and collision avoidance among neighboring agents can be ensured. Moreover, this method may prevent controller gain assignment (as addressed in [2, 3]) for ensuring existence of a unique equilibrium (formation) with $e_{ij} = 0$ and $\widetilde{Z}_{ijk} = 0$ for the closed-loop system since satisfaction of the PPBs (1) naturally encapsulates this.

Inspired by [5], by using proper nonlinear mapping functions, the problem of designing a controller with the constrained error conditions (1) can be transformed to solving a problem with boundedness of signals as the only requirement. However, since agent $i \geq 3$ moves in the plane and has three control directions at a time (two for the distances and one for the area), infeasibility in satisfying the three imposed constraints (1) may occur. Therefore, a primary challenge towards PPC design would be on designing feasible (consistent) error constraints (or PPBs) in (1) for agent $i \geq 3$. This requires state-dependent PPBs opposed to the conventional PPC designs that use merely time-dependent PPBs. As a first step, we will start analyzing the mentioned problem for three agent formations.

References

[1] K.-K. Oh, M.-C. Park, and H.-S. Ahn, "A survey of multi-agent formation control," *Automatica*, vol. 53, pp. 424–440, 2015.

[2] B. D. Anderson, Z. Sun, T. Sugie, S.-i. Azuma, and K. Sakurama, "Formation shape control with distance and area constraints," *IFAC Journal of Systems and Control*, vol. 1, pp. 2–12, 2017.

[3] T. Liu, M. de Queiroz, P. Zhang, and M. Khaledyan, "Directed formation control of n planar agents with distance and area constraints," in *2019 American Control Conference (ACC)*, pp. 1824–1829, July 2019.

[4] F. Mehdifar, C. P. Bechlioulis, F. Hashemzadeh, and M. Baradarannia, "Prescribed performance distance-based formation control of multi-agent systems (extended version)," *arXiv preprint arXiv:1911.07266*, 2019.

[5] C. P. Bechlioulis and G. A. Rovithakis, "Robust adaptive control of feedback linearizable mimo nonlinear systems with prescribed performance," *IEEE Transactions on Automatic Control*, vol. 53, no. 9, pp. 2090–2099, 2008.

[*] INMA, ICTEAM, UCLouvain, Louvain-la-Neuve, Belgium, (Emails: {farhad.mehdifar, julien.hendrickx}@uclouvain.be).
[†] School of Mechanical Engineering, National Technical University of Athens, Athens, Greece, (Email: chmpechl@mail.ntua.gr).

Formation Control for Circular Robots

Nelson P.K. Chan and Bayu Jayawardhana
DTPA, ENTEG, FSE, University of Groningen
Nijenborgh 4, 9747 AG Groningen, The Netherlands
Email: {n.p.k.chan, b.jayawardhana}@rug.nl

1 Introduction

In the present work, we revisit the formation control problem where the objective is to design control laws for a group of mobile robots such that they form a desired geometric shape. In literature, several constraints can be considered for defining the formation shape. In particular, the formation shape can be specified by the distance or the bearing between a subset of robot pairs [1]. Recently, other shape variables are as well being considered for defining the formation shape. Among others, the formation shape can as well be defined by the angle [2] between a robot and its two neighbors, or a ratio of the distances [3]. Herein, the robot is usually considered to be a point moving in the plane or the space. In addition, there is only one measurement available to a robot from its neighbors.

In this work, we consider the robots to have a circular shape and each robot can take two measurements for each of its neighbors. The internal angle obtained from these two relative measurements is taken as the control variable. We propose and analyse a gradient-based control law for solving the formation control problem.

2 Problem Formulation

We consider a group of N mobile robots moving in the plane. Each robot has a circular shape, and as such has a center denoted by $p_i \in \mathbb{R}^2$, and a radius $r_i \in \mathbb{R}$ for $i = 1, \ldots, N$. We assume the mobile robots to have the same radius, i.e., $r_i = r, \forall i$. The mobile robots are modeled by the kinematic equation

$$\dot{p}_i = u_i, i = 1, \ldots, N. \quad (1)$$

Each robot is able to obtain two relative 'point' measurements from each of its neighbors. An internal angle θ_{ij} can be obtained by utilizing these two relative 'point' measurements. In the current work, we assume each mobile robot to obtain two relative position measurements from each of its neighbors. The expression relating the internal angle θ_{ij} with the radius and the inter-center distance d_{ij} of the robots is

$$\cos\theta_{ij} = 1 - 2\left(\frac{r}{d_{ij}}\right)^2. \quad (2)$$

In terms of the available relative measurements z_{ijL} and z_{ijR}, we can write

$$\cos\theta_{ij} = \frac{z_{ijL}^\top z_{ijR}}{\|z_{ijL}\| \|z_{ijR}\|}. \quad (3)$$

For each pair $\{i, j\}$ of interacting mobile robots, a desired value $\theta_{ij}^\star$ is pre-defined. The goal is to design control laws for the mobile robots such that $\theta_{ij} \to \theta_{ij}^\star$ as time progresses.

3 Gradient-based Approach

In solving the formation control problem, we consider as potential function

$$V_{ij}(e_{ij}) = \frac{1}{2}\left(\frac{\cos\theta_{ij} - \cos\theta_{ij}^\star}{\cos\theta_{ij} - 0.5}\right)^2 = \frac{1}{2}\left(\frac{e_{ij}}{e_{ij} + c_{ij}}\right)^2. \quad (4)$$

with $e_{ij} = \cos\theta_{ij} - \cos\theta_{ij}^\star$ being the error signal and $c_{ij} = \cos\theta_{ij}^\star - 0.5$ with 0.5 being the value when the two robots are touching each other. The term in the denominator is included to ensure collision avoidance.

The gradient-based control law for each robot i in terms of the available measurements is of the form

$$\dot{p}_i = \sum_{j\in\mathcal{N}_i} 2\frac{e_{ij}c_{ij}}{(e_{ij}+c_{ij})^3}\sin^2\theta_{ij}\frac{z_{ij+}}{\|z_{ij+}\|^2}. \quad (5)$$

with $z_{ij+} = z_{ijL} + z_{ijR}$.

The following are properties of the proposed control law:

- The centroid of the formation is stationary, i.e., $p_{\text{cent}}(t) = p_{\text{cent}}(0), \forall t \geq 0$.

- The measurements taken by the robots can be done in the local coordinate frame and as such not aligned to a global coordinate frame.

- Local exponential convergence can be guaranteed when the initial formation is close to the desired formation.

References

[1] S. Zhao and D. Zelazo, "Bearing Rigidity Theory and Its Applications for Control and Estimation of Network Systems: Life Beyond Distance Rigidity," *IEEE Control Systems*, vol. 39, pp. 66–83, Apr. 2019.

[2] L. Chen, M. Cao, and C. Li, "Angle rigidity and its usage to stabilize planar formations,"

[3] K. Cao, Z. Han, X. Li, and L. Xie, "Ratio-of-Distance Rigidity in Distributed Formation Control," in *2018 15th International Conference on Control, Automation, Robotics and Vision (ICARCV)*, IEEE, Nov. 2018.

Simultaneous distributed localization, mapping and formation control of mobile robots based local relative measurement

Miao Guo [1,*], Bayu Jayawardhana [1], Jin Gyu Lee [2], Hyungbo Shim [3]

[1]ENTEG, Faculty of Science and Engineering, University of Groningen, The Netherlands.

[2]Control Group, Department of Engineering, University of Cambridge, United Kingdom.

[3] ARSI, Department of Electrical and Computer Engineering, Seoul National University, Korea.

[*]Corresponding author e-mail: M.guo@rug.nl

1 Abstract

Over the past decades, multi-robotic system (MRS) has been extensively studied because it is more robust and flexible in comparison with single robot. A number of applications of MRS can be found in (1). Precise localization plays an important role in multi-robotic system while fulfilling a certain task cooperatively. Normally, GPS signal can be obtained by mobile robots to maintain their formation and to steer the whole group. However, in certain circumstances (e.g. in a warehouse), the signals concerning global position information can not be provided for mobile robots. Thus, the problem of localizing a group of mobile robots in such environment while simultaneously maintaining a robust formation and performing group motion is challenging.

In this work, we consider n mobile robots and m static landmarks that have to solve three tasks simultaneously: namely, formation and localization tasks in a distributed way, and group motion in a centralized manner. Each agent can estimate positions of agents and landmarks by running distributed Kalman filter. Depending on whether its neighbors can be measured or not, each agent can choose to use either measurement or estimation to keep formation. Therefore the dynamics of mobile robots and landmarks can be described by

$$\dot{p}_i = u_i^1(k_1, p_c, p_c^*, \dot{p}_c^*) + u_i^2(k_2, x, \hat{x}_i, p_i^* - p_j^*) \quad (i = 1, \ldots, n) \tag{1}$$

$$\dot{m}_l = 0 \quad (l = 1, \ldots, m), \tag{2}$$

where $p_i \in \mathbb{R}^2$ denotes the position of i-th mobile robots and $m_l \in \mathbb{R}^2$ is the position of l-th landmark. The parameters k_1 and k_2 denote the control gain of maneuvering and maintaining formation respectively. The variable p_c is the position of centroid and $p_c^* \in \mathbb{R}^2$ is the desired position of centroid. The variable x is the state vector of the system, which consists of the collective position of landmarks and mobile robots. The information $p_i^* - p_j^*$ is the desired relative position between i-th agent and j-th agent. It is obviously that the formation graph can be divided into measurement graph and estimation graph and their relationship can be illustrated in Figure 1. Based on the above formulation, our control goal is to design a distributed Kalman filter that provides the estimated state $\hat{x}_i$ such that $\hat{x}_i \to x$ asymptotically for all i and a distributed control law $u_i = u_i^1 + u_i^2$ such that the centroid p_c asymptotically track the desired centroid p_c^* and the relative position $p_i - p_j$ converges to the desired relative position $p_i^* - p_j^*$ for all j that is a neighbor of the i-th agent.
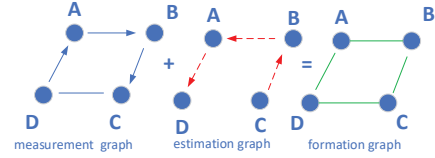
Figure 1: The relationship between measurement graph , estimation graph and formation graph.

2 Main results

The distributed Kalman filter we propose is

$$\dot{\hat{x}}_i = A\hat{x}_i + Bu + K_i(y_i - H_i\hat{x}_i) + \gamma W_i W_i^T \sum_{j \in \mathcal{N}_i} \alpha_{ij}(\hat{x}_j - \hat{x}_i)$$

$$K_i = Z_i \bar{P}_i \bar{H}_i^T R_i^{-1}$$

$$\dot{\bar{P}}_i = \bar{A}_i^{11}\bar{P}_i + \bar{P}_i(\bar{A}_i^{11})^T + \bar{G}_i Q \bar{G}_i^T - \bar{P}_i \bar{H}_i^T R_i^{-1} \bar{H}_i \bar{P}_i, \tag{3}$$

where $\hat{x}_i \in R^{2(n+m)}$ is the state of system estimated by i-th agent. Figure 2 shows the simulation results of a group of three mobile robots which maintains formation and maneuvers in a environment which consists of five landmarks.
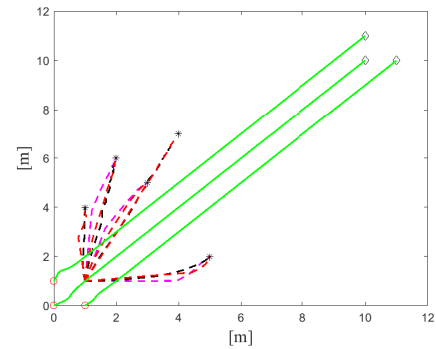
Figure 2: The dash lines denote the trajectories of positions of landmarks which are estimated by each agent.

References

[1] Arai, Tamio, Enrico Pagello, and Lynne E. Parker. "Advances in multi-robot systems." IEEE Transactions on robotics and automation 18.5 (2002): 655-661.

[2] M. Guo, B. Jayawardhana, Jin Gyu Lee, Hyungbo Shim. "Simultaneous distributed localization, mapping and formation control of mobile robots based local relative measurement." submitted to IFAC World Congress 2020.

Cooperative Passivity-Based Control for End-Effector Synchronisation

Oscar de Groot, Laurens Valk and Tamás Keviczky

Delft Center for Systems and Control, Delft University of Technology

Email: groot.oscar.de@gmail.com, laurensvalk@gmail.com, t.keviczky@tudelft.nl

Abstract

Passivity-based control is an established method for control of nonlinear mechanical systems such as robotic manipulators and Unmanned Aerial Vehicles (UAVs). The passivity property inherent to this control paradigm allows controllers to guarantee stability even when the underlying dynamics are nonlinear. In this work, we focus on end-effector synchronisation of a network of mechanical systems using passivity-based control methods. We specifically introduce two distributed cooperative control methods:

1. A unified cooperative Interconnection-and-Damping Assignment Passivity-Based Control (IDA-PBC) scheme for fully actuated and underactuated agents.

2. A novel passivity-based control scheme for output synchronisation of fully actuated systems with a stability guarantee in the presence of time-varying delays and packet loss.

Both methods share a number of properties. Both achieve a specified configuration (formation) in the end-effector coordinates. With leaders the agents settle at a desired reference, while without leaders the formation forms at an arbitrary point in configuration space. The inter-agent couplings are computed through gradient descend of a cooperative potential function that is passive by construction. The cooperative controllers are independent of the local system dynamics, which allows us to stably interconnect the controllers of systems for which a local solution exists.

To illustrate the efficacy of these approaches we compare the performance of both methods experimentally with and without time-varying delays and packet loss using a robotic manipulator and differential drive robots.

1 Cooperative IDA-PBC

In this work, we present a cooperative IDA-PBC [3] scheme for fully actuated and underactuated systems. We compose multi-agent system matrices from the individual single-agent matrices. The resulting cooperative IDA-PBC derivation then follows the single-agent procedure under mild assumptions. Appropriate selection of the communicated variable z, yields matching independent of the networked input and therefore guarantees stability and convergence to the minimum of the cooperative and local energy functions.

2 r-Passivity-Based Control

Based on the works [1] and [2], consider the scheme depicted in Figure 1, for end-effector synchronisation of fully actuated mechanical agents in the presence of time-varying delays and packet loss.
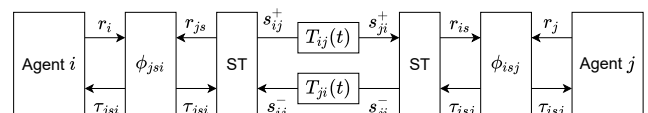
Figure 1: The multi-agent scheme as in [2] with modified outputs.

We modify the typical outputs r [1] as

$$r = \dot{z} + \lambda z, \qquad (1)$$

where $z = a(q)$ denote the end-effector coordinates. Velocities are required to achieve passivity, while the observability of the coordinates prevents drift due to loss of data. We show that the outputs (1) in the scheme from [2] leads to synchronisation of the end-effectors in the presence of arbitrary constant time delays. Each plant then needs to be passive with respect to the cooperative inputs and the outputs (1). We define the storage- and dissipation function

$$V = \frac{1}{2} r^T r + \frac{1}{2} \gamma \lambda z^T z, \qquad S = \gamma \dot{z}^T \dot{z}.$$

There exists a control law for fully actuated systems that shapes the plant dynamics as a strictly passive system with this storage- and dissipation function.

References

[1] Chopra, N. and Spong, M. W. (2005). On Synchronization of Networked Passive Systems with Time Delays and Application to Bilateral Teleoperation. In *SCIE Annual Conference*, pages 3424–3429, Okayama Japan.

[2] Chopra, N. and Spong, M. W. (2006). Output Synchronization of Nonlinear Systems with Time Delay in Communication. In *Proceedings of the 45th IEEE Conference on Decision and Control*, pages 4986–4992.

[3] Ortega, R., van der Schaft, A., Maschke, B., and Escobar, G. (2002). Interconnection and damping assignment passivity-based control of port-controlled Hamiltonian systems. *Automatica*, pages 585–596.

Passivity-based Velocity Tracking and Formation Control Without Velocity Measurements

Ningbo Li, J.M.A. Scherpen and A.J. van der Schaft
Jan C. Willems Center for Systems and Control, ENTEG, University of Groningen, The Netherlands
ningbo.li@rug.nl, j.m.a.scherpen@rug.nl and a.j.van.der.schaft@rug.nl

1 Abstract

This work presents an integrated approach for formation control and velocity tracking of a group of nonholonomic wheeled robots without velocity measurement. The solution is defined within the port-Hamiltonian framework, providing a clear interpretation of the results. The controller consists of a local nonlinear heading and velocity tracking controller combined with a distributed formation controller. The formation controller achieves formations by assigning virtual couplings in between the robots. The rate of convergence can be controlled by applying damping to the error in either the inertial velocity or the relative velocity of the vehicles. To avoid dependency on the unreliable velocity estimates we employ a dynamic extension to achieve the desired result.

2 Methodology

Considering a network of N wheeled robots, the dynamics of the wheeled robot are modeled as a rigid body with a nonholonomic constraint on its axle [1].

$$\begin{pmatrix} \dot{q}_i \\ \dot{p}_i^{rb} \end{pmatrix} = \begin{pmatrix} 0 & I_3 \\ -I_3 & -D_i^{rb} \end{pmatrix} \begin{pmatrix} \frac{\partial H_i^{rb}}{\partial q_i} \\ \frac{\partial H_i^{rb}}{\partial p_i^{rb}} \end{pmatrix} + \begin{pmatrix} 0 \\ F(q_i) \end{pmatrix} u_i \quad (1)$$

$$y_i = F^T(q_i) \frac{\partial H_i^{rb}}{\partial p_i^{rb}} \quad (2)$$

$$\sin \phi_i \dot{x}_{A,i} - \cos \phi_i \dot{y}_{A,i} = 0 \quad (3)$$

The control goals are that each wheeled robot tracks a desired forward velocity v^* along a desired heading ϕ^* and the whole group achieves a desired formation shape z^*.

The control goals can be divided into three parts. The first part is the heading control u_1, which is used to control the robot move along a desired heading. The second part is velocity tracking u_2 based on generalized canonical coordinate transformations. The main idea is to derive the error dynamics with respect to the reference velocity and then stabilize these dynamics. The third part is formation control u_3, which is a distributed formation controller, where robots exchange local information. The controller assigns virtual couplings between the front ends of the wheeled robots. Correspondingly the control input of the closed-loop system is

sum of the three controllers, which can be formulated as:

$$\begin{aligned} u &= u_1 + u_2 + u_3 \\ &= -k^\phi \tan \hat{\phi} - D^r v^* - G(\bar{q})(B \otimes I_2) K^v \bar{z} \quad (4) \\ &\quad - (D^t(G(\bar{q})(B \otimes I_2) + G(\bar{q})(B \otimes I_2)) \dot{\bar{z}} \end{aligned}$$

We wish to implement the input without relying on the velocity y and relative velocity $\dot{z}$. The term $D^t \bar{y}$ is used to improve the rate at which the system converges to v^*, and the term $\dot{\bar{z}}$ is used to improve the rate at which the system converges to the desired formation. To achieve this, we design a dynamic controller using the idea of dynamic extension [2].

$$\dot{z}^d := K_d^{-1} K_c (\bar{z} - z^d) \quad (5)$$

The new controller can be reformulated as:

$$\begin{aligned} u &= -k^\phi \tan \hat{\phi} - D^r v^* - G(\bar{q})(B \otimes I_2) K^v \bar{z} \\ &\quad - (D^t(G(\bar{q})B \otimes I_2) - G(\bar{q})(B \otimes I_2)) K_c (\bar{z} - z^d) \end{aligned}$$

$$(6)$$

Theorem 1. Consider the system (1)-(3) under a control law (6) with the assumption $\bar{\phi}(0) \in (-\pi/2, \pi/2)$, the closed-loop system achieves the control goals.

3 Conclusion

In this work, we consider the problem of formation control of a group of wheeled robots, while tracking a constant reference velocity along a prescribed heading. Our solution is a combination of a local nonlinear heading controller, a local velocity tracking controller, and a distributed formation controller. By relaxing the condition that all robots know the reference velocity, a dynamic extension is added to each robot to estimate its velocity, we have proven that our approach achieves the control objectives.

References

[1]   A. J. van der Schaft and D. Jeltsema, "Port-Hamiltonian systems theory: An introductory overview," *Foundations and Trends® in Systems and Control*, vol. 1, no. 2-3, pp. 173–378, 2014.

[2]   D. A. Dirksz and J. M. A. Scherpen, "On tracking control of rigid-joint robots with only position measurements," *IEEE Transactions on Control Systems Technology*, vol. 21, no. 4, pp. 1510–1513, 2012.

A Directed Spanning Tree Adaptive Control Framework for Time-Varying Formations

Dongdong Yue, Qi Li
School of Automation
Southeast University
Nanjing, China

Simone Baldi, Jinde Cao
School of Mathematics
Southeast University
Nanjing, China

Bart De Schutter
Delft Center for Systems and Control
Delft University of Technology
Delft, The Netherlands

Email: {d.yue, s.baldi, b.deschutter}@tudelft.nl

1 Introduction

In recent years, formation control of multi-agent systems has captured increasing attention due to applications in spacecraft formation flying, target seeking, search and rescue operations, to name a few [1]. By designing appropriate feasibility conditions, recent results on time-varying formation (TVF), and time-varying formation tracking (TVFT) have appeared as an extension to time-invariant formations. These designs rely on consensus-based methodologies to accomplish the formation in a *distributed* way (i.e. using local information only). If the design does not require any structural knowledge of the communication graph (e.g. the eigenvalues of the Laplacian matrix), then it is typically called *fully distributed*. Such designs have been proposed for undirected or detail-balanced/strongly-connected digraphs to address consensus, containment, or TVF problems. For more general digraphs, the directed spanning tree (DST) based distributed adaptive method was recently proposed to address consensus problems in a fully distributed way. However, fully distributed methods for TVF and TVFT problems are not yet available. In particular, in the presence of multiple leaders, it is impossible to have DSTs in the network since the leaders individually can not be influenced by any other agents. In this case, the problem of how to decouple the TVFT controller design and the network Laplacian spectra has not been addressed in the literature either. These observations motivate the work presented here.

2 Problem statements and control methodology

We consider TVF and TVFT problems for linear multi-agent systems over digraphs in a fully-distributed setting, i.e. without knowledge of the smallest eigenvalue of the Laplacian matrix associated to the communication graph. The solution to these problems relies on a unifying framework that generalizes the DST based adaptive method, which was originally limited to synchronization/consensus problems [2, 3]. For TVF without leaders, the control method consists in applying to each agent a distributed feedback control law with information of local state, local formation deviation, and neighboring formation deviations.

The DST-based adaptive control approach leads to a novel class of feasibility conditions, which are more efficient to check than the feasibility conditions in the state of the art. For TVFT with leader(s), the agents are not only required to span some formation, but also supposed to track a single leader, or some convex combinations of multiple leaders. The control methodology then degenerates to a distributed feedback control law with information of local formation deviation and neighboring formation deviations. More specifically, a generalized DST-based adaptive control approach is proposed, providing a natural unifying framework for the DST-based adaptive methods in the presence of one or more leaders. By updating only the coupling weights of the edges in the tree, or the generalized tree, all of the control designs can be decoupled from the communication Laplacian spectra. Necessary and sufficient conditions for the existence of solutions to the formation problems are derived. Asymptotic convergence properties of the formation errors are proved via graph theory and Lyapunov analysis.

References

[1] K.-K. Oh, M.-C. Park, and H.-S. Ahn, "A survey of multi-agent formation control," *Automatica*, vol. 53, pp. 424–440, 2015.

[2] W. Yu, J. Lu, X. Yu, and G. Chen, "Distributed adaptive control for synchronization in directed complex networks," *SIAM J. Control Optim.*, vol. 53, no. 5, pp. 2980–3005, 2015.

[3] Z. Yu, D. Huang, H. Jiang, C. Hu, and W. Yu, "Distributed consensus for multiagent systems via directed spanning tree based adaptive control," *SIAM J. Control Optim.*, vol. 56, no. 3, pp. 2189–2217, 2018.

Incremental Dissipativity Analysis of Nonlinear Systems using the Linear Parameter-Varying Framework

C. Verhoek, P.J.W. Koelewijn and R. Tóth
Control Systems Group, Eindhoven University of Technology
P.O. Box 513, 5600 MB, The Netherlands
Email: `c.verhoek@student.tue.nl`

1 Introduction and motivation

All physical systems are nonlinear (NL) when all details of their dynamic behavior is considered. Modeling and controlling these systems based on Linear, Time-Invariant (LTI) approximations around a steady-state condition has been a powerful method that could meet the required performance specifications in industrial applications so far. However, due to the growing performance demands together with increasing complexity of these systems, modeling and control tools of the LTI framework are becoming inadequate to use. Especially when the system is operated continuously in a transient mode, or with rapid transitions between operating points. Therefore, stability and performance analysis of NL systems becomes increasingly more important. Although a large variety of stability analysis tools are available for NL systems, there is no unified theory for general NL systems and a systematic performance analysis and shaping framework is largely missing. Moreover, the available analysis tools usually only give guarantees around the origin of the system, which is not suitable for e.g. reference tracking or disturbance rejection. Recent work [1] uses incremental analysis and the Linear Parameter-Varying (LPV) framework to give stability and performance guarantees for a predefined region of the state space using the incremental $\mathscr{L}_2$-gain. However, how general dissipativity theory [2] –to which stability and performance are closely related– is connected to the incremental framework is largely unknown. This research connects incremental dissipativity theory to general dissipativity, such that we can have convex stability and performance analysis of NL systems if we apply the LPV framework.

2 Notions of dissipativity

The class of systems that is considered in this research is the class of continuous, NL, time-invariant systems. The first, well-known notion of dissipativity, introduced in [2], states that if the system is dissipative, the energy in a system is always less (or equal) than the initial energy plus the energy supplied to the system. Choosing the storage function, representing the stored energy in the system, and the supply function, representing the supplied energy to the system, as quadratic functions, standardizes the analysis, but

usually restricts dissipativity to be a local property, i.e. only valid around an equilibrium point. An extended notion of dissipativity is incremental dissipativity, where dissipativity between two arbitrary trajectories of the considered system is examined. Hence, if a system is incrementally dissipative, any two arbitrary trajectories of a system will always converge towards each other, since the energy between the two trajectories dissipates. A recent notion of dissipativity is differential dissipativity. If a system is differentially dissipative, the energy in the infinitesimal tangent variations of a system trajectory tends to zero, i.e. the system converges to some reference trajectory. Now the question is, how do we link these notions of dissipativity and how can we link performance analysis in the incremental or differential framework to performance of the NL system?

3 Performance analysis of NL systems

To link the different notions of dissipativity, we consider quadratic storage and supply functions. Defining the differential form of the NL system, describing infinitesimal variations in a trajectory of the NL system, and working out the differential dissipation inequality (DIE) for the differential form of the NL system results in a matrix inequality that shows differential dissipativity of an NL system. Similarly, considering the difference in trajectories of an NL system, working out the DIE, and by applying mean-value theorem results, under some mild conditions, in the same matrix inequality. Moreover, it is proven that differential dissipativity implies incremental dissipativity. Furthermore, considering a forced equilibrium point of the NL system as a trajectory, it can be concluded that if a system is incrementally dissipative, the system is dissipative w.r.t. any arbitrary forced equilibrium point. By applying the LPV framework to the differential form of the NL system, the matrix inequalities become linear and thus differential, incremental and general dissipativity of the NL system can be examined with convex analysis.

References

[1] P. J. W. Koelewijn, R. Tóth, G. S. Mazzoccante, and H. Nijmeijer, "Nonlinear Tracking and Rejection using Linear Parameter-Varying Control," *Submitted to the IEEE Transactions on Control Systems Technology*, 2019.

[2] J. C. Willems, "Dissipative dynamical systems part I: General theory," *Archive for Rational Mechanics and Analysis*, 1972.

Trajectory convergence from coordinate-wise decrease of energy functions

Julien M. Hendrickx,
ICTEAM, UCLouvain, Belgium.
Email: `julien.hendrickx@uclouvain.be`

Balazs Gerencser
Alfred Rényi Institute of Mathematics, Hungary
Email: `gerencser.balazs@renyi.hu`

1 Abstract

We show a sufficient condition for convergence of a single trajectory based on each entry contributing non-positively to the evolution of an energy function along the trajectory.

2 Introduction

Classical approaches for establishing convergence based on an energy function V typically consider a dynamical system of the form $\dot{x} = f(x,t)$, and prove convergence of *all trajectories* (or all trajectories sufficiently close to some equilibrium point) under assumptions on $\nabla V(x) \cdot f(x,t)$ holding for all x and t. Particularly in cyber-physical systems or systems involving discrete computations or events, there may not exist a natural global evolution of the form $\dot{x} = f(x,t)$ defined outside of the specific trajectory considered. The speed $\dot{x}$ may indeed depend on various elements related to x (noise related to this history) communications with other systems, arbitrary events etc.

We follow here a different approach, establishing the convergence of a single trajectory based on a condition that is only required to hold along that specific trajectory. One can easily build examples of non-converging trajectories $y(t)$ satisfying $\frac{d}{dt}V(y(t)) < 0$ for all time. Hence some additional assumptions are needed. Our result show that *having each component of y contributing non-positively* to the evolution of $V(y(t))$ is sufficient for convergence.

3 Result

The following result generalizes Theorem 1(a) in [1], which only applied to quadratic energy functions V.

Theorem 1 *Let $V : \mathbb{R}^n \to \mathbb{R}$ be a twice-differentiable radially unbounded locally strongly convex function, and $y : \mathbb{R}_+ \to \mathbb{R}^n$ be an absolutely continuous function (so that $\dot{y}(t)$ exists a.e.) If for all t for which $\dot{y}(t)$ exists there holds*

$$\frac{\partial V}{\partial x_i}\dot{y}(t) \leq 0 \qquad \forall i = 1,\ldots,n. \tag{1}$$

Then $y^* = \lim_{t\to\infty} y(t)$ exists.

Theorem 1 does not have any implication about the convergence speed nor about the value of y^*, though one can easily deduce $V(y^*) \leq V(y(t))$ for all t. This apparent weakness is a direct consequence of the weakness of the assumptions and generality of the result: Observe indeed that (1) allows for constant trajectories with $\dot{y}(t) = 0$ or for trajectories stopping for an arbitrary long time before restarting, so no stronger conclusion could hold without stronger assumptions. Besides, the context in which the trajectory $y(t)$ exists may provide strong additional information about y^* once Theorem 1 guarantees its existence.

4 Future Works

Future works could relax the conditions of radial unboundedness and local strong convexity of V, extending and generalizing some results in [1] for positive semi-definite (SDP) quadratic functions. It was shown indeed Theorem 1 remains valid for energy functions of form $V = x^T L x$ with L the Laplacian of a connected graph, and which play a very important role in multi-agent applications. Somewhat weaker results about accumulation points of y were also obtained obtained for rank $n-1$ SDP quadratic functions $V = x^T A x$ under the surprising condition that no nontrivial vector of the kernel would contain any zero entry. All this suggests possible extensions of Theorem 1.

Acknowledgements

References

[1] J.M. Hendrickx, B. Gerencsér and B. Fidan, "Trajectory convergence from coordinate-wise decrease of quadratic energy functions, and applications to platoons", *IEEE Control Systems Letters*, 4(1), 151-156, 2019.

Incremental Stability based Analysis and Control of Nonlinear Systems using the LPV Framework

P.J.W. Koelewijn, R. Tóth and S. Weiland
Control Systems Group, Eindhoven University of Technology
P.O. Box 513, 5600 MB Eindhoven, The Netherlands
Email: {p.j.w.koelewijn,r.toth,s.weiland}@tue.nl

1 Introduction

The *Linear Parameter-Varying* (LPV) framework has been introduced to provide powerful tools for both analysis and controller synthesis of *Nonlinear* (NL) systems. It has allowed the systematic analysis and synthesis results from the *Linear Time-Invariant* (LTI) framework, such as $\mathscr{H}_2$ and $\mathscr{H}_\infty$ stability and performance, to be extended and used with LPV models, retaining their computational efficiency due to the convexity of the involved optimization problems. By means of the so-called 'embedding principle' the dynamics of an NL system can be represented in an LPV representation. Hence, this allows to apply the convex analysis and synthesis tools of the LPV framework to NL systems. Although the LPV framework has successfully been applied to a wide variety of applications, it has recently been shown that the current LPV analysis and synthesis methods are not always able to guarantee the desired stability and performance requirements for NL systems. In this paper we give an overview of our recent results and current research activities related to this problem.

2 Why the current LPV framework is inadequate

In [1] we have shown that in case reference tracking and disturbance rejection is considered, the current methods for analysis and synthesis in the LPV framework are inadequate to guarantee the desired stability requirements for NL systems. This is because the asymptotic stability results in the LPV framework only hold when the system is operating near the origin of the state-space. Hence, when a different equilibrium point is considered, e.g. when considering reference tracking and disturbance rejection, there are no guarantees that the desired stability and performance requirements are satisfied.

3 Appropriate notion of stability

In order to solve this an equilibrium independent notion of stability is required to guarantee the desired stability and performance requirements for NL systems, even when reference tracking and disturbance rejection is considered. One such notion is incremental stability, whereby stability is as-

(a) 'Standard' (asymptotic) stability.

(b) Incremental (asymptotic) stability.
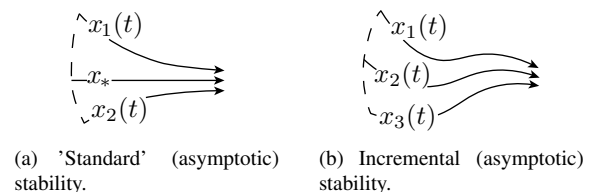
Figure 1: Considered notions of stability.

sessed with respect to different trajectories of the system instead of with respect to a specific fixed point, generally the origin, as in the case of 'conventional' stability, see also Fig. 1. Incremental (asymptotic) stability of an NL system, where the original system is referred to as the primal form, can then be assessed by assessing 'conventional' (asymptotic) stability of the so-called differential form of the system, i.e.

$$\dot{x}(t) = f(x(t)), \qquad \delta\dot{x}(t) = \frac{\partial f}{\partial x}(x(t))\delta x(t), \qquad (1)$$

where $x(t) \in \mathscr{X} \subseteq \mathbb{R}^{n_x}$ is the state of the primal form of the NL system and $\delta x(t) \in \mathbb{R}^{n_x}$ the state of the respective differential form of the NL system. Similar results can be derived in the discrete time case. By embedding the differential form in an LPV representation, the convex tools from the LPV framework can be used for incremental analysis of the NL systems. Moreover, in [2], we have developed convex synthesis tools for guaranteeing incremental ($\mathscr{L}_2$-gain) stability and performance requirements for continuous time NL systems. Current research developments are focussed on extending the incremental synthesis results to discrete time systems and developing a systematic framework for shaping the performance of the NL system when an incremental notion of performance is considered.

References

[1]   P. J. W. Koelewijn, G. Sales Mazzoccante, R. Tóth, and S. Weiland, "Pitfalls of Guaranteeing Asymptotic Stability in LPV Control of Nonlinear Systems," *Accepted to European Control Conference Saint Petersburg*, 2020.

[2]   P. J. W. Koelewijn, R. Tóth, and H. Nijmeijer, "Linear Parameter-Varying Control of Nonlinear Systems based on Incremental Stability," in *Proc. of the 3rd IFAC Workshop on Linear Parameter Varying Systems*, 2019.

Tuning Rules for Gradient Systems

Carmen Chan-Zheng[†], Pablo Borja, Jacquelien M.A Scherpen

ENgineering and TEchnology institute Groningen (ENTEG)

University of Groningen, The Netherlands

†c.chan.zheng@rug.nl

1 Abstract

A vast majority of control techniques (e.g., Passivity-based control) for physical systems are aimed to ensure the stability of the closed-loop system. However, in terms of practical implementation, these techniques might not be sufficient as these are not necessarily designed to achieve certain performance, i.e., to comply with the system's desired specifications. Addressing the performance is still an open problem, and therefore, we propose an approach to tune the gains for a particular nonlinear physical system class. We focus on a class in which can be described as a gradient system structure such as Port-Hamiltonian and Brayton-Moser systems. This is an important class since this covers a large variety of physical systems such as electrical networks, mechanical systems, etc. Our approach assumes that a control technique already stabilizes the nonlinear system, and then, we linearize the system. The linearized system is required to have a particular structure called *saddle point matrix* form, which can be obtained by a proper transformation. Next, we apply the tuning technique where a "no-overshoot" response is ensured. As an example, the proposed tuning rule is applied to a Brayton-Moser system.

2 Initial Results

Assuming that a stable linearized gradient system has the following structure:

$$\frac{d}{dt}\begin{bmatrix} \bar{x} \\ \bar{y} \end{bmatrix} = -\mathcal{N}\begin{bmatrix} \bar{x} \\ \bar{y} \end{bmatrix}, \quad \mathcal{N} = \begin{bmatrix} X & Z^\top \\ -Z & Y \end{bmatrix} \quad (1)$$

where $X = X^\top > 0 \in \mathbb{R}^{n \times n}$, $Z \in \mathbb{R}^{m \times n}$ has full rank, $Y = Y^\top \geq 0 \in \mathbb{R}^{m \times m}$, $\bar{x} \in \mathbb{R}^n$, $\bar{y} \in \mathbb{R}^m$ and $m \leq n$.

If $\lambda \in \mathbb{C}$ corresponds to an eigenvalue of system (1), then, $\mathscr{R}e(\lambda) < 0$ since it is stable by assumption. For a "no-overshoot" response, it is required that $\mathscr{I}m(\lambda) = 0$, i.e., the spectrum of $\mathcal{N}$ is positive real. The condition to satisfy $\mathscr{I}m(\lambda) = 0$ is proposed by the authors of [3]:

$$2||Z|| < \lambda_{min}(X) - \lambda_{max}(Y) \quad (2)$$

As an example, this condition is applied to tune a Brayton-Moser (BM) system. Brayton and Moser introduced some conditions in to ensure asymptotic stability for topologically complete nonlinear RLC-networks [1]. For sake of space, only the following condition is discussed:

$$||L^{1/2} R^{-1} \Gamma C^{-1/2}|| \leq 1 - \delta, \quad 0 < \delta < 1 \quad (3)$$

If (3) is satisfied then the following nonlinear system is asymptotically stable:

$$-\begin{pmatrix} -L(i) & 0 \\ 0 & C(v) \end{pmatrix}\frac{d}{dt}\begin{pmatrix} i \\ v \end{pmatrix} = \frac{\partial \mathscr{P}}{\partial z}\begin{pmatrix} i \\ v \end{pmatrix},$$

$$\mathscr{P}(i,v) := -\frac{1}{2}i^\top R i + G(v) + i^\top \Gamma v. \quad (4)$$

where $i \in \mathbb{R}^l$ and $v \in \mathbb{R}^c$ are the independent inductor currents and capacitor voltages, respectively. $L(i) = L^\top(i) > 0 \in \mathbb{R}^{l \times l}$ is the inductance matrix, and $C(v) = C^\top(v) > 0 \in \mathbb{R}^{c \times c}$ is the capacitance matrix, and lastly, $\mathscr{P} : \mathbb{R}^{l+c} \to \mathbb{R}$ is the *mixed-potential* function.

The variable δ from (3) is considered as a "fine-tuning" parameter [2]. To check the performance, consider the linearization of (4):

$$\frac{d}{dt}\begin{bmatrix} \bar{i} \\ \bar{v} \end{bmatrix} = -\underbrace{\begin{bmatrix} -L^{-1/2}P_{ii}L^{-1/2} & -L^{-1/2}P_{iv}C^{-1/2} \\ C^{-1/2}P_{vi}L^{-1/2} & C^{-1/2}P_{vv}C^{-1/2} \end{bmatrix}}_{:=\mathscr{A}}\begin{bmatrix} \bar{i} \\ \bar{v} \end{bmatrix} \quad (5)$$

where $\bar{i}$ and $\bar{v}$ is the linearized current and voltage variables, respectively. Note that the matrix $\mathscr{A}$ corresponds to the form of (1). Therefore, inspired by the work of the author [3], we have the following result:

Proposition 1. *Assuming that $G(v)$ is constant and (3) holds, then, the system described in (4) has no overshoot when $\frac{1}{2} \leq \delta < 1$.*

We aim to extend this applicability to other system domains, in particular, to propose tuning rules for underactuated mechanical systems.

References

[1] RK Brayton and JK Moser. A theory of nonlinear networks. i. *Quarterly of Applied Mathematics*, 22(1):1–33, 1964.

[2] Dimitri Jeltsema and Jacquelien MA Scherpen. Tuning of passivity-preserving controllers for switched-mode power converters. *IEEE Transactions on Automatic Control*, 49(8):1333–1344, 2004.

[3] Jörg Liesen and Beresford N Parlett. On nonsymmetric saddle point matrices that allow conjugate gradient iterations. *Numerische Mathematik*, 108(4):605–624, 2008.

Linear Parameter-Varying Embedding of Nonlinear Models Based on Polynomial Approximation

Arash Sadeghzadeh, Roland Tóth

[1] Control Systems Group, Eindhoven University of Technology, Eindhoven, The Netherlands

Emails: `a.sadeghzadeh@tue.nl`, `r.toth@tue.nl`

1 Introduction

The linear-parameter varying (LPV) methodology is a powerful tool to tackle model based controller synthesis problem for nonlinear systems [1]. However, the most challenging issue is to first obtain an LPV model for the nonlinear systems suitable for the LPV control synthesis. The present work considers this problem. The objective is to cast the LPV embedding problem into an optimization problem in which the scheduling variable selection, model complexity, and model accuracy are simultaneously taken into account. To obtain more accurate models, the required LPV model is considered to depend polynomially on the scheduling variables.

2 Problem Statement

Consider the continuous-time nonlinear system

$$\dot{x}(t) = F_1(x(t)) + G_1(x(t))u(t)$$
$$y(t) = F_2(x(t)) + G_2(x(t))u(t) \tag{1}$$

where $x(t) \in \mathcal{X} \subset \mathbb{R}^n$ is the state vector, $u(t) \in \mathbb{R}^m$ is the exogenous input, $y(t) \in \mathbb{R}^q$ is the system output. $\mathcal{X}$ is assumed to be a bounded polyhedron with known vertices including the origin. $F_1(x) : \mathcal{X} \to \mathbb{R}^n$, $F_2(x) : \mathcal{X} \to \mathbb{R}^q$, $G_1(x) : \mathcal{X} \to \mathbb{R}^{n \times m}$, $G_2(x) : \mathcal{X} \to \mathbb{R}^{q \times m}$ are static real-valued nonlinear analytic functions of x defined on $\mathcal{X}$. The ultimate goal in this paper is to embed this nonlinear system in a linear parameter-varying representation as follows:

$$\dot{x}(t) = A(\alpha(t))x(t) + B(\alpha(t))u(t),$$
$$y(t) = C(\alpha(t))x(t) + D(\alpha(t))u(t), \tag{2}$$

where $\alpha(t) = \begin{bmatrix} \alpha_1(t) & \alpha_2(t) & \cdots & \alpha_v(t) \end{bmatrix}^\top \in \mathbb{R}^{n_\alpha}$ is the scheduling variable vector and

$$\underline{\alpha}_i \leq \alpha_i(t) \leq \overline{\alpha}_i, \quad i = 1, \cdots, v$$

with $\underline{\alpha}_i, \overline{\alpha}_i \in \mathbb{R}$ that to be determined by the proposed approach. The objective here is to obtain an accurate

LPV model as possible for a pre-chosen number of scheduling variables, i.e. for all the admissible values of $x(t)$, the trajectories of $A(\alpha(t))x(t)$, $C(\alpha(t))x(t)$, $B(\alpha(t))$, and $D(\alpha(t))$ should be as close as possible to $F_1(x(t))$, $F_2(x(t))$, $G_1(x(t))$, and $G_2(x(t))$, respectively. Note that there exists a trade-off between the number v, functional dependency with respect to the scheduling variables, and the model accuracy.

3 Proposed Method

In the proposed approach, the state-space matrices of the LPV model (2) are designed such that they depend polynomially on the scheduling variables. The outline of the proposed algorithm is as follows:

• The nonlinear functions in (1) are approximated as polynomial functions of user-defined order using polynomial regression method, where argument selection to minimize the scheduling dimensions is also considered.

• The difference between the original nonlinear functions and their approximations, which are so-called residuals, are also considered as the scheduling variables to obtain more accurate models in addition to the appeared scheduling variables in the previous step.

• A principle component analysis (PCA) is utilized to reduce the likely high number of the scheduling variables resulting from previous steps, to obtain a model with minimal number of the scheduling variables.

This way, a polynomially dependent LPV model is obtained in which the scheduling variables consist of some of the state variables, and additionally, some variables which are the linear combinations of the residuals. Numerical studies reveal the capability of the proposed method to deliver more accurate LPV models with less number of the scheduling variables in comparison with exiting methods.

References
[1]   C. Hoffmann and H. Werner, "A Survey of Linear Parameter-Varying Control Applications Validated by Experiments or High-Fidelity Simulations," *IEEE Transactions on Control Systems Technology*, 23(2), 416-433, 2015.

Nearest Neighbor Control
For Incrementally Passive Nonlinear Systems
With Known Constant Input

M. Z. Almuzakki[1,*], B. Jayawardhana[1], & A. Tanwani[2]

[1]Engineering and Technology Institute Groningen, University of Groningen, Groningen 9747AG, the Netherlands.
[2]Laboratory for Analyses and Architecture of Systems (LAAS) – CNRS, Université de Toulouse, France.
*Corresponding author e-mail: m.z.almuzakki@rug.nl.

1 Abstract

In this work, we study the problem of practical output-feedback stabilization of incrementally passive nonlinear systems with respect to a known constant input using a finite set of control actions. A preliminary study on practical stabilization around the origin has been conducted in [1] where, under some passivity and observability assumption on the system, and for a given set of discrete control actions, a nearest-neighbor control law can be used to globally practically stabilize the system. Moreover, the study give an insight that it is sufficient to have $m+1$ nonzero control actions, with m being the input dimension, in addition to the zero control action in order to achieve global practical stabilization for a passive system.

In many control applications, the desired equilibrium point of the system in study may not be equal to zero. Instead, it may corresponds to an arbitrary constant input. For these cases, the notion of incremental systems with respect to constant inputs can be used to design the appropriate control law to stabilize the system around the desired equilibrium point, see for example [2]. Furthermore, we are interested in implementing the nearest-neighbor control law for practical stabilization around the desired, not necessarily zero, equilibrium point. The natural question that arise from this problem is how to adapt the conditions in [1] for incrementally passive systems with respect to constant input and how to map the output such that the stability requirements are satisfied.

The systems considered in this work are given by

$$\Sigma : \begin{cases} \dot{x} & = f(x) + g(x)u \\ y & = h(x) \end{cases} \tag{1}$$

where the state $x(t) \in \mathbb{R}^n$, the output $y(t) \in \mathbb{R}^m$ and the input $u(t) \in \mathcal{U} := \{0, u_1, \dots, u_p\}$ with $u_i \in \mathbb{R}^m$ for all $i = 1, \dots, p$. The function $f, g,$ and h are assumed to be $\mathcal{C}^1$ differentiable, $f(0) = 0$, $g(x)$ is full-rank for all x and $h(0) = 0$.

In [1], the assumptions imposed in order to practically stabilize Σ around the origin are: (i) the system Σ is passive with proper storage function H satisfying $\dot{H} \leq y^\top u$; (ii) the system Σ with $u = 0$ is large-time norm-observable for some $\tau > 0$ and $\gamma \in \mathcal{K}_\infty$ [3]; and (iii) $0 \in \text{int}(\text{conv}(\mathcal{V}))$ for some $\mathcal{V} \subseteq \mathcal{U}$. In this work, the assumptions (i), (ii), and (iii) above are adapted in the following:

(A1) for any steady-state pair

$$(x^*, u^*) \in \{(x^*, u^*) \in \mathbb{R}^n \times \mathbb{R}^m \mid f(x^*) + g(x^*)u^* = 0\},$$

the system Σ is incrementally passive with respect to u^*, with proper storage function H_0 satisfying $\dot{H}_0 \leq \bar{y}^\top \bar{u}$, where $\bar{(\cdot)} = (\cdot) - (\cdot)^*$ and $y^* = h(x^*)$;

(A2) the incremental system with $u = u^*$, i.e. the system

$$\begin{cases} \dot{\bar{x}} & = f(\bar{x} + x^*) - f(x^*) + (g(\bar{x} + x^*) - g(x^*))u^*, \\ \bar{y} & = h(\bar{x} + x^*) - h(x^*), \end{cases}$$

is large-time norm-observable for some $\tau > 0$ and $\gamma \in \mathcal{K}_\infty$ [3]; and

(A3) for a given discrete set $\mathcal{U}$, $u^* \in \text{int}(\text{conv}(\mathcal{V}))$ for some $\mathcal{V} \subseteq \mathcal{U}$.

Proposition 1.1. *Consider the system Σ satisfying (A1) and (A2), along with a discrete set $\mathcal{U} \supset \mathcal{V}$ satisfying (A3) so that there exists a scalar δ such that for each $y \in \mathbb{R}^m$,*

$$\|y - u^*\| > \delta \Rightarrow \exists\, v_i \in \mathcal{V} \text{ s.t. } \|v_i + y - 2u^*\| < \|y - u^*\|.$$

For a given $\varepsilon > 0$ assume that $\gamma(\delta) \leq \varepsilon$. Then by defining

$$\phi(y) := \arg\min_{v \in \mathcal{U}} \{\|v + y\|\} \tag{2}$$

the control law $u = \phi(\bar{y} - u^*)$ globally practically stabilizes Σ with respect to $\mathbb{B}_\varepsilon(x^*)$ (ball with radius ε centered at x^*).

References

[1] B. Jayawardhana, M. Z. Almuzakki, and A. Tanwani (2019). *Practical Stabilization of Passive Nonlinear Systems with Limited Control.* 11th IFAC Symposium on Nonlinear Control Systems 2019. IFAC-PapersOnLine, 52(16), 460–465.

[2] B. Jayawardhana, R. Ortega, E. Garcia Canseco, and F. Castaños (2007). *Passivity of nonlinear incremental systems: application to PI stabilization of nonlinear RLC circuits.* Systems and Control Letters, 56(9-10), 618–622.

[3] J.P. Hespanha, D. Liberzon, D. Angeli, and E.D. Sontag (2005). *Nonlinear Norm-Observability Notions and Stability of Switched Systems.* IEEE Trans. Autom. Control, 50(2), 154–168.

Graphical modeling for supervisor synthesis

F.F.H. Reijnen, J.M. van de Mortel-Fronczak, M.A. Reniers, J.E. Rooda
Control Systems Technology Group, Department of Mechanical Engineering
Eindhoven University of Technology
P.O.Box 513 5600 MB Eindhoven, The Netherlands

1 Introduction

High-tech systems have become increasingly complex due to the increase in required functionality and required safety. As a result, supervisory controllers for these systems are getting more complex as well. Formal methods, such as supervisor synthesis introduced in [1], can help to overcome this growing complexity. A discrete-event model of the plant (representing what the system can do) and a model of the control requirements (representing what the system may do) are used to synthesize a correct-by-construction supervisor that adheres to the requirements and is controllable, non-blocking, and maximally permissive.

In this paper, the design of supervisors for a family of similar systems is investigated. Inspired by the work of [2], standardized modeling components (called modules) are used.

2 Modeling method

The proposed modeling method is as follows. When a supervisor for a system has to be synthesized, firstly, the subsystems in the plant are modeled by instantiating modules from a library. The module can be customized via parameters. Secondly, the requirements model is partitioned into internal requirements, i.e., requirements inside a module, and external requirements, i.e., requirements between modules. The internal requirements are also standardized. The external requirements are manually modeled. For each module, a set of external events and external states is defined that can be used in the model of the external requirements. A supervisor for the system can now be synthesized from the discrete-event plant (composed out of the modules), the internal requirements, and the external requirements.

A prototype tool has been developed for the design of supervisors for movable bridges. This prototype is used to generate model code that serves as input for synthesis in the CIF toolset [3]. The tool consists of a graphical interface, shown in Figure 1, where a user can instantiate components on a canvas, using the mouse cursor, an area where requirements can be modeled, and a model library.

3 Case study

To demonstrate the method, the tool has been used to model a family of seventeen bridges located in the Wilhelmina canal, the Netherlands.
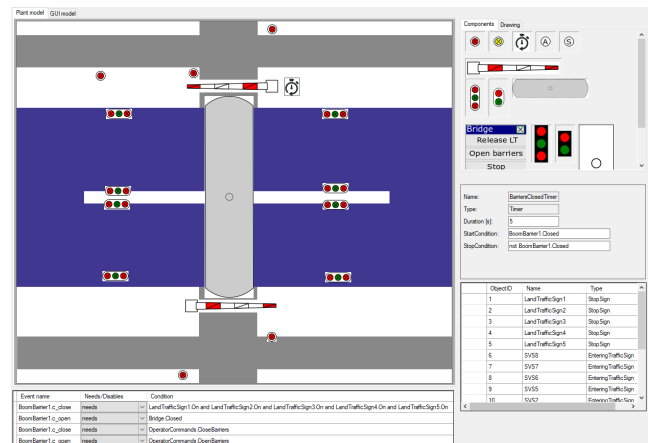
Figure 1: The interface of the tool, displaying the Oisterwijksebaan bridge in Tilburg, the Netherlands.

It was possible to model the bridges with the modules present in the library. After modeling the external requirements, the CIF toolset was able to synthesize a supervisor for each of the bridges. Monolithic synthesis has been used. The synthesis takes a few seconds. The results show that this method is suitable for designing supervisors for a family of movable bridges.

Acknowledgements

References

[1]   P. Ramadge and W. Wonham, "Supervisory control of a class of discrete event processes", in SIAM Journal on Control and Optimization, 25(1), pp. 206-230, 1987.

[2]   L. Grigorov, B. Butler, J. Cury, and K. Rudie, "Conceptual design of discrete-event systems using templates", in Discrete Event Dynamic Systems, 21(2), pp. 257-303, 2011.

[3]   D. van Beek, W. Fokkink, D. Hendriks, A. Hofkamp, J. Markovski, J. van de Mortel-Fronczak, M. Reniers, "CIF 3: Model-based engineering of supervisory controllers", in Proceedings of TACAS, Springer, pp 575–580, 2014.

Model reduction for supervisor synthesis

L. Moormann[1], J.M. van de Mortel - Fronczak[1], W.J. Fokkink[2], J.E. Rooda[1]
[1]Eindhoven University of Technology and [2]Vrije Universiteit Amsterdam
l.moormann@tue.nl

1 Introduction

The design of supervisory controllers for cyber-physical systems is an increasingly complex task due to the rising demand for functionality and safety. Through the use of formal methods, such as synthesis-based engineering, correct by construction supervisory controllers can be synthesized. To perform synthesis, first a discrete-event model is created that specifies what the system *can* do. This model is called the plant. Second, requirement models are created to specify what the system *may* do.

In [1], it is shown that under certain conditions the models can be reduced before synthesis, or that synthesis can be skipped entirely. In this work, the method presented there is extended to further reduce the plant and the requirement models, subsequently the method is applied in a case study.

2 Method

The method of [1] uses directed graphs, such as the one shown in Figure 1. In this graph, the vertices indicate components of the plant models and edges indicate dependencies between these components. The edges are based on the requirement models: there is an edge from the vertex of component A to the vertex of component B if there exists a requirement for component B that depends on component A. Cycles in the graph are indicated with red arrows. In [1], it is shown that synthesis can be skipped if the directed graph of a system contains no overlapping extended strongly connected components. Furthermore, if synthesis is needed, then all vertices without outgoing edges can be omitted during synthesis.

Models that contain dependency cycles can be reduced further by using the theory from [2]. In [2], symmetry is formally defined for discrete-event systems for the purpose of model reduction. This definition can be applied to the directed graphs of [1]. If the component models and requirement models of two vertices are symmetric, only one vertex needs to be included during synthesis. If synthesis for the reduced model does not add any new restrictions, then synthesis can be skipped entirely for the complete system.

3 Results

The proposed method has been applied to a case study in which a supervisory controller is designed for the Eerste Heinenoordtunnel (EHT), a roadway tunnel in the Netherlands. Figure 1 shows the initial graph of this model. This initial graph contains 369 vertices and 413 edges.
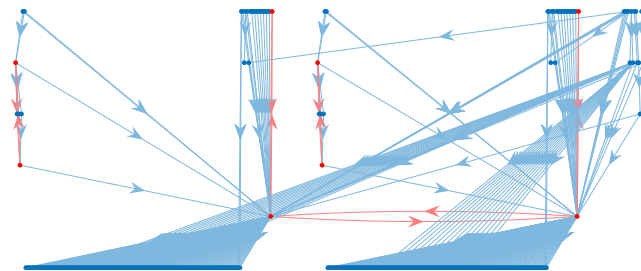
Figure 1: Directed graph of the initial EHT model.

First, the method from [1] is applied to reduce the model to 51 vertices and 73 edges. Second, the addition to this method is applied to reduce the model further to 21 vertices and 28 edges. Figure 2 shows this reduced graph.
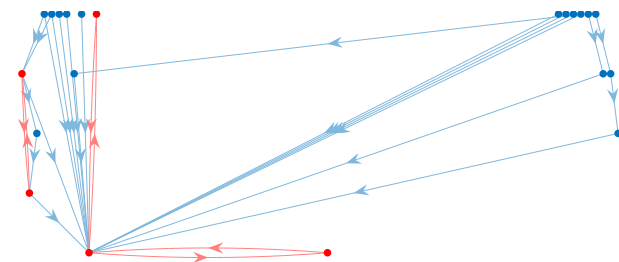
Figure 2: Directed graph of the reduced EHT model.

An attempt has been made to synthesize supervisors for the three models. Due to memory issues, no supervisor could be synthesized for the initial model. After model reduction, a supervisor has been synthesized for the two reduced models.

4 Conclusions and future work

A method has been proposed to extend the model reduction method of [1] for the purpose of supervisor synthesis. This method has been applied successfully to a case study. Future research will focus on possibilities to further reduce the number of vertices and edges in the model.

Acknowledgments

References

[1]   M.A. Goorden et al., "Model properties for nonblocking modular supervisors", Submitted to *IEEE Transactions on Control Systems Technology*

[2]   L. Moormann et al., "Efficient validation of supervisory controllers using symmetry reduction", Submitted to *Workshop on Discrete Event Systems 2020*

Supervisory Control for Product Lines with Dynamic Feature Configuration

Sander Thuijsman and Michel Reniers

Department of Mechanical Engineering

Eindhoven University of Technology, The Netherlands

Email: `s.b.thuijsman@tue.nl`

1 Introduction

In modern product development, companies often do not design products one-by-one anymore. Instead, they design *product lines*. By applying *product line engineering*, companies exploit the variability between possible configurations of products. By doing so, they increase product individualization, reduce development costs, reduce time-to-market, and enhance product quality [1].

In *supervisory control theory*, the uncontrolled system and a specification of its behavioral requirements are modeled. This model is then used to perform *supervisor synthesis*; an algorithmic computation that generates a correct-by-construction supervisory controller for the system in accordance with the requirements. Ter Beek et al. [2] were the first to apply product line engineering to supervisory control. They provided an approach to model product lines CIF 3 using *feature models*. A supervisor is generated that contains the behavior for each valid product configuration.

The product configuration might change dynamically. For instance because a component or a component is upgraded. Ter Beek et al. [2] only consider a static product configuration. We extend their methodology for product lines with dynamic (re-)configuration.

2 Modeling of feature model

In Figure 1 a feature model for a wiper system is shown, taken from [3]. This model defines that the system consists out of a sensor, a wiper, and optionally a permanent wiping feature. The sensor and wiper both come in alternatively a low- or high quality version. The low quality sensor can only detect whether it rains or not, while the high quality sensor can also detect how heavy it rains. The low quality wiper can only be on and off, for the high quality wiper the speed can be set. An example of a valid product instance is a wiper system containing a low quality sensor, a high quality wiper, and no permanent wiping feature.

Figure 1 also shows a variable name for each of the features. This is a Boolean variable that is true if the feature is present and false otherwise. These variables can be used to construct logical expressions to represent the feature model in CIF 3. For example, the following expression evaluates to true if both the sensor and wiper are present: `r ⇔ (s and w)`.
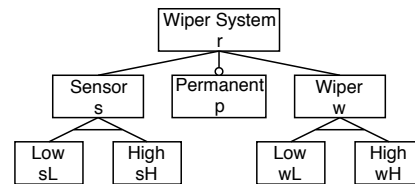
Figure 1: Feature model for wiper system.

3 Modeling of behavior

The uncontrolled behavior of the components is modeled using automata in `CIF 3`. Components are restricted so that they only execute behavior when they are present. Inter-component requirements can be formulated, and be based on their presence. For example, *quickwipe* needs `wH and ((sH and detected_heavy) or (sL and detected))`. To allow for reconfiguration, *come* and *go* events are added to the model. When these events occur, the presence value of the component is updated. It is possible that due to these events the configuration is invalid temporarily. There are multiple ways the modeler can deal with this. For example, it is possible to simply disallow all or some particular events, or apply additional requirements.

4 Result

Synthesis is performed on the combined feature and behavioral model. A supervisory controller is obtained that has different sets of states representing different valid configurations, and these sets are connected by the *come* and *go* events for reconfiguration.

Acknowledgment

References

[1] Pohl, K., Böckle, G., and van der Linden, F. (2005). *Software Product Line Engineering: Foundations, Principles and Techniques.* Springer-Verlag, Berlin, Heidelberg.

[2] ter Beek, M., Reniers, M., and de Vink, E. (2016). Supervisory controller synthesis for product lines using CIF 3. In *Leveraging Applications of Formal Methods, Verification and Validation: Foundational Techniques*, 856-873.

[3] Classen, A. (2010). *Modelling with FTS: a collection of illustrative examples.* Technical report, University of Namur.

Correct-by-design control synthesis for stochastic systems

B.C. van Huijgevoort [1] and S. Haesaert[1]

Abstract
Verified control synthesis of continuous stochastic systems is in general a difficult and computationally expensive task. In this work, we reduce the conservatism of this synthesis to make the computations more effective.

Introduction: Airplanes, cars, and power systems are examples of safety-critical control systems. These systems are often best described by stochastic discrete-time models. For these systems, we are interested in the design of controllers that provably satisfy formal specifications. To enable this correct-by-design control synthesis, finite-state models can be computed that approximate the original, continuous-state models with bounded deviations. Leveraging these bounds, we can use the finite-state models to synthesize certified controllers for the original continuous-state models. Computing both the finite-state models and the corresponding error bounds is in general difficult, time consuming and conservative. To reduce this conservatism we tailor this abstraction procedure to the specification. More specifically, we design the error bounds, expressed via simulation relations, between the original and abstract model in a specification guided fashion.
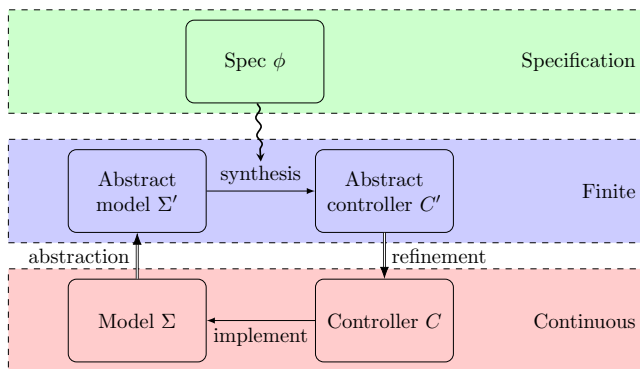
Figure 1: Illustration of correct-by-design control synthesis

Problem statement: Consider a discrete-time stochastic system Σ whose behaviour can be described by stochastic difference equations. For this system, we want to design a controller C such that the composed system $\Sigma \times C$ satisfies a formal specification ϕ with a high probability. This specification can be given as a temporal formula to represent either simple specifications over the state space of the system such as reach-avoid, invariance, liveness or more complex combinations thereof. Given specification ϕ, the synthesis

problem becomes

$$\sup_{C} \mathbb{P}(\Sigma \times C \vDash \phi). \tag{1}$$

However, for continuous-state models there does not exist an analytical solution to this problem.

Approach: In order to perform control synthesis for stochastic models with guarantees, we approximate the continuous-state models by finite-state Markov Decision Processes Σ', for which it is possible to verify certain temporal logic specifications. This method is known as correct-by-design control synthesis [1] and is schematically shown in Figure 1. The top *specification* layer gives the desired behaviour of the controlled system using temporal logic and is used to synthesize an abstract controller over the abstract, finite-state model. This controller is refined from the *finite* layer to the *continuous* layer, leading to controller C. To bound the approximation error caused by using a finite-state model, we use simulation relations [2] that bound deviations in the output ε and in the probability δ. Therefore, the computation of the satisfaction probability of ϕ, $\Sigma \times C \vDash \phi$, is replaced by a robust computation [3] that yields a lower bound, that is,

$$\mathbb{R}^{\varepsilon,\delta}(\Sigma' \times C' \vDash \phi) \leq \mathbb{P}(\Sigma \times C \vDash \phi). \tag{2}$$

The deviation bounds increase the conservatism of this robust computation leading to a lack of accuracy and a smaller chance of finding a controller. In this work, we design the error bounds between the original and abstract model in a specification-guided manner. The approach can now be mathematically formulated as follows

$$\begin{aligned}
&\sup_{\varepsilon,\delta} \sup_{C'} \quad \mathbb{R}^{\varepsilon,\delta}(\Sigma' \times C' \models \phi) \\
&\text{subject to} \quad \Sigma' \preceq_{\varepsilon,\delta} \Sigma.
\end{aligned} \tag{3}$$

Satisfying (3) implies that the lower bound of the satisfaction probability of the specification is maximized with respect to the specification.

References

[1]   M. Mazo, A. Davitian, and P. Tabuada. "Pessoa: A tool for embedded controller synthesis." *International Conference on Computer Aided Verification*, 2010

[2]   S. Haesaert, S. Soudjani, and A. Abate. "Verification of general Markov decision processes by approximate similarity relations and policy refinement." *SIAM Journal on Control and Optimization*, 2017.

[3]   S. Haesaert, S. Soudjani, and A. Abate. "Temporal logic control of general Markov decision processes by approximate policy refinement." *IFAC-PapersOnLine*, 2018

[1]Control Systems group, Eindhoven University of Technology, Email: b.c.v.huijgevoort@tue.nl

Synthesis of efficient failure-recovering supervisors

N. Paape*, J.M. van de Mortel-Fronczak*, L. Swartjes**, M.A. Reniers*
* Eindhoven University of Technology and ** Vanderlande Industries B.V.
(Email: n.paape@tue.nl)

1 Problem statement

In automated systems, supervisory controllers — or in short supervisors — are utilized to guarantee machine safety and specified functionality. These properties need to be guaranteed when system behavior is nominal, but also when faults occur in the system. However, designing valid supervisors for such systems is becoming increasingly more complex.

As shown in [1], a system and its supervisor can usually be approximated as *discrete-event systems* (DES), with the system generating uncontrollable events at discrete instances in time, and the supervisor enabling or disabling controllable events to guarantee machine safety and functionality.

In [2], a method is proposed to synthesize fault-tolerant supervisors using extended finite-state automata and state-based requirement models. However, we identified a subclass of faults — *failures* — for which this methodology results in a supervisor which is overly restrictive; if all *critical* (unsafe after failure) states are made unreachable, then as a result specified functionality gets disabled too.

To give an example, suppose there is a system with two (controllable) components: a conveyor and a sorter. The system has one (uncontrollable) diagnoser which detects if the sorter has jammed. The automata of these components are depicted graphically in Figure 1. Suppose a safety requirement is that the system is unsafe if a jam failure occurs when either the conveyor is on, or the sorter is sorting. The resulting fault-tolerant supervisor is too restrictive as the conveyor is not allowed to turn on, nor may the sorter sort.

2 Our contribution

We developed a procedure for the synthesis of *efficient failure-recovering supervisors*. In a system under control of an efficient failure-recovering supervisor, quick and controllable recovery from a failure is guaranteed.

(a) Conveyor   (b) Sorter
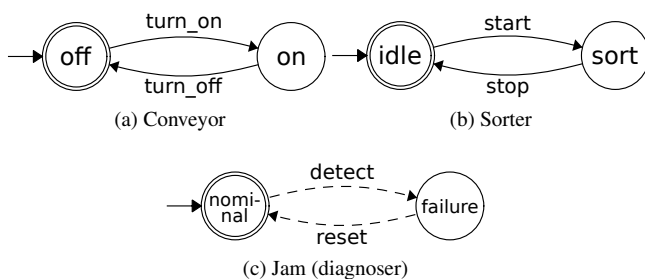
(c) Jam (diagnoser)

Figure 1: The system components and the jam diagnoser.
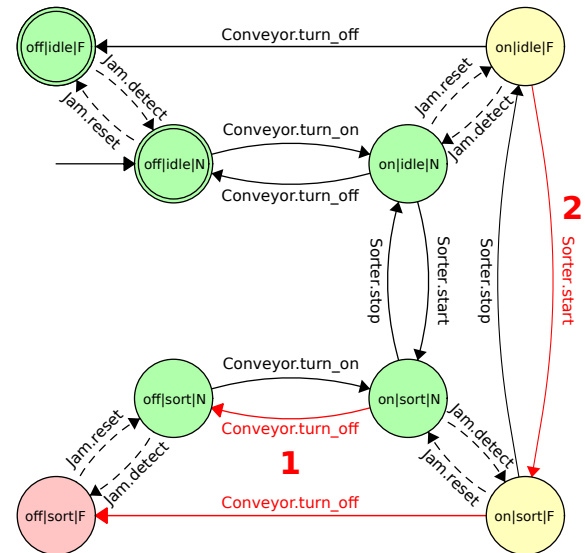
Figure 2: Efficient failure-recovering supervisor synthesis.

For every possible failure, a *recovery objective* is defined; a condition which must be fulfilled as quickly as possible after the failure is detected. All post-failure states in which this objective is not satisfied are defined as critical states.

For all critical states in a system, the efficient failure-recovering supervisor enforces the shortest path of controllable events to a state in which the recovery objective is satisfied. If no such path exists, then the state is regarded *unrecoverable*, and it is made unreachable by the supervisor.

An example is given in Figure 2, in which efficient failure-recovering supervisor synthesis is displayed for a hypothetical sorting system (the requirements it adheres to are omitted due to space limitations). In the figure, noncritical states are green, recoverable critical states are yellow, and unrecoverable critical states are red. The recovery objective for the jam failure is that the conveyor must be off, and sorter must be idle. In the synthesized supervisor, the red transitions indicated by a 1 are disabled as to make unrecoverable states unreachable, and the red transition indicated by a 2 is disabled to allow only the shortest failure-recovery paths.

References

[1]   W.M. Wonham and K. Cai, "Supervisory Control of Discrete-Event Systems," Communications and Control Engineering, Springer International Publishing, 2019.

[2]   F.F.H. Reijnen, M.A. Reniers, J.M. van de Mortel-Fronczak and J.E. Rooda, "Structured Synthesis of Fault-Tolerant Supervisory Controllers," IFAC-PapersOnLine, 51(24), pp. 894-901, 2018.

Strategies of drug dosing based on pharmacokinetic models

Pauline Thémans[*], Flora T. Musuamba[†], and Joseph J. Winkin[*]

[*]Namur Institute for Complex Systems (naXys) and Department of Mathematics,
University of Namur, Rempart de la Vierge 8, B-5000 Namur, Belgium
Email: `pauline.themans@unamur.be`, `joseph.winkin@unamur.be`
[†]Federal Agency for Medicines and Health Products, Brussels, Belgium
Email: `flora.musuambaTshinanu@fagg-afmps.be`

1 Context

Pharmacokinetics (PK) is a particular field of clinical pharmacology that studies how a drug evolves after administration to an organism. In particular, it aims to quantify the interation between the dose and the drug exposure in patients (concentration-time profile) through mathematical models. The aim of this contribution is to report analytical and individual-based methods for effective antibiotic dose selection, that are based on tools from systems and control theory (see [1]). These methods are designed to ensure their applicability in clinical practice. Treatments given by constant intravenous infusion at regular dosing intervals are considered. Results are exemplified by a case study for which numerical results are reported, namely *meropenem*, a β-lactam antibiotic used for treating severe infections.

2 Population pharmacokinetic models

Pharmacokinetic models were fitted to observed (systemic and sparse infection-site) concentrations in patients with severe nosocomial pneumonia. They are linear finite-dimensional linear state-space representations. Fitting and predictive performances were evaluated by internal and external validations, including numerical and visual tools (bootstraping, diagnostic scatter plots, etc.). A brief system analysis proves that such models are nonnegative and stable. The developed models are used as starting point to design control strategies which provide guidelines (decision-making aid) for drug dosing in patients, based on relevant patient's characteristics (covariates) and on any other practical condition (target exposure for efficacy, dosing interval, infusion duration, price, etc.). A fundamental challenge is to deal with the random components included in the PK models, describing the interindividual variability (IIV) in drug concentrations (see e.g. [2]).

3 Individualized drug dosing

Meropenem is a time-dependent antibiotic, meaning that treatment afficacy is measured in terms of percentage of the time between two doses that the drug concentration is maintained above a target minimal level (MIC).

In the scientific litterature, dosing of antibiotics is frequently based on Monte Carlo simulations from a mathematical pharmacokinetic model to assess the probability of target attainment (PTA), regarding a given PK/PD target (e.g. 100%T>MIC), at a population level. These probabilities can be compared between different dosing regimens to select the "optimal" one for the population under study (see e.g. [3]).

In the PhD work of the first author, an alternative *analytical* method for dosing recommendation is proposed, in contrast to the *empirical* analysis described above. Moreover, this method is designed to compute a dose at a *patient level*, in contrast to *population level*. Some parameters, namely the dosing interval and the duration of the infusion, would be clinician's decisions. An input-output analysis leads to a formula which determines the amount of drug to administrate (dose), given the covariates (patient level) and the practical conditions (see [1]). It can be seen as an open-loop control law. This input-output formula can then been incorporated into a "worst-case" analysis to deal with the variability and the unknown realization of the random variables. This obviously leads to a more conservative value. Finally, the design of an (estimated) state feedback, based on measurements of concentration equally spaced in time, is also considered.
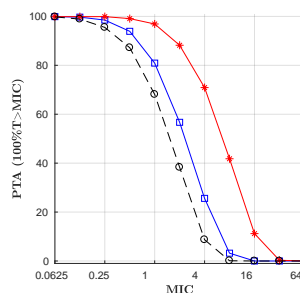
PTA based on model predictions for a virtual patient: blue line with squares, red line with stars and black line with circles correspond to the doses associated to the nominal model, the "worst-case" and the provider recommendation, respectively.

References

[1]   P. Thémans, F. T. Musuamba, J. J. Winkin. Model-based strategies of drug dosing for pharmacokinetic systems. 2019 (submitted).

[2]   D. R. Mould and R. N. Upton. Basic concepts in population modeling, simulation, and model-based drug development-part 2: Introduction to pjarmacokinetic modeling methods. *CPT Pharmacometrics Syst Pharmacol*, 2(4):1-14, 2013.

[3]   F. Frippiat, F. T. Musuamba, et al. Modelled target attainment after meropenem infusion in patients with severe nosocomial pneumonia: The PROMESSE study. *Journal of Antimicrobial Chemotherapy*, 70(1):207-216, 2015.

Dynamical analysis of an age-dependent SIR epidemic model

Candy Sonveaux and Joseph J. Winkin

Namur Institute for Complex Systems (naXys) and Department of Mathematics
University of Namur, rempart de la Vierge 8, B-5000 Namur, Belgium
Email: candy.sonveaux@unamur.be, joseph.winkin@unamur.be

Epidemic models aim to describe the evolution of diseases in order to have a better understanding of these processes. Those models allow the comparison, planification and implementation of some prevention, therapy or control programs. Here, we are interested in vaccination as control policy.

In our work, an adapted version of the well-known SIR model of Kermack and McKendrick [5] is used. Thus the population is assumed to be divided in three disctinct classes : the group S of uninfected individuals susceptible to catch the disease; the group I of infected individuals who can transmit the disease and the group R of recovered individuals who are permanently immune to the disease. This is the main assumption in a SIR model, which is a simple but validated and widespread model.

The particularity of this work is to take account of the importance of the individuals age in the model. It is motivated by the fact that several factors in diseases propagation depend on the age of the individuals, vaccination being one of them.
The dynamics of the disease propagation are based on the model described in [1]. Here proportions are used, as suggested in [2, Chapter 6]. The dynamics are given by this set of integro-partial differential equations, for $t \geq 0$ and $a \in [0, L]$,

$$
\begin{cases}
\partial_t s(t,a) + \partial_a s(t,a) = -\theta(a) s(t,a) \\
\qquad\qquad - \beta(a) \int_0^L i(t,b) P(t,b)\, db\, s(t,a), \\
\\
\partial_t i(t,a) + \partial_a i(t,a) = -\gamma(a) i(t,a) \\
\qquad\qquad + \beta(a) s(t,a) \int_0^L i(t,b) P(t,b)\, db
\end{cases}
\tag{1}
$$

under initial conditions $s(0,a) = s_0(a)$, $i(0,a) = i_0(a)$ and boundary conditions $s(t,0) = 1$, $i(t,0) = 0$. The parameters $\theta(a)$ and $\beta(a)$ are the vaccination rate, which is the control variable, and the disease transmission rate between s and i individuals, respectively. Both are assumed to be dependent on the individuals age. Moreover, L is the maximal life duration in the considered population P. Finally, the proportion of recovered indiviuals is given by $r(t,a) = 1 - s(t,a) - i(t,a)$.

The first main goals of this research are to study the well-posedness of model (1) and to perform the stability analysis of its equilibria. This was performed by applying techniques and results from [3] and [4] to model (1). We re-

port the existence and uniqueness of a nonnegative solution for the system by using a semigroup formulation of model (1) and a theorem applied to a specific semilinear Cauchy problem. Moreover, the model is realistic in the sense that the quantities s and i are in $[0,1]$. A treshold condition for the disease to become endemic has been found. By using semigroup theory and linear operator spectrum theory, it is shown that, under this treshold, known as the basic reproduction number of the infection, there is only one stable equilibrium corresponding to the disease-free case. Above the treshold, there are two equilibria, the disease-free one and an endemic one. We proved that the disease-free equilibrium is locally unstable, whereas the non-trivial endemic one is asymptotically stable.

In a future work perspective, in view of the stability analysis, it seems natural to try to find an appropriate vaccination policy, in order to stabilize the system around the disease-free equilibrium. Moreover those developments could be extended to study the stabilization of more general semilinear systems that are affine with respect to the control variable.

References

[1] G. Bastin and J-M. Coron. *Stability and boundary stabilization of 1-D hyperbolic systems*. pp. 40-43. coll. PNLDE Subseries in Control. Birkhauser, Switzerland, 2016.

[2] H. Inaba. *Age-Structured population dynamics in demography and epidemiology*. Springer, 2017.

[3] H. Inaba. *Treshold and stability results for an age-structured epidemic model*. Journal of mathematical biology. pp. 411-434, 1990.

[4] H. Inaba. *Mathematical analysis of an age-structured SIR epidemic model with vertical transmission*. Discrete and continuous dynamical systems - Series B, pp. 69-96, 2006.

[5] W. O. Kermack and A. G. McKendrick. *A contribution to the mathematical theory of epidemics*. Proceedings of the Royal Society London A. 115. pp. 700-721, 1927.

Luenberger observer design for a dynamic biotechnological model with embedded linear program

Kobe De Becker, Kristel Bernaerts, Steffen Waldherr

Bio- & Chemical Reactor Engineering and Safety (CREaS), KU Leuven

Celestijnenlaan 200f, 3001 Leuven, `kobe.debecker@kuleuven.be`

In this work, we focus on developing an observer method for dynamic enzyme-cost flux balance analysis (deFBA) models. This modelling framework [1] predicts dynamic extracellular metabolite concentration profiles, intracellular reaction fluxes and the biomass composition including enzyme amounts. A deFBA model is formulated as a set of linear ODEs, based on mass balancing, with a linear programming (LP) problem embedded in the right-hand side [2]. The governing set of ODEs is written as

$$\dot{x} = Sv^*(x) + Ax + Gu, \tag{1}$$

with x the extracellular metabolite and biomass component amounts, S_{exch} the stoichiometric matrix selecting for exchange fluxes. Ax describes transport on the reactor scale and Gu represents the influence of known inputs u. $v^*(x)$ are the optimal reaction fluxes which are calculated as part of the argument of an LP problem from which the right-hand side depends directly on the state vector x. The optimal fluxes v^* are linear with respect to the process states x

$$v^*(x) = T_i B_i^{-1} E x, \; x \in \mathcal{M}_i, \tag{2}$$

with B_i the optimal feasible basis of the LP problem and $\mathcal{M}_i$ the set of states x that correspond to this optimal basis B_i. As the optimal feasible basis changes during integration, the system is said to be in different modes, characterized by the set $\mathcal{M}_i$. T_i and E are a mode-dependent and a mode-independent selection matrix for fluxes and states respectively. This results in the model equations

$$\dot{x} = S_{exch} T_i B_i^{-1} E x + Ax + Gu, \; x \in \mathcal{M}_i, \tag{3}$$

The challenge in designing an observer for the above mentioned system is the mode-switching behaviour of the system and the unknown system modes of the set $\mathcal{M}_i$. A preliminary list of system modes is constructed by running the model simulation multiple times with different initial estimates. For each of these modes a Luenberger observer is designed according to

$$\dot{\hat{x}}_i = S_{exch} T_i B_i^{-1} E \hat{x}_i + A\hat{x}_i + Gu + L_i(y - C\hat{x}_i), \tag{4}$$

with the ^-sign indicating estimates, y the measurements and C the measurement matrix. L_i is the observer gain for mode i. Gain determination happens by simultaneous stabilization of the observer error dynamics for all detectable modes that are in the preliminary list of modes. For each
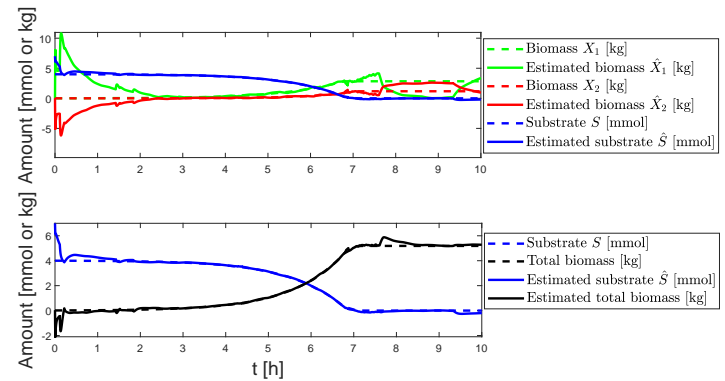
Figure 1: (Top) State estimations (full lines) and true noiseless system values (dashed lines), (Bottom) Output estimations (full lines) and noiseless output measurements (dashed lines), taken from [2]

of the Luenberger observers in the bank of observers, a moving average error between the estimated and measured output. The mode with the lowest moving average error is estimated to be the current observer mode with index $\hat{k}$ and corresponding basis $B_{\hat{k}}$. An overall Luenberger observer is run according to (3) with $\hat{k}$ as the mode estimate. The overall observer dynamics are updated each time the optimal mode estimate changes.

The observer design is applied on a small-scale model consisting of two bacterial species, X_1 and X_2. The second species grows on a product produced by the first species. The initial substrate S and the total biomass amount $X_1 + X_2$ are measured. Gaussian white noise is added to the actual system values with a signal to noise ratio of 40 dB. From the results in Figure 1 it is clear that the measured outputs are correctly estimated. The three process states are correctly estimated during exponential growth. During the stationary phase of the process, state estimations are not accurate due to the system running into undetectable modes.

[1] Waldherr S., Oyarzun D. A. and Bockmayr A. (2015). Dynamic optimization of metabolic networks coupled with gene expression. Journal of Theoretical Biology. 365.

[2] De Becker K., Bernaerts K., Waldherr S. (2020). Luenberger observer design for a dynamic system with embedded linear program, applied to bioprocesses. Submitted.

Particle filter design for an agent-based crop model

Jorge Lopez-Jimenez[1,2], Nicanor Quijano[1], and Alain Vande Wouwer[2]

[1]Department of Electronics and Electrical Engineering, Universidad de los Andes, Bogota, Colombia
[2]Automatic Control Laboratory, University of Mons, Boulevard Dolez 31, Mons, Belgium , Email:
`jorgealfredo.lopezjimenez@umons.ac.be`

1 Introduction

Traditionally, crop models allows the prediction of biomass growth and yield. However, there are two main issues with large-scale crop systems for biomass prediction: 1) land heterogeneity, and 2) environmental variations under climate change. An agent-based model (ABM) can address these two problems. ABMs have flexibility, modularity and are built on rules of behaviour. This type of model has been used in different contexts and has proved effective. Nevertheless, there is no standard mathematical formalization of ABMs which makes it difficult to apply classical state estimation.

The purpose of this work is to present an ABM, with a heterogeneous set of agents which are space and time aware, and the design of a particle filter for data assimilation.

2 The Model

An ABM with three state variables is considered: 1) the water content in every patch of homogeneous soil (W), 2) the cumulative temperature (TT), and 3) the biomass (B). The reason of the choice of these variables is that remote sensing can provide information about all of them and it is possible to combine with on field measurements [1].

The simulator is developed in Matlab. The first step is the processing of an aerial image of the field. A grid is constructed over the field, where every patch in the grid correspond to a homogeneous portion of crop, and in turn, an agent. The behaviour of an agent x_i is related to its internal mechanistic functions, and the exchanges with its neighbours. The evolution of every agent is given by

$$\dot{x}_i = f_i(x_i, E, U_i, \theta_i) + g_i(\mathcal{N}(x_i)), \qquad (1)$$

where $f_i(\cdot)$ is a function of the evolution of state variables of agent x_i, E is the vector of the explanatory variables (i.e. environmental inputs such as temperature, and precipitations), U is the vector of management inputs (i.e. irrigation), and θ_i is the set of parameters. $g_i(\cdot)$ describes the exchanges with the neighbours of x_i.

3 Particle Filter

A particle filter (PF) is used to assimilate the incoming data, and the estimation of the three state variables. A set of particles representing state vectors is propagated in parallel, such that each state vector represents one realization of the non-linear model. The state equation for each particle in the filter is [2]:

$$x_t^{i-} = f(x_{t-1}^{i+}, u_{t-1}^i, \theta_{t-1}^+, t-1) + \eta_{t-1}^i \qquad (2)$$

where $f_i(\cdot)$ is the non-linear model, x_t^{i-} is the state of the ith particle prior to the update time t, x_{t-1}^{i+} is the posterior state of the ith particle at time $t-1$, u_{t-1}^i represents the environmental and management inputs, θ_{t-1}^+ represents the model parameters, and η_{t-1}^i is the model error.

A Sequential Monte Carlo (SMC) filter is considered instead of the traditional Sequential Importance Resampling (SIR) filter, as it is required to counteract degeneracy. Finally, two techniques of resampling are tested, the PF with residual resampling and the PF with residual resampling and uniform parameter replacement [2].The diagram of the whole process is shown in Fig. 1.
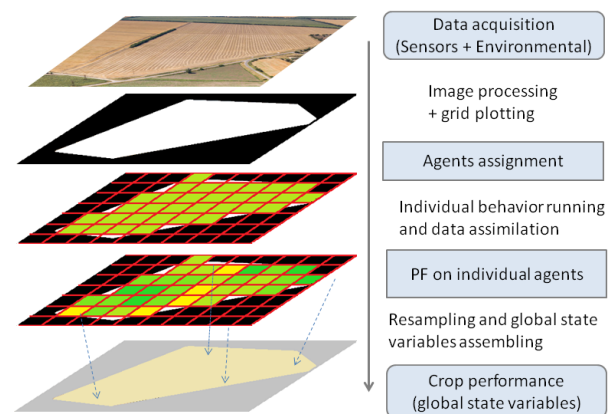
Figure 1: Diagram of the process.

References

[1] I. Campos, L. Gonzalez-Gomez, J. Villodre, J. Gonzalez-Piqueras, A. Suyker, and A. Calera "Remote sensing-based crop biomass with water or light-driven crop growth models in wheat commercial fields," Field crops research. Elsevier, 2018.

[2] K. Nagarajan, J. Judge, W. Graham, and A. Monsivais-Huertero, "Particle filter-based assimilation algorithms for improved estimation of root-zone soil moisture under dynamic vegetation conditions,"Advances in water resources, Elsevier, 2011.

Surrogate Modelling of Activated Sludge Wastewater Treatment Plant

M.A. Prawira Negara[1], A.K. Geurkink[2], K.J. Keesman[3], G.J.W. Euverink[2], B. Jayawardhana[2]

[12]Engineering and Technology Institute of Groningen, University of Groningen

[3]Mathematical and Statistical Methods - Biometris, Wageningen University & Research

[1]m.a.prawira.negara@rug.nl
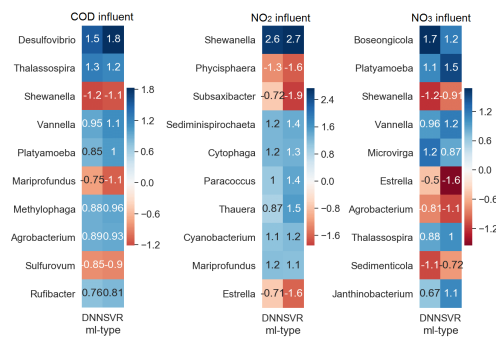
Figure 1: Correlation Analysis Result
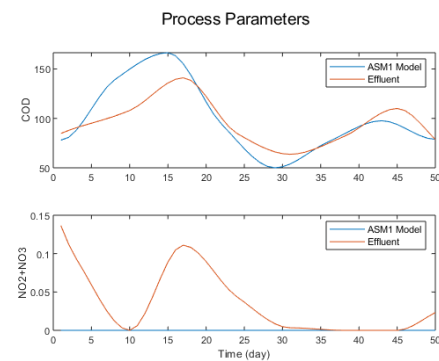
Figure 2: ASM1 model Result

1 Introduction

It has been recognized that wastewater forms a significant part of waste from human activities and it requires treatment before it is environmentally safe to be discharged to the natural water resources [1]. While the concept is simple, the control of the treatment process is very complex because of a large number of variables that affects it [2]. There are a number of established models for describing the process dynamics in WWTP such as the well-studied Activated Sludge Models [3]. These ASM models are lumped dynamical models where the influence of the activated sludge is lumped to the kinetic laws of few process variables. The unknown parameters are a fusion of metabolic activities of various microorganisms which have a large degree of uncertainties. This modelling approach prevents the direct use of the models for a deeper understanding of the processes and for optimization and control at the microbiology of a WWTP. For improving the reliability and applicability of these models, the knowledge and real-time information of the microorganism population are indispensable for enriching the ASM models.

2 Correlation Analysis (SVR)

In [4] by analyzing the (local) sensitivity of each modeled process parameter to each genus (NGS data), an indication of the influence of the microbial structure on process performance was found. The result of the correlation analysis can be seen in Figure 1.

3 WWTP Modelling: ASM1 Model

Using the well known ASM1 [1], we able to model the two activated sludge reactor tanks in the system. The ASM1 is able to model a different way of nitrogen removal than normally used. The aeration process, which normally happens at the first step, is happening at the second tank. In Figure 2, we can see the simulation result of the model.

4 Future Works

The next thing to do is to use the result of the correlation analysis into the model that we have. We will include the use of NGS data into the ASM1 model.

References

[1] M. Henze and Y. Comeau. *Biological Wastewater Treatment*. IWA Publishing, London, 2008.

[2] P.S. Davies. *The Biological Basis of Wastewater Treatment*. Strathkelvin Instruments Ltd, Motherwell, 2005.

[3] M. Henze, W. Gujer, T. Mino, and M. van Loosdrecht. *Activated Sludge Models ASM1, ASM2, ASM2d and ASM3*. IWA Publishing, London, 2000.

[4] M.A.P. Negara, E. Cornelissen, A.K. Geurkink, G.J.W. Euverink, and B. Jayawardhana. Next generation sequencing analysis of wastewater treatment plant process via support vector regression. *IFAC PapersOnline*, 52-23:37–42, 2019.

Mathematical modelling of malaria transmission considering the influence of current prevention and treatment

Ousmane Diao

SST/ICTM/INMA, UCLouvain

Avenue Georges Lemaître 4-6 bte L4.05.01

1348 Louvain-la-Neuve

ousmane.diao@uclouvain.be

1 Introduction

Malaria is a parasitic infection transmitted by a mosquito (female Anopheles) which is very deadly for humans. Human transmission can also occur by blood transfusion, needles sharing or from an infected mother (congenitally) [1]. This infection constitutes a major public health problem in many parts of the world, particularly in Africa. According to the Senegal's National Malaria Control Program of 2016, 349 540 malaria cases were confirmed as well as 325 deaths related to the disease. Children under 5 years are the most vulnerable with 21.5% of clinical signs and 30.77% of deaths. Many strategies have been developed to reduce morbidity and mortality, e.g., insecticide-treated bed-nets (ITNs), vaccines, Artemisinin-based combination therapy (ACT) and indoor residual spraying (IRS). Mathematical modelling may play an important role in the operation and optimization of these aforementioned strategies [2].

2 Model formulation

Based on several cases of malaria that have occurred, various studies have emerged that construct a mathematical model for malaria based on Ross approch [3]. Indeed, it can help to understand and to identify the relationship of transmission dynamic, to quantify the epidemiological parameters, to assist in future planning and to give appropriate control measures. In this work, we adopt a SEIRS-SEI model based on the approch in [3, 4] which considers two currents of prevention: bed-net coverage (b) and spraying use (a), and a current of treatment: effectiveness of Antimalarial Drugs (ψ). This model is then used to assess the effects of these components on the transmission dynamic. The derivative system of the parasite transmission is given by:

$$\begin{cases} \frac{ds_h}{dt} = \Lambda_h + \gamma r_h - (\mu_h + \theta + \lambda_h)s_h \\ \frac{de_h}{dt} = \lambda_h s_h - (\mu_h + \alpha)e_h \\ \frac{di_h}{dt} = \alpha e_h - (\mu_h + \nu + k\psi)i_h \\ \frac{dr_h}{dt} = k\psi i_h + \theta s_h - (\mu_h + \gamma)r_h \\ \frac{ds_v}{dt} = \Lambda_v - (\mu_v + \lambda_v)s_v \\ \frac{de_v}{dt} = \lambda_v s_v - (\mu_v + \omega)e_v \\ \frac{di_v}{dt} = \omega e_v - \mu_v i_v \end{cases}$$

Using the Van Den Driessche and Watmough method, the basic reproduction number (the average number of secondary infections that occur when one infective individual is introduced into a completely susceptible host population) R_0 is defined by:

$$R_{0(a,b,\psi)} = \frac{\beta_{max}(1-b)}{\mu + (a+b)\mu_{max}}\sqrt{\frac{p_1 p_2 \Lambda_v \Lambda_h(\mu_h+\gamma)}{\mu_h(\mu_h+\nu+k\psi)(\mu_h+\theta+\gamma)}}$$

3 Results

The results show that the basic reproduction number R_0 decreases for a high level of interventions. It indicates also that an high bed-net coverage ($> 80\%$) reduces consequently malaria transmission and can lead to the disappearance of the disease if we maintain this level and combine with an effective treatment and continuous spraying use.

Figure 1: Variation of R_0
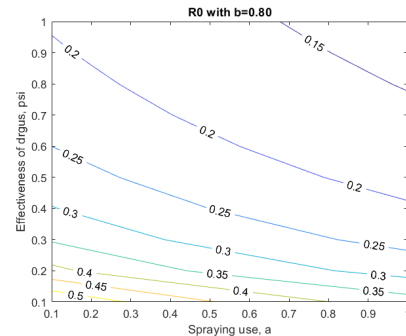
References

[1] R. G. Putri *et al.*, "Sirs-si model of malaria disease with application of vaccines, anti-malarial drugs, and spraying", *IOSR Journal of Mathematics (IOSR-JM)*, 10, 2014.

[2] Roll Back Malaria, "Mathematical modeling by control and elimination of malaria", *Collection et Impact*, 48(5), 2010.

[3] Resmawa and al, "Model seirs-sei of malaria disease with application of vaccinesandanti-malarialdrugs" *IOSR Journal of Mathematics (IOSRJM)*, 13(3):85–91, 2017.

[4] Abdulaziz Y.A. Mukhtar and al, "Modeling the effect of bed-net coverage on malaria transmission in south Sudan", *PLOS ONE*, 2018.

Distributed Model Predictive Control for Linear Systems under Time-varying Communication

Bo Jin
Faculty of Science and Engineering
University of Groningen
Nijenborgh 4
9747 AG Groningen
The Netherlands
Email: b.jin@rug.nl

Ming Cao
Faculty of Science and Engineering
University of Groningen
Nijenborgh 4
9747 AG Groningen
The Netherlands
Email: m.cao@rug.nl

1 Abstract

We study the distributed model predictive control (DMPC) problem for a network of linear discrete-time subsystems under time-varying communication networks where the system dynamics are decoupled and the system constraints are coupled. A novel distributed optimization algorithm is proposed to solve the dual problem of the DMPC optimization problem in a fully distributed way. We prove that the sequences of the primal and dual variables converge to their optimal values. Finally, the effectiveness of the proposed ADMM algorithm is verified via an example.

2 Problem Formulation

Consider a system consisting of M subsystems, and each subsystem i is modeled as $x^i(t+1) = A^i x^i(t) + B^i u^i(t)$, $i \in \mathbb{Z}^M$, where $x^i(t)$ and $u^i(t)$ represent the state and input at time t, respectively. Each subsystem is subject to a local state constraint and a local input constraint: $x^i(t) \in X^i, u^i(t) \in U^i$, where $X^i \subset \mathbb{R}^{n_i}$ and $U^i \subset \mathbb{R}^{m_i}$ are polytopes containing the origin in their interiors. In addition, all of these subsystems have to satisfy a global constraint: $\sum_{i=1}^{M} (\Psi_x^i x^i(t) + \Psi_u^i u^i(t)) \le 1_p$, with $\Psi_x^i \in \mathbb{R}^{p \times n_i}$ and $\Psi_u^i \in \mathbb{R}^{p \times u_i}$ are some constant matrices.

3 Stochastic distributed ADMM algorithm

For the above system, a global optimization problem is formulated as

$$\text{\textbf{Problem 1}}: \quad \min_{\{u^i, i \in \mathbb{Z}^M\}} \sum_{i=1}^{M} J^i(x^i, u^i), \text{s. t.}$$

$$u^i \in U^i(x^i), \forall i \in \mathbb{Z}^M \tag{1}$$

$$\sum_{i=1}^{M} f^i(x^i, u^i) \le b(\varepsilon). \tag{2}$$

J^i is the local objective function, Equation (1) and (2) are designed to consider the local and global constraints respectively.

Letting λ be the dual variable for the coupled constraint (2), the dual problem of Problem 1 is as follows:

$$\text{\textbf{Problem 2}}: \min_{\lambda \ge 0} \sum_{i=1}^{M} g_i(\lambda),$$

where $g_i(\lambda) = \max_{u^i \in U^i(x^i)} -J^i(x^i, u^i) - \lambda^T \ (f^i(x^i, u^i) - \frac{b(\varepsilon)}{M})$. Then, we propose an push-sum based distributed optimization algorithm to solve the above optimization problem in a fully distributed manner. We prove the primal and dual variables converge. The push-sum based dual gradient algorithm is given as:

$$\omega^{i,k+1} = \sum_{j \in \mathcal{N}_{in}^{i,k}} \frac{z^{j,k}}{d^{j,k}}, \tag{3}$$

$$y^{i,k+1} = \sum_{j \in \mathcal{N}_{in}^{j,k}} \frac{y^{j,k}}{d^{j,k}}, \tag{4}$$

$$\lambda^{i,k+1} = \frac{\omega^{i,k+1}}{y^{i,k+1}}, \tag{5}$$

$$u_p^{i,k+1} = \arg\min_{u_p^i \in \mathcal{U}_p^i} J^i(x^i, u_p^i) + \lambda^{i,k+1}(f^i(x^i, u_p^i) - \frac{b(\varepsilon)}{M}), \tag{6}$$

$$z^{i,k+1} = \left[\omega^{i,k+1} + \alpha^{k+1} M(f^i(x^i, u_p^{i,k+1}) - \frac{b(\varepsilon)}{M}) \right]^+. \tag{7}$$

4 Numerical example

Fig. 1 and Fig. 2 show the trajectories of the input and the dual variable $\lambda^{1,k}$ respectively.
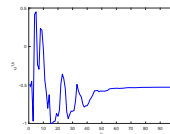
Figure 1: Convergence of $u^{1,k}$
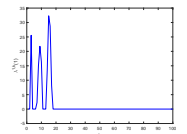
Figure 2: Convergence of the second element of $\lambda^{1,k}$

Real Time Iterations for Mixed-Integer Model Predictive Control [1]

Massimo De Mauri[2]
massimo.demauri@kuleuven.be

Wim Van Roy[2]
wim.van.roy@atlascopco.com

Goele Pipeleers[2]
goele.pipeleers@kuleuven.be

1 Abstract

The work to be presented deals with mixed-integer non-linear Model Predictive Control (MPC). MPC is generally regarded as an efficient yet powerful approach to rapidly find close-to-optimal solutions to complex optimal control problems. Nevertheless, when applied to models involving discrete variables, MPC suffers from the exponential complexity of mixed-integer non-linear programming. In practice, mixed-integer non-linear MPC may result ill suited for fast real-time applications.

MPC finds a solution to a discrete-time optimal control problem P over a time interval $[t_0, T]$ iteratively solving P over small portions of such interval. MPC starts by computing an optimal control sequence for the first few time steps of the original time interval. Then, at each iteration, the set of time steps to consider is shifted of one place forward and a new control sequence is computed. The algorithm keeps iterating until obtaining a complete control sequence for the original control problem. One important characteristic of MPC is fact that the sub-problem to solve at iteration $k+1$ is very similar to the one solved at iteration k. This characteristic has been successfully exploited in order to speed up Non-Linear MPC ([3]) giving rise to the class of techniques generally referred to as Real-Time Iterations (RTI) for MPC. Despite the success of RTI techniques in the continuous domain, there is still little similar literature in the mixed-integer context ([4]).

The presentation will introduce the "Mixed-Integer Real Time Optimal Control" (MIRT-OC) algorithm: an innovative mixed-integer MPC technique characterized by an extensive reuse of the information generated during one MPC iteration in order to reduce the computational cost of the subsequent iteration.

MIRTOC takes advantage of the fact that in B&B it is possible to add constraints to the problem that is in process to be solved without invalidating the information generated before the constraints addition. MIRTOC starts by defining an initial linear/quadratic relaxation of the first MPC problem and begins to solve it via B&B. Each time a new feasible solution is found for the current relaxation the constrain set of such relaxation is enriched by the addition of new linear constraints that will reduce the relaxation conservativism. Eventually, the relaxation becomes accurate enough to yield the same global optimum than the original non-linear problem. At this point (or earlier if a time limit is imposed), the first control action of the obtained optimal control sequence is stored (or applied to the plant) and the time window is shifted of one time step forward. We will call such operation "MPC-shift". Under reasonable working assumptions, MIRTOC expresses each MPC-shift as a set of constraint additions and doing so it is capable of integrating the MPC-shifts into the B&B structure.

The advantage in using MIRTOC to tackle mixed-integer non-linear MPC lies in the fact that the last obtained relaxation for the k-th MPC subproblem along with a large part of the B&B tree built during the solution process is propagated to the $(k+1)$-th subprolem. Moreover, the algorithm offers a natural way to propagate forward all collected the heuristic and branching information. As a consequence, using MIRTOC each MPC iteration may result much computationally cheaper than in the classical MPC approach.

In practical terms, as shown by the collected empirical data, the proposed algorithm provides sizeable computational savings and it may represent an important step towards a true real-time mixed-integer non-linear MPC scheme.

References

[1]   I. Quesada & I.E. Grossmann,"An LP/NLP based branch and bound algorithm for convex MINLP optimization problems", Computers & Chemical Engineering, 1992.

[2]   J.B. Rawlings, D.Q. Mayne & M. Diehl. "Model Predictive Control: Theory, Computation, and Design", Nob Hill Publishing, 2018 (2nd ed.).

[3]   M. Dihel, H.G. Bock & J.P. Schlder, "A real-time iteration scheme for Nonlinear optimization in optimal feedback control", Control Optimization, 2005.

[4]   P. Hespanhol, R. Quirynen & S. Di Cairano, "A Structure Exploiting Branch-and-Bound Algorithm for Mixed-Integer Model Predictive Control", European Control Conference, 2019.

[5]   M. De Mauri, V. Van Roy. OpenBB (Software), "https://github.com/MassimoDeMauri/OpenBB.jl".

[2]MECO Research Team, Department Mechanical Engineering, KU Leuven and DMMS lab, Flanders Make, Leuven, Belgium.

Imprecise Probabilistic MPC (iMPC) for systems with non-deterministic uncertainty

Frederik Debrouwere, Keivan Shariatmadar and Mark Versteyhe
Department of Mechanical Engineering, M-Group KU Leuven Campus Bruges

1 Introduction

Model Predictive Control (MPC) has shown significant success for high-performance control of complex systems [3]. Robust MPC (RMPC) schemes have been developped in the past to allow for the systematic handling of deterministic uncertainties. These RMPC frameworks are capable of accounting for interval-member uncertainties where a probability density of the uncertainty is unknown or unused [1]. This however renders highly conservative control actions in reality. Furthermore, in real world applications, many of the uncertainties should however be considered to be probabilistic. To cope with this type of uncertainty, Stochastic MPC (SMPC) schemes were developped, where typically this probabilistic nature is modelled by means of a (stochastic) probability distribution (PDF) be it either standard descriptions of probability (e.g. Gaussian) or using sample based probability density functions. Including this probability may lead to less conservative control actions compared to RMPC.

Although a lot of physical phenomena occurring in real life exhibit some probabilistic nature, it is unfair and unrealistic to model them as a single probability distribution, since these phenomena are inherently non-deterministic. Indeterminism means that the probability density function of a parameter is not fixed (e.g. over time or over different products) but is undetermined.

When developing a controller, a classical but conservative way to deal with this uncertainty is to use minimum and maximum bounds on the values that these parameters can take, i.e. the RMPC approach. Although the stochastic MPC results in less conservative control, the underlying stochastic models are not a true description of the underlying uncertainty. Then, Stochastic MPC based on such a description (the overall average PDF) would violate the probabilistic set of bounds as it underestimates the true bounds.

Interval approaches in RMPC hence result in conservatism, as the probability is neglected the interval is a large overestimation of the reality, whilst stochastic approaches in SMPC result in the possibility that constraints are violated as the used stochastic model might be an underestimation of reality.

2 Approach

The authors believe that more advanced uncertainty models, such as probability boxes [2], based on the theory of imprecise belief [4] should be incorporated in order to obtain a less conservative control law, by modelling the uncertainty more realistically.

The authors hence propose to modify the current state of the art stochastic tube SMPC algorithm which make use of the explicit probability distributions.The resulting control law is referred to as non-determinisitic *imprecise* MPC (iMPC).

3 Conclusion

This work shows that in many cases we can write more performant controllers than classical robust MPC when we are able to write bounds on the level of indeterminism in uncertainty. The burden of the computational effort is offline and is only slightly higher than needed for stochastic MPC. Online, the optimization algorithm does not differ much from the implementation of SMPC.

We have observed the improvement potential when we take a realistic representation of uncertainty, leading to more reliable and less conservative control actions.

4 Acknowledgements

References

[1] Mark Cannon Basil Kouvaritakis. *Model Predictive Control: Classical, Robust and Stochastic*. Springer, 2015.

[2] Scott Ferson, Vladik Kreinovich, Lev Ginzburg, Davis S. Myers, and Kari Sentz. Constructing probability boxes and dempster-shafer structures. 04 2003.

[3] Manfred Morari and Jay H. Lee. Model predictive control: past, present and future. *Computers and Chemical Engineering*, 23(4):667 – 682, 1999.

[4] P. Walley. *Statistical Reasoning with Imprecise Probabilities*. Chapman & Hall/CRC Monographs on Statistics & Applied Probability. Taylor & Francis, 1991.

Short-Horizon MPC of Large-Scale Thermal Systems[*]

T.J. Meijer[1,†], V.S. Dolk[2], Bram de Jager[1] and W.P.M.H. Heemels[1]

[1] Control Systems Technology Group, Eindhoven University of Technology, Eindhoven, The Netherlands

[2] ASML Research Mechatronics and Control, Veldhoven, The Netherlands

[†] Email: t.j.meijer@tue.nl

1 Introduction

In the production of integrated circuits (ICs), optical elements are used to guide light along a desired path. This light induces undesired thermal loads and deformations in the optical elements causing the accuracy with which the light follows the desired path to deteriorate. Therefore, it is required to actively suppress these deformations using thermal actuators which compensate for the thermal loads.

Model predictive control (MPC) is adopted to control these thermal actuators within their limited operating range and to account for the presence of strict performance constraints. To ensure that the constraints remain satisfied a prediction model with a finite horizon is used. To achieve satisfactory performance and to be able to apply much of the existing MPC theory and many related algorithms, it is crucial that the prediction horizon is sufficiently long for the relevant system dynamics to appear in the prediction model, e.g. [1]. The dynamics of thermal systems are typically described using large-scale models originating from a finite-element method. Due to limited computational power, it is infeasible to select the prediction horizon long enough for all the dynamics in this large-scale model to appear in the prediction model. In this study, an algorithm is proposed to determine the dynamics seen by the MPC for a certain prediction horizon.

2 Problem formulation

Consider a minimal discrete-time LTI state-space realization

$$x_{k+1} = Ax_k + Bu_k, \tag{1a}$$
$$z_k = Cx_k, \tag{1b}$$

where $x_k \in \mathbb{R}^n$, $u_k \in \mathbb{R}^m$ and $z_k \in \mathbb{R}^p$ represent the states (nodal temperatures), actuator inputs and performance outputs at time $k \in \mathbb{N}$. At every sampling instance k, the controller solves the following finite-horizon optimal control problem given the current (estimated) state x_k:

$$\min_{\boldsymbol{x}_k \boldsymbol{u}_k} \quad \frac{1}{2} \sum_{i=0}^{N} x_{i|k}^T C^T Q C x_{i|k} + u_{i|k}^T R u_{i|k},$$
$$\text{s.t.} \quad x_{i+1|k} = Ax_{i|k} + Bu_{i|k}, \quad i \in \mathbb{N}_{\leq N-1}, \tag{2}$$
$$M x_{i|k} + J u_{i|k} \leq c, \quad i \in \mathbb{N}_{\leq N}.$$

Here, the sequences of future outputs, states and inputs are denoted $\boldsymbol{x}_k := \{x_{1|k}, \ldots, x_{N|k}\}$ and $\boldsymbol{u}_k := \{u_{0|k}, \ldots, u_{N-1|k}\}$ respectively, N denotes the prediction horizon and Q and R are weighting matrices.

As mentioned before, the MPC controller only anticipates dynamics which appear within its prediction horizon. How to determine which dynamics are "seen" by the controller?

3 Proposed method

The optimal solution to (2) depends only on states which are both N-step controllable and N-step observable. For the sake of compactness, the controllability index is assumed to be 3. The pair (A, B) can be brought to so-called controllability staircase form (CSCF), given by

$$x_{k+1} = \begin{bmatrix} A_{11} & A_{12} & A_{13} \\ A_{21} & A_{22} & A_{23} \\ 0 & A_{32} & A_{33} \end{bmatrix} x_k + \begin{bmatrix} B_1 \\ 0 \\ 0 \end{bmatrix} u_k, \tag{3}$$

using orthogonal similarity transformations [2]. Here, $B_1 \in \mathbb{R}^{n_1 \times m}$ and $A_{ij} \in \mathbb{R}^{n_i \times n_j}$. B_1, A_{21} and A_{32} are full row rank.

Based on the CSCF, the first $r = \sum_{i=1}^{N} n_i$ states are N-step controllable after which the state is truncated. Duality between controllability and observability is exploited to compute the N-step observable states of the truncated system. Truncating once more results in a system with only the N-step controllable and observable states of (1) and captures the dynamics "seen" by the MPC. The algorithm is applied to a simple numerical example.

References

[1] J. Yang, T. Meijer, V. Dolk, B. de Jager, and W. Heemels, "A System-Theoretic Approach to Construct a Banded Null Basis to Efficiently Solve MPC-Based QP Problems," in *IEEE Conference on Decision and Control (CDC) 2019, Nice, France*, December 2019.

[2] A. Varga, "Numerically stable algorithm for standard controllability form determination," *Electronics Letters*, vol. 17, no. 2, pp. 74–75, January 1981.

Optimal control of hybrid systems: dual dynamic programming approach

Benoît Legat[1], Jean Bouchat[2], Raphaël M. Jungers[3]

UCLouvain

B-1348 Louvain-la-Neuve

Belgium

Email: benoit.legat@uclouvain.be,
jean.bouchat@uclouvain.be,
raphael.jungers@uclouvain.be

The capability of hybrid systems to encode both continuous dynamics and discrete events in the same mathematical model renders them essential in fields such as robotics, automotive control or air traffic management. However, with their ability to model complex systems comes substantial challenges for controlling them. In this work, we study finite horizon optimal control problems with convex cost function on hybrid systems.

We introduce an algorithm that under-approximates the value function using a piecewise convex polyhedral function. Dual dynamic programming is used to generate lower bounds for the value function that are used to refine the value function approximation. As computing an accurate approximating of the value function in the whole state space is intractable, we aim to only generate an accurate approximation along the optimal trajectory.

As the optimal trajectory is unknown, the method alternates between 1) a search for a sub-optimal trajectory according to the current piecewise polyhedral lower bound of the value function using Model Predictive Control (MPC), the *forward pass*, and 2) a refinement of the polyhedral lower bound of the value function along the trajectory, the *backward pass*.

Figure 1 illustrates how the algorithms explores different trajectories before converging. Due to the non-convexity of the value function, the backward pass cannot always refine the polyhedral lower bound so that its value matches the actual cost of the forward pass. This duality gap between the lower bound of the backward pass and the upper bound of the forward pass may prevent the method from converging to the optimal trajectory. This gap can be reduced by subdividing the regions of the piecewise polyhedral functions along the trajectory the algorithm converges to.

This lack of exploration of the state space due to an over-
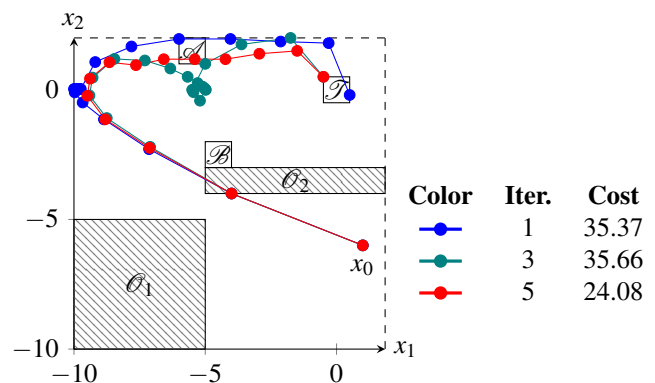
(a) Continuous state trajectories.

Figure 1: Results for the hybrid system introduced in [1], see Figure 4.7 of [3]. The MPC of the forward pass has an horizon $N = 3$. Note that all iterations subsequent to the fifth result in trajectories which are the same as the latter.

exploitation of the approximate lower bound is a common theme in reinforcement learning known as the *exploration-exploitation trade-off*, notably encountered in the multi-armed bandit problem [2, Section 1.5]. We can observe that a small horizon for the MPC is in favor of exploitation while a longer horizon increases exploration. Additionally, computing several sub-optimal trajectories instead of a single one in the forward pass would improve exploration.

References

[1] Ebru Aydin Gol, Mircea Lazar, and Calin Belta. "Language-guided controller synthesis for linear systems". In: *IEEE Transactions on Automatic Control* 59.5 (2014), pp. 1163–1176.

[2] Dimitri P Bertsekas. *Dynamic programming and optimal control*. Vol. 1. 2. Athena Scientific Belmont, MA, 1995.

[3] Jean Bouchat and Raphaël M Jungers. "Reinforcement learning for the optimal control of hybrid systems". MA thesis. UCLouvain, June 2020.

Optimal irrigation management for large-scale precision farming using model predictive control

A.T.J.R. Cobbenhagen, D.J. Antunes, M.J.G. van de Molengraft and W.P.M.H. Heemels

Control Systems Technology group, Department of Mechanical Engineering

Eindhoven University of Technology

P.O. Box 513, 5600 MB, Eindhoven, The Netherlands

Email: `a.t.j.r.cobbenhagen@tue.nl`

1 Introduction and problem description

Agriculture is responsible for 69% of annual water withdrawal globally, to which irrigation has a large contribution [1]. It is therefore important to intelligently apply water to arable fields in order to reduce this demand. An intelligent irrigation system is also beneficial to the farmer as a better division of irrigation over field can improve yields and profit margin.

This paper considers the set-up where there are many more fields ($\approx 100 - 1000$) than agents (≈ 10) that can provide irrigation to arable fields in order to produce crops. A similar set-up was considered in the previous works [2, 3].

The objective is to develop a framework that maximizes a profit function that is dependent on the state of the crops at the end of the growing season (i.e., harvest), the amount of irrigation applied and the amount of irrigation actions by agents. These actions are subject to constraints on the agent allocation. The proposed framework should be scalable to large-scale operations.

2 Proposed framework

The proposed framework computes the optimal irrigation actions with respect to the profit function and the allocation constraints in a receding horizon fashion, where a discrete-time crop growth model is used for prediction. The states in the model include biomass, leaf area index, soil water content, and others. Typical prediction horizons are 7 to 10 days long and the control horizon is one day long.

A simplified crop/soil-water relationship is modelled in the constraints of the optimization problem. For each field $j \in \{1, 2, ..., M\}$ (M is the number of fields), a reduction factor $\theta_t^j \in [0,1]$ is introduced at each time $t \in \mathscr{T} := \{1, 2, ..., T\}$ (where T is the length of growing season) such that the actual growth G_t^j at time $t \in \mathscr{T}$ is equal to $\theta_t^j \hat{G}_t^j$, where $\hat{G}_t^j$ is the maximum potential growth given by the crop growth model. The dependency of θ_t^j on the soil-water content is shown in Figure 1 and it is modelled by linear constraints in the framework.

Furthermore, the framework makes use of a linear relationship (as shown in [3]) between the crop growth within the prediction horizon and the yield at the end of the season.
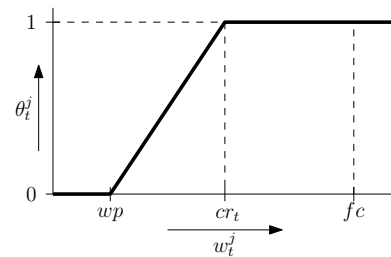
Figure 1: Dependency of θ_t^j on the soil water content w_t^j.

3 Properties of proposed framework

The approximation of the soil water/crop growth interaction mentioned above allows the use of complex crop growth models for the prediction without affecting the computation times of the optimization greatly. In fact, a wide variety of established crop growth models can be used in the proposed framework under mild conditions.

The proposed framework takes into account:
1. weather predictions,
2. water-carrying capacity of agents,
3. scheduling of refilling of water to agents at farm,
4. maximum rate of irrigation application to fields,
5. travel distance of agents,
6. operation costs of agents,
7. water costs.

The framework can be used for different objectives such as maximization of profit or minimization of water use and/or irrigation actions. For instance, in [3] it was shown that (for a similar version of the proposed framework in this paper) it is possible to have an increase of 19% in profit whilst reducing irrigation by 30% and irrigation moments by 41% at the expense of a yield loss of only 5% compared to a heuristic.

References

[1] WWAP (UNESCO World Water Assessment Programme), "The United Nations World Water Development Report 2019," Paris, UNESCO, 2019.

[2] A. T. J. R. Cobbenhagen, D. J. Antunes, M. J. G. van de Molengraft, and W. P. M. H. Heemels, "Heterogeneous multi-agent resource allocation through multi-bidding with applications to precision agriculture," IFAC-PapersOnLine, vol. 51, no. 23, pp. 194–199, 2018.

[3] L. P. A. Schoonen, A. T. J. R. Cobbenhagen, and W. P. M. H. Heemels, "Optimal irrigation management for large-scale arable farming using model predictive control," IFAC-PapersOnLine, vol. 52, no. 30, pp. 56–61, 2019.

Optimal Experiment Design for a Wafer Stage:
A Sequential Relaxation Approach

Nic Dirkx[1,2] , Jeroen van de Wijdeven[1], Tom Oomen[2]

[1] *ASML Research Mechatronics & Control, Veldhoven, The Netherlands*
[2]*Eindhoven University of Technology, Department of Mechanical Engineering, Control Systems Technology, The Netherlands*

1 Background

Ever-increasing performance requirements for high-precision positioning systems such as wafer scanners requires the availability of accurate models [1]. Frequency Response Function (FRF) identification from experimental data is considered a fast, inexpensive, and accurate method to obtain such models [2].

2 Problem

The choice of input signal determines the quality of the identified FRF, which motivates the employment of Optimal Experiment Design (OED) strategies. OED involves the optimization of the inputs to maximize the model accuracy within the available resources [3]. For Multiple Inputs Multiple Outputs (MIMO) systems, OED does not only require appropriate design of the magnitudes of the input signals, but also their directions. Furthermore, the design must address the specific constraints that are relevant for the considered system. For wafer stages, these constraints are typically related to specific elements of the systems, e.g., a power limitation for a specific actuator or a limitation of a local displacement.

The aim of this research is to develop OED methods that explicity address directionality in excitation design within element-wise power constraints.

3 Approach

The OED problem is formulated as the constrained minimization of a cost function $\mathscr{J}(\Phi_w)$ related to the FRF accuracy over the input spectrum Φ_w:

$$
\begin{aligned}
\text{minimize} \quad & \mathscr{J}(\Phi_w) \\
\text{subject to} \quad & g(\Phi_w) \leq 0 \\
& \text{rank}(\Phi_w) = 1.
\end{aligned}
\tag{1}
$$

Here, the combination of $g()$ and the rank constraint function forms the set of element-wise power constraints. Due to the rank constraint, problem (1) is non-convex and hard to solve in most cases.

A Sequential Relaxation (SR) algorithm is proposed that replaces the rank constraint in (1) by an approximate convex function, and then solves the resulting sequence of convex optimization problems. The solution of the SR algorithm is guaranteed to converge to a local minimum of the original non-convex problem (1).

[1]E-mail: nic.dirkx@asml.com

4 Results

The developed method is experimentally tested for the identification of the 4×4 dynamics of a wafer stage, see Fig. 1. The system is subject to element-wise output power constraints. Three different excitation designs are compared:

R1) Preliminary design, using a uniform excitation power distribution.

R2) Traditional optimized single input design approach with optimized excitation magnitude, but non-optimized directions.

R3) Optimal multivariable design using the SR algorithm, with optimized magnitudes and directions.

Fig. 1 shows entry (1,1) of the resulting FRFs, including 95% confidence regions (shades) and standard deviations (dashed). The multivariable design (R3) achieves a factor 2 lower standard deviation compared to the traditional approach (R2) by exploiting directionality in the design.
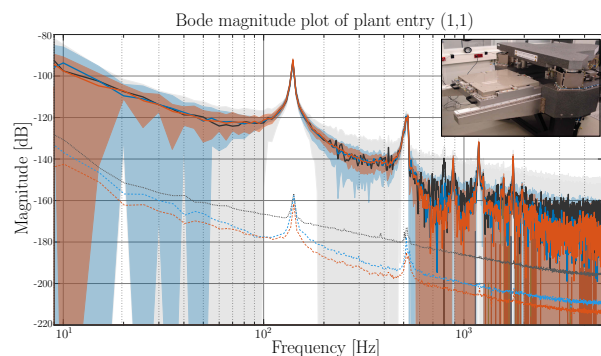
Figure 1: Identified FRFs using design R1 (black), R2 (blue), and R3 (red). Top right: wafer stage setup.

5 Ongoing work

Ongoing research includes development of methods for:

- dealing with peak amplitude constraints
- standard plant identification, including identification of unmeasurable performance variables.

References

[1] T. Oomen, "Advanced Motion Control for Precision Mechatronics: Control, Identification, and Learning of Complex Systems," *IEEJ Journal of Industry Applications*, 7, 127-140. 2018.

[2] R. Pintelon, J. Schoukens, "System identification: a frequency domain approach," *J. Wiley*, 2012

[3] H. Hjalmarsson, "From experiment design to closed-loop control," *Automatica*, 41(3), 2005

A Novel LPV/LTV Method for Nonlinear System Identification

Mehrad Sharabiany, John Lataire, Rik Pintelon
Dept. ELEC, Vrije Universiteit Brussel (VUB),
Pleinlaan 2 - 1050 Brussels, Belgium
Email: mehrad.ghasem.sharabiany@vub.be, John.Lataire@vub.be, Rik.Pintelon@vub.ac.be

1 Introduction

The identification and control of LTI systems is well established among engineers. So, not surprisingly, there are many nonlinear system identification methods based on an integration of local LTI models. Among them, LPV modeling approaches have received a lot of attention from the community. For LPV systems, there is a (set of) scheduling parameter(s) (p) which is constant for a local LTI model. There are two major LPV identification approaches: local and global [2]. In this paper, we propose a novel Global LPV modeling paradigm for nonlinear systems. Then, we model a pendulum which is followed by the simulation results.

2 Approach

The proposed identification method is as follows: the system is excited with a combined large-amplitude slow signal and a small-amplitude rapid signal. After de-trending, it can be proved that it is possible to approximate the system with an LTV model. This LTV model is estimated by the algorithm proposed in [1]. It is known that any LPV model is inherently an LTV model too. Therefore, the coefficients of that linear time-varying system can be considered as the coefficients of the corresponding LPV model. The main idea is that the large input and output signals themselves can be used as scheduling parameters. So, the LTV coefficients must somehow be related to the scheduling trajectory (i.e. the large signal input and outputs). In this way, there is no need for an extra independent scheduling variable. Also, there is no difficulty in the measurement of the scheduling parameters.(See Figure 1.)

The underlying maths come from a Taylor series expansion of a nonlinear function around a trajectory. In this case, the coefficients of the LPV/LTV system are obtained via linearization of the plant around the large signal trajectory.

3 Illustrative example and results

The proposed method is examined on a fixed-length pendulum which revolves a whole cycle. First, a ramp trajectory (from $-3\pi/4$ to $5\pi/4$) is used for acquiring the LTV system. The LTV model is estimated from the small signal input/output data. Then, a static Neural Network maps large signals to LTV models coefficients. Validation is accomplished by exciting the system with various different trajec-
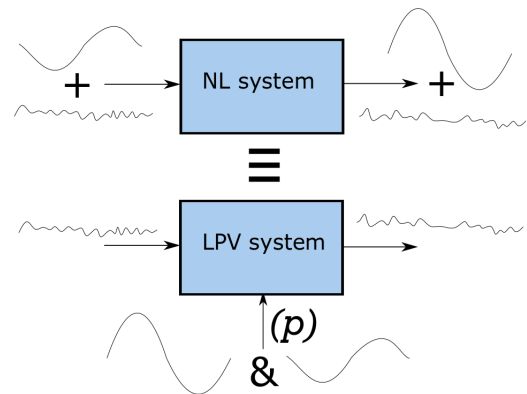
Figure 1: Proposed LPV system arrangement

tories. The estimated and true trajectories for validation are in good agreement. (e.g. see Figure 2)
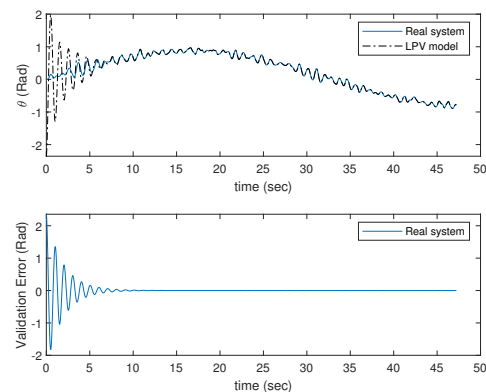
Figure 2: Validation Simulation Results VS Real Sytem Output

References

[1]   J. Lataire, R. Pintelon, D. Piga, and R. Tóth. Continuous-time linear time-varying system identification with a frequency-weighted kernel based estimator. *IET Control Theory & Applications*, 11(4):457 – 465, Feb. 2017.

[2]   R. Tóth. *Modeling and Identification of Linear Parameter-Varying Systems*, volume 403 of *Lecture Notes in Control and Information Sciences*. Springer-Verlag, Berlin Heidelberg, first edition, 2010.

Nonlinear Data-driven Identification of a Thermo-electric System

Jean-Philippe Noël, Enzo Evers, Tom Oomen
Control Systems Technology Group, Eindhoven University of Technology
j.m.m.g.noel, e.evers, t.a.e.oomen @tue.nl

1 Introduction and motivation

Thermo-electric coolers based on the Peltier effect are a popular actuation option in high-precision systems where active heat exchanges are required [1]. State-of-the-art modelling in the field is largely performed by relying on first principles. This contribution presents a data-driven approach to modelling the nonlinear dynamics of Peltier elements.

2 Identification procedure

The adopted identification methodology proceeds in two steps. Firstly, a nonparametric analysis is achieved in the frequency domain, with the objective of quantifying the amount of nonlinear distortions affecting the system output spectrum at a given excitation amplitude. A discrimination between distortions originating from odd (symmetric) and even (asymmetric) nonlinearities is also made possible by the use of special multisine excitation signals [2]. Secondly, a nonlinear state-space model is identified from data. The identification is carried out in the frequency domain again, by minimising an unweighted least-squares cost function. The nonlinear model terms are function of the measured current at the system input side, following the prior knowledge that a Joule effect, which is related to dissipation in heat conduction, is the dominant source of nonlinearity in a Peltier element dynamics when excited over a reasonably small temperature range.

3 Identification results

Fig. 1 depicts the nonparametric analysis of an input-output data set measured under a multisine excitation signal with a root-mean-squared amplitude of 0.64 A. In the frequency domain, this signal contains no power at the even lines to detect asymmetric nonlinearities, and randomly leaves odd lines unexcited to detect symmetric nonlinearities. Fig. 1 reveals that a substantial even nonlinearity (blue) distorts the system output spectrum (grey), as opposed to the marginal amplitudes of the odd distortions (yellow) and noise disturbances (black). The result of the nonlinear state-space modelling step is provided in Fig. 2. The identified model incorporates a quadratic input term in the state equation, reflecting the outcome of the nonparametric analysis in Fig. 1. This model features 5 state variables and overall comprises 41 parameters. The associated residual in Fig. 2 (green) is seen to be 10 to 20 dB below the corresponding linear modelling error level (blue) over the frequency range from DC to 0.1 Hz.
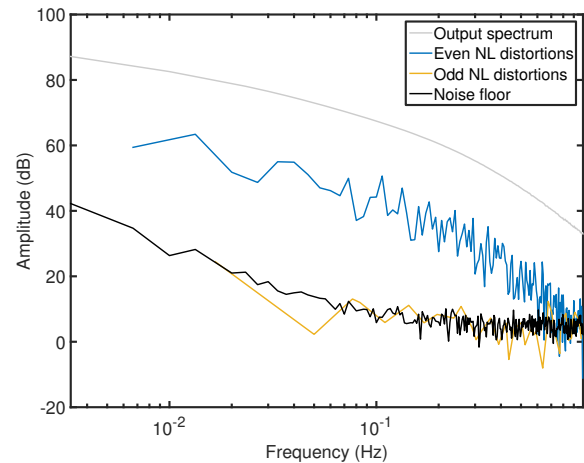
Figure 1: Nonparametric analysis of test data.
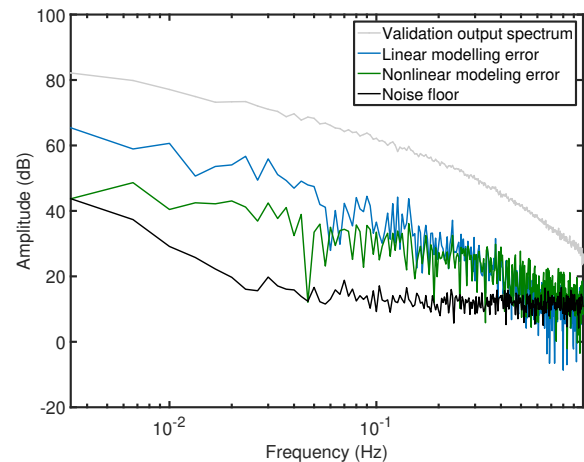
Figure 2: Parametric nonlinear modelling in state space.

4 Conclusion and outlook

On-going investigations focus on identifying the Peltier dynamics over larger temperature ranges, and on exploiting the resulting data-driven models for designing feedback linearisation controllers.

References

[1]   R. van Gils, *Peltier for precision actuation*, Mikroniek 59(2), 5-10, 2019.

[2]   J. Schoukens, L. Ljung, *Nonlinear system identification: a user-oriented road map*, IEEE Control Systems Magazine 39(6), 28-99, 2019.

Consistent identification of dynamic networks subjected to white noise using Weighted Null-Space Fitting[1]

Stefanie Fonken
Control Systems Group,
Department of Electrical Engineering,
Eindhoven University of Technology,
The Netherlands
Email: s.j.m.fonken@student.tue.nl

Mina Ferizbegovic and Håkan Hjalmarsson
Department of Automatic Control,
School of Electrical Engineering,
KTH Royal Institute of Technology,
Stockholm, Sweden
Email: {minafe, hjalmars}@kth.se

1 Introduction

Identification of dynamic networks with the prediction error method (PEM) suffers from issues with local minima. Therefore, the aim is to formulate a method to simultaneously estimate all modules of a given structure, without the need to solve non-convex optimization problems, under the assumption of known topology. This abstract summarizes the results of [1], which addresses the above problem.

2 Problem statement

A rational linear dynamic network consists of L nodes. Following [2], the network is expressed as

$$\begin{bmatrix} w_1(t) \\ \vdots \\ w_L(t) \end{bmatrix} = G(q) \begin{bmatrix} w_1(t) \\ \vdots \\ w_L(t) \end{bmatrix} + R(q) \begin{bmatrix} r_1(t) \\ \vdots \\ r_M(t) \end{bmatrix} + \begin{bmatrix} e_1(t) \\ \vdots \\ e_L(t) \end{bmatrix}, \quad (1)$$

where $G(q)$ is an off-diagonal matrix with its elements being stable and strictly proper rational transfer functions. In addition, the elements of $R(q)$ contain stable and proper rational transfer functions. Both $R(q)$ and $G(q)$ can also have zero entries. Moreover, $e(t)$ is an unmeasured white noise sequence with $e_i(t) \sim \mathcal{N}(0, \sigma_{e_i}^2)$. The parameter vector θ to estimate, consists of the numerator and denominator coefficients of $G_{ij}(q)$ and $R_{ij}(q)$.

3 Weighted Null-Space Fitting

The Weighted Null-Space Fitting (WNSF) method [3] is a three-step least-squares method, originally developed for single-input-single-output (SISO) systems. This method has been extended to the dynamic network setup in (1) in [1]. The first step of the WNSF method for networks is an intermediate step, a non-parametric (high-order) autoregressive exogenous (ARX) model estimates the finite impulse responses (FIR) of $G_{ij}(q)$ and $R_{ij}(q)$. The second step aims to reduce the non-parametric model to a parametric model, resulting in the initial estimate $\hat{\theta}_N^{(0)}$. In the third step, the parametric model is re-estimated giving $\hat{\theta}_N^{(1)}$. Both the second and third step use the estimation error covariance as

weighting in the least squares to reduce the variance on the consistent estimates of θ. Since finite sample size N is used, it could be beneficial to iterate the last step using available $\hat{\theta}_N^{(k)}$ to compute $\hat{\theta}_N^{(k+1)}$.

4 Results

We compare the performance of the second and third step of the WNSF method for networks with the PEM initialized at the true parameters as shown in Fig. 1, where $\hat{\theta}_N^{final}$ indicates the final value for iteration $\hat{\theta}_N^{k+1}$. The model considered has $G(q)$ with an arbitrary topology and $R(q)$ a diagonal matrix, both square matrices with 6×6 dimension. Moreover, the order of the transfer functions range from one to six. PEM provides asymptotically efficient estimates when converging to a global minimum. The simulation results suggest that the WNSF method for networks has the same large sample properties as the PEM.
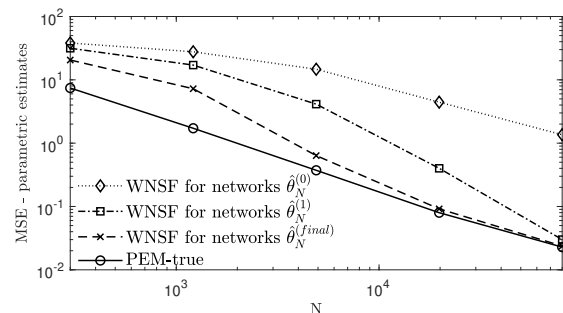
Figure 1: MSE between $\hat{\theta}_N$ and θ_0 as function of sample size N, averaged over 100 Monte Carlo runs

References

[1]   S.J.M. Fonken, M. Ferizbegovic and H. Hjalmarsson, "Consistent identification of dynamic networks subjected to white noise using Weighted Null-Space Fitting," *Submitted to 21st IFAC World Congress.*

[2]   P.M.J. Van den Hof, A.G. Dankers, P.S.C. Heuberger and X. Bombois, "Identification of dynamic models in complex networks with prediction error methods: basic methods for consistent module estimates," *Automatica*, vol. 49(10), pp. 2994–3006, 2013.

[3]   M. Galrinho, C.R. Rojas and H. Hjalmarsson, "Parametric identification using Weighted Null-Space Fitting," *IEEE Transactions on Automatic Control*, vol. 64(7), pp. 2798–2813, 2019.

Identification and identifiability of physical networks[1]

E.M.M. Kivits and P.M.J. Van den Hof

Control Systems Group, Department of Electrical Engineering

Eindhoven University of Technology, P.O. Box 513, 5600 MB Eindhoven, The Netherlands.

Email: `e.m.m.kivits@tue.nl` and `p.m.j.vandenhof@tue.nl`

1 Physical network

Physical networks are interconnections of physical components. These networks are typically depicted by undirected dynamical graphs, where the components interact through the differences of node signals. For system identification purposes, these networks are described by directed module representations with additional structural conditions, which incorporate the symmetry of the physical components [1].

Mathematically, the node signals $w(t)$ are described by

$$w(t) = G(q)w(t) + R(q)r(t) + H(q)e(t), \qquad (1)$$

with excitation signals $r(t)$, white noise proces $e(t)$ and with

$$G(q) = Q^{-1}(q)P(q), \qquad R(q) = Q^{-1}(q)F,$$
$$H(q) = Q^{-1}(q)Q(\infty)C(q), \qquad (2)$$

with $Q(q)$ a diagonal polynomial matrix, $P(q)$ a hollow and symmetric polynomial matrix, F a diagonal, binary, known matrix, $C(q)$ a monic, stable and stably invertible rational matrix, and $Q(\infty) = \lim_{z \to \infty} Q(z)$. Here, $H(q)$ is scaled with $Q(\infty)$ in order to redefine the noise model to be monic.

2 Identification aspects

Performing system identification to (1) leads to some additional aspects due to the structure conditions (2).

Scaling The symmetrical nature of the physical components induces structure in the modules and therefore, the modules should not be parameterised independently. In addition, the denominator polynomial matrix $Q(q)$ is not monic and cannot be scaled to be monic as this destroys the symmetric structure in $P(q)$. This *scaling* aspect introduces an additional degree of freedom that needs to be identified.

Direct feedthrough The physical structure together with the discretisation method lead to direct feedthrough terms in all modules, which lead to algebraic loops in the network. Therefore, the node signals at time moment t cannot be used for identifying the parameters of (1)-(2). To identify these parameters, prediction error methods are used with predictor

$$\hat{w}(t|t-1) := \mathbb{E}\left\{ w(t) \mid w^{t-1}, r^t \right\}, \qquad (3)$$

where w^i refers to the past of $w(t)$ up until time moment i.

Non-linear optimisation The predictor (3) leads to the prediction error

$$\varepsilon(t, \theta) := A(\infty, \theta)^{-1}C^{-1}(q, \theta)\left[A(q, \theta)w(t) - Fr(t)\right], \quad (4)$$

with $A(q, \theta) = Q(q, \theta) - P(q, \theta)$. This prediction error is non-affine in the parameters θ, because the polynomial $A(q, \theta)$ is not monic as $A(\infty, \theta) \neq I$. As a result, the optimisation problem of minimising a quadratic identification criterion becomes in general non-convex and is only convex if $C(q)A(\infty) = I$.

3 Approach towards identifiability

In identifiability analysis for dynamic networks, typically independent parameterisations of all modules are assumed. This assumption is not satisfied for physical networks.

Rank conditions A number of literature results on identifiability of dynamic networks are based on rank conditions on the transfer function matrix of the network [2]. Extending these results to physical networks mainly consists of incorporating the symmetric structure (i.e. dependent parameterisations) in the rank conditions.

Markov parameters There exists a result on identifiability of symmetric first order systems [3], which is based on Markov parameters. The main challenges in generalising this result to physical networks are caused by the non-monicity of the polynomial matrices, the number of matrices involved and the zero-structure in these matrices.

References

[1] E.M.M. Kivits, P.M.J. Van den Hof, "A dynamic network approach to identification of physical systems," In *Proc. 58th IEEE Conference on Decision and Control*, 4533-4538, 2019.

[2] H.H.M. Weerts, P.M.J. Van den Hof, A.G. Dankers, "Identifiability of linear dynamic networks," *Automatica*, Volume 89, 247-258, 2018.

[3] H.J. van Waarde, P. Tesi, M.K. Camlibel, "Identifiability of undirected dynamical networks: A graphtheoretic approach," *IEEE Control Systems Letters*, 2(4), 683-688, 2018.

Representing Music Using MIMO Models for Genre Clustering

Bram Geelen   Bart De Moor

KU Leuven, Department of Electrical Engineering (ESAT), Stadius Center for Dynamical Systems,
Signal Processing and Data Analytics
bram.geelen@esat.kuleuven.be; bart.demoor@esat.kuleuven.be

1 Overview

We present a method to analyse musical works, by representing melodies as time series of pitch class activations. For any musical work - represented as audio or as a digital score - we can create a *beat-aligned chromagram*, which describes the activity of the twelve *pitch classes* (A, A#, ..., G#) at every beat. Previous work has shown that simple statistical descriptors of such a chromagram can be used to perform adequate genre classification [3], yet these descriptors do not incorporate the pitch class transitions - which are essential to the *harmonical progression* of a song - into the song representation. If we construct an AR model of these transitions, we exactly create a model of how the melody and harmonies progress throughout the song. With the (flattened) matrices of the AR model of every song, we can perform a simple genre clustering using off-the-shelf methods.

2 Clustering beat-aligned chromagrams

To construct the desired state representation from an audio source, we must first create the *constant-Q spectrogram* of the analysed song [1]. This is very similar to a short-time Fourier Transform, in that N narrow-band filters are convolved with the input signal, yet with *harmonically* spaced frequencies instead of linearly spaced. A chromagram aggregates the activities of the result into bins of each of the 12 musical *pitch classes*. Next, we locate the *beats* in the song, with the beat tracking algorithm proposed by Ellis [2]. Then we simply average the activity of of the pitch classes within each beat, to receive the beat-aligned chromagram.

We can also create a beat-aligned chromagram from digital music score representations such as .midi-files, by first identifying the beat of the song (often this is inherently part of the score), and subsequently aggregating per beat the activity of the 12 pitch classes throughout the song.

We then wish to represent the harmonic progression of the song as a vector, to ease the further work of clustering the corpus. We do this by looking at the beat-aligned chromagram as a time series of vector states X_t (with every vector representing a single beat), and constructing a simple rank-one MIMO AR model M;

$$X_{t+1} = M \cdot X_t$$

We can then flatten the matrix M to receive the vector representation we want. Note that we can increase the accuracy of this model by increasing its rank, yet this will result in

a worse song representation; a least-squares solution for M could differ heavily between similar songs, especially with high correlation in the input space. To alleviate this problem, we can simply *correlate* the pitch class activities from one state to the next. This means we *don't* create a higher-order AR model, but only analyse how every pitch class activation is correlated with every pitch class in the next beat (or k beats *further*). Thus, we create a correlation matrix M from the beat-aligned chromagram X (of shape $(T, 12)$) as follows;

$$M_{ij} = corr(X_{1:T-k,i}, X_{k:T,j})$$

In this presentation, we will show how to interpret both the beat-aligned chromagrams as well as the correlation matrices, and demonstrate how they differ between genres. We will also show how the representations perform in benchmark genre classification datasets, when combined with off-the-shelf classifying models.

References

[1] Judith C Brown. Calculation of a constant q spectral transform. *The Journal of the Acoustical Society of America*, 89(1):425–434, 1991.

[2] Daniel PW Ellis. Beat tracking by dynamic programming. *Journal of New Music Research*, 36(1):51–60, 2007.

[3] Alexander Schindler and Andreas Rauber. Capturing the temporal domain in echonest features for improved classification effectiveness. In *International Workshop on Adaptive Multimedia Retrieval*, pages 214–227. Springer, 2012.

Repetitive control to improve pressure tracking performance in mechanical ventilation of sedated patients

Joey Reinders[1,2], Ruben Verkade[2], Bram Hunnekens[2], Nathan van de Wouw[1,3], and Tom Oomen[1]

1 Department of Mechanical Engineering, Eindhoven University of Technology, Eindhoven

2 DEMCON Advanced Mechatronics, Best

3 Department of Civil, Environmental & Geo-Engineering, University of Minnesota, U.S.A.

Email: j.m.f.reinders@tue.nl

Mechanical ventilation

Mechanical ventilation is used in Intensive Care Units (ICUs) to save lives of patients unable to breathe on their own. Mechanical ventilation supports patients by ensuring adequate oxygenation and carbon dioxide elimination. Mechanical ventilators attached to the patient, as depicted schematically in Figure 1, are used to ensure airflow in and out of the lungs. For a fully sedated patient this is achieved by generating a pressure profile as shown in Figure 2. This results in the desired flow of air in and out of the lungs.

Control problem

This paper considers Pressure Controlled Mandatory Ventilation (PCMV) of fully sedated patients. The goal in PCMV is to track a given airway pressure reference repeatedly. This reference is exactly periodic with a known period length which is preset by the clinician. Besides this reference pressure, no patient breathing effort is considered.

Controller design for mechanical ventilation is challenging because of the large plant variations. One control system should accurately track the desired target pressure for a large variety of patients (ranging from neonates to adults), hoses, and filters. Therefore, the aim is to exploit the repetitive nature of the target signal to achieve accurate performance for this variety of plants. This is achieved in the following section by using Repetitive Control (RC) [1].

Repetitive controller design

Next, a single repetitive controller that achieves accurate pressure tracking for a wide variety of patients is designed. A detailed explanation of this design process can be found in [2] and [3]. To design the RC filters, a Frequency Response Function (FRF) of the complementary sensitivity is identified for different patients. The mean of these FRFs is used to design the learning filter. Next, a robustness filter is designed such that the SISO RC stability criterion is guaranteed for every individual patient. In the next section, the improvement in performance compared to traditional PID control is shown by means of an experimental case study.

Experimental results

In Figure 2, the results of an experimental case study are shown. In this case study an adult patient with a typical tar-
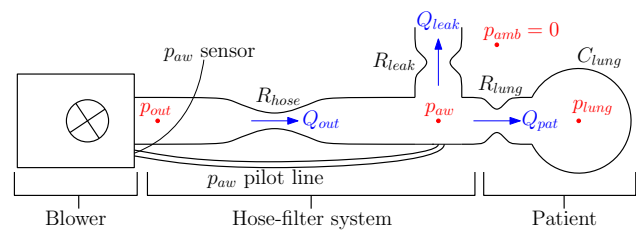
Figure 1: Schematic representation of the blower-hose-patient system, with the corresponding resistances, lung compliance, pressures, and flows.
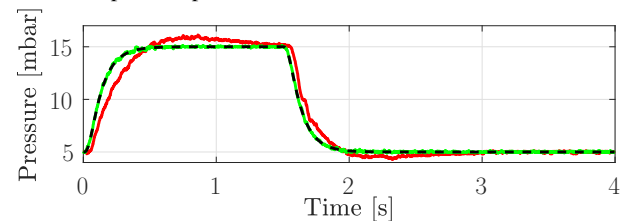
Figure 2: Results of an experimental case study, showing the target pressure (- - -), the airway pressure with a PID controller (——), and the airway pressure with the converged RC controller (——).

get pressure is considered. The patient is emulated using a mechanical lung simulator and the Demcon Macawi ventilation module is used. Figure 2 clearly shows that the rise-time of the PID controller is rather slow and it shows significant overshoot. The converged repetitive controller shows almost perfect tracking. In terms of the error 2-norm, the tracking error is reduced by a factor 10. Other patient types show similar results.

Concluding, it is shown that repetitive control can significantly improve pressure tracking performance in ventilation of fully sedated patients.

References

[1]   S. Hara, Y. Yamamoto, T. Omata and M. Nakano, "Repetitive control system: a new type servo system for periodic exogenous signals," in *IEEE Transactions on Automatic Control*, vol. 33, no. 7, pp. 659-668, July 1988.

[2]   J. Reinders, R. Verkade, B. Hunnekens, N. van de Wouw, and T. Oomen, "Improving mechanical ventilation for patient care through repetitive control," Submitted for conference publication.

[3]   L. Blanken, S. Koekebakker, T. Oomen, "Multivariable Repetitive Control: Decentralized Designs with Application to Continuous Media Flow Printing," in *IEEE/ASME Transactions on Mechatronics*, 2020. (Early Access)

Generic Signal Parametrizations for Low-Dimensional Learning Control

Jeroen Willems, Edward Kikken, Bruno Depraetere & Sorin Bengea

DecisionS lab, Flanders Make, Leuven, Belgium. E-mail: firstname.lastname@flandersmake.be

1 Introduction

Iterative learning control (ILC) can yield superior performance for repetitive tasks while only requiring approximate models, making this control strategy very appealing for industry. However, for non-linear systems it involves solving of optimization problems, which limits the industrial uptake, especially for learning online to compensate for variations throughout the system's lifetime. Industry avoids this problem by designing simple rule-based learning schemes. Based on insight they parametrize the control law and define rule-based strategies to update the parameters based on observable output features. However, these are often designed in an ad-hoc manner, which potentially limits performance.

In this paper, we will couple a low-dimensional parametrized learning control algorithm with a generic signal parametrization method on the basis of autoencoders. This will allow high control performance, while limiting implementational complexity and maintaining interpretability, paving the way for a higher industrial uptake of learning control for non-linear systems.

2 ILC Approach and Parametrization Choice

The main idea [1] is to translate the full nonlinear optimization problem of nonlinear ILC [2], into learning good input parameters $\mathbf{p}_i$ based on output parameters $\mathbf{p}_o$, so the learning can be reduced to a low-dimensional and simpler operation that can easily be run online. The translation from full in- and outputs $\mathbf{u}$ and $\mathbf{y}$ to a few characterizing parameters $\mathbf{p}_i$ and $\mathbf{p}_o$ is done using input and output parametrizations T_{input} and T_{output}. To design these T_{input} and T_{output}, we propose a generic non-linear machine-learning parametrization method that achieves high-accuracy with limited user configuration: 1D convolutional autoencoders, a 1D version of the well-known 2D autoencoder, see [3].

Once the parametrizations are chosen the ILC is reduced to a simple strategy for updating the parameter values. We will use the generic (yet slow) approach of estimating the Jacobian relating changes in input parameters to changes in output parameters, and calculate our ILC parameter updates with this. The proposed ILC scheme is depicted in Figure 1.
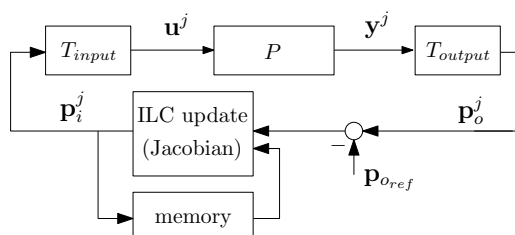
Figure 1: Overview of the simple learning framework.

3 Simulation results, Conclusions and Future Work

The approach is applied to a simulated slider-crank setup where each parametrization consists of 4 input and 4 output parameters. The control goal is to perform one revolution of the crank (reference tracking). The resulting mean absolute error (MAE) is shown in Figure 2. We have compared our approach with autoencoders with ones based on limited rank Singular Value Decomposition (SVD) and an engineered solution will be applied, and we can draw several conclusions:

- The SVD-based approach converges the fastest (4 iterations), but results in the highest tracking error, due to e.g. imperfect signal reconstruction.
- The autoencoder-based parametrization achieves a lower tracking error, and converges after 6 iterations, due to e.g. enhanced reconstruction capabilities.
- The engineered parametrization approach achieves the lowest tracking error and converges relatively fast. The downside is that the performance of such an approach is very dependent on the chosen parametrization.
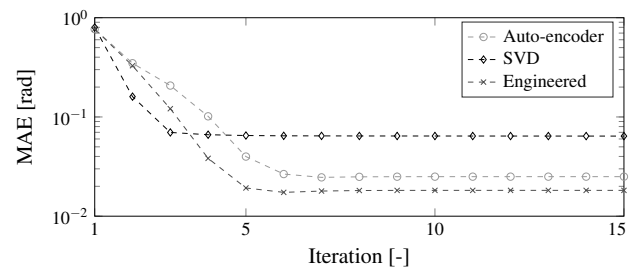
Figure 2: MAE as a function of iterations.

Future work is aimed at a 'learning control relevant' autoencoder, which optimizes not only signal reconstruction, but also improves convergence of the learning. Next to that we also aim to improve the Jacobian estimation, combining the normal learning experiments with models to avoid needing to perform experiments dedicated for Jacobian estimation.

References

[1] Willems, Jeroen, et al. "Learning control in practice: Novel paradigms for industrial applications." 2018 IEEE Conference on Control Technology and Applications (CCTA). IEEE, 2018.

[2] Volckaert, Marnix, et al. "A two step optimization based iterative learning control algorithm." ASME 2010 Dynamic Systems and Control Conference. American Society of Mechanical Engineers Digital Collection, 2010.

[3] Vincent, Pascal, et al. "Extracting and composing robust features with denoising autoencoders." Proceedings of the 25th international conference on Machine learning. ACM, 2008.

Gaussian Process Repetitive Control for Suppressing Spatial Disturbances: With Application to a Substrate Carrier System

Noud Mooren [1,*], Gert Witvoet [1,2], Tom Oomen [1]

[1]Eindhoven University of Technology, Dept. of Mechanical Engineering, Control Systems Technology, The Netherlands

[2] TNO Technical Sciences, Optomechatronics Departments, Delft, The Netherlands. *Email: n.f.m.mooren@tue.nl

1 Background

Motion systems are often subject to disturbances such as, cogging, commutation errors, gearings and imbalances, which are position-dependent disturbances, i.e., induced by an underlying cause in the spatial domain, see [1]. In the case that a rotary system operates with a constant operating velocity, or a linear system performs a repetitive motion task, these disturbances appear periodic in the time domain. However, if the operating conditions deviate, the disturbances appears a-periodic in the time domain while being periodic in the spatial domain [2].

2 Problem formulation

Classical repetitive control (RC) is not effective for disturbances that appear with varying period or a-periodic in the time domain [3]. This implies that classical RC with a memory loop in the time domain is not applicable to the aforementioned motion systems. The aim of this paper is to develop an RC approach for position-dependent disturbances.

3 Spatial Repetitive Control

The key idea is to construct a memory loop in the spatial domain. This is done by means of a Gaussian Process (GP) [4]. The time-domain signals are transformed to the spatial domain and stored in the GP, see Fig. 1. Furthermore, a suitable periodic kernel is developed to include periodicity and enforce smoothness in the GP. In addition, RC is developed using the traditional design philosophy [3].

4 Simulation case study

A simulation study is performed to show that classical RC fails if the disturbance period varies, whereas, the spatial
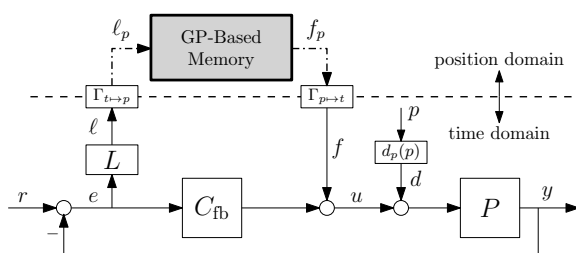
Figure 1: Spatial RC framework, with learning filter *L*.
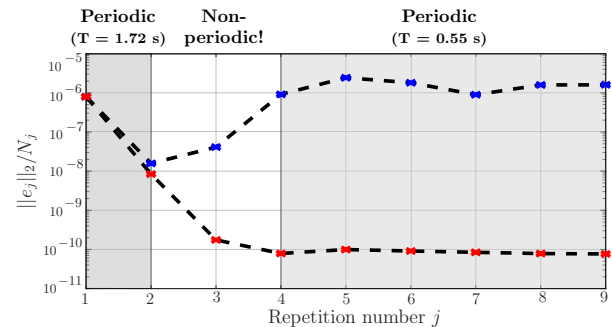
Figure 2: The 2-norm of the error with classical RC ($\times$) and spatial RC ($\times$). The disturbance is periodic at first, then non-periodic (after $j = 2$) and becomes periodic again (after $j = 4$) with a different period time.

RC approach is able to deal with these varying disturbances successfully as shown in Fig. 2.

5 Conclusions & Ongoing research

A new spatial RC approach is presented for rejection of disturbances that are periodic in a spatial domain and may appear a-periodic in the time domain. Furthermore, it deals efficiently with the non-equidistant observations through a GP-based memory loop. The potential of this methods is shown and ongoing work aims at the implementation on a substrate carrier system.

6 Acknowledgments

References

[1]   Ahn, H.S., Chen, Y., and Dou, H. (2005). State-periodic adaptive compensation of cogging and coulomb friction in permanent magnet linear motors, In Proceedings of the American Control Conference, 3036-3041

[2]   Chen, C.L. and Chiu, G.T.C. (2008). Spatially periodic disturbance rejection with spatially sampled robust repetitive control. Journal of Dynamic Systems, Measurement, and Control, 130(2), 021002.

[3]   Longman, R.W. (2010). On the theory and design of linear repetitive control systems. European Journal of Control, 16(5), 447-496.

[4]   Williams, C.K. and Rasmussen, C.E. (2006). Gaussian processes for machine learning. MIT press Cambridge, MA, 2

Balancing on-sample and intersample behavior in sampled-data system inversion

Wataru Ohnishi[1,2], Jurgen van Zundert[3], Hiroshi Fujimoto[1], Tom Oomen[2]

[1]The University of Tokyo, Graduate School of Engineering, Japan. Email: ohnishi@koseki.t.u-tokyo.ac.jp
[2]Eindhoven University of Technology, Department of Mechanical Engineering, The Netherlands
[3]Demcon Advanced Mechatronics, Best, The Netherlands

1 Introduction

System inversion is essential in feedforward and learning control. Ideally, perfect tracking can be achieved by exact system inversion. Due to a digital controller implementation, the system inversion has to be performed in the discrete-time domain.

2 Description

Zeros discretized by zero-order-hold can be classified as two types: 1) intrinsic zeros corresponding to the system dynamics; or 2) discretization zeros due to signal sampling [1]. If the plant relative order is even, one of the discretization zero(s) is located close to $z = -1$ [2]. The system inversion for zero at $z \simeq -1$ brings high-oscillating control input [3] and results in poor inter-sample performance [4].

3 Approach

To balance the on-sample and inter-sample tracking error, a novel sampled-data system inversion shown in Figure 1 is proposed. The single-rate inversion achieves exact tracking on sample at the cost of poor inter-sample performance, whereas multi-rate inversion achieves better inter-sample performance compromising on-sample tracking error (at control period T_u). In the developed approach, the system is decomposed into two parts and the inversion is applied separately.

4 Results

The developed approach is applied to a positioning system shown in Figure 2 with non-equidistant sampling. As shown in Figure 3, the proposed inversion yields the better performance compared with the existing approach. It is concluded that the proposed approach exploits additional degrees of freedom for discrete-time system inversion and demonstrates better performance.

References

[1]   T. Hagiwara, T. Yuasa, and M. Araki, "Stability of the limiting zeros of sampled-data systems with zero-and first-order holds," *International Journal of Control*, vol. 58, no. 6, pp. 1325–1346, 1993.

[2]   K. Åström, P. Hagander, and J. Sternby, "Zeros of sampled systems," *Automatica*, vol. 20, no. 1, pp. 31–38, 1984.
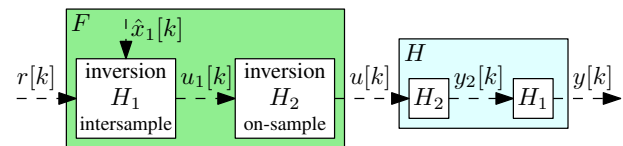
Figure 1: Block diagram of the proposed approach. The discrete-time system H is decomposed into H_1 and H_2. Multi-rate inversion is applied to H_1 for the purpose of inter-sample behavior. Single-rate inversion is applied to H_2 for the purpose of on-sample behavior.
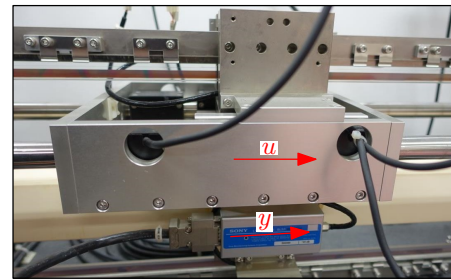
Figure 2: Motion system used in simulations and for experimental validation.
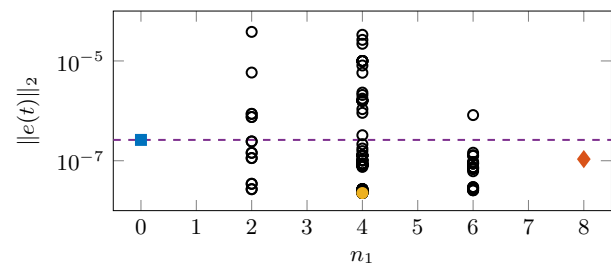
Figure 3: Continuous-time versus on-sample error in simulations. The approach balances the intersample behavior and the on-sample behavior for continuous-time performance.

[3]   K. L. Moore, S. P. Bhattacharyya, and M. Dahleh, "Capabilities and limitations of multirate control schemes," *Automatica*, vol. 29, no. 4, pp. 941–951, 1993.

[4]   J. van Zundert, W. Ohnishi, H. Fujimoto, and T. Oomen, "Improving Intersample Behavior in Discrete-Time System Inversion: With Application to LTI and LPTV Systems," *IEEE/ASME Transactions on Mechatronics*, vol. 25, no. 1, pp. 55–65, 2020.

Multi-System Iterative Learning Control: extending ILC towards Interconnected Systems.

Daniele Ronzani, Armin Steinhauser and Jan Swevers
MECO Research Team, Dept. Mechanical Engineering, KU Leuven
DMMS lab, Flanders Make
Celestijnenlaan 300B, 3001 Heverlee, Belgium
firstname.lastname@kuleuven.be

1 Introduction

Traditionally, iterative learning control (ILC) is employed to improve the performance of a repetitive task by learning on a single system. However, in the context of Cyber-Physical Systems (CPS) and Industry 4.0, mechatronic systems are interconnected and could therefore exploit knowledge learned by other machines systematically. For instance, the commissioning of a new fleet of similar machines, that has to learn how to optimally perform the same task, or the addition of a new system to a tuned fleet, are possible scenarios where learning and sharing a common model could lead to an improvement of performance and/or reduction of commissioning time.

This work present the Multi-System Iterative Learning Control (MSILC) algorithm that aims to extend traditional ILC towards multiple systems.

2 Algorithm

The MSILC approach is based on a generic nonlinear norm-optimal ILC method that, as shown in [1], can be interpreted as a two-step procedure: first compute an explicit model correction and subsequently invert the corrected system dynamics. Specifically, the MSILC further exploit the model correction step by calculating a common correction—shared between all systems—and a correction specific to each system, as shown in Figure 1. The MSILC algorithm, is implemented as a custom class of RoFaLT [2], `MultiSystemsILC`, and is available on GitLab [1]. The software provide a and generic tool for an optimization, model-based nonlinear ILC.

The approach is theoretically analyzed and categorized in the field of linear ILC through the well known framework of filter design. The MSILC iteration-domain dynamics can be equivalently represented by the update law (1) for the next iteration $i+1$ of a system k belonging to a fleet of K systems. The parameter ϕ, resulting from the regularization in the delta correction step, provide a tuning knob to trade-off between a single-system
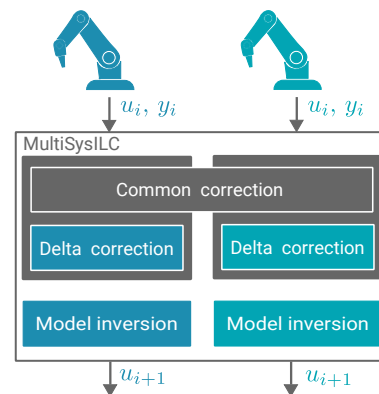
Figure 1: Illustration of the MSILC algorithm.

norm-optimal update law (1a) and a common norm-optimal update law. The filters $\mathcal{L}$ and $\mathcal{Q}$ are designed by means of the regularization parameter in the model inversion step of the algorithm.

$$u_{i+1}^k = \phi\, \mathcal{Q}\big(u_i^k + \mathcal{L}\, e_i^k\big) \tag{1a}$$

$$+ (1-\phi)\frac{1}{K}\sum_j^K \mathcal{Q}\big(u_i^j + \mathcal{L}\, e_i^j\big), \tag{1b}$$

3 Numerical study

The functioning of the approach is discussed through a numerical study of a fleet of positioning stages with measurement affected by iteration-varying disturbances. The results demonstrate the increase of the fleet performance achieved by using a trade-off between a single-system and common update law.

References

[1]   M. Volckaert, J. Swevers, and M. Diehl, A Two Step Optimization Based Iterative Learning Control Algorithm, ASME 2010 Dyn. Syst. Control Conf. Vol. 1, pp. 579-581, Jan. 2010.

[2]   A. Steinhauser, T. D. Son, E. Hostens, and J. Swevers, RoFaLT : An Optimization-based Learning Control Tool for Nonlinear Systems, 2018 IEEE 15th Int. Work. Adv. Motion Control, pp. 198-203, Mar. 2018.

[1]https://gitlab.mech.kuleuven.be/meco-software/multisystem-ilc

Intermittent Sampling in Iterative Learning Control: a Monotonically-Convergent Gradient-Descent Approach with Application to Time Stamping

Nard Strijbosch
Eindhoven University of Technology
Control Systems Technology
Email: n.w.a.strijbosch@tue.nl
P.O. Box 513, 5600 MB Eindhoven
The Netherlands

Tom Oomen
Eindhoven University of Technology
Control Systems Technology
Email: t.a.e.oomen@tue.nl
P.O. Box 513, 5600 MB Eindhoven
The Netherlands

1 Background: Iterative Learning Control

Iterative learning control (ILC) can significantly improve the performance in control applications by learning from past experiments. A mature framework has been developed in the past decades for disturbances that are iteration-invariant acting on LTI dynamical systems [1].

2 Problem Formulation

The standard assumption that a measurement signal is available at each sample in iterative learning control (ILC) is not always justified, e.g., in systems with data dropouts or when exploiting time-stamped data from incremental encoders [2]. When designing an ILC algorithm for this type of systems, where only intermittent data is available to the ILC algorithm, a few challenges arise:

- monotonic convergence is not defined due to varying lengths of error signals,
- computation time for an explicit ILC update explodes due to exponentially growing number of possible data points.

3 Decentralized Intermittent ILC

To address this, a new notion of monotonic convergence is defined and a decentralized ILC approach is developed where both theoretical and design aspects are fully commenced, in addition to its application on state-of-the-art applications [3]. The developed ILC framework guarantees monotonic convergence of the sequence of control input signals for all possible time-stamp sequences. Moreover, a decentralized design approach is developed that consists of designing a single diagonal matrix that should only suffice a single LMI. This approach is computationally efficient due to its independence of the number of time-stamp sequences. Moreover, this approach delicately connects to existing gradient-descent based ILC algorithms.

4 Results

When applying the decentralized ILC controller to a mass-spring-damper system from which exact time-stamped data is available the results presented in Figure 1 are obtained. It
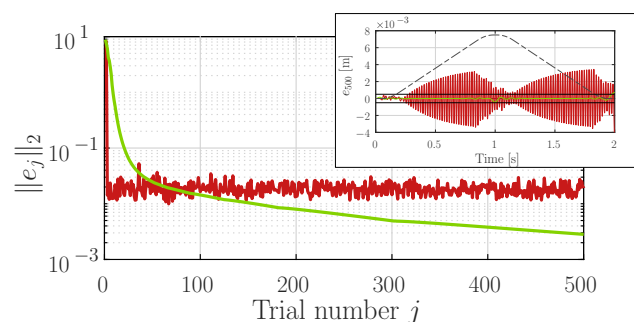
Figure 1: Error norm $\|e_j^h\|_2$ when applying traditional quantized ILC (—) and when applying the decentralized ILC controller (—). Error e_{500} at trial 500 after applying traditional quantized ILC (—) and after applying the decentralized ILC controller (—).

can be observed that each iteration the time instances of the available data are varying. Nonetheless, the ILC algorithm is capable of reducing the error significantly, and monotonic convergence of the input signal is guaranteed.

5 Ongoing research

Future research focuses on extending the ILC framework to a wider range of systems and applying the developed framework to experimental setups.

Acknowledgements

References

[1]   D. A. Bristow, M. Tharayil, and A. G. Alleyne, "A survey of iterative learning control," *IEEE Control Systems Magazine*, vol. 26, pp. 96–114, June 2006.

[2]   N. Strijbosch and T. Oomen, "Beyond quantization in iterative learning control: Exploiting time-varying time-stamps," in *American Control Conference 2019, Philadelphia, USA*, 2019.

[3]   N. Strijbosch and T. Oomen, "Intermittent Sampling in Iterative Learning Control: a Monotonically-Convergent Gradient-Descent Approach with Application to Time Stamping," in *Conference on Decision and Control 2019, Nice, France*, 2019 .

Distributed H_2 Suboptimal Filter Design
for Linear Systems

Junjie Jiao, Harry L. Trentelman, and M. Kanat Camlibel

Bernoulli Institute for Mathematics, Computer Science and Artificial Intelligence,

University of Groningen, The Netherlands

j.jiao@rug.nl, h.l.trentelman@rug.nl, m.k.camlibel@rug.nl

Motivation and Problem Statement

Consider the finite-dimensional linear time-invariant system

$$\begin{aligned}
\dot{x} &= Ax + Ed, \\
y &= Cx + Dd, \\
z &= Hx,
\end{aligned} \tag{1}$$

where $x \in \mathbb{R}^n$ is the state, $d \in \mathbb{R}^q$ the external disturbance, $y \in \mathbb{R}^r$ the measured output and $z \in \mathbb{R}^p$ the output to be estimated. The matrices A, C, D, E and H have suitable dimensions. The standard optimal filtering problem for (1) is to find a filter that takes y as input and returns an optimal estimate ζ of z, while the filter state asymptotically tracks the state x of (1). Here, 'optimal' means that the H_2 norm of the transfer matrix from d to the estimation error $z - \zeta$ is minimized over all such filters. In this problem setting, a standing assumption is that one single filter is able to acquire the complete measured output y of the system.

In the present work, we relax this assumption. More specifically, we consider the case that the complete measured output y of (1) is not available to one single filter, but is observed by N local filters. In this case, for $i = 1, 2, \ldots, N$, the ith local filter only acquires

$$y_i = C_i x + D_i d,$$

where $y_i \in \mathbb{R}^{r_i}$, $C_i \in \mathbb{R}^{r_i \times n}$, $D_i \in \mathbb{R}^{r_i \times q}$ and $C = \text{col}(C_i)$, $D = \text{col}(D_i)$. Clearly, the original output y of (1) has then been partitioned as $y = (y_1^\top, y_2^\top, \ldots, y_N^\top)^\top$ with $\sum_{i=1}^{N} r_i = r$. In this work it will be a standing assumption that the pair (C, A) is detectable. We will also assume that none of the pairs (C_i, A) is detectable itself.

In our case, each local filter makes use of the portion of the measured output that it acquires and then communicates with its neighboring local filters by exchanging filter state information. In this way, the local filters will together form a distributed filter. More concretely, we propose a distributed filter of the form

$$\begin{aligned}
\dot{w}_i &= Aw_i + G_i(y_i - C_i w_i) + F_i \sum_{j=1}^{N} a_{ij}(w_j - w_i), \\
\zeta_i &= Hw_i, \quad i = 1, 2, \ldots, N,
\end{aligned} \tag{2}$$

where $w_i \in \mathbb{R}^n$ is the state of the ith local filter and $\zeta_i \in \mathbb{R}^p$ is the associated output. The matrices $G_i \in \mathbb{R}^{n \times r_i}$ and $F_i \in \mathbb{R}^{n \times n}$ are local filter gains to be designed. The coefficients a_{ij} are the entries of the adjacency matrix $\mathscr{A}$ of the communication graph. In this work, it will be a standing assumption that this graph is a strongly connected weighted directed graph.

For the ith local filter, we introduce the associated local state estimation error e_i and local output estimation error η_i as

$$e_i := x - w_i, \quad \eta_i := z - \zeta_i, \quad i = 1, 2, \ldots, N.$$

The dynamics of the ith local error system is then given by

$$\begin{aligned}
\dot{e}_i &= (A - G_i C_i)e_i + F_i \sum_{j=1}^{N} a_{ij}(e_j - e_i) + (E - G_i D_i)d, \\
\eta_i &= He_i, \quad i = 1, 2, \ldots, N.
\end{aligned}$$

Denote $e = (e_1^\top, e_2^\top, \ldots, e_N^\top)^\top$, $\eta = (\eta_1^\top, \eta_2^\top, \ldots, \eta_N^\top)^\top$, $\bar{A} := \text{blockdiag}(A - G_i C_i)$, $\bar{F} := \text{blockdiag}(F_i)$ and $\bar{E} := \text{col}(E - G_i D_i)$. The global error system is then given by

$$\begin{aligned}
\dot{e} &= \left(\bar{A} - \bar{F}(L \otimes I_n)\right)e + \bar{E}d, \\
\eta &= (I_N \otimes H)e,
\end{aligned} \tag{3}$$

where $L \in \mathbb{R}^{N \times N}$ is the Laplacian matrix of the communication graph. The impulse response of (3) from d to η is equal to $T_d(t) = (I_N \otimes H)e^{(\bar{A} - \bar{F}(L \otimes I_n))t}\bar{E}$. Furthermore, we introduce the global H_2 cost functional

$$J = \int_0^\infty \text{tr}\left[T_d^\top(t)T_d(t)\right]dt. \tag{4}$$

The distributed H_2 optimal filtering problem is then the problem of minimizing the H_2 cost functional (4) over all distributed filters (2) such that the global error system (3) is internally stable. Note that (4) is a function of the local gain matrices $F_1, F_2, \ldots, F_N$ and $G_1, G_2, \ldots, G_N$. Unfortunately, due to the particular form of (2), this optimization problem is, in general, non-convex and it is unclear whether a closed-form solution exists. Therefore, instead of trying to find an *optimal* solution, we will address a version of this problem that only requires *suboptimality*.

The aim of this work is to design filter gains such that the corresponding distributed filter is H_2 suboptimal in the sense that the error system (3) is internally stable and the H_2 performance (4) is smaller than an a priori given tolerance.

Lower bound performance for averaging algorithms in open multi-agent systems

Charles Monnoyer de Galland and Julien M. Hendrickx

ICTEAM Institute, UCLouvain, B-1348 Louvain-la-Neuve, Belgium.

Email: { `charles.monnoyer, julien.hendrickx` } @uclouvain.be

1 Introduction

We consider *open* multi-agent systems, *i.e.*, systems where arrivals and departures of agents happen at a timescale similar to that of the process, so that they cannot be neglected. In that context, we derive *fundamental limitations* on the performance of algorithms estimating the average of the values held by the agents presently in the system.

Most results stated on multi-agent systems assume that their composition remains unchanged throughout the whole process. This assumption is getting increasingly challenged by the growing size of the systems, making small individual probabilities of arrivals or departures within the system non-negligible. Such systems can also naturally arise when the process is slow enough, e.g. multi-vehicle systems where vehicles share a stretch of road for a time. In such configurations, analyses and algorithm design become challenging as the state, size, and at some extent objective pursued by the system vary over time, preventing it to achieve the usual convergence. On top of that, results obtained for closed systems do not easily extend to open ones [1, 2].

Little work exists around open systems, including simulation-based analyses [3] or through size-independent quantities [1], and algorithm design for MAX consensus [2]. In this work, we extend the results presented in [4] by proposing a general formulation of fundamental performance limitations for algorithms that can be implemented under some restrictions on the exchange of information within the system, and apply it to the Gossip algorithm.

2 Problem statement

We consider a multi-agent system constituted of N agents labelled from 1 to N, where each agent j owns a constant intrinsic value x_j drawn from some zero-mean distribution of variance σ^2. Random replacements happen according to a Poisson process of rate λ_r, resulting in the attribution of a new value to the replaced agent so that the system is open and its size is constant. We provide agents with some knowledge about the dynamics of the system and assume they can collect information about the state of the other agents at some times, so that it is possible to implement algorithms that estimate the time-varying average of the intrinsic values of the system $\bar{x}(t) := \frac{1}{N}\sum_{j=1}^{N} x_j(t)$. Our objective is to characterize lower bounds on the performance of such algorithms by bounding their Mean Square Error (MSE).

3 Results

In order to derive a lower bound on the MSE, we define the algorithm that achieves optimal performance under restrictions on the way agents acquire information about each other. This leads to expression (1) where $f_j(s)$ is a probability function related to the age of such information about some agent j.

$$\mathbb{E}\left[C(t)\right] \geq \frac{N-1}{N^2}\left(1 - \int_0^t f_j(s)e^{-2\lambda_r s}\, \mathrm{d}s\right)\sigma^2 \quad (1)$$

This bound is valid for any algorithm that can be implemented under the restrictions it considers. An illustration of this is presented in Figure 1 (with λ_c the pairwise interaction rate between the agents), which compares the performance of the Gossip algorithm obtained through simulations with several instantiations of (1) through restrictions that allow implementing the Gossip algorithm.
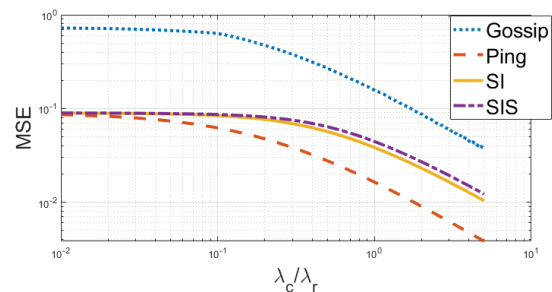
Figure 1: MSE comparison showing the validity of (1) for the Gossip performance (blue), where *Ping*, *SI* and *SIS* refer to valid models to instantiate $f_j(s)$ in (1).

References

[1] J. M. Hendrickx and S. Martin, "Open multi-agent systems: Gossiping with deterministic arrivals and departures," in *Proceedings of the 56th IEEE CDC*, pp. 1094–1101, 09 2016.

[2] M. Abdelrahim, J. M. Hendrickx, and W. M. Heemels, "Max-consensus in open multi-agent systems with gossip interactions," in *Proceedings of the 56th IEEE CDC*, 12 2017.

[3] P. Sen and B. K. Chakrabarti, *Sociophysics: an introduction.* Oxford University Press, 2013.

[4] *arXiv e-prints*, p. arXiv:1909.02475 [cs.MA], Sep 2019.

On the inclusion of human cognitive mechanisms in social diffusion

Lorenzo Zino, Mengbin Ye, and Ming Cao[1]

Faculty of Science and Engineering, ENTEG, University of Groningen

Groningen, 9747 AG, The Netherlands, Emails: {lorenzo.zino, m.ye, m.cao}@rug.nl

1 Introduction

Social diffusion is a fundamental phenomenon in social communities. Evolutionary game theory has been extensively used to capture salient features of diffusion processes and study their evolution [1]. However, unlike other kinds of diffusion processes (e.g., epidemics outbreaks), social diffusion involves human decision making, which is characterized by complex behavioral mechanisms that cannot be neglected in the design of a realistic agent-based model.

Motivated by these reasons and inspired by sociopsychological literature and empirical evidence from experimental data, we propose a mathematical model for social diffusion. Building on a standard coordination game, we develop our model by incorporating two inherent features of human behavior: *inertia* and *trend-seeking*. The former being the inclination of individuals to be consistent with their previous choices, the latter being their tendency to be influenced by dynamic trends.

2 Social Diffusion Model

The game is played by a set $V = \{1, ..., n\}$ of $n \geq 2$ players. Each player $i \in V$ can choose between two alternative strategies: the *status quo* (0) and the *innovation* (1). At each discrete time-step, players revise their strategy, denoted by $x_i(t)$, following a log-linear learning [1]. Specifically, $Pr[x_i(t+1) = x] \propto \exp\{\beta_i \pi_i(x)\}$, where β_i quantifies the level of noise in the decision process and $\pi_i(x)$ is the payoff of player i for adopting strategy x, which is given by

$$
\pi_i(x) = \frac{b_i}{n-1}[x, 1-x] \sum_{j \in V \setminus \{i\}} \begin{bmatrix} x_j(t) \\ 1-x_j(t) \end{bmatrix} \\
+ k_i[x, 1-x] \begin{bmatrix} x_i(t) \\ 1-x_i(t) \end{bmatrix} + r_i[x, 1-x] \begin{bmatrix} \hat{x}_i(t) \\ 1-\hat{x}_i(t) \end{bmatrix},
\tag{1}
$$

where $b_i + k_i + r_i = 1$ are nonnegative scalar constants and $\hat{x}_i(t) = \left[1 + \sum_{j \in V \setminus \{i\}} (x_j(t) - x_j(t-1))\right]/2(n-1)$. The first term of (1) is a standard coordination game mechanism, as in [1]. The extension of coordination games occurs through the inclusion of two novel terms. The former captures *inertia*: players receive a higher payoff for sticking with their current strategy. The latter encapsulates *trend-seeking*: the payoff for playing a strategy is improved whenever its fraction of adopters has increased in the previous time-step.
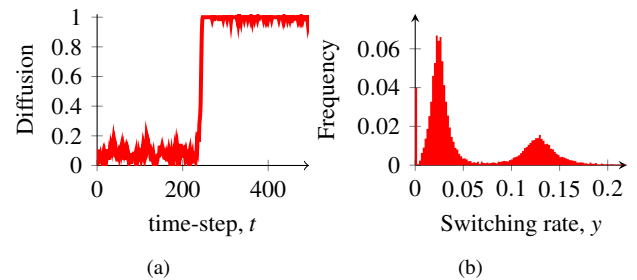
Figure 1: Results of the Monte Carlo simulations.

Social diffusion is modeled by introducing in a population that plays the status quo a small fraction of innovators, which stubbornly chose the innovation, following [2].

3 Results

From an extensive campaign of Monte Carlo simulations (see Fig. 1), we observe that our model is able to capture three key features, which have been widely observed in many social diffusion phenomena in the literature and in experimental trials conducted by our research group [3]. Specifically, at the macroscopic (societal) level, we observe that the take-off time of the diffusion process may be strongly delayed, but, once the tipping point is reached, innovation explosively diffuse in few steps. At the microscopic (individual) level, we observe a moderate and heterogeneous switching activity. Extensive comparisons of this model with a standard coordination game suggest that the introduction of the two additional terms to account for inertia and trend-seeking are necessary for the the synchronous presence of all these real-world features.

References

[1] G. E. Kreindler and H. P. Young, "Rapid innovation diffusion in social networks," *Proc. Natl. Acad. Sci. USA*, vol. 111, no. 3, pp. 10 881–10 888, 2014.

[2] D. Centola, J. Becker, D. Brackbill, and A. Baronchelli, "Experimental evidence for tipping points in social convention," *Science*, vol. 360, no. 6393, pp. 1116–1119, 2018.

[3] H. Risselada, J. W. Bolderdijk, Ž. Mlakar, B. M. Fennis, M. Ye and L. Zino, "Releasing the brake: How disinhibition frees people and facilitates innovation diffusion," *Submitted to EMAC 2020*.

Nash equilibrium seeking under partial-decision information

Mattia Bianchi
DCSC
Tu Delft
m.bianchi@tudelft.nl

Giuseppe Belgioioso
Control Systems Group
TU Eindhoven
g.belgioioso@tue.nl

Sergio Grammatico
DCSC
TU Delft
s.grammatico@tudelft.nl

1 Introduction

Noncooperative games arise in several network domains, where multiple selfish decision-makers, or agents, aim at optimizing their individual, yet correlated, objective functions. Mathematically, a game is represented by the set of problems:

$$\forall i \in \mathcal{N} : \quad \underset{y_i}{\operatorname{argmin}} \, J_i(y_i, x_{-i}), \tag{1}$$

where $\mathcal{N}$ is the set of agents, and the cost function J_i of each agent depends not only on its strategy, but also on the decisions x_{-i} of all the competitors. The topic has received increased attention with the spreading of multi-agent systems, due to the numerous engineering applications, ranging from communication networks and demand-side management in the smart grid, to charging/discharging of electric vehicles and demand response in competitive markets.

From a game-theoretic perspective, the challenge is to design distributed Nash equilibrium (NE) seeking algorithms, using the limited knowledge available to each agent. A Nash equilibrium is a collective strategy $x^* = \operatorname{col}((x_i^*)_{i \in \mathcal{N}})$ from which no agent has an incentive to deviate, i.e.,

$$\forall i \in \mathcal{N} : \quad x_i^* \in \underset{y_i}{\operatorname{argmin}} J_i\left(y_i, x_{-i}^*\right).$$

Typically the assumption is made that each agent can access the decisions of all the competitors, for example in the presence of a coordinator that broadcast the data to the network [1]. However the existence of a central node with bidirectional communication with all the agents is impractical for many applications. Therefore, in recent years, fully distributed algorithms have been explored, that allow to compute NEs relying on local data only. Specifically, we consider a partial-decision information scenario, where the agents engage in nonstrategic information exchange with their neighbors over a communication network; based on the data received, they can estimate the strategies of all other agents, and eventually reconstruct the true values.

2 Contributions

To deal with the partial-decision information scenario, most of the results available resort to (projected) gradient and consensus dynamics, [2], [3]. The main drawback is that, usually, small (or diminishing) step sizes have to be chosen, affecting the speed of convergence. Therefore, we propose

a novel, a fully distributed, single layer, fixed step sizes NE seeking algorithm, where each agent updates its strategy based on a proximal best-response augmented with consensual terms. We establish geometric convergence, under strong monotonicity and Lipschitz continuity of the game mapping, by recasting our algorithm as a proximal-point iteration [4, §23], opportunely preconditioned to distribute the computation among the agents. This operator-theoretic interpretation proves very powerful. First, it allows to demonstrate the convergence of our algorithm even if the proximal operator is computed inexactly by the agents. Secondly, it favors the implementation of well-known accelerations scheme that can enhance the convergence speed. We demonstrate, both by comparing the theoretical rates and in numerical simulations, that our algorithm outperforms the existing gradient-based dynamics in terms of the number of iterations needed for the convergence, resulting in a considerable reduction of the communication burden.

References

[1] F. Facchinei and C. Kanzow, "Generalized Nash equilibrium problems," *Annals of Operations Research*, vol. 175, pp. 177–211, 2010.

[2] L. Pavel, "Distributed GNE seeking under partial-decision information over networks via a doubly-augmented operator splitting approach," *IEEE Transactions on Automatic Control, DOI: 10.1109/TAC.2019.2922953*, 2019.

[3] J. Koshal, A. Nedic, and U. V. Shanbhag, "Distributed algorithms for aggregative games on graphs," *Operations Research*, vol. 64, pp. 680–704, 2016.

[4] H. H. Bauschke and P. L. Combettes, *Convex analysis and monotone operator theory in Hilbert spaces*. Springer, 2017, vol. 2011.
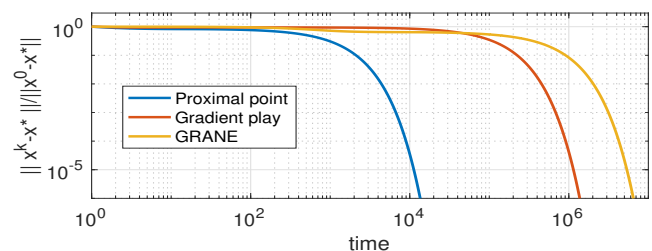
Figure 1: Comparison of the proximal-point algorithm with two gradient-based algorithms studied in literature.

Charging plug-in electric vehicles: a game theoretic approach

Carlo Cenedese
ENTEG
Groningen University, The Netherlands
c.cenedese@rug.nl

Filippo Fabiani
Department of Engineering Science
University of Oxford, United Kingdom
filippo.fabiani@eng.ox.ac.uk

Michele Cucuzzella
ENTEG
Groningen University, The Netherlands
m.cucuzzella@rug.nl

Jacquelien M. A. Scherpen
ENTEG
Groningen University, The Netherlands
j.m.a.scherpen@rug.nl

Ming Cao
ENTEG
Groningen University,The Netherlands
m.cao@rug.nl

Sergio Grammatico
Delft Center for Systems and Control
TU Delft, The Netherlands
s.grammatico@tudelft.nl

1 The problem of charging plug-in electric vehicles

Plug-in Electric Vehicles (PEVs) represent a promising alternative to the conventional fuel-based transportation [1]. However, they require a "smart" charge/discharge coordination to prevent undesired electricity demand peaks and congestion in the low-voltage distribution grid [2]. Indeed, a fleet of PEVs can serve as a *mobile extension* of the grid, mitigating the intermittent behavior of renewable energy sources by storing (or providing) energy when the generation is higher (or lower) than the load demand. These capabilities are known as " grid-to-vehicle" (g2v) and "vehicle-to-grid" (v2g), respectively [3]. In this context, a key role is played by the "fleet manager" or "aggregator", which is partially responsible for providing charging services to the PEVs, coordinating the charge/discharge schedule to fulfill the needs of the PEVs owners and (desirably) providing ancillary services to the distribution system operator [1, 2].

An attracting framework that suitably condenses both individual interests and intrinsic limitations related to the shared facilities is represented by noncooperative game theory whose equilibrium solution represents the best charging strategy of each PEV.However, most of the models adopted in the literature do not describe the natural discrete operations of each PEV, e.g., being plugged-in or plugged-out from one of the available charging points, in g2v or in v2g mode.This work presents an innovative solution to deal with these shortcomings by introducing integers variables in the model and a dynamical price of the energy. The introduction of integer decision variables enables us to model the inherent operating modes of the overall process, e.g. when a PEV is connected to one of the available charging points. Furthermore, the imposed logic constrains increase the safety and efficiency of the algorithm, ensuring that (i) the needs of the PEVs owners are fulfilled, (ii) the PEVs are not persistently connected to and disconnected from the grid among consecutive time intervals, (iii) the power required by both the PEVs and non-PEV loads does not exceed the grid capacity and (iv) the number of vehicles that can charge/discharge at the same time does not exceed the number of available charging points. The energy price is decided by the aggregator as a function of the total energy demand in the grid and this choice allows to coordinate the charging of PEVs in a decentralized fashion with the aim of filling the night-time valley in the demand. As a technical tool we used Mixed-Integer Generalized Potential Game, with an exact potential function, that we proved to converge to a mixed integer generalized Nash equilibrium of the game, if a sequential best-response algorithm is applied (All the technical details can be found in [4]).

References

[1]   J. Hu, H. Morais, T. Sousa, and M. Lind, "Electric vehicle fleet management in smart grids: A review of services, optimization and control aspects," *Renewable and Sustainable Energy Reviews*, vol. 56, pp. 1207–1226, 2016.

[2]   R. J. Bessa and M. A. Matos, "Economic and technical management of an aggregation agent for electric vehicles: A literature survey," *European Transactions on Electrical Power*, vol. 22, no. 3, pp. 334–350, 2012.

[3]   E. Sortomme and M. A. El-Sharkawi, "Optimal scheduling of vehicle-to-grid energy and ancillary services," *IEEE Transactions on Smart Grid*, vol. 3, no. 1, pp. 351–359, 2012.

[4]   C. Cenedese, F. Fabiani, M. Cucuzzella, J. Scherpen, M. Cao, and S. Grammatico, "Charging plug-in electric vehicles as a mixed-integer aggregative game," in *2019 IEEE 58th CDC*.   IEEE, 2019.

Autocratic strategies for infinitely repeated N-player games with arbitrary actions spaces

Emin Martirosyan†, Alain Govaert, Ming Cao

ENgineering and TEchnology institute Groningen (ENTEG)

University of Groningen, The Netherlands

Email: †e.n.martirosyan@rug.nl

1 Introduction

In many complex systems consisting of large numbers of selfish individuals, analysis of emerging behavior is a problem particularly addressed game theory. For example, social dilemma games model interactions among players where each one decides whether to sacrifice her own good in favor of the greater good. Different mechanisms and strategies were introduced to enable individuals to follow a particular behavior [1], [2]. We introduce an autocratic strategy for N-player games with arbitrary action spaces that allows a focal player to unilaterally enforce a linear relationship between her own payoff and the co-players' payoffs. In other words, it is a strategy that empowers a player a large control over the distribution of the payoffs. As an example, the proposed strategy is applied to a social dilemma game, namely the public goods game.

2 Autocratic strategy

Consider N-player iterated games with the actions spaces S_i and payoff functions $u_i(x_i, x_{-i})$ for $i \in \{1, \dots, N\}$. Players interact infinitely many times, deriving a payoff discounted by $\lambda \in (0,1)$ at each round determined by their payoff functions. Then, the average payoff of player i is

$$\pi_i = (1-\lambda) \sum_{t=0}^{\infty} \lambda^t u_i(x_i^{(t)}, x_{-i}^{(t)}), \tag{1}$$

where $x_i^{(t)}$ is an action of player i and $x_{-i}^{(t)}$ is an action profile of i's opponents played at round t. Each player uses a memory-one strategy σ_i (a strategy that describes a reaction of a player to an action profile played in the last round).

Theorem 1. Suppose that $\sigma_i[x_i, x_{-i}]$ is a memory-one strategy for player i and let σ_i^0 be player i's initial strategy. If, for some bounded function $\psi(\cdot)$ and fixed $\alpha, \gamma \in \mathbb{R}$, $\beta = \{\beta_j \in \mathbb{R} \mid j \neq i\}$, the equation

$$
\begin{aligned}
&\alpha u_i(x_i, x_{-i}) + \sum_{j \neq i} \beta_j u_j(x_i, x_{-i}) + \gamma = \psi(x_i) \\
&- \lambda \int_{s \in S_i} \psi(s) \, d\sigma_i[x_i, x_{-i}](s) - (1-\lambda) \int_{s \in S_i} \psi(s) \, d\sigma_i^0(s),
\end{aligned}
\tag{2}
$$

holds for all $(x_i, x_{-i}) \in S_i \times S_{-i}$, then (σ_i, σ_i^0) enforce the linear payoff relationship

$$\alpha \pi_i + \sum_{j \neq i} \beta_j \pi_j + \gamma = 0 \tag{3}$$

for any strategies of i's $N-1$ opponents.

In fact, Theorem 1 is difficult to apply because the integral term in (2), $\int_{s \in S_i} \psi(s) \, d\sigma_i[\mathbf{x}](s)$, in general cannot be solved explicitly. Thus, we show that under specific conditions, an autocratic strategist can use (σ_i, σ_i^0) concentrated on a finite set of points of S_i and unilaterally enforce the linear payoff relationship.

3 Example: Public Goods Game

Each of the N players makes a decision - whether or not to contribute to a public pot. Every player $i = \{1, \dots, N\}$ contributes $x_i \in [0,1]$. Her payoff function is given by

$$u_i(x_i, x_{-i}) = \frac{rc \sum_{k=1}^{N} x_k}{N} - cx_j \tag{4}$$

with $1 < r < N$ and $c > 0$.

Constructing a two-point autocratic strategy concentrated only at $x_i = 0$ and $x_i = 1$ and using the following parameterization

$$
\begin{aligned}
\rho &= -\sum_{j \neq i} \beta_j, & \chi &= \frac{\alpha}{\rho}, \\
\omega_{j \neq i} &= -\frac{\beta_j}{\rho}, & l &= -\frac{\gamma}{\alpha + \rho},
\end{aligned}
\tag{5}
$$

we analyze the existence of the following special types of autocratic strategies presented in the table below.

Autocratic strategy	Parameters value
Fair	$\chi = 1$
Generous	$l = rc - c$ and $0 < \chi < 1$
Extortionate	$l = 0$ and $0 < \chi < 1$

The results suggest that the fair strategy does not exist in the N-player public goods game with $\lambda \in (0,1)$. On the other hand, the existence of the generous and extortionate strategies requires the autocratic player making $x_i = 1$ and $x_i = 0$ contributions in $t = 0$, respectively.

References

[1] Press, William & Dyson, Freeman. (2012). Iterated Prisoners Dilemma Contains Strategies That Dominate Any Evolutionary Opponent. Proceedings of the National Academy of Sciences of the United States of America. 109.

[2] Nowak, Martin & Sigmund, Karl. (2005). Evolution of Indirect Reciprocity. Nature. 437.

Memristors as building blocks for neuromorphic computing

Anne-Men Huijzer, Bart Besselink
Bernoulli Institute for Mathematics, Computer Science and Artificial Intelligence
CogniGron - Groningen Cognitive Systems and Materials Center
University of Groningen
m.a.huijzer@rug.nl, b.besselink@rug.nl

1 Introduction

Digital computers are build based on the Turing machine and employ the so-called von Neumann architecture. Here, computation and memory storage take place in different regions of the device, which leads to a high use of energy. This, in addition to the stagnating developments in the processing speed of the devices, motivates the interest in new computing paradigms such as neuromorphic computing. This computing paradigm is inspired by the human brain and hopes to learn from the efficiency of it, which is believed to be a consequence of the co-location of memory and computing.

Suggested building blocks for neuromorphic computing are memristors [2], i.e. resistors with memory storage, because of their nonlinearity and ability to store information. These characteristics give the devices a high potential to mimic synapses, the connection between different neurons, in the human brain.

2 Memristors

Memristors are introduced as a new two-terminal circuit element by Leon Chua in the early 1970s [1]. They can be described as a relationship between the charge $q(t) = \int_{-\infty}^{t} i(\tau)d\tau$ and flux-linkage $\varphi = \int_{-\infty}^{t} v(\tau)d\tau$ as

$$\dot{x}(t) = f(x(t)),$$
$$i(t) = G(x(t))v(t). \qquad (1)$$

Here, $i(t)$ and $v(t)$ are equal to the current through and the voltage across the device in the case of a voltage-controlled memristor, and opposite in the case of a flux-controlled device. The function G is continuous and represents the memristance and memductance of the device in the case of a voltage- and flux-controlled memristor, respectively. Memristors are characterized by a hysteresis loop going through the origin in an $i(t)$, $v(t)$ diagram, as shown in Figure 2. In addition to single memristors, memristor networks, i.e. electrical networks in which each edge corresponds to a memristor, are considered. It can be shown that these networks are also characterized by a hysteresis loop going through the origin. By developing tools for the modelling and analysis of the external behavior of such networks, we want to investigate whether networks of memristors exhibit a richer
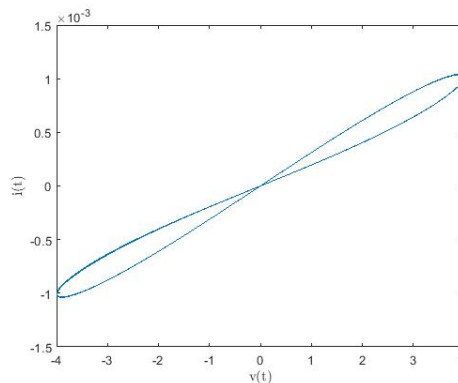
Figure 1: Simulation result obtained for (1) with $f(x(t)) = v(t)$ and $G(x(t)) = 1.884x(t) + 0.25$. The diagram shows the relation between $v(t)$ and $i(t)$ obtained for the input $v(t) = 4\sin(40\pi t + \pi/3)$.

dynamical behavior than a single memristor. To this end, we utilize graph theory and extend the notions of Kron reduction and effective resistance, as described in [3], to memristor networks. By considering the external behavior of memristor networks we can compare the dynamics of a memristor network with the dynamics of a single memristor.

3 Results

Simulation results of the external behavior of memristor networks with a varying number of memristors and network structure show that the dynamic behavior of memristor networks differs from that of a single memristor. This suggests that proper design of the structure of memristor networks can be used to achieve desired memristor behavior needed for using these devices as building blocks for neuromorphic computing, i.e. needed to mimic the dynamical behavior of a synapse in the human brain.

References

[1]   L. Chua, "Memristor-the Missing Circuit Element," IEEE Transactions on circuit theory, vol. 18, no. 5, pp. 507-519, 1971.

[2]   T. Chang, Y. Yang, W. Lu, "Building Neuromorphic Circuits with Memristive Devices," IEEE Circuits and Systems Magazine, vol. 13, no. 2, pp. 56-73, 2013.

[3]   F. Dörfler, F. Bullo, "Kron Reduction of Graphs With Applications to Electrical Networks," IEEE Transactions on Circuits and Systems, vol. 60, no. 1, pp. 150-163, 2013.

A forward approach to controllability of switched DAEs

P. Wijnbergen
Bernoulli Institute, RUG
Email: `p.wijnbergen@rug.nl`

S. Trenn
Bernoulli Institute, RUG
Email: `s.trenn@rug.nl`

Introduction

In this note we consider *switched differential algebraic equations* (switched DAEs) of the following form:

$$E_\sigma \dot{x} = A_\sigma x + B_\sigma u, \qquad (1)$$

where $\sigma : \mathbb{R} \to \mathbb{N}$ is the switching signal and $E_p, A_p \in \mathbb{R}^{n \times n}$, $B_p \in \mathbb{R}^{n \times m}$, for $p, n, m \in \mathbb{N}$. In general, trajectories of switched DAEs exhibit jumps (or even impulses), which may exclude classical solutions from existence. Therefore, we adopt the *piecewise-smooth distributional solution framework* introduced in [2]. We study controllability of (1) on the interval $[t_0, t_f]$ where (1) is controllable if for all initial values there exists an input such that $x_u(t_f^-, x_0) = 0$. Furthermore, we assume that the switching signal only has finitely many switches in that interval and assume that the switching signal is of the form $\sigma(t) = p$ if $t \in [t_p, t_{p+1})$.

Problem setting

Necessary and sufficient conditions for controllability of a switched DAE are given in [1]. However, these conditions involve a backward approach, where all calculations redone again if the length of the interval increases. This abstract introduces necessary and sufficient conditions for controllability of switched DAEs that only depend on calculations that run forward in time.

Since controllability implies the existence of an input such that the state is zero at t_f^- for any initial condition, it means that $\min_u x_u(t_f^-, x_0) = 0$ for all x_0. Hence in order to verify whether the system is controllable, we compute the minimum norm of the state at the end of the interval $[t_0, t_f]$. To that extent, we first introduce certain projectors for a given switched DAE. Let $\mathcal{C}_i$ be the controllable space of the ith mode. Then $\Pi_{\mathcal{C}_i^\perp}$ is the projector onto $\mathcal{C}_i^\perp$ along $\mathcal{C}_i$. These projectors project solutions on the interval (t_i, t_{i+1}) to elements of the augmented consistency space of the ith mode. This allows us to compute the x_0-uncontrollable orthogonal subspace, defined as follows.

Definition 1 *Consider the system* (1). *The x_0-uncontrollable orthogonal subspace Ψ_i is defined by the following sequence*

$$\Psi_0 = \operatorname{im} \Pi_{\mathcal{C}_0^\perp} e^{A_0^{diff}(t_1 - t_0)} \Pi_0,$$

$$\Psi_{i+1} = \operatorname{im} \Pi_{\mathcal{C}_{i+1}^\perp} e^{A_{i+1}^{diff}(t_{i+1} - t_i)} \Pi_{i+1} \Psi_i.$$

In addition to the x_0-uncontrollable orthogonal subspace we also introduce the reachable space, which can be computed by the algorithm given by Proposition 1.

Definition 2 *Consider the system* (1). *The time t_i reachable space is defined by*

$$\mathcal{R}^{[0,t_i]} = \{x \in \mathbb{R}^n \mid \exists u \ s.t. \ x_u(t_i, 0) = x\}.$$

Proposition 1 *Consider the following sequence of sets:*

$$\mathcal{S}_0 = \mathcal{C}_0,$$

$$\mathcal{S}_{i+1} = e^{A_{i+1}^{diff}(t_{i+2} - t_{i+1})} \Pi_{i+1} \mathcal{S}_i + \mathcal{C}_{i+1},$$

then we have $\mathcal{S}_i = \mathcal{R}^{[0,t_{i+1}]}$ for $i \in \{0, 1, ..., n\}$.

It turns out that we can decompose a solution, evaluated before the switching instance, as follows.

Lemma 1 *Consider the system* (1). *If $x_u(t, x_0)$ is a solution of* (1)*, then we can compose the solution befor each switching instance as follows.*

$$x_u(t_i^-, x_0) = \psi + \eta, \qquad \psi \in \Psi_{i-1}, \eta \in \mathcal{R}^{[t_0, t_i)}$$

Main result

If the system is controllable, there must exist an input such that $x_u(t_f^-, x_0) = 0$. In terms of the decomposition of Lemma 1 this yields the following theorem.

Theorem 1 *Consider the switched DAE* (1). *The initial condition $x_0 \in \mathcal{R}$ of the switched system is controllable if and only if $\Psi_n \subseteq \mathcal{R}^{[t_0, t_f)}$.*

Note that if the conditions in Theorem 1 are satisfied for all basis vectors of the state-space, then the condition is satisfied for all elements of the state-space. Furthermore, both the computation of the Ψ_n and $\mathcal{R}^{[t_0, t_f)}$ run forward in time, allowing for an extension of $[t_0, t_f)$ without much computational effort.

References

[1] Ferdinand Küsters, Markus G.-M. Ruppert, and Stephan Trenn. Controllability of switched differential-algebraic equations. *Syst. Control Lett.*, 78(0):32 – 39, 2015.

[2] Stephan Trenn. *Distributional differential algebraic equations*. PhD thesis, Institut für Mathematik, Technische Universität Ilmenau, Universitätsverlag Ilmenau, Germany, 2009.

A New Framework for Control of Multi-agent Systems over Wireless

Matthias Pezzutto
Department of Information Engineering
University of Padova
via Gradenigo 6B, Padova, Italy.
matthias.pezzutto@phd.unipd.it

Emanuele Garone
Ecole Polytechnique de Bruxelles
Université Libre de Bruxelles
avenue Franklin Roosevelt 50, Bruxelles, Belgium.
egarone@ulb.ac.be

1 Abstract

Our work aims to devise a valid and reliable strategy for control of multi-agent systems. We propose a novel layer structure which features, from top to bottom, a high-level motion planner, a scheme in charge of the supervision of the agents, a wireless network to enable communications, and a local control layer on the top of the physical systems. The key role is played by the supervision scheme, which transforms a rough trajectory into the accurate local reference signals for each agent taking into account coordination aspects, constraints, and unreliability due to the wireless communication. We propose a novel sequential distributed Reference Governor with a mechanism to efficiently overcome packet losses due to the network.

2 Motivation

As to date different solutions already exist to deal with multi-agent systems. A first large body of literature does not make use of a communication network. In these works, a leader knows the desired trajectory while the other agents follow it exploiting a suitable sensing apparatus (e.g. cameras, force sensors). This approach is mainly used for formation control but it is not suitable to address more complicated tasks like cooperative manipulation. To overcome this limitation, the communications of current states and future intentions are considered by other works. For example, several algorithms exploit a central unit that collects information from the agents and transmits the suitable trajectories. Similar strategies but with a distributed fashion also exist. These works usually consider ideal communication links ensuring that the computing unit has always a perfect knowledge of the system (or of the neighbours), but this assumption is not verified in many multi-agent systems (e.g. mobile robots) where wireless networks come into play. Indeed, it is known that wireless communications are not completely reliable due to the intrinsic nature of the wireless mean, that is affected by interferences and external noise: packets containing the states and the commands can be delayed or even lost. A large body of literature has faced up control over wireless but stability requirements turn out to be too strict to fully remotely control plants using existing networks with an adequate safety margin. Our layer structure overcomes the limitations of the aforementioned approaches to improve existing results in multi-agent control.
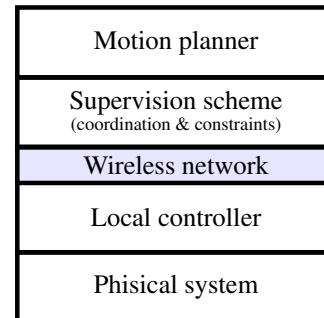
Figure 1: Proposed layer structure

3 The layer structure

The proposed layer structure is reported in Fig. 1. The highest layer is the motion planner, which provides to the lower layer an high-level trajectory or a simple set-point. The supervision scheme computes the reference signals for the agents while managing constraints, coordination, and unreliable links. The wireless network puts in communication the supervision layer and the local control layer. Local controllers are designed to achieve stability and desired performances of the physical system, namely the lowest layer.

The main focus of our research is on the supervision scheme, for which we propose to use a distributed sequential Reference Governor. We consider a problem formulation similar to [3] but focusing on the case in which few agents are present (our target application is load transportation) and taking into account packet losses [2]. With slight changes of [1], we find the solution for the case with two agents. Currently we are working to manage the larger information asymmetry due to a number of agents greater than two.

References

[1]   M. Pezzutto, E. Garone, L. Schenato, "Reference governor for constrained control over lossy channels." IEEE Control Systems Letters 4(2), 271-276. 2020.

[2]   L. Schenato, "Optimal estimation in networked control systems subject to random delay and packet drop." IEEE Transactions on Automatic Control 53(5), 1311-1320. 2008.

[3]   A. Casavola, E. Garone, F. Tedesco, "A distributed multi-agent command governor strategy for the coordination of networked interconnected systems." IEEE Transactions on Automatic Control 59(8), 2099-2112. 2014.

Robust $\mathscr{H}_\infty$-controller design for uncertain time-delay systems

Pieter Appeltans and Wim Michiels

NUMA, KU Leuven, Celestijnenlaan 200a - box 2402, B-3001 Leuven, Belgium

{pieter,wim}.{appeltans,michiels}@cs.kuleuven.be

1 Abstract

This work considers dynamical systems with state delay and uncertain state matrices:

$$
\begin{cases}
\dot{x}(t) = \sum_{k=0}^{K} (A_k + Q_k \delta R_k) x(t - \tau_k) + B^1 w(t) + B^2 u(t) \\
z(t) = C^1 x(t) + D^{11} w(t) + D^{12} u(t) \\
y(t) = C^2 x(t) + D^{21} w(t) + D^{22} u(t)
\end{cases}
\tag{1}
$$

with $x \in \mathbb{R}^n$ the state; $w \in \mathbb{R}^{m_1}$ the performance input; $u \in \mathbb{R}^{m_2}$ the control input; $z \in \mathbb{R}^{p_1}$ the performance output; $y \in \mathbb{R}^{p_2}$ the observable output; A_k, Q_k and R_k for $k = 0 \ldots K$, B^1, B^2, C^1, C^2, D^{11}, D^{12}, D^{21} and D^{22} real-valued matrices of appropriate dimension; $\delta \in \mathbb{R}^{q \times r}$ a real-valued uncertainty bounded in Frobenius norm by $\bar{\delta}$ and $0 = \tau_0 < \tau_1 < \cdots < \tau_K$ real-valued delays. This system is controlled using a dynamical controller of order n_c:

$$
\begin{cases}
\dot{\xi}(t) &=& F\xi(t) + Gy(t) \\
u(t) &=& H\xi(t) + Ky(t)
\end{cases}
\tag{2}
$$

with $\xi \in \mathbb{R}^{n_c}$ the state of the controller and F, G, H, and K real-valued matrices of appropriate dimension. If $I - D^{22} K$ is invertible, then the closed-loop of (1) and (2) can be written in the following form:

$$
\begin{cases}
\dot{x}^{cl}(t) = \sum_{k=0}^{K} \left(A_k^{cl}(\mathbf{p}) + Q_k^{cl} \delta R_k^{cl} \right) x^{cl}(t - \tau_k) + B^{cl}(\mathbf{p}) w(t) \\
z(t) = C^{cl}(\mathbf{p}) x^{cl}(t) + D^{cl}(\mathbf{p}) w(t),
\end{cases}
\tag{3}
$$

with $x^{cl} = \begin{bmatrix} x^T & \xi^T \end{bmatrix}^T$ and $\mathbf{p} = \mathrm{VEC}(F, G, H, K)$, a vector containing all elements of the controller matrices. The associated performance input-output transfer function is equal to:

$$
\begin{aligned}
T(s; \delta, \mathbf{p}) =& C^{cl}(\mathbf{p}) \left(Is - \sum_{k=0}^{K} (A_k^{cl}(\mathbf{p}) + Q_k^{cl} \delta R_k^{cl}) e^{-s\tau_k} \right)^{-1} B^{cl}(\mathbf{p}) \\
&+ D^{cl}(\mathbf{p}).
\end{aligned}
$$

If (3) is internally, exponentially stable for particular realisations of δ and $\mathbf{p}$, then the $\mathscr{H}_\infty$-norm of the associated transfer function quantifies the worst-case energy gain of the system and is hence an important performance measure:

$$
\|T(\cdot; \delta, \mathbf{p})\|_{\mathscr{H}_\infty} := \sup_{\omega \in \mathbb{R}^+} \sigma_1\left(T(j\omega; \delta, \mathbf{p}) \right) = \sup_{\substack{w \in \mathscr{L}_2 \\ w \neq 0}} \frac{\|z\|_{\mathscr{L}_2}}{\|w\|_{\mathscr{L}_2}}
\tag{4}
$$

with $\sigma_1(\cdot)$ the largest singular value, $\mathscr{L}_2$ the space of square integrable signals and $\|\cdot\|_{\mathscr{L}_2}$ the associated norm. The robust $\mathscr{H}_\infty$-norm is defined as the worst-case $\mathscr{H}_\infty$-norm over all realisations of the uncertainty δ:

$$
\begin{aligned}
\|T(\cdot; \cdot, \mathbf{p})\|_{\mathscr{H}_\infty}^{\bar{\delta}} &= \max_{\delta \in \mathbb{R}^{q \times r}, \|\delta\|_F \leq \bar{\delta}} \|T(\cdot; \delta, \mathbf{p})\|_{\mathscr{H}_\infty} \\
&= \max_{\substack{\delta \in \mathbb{R}^{q \times r} \\ \|\delta\|_F \leq \bar{\delta}}} \sup_{\omega \in \mathbb{R}^+} \sigma_1\left(T(j\omega; \delta, \mathbf{p}) \right).
\end{aligned}
\tag{5}
$$

The goal of this work is to find controller parameters $\mathbf{p}$ such that this robust $\mathscr{H}_\infty$-norm is minimized. These minimizing parameters will be found by solving the non-smooth non-convex minimization problem

$$
\mathbf{p}^\star = \arg\min_{\mathbf{p}} \|T(\cdot; \cdot, \mathbf{p})\|_{\mathscr{H}_\infty}^{\bar{\delta}}
$$

using HANSO [3]. This requires the evaluation of $\|T(\cdot; \cdot, \mathbf{p})\|_{\mathscr{H}_\infty}^{\bar{\delta}}$ and its derivative with respect to the control parameters when these derivatives exist. The former can be computed using the recently developed method presented in [1] which uses the relation between the robust $\mathscr{H}_\infty$-norm and the robust distance to instability of an associated eigenvalue problem. The derivatives can be computed at points for which the δ and ω that maximize (5) are unique and the associated maximal singular value is simple.

The presented theory can also be generalised to systems with delays in the input, output and direct feed-through terms. However, for such systems the $\mathscr{H}_\infty$-norm of a particular realisation of the closed loop might be sensitive to arbitrary small delay changes. In that case it is better to consider the (robust) strong $\mathscr{H}_\infty$-norm [2]. Also systems with uncertainties on the delays, multiple uncertainties, and uncertainties in the input, output and direct feed-through matrices can be considered. More detail on how to compute the robust strong $\mathscr{H}_\infty$-norm of these systems can be found in [1]. The controller can subsequently be designed using the non-smooth optimization approach outlined above.

References

[1] Pieter Appeltans and Wim Michiels. A pseudo-spectra based characterisation of the robust strong H-infinity norm of time-delay systems with real-valued and structured uncertainties. *arXiv preprint arXiv:1909.07778*, 2019.

[2] Suat Gumussoy and Wim Michiels. Fixed-order H-Infinity control for interconnected systems using delay differential algebraic equations. *SIAM Journal on Control and Optimization*, 49(5):2212–2238, 2011.

[3] Michael L. Overton. Optimization, HANSO: a hybrid algorithm for nonsmooth. *Available from cs.nyu.edu/overton/software/hanso*, 2009.

Strong structural properties of structured linear systems

B. M. Shali,	H. J. van Waarde,	M. K. Camlibel,	H. L. Trentelman
b.m.shali@rug.nl	h.j.van.waarde@rug.nl	m.k.camlibel@rug.nl	h.l.trentelman@rug.nl

Bernoulli Institute, University of Groningen, The Netherlands

1 Introduction

The concept of structure for linear systems was introduced by Lin in [1] in order to obtain more realistic models of physical systems. Lin recognizes that most of the parameters in a physical model are known only with the approximation of some errors of measurement, and only some are known precisely. The latter typically happens for entries which are equal zero, indicating no physical relationship between variables. With this in mind, the novel idea introduced in [1] is that the entries of the system matrices are not known precisely, but are known to be fixed zeros or arbitrary real numbers. This pattern of fixed zeros gives the system its structure, and is what makes it a structured system. We will also consider entries that are known to be nonzero real numbers, which proves to be useful in some applications. For example, when modelling a network of scalar linear systems, the entries of the system matrices are fixed zeros for missing links, nonzero real numbers for existing links, and arbitrary real numbers for unknown or faulty links.

We will follow the approach taken in [2] and use pattern matrices to define structured systems. Then we will define strong structural properties and characterize them using the pattern matrices that describe a structured system.

2 Pattern Matrices

A matrix with entries from the set $\{0, *, ?\}$ is called a *pattern matrix*. The *pattern class* $\mathscr{P}(\mathscr{A})$ of a pattern matrix $\mathscr{A} \in \{0, *, ?\}^{m \times n}$ is defined as the set

$$\{A \in \mathbb{R}^{m \times n} \mid A_{ij} = 0 \text{ if } \mathscr{A}_{ij} = 0 \text{ and } A_{ij} \neq 0 \text{ if } \mathscr{A}_{ij} = *\}.$$

In other words, an entry of the pattern matrix $\mathscr{A}$ indicates a fixed zero (0), nonzero ($*$) or arbitrary (?) real number in the corresponding entry of the real matrices in the pattern class of $\mathscr{A}$. Addition and multiplication for the set $\{0, *, ?\}$ can be defined in a natural way, from which addition and multiplication for pattern matrices is defined as usual.

3 Strong Structural Properties

Let (A, B, C, D) denote the linear time-invariant system

$$\dot{x} = Ax + Bu, \qquad y = Cx + Du,$$

with state x, input u and output y. In the context of control, we are typically interested in the system-theoretic properties of (A, B, C, D). If the entries of A, B, C and D are known precisely, then we have a variety of tests and conditions to check if (A, B, C, D) possesses a given system-theoretic property.

Now, suppose that the entries of the matrices A, B, C and D are not known precisely, but are known to be fixed zeros, nonzero or arbitrary real numbers. In other words, we know that $A \in \mathscr{P}(\mathscr{A})$, $B \in \mathscr{P}(\mathscr{B})$, $C \in \mathscr{P}(\mathscr{C})$ and $D \in \mathscr{P}(\mathscr{D})$ for some known pattern matrices $\mathscr{A}, \mathscr{B}, \mathscr{C}$ and $\mathscr{D}$. This naturally leads to a family of systems (A, B, C, D) as A, B, C and D range over the corresponding pattern classes. This family is called a *structured system* and is denoted by $(\mathscr{A}, \mathscr{B}, \mathscr{C}, \mathscr{D})$. Note that the system (A, B, C, D) is sure to possess a given system-theoretic property if and only if it possesses that property for all $A \in \mathscr{P}(\mathscr{A})$, $B \in \mathscr{P}(\mathscr{B})$, $C \in \mathscr{P}(\mathscr{C})$ and $D \in \mathscr{P}(\mathscr{D})$. Then that property is more appropriately attributed to $(\mathscr{A}, \mathscr{B}, \mathscr{C}, \mathscr{D})$, and is referred to as a *strong structural property*.

We would like to derive tests and conditions to check if $(\mathscr{A}, \mathscr{B}, \mathscr{C}, \mathscr{D})$ possesses a given strong structural property. This has already been done in [2] for strong structural controllability. We can extend the results from [2] to output controllability, input-state observability and left invertibility. Recall that a system (A, B, C, D) is output controllable if and only if the matrix $\begin{bmatrix} D & CB & CAB & \cdots & CA^{n-1}B \end{bmatrix}$ has full row rank, where n is the dimension of the state. Using this, we obtain the following result.

Theorem 1. *The structured system $(\mathscr{A}, \mathscr{B}, \mathscr{C}, \mathscr{D})$ is strongly structurally output controllable if the pattern matrix $\begin{bmatrix} \mathscr{D} & \mathscr{C}\mathscr{B} & \mathscr{C}\mathscr{A}\mathscr{B} & \cdots & \mathscr{C}\mathscr{A}^{n-1}\mathscr{B} \end{bmatrix}$ has full row rank.*

Similarly, we can derive necessary and sufficient conditions for strong structural input-state observability, as well as a couple of distinct sufficient conditions for strong structural left invertibility. Finally, we can provide graph-theoretic algorithms to check if those conditions are satisfied.

References

[1]   C.-T. Lin, "Structural controllability," *IEEE Transactions on Automatic Control*, vol. 19, pp. 201–208, 1974.

[2]   J. Jia, H. J. van Waarde, H. L. Trentelman, and M. K. Camlibel, "A Unifying Framework for Strong Structural Controllability," arXiv:1903.03353, 2019.

Model reduction of switched systems in time-varying approach

Md Sumon Hossain, Stephan Trenn
Bernoulli Institute for Mathematics, Computer Science, and Artificial Intelligence,
University of Groningen, The Netherlands
Emails: `s.hossain@rug.nl, s.trenn@rug.nl`

1 Introduction

Consider switched linear systems of the form:

$$S_\sigma : \begin{cases} \dot{x}(t) = A_\sigma x(t) + B_\sigma u(t), & x(t_0) = \mathbf{0}, \\ y(t) = C_\sigma x(t), \end{cases} \quad (1)$$

where $\sigma : \mathbb{R} \to M = \{0, 1, 2, \cdots, s\}$ with finitely many switching times $t_0 < t_1 < t_2 < t_3 < \cdots < t_s$. The system matrices are $A_i \in \mathbb{R}^{n \times n}$, $B_i \in \mathbb{R}^{n \times m}$, $C_i \in \mathbb{R}^{p \times n}$, $D_i \in \mathbb{R}^{n \times m}$, where $i \in M$. Here, the i-th mode is active in the interval $[t_i, t_{i+1})$, for $i = 1, \cdots, s$.

Recently, many works have been done on model order reduction (MOR) of switched linear systems. We view here the switched system as a special *time-varying* system and aim for a (time-varying) model-reduction depending on a given (known) switching signal. A model reduction approach is proposed for piecewise constantly switched systems, based on balancing based MOR method for linear time-varying systems, for details see [1].

2 Problem setting

The available balanced truncation methods for time-varying system assume that the coefficient matrices are at least continuous. However, the switched system (1) seen as a time-varying system has *discontinuous* coefficient matrices, so we propose (continuously) time-varying approximation:

$$S_\varepsilon : \begin{cases} \dot{x}(t) = A_\varepsilon(t) x(t) + B_\varepsilon(t) u(t), & x(t_0) = \mathbf{0}, \\ y(t) = C_\varepsilon(t) x(t), \end{cases} \quad (2)$$

where, for example $A_\varepsilon(.)$ is defined as follows:

$$A_\varepsilon(t) = \begin{cases} A_i + \frac{t - t_i}{\varepsilon}(A_{i+1} - A_i) & : t \in [t_i, t_i + \varepsilon], \\ A_{i+1} & : t \in (t_i + \varepsilon, t_{i+1}] \end{cases}.$$

3 Model reduction

At first we compute the time-varying controllability and observability Gramians $P(t)$ and $Q(t)$ respectively. Let the time-varying system (2) is boundedly completely controllable and observable on $[t_0, t_f]$. Then there exists a time-varying coordinate transformation T such that

$$T(t)^{-1} P(t) T(t)^{-\top} = T(t)^\top Q(t) T(t) = \Pi(t),$$

for all $t \in [t_0, t_f]$. In fact, $T(t) = R(t) U(t) \Pi(t)^{-1/2}$, $T(t)^{-1} = \Pi(t)^{-1/2} V(t)^\top L(t)^\top$, where $U(t) \Pi(t) V(t)^\top = svd(R(t)^\top L(t))$, and where $R(t) R(t)^\top = P(t)$ and $L(t) L(t)^\top = Q(t)$ are the Cholesky decompositions of P and Q, respectively.

Using the projection matrices, we compute reduced system:

$$\hat{S}_\varepsilon : \begin{cases} \dot{\hat{x}}(t) = \hat{A}_\varepsilon(t) \hat{x}(t) + \hat{B}_\varepsilon(t) u(t), & \hat{x}(t_0) = \mathbf{0}, \\ \hat{y}(t) = \hat{C}_\varepsilon(t) \hat{x}(t), \end{cases} \quad (3)$$

where the system matrices are $\hat{A}_i \in \mathbb{R}^{r \times r}$, $\hat{B}_i \in \mathbb{R}^{r \times m}$, $\hat{C}_i \in \mathbb{R}^{p \times r}$, $D_i \in \mathbb{R}^{r \times m}$, for $i \in M$ and $r \ll n$.

4 Results

Consider a randomly generated SISO switched linear system

$$A_1 = \begin{bmatrix} -0.74 & 0.3 & 0.2 & -0.01 & -0.06 \\ 0.965 & -1.43 & -0.5 & 0.8 & -0.26 \\ 0.922 & -0.0487 & -0.44 & 0.03 & 0.054 \\ -0.98 & 0.28 & 0.31 & -0.764 & 0.07 \\ -0.634 & -1.26 & 0.534 & 0.662 & -0.48 \end{bmatrix}, B_1 = \begin{bmatrix} 2 \\ 1.4 \\ 1.1 \\ -0.06 \\ 0.08 \end{bmatrix},$$

$$C_1 = \begin{bmatrix} 2.5 & 2 & 1.6 & 0.02 & -0.03 \end{bmatrix}, A_2 = A_1 - 0.5 * I_5,$$

$$B_2 = \begin{bmatrix} 2.5 & 1.8 & .3 & 0.6 & -1 \end{bmatrix}^T, C_2 = \begin{bmatrix} 1.5 & 1.4 & .7 & 0.1 & 0.2 \end{bmatrix}, \varepsilon = 10^{-3}.$$

Consider switching times are $t_1 = 2s, t_2 = 4s$. Applying proposed technique, we compute first order reduced system. Figure 1 shows that the first order reduced system gives good approximation of original system.
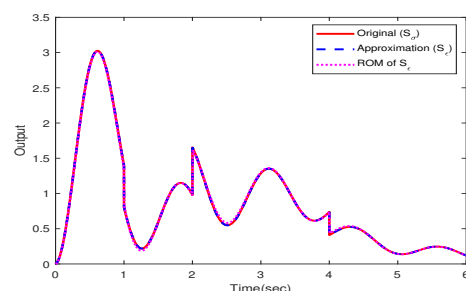
Figure 1: Comparison between the output of original system, proposed approximation and 1st order reduced system.

References

[1] N. Lang, J. Saak, T. Stykel "Balanced truncation model reduction for linear time-varying systems," Math. and Comp. Mod. of Dyn. Sys., 22, p. 267-281, 2016.

On co-designing active seismic control of a tall building with actuator selection

Taranjitsingh Singh, Jan Swevers and Goele Pipeleers
MECO Research Team, Department of Mechanical Engineering, KU Leuven
DMMS Lab, Flanders Make, Leuven, Belgium
Email: taranjitsingh.singh@kuleuven.be

1 Introduction

$\mathcal{H}_\infty$ output feedback control design have a capability of designing stable and high performance feedback controllers for multivariable systems which is in demand. For e.g, design of an active seismic controller for tall buildings. Century park tower in Tokyo is equipped with active tuned mass dampers (ATMDs) on 4 floors [1]. A question arises whether a better seismic control performance is achieved with a different ATMD location scheme.

Feedback control design for all the possible combinations of actuators is expensive. We need a computationally inexpensive method for co-design that avoids solving all combinations. One such method is formulating the co-design problem as a Mixed Boolean Semi-definite Programming (MBSDP) and solve it using Branch and Bound (BNB) algorithm [2].

2 Modeling of a $n-$floor building

The modeling of a tall building of n-floors is shown in the Figure. 1. The dynamic model is constructed from the state

$$\mathcal{A} = \Pi \begin{bmatrix} 0_{n \times n} & I_n \\ -M^{-1}K_s & -M^{-1}C_d \end{bmatrix} \Pi^{-1},$$
$$\mathcal{B}_u = \Pi \begin{bmatrix} 0_{n \times p} \\ M^{-1}T_u \end{bmatrix}, \mathcal{B}_w = \Pi \begin{bmatrix} 0_{n \times 1} \\ -1_{n \times 1} \end{bmatrix}$$
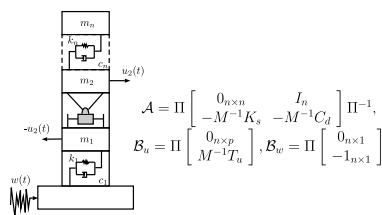
Figure 1: model with masses, stiffness and as damping coefficients, with u_i as actuator inputs and w as disturbance.

space matrices given in eq in Figure. 1, with M, K_s, C_d and T_u as mass, stiffness, damping and control location matrix respectively and Π as the state transition matrix with inputs as actuation forces and outputs as interstory accelerations.

3 Co-design of the building

For the co-design, a 20-story building is considered and the parameters are taken from [3]. The aim is to design an active seismic feedback control by reducing the vibrations on interstory accelerations with minimizing actuator efforts. The

optimization problem which is solved using BNB is shown as

$$\begin{aligned} \text{minimize:} \quad & \gamma \\ \text{subject to:} \quad & \text{LMIs} < 0, \quad \text{Big-M reformulation} \\ & \|a\|_1 = 4, a_{20} = 1 \end{aligned} \quad (1)$$

Here, LMIs are the linear matrix inequalities for $\mathcal{H}_\infty$ controller synthesis, Big-M reformulations are responsible for decoupling MBSDP variables, and other constraints imply choosing optimal 4 floor locations, with the location on the top floor is fixed.

As a result, the algorithm selects the first 3 floors as a global solution with 33.60% faster that exhaustive search. The maximum singular value is reduced to 20.47% using 4 actuators for active seismic control. The time response in Figure. 2 is shown for earthquake distubances from Kobe and Chichi for the roof accelerations. For Kobe, the average rms reduction for all floors is 24.75% and for Chichi is 31.67% using active seismic control.
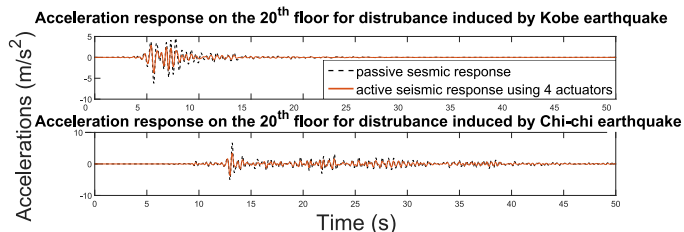
Figure 2: Time response for interstory acceleration in 20th floor for Kobe and Chichi earthquakes

References
[1]   Y. Ikeda, "Active and semi-active control of buildings in japan," *Journal of Japan Association for Earthquake Engineering*, vol. 4, no. 3, pp. 278–282, 2004.
[2]   T. Singh, M. De Mauri, W. Decré, J. Swevers, and G. Pipeleers, "Combined $\mathcal{H}_\infty/\mathcal{H}_2$ controller design and optimal selection of sensors and actuators," *IFAC-PapersOnLine*, vol. 51, no. 25, pp. 73–77, 2018.
[3]   F. Palacios-Quiñonero, J. Rubió-Massegú, J. Rossell, and J. Rodellar, "Design of distributed multi-actuator systems with incomplete state information for vibration control of large structures," *Designs*, vol. 2, no. 1, p. 6, 2018.

High pixel number deformable mirror concept utilizing piezoelectric hysteresis for stable shape configurations

A.E.M. Schmerbauch[1*], M.A. Vasquez Beltran[1], A.I. Vakis[2], B. Jayawardhana[1], R. Huisman[3]

University of Groningen, Engineering and Technology Institute Groningen, Discrete Technology and Production Automation[1]

University of Groningen, Engineering and Technology Institute Groningen, Computational Mechanical and Materials Engineering[2]

SRON Groningen, Kapteynborg, Landleven 12, 9747 AD Groningen[3]

Email[*]: a.e.m.schmerbauch@rug.nl

1 Introduction

Deformable mirrors (DMs) are instruments used for wavefront correction in advanced imaging systems. In this work, we develop a control method for the mirror deflection of a new concept of DM termed a hysteretic deformable mirror (HDM) (Figure 1), whose actuation mechanism consists of multilayered piezoelectric actuators with high hysteresis. By exploiting the hysteresis behavior, which is often undesired in most high-precision systems, high pixel (actuator) numbers can be realised that allow for high spatial frequency wavefront correction. The HDM exploits the memory introduced by the actuators' hysteresis to enable the deflection control in a "set and forget" manner. The simple electrode layout in every layer of actuators allows the multiplexing of a single control signal for the complete HDM.
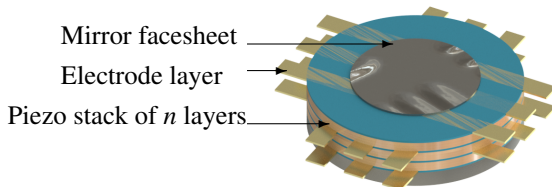
Figure 1: Concept of the hysteretic deformable mirror.

2 Modeling the mirror facesheet

We obtain a mechanical model to describe the relation between the mirror facesheet deflection z and the pressures q applied by the actuators. We consider the Poisson equation in polar coordinates (r,ϕ) for small surface displacements for a membrane under tension [1, 2]. Incorporating the HDM's particular arrangement of the electrodes into the solution to Poisson's equation leads to

$$z(r,\phi,r',\phi') = C \iint_A \mathscr{F}(r,\phi,r',\phi'(r'))\, q(r',\phi')\, d\phi'\, dr' \quad (1)$$

with $A = \{(r',\phi')|\phi_1(r') \leq \phi' \leq \phi_2(r'), 0 \leq r' \leq 1\}$ where

$$\mathscr{F}(r,\phi,r',\phi'(r')) = \begin{cases} f_1(r,\phi,r',\phi'(r')) & \text{if } 0 < r' < r \\ f_2(r,\phi,r',\phi'(r')) & \text{if } r < r' < 1. \end{cases}$$

The solutions of Equation (1) can be written in matrix form

$$\mathbf{z} = \mathscr{M}\Phi \quad (2)$$

where $\mathscr{M}$ contains the coefficients derived from the solutions to Poisson's equation and Φ the pressure of each actuator. Equation (2) can be solved in the least-square sense to minimize the root-mean square deviation between the desired and computed pressures to obtain the actuators' pressure which can reproduce best the Zernike polynomials [3]. These pressures are used as reference for the control algorithm.

3 Controlling the mirror deflection

To control the mirror deflection, we propose an iterative algorithm that drives sequentially the remnant pressure of each actuator to its reference value. Our model assumes a particular coupling between the pixels, and a control signal that must address all the actuators within a time interval $[0,T]$. For given initial conditions, the remnant of the j-th actuator can be expressed by

$$\gamma_j(u_j) = \big(\Phi_j(u_j)\big)(T) - \big(\Phi(u_j)\big)(0).$$

The control objective is to find the inputs u_j^* that drive each remnant γ_j to a reference value γ_j^*. Inspired by the Iterative Learning Control methodology, an iterative algorithm of the form

$$w_j^{i+1} = w_j^i + c e_j^i$$

where $e_j^i = \gamma_j^i - \gamma_j^*$ and c is a control parameter, finds the factors w_j that drive each actuators' remnant to its reference.

References

[1] P. M. Morse and H. Feshbach, Methods of Theoretical Physics, Part II, McGraw-Hill, New York, 1953.

[2] E. S. Claflin and N. Bareket, Configuring an electrostatic membrane mirror by least-squares fitting with analytically derived influence functions, J. Opt. Soc. Am. A3, pp. 1833-1839, 1986.

[3] V. Lakshminarayanan and A. Fleck, Zernike polynomials: a guide, Journal of Modern Optics, vol. 58:7, pp. 545-561, 2011.

Ageing-Aware Charging of Lithium-ion Batteries Using an Electrochemistry-Based Model with Capacity-Loss Side Reactions

Z. Khalik   H.J. Bergveld   M.C.F. Donkers

departement of Electrical Engineering, Eindhoven University of Technology

{z.khalik, h.j.bergveld, m.c.f.donkers}@tue.nl

1 Introduction

Lithium-ion batteries are commonly charged using a so-called constant-current-constant-voltage (CC-CV) protocol, where the battery is initially charged at a set constant current, followed by a phase where the battery is kept at a constant voltage, until the current drops to a certain value. This current limit and voltage limit are determined by a trade-off between a short charging time and long cycle life. Namely, besides the main chemical reaction, i.e., the one that stores energy in the battery, several side reactions occur that eventually lead to capacity fade and power fade. Shortening the charging times without affecting the longevity of the battery is of interest, particularly for electric vehicles, where the relatively long charging times (when compared to refueling time of a conventional vehicle) contribute to so-called range anxiety.

A traditional approach to achieve short charging times, while limiting ageing, has been to improve on the CC-CV protocol by introducing additional CC or CV stages, which are referred to as multi-stage charging protocols. However, the selection of current and voltage limits is not trivial. To find the limits that provide a good trade-off between battery ageing and charging time, typically, many experiments need to be performed. A more recent trend lies in the use of model-based control to systematically make the trade-off between battery ageing and charging time. The models used can vary from empirical models, such as the equivalent-circuit model to electrochemistry-based models that describe the main electrochemical reaction (i.e., the reaction that leads to storing energy) such as the Doyle-Fuller-Newman (DFN) model. These models can be extended with ageing models, e.g. [1], where the DFN model is extended with a side-reaction model describing the loss of Li-ions, such that ageing can be directly incorporated into the model-based controller.

2 Ageing-Aware Charging Protocol Design

We present a model-based design method for multi-stage charging protocols, where this leads to a trade-off between charging times and ageing. The results are leveraged by the recent development of a highly efficient implementation of the DFN model [2]. While we will focus on multi-stage charging protocols in this paper, extensions to full model-based charging can be done based on the model implemen-
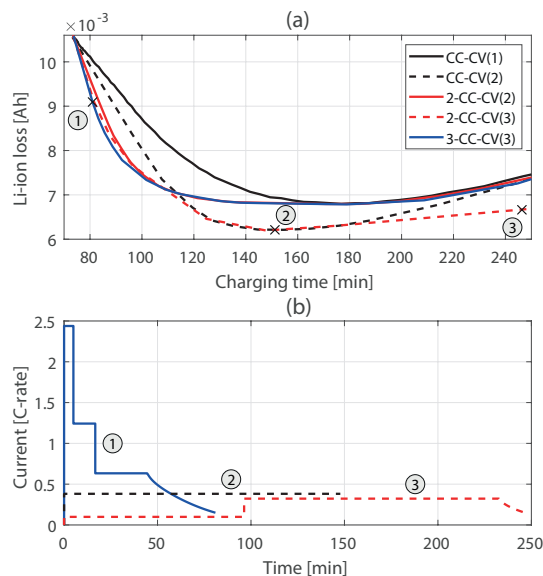
Figure 1: In (a), a comparison of degradation vs charging time of several charging protocols is shown. In (b), selected current profiles at several points on (a) are shown.

tation presented in this paper.

In Fig. 1, the trade-off between Li-ion loss and charging time for several multi-stage charging protocols is shown. The notation used to denote the multi-stage charging protocols is N-CC-CV(D), where N denotes the number of CC stages, and D denotes the amount of design-adjustable variables. In order to obtain these results, the design-adjustable parameters for the charging protocols have been varied over a range of values, from which only the points are shown where minimal Li-ion loss occurs for a given charging time. We observe that a better trade-off between ageing and charging time than the CC-CV protocol can be obtained by considering additional CC stages.

References

[1] Ramadass, P., Haran, B., Gomadam, P.M., White, R., Popov, B.N., "Development of First Principles Capacity Fade Model for Li-Ion Cells", J. Electrochem. Soc., 2004.

[2] Khalik, Z., Bergveld, H.J., Donkers, M.C.F., "On Trade-offs Between Computational Complexity and Accuracy of Electrochemistry-based Battery Models", Conf. Decision & Control, 2019.

Motion control of Piezo-electric actuators for nanopositioning

C.P. Bosman Barros[1], H. Butler[1], R. Tóth[1], K. van Berkel[2]

[1] Control Systems Group, Electrical Engineering, Eindhoven University of Technology

[2] ASML Netherlands B.V., Veldhoven, The Netherlands

Email: c.p.bosman.barros@tue.nl

1 Introduction

Implementation of next generation lithography systems and e-beam metrology systems using a dual-stage configuration with piezo-electric actuators for short-stroke positioning is currently considered to be the next technological step in semi-conductor manufacturing. This is expected to lead to mass reduction and avoidance of electromagnetic fields at the exposure area.

2 Problem description

In this work, a simplified one-dimensional rigid body model of a piezo-electric actuator connected to a long-range stage presented in [1] is considered and the control objective is to position the wafer table according to a given reference trajectory with nanometer accuracy.

Due to the high stiffness of piezo-actuators provided connection, the major challenge of motion control design is preventing the disturbance forces present at the long-stroke stage from acting on the wafer table. The selection of the control architecture directly impacts on the performance of the overall system and needs to be chosen carefully.
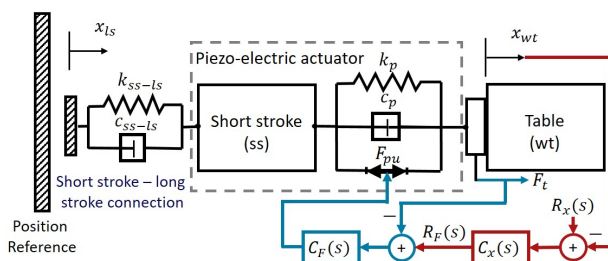
Figure 1: Schematic of the proposed control architecture.

Concerning the controller design, due to high sampling rate and restricted computational resources, only fixed structure and low-order control laws are considered. Additionally, as the hysteresis and creep effects are not

considered in the model, the closed loop system has to be robust against model uncertainty.

3 Control architecture and design

To deal with the wide frequency range high transmissibility from x_{ls} to x_{wt}, caused by the high stiffness connection, we propose the control architecture in Fig. 1.

For the inner loop, the force F_t contains the information of the forces transmitted through the stiff connection and is measured. To suppress lightly damped resonance frequencies, different damping control methods have been investigated and compared, specifically integral force feedback, positive position feedback and integral resonant control. Based on the comparison, a force feedback scheme is chosen which aims at decoupling the wafer table from the long stroke for low frequencies, while also providing damping.

Loop shaping is used to design a tracking controller and implemented in the outer loop to enforce tracking of the reference signal, thereby reducing the positioning errors due to other disturbances. The measurement of the position x_{wt} is used for this loop, therefore the proposed control architecture consists of a cascade controller with an inner and an outer feedback control loop, as depicted in Fig. 1.

4 Conclusions

In this work, a one-dimensional rigid body model for the short-range stage is considered and a feedback cascade control architecture is proposed. Next steps include the investigation of what type of sensor is adequate and how well does it need to perform, the design of feedforward controllers and implementation of the control designs in a real set-up.

References

[1] Bosman Barros, C.P. et al. *Modeling and control of a piezo-electric short-range stage.* 38th Benelux Meeting on Systems and Control, 2019.

Effects of Laser Surface Texturing on the Non-Steady Friction Behaviour

Kristof Driesen, Frederik Debrouwere, Stijn Debruyne and Mark Versteyhe

M-Group, Departement of Mechanical Engineering

KU Leuven University

Spoorwegstraat 12, 8200 Brugge

Belgium

Email: `<firstname>.<lastname>@kuleuven.be`

1 Introduction

Modern machines depend on high-speed and high accuracy motion control for achieving their intended task. Friction however has a severe effect on system performance by its negative side effects, like energy losses and non-linear behaviour kinematics.

Previous research was focused (i) on reducing the Coefficients Of Friction (COF) and (ii) on modelling these frictional effects and taking them into account in the control loop [1]. Multiple advanced behavioural friction models where developed (Dahl, LuGre, Leuven, ...) to describe friction instabilities [2]. The parameters of these models need to be identified by means of complicated estimators on experimental obtained data which lead to difficulties for their application [3].
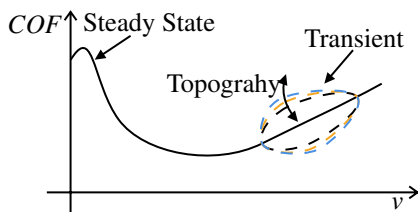
Figure 1: COF - velocity relationship: steady-state (solid line) and transient (dashed line)

2 Motivation for the research

A large and growing body of literature has investigated the influence of surface topography (roughness and engineered surfaces) on static and kinetic COF of lubricated and dry contacts [4]. It has conclusively been shown that a modified surface topography has the potential to improve the steady state frictional response of *lubricated contacts* as per [5]. To date, several studies have investigated the influence of surface topography on dry contacts nevertheless the relation remains unclear. Research within dry contacts is mostly descriptive in essence and often only reports experimental results. Some authors combined coatings, solid lubricants and textures to obtain beneficial effects over a large operation area [6]. Ga-

chot et al. [4] identifies the main influence factors on the COF as follows: (i) geometry of the texture, (ii) area density, (iii) aspect ratio and (iv) relative direction of the surface texture compared to the sliding direction. Many authors report huge differences in the steady state COF yet the influence on the non-steady state frictional behaviour is left mainly undocumented.

3 Approach

In this work initial experimental work is reported to assess the influence of surface topography on the non-steady frictional behaviour (ex. frictional instability, presliding behavior, ...) of lubricated metallic surfaces. The outcome should lead to a paradigm shift: instead of correcting unfavourable friction behaviour through advanced servo-control, this work has the intention to lay the basis of adapting the non-steady frictional behaviour to meet design specifications.

References

[1] Frederik Debrouwere, Mark Versteyhe, and Stijn Debruyne. Including the stribeck friction curve in optimal path following motions. pages 1–6. University of Strathclyde, 2018.

[2] Farid Al-Bender, Vincent Lampaert, and Jan Swevers. Modeling of dry sliding friction dynamics: From heuristic models to physically motivated models and back. *Chaos: An Interdisciplinary Journal of Nonlinear Science*, 14(2):446–460, 2004.

[3] M. Boegli, T. De Laet, J. De Schutter, and J. Swevers. A smoothed gms friction model for moving horizon friction state and parameter estimation. In *2012 12th IEEE International Workshop on Advanced Motion Control (AMC)*, pages 1–6, March 2012.

[4] Carsten Gachot, A. Rosenkranz, S. M. Hsu, and H. L. Costa. A critical assessment of surface texturing for friction and wear improvement. *Wear*, 372-373:21–41, 2017.

[5] Philipp G. Grützmacher, Francisco J. Profito, and Andreas Rosenkranz. Multi-scale surface texturing in tribology—current knowledge and future perspectives. *Lubricants*, 7(11), 2019.

[6] P. Basnyat, B. Luster, C. Muratore, A.A. Voevodin, R. Haasch, R. Zakeri, P. Kohli, and S.M. Aouadi. Surface texturing for adaptive solid lubrication. *Surface and Coatings Technology*, 203(1):73 – 79, 2008.

Quadratic Tracking Control of Photopolymerization for Additive Manufacturing

K.H.J. Classens[1], T.M. Hafkamp[1], S. Westbeek[1], J.J.C. Remmers[1] and S. Weiland[2]

[1]Dept. of Mechanical Engineering, Eindhoven University of Technology, The Netherlands
[2]Dept. of Electrical Engineering, Eindhoven University of Technology, The Netherlands

{k.h.j.classens,t.m.hafkamp,s.westbeek,j.j.c.remmers,s.weiland}@tue.nl

1 Background

Rapid prototyping has flourished over the past decade and quickly matured into industrialized additive manufacturing (AM), also know as 3-D printing. AM through photopolymerization is a prominent technique in which a photopolymer is selectively solidified towards a near net shape part, often in a layer-wise process. The technique of photopolymerization comprises the processes where liquid photopolymers are selectively cured by delivering some type of light, typically ultraviolet (UV).

2 Problem

Although photopolymerization-based AM is increasingly being used in the manufacturing industry, several challenges are still faced in order to improve repeatable product quality. It is commonly recognized that an in-depth understanding and monitoring of the curing process and the control thereof has a great potential to lead to end products of better quality [1]. This motivates the research on closed-loop control of the curing process and the build-up of material properties. A roadmap to improve repeatable product quality is depicted in Figure 1 [2]. This work mainly focuses on the 0-D SISO case in which the system boundary is drawn at (sub-)voxel scale. There is little consensus about strategies to achieve beneficial material properties to improve product quality. In order to move to a higher dimensional problem and to cope with varying control objectives, a flexible control architecture is desired.
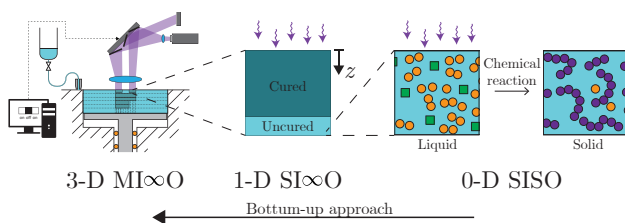
Figure 1: Roadmap to improve product quality [2].

3 Approach

This work mainly focuses on tracking control of the curing degree, p, which is a measure for the progress of the polymerization reaction. The time-evolution is typically described by a nonlinear first order differential equation. An extension to the quadratic tracking framework is introduced

to anticipatively control this nonlinear system. For this purpose, an updating strategy is proposed based on sequential linearization of the nonlinear model. First, the controlled system is validated by means of simulation and subsequently the controlled system is experimentally validated on the set-up described in [3].

4 Results and Outlook

The experimentally obtained closed-loop tracking response of a sigmoid-shaped reference signal is depicted in Figure 2. The work can be considered as a twofold proof of principle. Firstly, the potential of model-based control of the material property evolution is demonstrated. Secondly, the extension to the quadratic tracking framework is validated. Two extensions are proposed in [4]. The domain can be extended to 1-D SI∞O and a control-oriented model is proposed that includes temperature, strain and stress evolution.
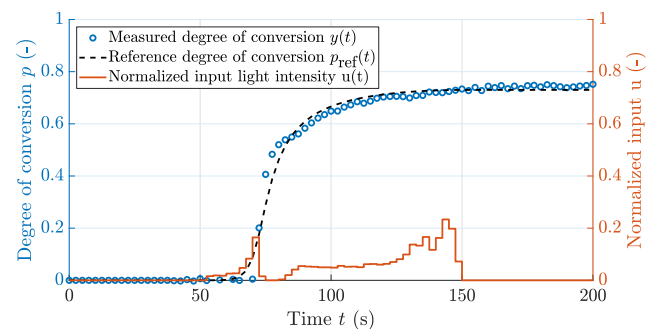
Figure 2: Experimental closed-loop curing response.

References

[1]   Y. Huang *et al.*, "Additive Manufacturing: Current State, Future Potential, Gaps and Needs, and Recommendations." *Journal of Manufacturing Science and Engineering*, vol. 137, 2015.

[2]   T.M. Hafkamp *et al.*, "A feasibility study on process monitoring and control in vat photopolymerization of ceramics." *Mechatronics*, vol. 56, 2018.

[3]   T.M. Hafkamp *et al.*, "Real-time feedback controlled conversion in vat photopolymerization of ceramics: A proof of principle." *Additive Manufacturing*, vol. 30, 2019.

[4]   K.H.J. Classens, "Multiphysical Modeling and Control of Photopolymerization for Additive Manufacturing," Master's thesis, Eindhoven University of Technology, Eindhoven, 2019.

Linear Predictors for Interconnected Systems: a Koopman Operator Approach.

Camilo Garcia-Tenorio[1,2], Eduardo Mojica-Nava[1], and Alain Vande Wouwer[2]

[1]Engineerings Faculty, National University, Carrera 30 No. 45-03, Bogotá, Colombia
[2]Control Department, Mons University, Boulevard Dolex 31, Mons, Belgium
[1,2]Email: {cagarciate, eamojican}@unal.edu.co,
Alain.Vandewouwer@umons.ac.be

1 Introduction

In large scale interconnected systems, the uncertainty of the internal structure and critical parameter values plays an essential role in the individual subsystem's stability. A common approach in such systems is to have a centralized decision-making (controller) scheme. The problem arises when the operating environment is poorly known, and the centrality presupposition fails to hold either by a lack of information or computing power. In the case where local measurements of the states and measurements of the input from neighboring systems are present, data-driven local predictors provide a tool for analyzing local stability. We propose the development of linear local predictors based on the approximation of the Koopman operator for inputs via the extended dynamic mode decomposition (EDMD) algorithm [1]. This kind of predictors has the advantages of capturing the nonlinear dynamics in extended function spaces and the presence of the spectrum of the operator for the stability analysis.

2 Model

Consider the interconnection of two Duffing equations. These systems have the same structure with different parameterizations and interconnected via the first state variable as in

$$\dot{x}_{1,1} = x_{1,2} + g_1 x_{2,1}$$
$$\dot{x}_{1,2} = -\delta_1 x_{1,2} - \beta_1 x_{1,1} - \alpha_1 x_{1,1}^3$$
$$\dot{x}_{2,1} = x_{2,2} + g_2 x_{1,1}$$
$$\dot{x}_{2,2} = -\delta_2 x_{2,2} - \beta_2 x_{2,1} - \alpha_2 x_{2,1}^3, \qquad (1)$$

where the parametrization used for the subsystems is: $\alpha = (0.5, -0.5)$, $\beta = (1, -1)$ and $\delta = (1, 1)$, and the interconnection weight between the systems is $g = (0.5, 0.8)$.

3 Method & Results

To find a local linear predictor for each of the subsystems in (1) from a series of simulated trajectories, we propose a Koopman operator approach based on the extension of the EDMD algorithm that accounts for inputs and control [2]. The information provided to each of the linear predictors is the local information of its states and the interconnection input, i.e., the first state of the neighboring system without the interconnection's weight.

The approach yields two linear predictors of order 125 with embedded nonlinear dynamics of the local and interconnection states, and the interconnection weight, i.e., there is no need to know the strength of the interaction, only the topology. Figure 1 shows the result of the application of the proposed method from a set of 200 initial conditions and 20 data-points per simulation for a total of 4000 data snapshots on a 2s time frame, where 80% are for calculating the approximation and the remaining for testing. The comparison of the numerically simulated trajectories and the evolution of the predictor $g(x)$ from the same initial conditions gives the method's accuracy.
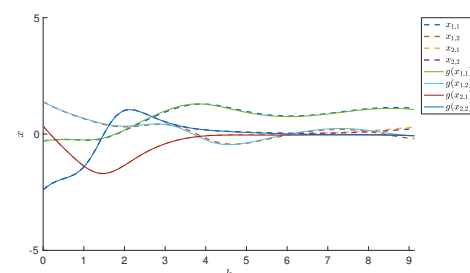
Figure 1: States vs. time of interconnected Duffing equations with decentralized linear predictor.

References

[1] M. Williams, I. Kevrekidis, C. Rowley "A Data-Driven Approximation of the Koopman Operator: Extending Dynamic Mode Decomposition," Journal of Nonlinear Science, vol. 25, no. 6, pp. 1307–1346, 2015.

[2] J. Proctor, S. Brunton, and J. Kutz, "Generalizing Koopman Theory to Allow for Inputs and Control," SIAM Journal on Applied Dynamical Systems, vol. 17, no. 1, pp. 909-930, 2018.

Two methods to approximate the Koopman operator with a reservoir computer

Marvyn Gulina and Alexandre Mauroy

Namur Institute for Complex Systems (naXys) and Department of Mathematics,
University of Namur, Rempart de la vierge 8, B-5000 Namur, Belgium
Email: marvyn.gulina@unamur.be and alexandre.mauroy@unamur.be

1 Introduction

The Koopman operator provides an alternative framework to describe the evolution of nonlinear systems in a purely linear fashion. Let us consider an autonomous dynamical system $x(t+1) = F(x(t))$ where $x \in \mathscr{X}$ is the state space and $F : \mathscr{X} \to \mathscr{X}$ is a nonlinear map. The Koopman operator is defined as the composition $\mathscr{K} f = f \circ F$ where $f : \mathscr{X} \to \mathbb{C}$ is an *observable* that belongs to a Banach space [1].

Since the Koopman operator is infinite-dimensional, it is natural and often necessary to compute its finite-dimensional approximation. This approximation is given by the *Koopman matrix*, which represents the projection of the operator onto a subspace spanned by the basis functions, also called *dictionary*. A finite-dimensional approximation of the Koopman operator can be obtained from data through the so-called Extended Dynamic Mode Decomposition (EDMD) algorithm [2].

Recently *dictionary learning* methods for EDMD have been proposed to provide a set of functions that yields the best representation of the Koopman operator. In particular, [3] has considered a feed-forward network for this purpose.

In this work, we propose to use a reservoir computer [4, 5] instead of a feed-forward network. This allows to train the dictionary with a dynamical network rather than with a static one. The reservoir computer is a discrete-time neural network which consists of three layers: the inputs, the reservoir, and the outputs (see [6] for a review). It is noticeable that the outputs are obtained through *linear* combinations of the states and *only* the output weights are trained. This is a key computational advantage of the reservoir computer that we exploit.

2 Two methods

We propose two methods to approximate the Koopman operator with a reservoir computer.

Our first method is to apply EDMD directly on the internal states of the reservoir. This method is efficient but provides a large Koopman matrix, since the number of internal states is typically large. This motivates our second method, which fully exploits the reservoir computer framework.

In order to reduce the size of the Koopman matrix, our a second method uses the outputs of the reservoirs as dictionary functions. These outputs are trained through the following optimization problem

$$\min_{W_{out}, K} \sum_{t=1}^{T-1} \| W_{out} s(t+1) - K W_{out} s(t) \|^2 \qquad (1)$$

where W_{out} is the output weights matrix, K the Koopman matrix and $s(t)$ is the vector of internal states of the reservoir at time t.

The optimization is solved with two alternating steps:

1. Computation of the Koopman matrix: fix W_{out} and optimize K using the least squares method ;

2. Dictionary learning: fix K and optimize W_{out} to minimize the norm of $W_{out} s(t+1) - K W_{out} s(t)$.

The second step of the method amounts at solving a Sylvester equation of the form $AX + XB = C$. We propose two different least squares techniques to solve the equation, which we will discuss.

It is noticeable that the second method can be seen as a compromise between our first method and linear DMD.

We will illustrate these two methods in the context of spectral analysis and prediction.

References

[1] B.O. Koopman, 1931
Proc. Natl. Acad. Sci. U. S. A. **17**(5), 315 (1931)

[2] M. Williams, I. Kevrekidis, and C. Rowley, 2015.
J Nonlinear Sci (2015) 25:1307–134.

[3] Q. Li, F. Dietrich, E. Bollt, I. Kevrekidis, 2017.
Chaos **27**, 103111 (2017)

[4] H. Jaeger, GMD Report **148** (2010).

[5] P. Antonik, M. Gulina, J. Pauwels, S. Massar, 2018.
Phys. Rev. E **98**, 012215 (2018)

[6] M. Lukǒsevičius, H. Jaeger, and B. Schrauwen, 2012.
Künst. Intell. **26**, 365 (2012).

Koopman operator approach applied to switched nonlinear systems

Christian Mugisho Zagabe and Alexandre Mauroy

Namur Institute for Complex Systems (naXys), Department of Mathematics

University of Namur, Rempart de la Vierge 8, B-5000 Namur, Belgium

Email: christian.mugisho@unamur.be and alexandre.mauroy@unamur.be

1 Introduction

The Koopman operator approach describes a dynamical system through the evolution of an observable defined on the state space. In the continuous-time setting, the infinitesimal generator of the semigroup of Koopman operators leads to a linear (but infinite-dimensional) representation of the system. This approach can be used for stability analysis. As shown in [1], there is a strong connection between global stability properties of the nonlinear system and linear stability properties of the Koopman operator.

Our goal is to exploit the Koopman operator approach to study the stability properties of switched nonlinear systems. A switched system is a collection of subsystems that alternate according to a given commutation law. Uniform stability of switched linear systems (i.e. under any law of commutation) was considered in [2]. The authors proved that a switched linear system is globally uniformly asymptotically stable (GUAS) if the matrices describing the subsystems are stable and generate a solvable Lie algebra. In [3], the author proposed an open problem on the nonlinear case and suggested to find the conditions on the Lie algebra generated by the subsystems vector fields under which the switched system is GUAS. We will report on advances on this problem in the context of the Koopman operator approach.

2 Lie group framework and relationship between finite and infinite-dimensional systems

We exploit the relationship between a finite-dimensional dynamical system $\dot{x} = F(x)$ on $X \subset \mathbb{R}^n$ and its infinite-dimensional representation $\dot{f} = L_F f$ in spaces of observables $\mathscr{F} = C^k(X), 0 \leq k \leq \infty$. Note that L_F is the infinitesimal generator of the semigroup of Koopman operators. Instead of describing a dynamical system with a diffeomorphism $\varphi : X \to X$, we use an automorphism $U_\varphi : C^k(X) \to C^k(X)$ acting on f according to $U_\varphi f = f \circ \varphi$. The set of diffeomorphisms $Diff^k(X)$ and the set of automorphisms $Aut\left(C^k(X)\right)$ can be interpreted as Lie groups, which are isomorphic under some technical conditions. Their respective Lie algebras $Vect^k(X)$ and $Der\left(C^k(X)\right)$ allows us to see the vector field F on X as a derivation L_F on $C^k(X)$ acting on f according to $L_F f = F \cdot \nabla f$. Note that the Lie algebras isomorphism $Vect^k(X) \to Der\left(C^k(X)\right)$ is well-known. This is summarized in the following diagram:

$$
\begin{array}{ccc}
\text{Lie groups :} & Diff^k(X) \xrightarrow{\ \ \ } Aut\left(C^k(X)\right) \\
& \ \ \varphi \qquad\qquad U_\varphi \\
& \text{Lie} \top \qquad\qquad \top \text{Lie} \\
& F \qquad\qquad\ L_F \\
\text{Lie algebras :} & Vect^k(X) \xrightarrow{\ \ \ } Der\left(C^k(X)\right)
\end{array}
$$

Consider the switched nonlinear system $\dot{x} = F_\sigma(x)$, where $\sigma : t \mapsto \sigma(t) \in \{1,...,m\}$ is the commutation law. The Koopman operator approach allows us to describe the system as a linear infinite-dimensional switched system $\dot{f} = L_{F_\sigma} f$. It follows that studying the stability properties of the switched nonlinear system is equivalent to studying the stability properties of the switched infinite-dimensional system.

3 Common Lyapunov function for switched linear systems

Showing the GUAS property amounts to finding a common Lyapunov function (CLF) for the subsystems [4]. For finite-dimensional linear systems $\dot{x} = A_i x$, with $A_i \in \mathscr{A}$, the existence of a CLF is guaranteed if the (stable) matrices A_i are simultaneously triangularizable, i.e. if there exists an $\mathscr{A}$-invariant maximum flag [2]. We study the validity of the extension of the result to infinite dimension, i.e. if $\mathscr{A}$ is a collection of stable simultaneously triangularizable operators, then there exists a common Lyapunov functional for the infinite-dimensional linear systems $\dot{f} = L_{F_i} f$, with $L_{F_i} \in \mathscr{A}$. This extension can be related to the open problem in [3] since one can connect simultaneous triangularization to generalized notions of nilpotency and solvability in infinite dimension (see e.g. [5]).

Considering a geometric version of the proof for the finite-dimensional case, we will report on current challenges and progress toward the infinite-dimensional result.

References

[1] A. Mauroy and I. Mezić, *Global stability analysis using the eigenfunctions of the Koopman operator*, IEEE Transactions on Automatic Control, vol. 61, pages 3356-3369, 2016.

[2] D. Liberzon, J. Hespanha and A. Morse, *Stability of switched linear systems: a Lie-algebraic conditions.* Systems and Control Letters, vol. 37, pages 117-122, 1999.

[3] D. Liberzon, *Lie algebras and stability of switched nonlinear systems* In V. Blondel and A. Megretski, *Unsolved Problems in Mathematical Systems and Control Theory,* pages 203-207, Princeton University Press, 2004.

[4] D. Liberzon, *Switching in Systems and Control*, Birkhauser, Boston, 2003.

[5] A. Katavolos and H. Radjavi, *Simultaneous Triangularization of Operators on a Banach Space*, Journal of the London Mathematical Society (2) 41, pages 547-554, 1990.

Numerical Gaussian process Kalman filtering

Armin Küper and Steffen Waldherr

Department of Chemical Engineering

KU Leuven

3000, Leuven, Belgium

Email: {armin.kuper, steffen.waldherr}@kuleuven.be

Gaussian processes (GPs) are distributions over functions, fully defined through a mean function and a covariance function. With GPs one can do non-parametric regression [4]. Regression on spatiotemporal data can be done through so-called numerical Gaussian processes [2]. In this framework, the covariance functions are constructed from the time-discretised spatiotemporal model structure. In this way, tedious spatial discretisation is circumvented.

We present numerical Gaussian process Kalman filtering (GPKF) as a novel method for state estimation in infinite-dimensional systems [1]. Numerical GPs can be embedded into the well-known Kalman filter equations [3] since the states evolve linear and are Gaussian distributed. As a result, we can do Kalman filtering with Gaussian processes for infinite-dimensional systems. Furthermore, process and measurement noise levels are learned online on the data stream, therefore eliminating trial and error fine-tuning of the Kalman filter.

We use the advection equation

$$\frac{\partial n}{\partial t}(t,x) = -g\frac{\partial n}{\partial x} \tag{1}$$

with velocity g, to showcase the capability of the numerical GPKF. Measurements are obtained as noisy point evalua-

Figure 2: Estimation of process and measurement noise standard deviation.

tions of the ground truth solution. Fig. 1 shows temporal snapshots of the numerical GPKF estimations, while noise level estimations are illustrated in Fig. 2. All figures are taken from [1].

References

[1] Armin Küper and Steffen Waldherr. Numerical gaussian process kalman filtering. *arXiv preprint arXiv:1912.01234*, 2019.

[2] Maziar Raissi, Paris Perdikaris, and George Em Karniadakis. Numerical gaussian processes for time-dependent and nonlinear partial differential equations. *SIAM Journal on Scientific Computing*, 40(1):A172–A198, 2018.

[3] Simo Särkkä. *Bayesian filtering and smoothing*, volume 3. Cambridge University Press, 2013.

[4] Christopher KI Williams and Carl Edward Rasmussen. *Gaussian processes for machine learning*, volume 2. MIT Press Cambridge, MA, 2006.

Figure 1: Temporal snapshots of ground truth solution (black) and posterior estimate (blue) along with two times the standard deviation. Blue circles indicate noisy measurements.

Gaussian process regression for time-series estimation

Georgios Birpoutsoukis, Julien M. Hendrickx
ICTEAM, UCLouvain, B1348 Louvain la Neuve, Belgium
e-mail: georgios.birpoutsoukis@uclouvain.be

1 Introduction

Estimation of AutoRegressive (AR) and AutoRegressive Moving Average (ARMA) models is proposed in a Bayesian framework using a Gaussian Process Regression (GPR) approach. Stability of the time-series is exploited during the model parameter estimation. Models of enhanced predictability can be obtained, even in the case of large model orders. It is shown that the proposed approach is strongly linked with the Prediction Error (PE) model estimation approaches, if the estimated parameters are regularized. The method is extended to the estimation of ARMA processes.

2 Model structure and parameter estimation

Based on data measured from a stochastic process, the objective is to describe its dynamics and predict the process evolution. It is assumed that the true process is exactly described by the discrete-time AR model structure:

$$\phi(q)\, y_t = e_t \Rightarrow (1 + \sum_{j=1}^{n_{AR}} \phi_j q^{-j}) y_t = e_t \Rightarrow y_t = H_{AR}\, e_t$$

where $y_t \in \mathbb{R}$ is the measured output at t, $e_t \in \mathbb{R}$ is the innovation at t, n_{AR} is the AR order, $\phi_j \in \mathbb{R}, j = 1, \ldots, n_{AR}$ are the AR model coefficients, and q is an operator such that $q^{-j} y_t = y_{t-j}$. The innovation e_t is assumed to be a realization of an i.i.d. Gaussian white noise process with variance σ_e^2, and that H_{AR} and H_{AR}^{-1} are stable. If N points of the process output $y_t, t = 1, \ldots, N$ are collected, $Y = [y_{n_{AR}+1} \cdots y_N]^T \in \mathbb{R}^{N-n_{AR}}$, $E = [e_{n_{AR}+1} \cdots e_N]^T \in \mathbb{R}^{N-n_{AR}}$ and $\beta = [\phi_1 \cdots \phi_{n_{AR}}]^T$, then the AR process can be written as $Y = K\beta + E$, where $K \in \mathbb{R}^{(N-n_{AR}) \times n_\beta}$ is the regressor appropriately structured and $\beta \in \mathbb{R}^{n_\beta}$ contains the parameters of the model. The objective is to estimate β using the measured output data. Towards this direction, we assume that the parameter vector β is a zero mean Gaussian random variable with covariance $\Sigma_\beta \in \mathbb{R}^{n_\beta \times n_\beta}$, i.e. $\beta \sim \mathcal{N}(0, \Sigma_\beta)$. Assuming that the elements in K are known and given that $Y = K\beta + E$, $E \sim \mathcal{N}(0, \sigma_e^2 I_N)$, I_x denoting the identity matrix of size x, then β and Y are jointly Gaussian variables [1], and the posterior distribution of β conditioned on the process data Y is given by $\beta|Y \sim \mathcal{N}(\hat{\beta}^{apost}, \Sigma_\beta^{apost})$ where:

$$\hat{\beta}^{apost} = (K^T K + \sigma_e^2 \Sigma_\beta^{-1})^{-1} K^T Y$$

$$\Sigma_\beta^{apost} = ((\sigma_e^2 (K^T K)^{-1})^{-1} + \Sigma_\beta^{-1})^{-1}$$

Different types of structures can be used for the prior covariance matrix Σ_β of the parameter vector β, in order to impose exponential decay (stability) and correlation, such as the Diagonal Correlated (DC) and Tuned-Correlated (TC) structure [1].

3 Results

The GPR method is illustrated on the estimation of a 20th order AR process ($n_\beta = 20$) and compared to the PE method. 50 Monte Carlo (MC) simulations are carried out where, at each iteration a new realization of e_t with variance $\sigma_e^2 = 1$ is used to generate the AR output data and estimate the model parameters. Different values of the data length N are considered in order to observe the evolution of the performance for both methods. To evaluate the performance of
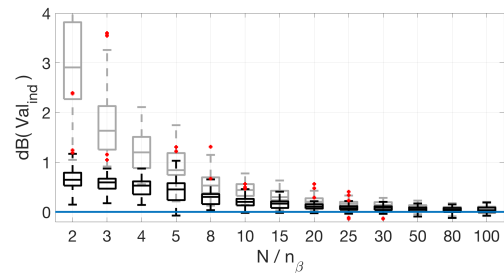
Figure 1: Monte Carlo simulation results. Black: GPR performance. Grey: PE performance.

the models, a new validation dataset is considered of length $N_{val} = 10000$ samples, of data not used during model estimation. The model performance is evaluated with the index $\text{Val}_{ind} = \frac{1}{N_{val}} \sum_{1}^{N_{val}} (y_t - \hat{y}_{t/t-1})^2$. The results are depicted in Fig.1. It is clear that the GPR method outperforms the PE method in terms of predictability, measured using Val_{ind}. It should be noted that a number of models obtained with the PE method are not in the figure due to their bad performance and the very high value of Val_{ind}.

Table 1: Improvement of median values of Val_{ind}.

N/n_β	2	3	5	10	20
Perf. Improv.	40.6%	21.3%	8.5%	5.3%	2.2%

4 Acknowledgments

References

[1]   Chen, T., Ohlsson, H., & Ljung, L. On the estimation of transfer functions, regularizations and Gaussian processes - revisited. Automatica, 48(8):1525-1535, 2012.

LPV Modeling Using the Koopman Operator

Lucian Cristian Iacob, Roland Tóth and Maarten Schoukens
Control Systems Group, Eindhoven University of Technology
P.O Box 513, 5600 MB, Eindhoven, The Netherlands
Email: {l.c.iacob, r.toth, m.schoukens}@tue.nl

1 Introduction and Motivation

Linear parameter-varying (LPV) models have been introduced to describe nonlinear (NL) and time-varying (TV) systems and make use of powerful results of linear control theory. LPV systems extend the notion of linear time invariant (LTI) systems, with the difference that the input/output relations change depending on a scheduling parameter. The goal is to efficiently convert a nonlinear model to an LPV representation with minimal complexity and conservativeness and preserving the system properties. A novel approach for modeling nonlinear systems in terms of a quasi-linear representation is based on the Koopman operator theory. Typically, an infinite-dimensional operator is obtained that requires an approximation for practical applications. Based on the resulting model, an LPV description can be obtained using a velocity-based linearization, which is valid at every operating point [3].

2 Problem formulation

Consider a discrete-time nonlinear system given in the general form:

$$x_{k+1} = f(x_k, u_k) \tag{1}$$

with $x \in \mathbb{R}^n$ the states of the system and $u \in \mathbb{R}^m$ the control inputs. The Koopman operator $\mathcal{K} : \mathcal{F} \to \mathcal{F}$ is a linear operator defined on a space $\mathcal{F}$ of scalar observables. An observable belonging to $\mathcal{F}$ is defined as $\phi : \mathbb{R}^{n+m} \to \mathbb{R}$, which is a scalar function along the trajectories of the nonlinear system [1]. The Koopman operator $\mathcal{K}$ is infinite dimensional and acts on functions of the state and input. It propagates ϕ one step forward in time:

$$\mathcal{K}\phi(x_k, u_k) = \phi(f(x_k, u_k), u_{k+1}). \tag{2}$$

In practice, the Koopman operator needs to be approximated. Several approaches are based on the Dynamic Mode Decomposition (DMD) [1] and the Least Squares (LS) method [2]. The present work focuses on the latter. A vector of observables is introduced, as suggested in [2]:

$$\Psi(x, u) = \left[x^\top, u^\top, \phi_{n+m+1}(x, u), \ldots, \phi_N(x, u) \right] \tag{3}$$

with N being the number of observables. The last $N - (n+m)$ observables are chosen as basis functions. A comparison between polynomial and Fourier basis is given in

[2]. The approximated Koopman operator $K \in \mathbb{R}^{N \times N}$ advances Ψ one step forward in time:

$$\Psi_{k+1} = \Psi_k K + e_k \tag{4}$$

where $e_k(x_k, u_k)$ is the residual error and $\Psi_k = \Psi(x_k, u_k)$. A LS algorithm can be used to minimize the residual and compute K by using snapshots of data at (x_τ, u_τ) and $(x_{\tau+1}, u_{\tau+1})$. As described in [2], the dynamics are approximated through the following relation:

$$x_{k+1} \approx \hat{K}^\top \Psi_k^\top \tag{5}$$

with $\hat{K}^\top \in \mathbb{R}^{n \times N}$ being the truncation of $\mathcal{K}$ to the first n columns. Next, Eq. (5) is linearized using the velocity-based technique [3], yielding:

$$\Delta x_{k+1} \approx \underbrace{\hat{K}\frac{\partial \Psi_k^\top}{\partial x}}_{A(\rho_k)} \Delta x_k + \underbrace{\hat{K}\frac{\partial \Psi_k^\top}{\partial u}}_{B(\rho_k)} \Delta u_k \tag{6}$$

with $\rho_k = \left[x_k^\top, u_k^\top \right]^\top$. Eq. (6) represents a discrete-time LPV model. Such a velocity form-based LPV description is highly useful for control synthesis, with guaranteed stability and performance (see [4]).

Future work intends to investigate different methods of computing the Koopman operator and the numerical implementation for a test system. This includes a review of the available approximation algorithms, the choice of the basis functions, and the possible ways to transform the resulted Koopman model into an LPV description. Furthermore, an analysis of the limitations of the proposed method and its connection to Reproducing Kernel Hilbert Space methods (RKHS) will be carried out.

References

[1]   M. Korda, I. Mezić, "Linear predictors for nonlinear dynamical systems: Koopman operator meets model predictive control", arXiv:1611.03537, Mar 2018.

[2]   I. Abraham et al, "Model-Based Control Using Koopman Operators", arXiv:1709.01568, September 2017.

[3]   G. Cai et al, "A Velocity-Based LPV Modeling and Control Framework for an Airbreathing Hypersonic Vehicle", *International Journal of Innovative Computing, Information and Control*, Vol. 7, Nr. 5(A), May 2011.

[4]   P. S.G. Ciseneros et al, "Constrained Predictive Control of a Robotic Manipulator using quasi-LPV representations", IFAC PapersOnLine 52-26, 2018.

Exact Gradient Methods with Memory

Mihai I. Florea
Mathematical Engineering (INMA)
Catholic University of Louvain (UCL)
Avenue Georges Lemaître, 4 - bte L4.05.01, B - 1348
Louvain-la-Neuve, Belgium
Email: mihai.florea@uclouvain.be

1 Background

A black-box first-order method has access at every iteration to the starting point and all the previously obtained gradient information. Recently, the Gradient Method (GM) has been enhanced in [1] by maintaining a piece-wise linear model constructed using a bundle of past gradients and function values. The simulation results in [1] show that the Inexact Gradient Method with Memory (IGMM) based on this construction markedly outperforms GM even with small bundles, often requiring an order of magnitude fewer iterations to reach the same objective accuracy.

However, the piece-wise linear model cannot be minimized exactly for non-trivial bundles, introducing a new algorithm parameter in the form of the tolerance δ. When minimizing composite functions wherein the smooth part of the objective is relatively smooth with respect to a distance generating function (DGF), the need for a bound on inexactness imposes additional conditions on the DGF and narrows the range of problems to which IGMM can be applied. In addition, δ carries over to the worst-case convergence rate.

2 An Accurate Descent Rule

By incorporating the maximum between a lower linear model of the objective smooth part and the linear model generated by GM at the current point, we can construct an at most two-piece model that can be solved exactly. The complexity of this computation is negligible, and can be performed in constant time.

This model constitutes the second stage in a two-level system. When the first stage is based on a piece-wise linear model, our system yields an *exact* descent rule as in GM and models the objective function with the accuracy of IGMM.

However, unlike IGMM, out system does not impose additional conditions on the DGF. Moreover, the exact descent rule does not impose any quality requirements on the first stage, eliminating the need to define a tolerance parameter altogether.

The simplicity of our model can be mirrored in the linesearch stopping criterion, which also becomes of negligible computational complexity when compared to that of IGMM.

3 Exact Gradient Methods with Memory

By iterating the descent step, we obtain an Exact Gradient Method with Memory (EGMM). The exactness of the descent rule eliminates tolerance parameters such as δ from the convergence analysis, yielding a worst-case rate of $O(1/k)$. EGMM is as broadly applicable as the Bregman Distance Gradient Method (NoLips). Recent results in [2] suggest that EGMM may be optimal on the problem class it addresses, up to a constant factor that is asymptotically equal to 2. EGMM is also by design monotone, which leads to a stable convergence behavior.

We have further used the descent property to accelerate EGMM. The resulting Accelerated Gradient Method with Memory (AGMM) is applicable to one of the widest problem classes for which acceleration is currently known to be attainable [2]. The absence of the δ term prevents the accumulation of errors and leads to a worst-case rate of $O(1/k^2)$, equal to that of the Fast Gradient Method (FGM).

4 Simulation Results

The flexibility in the first stage of our system has allowed us to implement EGMM with a high target accuracy for solving the inner problem while limiting the number of inner iterations. In our preliminary computational experiments, EGMM was able to significantly outperform IGMM, sometimes achieving the same objective accuracy using an order of magnitude fewer iterations. AGMM also consistently overtakes FGM, even with small bundles.

5 Acknowledgements

References

[1] Yurii Nesterov and Mihai I. Florea. Gradient methods with memory. *CORE Discussion Papers*, 2019(22), 2019.

[2] Radu A. Dragomir, Adrien Taylor, Alexandre d'Aspremont, and Jérôme Bolte. Optimal complexity and certification of Bregman first-order methods. *arXiv preprint arXiv:1911.08510*, 2019.

The Proximal Augmented Lagrangian Method for Nonconvex Quadratic Programs

Ben Hermans
MECO Research Team, Department Mechanical
Engineering, KU Leuven
DMMS lab, Flanders Make, Leuven, Belgium
Email: ben.hermans2@kuleuven.be

Andreas Themelis and Panagiotis Patrinos
KU Leuven, Leuven, Belgium
Department of Electrical Engineering,
Division ESAT-STADIUS

1 Introduction

A quadratic program (QP) is an optimization problem of the following form:

$$\underset{x \in \mathbb{R}^n}{\textbf{minimize}} \quad f(x) = \tfrac{1}{2}x^\top Q x + q^\top x,$$

$$\textbf{subject to} \quad Ax \in C,$$

with $Q \in \mathbb{R}^{n \times n}$, $q \in \mathbb{R}^n$, $A \in \mathbb{R}^{m \times n}$, $C = \{z : \ell \le z \le u\}$ and $\ell, u \in \mathbb{R}^m$ with their components satisfying $-\infty \le \ell_i \le u_i \le \infty$, $i = 1, \dots, m$. QPs arise in many domains of numerical optimization, such as finance, machine learning, (linear) model predictive control (MPC), etc. Furthermore, sequential quadratic programming (SQP) is a popular technique for nonlinear optimization, in which the problem is approximated by a QP at every iteration. Therefore, substantial research has been performed to efficiently and robustly solve QPs. State-of-the-art solvers rely typically on interior point methods, active-set methods or proximal algorithms.

In previous work [1], we introduced QPALM, a proximal augmented Lagrangian method (ALM) solver for convex QPs. In this work, we extend QPALM to deal also with nonconvex QPs, when Q is nonpositive definite. Nonconvex QPs arise for example in mixed integer-linear [2] and in mixed integer-quadratic programs [3], which has applications in hybrid MPC, and as a result of applying SQP to a general nonlinear, nonconvex optimization problem.

2 Methodology

By introducing a slack vector $z = Ax$, we apply the proximal ALM where the equality constraints are relaxed. The inner subproblem is a minimization of the proximal augmented Lagrangian, which after elimination of z is given by

$$\varphi_k(x) = f(x) + \tfrac{1}{2} \operatorname{dist}^2_{\Sigma_k, C}(Ax + \Sigma_k^{-1} y^k) + \frac{1}{2\gamma_k} \|x - x^k\|^2, \quad (1)$$

with Σ_k a diagonal matrix with penalty parameters, γ_k the proximal penalty parameter, and $\operatorname{dist}_{\Sigma, C}(z) = \min\{\|w - z\|_\Sigma \mid w \in C\}$. As in [1], one element of the generalized hessian of (1) is then given by

$$H_k(x) = Q + \frac{1}{\gamma_k} I + A_{J_k(x)}^\top (\Sigma_k)_{J_k(x)} A_{J_k(x)}, \quad (2)$$

with $J_k(x) = \{i \mid (Ax + \Sigma_k^{-1} y^k) \notin [\ell_i, u_i]\}$ the set of active constraints, and where $A_{J_k(x)}$ is the stacking of the j-th rows of A with $j \in J_k(x)$. The key observation here is that, as the last term in (2) is positive semidefinite, $H_k(x)$ will be positive definite by choosing $\gamma_k < \frac{1}{|\lambda_{\min}(Q)|}$, with $\lambda_{\min}(Q)$ the minimum eigenvalue of Q. Therefore, the approach in [1] can be followed if one sticks to this choice of the proximal penalty parameter. Theoretical convergence to a stationary point can be shown with only minor modifications to the algorithm.

A key issue, however, is to either compute or find an appropriate upper bound on $|\lambda_{\min}(Q)|$. Numerical experiments show that overly small values of γ_k to certainly satisfy the inequality, slow down the convergence in practice. Therefore, a trade-off is necessary between the accurate computation of the minimum eigenvalue and the convergence speed of the resulting algorithm. In QPs arising in practice, Q is often large and sparse. As such, direct methods based on dense linear algebra will be too slow for our purpose. Iterative methods, which typically find only a few specific eigenvalues and rely on matrix-vector multiplications, are more suited. For example, the single-vector version of the locally optimal block preconditioned conjugate gradient (LOBPCG) method [4] can efficiently find the minimum eigenvalue of a symmetric matrix. A dedicated implementation of this algorithm is written in C and added to the QPALM repository.[1]

References

[1] B. Hermans, A. Themelis, and P. Patrinos, "QPALM: A Newton-type Proximal Augmented Lagrangian Method for Quadratic Programs," in *58th IEEE Conference on Decision and Control*, Dec. 2019.

[2] M. Raghavachari, "On connections between zero-one integer programming and concave programming under linear constraints," *Operations Research*, vol. 17, no. 4, pp. 680–684, 1969.

[3] D. Axehill, *Integer quadratic programming for control and communication*. PhD thesis, Institutionen för systemteknik, 2008.

[4] A. V. Knyazev, "Toward the optimal preconditioned eigensolver: Locally optimal block preconditioned conjugate gradient method," *SIAM journal on scientific computing*, vol. 23, no. 2, pp. 517–541, 2001.

---

[1] https://github.com/meco-group/QPALM

Co-design of a Continuous Variable Transmission Using a Sequential Quadratic Programming based control optimization

C.A.Fahdzyana*, M.C.F. Donkers†, T. Hofman*

*Dept. of Mechanical Engineering, † Dept. of Electrical Engineering

Eindhoven University of Technology

5612 AZ Eindhoven, The Netherlands

Email: c.a.fahdzyana@tue.nl, m.c.f.donkers@tue.nl, t.hofman@tue.nl

1 Introduction

One way to improve vehicle driveline efficiency is by utilizing a continuously variable transmission (CVT), which allows the propulsion source (i.e., engine and/or EM) to be operated at the optimal operating points. In this work, an integrated plant and control system design (co-design) for a CVT system is performed. The goal is to achieve a new CVT design with lower mass and dimensions (related to cost reduction), while also minimizing the clamping force (for energy saving and to prevent damage) and the error for ratio trajectory tracking. Here, we propose a Sequential Quadratic Programming (SQP) based control optimization strategy [1] for integrated plant and control system design. The combined plant and control optimization will be solved by utilizing the nested approach [2].

2 CO-DESIGN

We formulate the (nonlinear) optimization problem for the integrated plant and control design problem of the CVT such that

$$\min w_p \underbrace{M_v}_{J_p} + w_c \underbrace{\int_{t_o}^{t_f} q\left(r_{g,r}(t) - r_g(t)\right)^2 + r\,u(t)\,\mathrm{d}t}_{J_c}, \quad (1)$$

subject to a set of design constraints, given by:

$$\mathbf{g}(\mathbf{x_p}) \leq \mathbf{0},\, \mathbf{h}(\mathbf{x_p}) = \mathbf{0},\, \mathbf{g}(\mathbf{x_p}, \mathbf{x_c}) \leq \mathbf{0},\, \mathbf{h}(\mathbf{x_p}, \mathbf{x_c}) = \mathbf{0}, \quad (2)$$

where $\mathbf{x_i}$ and J_i are the design parameters as well as the objective, respectively, for $i \in \{p, c\}$. The general formulation of SQP algorithm is given by [1]:

$$
[x_k^{i+1}, u_k^{i+1}] = \operatorname*{argmin}_{x_k, u_k} \frac{1}{2} \begin{bmatrix} x_k - x_k^i \\ u_k - u_k^i \end{bmatrix}^\top R_k \begin{bmatrix} x_k - x_k^i \\ u_k - u_k^i \end{bmatrix}
$$
$$
+ \left(H_k \begin{bmatrix} x_k \\ u_k \end{bmatrix} + F_k\right)^\top \begin{bmatrix} x_k \\ u_k \end{bmatrix}, \quad (3)
$$

subject to:

$$x_{k+1} = f(x_k^i, u_k^i) + \nabla f(x_k^i, u_k^i) \begin{bmatrix} x_k - x_k^i \\ u_k - u_k^i \end{bmatrix} \quad (4)$$

$$\underline{x}_k \leq x_k \leq \bar{x}_k,\, \underline{u}_k \leq u_k \leq \bar{u}_k \quad (5)$$

where x is the state variable, u is the control input, $f(x, u)$ is the nonlinear plant dynamics. The results are depicted in Fig. 1 and Table 1.
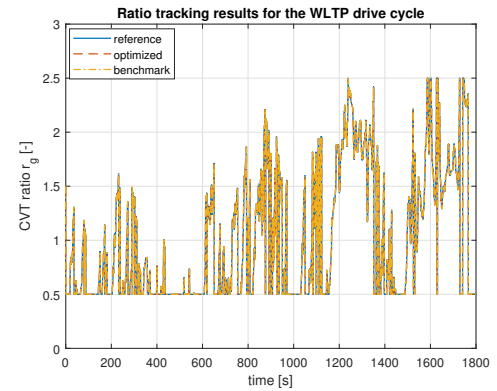
Figure 1: Ratio tracking results for the WLTP cycle

Table 1: Results of Optimization

parameter	description	benchmark	optimized	unit
J_p	plant objective	7.1	4.4	kg
J_c	control objective	2.9	2.9	$\cdot 10^3$
β	wedge angle	11	8.14	^{o}
a	Center distance	171	145.2	mm

3 CONCLUSIONS

In this paper, we have presented an SQP-based algorithm to solve the nonlinear control optimization problem for an integrated plant and control system design (co-design) of a CVT system. It is concluded that the current CVT variator design can be reduced in terms of size and weight without compromising performance, i.e., tracking the required ratio trajectory.

References

[1] J. Nocedal S. J. Wright. Numerical Optimization. *Springer*, 2006.

[2] H.K. Fathy, Combined Plant And Control Optimization: Theory, Strategies and Applications. *PhD Thesis*, University of Michigan, 2003.

Transition-time optimization for multi-actor dynamical systems

Wim Van Roy*, Joris Gillis, Goele Pipeleers and Jan Swevers

MECO Research Team, KU Leuven DMMS lab, Flanders Make

Celestijnenlaan 300, 3001 Leuven

*Email: wim.van.roy@kuleuven.be

1 Introduction

Switching decisions often play an important role in the efficiency of systems in real-world control applications such as chemical processes, heating systems or energy production and conversion systems. For these model-based (non-)linear control applications it is important to take the discrete nature of switches efficiently into account leading to a Mixed Integer Non-linear or Mixed Integer Linear problem for which commercial solvers such as *GUROBI* [1] can be used. Despite the large number of techniques such as several heuristics, branch-and-bound and optimal cutting planes, these problems are often hard to solve in real-time due to the discrete nature of the problem. Especially when the number of possible switches is large due to several actors that can switch from state.

However, when the sequence of the switches is approximately known, these problems can also be translated into non-linear problems removing the need to handle the mixed integer values. This can potentially reduce the calculation time considerably. We will discuss two alternative techniques for this approach. The first approach is the switching time optimization as presented by [2]. The second approach is a switching moment optimization.

2 Approach

2.1 Switching time optimization

The problem can be reformulated as a multi-stage system in which each stage represents a combination of states of the actors in the system as described by S. Sager[2]. Each state switch from an actor will lead to a new stage. This leads to a multistage optimal control problem (MSOCP).

2.2 Switching moment optimization

Alternatively, a state switch can be represented by a switching function. A switching functions should give a "1" when the state is active, otherwise a "0" value. This behaviour can be approximated by a sigmoid function, such as the following logistic function.

$$\sigma(x) = \frac{1}{1 + e^{-x}}$$

The states of an actor will then be represented as a sum of sigmoid functions.

$$S_{m,i}(t) = \sum_{j=0}^{n_{s,m}} w_{m,i,j} \sigma \left(\frac{t - t_{m,j}}{\Delta t_{m,j}/4} \right)$$

With $S_{m,i}$ the i-th state of actor m with their corresponding weights $w_{m,i,j} \in \{-1, 0, 1\}$ for each j-th switch, $n_{s,m}$ the number of switches for actor m and for each switch, a ramp time $\Delta t_{n,j}$ and switching time $t_{n,j}$. The switching times can subsequently be part of the resulting optimization problem.

3 Comparison

Both approaches will be compared using practical examples using *CasADi*[3]. It turns out that the switching time optimization calculation has on average a calculational advantage compared to the switching moment optimization. However, when the sequence of the switches is not known upfront, the switching moment optimization has a clear advantage. It is capable of deriving the optimal start-up sequence without the need of a branch-and-bound algorithm.

References

[1] LLC Gurobi Optimization, "Gurobi optimizer reference manual", 2019.

[2] S. Sager, *Numerical methods for mixed-integer optimal control problems.* Der andere Verlag Tönning, 2005.

[3] J. A. E. Andersson, J. Gillis, G. Horn, J. B. Rawlings, and M. Hiegl, "CasADi - A software framework for nonlinear optimization and optimal control," *Mathematical Programming Computation*, vol. 11, no.1 pp. 1-36, 2019.

Effortless modeling of optimal control problems with rockit

Joris Gillis   Bastiaan Vandewal   Goele Pipeleers
Jan Swevers
MECO Research Team, Department Mechanical Engineering, KU Leuven
DMMS lab, Flanders Make, Leuven, Belgium
Email: {firstname}.{lastname}@kuleuven.be

1 Introduction

A host of complementary research fields connected to mechatronics can be approached through optimal control problems (OCP): system identification, iterative learning, motion planning, model predictive control, etc.

We present rockit[1] (rapid optimal control kit), an open-source Python package that facilitates the definition, solving and post-processing of continuous-time nonlinear OCPs. While CasADi [1, 2], which is used internally in rockit, offers superior flexibility in all three modeling aspects, rockit conveniently abstracts away implementation details from application experts and students.

We illustrate rockit's main components with the help of code snippets, runnable in a Python environment empowered with `pip install rockit-meco`.

2 Definition of OCP

The `Ocp` class represents an optimal control problem:

```
from rockit import *
ocp = Ocp(t0=0, T=10) # Horizon of 10s
```

Symbols for states and controls can be defined and combined into time-dependent expressions a.k.a. *signals*:

```
x = ocp.state()
y = ocp.state()
u = ocp.control()
e = (1 - y**2)
```

System dynamics can be associated with each state:

```
ocp.set_der(x, e * x - y + u)
ocp.set_der(y, x)
```

A Lagrange objective functional term can be specified by providing a *signal* as integrand:

```
ocp.add_objective(
  ocp.integral(x**2 + y**2 + u**2))
```

A Mayer term can be added by requesting evaluation of a signal at $t_f = t_0 + T$, i.e. the end of the OCP horizon:

```
ocp.add_objective(ocp.at_tf(x**2))
```

Path constraints, valid over the entire time-domain, can be specified with (in)equalities on signals[2]:

```
ocp.subject_to(x >= -0.25)
ocp.subject_to(-1 <= (u <= 1 ))
```

Boundary constraints are created with evaluated signals:

```
ocp.subject_to(ocp.at_t0(x) == 0)
ocp.subject_to(ocp.at_t0(y) == 1)
```

3 Solving and post-processing

Only direct solution methods are currently implemented, e.g. multiple shooting with explicit Runge-Kutta:

```
ocp.method(
  MultipleShooting(N=10, intg='rk'))
```

The OCP can be solved after specifying a nonlinear solver:

```
ocp.solver('ipopt')
sol = ocp.solve()
```

Optimized signals can be evaluated on the control grid:

```
t, xs = sol.sample(x, grid='control')
```

A polynomial interpretation of integrator output enables signal introspection at a much refined grid:

```
sample(x, grid='integrator', refine=100)
```

4 Addendum

Rockit v0.1.8 supports matrix-valued states and controls, time-dependent differential-algebraic equations, free start- and end-time problems, non-uniform grids and multi-stage problems. Rockit offers a zero-cost abstraction mode: parametric OCPs can be exported to CasADi Functions and hence to C code and Simulink.

References

[1]   Joel A. E. Andersson, Joris Gillis, Greg Horn, James B. Rawlings, and Moritz Diehl. CasADi: a software framework for nonlinear optimization and optimal control. *Mathematical Programming Computation*, Jul 2018.

[2]   Joris Gillis. Effortless nlp modeling with casadi's opti stack. In *Book of Abstracts – 37th Benelux Meeting on Systems and Control*, page 186, March 2018.

---

[1]https://gitlab.mech.kuleuven.be/meco-software/rockit

[2]The parentheses in the two-sides inequality is a workaround for an unfortunate restriction in the Python language.

Local Spline Relaxation for Multiple Shooting

Bastiaan Vandewal, Joris Gillis and Jan Swevers

MECO Research Team, Department of Mechanical Engineering, KU Leuven, Belgium

DMMS Lab, Flanders Make, Leuven, Belgium

Email: bastiaan.vandewal@kuleuven.be

1 Introduction

Calculating collision-free motion trajectories through environments with obstacles is of highest priority in autonomous mobile systems. The constraints that define these trajectories should hold during the entire motion time. Whereas time gridding can be used to refine the grid, it only defines constraints on a finite set of time samples and as such those constraints can be violated in between these grid points. By constraining a continuous approximation of the trajectory, those path constraints are satisfied at all time instances [1].

This abstract presents a comparison between the classical time gridding approach and a new motion planning approach, Local Spline Relaxation (LSR), that piecewise parameterizes the trajectories as fourth order polynomials based on Runge-Kutta's fourth order integration scheme [2]. All calculations have been made with Rockit[1], a toolbox for modeling optimal control problems (OCP).

2 Local Spline Relaxation

Figure 1 shows the state trajectory for an OCP, where one of the states is constrained to be larger than -0.25. This constraint is clearly not satisfied in between those gridded points. By applying spline relaxation techniques, the constraints are enforced over the entire time domain as can be seen in the same figure. Although the constraint is now satisfied, some conservativeness has been introduced.
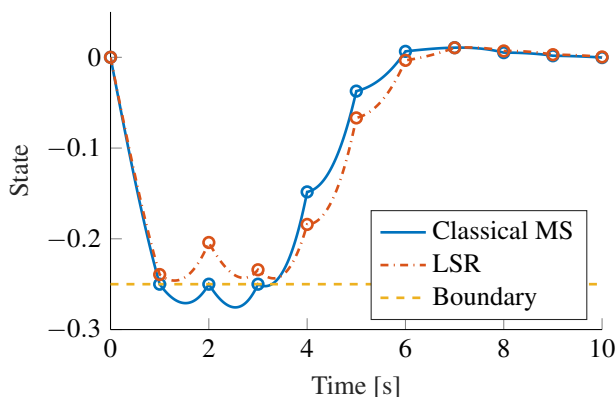
Figure 1: Comparison of constraint violation for classical multiple shooting and constraint satisfaction for LSR.

---

[1] Available online at https://github.com/meco-group/rockit

3 Comparison

The number of integration steps per control interval M ranges from 1 to 10, while all other parameters are kept the same. The comparison of the minimal distance to the boundary (represented by 0) can be found in Figure 2.
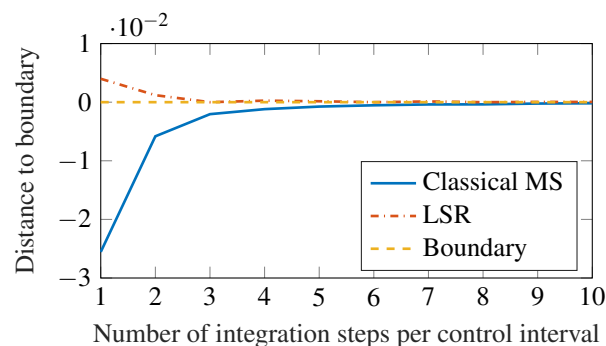
Figure 2: Comparison of minimal distance to the boundary for classical multiple shooting and LSR with varying M.

The violation of the constraint for the classical multiple shooting strongly reduces with rising amount of integration steps per control interval, but never fully disappears. To the contrary, the conservativeness introduced by LSR is only small, strongly reduces with higher amount of integration steps and even becomes neglectable for $M = 3$. The calculation time for low M is only slightly higher for LSR and the same distance to the boundary can be found using the same amount of calculation time.

References

[1]   W. Van Loock, G. Pipeleers, and J. Swevers, "Optimal motion planning for differentially flat systems with guaranteed constraint satisfaction." Proceedings of the 2015 Americal Control Conference (ACC), Chicago, 2015.

[2]   B. Vandewal, J. Gillis, E. Rademakers, G. Pipeleers and J. Swevers, "Obstacle Avoidance in Path Following using Local Spline Relaxation." in IEEE 16th International Workshop on Advanced Motion Control, 2020 (accepted).

Data-driven distributionally robust LQR with multiplicative noise

Peter Coppens[1]
peter.coppens@kuleuven.be

Mathijs Schuurmans[1]
mathijs.schuurmans@kuleuven.be

Panagiotis Patrinos[1]
panos.patrinos@kuleuven.be

[1]STADIUS, Department of Electrical Engineering (ESAT), KU Leuven, Leuven, Belgium.

1 Introduction

We develop controllers for linear systems with time-varying parametric uncertainty. These may cover a wide range of systems. In our case the uncertainty varies stochastically. Most existing approaches then assume that the distribution of w is known [1], which is not the case in many practical applications. To this end, we adopt a data-driven distributonally robust (DR) approach [2] towards solving the infinite-horizon Stochastic Linear Quadratic Regulator (SLQR) problem. To do so we minimize the expected cost for the worst-case distribution in a so-called ambiguity set computed based on the available data such that it contains the true distribution with high probability. The result is then a controller that is mean square stabilizing with high probability.

2 Methodology

The dynamics of the linear system with stochastic parameteric uncertainty are described by:

$$x_{k+1} = A(w_k)x_k + B(w_k)u_k$$

$$\text{with} \quad A(w) = A_0 + \sum_{i=1}^{n_w} w^i A_i, \quad B(w) = B_0 + \sum_{i=1}^{n_w} w^i B_i,$$

with $x_k \in \mathbb{R}^{n_x}$ the state, $u_k \in \mathbb{R}^{n_u}$ the input and $w_k \in \mathbb{R}^{n_w}$ an indepent identically distributed copy of a random vector w distributed according to $\mathbb{P}_w$. By w^i we denothe the i'th element of w. From earlier results in literature [1] it is clear that only the mean $\mu = \mathbb{E}[w]$ and the covariance $\Sigma = \mathbb{E}[ww^\top]$ affect the optimal controller. As such we estimate these from M offline samples using $\hat{\mu} = \sum_{n=0}^{M} w_n$ and $\hat{\Sigma} = \sum_{n=0}^{M}(w_n - \hat{\mu})(w_n - \hat{\mu})^\top$. By combining results from [3, 4, 2] we then produce an ambiguity set:

$$\mathscr{A} = \left\{ \mathbb{P}_v \in \mathscr{M} \; \middle| \; \begin{array}{l} (\mathbb{E}_{\mathbb{P}_v}[v] - \hat{\mu})^\top \hat{\Sigma}^{-1}(\mathbb{E}_{\mathbb{P}_v}[v] - \hat{\mu}) \le r_\mu^2 \\ \mathbb{E}_{\mathbb{P}_v}\left[(w - \mu)(w - \mu)^\top\right] \le r_\Sigma \hat{\Sigma}, \end{array} \right\},$$

with $\mathbb{P}_v$ the distribution of v and $\mathscr{M}$ the set of probability measures defined on $(\mathbb{R}^{n_w}, \mathscr{B})$, with $\mathscr{B}$ the Borel σ-algebra of $\mathbb{R}^{n_w}$. The radii r_μ and r_Σ are calculated such that $\mathbb{P}[\mathbb{P}_w \in \mathscr{A}] \ge 1 - \beta$, with β some tunable parameter. To do so we need to assume that w is a sub-Gaussian random vector. The distributionally robust LQR problem is then:

$$
\begin{aligned}
\underset{u_0, u_1, \dots}{\textbf{minimize}} \quad & \max_{\mathbb{P}_v \in \mathscr{A}} \mathbb{E}_{\mathbb{P}_v}\left[\sum_{k=1}^{\infty} x_k^\top Q x_k + u_k^\top R u_k \right] \\
\textbf{subj. to} \quad & x_{k+1} = A(v_k)x_k + B(v_k)u_k, \quad k \in \mathbb{N} \\
& x_0 = \bar{x},
\end{aligned}
\tag{1}
$$
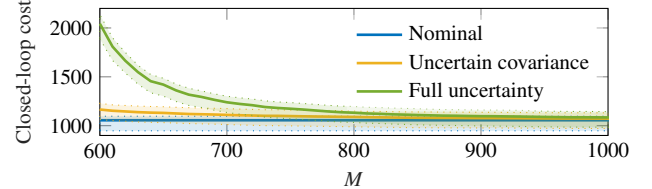
Figure 1: Mean and 0.3-confidence interval of the closed-loop cost versus sample size for controllers.

with $Q > 0$, $R > 0$ and v_k i.i.d. random vectors with distribution $\mathbb{P}_v$. When $r_\mu = 0$ it is possible to show that the solution to (1) is equal to the solution of the classical LQR problem, where we assume that the covariance of w is given by $r_\Sigma \hat{\Sigma}$. This solution is evaluated by solving a semidefinite program, which is a generalization of the one derived in [5]. For the case where $r_\mu > 0$ it is only possible to solve (1) suboptimally by using results from robust optimization [6]. We also verify that both of these controllers are mean square stabilizing with probability at least $1 - \beta$.

Since the estimates $\hat{\mu}$ and $\hat{\Sigma}$ become more accurate as more data is gathered, r_μ and r_Σ decrease and therefore the controller converges to the optimal controller for the true distribution of w. This behaviour was confirmed experimentally by calculating the optimal controllers for a double integrator with stochastically varying parameters. The result is depicted in Figure 1.

References

[1]   T. Morozan. Stabilization of some stochastic discrete-time control systems. *Stoch. Anal. Appl.*, 1(1):89–116, 1983.

[2]   E. Delage and Y. Ye. Distributionally robust optimization under moment uncertainty with application to data-driven problems. *Oper. Res.*, 58(3):595–612, 2010.

[3]   D. Hsu, S. Kakade, and T. Zhang. Tail inequalities for sums of random matrices that depend on the intrinsic dimension. *Electron. Commun. Probab.*, 17(52):1–13, 2012.

[4]   D. Hsu, S. M. Kakadey, and T. Zhang. Tail inequalities for sums of random matrices that depend on the intrinsic dimension. *Electron. Commun. Probab.*, 17(14), 2012.

[5]   V. Balakrishnan and L. Vandenberghe. Semidefinite programming duality and linear time-invariant systems. *IEEE Trans. on Autom. Control*, 48(1):30–41, 2003.

[6]   A. Ben-Tal, L. El Ghaoui, and A. Nemirovski. Robustness. In *Handbook of Semidefinite Programming*, pages 139–162. 2000.

Data informativity for system analysis and control part 1: analysis

Jaap Eising, Henk J. van Waarde, Harry L. Trentelman, and M. Kanat Camlibel

University of Groningen

Introduction

Model-based control is one of the main paradigms within the field of systems and control. In many instances, however, a system model is not known a priori and has to be identified from measured data. This naturally leads to a two-step procedure of system identification followed by control design. In contrast, data-driven analysis and control aims at analysing system properties and constructing controllers directly on the basis of data, without explicitly identifying a system model. Several interesting results following this data-driven paradigm [1, 2, 3, 4] make use of persistently exciting data. However, the assumption of persistency of excitation is rather strong, and is conservative for many analysis and design problems.

Our paper [5] introduces a general framework for data-driven analysis and control that works with data that are not necessarily persistently exciting. In particular, the paper provides necessary and sufficient conditions on the data under which certain analysis and design problems can be solved. The results are interesting since they reveal that analysis and control may be possible in situations where (unique) system identification cannot be performed. In this first talk, we will highlight our analysis results.

Results

Consider the discrete-time linear system

$$x(t+1) = A_s x(t) + B_s u(t). \tag{1}$$

We will consider data consisting of input and state measurements and define the matrices:

$$U_- := \begin{bmatrix} u(0) & u(1) & \cdots & u(T-1) \end{bmatrix}, \; X := \begin{bmatrix} x(0) & x(1) & \cdots & x(T) \end{bmatrix}.$$
$$X_- := \begin{bmatrix} x(0) & x(1) & \cdots & x(T-1) \end{bmatrix}, X_+ := \begin{bmatrix} x(1) & x(2) & \cdots & x(T) \end{bmatrix},$$

Say we are interested in verifying whether the 'true' system (1) is controllable or stabilizable, based on the data (U_-, X). We can only conclude that the 'true' system has a property if *all* systems generating the measurements (U_-, X) have this property. We denote the set of all systems of the form (1), compatible with these data as

$$\Sigma_{i/s} := \left\{ (A, B) \mid X_+ = \begin{bmatrix} A & B \end{bmatrix} \begin{bmatrix} X_- \\ U_- \end{bmatrix} \right\}.$$

Since we are interested in controllability and stabilizability, we introduce the sets

$$\Sigma_{cont} := \{(A,B) \mid (A,B) \text{ is controllable}\},$$
$$\Sigma_{stab} := \{(A,B) \mid (A,B) \text{ is stabilizable}\},$$

which leads to the following definition:

Definition 1 We say that the data (U_-, X) are *informative for controllability* if $\Sigma_{i/s} \subseteq \Sigma_{cont}$ and *informative for stabilizability* if $\Sigma_{i/s} \subseteq \Sigma_{stab}$.

In the following theorem from [5], we give necessary and sufficient conditions for the above notions of informativity. Note that controllability and stabilizability are assessed purely on the basis of data.

Theorem 2 (Data-driven Hautus tests) *The data (U_-, X) are informative for controllability if and only if*

$$\text{rank}(X_+ - \lambda X_-) = n \quad \forall \lambda \in \mathbb{C}. \tag{2}$$

Similarly, the data (U_-, X) are informative for stabilizability if and only if

$$\text{rank}(X_+ - \lambda X_-) = n \quad \forall \lambda \in \mathbb{C} \text{ with } |\lambda| \geqslant 1. \tag{3}$$

The study of other system-theoretic properties such as stability can be done along the same lines, and will be discussed in more detail during the talk.

References

[1]   I. Markovsky and P. Rapisarda, "Data-driven simulation and control," *International Journal of Control*, vol. 81, no. 12, pp. 1946–1959, 2008.

[2]   J. Coulson, J. Lygeros, and F. Dörfler, "Data-enabled predictive control: In the shallows of the DeePC," in *Proceedings of the European Control Conference*, June 2019, pp. 307–312.

[3]   J. Berberich, J. Köhler, M. A. Müller, and F. Allgöwer, "Data-driven model predictive control with stability and robustness guarantees," *Available online at https://arxiv.org/abs/1906.04679*, 2019.

[4]   C. De Persis and P. Tesi, "Formulas for data-driven control: Stabilization, optimality and robustness," *Available online at https://arxiv.org/pdf/1903.06842.pdf*, 2019.

[5]   H. J. Van Waarde, J. Eising, H. L. Trentelman, and M. K. Camlibel, "Data informativity: a new perspective on data-driven analysis and control," *Available online at https://arxiv.org/abs/1908.00468*.

Data informativity for system analysis and control part 2: design

Henk J. van Waarde, Jaap Eising, Harry L. Trentelman, and M. Kanat Camlibel
University of Groningen

Introduction

Model-based control is one of the main paradigms within the field of systems and control. In many instances, however, a system model is not known a priori and has to be identified from measured data. This naturally leads to a two-step procedure of system identification followed by control design. In contrast, data-driven analysis and control aims at analysing system properties and constructing controllers directly on the basis of data, without explicitly identifying a system model. Several interesting results following this data-driven paradigm [1, 2, 3, 4] make use of persistently exciting data. However, the assumption of persistency of excitation is rather strong, and is conservative for many analysis and design problems.

Our paper [5] introduces a general framework for data-driven analysis and control that works with data that are not necessarily persistently exciting. In particular, the paper provides necessary and sufficient conditions on the data under which certain analysis and design problems can be solved. The results are interesting since they reveal that analysis and control may be possible in situations where (unique) system identification cannot be performed. In this second talk, we will highlight our results on control design.

Results

As in part 1, consider the discrete-time linear system

$$x(t+1) = A_s x(t) + B_s u(t). \qquad (1)$$

Let the input/output data obtained from (1) be given by:

$U_- := \begin{bmatrix} u(0) \ u(1) \ \cdots \ u(T-1) \end{bmatrix}$, $X := \begin{bmatrix} x(0) \ x(1) \ \cdots \ x(T) \end{bmatrix}$.

$X_- := \begin{bmatrix} x(0) \ x(1) \ \cdots \ x(T-1) \end{bmatrix}$, $X_+ := \begin{bmatrix} x(1) \ x(2) \ \cdots \ x(T) \end{bmatrix}$,

Suppose that we are interested in designing a stabilizing state feedback $u = Kx$ for the 'true' system (1), using the data (U_-, X). We can only conclude that the true system is stabilized by this control law if *all* systems generating the measurements (U_-, X) are stabilized. We denote the set of all systems of the form (1), compatible with the data as

$$\Sigma_{\text{i/s}} := \left\{ (A,B) \mid X_+ = \begin{bmatrix} A & B \end{bmatrix} \begin{bmatrix} X_- \\ U_- \end{bmatrix} \right\}.$$

We now have the following definition and characterization of data informativity for stabilization.

Definition 1 We say that the data (U_-, X) are informative for stabilization by state feedback if there exists a feedback gain K such that $A + BK$ is stable for all $(A,B) \in \Sigma_{\text{i/s}}$.

Theorem 2 *The data (U_-, X) are informative for stabilization by state feedback if and only if there exists a right inverse $X_-^\dagger$ of X_- such that $X_+ X_-^\dagger$ is stable.*

Moreover, K is such that $A + BK$ is stable for all systems $(A,B) \in \Sigma_{\text{i/s}}$ if and only if $K = U_- X_-^\dagger$, where $X_-^\dagger$ satisfies the above properties.

Note that it is not immediately clear how to compute a suitable right inverse $X_-^\dagger$ in Theorem 2. The following theorem resolves this issue by showing that $X_-^\dagger$ can be found by solving a data-based linear matrix inequality.

Theorem 3 *The data (U_-, X) are informative for stabilization by state feedback if and only if there exists a matrix $\Theta \in \mathbb{R}^{T \times n}$ satisfying*

$$X_- \Theta = (X_- \Theta)^\top \quad and \quad \begin{bmatrix} X_- \Theta & X_+ \Theta \\ \Theta^\top X_+^\top & X_- \Theta \end{bmatrix} > 0. \qquad (2)$$

Moreover, K is such that $A + BK$ is stable for all systems $(A,B) \in \Sigma_{\text{i/s}}$ if and only if $K = U_- \Theta (X_- \Theta)^{-1}$ for some matrix Θ satisfying (2).

As we will discuss during the talk, it is possible to characterize informativity and to find controllers for several other problems. We will also discuss robustness with respect to unknown disturbances, and design using input/output data.

References

[1]   I. Markovsky and P. Rapisarda, "Data-driven simulation and control," *International Journal of Control*, vol. 81, no. 12, pp. 1946–1959, 2008.

[2]   J. Coulson, J. Lygeros, and F. Dörfler, "Data-enabled predictive control: In the shallows of the DeePC," in *Proceedings of the European Control Conference*, June 2019, pp. 307–312.

[3]   J. Berberich, J. Köhler, M. A. Müller, and F. Allgöwer, "Data-driven model predictive control with stability and robustness guarantees," *Available online at https://arxiv.org/abs/1906.04679*, 2019.

[4]   C. De Persis and P. Tesi, "Formulas for data-driven control: Stabilization, optimality and robustness," *Available online at https://arxiv.org/pdf/1903.06842.pdf*, 2019.

[5]   H. J. Van Waarde, J. Eising, H. L. Trentelman, and M. K. Camlibel, "Data informativity: a new perspective on data-driven analysis and control," *Available online at https://arxiv.org/abs/1908.00468*.

Informativity for data-driven moment matching

A.M. Burohman, B. Besselink, J.M.A. Scherpen, M.K. Camlibel

Jan C. Willems Center for Systems and Control, Center for Data Science and Systems Complexity,

University of Groningen, The Netherlands

Email: {a.m.burohman; b.besselink; j.m.a.scherpen; m.k.camlibel}@rug.nl

1 Introduction

In the field of model reduction, moment matching techniques are an efficient tool to obtain a reduced-order model on the basis of the original high-order model, see [1, 2]. In this abstract however, we assume that we only have access to input-output data generated from the system (and not the model itself). We are interested in approximating the system by a lower-order model matching its moment(s) using this data only. We note that this framework does not need to uniquely identify the system as in [3]. Instead, we characterize the set of all systems explained by the data and all systems having the same moment at a given interpolation point. Based on those sets, we introduce a new concept called data informativity for moment-matching at the given interpolation point. Then, we look for the conditions under which the data is informative for this new concept.

2 Main Result

Consider the input-output data (U, Y) where

$$U = \begin{bmatrix} u_0 & u_1 & \dots & u_T \end{bmatrix}, \quad Y = \begin{bmatrix} y_0 & y_1 & \dots & y_T \end{bmatrix},$$

for some integer $T > 0$, generated from an unknown discrete-time linear system of the form

$$
\begin{aligned}
y_{t+n} &+ p_{n-1} y_{t+n-1} + \cdots + p_1 y_{t+1} + p_0 y_t \\
&= q_n u_{t+n} + q_{n-1} u_{t+n-1} + \cdots + q_1 u_{t+1} + q_0 u_t,
\end{aligned}
\tag{1}
$$

with t the discrete-time variable. After defining the row vectors q and p to be the collection of the parameters of (1), it is clear that (1) explains the data (U, Y) if and only if

$$\begin{bmatrix} q & -p \end{bmatrix} \begin{bmatrix} H_n(U) \\ \bar{H}_n(Y) \end{bmatrix} = \begin{bmatrix} y_n & \dots & y_T \end{bmatrix} \tag{2}$$

where $H_n(V) \in \mathbb{R}^{(n+1) \times (T-n+1)}$ is the Hankel matrix of V of depth n and $\bar{H}_n$ equals H_n with its last row removed. Now, we can define

$$\Sigma_{U,Y} := \left\{ \begin{bmatrix} q & -p \end{bmatrix} \in \mathbb{R}^{1 \times (2n+1)} \middle| \quad (2) \quad \text{holds} \right\} \tag{3}$$

as the set containing all systems explaining the data (U, Y).

Given an interpolation point $\sigma \in \mathbb{C}$, the number $M_0 \in \mathbb{C}$ is said to be a 0-th moment at σ of (1) if it is a solution to

$$P(\sigma) M_0 = Q(\sigma), \tag{4}$$

where $P(z) = z^n + p_{n-1} z^{n-1} + \cdots + p_1 z + p_0$ and $Q(z) = q_n z^n + q_{n-1} z^{n-1} + \cdots + q_1 z + q_0$. Condition (4) can be written as

$$\begin{bmatrix} q & -p \end{bmatrix} \begin{bmatrix} \gamma_n(\sigma) \\ M_0 \gamma_{n-1}(\sigma) \end{bmatrix} = M_0 \sigma^n, \tag{5}$$

where $\gamma_\ell(z) := \begin{bmatrix} 1 & z & \cdots & z^\ell \end{bmatrix}^T$. Then, the expression (5) allows for defining

$$\Sigma_{\sigma, M_0} := \left\{ \begin{bmatrix} q & -p \end{bmatrix} \in \mathbb{R}^{1 \times (2n+1)} \middle| \quad (5) \quad \text{holds} \right\} \tag{6}$$

as the set of all systems that have 0-th moment M_0 at σ.

Definition 1. The data set (U, Y) is informative for 0-th moment matching at σ if there exists a unique M_0 such that $\Sigma_{U,Y} \subseteq \Sigma_{\sigma, M_0}$.

Then, in this abstract, we aim to provide necessary and sufficient conditions on the data (U, Y) such that it is informative for 0-th moment matching at σ.

Theorem 1. *The data (U, Y) is informative for 0-th moment matching at σ if and only if*

$$\text{rank} \begin{bmatrix} H_n(U) & 0 & \gamma_n(\sigma) \\ H_n(Y) & \gamma_n(\sigma) & 0 \end{bmatrix} = \text{rank} \begin{bmatrix} H_n(U) & 0 \\ H_n(Y) & \gamma_n(\sigma) \end{bmatrix} \tag{7}$$

and

$$\text{rank} \begin{bmatrix} H_n(U) & 0 \\ H_n(Y) & \gamma_n(\sigma) \end{bmatrix} = \text{rank} \begin{bmatrix} H_n(U) \\ H_n(Y) \end{bmatrix} + 1. \tag{8}$$

When (7) and (8) hold, computing M_0 is straightforward. Finding the reduced-order model satisfying moment matching can be regarded as a rational interpolation problem of the pair (σ, M_0). The extension considering higher-order moments also has been studied and results in similar conditions.

References

[1] A. C. Antoulas, *Approximation of Large-scale Dynamical Systems*. SIAM, 2005.

[2] A. Astolfi, "Model reduction by moment matching for linear and nonlinear systems," *IEEE Transactions on Automatic Control*, vol. 55, no. 10, pp. 2321–2336, 2010.

[3] M. Verhaegen and V. Verdult, *Filtering and System Identification: A Least Squares Approach*. Cambridge University Press, 2007.

Data-Driven Rational LPV Controller Synthesis for Unstable Systems using Frequency Response Functions

Tom Bloemers[1], Roland Tóth[1] and Tom Oomen[2]

[1]Department of Electrical Engineering, Eindhoven University of Technology

[2]Department of Mechanical Engineering, Eindhoven University of Technology

Email: {t.a.h.bloemers, r.toth, t.a.e.oomen}@tue.nl

1 Introduction

The current state-of-the-art control design techniques for Linear Parameter-Varying (LPV) systems rely on the availability of parametric models of the to be controlled system. In practice, these models can be difficult to obtain and are often too complex for control design. Although data-driven controller synthesis based on Frequency Response Functions (FRF) enables a systematic design approach within the LTI framework, at present these methods are limited when applied to LPV systems. In [1], first steps towards data-driven frequency domain controller design for LPV systems have been presented. Here an LPV finite impulse response controller is synthesized, where stability is characterized in terms of a Nyquist constraint.

2 Problem formulation

Many control systems are operating condition dependent, for example a nonlinear system that operates along a trajectory. This dependency is here represented by a scheduling variable $p[k] \in \mathbb{P}$, where $\mathbb{P}$ is the scheduling domain. The goal is to synthesize a data-driven fixed-order rational LPV controller $K = RS^{-1}$, depicted in Figure 1, for which the signal relations are as follows:

$$u[k] = \sum_{j=0}^{n_{\mathrm{r}}} r_j(p[k])e[k-j] - \sum_{i=1}^{n_{\mathrm{s}}} s_i(p[k])u[k-i], \quad (1)$$

where the controller coefficient functions r and s are evaluated along the trajectory of p.
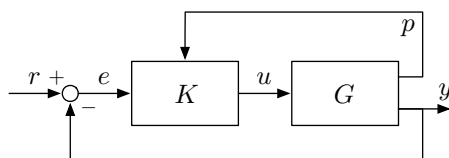
Figure 1: LPV representation of the closed-loop interconnection. K is the LPV controller and G is a nonlinear system.

3 Methodology

Inspired by [1, 2], the main contribution of this paper is a synthesis procedure for rational LPV control design for unstable systems, based on so-called frozen FRFs. The main idea is to factorize the plant and controller as coprime factorizations over $\mathcal{RH}_\infty$ and utilize the main-loop theorem to derive convex conditions on local stability and $\mathcal{H}_\infty$ performance.

4 Results

The resulting approach is applied to an inverted pendulum, where the angular position of the pendulum introduces nonlinear dynamics. A 5th order controller is designed where the coefficient functions r and s are chosen to have affine static dependence on the scheduling p. The proposed method results in a stabilizing controller that achieves sufficient performance around the operating points, for which the step responses are shown in Figure 2.
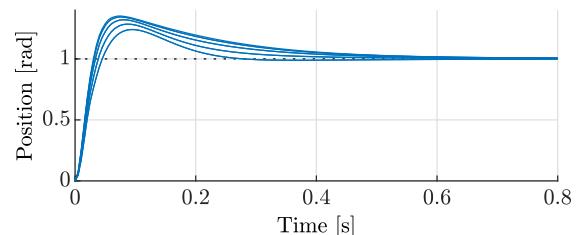
Figure 2: Local step responses of the inverted pendulum using 5th order rational data-driven LPV control design. The step responses are evaluated on a grid $\mathcal{P} \subset \mathbb{P}$ consisting of 9 grid-points.

5 Outlook

Currently, the proposed data-driven LPV synthesis guarantees performance and stability locally. Future work aims at the development of global performance and stability guarantees based approach.

References

[1]   T. Bloemers, R. Tóth, and T. Oomen,"Towards Data-Driven LPV Controller Synthesis Based on Frequency Response Functions," In Proc. of the 58th IEEE Conference on Decision and Control, Nice, France, December 2019.

[2]   A. Karimi, A. Nicoletti, and Y. Zhu,"Robust $\mathcal{H}_\infty$ controller design using frequency-domain data via convex optimization," International Journal of Robust and Nonlinear Control, vol. 28, no. 12, pp. 3766-3783, 2018.

A data-driven approach to distributed control[*]

Tom R. V. Steentjes, Mircea Lazar, Paul M. J. Van den Hof
Eindhoven University of Technology, The Netherlands
E-mail addresses: {t.r.v.steentjes, m.lazar, p.m.j.vandenhof}@tue.nl

1 Introduction

For many practical control applications, such as smart grids, smart buildings and vehicle platoons, models are not readily available, but data can be used to enable the controller design. Performance-oriented modelling on the basis of data has been addressed in the field of 'identification for control' [1]. Alternatively, the optimal synthesis of controllers on the basis of data without intermediate model construction was considered in [2] and led to the field of direct methods for data-driven controller design [3]. Both fields have only considered unstructured plants and controllers so far, to the best of the authors' knowledge. In this work, we consider the direct synthesis of a distributed controller for interconnected systems from data.

To illustrate the data-driven design of distributed controllers, we consider two processes that are interconnected. The application to more than two subsystems over arbitrary graphs is relatively straightforward and can be performed *mutatis mutandis*. The key steps to extend the data-driven controller design in [2] to the distributed case are (i) determining the *ideal distributed controller* and (ii) relating a global performance criterion to a *network identification problem*.

2 Problem formulation

We assume that the interconnected system consists of two processes $\mathcal{P}_1$ and $\mathcal{P}_2$ described by

$$\begin{cases} y_i(t) = G_i(q)u_i(t) + W_i(q)s_i(t), \\ o_i(t) = F_i(q)y_i(t), \end{cases} \quad i = 1, 2,$$

and $e_i = r_i - y_i$, interconnected through $s_2 = o_1$ and $s_1 = o_2$, with G_i, W_i and F_i rational transfer functions and q is the forward shift: $qx(t) = x(t+1)$. We assume that these transfer functions are not known. For each system, it is desired that y_i tracks the reference signal r_i. We consider an interconnected system that incorporates control specifications for the controlled network, as a structured analogy to the common reference model in e.g. [2]. This is depicted in Figure 1 as the interconnection of $\mathcal{K}_1$ and $\mathcal{K}_2$. The objective is to minimize the difference between the outputs y_i and the outputs y_i^d of the structured reference model, corresponding
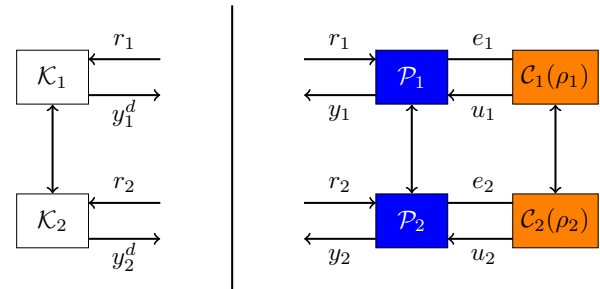
Figure 1: Structured reference model (left) and closed-loop network with distributed controller (right).

to the minimization of the performance criterion

$$J_d(\rho_1, \rho_2) = \bar{E}[y_1^d(t) - y_1(t)]^2 + \bar{E}[y_2^d(t) - y_2(t)]^2,$$

where ρ_i is the parameter that corresponds to controller $\mathcal{C}_i$.

3 Approach

The controller that admits the same interconnection structure as the process and achieves $J_d(\rho_1, \rho_2) = 0$, is the ideal distributed controller. This controller provides a possible parametrization with controller classes $\{\mathcal{C}_i(\rho_i)\}$ that contain the ideal controller subsystems. We will describe a procedure to obtain this controller explicitly.

On the basis of input-output data collected from the interconnected system, we construct virtual signals via the structured reference model, leading to a virtual experiment setup. We will show that the virtual experiment setup leads to a network identification problem with a criterion that has the same global optimum as the performance criterion J_d, when the controller class contains the ideal distributed controller. This implies that the distributed-controller synthesis problem can be formulated as a network identification problem.

References

[1] P. M. J. Van den Hof and R. J. P. Schrama. Identification and control: Closed-loop issues. *Automatica*, 31(12):1751 – 1770, 1995.

[2] M. C. Campi, A. Lecchini, and S. M. Savaresi. Virtual reference feedback tuning: a direct method for the design of feedback controllers. *Automatica*, 38(8):1337 – 1346, 2002.

[3] A. S. Bazanella, L. Campestrini, and D. Eckhard. *Data-Driven Controller Design: The H_2 Approach*. Communications and Control Engineering. Springer Netherlands, 2011.

Generalized sensing and actuation schemes for consistent local module identification in dynamic networks[1]

Karthik R. Ramaswamy [a], Paul M.J. Van den Hof [a], and Arne G. Dankers [b]

[a]Department of Electrical Engineering, Eindhoven University of Technology

[b]Department of Electrical and Computer Engineering, University of Calgary

Email: {k.r.ramaswamy, p.m.j.vandenhof}@tue.nl, adankers@hifieng.com

1 Introduction

For identifying a target module that is embedded in a dynamic network with known interconnection structure, different sets of conditions are available for the set of node signals to be measured and the set of excitation signals to be applied at particular node locations. In earlier works, sufficient conditions are provided, which depend on the identification method, either being an indirect method [2] where external signals are used as inputs or the direct method [1] where node signals are used as inputs. However, there are certain restrictions offered by these methods on selection of node signals (sensor selection) and excitation of particular nodes (actuation schemes). This demands a new identification method that provides flexibility in the sensor selection and actuation schemes [3].

2 Restrictions in existing methods
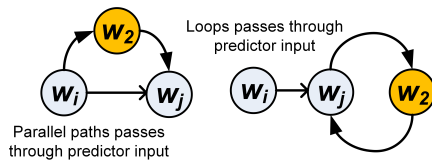
Figure 1: Figure depicting the parallel path and loop conditions in Direct method [1]. Nodes in yellow are measured and in grey are non-measured.

The direct method demands that all parallel paths from the input of the target module to its output and all loops through the output node should pass through a measured node signal that is included as a predictor input (see figure 1). This requirement ensures that the identified module using the direct method corresponds to the target module. However, in practical situations, there can be parallel paths and loops that might have all nodes non-measured (sensor placement problem). Indirect methods demand certain nodes to be excited in order to identify the target module. In certain situations it might not be possible to actuate these nodes (actuation problem).

3 Philosophy

We relax the parallel path and loop conditions by combining both direct and indirect approaches. This is done by including both node signals and external excitation signals as predictor inputs, using a MIMO identification approach and allowing post-processing of the module estimates.

4 Approach

Any violation of the parallel path/loop condition can be handled by exciting a node in the parallel path/loop respectively, including the excitation signal in the predictor input, and by measuring a descendant node from the excited node, different from the output of the target module, and by including this descendant node in the predicted output (see figure 2 for an illustration). As an alternative, violation of the loop condition can also be handled by exciting the output of the target module.
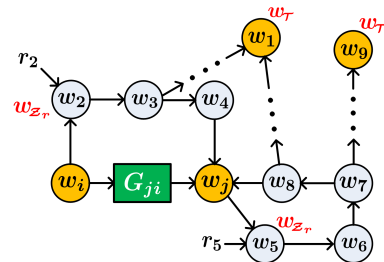
Figure 2: Violation of the parallel path condition is resolved by exciting w_2 with r_2 and including it as an input, and by measuring the descendant w_1 and including it as an output. Violation of the loop condition is handled by exciting w_5 with r_5 and including it as an input, and by measuring the descendant w_9 and including it as an output. Each excitation for these parallel path/loops should have at least one independent descendant measured.

References

[1] A. G. Dankers, P. M. J. Van den Hof, P. S. C. Heuberger, and X. Bombois. Identification of dynamic models in complex networks with prediction error methods: Predictor input selection. *IEEE Trans. on Automatic Control*, 61(4):937–952, 2016.

[2] M. Gevers, A.S. Bazanella, and G. Vian da Silva. A practical method for the consistent identification of a module in a dynamical network. *IFAC-PapersOnLine*, 51-15:862–867, 2018. Proc. 18th IFAC Symp. System Identif. (SYSID2018).

[3] K. R. Ramaswamy, P. M. J. Van den Hof, and A. G. Dankers. Generalized sensing and actuation schemes for local module identification in dynamic networks. In *Proc. 58th IEEE Conf. on Decision and Control (CDC)*, pages 5519–5524, 2019.

Allocation of Excitation Signals for Generic Identifiability of Dynamic Networks [1]

Xiaodong Cheng, Shengling Shi, and Paul M.J. Van den Hof
Department of Electrical Engineering
Eindhoven University of Technology
PO Box 513, 5600 MB Einhoven, The Netherlands
Email: {x.cheng, s.shi, P.M.J.vandenhof}@tue.nl

1 Introduction

We study dynamic networks in the form of

$$w(t) = G(q)w(t) + R(q)r(t), \qquad (1)$$

where q^{-1} is the delay operator, $w(t) \in \mathbb{R}^L$ and $r(t) \in \mathbb{R}^K$ are vectors of measured internal signals and external excitation signals, respectively. The topology of the underlying graph $\mathcal{G}$ is known. Let $\mathcal{R}$ be a subset of vertices that are excited by the external signals $r(t)$, and $K := |\mathcal{R}|$. We are then interested in question: where to allocate the excitation signals in the network such that it is *generically identifiable* [1, 2].

2 Disjoint Pseudotrees

A connected directed graph $\mathcal{T}$ is called a (directed) **pseudotree** if $|\mathcal{N}_i^-| \le 1$, for all $i \in V(\mathcal{T})$.

Consider two pseudo-trees $\mathcal{T}_1$ and $\mathcal{T}_2$ as subgraphs of a directed graph $\mathcal{G}$. $\mathcal{T}_1$ and $\mathcal{T}_2$ are called **disjoint** in $\mathcal{G}$ if the following two conditions hold: (1) $E(\mathcal{T}_1) \cap E(\mathcal{T}_2) = \emptyset$; (ii) For each $j \in V(\mathcal{T}_1) \cup V(\mathcal{T}_2)$, all the edges in $E(\mathcal{T}_1) \cup E(\mathcal{T}_2)$ that are incident from j are included in $E(\mathcal{T}_1)$ or $E(\mathcal{T}_2)$.

In Fig. 1, pseudo-trees in (a) and (b) are are not disjoint, since the outgoing edges from the gray vertices are assigned to different pseudo-trees, while the pseudo-trees in (c) and (d) are disjoint pairs.

3 Generic Identifiability

A condition for generic identifiability is provided in [3]:

Theorem 1 *The network $\mathcal{G}$ is generically identifiable if there exists K disjoint pseudotrees that covering all the edges of $\mathcal{G}$ (i.e., $E(\mathcal{T}_1) \cup \cdots \cup E(\mathcal{T}_K) = E(\mathcal{G})$), and at least one root of each pseudotree is excited.*

The method for allocation of excitation signals is: find the minimal number of pseudo-trees covering all the edges, and allocate an excitation signal to a root of each pseudo-tree.
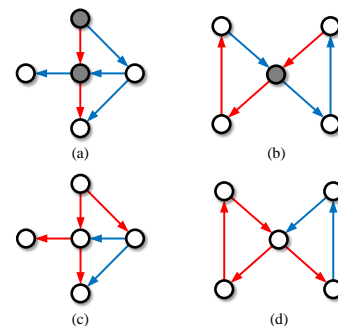
Figure 1: Illustration of disjoint pseudo-trees
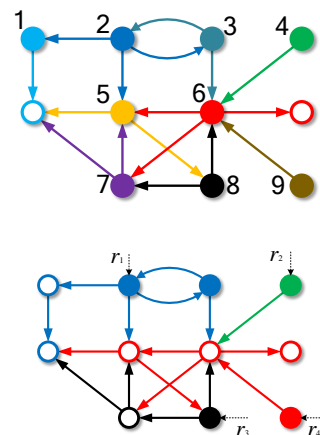
Figure 2: Allocation of excitation singles

References

[1] H. H. M. Weerts, P. M. J. Van den Hof, and A. G. Dankers, "Identifiability of linear dynamic networks," *Automatica*, vol. 89, pp. 247–258, 2018.

[2] J. M. Hendrickx, M. Gevers, and A. S. Bazanella, "Identifiability of dynamical networks with partial node measurements," *IEEE Transactions on Automatic Control*, vol. 64, no. 6, pp. 2240–2253, June 2019.

[3] X. Cheng, S. Shi, and P. M. Van den Hof, "Allocation of excitation signals for generic identifiability of linear dynamic networks," *arXiv preprint arXiv:1910.04525*, 2019.

Model Order Selection for Robust-Control-Relevant Identification

Paul Tacx, Robin de Rozario, Tom Oomen
Eindhoven University of Technology
Department of Mechanical Engineering
Control Systems Technology group
P.O. Box 513, 5600 MB Eindhoven, The Netherlands
Email: `p.j.m.m.tacx@student.tue.nl` & `t.a.e.oomen@tue.nl` & `r.d.rozario@tue.nl`

1 Background

Next-generation motion systems are envisioned to be lightweight due to increasing demands regarding throughput and precision. Typically, lightweight motion systems exhibit flexible dynamic behavior within the control bandwidth. In general, flexible dynamic behavior is not aligned with the degrees of freedom. As a result, next-generation motion systems are envisioned to be inherently multivariable. Hence, designing controllers through loop-shaping-based techniques becomes practically infeasible.

2 Problem

Model-based control effectively deals with multivariable systems. However, a model is an approximation of reality. Therefore, a model cannot encompass the complete behavior a true system. Robust control takes modeling errors explicitly into account by considering a model set that encompasses the true system. Regarding the model set, three requirements arise, the model set should (R1) encompass the true system, (R2) minimize the worst-case performance criterion and (R3) facilitate implementation: low-order models. The aim of this research is to develop an identification framework that enables R1, R2 and R3.

3 Approach

In [1], a robust-control-relevant model set is introduced by connecting the robust controller synthesis to the identification step thereby satisfying R1 and R2. However, for the proposed approach, it is unknown how to select the order of the model set. As a result, high-order models are typically selected which hampers successful implementation. The key step in this research is the development of an order selection procedure that enables R1, R2 and R3. The proposed procedure is based on a deterministic interpretation of order selection for the statistical framework [2].

4 Results

The developed approach was applied to a sixth-order mass-spring-damper system. The optimal model order is investigated for a range of bandwidth scenarios in Fig. 1. The robust-control-relevant model set with optimal model order for a bandwidth of 3.2 Hz is depicted in Fig. 2. The simulations show that in most cases a low-order model suffices for control purposes.
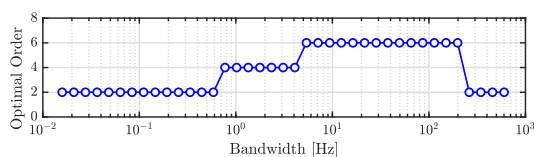
Figure 1: Optimal model order as function of the desired bandwidth.
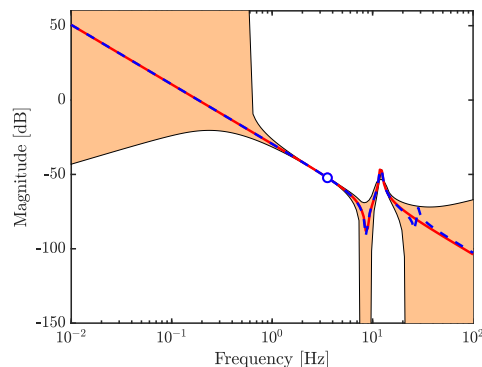
Figure 2: Bode magnitude diagram of the nominal model (——), the true system (- - -) and the robust-control-relevant model set (■). The desired bandwidth is indicated by (○).
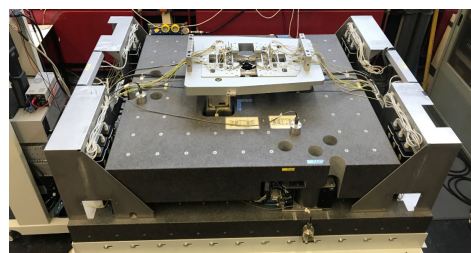
Figure 3: Reticle stage setup at the motion lab of the TU/e.

5 Outlook

Current research focuses on applying the proposed algorithm in overactuation and oversensing on the reticle stage of the TU/e, see Fig. 3.

References

[1]   Oomen, T., van Herpen, R., Quist, S., van de Wal, M., Bosgra, O. and Steinbuch, M., 2013. Connecting system identification and robust control for next-generation motion control of a wafer stage. IEEE Transactions on Control Systems Technology, 22(1), pp.102-118.

[2]   Stoica, P. and Selen, Y., 2004. Model-order selection: a review of information criterion rules. IEEE Signal Processing Magazine, 21(4), pp.36-37.

Time-Varying Ankle Joint Stiffness Identification during Cyclic Movement

Ronald C. van 't Veld[1], Alejandro Moya Esteban[1] and Alfred C. Schouten[1,2]

[1] Department of Biomechanical Engineering, University of Twente, Enschede, The Netherlands

[2] Department of Biomechanical Engineering, Delft University of Technology, Delft, The Netherlands

Email: {r.c.vantveld,a.moyaesteban,a.c.schouten}@utwente.nl

1 Introduction

Human limb mechanical properties can be quantified using joint impedance, the dynamic relation between joint angle deviations and corresponding joint torque, with joint stiffness as its position-dependent component. Joint stiffness is key in postural control and movement and well understood within (quasi-)static conditions [1]. However, muscle and joint mechanics change during movement, consequently also the joint stiffness changes [2]. Monitoring and understanding the continuous modulation of joint stiffness during movement in able-bodied subjects has several technical and clinical applications. For example, it can be applied to the design of next-generation biomimetic prostheses and exoskeletons or to advance clinical assessment and decision making. The goal of this study is to develop an experimental protocol to assess how humans modulate ankle joint stiffness during cyclic movement.

2 Methods

Six healthy adults (5 male, 24.2±1.0y) participated in this study. Participants were seated with their right foot connected to a single axis actuator using a footplate. The experiment consisted of three conditions: a 5Nm amplitude sinusoidal torque tracking task against a rigid actuator (static posture), and a 0.15rad amplitude slow (0.3Hz) and fast (0.6Hz) sinusoidal position tracking task against a virtual spring resulting in a torque amplitude of approximately 9Nm (dynamic posture). Additionally, pseudo-random binary sequence (PRBS) perturbations were applied during the tasks (±0.015 rad, 0.15s switching time). System identification was performed using an ensemble-based, linear time-varying (LTV) algorithm, which produced ankle joint stiffness estimates by means of multiple short segments of the torque and angle recordings [2].

3 Results and Discussion

The results across subjects and conditions show two maximum stiffness peaks followed by periods of decreased stiffness, see Fig. 1. The two stiffness peaks correspond to the two phases with increased ankle deflection and increased voluntary torque exerted by the human. The average estimated joint stiffness magnitude across conditions ordered
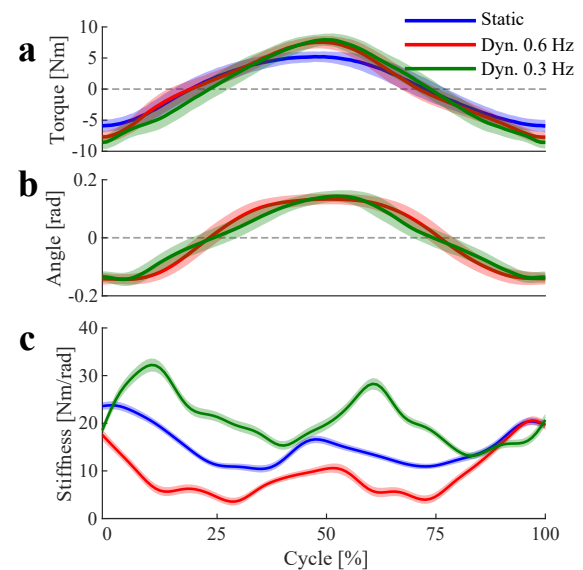
Figure 1: Ensemble mean ±1 sd of *(a)* measured ankle torque and *(b)* measured ankle angle around the neutral angle. *(c)* Mean ±1 sd of estimated ankle joint stiffness over 35 repetitions of MS algorithm. Data from representative subject, adapted from [3].

from low to high was: fast dynamic, static and slow dynamic posture. Our results highlight the variability in stiffness modulation strategies across conditions, especially across movement frequency.

References

[1] R. E. Kearney and I. W. Hunter, "System Identification of Human Joint Dynamics," *Critical Reviews in Biomedical Engineering*, vol. 18, no. I, pp. 55–87, 1990.

[2] D. Ludvig, M. Plocharski, P. Plocharski, and E. J. Perreault, "Mechanisms Contributing to Reduced Knee Stiffness during Movement," *Experimental Brain Research*, vol. 235, no. 10, pp. 2959–2970, 2017.

[3] A. Moya Esteban, R. C. van 't Veld, C. P. Cop, G. Durandau, M. Sartori, and A. C. Schouten, "Estimation of Time-Varying Ankle Joint Stiffness Under Dynamic Conditions via System Identification Techniques," *41st Annual International Conference of the IEEE EMBC*, pp. 2119–2122, 2019.

A Column Space Based Approach to Solve Multiparameter Eigenvalue Problems

Christof Vermeersch and Bart De Moor, *Fellow, IEEE & SIAM*
Center for Dynamical Systems, Signal Processing, and Data Analytics (STADIUS),
Dept. of Electrical Engineering (ESAT), KU Leuven
`{christof.vermeersch,bart.demoor}@esat.kuleuven.be`

1 Introduction

Multiparameter eigenvalue problems (MEPs) emerge both in nature and science [1]. More particularly, they often arise in systems and control, e.g., the least-squares realization of linear time-invariant models [2] and the globally optimal identification of autoregressive moving-average models [3]. A multidimensional realization problem in the null space of the block Macaulay matrix that contains the MEP results in a standard eigenvalue problem, of which the eigenvalues and -vectors yield the solutions of the MEP. Since this null space based algorithm uses established numerical linear algebra tools, like the singular value and eigenvalue decomposition, it finds the solutions within machine precision. In this research, we propose a new, complementary approach to solve MEPs, which considers the column space of the block Macaulay matrix instead of its null space.

2 Research methodology

An MEP extends the typical structure of the well-known standard eigenvalue problem [1]:

$$\left(\sum_{\omega} A_{\omega} \omega \right) z = 0, \tag{1}$$

where $\omega(\lambda_1, \ldots, \lambda_n) = \lambda_1^{k_1} \cdots \lambda_n^{k_n}$ is a monomial function of the n eigenvalues $\lambda_1, \ldots, \lambda_n \in \mathbb{C}$ and the vector $z \in \mathbb{C}^q$ is the eigenvector. The matrices $A_{\omega} \in \mathbb{R}^{p \times q}$ contain the corresponding coefficients. Contrary to standard eigenvalue problems, the available literature about solving MEPs remains quite limited. Typically, numerical optimization methods are used to find (approximations of) the eigenvalues and -vectors. Algebraic approaches, on the other hand, confine themselves mostly to linear or quadratic two-parameter eigenvalue problems. Vermeersch and De Moor [3] have shown that a multidimensional realization problem in the null space of the block Macaulay matrix that contains this MEP results in a standard eigenvalue problem, which yields the solutions of the MEP. Instead of the null space, we consider the column space of the block Macaulay matrix and work on the data directly. The complementarity between both spaces yields an alternative approach to solve MEPs, without the need to construct a numerical basis of the null space.

3 Presentation outline

In our presentation, we will explain how we can find the solutions of an MEP via a multidimensional realization problem in the column space of the block Macaulay matrix. Furthermore, the presentation will elaborate on this block Macaulay matrix and the complementarity between its null space and column space.

References

[1] Frederick V. Atkinson. *Multiparameter Eigenvalue Problems*, volume 82 of *Mathematics in Science and Engineering*. Academic Press, New York, NY, USA, 1972.

[2] Bart De Moor. Least squares realization of LTI models is an eigenvalue problem. In *Proc. of the 18th European Control Conference (ECC)*, pages 2270–2275, Naples, Italy, 2019.

[3] Christof Vermeersch and Bart De Moor. Globally optimal least-squares ARMA model identification is an eigenvalue problem. *IEEE Control Systems Letters*, 3(4):1062–1067, 2019.

Unsupervised Wind Turbine Anomaly Detection
A Weighted Cepstral Distance Application

Oliver Lauwers   Bart De Moor

KU Leuven, Department of Electrical Engineering (ESAT), Stadius Center for Dynamical Systems,
Signal Processing and Data Analytics.
oliver.lauwers@kuleuven.be; bart.demoor@kuleuven.be

1 Introduction

The (power) cepstrum of a signal is a technique stemming from the field of *homomorphic signal processing* [5]. In this presentation, we use the weighted cepstral distance [1, 2, 4] to do unsupervised anomaly detection in wind turbines.

2 SISO cepstrum

The *power cepstrum coefficients* of a univariate signal $y(k)$, with k denoting time, are defined as [5]

$$c_y(k) = \mathscr{F}^{-1}(\log \Phi_y(e^{i\omega})), \tag{1}$$

with $\Phi_y(e^{i\omega}) = |Y(e^{i\omega})|^2$ the *power spectrum* of the signal (and $Y(e^{i\omega})$ the *Fourier transform* of the signal), and $\mathscr{F}^{-1}$ denoting the *inverse Fourier transform* operator.

A signal from a stochastic system, given in z-domain as

$$Y(z) = \frac{b(z)}{a(z)} U(z), \tag{2}$$

with $U(z)$ describing white noise, $a(z)$ the pole polynomial with the poles α_i as roots and $b(z)$ the pole polynomial with the poles β_i as roots, has cepstrum coefficients

$$c_y(k) = \sum_{j=1}^{p} \frac{\alpha_j^{|k|}}{|k|} - \sum_{j=1}^{q} \frac{\beta_j^{|k|}}{|k|}, \quad \forall k \neq 0. \tag{3}$$

The cepstrum is a characteristic of the dynamics of the generative system of the time series. A distance measure can be defined [1, 2, 4] on the cepstral coefficients as

$$d_c((y_1, u_1), (y_2, u_2)) = \sum_{k=0}^{\infty} k((c_{y_1} - c_{u_1}) - (c_{y_2} - c_{u_2}))^2, \tag{4}$$

with (y_1, u_1) and (y_2, u_2) the output/input-signal pairs of the respective systems. This distance measure can be interpreted in terms of model parameters and subspace angles between the output spaces of the systems.

An extension of the power cepstrum to multiple input multiple output (MIMO) systems was presented in [3]. However, an extension of the distance measure above to this case proves to be difficult, theoretically. We will focus on the details of why this is so in the presentation, and corroborate our results with an application on wind turbine anomaly detection.

3 Wind Turbine Anomaly Detection

Wind turbines have several built-in sensors, which are governed by a supervisory control and data acquisition (SCADA) system. In this presentation, we use open-source SCADA data from EDF [6], and focus on the topic of anomaly detection. We present an unsupervised anomaly detection method.

References

[1] *Subspace angles between ARMA models*, De Cock, Katrien and De Moor, Bart, Systems & Control Letters, 46 (4), pp.265–270, 2002

[2] *A Time Series Distance Measure for Efficient Clustering of Input/Output Signals by Their Underlying Dynamics*, Lauwers, Oliver and De Moor, Bart, IEEE Control Systems Letters, 14 June 2017

[3] *A Multiple-Input Multiple-Output Cepstrum*, Lauwers, Oliver and Agudelo, Oscar Mauricio and De Moor, Bart, IEEE Control Systems Letters, 2 (2), pp. 272 – 277, 2018

[4] Martin, Richard J,*A metric for ARMA processes*, IEEE Transactions on Signal Processing, 48 (4), pp. 1164–1170, 2000

[5] Oppenheim, A., Schafer, R., *Digital Signal Processing* (1st Edition), 1975, Pearson, New jersey

[6] *Hack the Wind 2018*, https://opendata.edp.com/pages/hackthewind/description

Commutation-Angle Iterative Learning Control for Walking Piezo-Stepper Actuators

Leontine Aarnoudse [1,*], Nard Strijbosch [1], Edwin Verschueren [2], Tom Oomen [1]

[1]Control Systems Technology, Eindhoven University of Technology, P.O. Box 513, 5600MB Eindhoven, The Netherlands

[2]Thermo Fisher Scientific, Achtseweg Noord 5, 5651GG Eindhoven, The Netherlands. *Email: l.i.m.aarnoudse@tue.nl

1 Background

Iterative learning control (ILC) can compensate repeating disturbances in control applications by modifying a feedforward input signal based on preceding experiments [1]. During the walking motion of a piezo-stepper actuator, engagement and release between the piezo elements and the mover lead to position disturbances that are repeating in the domain in which the actuating waveforms are repeating, known as the commutation-angle or α-domain [2]. For varying velocities, the temporal domain error profile caused by these disturbances is varying. Since typical ILC approaches amplify trial-varying disturbances [3], temporal domain ILC is not suited for a piezo-stepper actuator and an α-domain approach is needed instead.

2 Problem Formulation

The position disturbances for a piezo-stepper actuator are repeating in the α-domain for varying drive frequencies, but the number of samples within a step and the distance between the samples is varying, as shown in Figure 1. The aim of this research is to develop an ILC framework that is applicable to systems such as a piezo-stepper actuator that involve both position domain disturbances and intermittent sampling.

3 Approach

Since the sampling is iteration-varying, ILC cannot be applied directly to the sampled input and error signals. Therefore, the input and error signals are parameterized using radial basis functions [4], ch.14. An optimal ILC update law for continuous signals in the α-domain is developed to determine the input parameters for each iteration. Conditions for monotonic convergence of the sequence of parameter vectors are determined.

4 Experimental Results and Conclusions

The feasibility of the developed ILC framework is validated experimentally using a piezo-stepper actuator walking at varying drive frequencies. The α-domain repeating disturbance is compensated, leading to significant improvements in the positioning accuracy and jogging smoothness of the actuator.
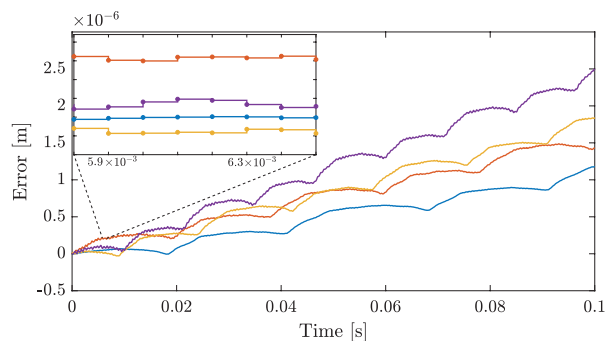
(a) Disturbance as a function of time.
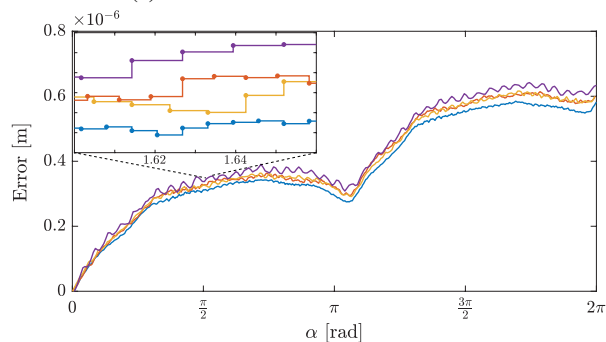
(b) Disturbance as a function of the commutation angle α.

Figure 1: Disturbances for a piezo-stepper for drive frequencies 20 Hz (—), 25 Hz (—), 30 Hz (—) and 40 Hz (—). In the temporal domain (a) the sampling is equidistant but the disturbance is drive-frequency dependent. In the α-domain (b) the sampling is non-equidistant for varying drive frequencies, but the disturbances are similar.

References

[1] D.A. Bristow, M. Tharayil, and A.G. Alleyne, "A survey of iterative learning control," *IEEE Control Syst.,* 26(3), 96-114, 2006.

[2] N. Strijbosch, P. Tacx, E. Verschueren, and T. Oomen, "Commutation angle iterative learning control: enhancing piezo-stepper actuator waveforms," In *IFAC Symp. Mechatron. Syst.,* Vienna, Austria, 2019.

[3] T. Oomen and C.R. Rojas, "Sparse iterative learning control with application to a wafer stage: achievable performance, resource efficiency, and task flexibility," *Mechatronics*, 47, 134-147, 2017.

[4] K.P. Murphy, *Machine Learning: A Probablistic Perspective*. Cambridge: The MIT Press, 2012.

Model-based similarity assessment for nonlinear systems

Armin Steinhauser and Jan Swevers
MECO Research Team, Dept. Mechanical Engineering, KU Leuven
and
DMMS lab, Flanders Make
Email: `first.lastname@kuleuven.be`

1 Introduction

With the development and implementation of concepts like *Industry 4.0*, an overwhelming amount of data is centrally available that allows for a comprehensive data analysis. This paper focuses on the valuation of system similarity, which is of utmost importance when considering applications where a (potentially high) number of systems is supposed to collaborate, or a new system is supposed to be initialized based on data from similar systems that are already deployed. Similarity can be defined in numerous ways [1]—however, assuming that a model is given and seeking for a generic approach, we focus on deriving a model-based similarity measure for arbitrary systems.

2 Outline of the approach

Let $\mathcal{S} = \{\sigma_i : i = 1, \ldots, I\}$ be a finite set of systems with consistent number of inputs and outputs, and assume a compliant model given in discrete time

$$\mathcal{M} := \begin{cases} x_{k+1} = f(x_k, u_k), \\ y_k = h(x_k, u_k), \end{cases} \tag{1}$$

where a subscript $k \in \{0, \ldots, N-1\}$ denotes time instances, $u_k \in \mathbb{R}^{n_u}$ are inputs, $y_k \in \mathbb{R}^{n_y}$ are outputs and $x_k \in \mathbb{R}^{n_x}$ are states. The arbitrary, possibly nonlinear maps f and h are the system dynamics and output equations, respectively. Presuming that measurements are generated by one and the same input signal for all systems, their state trajectories $\mathcal{X} = \{\chi_i = (x_0, \ldots, x_{N-1})_i^T : i = 1, \ldots, I\}$ are estimated, exploiting the fact that all necessary data is readily available. Let $\chi_r \in \mathcal{X}$ be the estimated state trajectory of a reference system $\sigma_r \in \mathcal{S}$, then the proposed similarity measure $\rho : \mathcal{X} \to [0, 1]$, based on an $L_{2,1}$-norm of the difference of the state trajectories, reads

$$\rho(\chi_i) = 1 - \frac{1}{\rho_{\max}} \|\chi_r - \chi_i\|_{2,1} \tag{2}$$

with $\rho_{\max} = \max(\{\|\chi_r - \chi\|_{2,1} : \chi \in \mathcal{X}\})$. The measure is thus normalized w.r.t. σ_r, satisfying

$$\rho(\chi_r) = 1 \quad \text{and} \quad 0 \leq \rho(\chi_i) \leq 1 \ \forall i. \tag{3}$$

Note that the model, the employed estimator and also the chosen input signal will affect the result of the similarity assessment.

3 Simulation study

We consider the nonlinear dynamics of a Van der Pol oscillator with varying gains of the input and the nonlinearity. Recording the responses to an exemplary input signal yields the similarity map depicted in Fig. 1. Based on this similar-
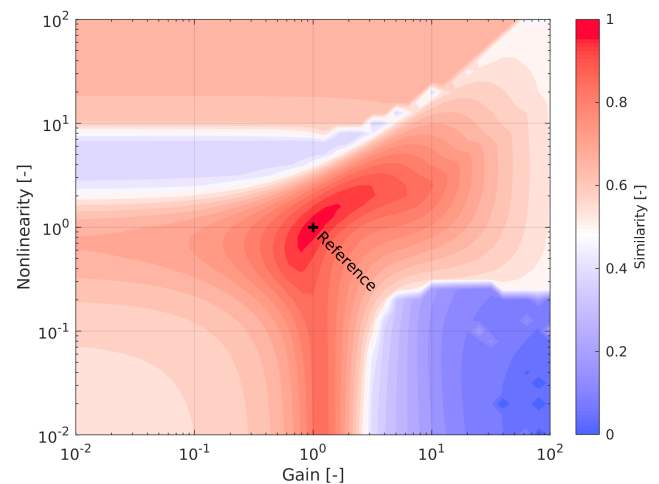
Figure 1: Similarity map for Van der Pol oscillator; the reference system features unit gains.

ity assessment, we show an exemplary use case in the field of learning control, where the similarity measure is used to decide if previously obtained results should be utilized to initialize the learning process of newly added systems. We further investigate the impact of different models and input signals, and compare the obtained similarity results with alternative approaches to illustrate the properties of the proposed approach.

References

[1] Pham, D.T. and Afify, A.A., "Clustering techniques and their applications in engineering," *Proc. IMechE Part C: Journal of Mechanical Engineering Science*, 221(11):1445–1459, 2007.

Similarity assessment for efficient initialization of new controllers

Rian Beck, Jeroen Willems, Edward Kikken, Sorin Bengea & Bruno Depraetere
DecisionS core lab, Flanders Make, mail: firstname.lastname@flandersmake.be

1 Motivation

Learning control can find good control values for a machine being commissioned. Unfortunately learning typically has to start from scratch. A model could be used to initialize, but for many learning applications these are not very good, as the learning is done precisely to compensate for this model-plant mismatch. As a result, often **learning starts from a bad initial guess**, leading to (i) a **long convergence process** with a high commissioning cost, and (ii) during the convergence possibly **poor results and dangerous operation**.

When the machine to be commissioned is similar to existing machines in the fleet, an option is to **'hot-start'** the learning. A possible approach to hot-start is to **find the most similar machine** in the existing fleet and to use the control values for this machine as an initial guess when starting the learning. Other methods based on for example transformations can be considered, but even those will benefit from using data from the most similar machines. In this work we therefore focus on similarity assessment only, with the intent of afterwards using the result for hot-starting.

Although we consider similarity between machines the methodology can also be applied to a single machine executing different tasks at different speeds and conditions.

2 Methods and challenges for similarity assessment

If all machines have been excited with the same inputs, we can directly **compare output signals**. A suitable metric for comparison still has to be chosen though, as machines which are similar up to a static offset could be seen as very different with a 2-norm even though they could be a good starting point for learning. Similarly, if all machines have performed the same task (and achieved the same output) we can **compare input signals**, but the same challenges remain.

Another option is to **compare model parameters** for physical models estimated for the different machines. This seemingly easy method can deal with machines excited with different data, but if there is more than 1 model parameter we have a multi-dimensional comparison, and we need to deduce a single comparable value. More importantly, since we are using learning control the models can also be so poor that hot-starting based on them can even make things worse.

When there is no similarity in the data nor good models, a different approach has to be taken. One possible option is to use the model-based approach but with **data-driven models** such as neural networks trained on the available data. The parameters for the networks can then be compared directly,
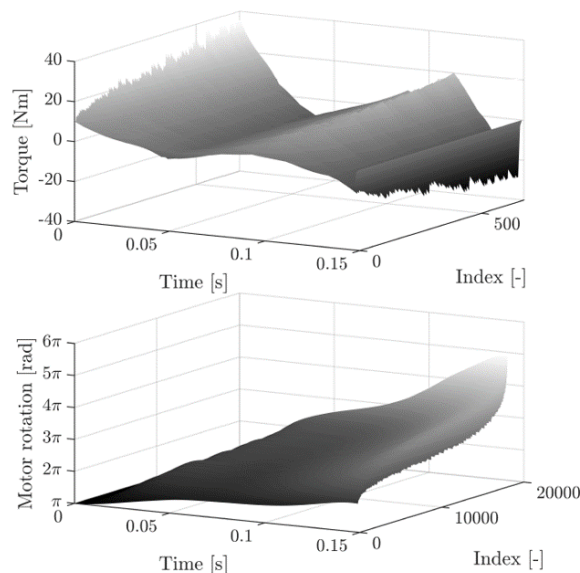
Figure 1: Illustration of simulated in- and output signals for many similar but non-identical machines.

or more preferably used to calculate input or outputs to allow comparing signals like in the first approach. In order to successfully model the input-output behavior of the machine an appropriate neural network structure has to be chosen. LSTM (Long Short-Term Memory) or NARX (Nonlinear Autoregressive Network with Exogeneous Inputs) network structures can be chosen, as these are well able to the capture the machine dynamics.

3 Discussion

In this talk we will evaluate and compare several methods for similarity assessment, and illustrate them on a **slider crank simulation example** using the generated dataset shown in Fig. 1. Given the intent of initializing learning control we will consider machines more similar if using the optimal control for machine A as an initial guess for machine B leads to a better result, and/or a lower number of iterations needed afterwards to converge to the optimal input for machine B. We will show that the data-driven methods can always be used, and are thus suitable for generic industrial usage, but that often better results can be achieved with the other specific methods if suitable data is available.

On the Role of Models in Learning Control:
Actor-Critic Iterative Learning Control

Maurice Poot [1,*], Jim Portegies [2], Tom Oomen [1]

[1]Control Systems Technology Group, Dept. of Mechanical Engineering, Eindhoven University of Technology, The Netherlands

[2]CASA, Dept. of Mathematics and Computer Science, Eindhoven University of Technology, The Netherlands. *Email: `m.m.poot@tue.nl`

1　Background

Learning has large benefits for control applications, including high-tech mechatronic systems, by greatly improving the accuracy using data from past tasks. Norm-Optimal Iterative Learning Control (NOILC) exploits model knowledge for fast and safe learning [1]. Obtaining a model of a system leads to undesired user-intervention. In reinforcement learning (RL), many model-free learning techniques are developed that show promising convergence properties [2, 3].

2　Problem formulation

Although ILC methods often have fast and safe convergence properties and exceptional performance, these methods require an explicit system model. The aim of this research is to investigate model-based and model-free learning for mechatronic systems from the perspective of prior model-knowledge and sample complexity and to develop a model-free approach to learn the optimal feedforward signal from experiment data.

3　Approach

A model-free approach to learn the optimal feedforward signal is developed and is called actor-critic iterative learning control (ACILC). ACILC exploits the use of feedforward parameterization with basis functions such that implicit model knowledge can be incorporated and uses the actor-critic algorithm of RL [2, 3] to learn the feedforward parameters without explicitly using a system model.

4　Results

Initial results for positioning of a consumer printer demonstrate the model-free performance of ACILC in comparison to NOILC [1] with basis functions that uses an explicit system model. In Figure 1, the cost per trial is shown, demonstrating that ACILC achieves the same optimal cost as NOILC in 20 trials for the same basis functions. The cost of ACILC varies significantly in the first trials due to exploration necessary for learning, while the cost of the NOILC method converges in one step due to the use of a model.
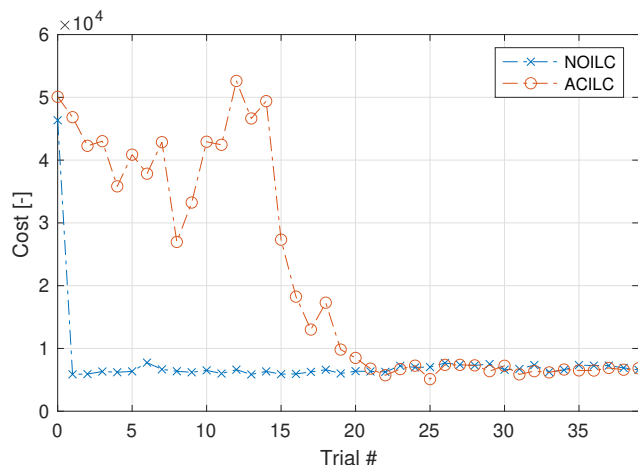
Figure 1: Cost per trial for model-based NOILC with basis functions and model-free ACILC experiments.

5　Conclusion and outlook

The developed ACILC framework is a model-free framework capable of learning the optimal feedforward signal with little implicit model knowledge incorporated in the basis functions. Future research focuses on tuning of the actor-critic parameters and extending the basis functions to further improve the convergence performance.

6　Acknowledgements

References

[1]　Oomen, T. (2018). Learning in machines: towards intelligent mechatronic systems through iterative control. *Mikroniek*, 6, 5-11.

[2]　Grondman, I., Buşoniu, L., Lopes, G., and Babuška, R. (2012). A survey of actor-critic reinforcement learning: standard and natural policy gradients. *IEEE Trans. on Systems, Man, and Cybernetics, Part C (Appl. and Rev.)*, 42(6), 1291-1307.

[3]　Recht, B. (2019). A tour of reinforcement learning: the view from continuous control. *Annual Review of Control, Robotics, and Autonomous Systems*, 2, 253-279.

From Reward Function to Cost Function: Modified Stage Costs in MPC Inspired by Reinforcement Learning

Dingshan Sun
Delft Center for Systems and Control
Delft University of Technology
d.sun-1@tudelft.nl

Anahita Jamshidnejad
Department of Control and Operations
Faculty of Aerospace Engineering, TU Delft
a.jamshidnejad@tudelft.nl

Bart De Schutter
Delft Center for Systems and Control
Delft University of Technology
b.deschutter@tudelft.nl

1 Introduction

Reinforcement learning (RL) is a machine learning technology that iteratively learns an optimal policy for agents that is a mapping from states to actions, while they interact with the environment. The reward function is an essential component in RL, representing the reward an agent receives when it takes a certain action at a given state. The design of the reward function can significantly influence the process and results of the policy learning process. A misspecified reward function may give rise to various problems, such as getting stuck in local optima, slow learning processes, and reward hacking, which means the agent tries to maximize a reward function that does not lead to the designer's goals. We intend to borrow the reward function design methods from RL, and apply them in designing the objective function for MPC. More specifically, we will transform the design objective of MPC into stage costs, similar to the way the final goal is transformed into rewards in RL, expecting a better performance with faster convergence in practical usage.

In this presentation, we introduce the typical reward function design methods of RL, and propose potential solutions to achieve our aim.

2 Reward function design in RL

RL has been applied in a multitude of scenarios, from industrial applications, like robot control, residential applications, like electric water heater control, to infrastructural applications, like traffic signal control and smart grid control. Depending on the applications and tasks that are considered, the formulation of the reward function varies greatly. Generally, according to the distribution of the rewards along the states, reward functions can be classified as sparse and dense, where sparse rewards means only a few states and actions are given a reward among large state space while dense rewards generally means all the states has a reward. Although dense reward functions provide more information about the learning process, they are much more difficult to construct than sparse functions. It is thus necessary to supply domain knowledge of specific tasks to accelerate the learning process and to provide more accurate information to steer the agent towards the designer's intentions [1].

Typically, domain knowledge is utilized implicitly via multiple sub-goals and a progress estimator [2]. During the implementation of RL in practice, the tasks and environments are usually complicated and many practical issues should be considered. For example, consider a formation of robots that are required to finish a task including starting from a home position, moving towards the task zone, grasping objects, returning, and dropping them at the home position, while avoiding collision with each other. To finish such a complex task, sub-goals or stage goals are needed to guide the robots to finish their tasks in a desired order. The robots get positive rewards for desired actions like grasping objects in the task zone or dropping objects at the home position, and negative rewards for undesired actions, like grasping objects at the home position. Furthermore, progress estimators are needed to give feedback to the agents while they are working towards achieving the task when the state space is large and completing the task takes a long time. To illustrate this, a progress estimator can be used to provide distance information for the agent during homing progress. Based on the distance from the agent to the home position, a progress estimator gives positive rewards to the current state-action pair, thus stimulating the homing process. Similarly, the agent will get negative rewards if it is moving towards an obstacle, to avoid the collision.

3 Intended approach

Just as in RL, the cost functions, including the terminal cost, in MPC can also be regarded as representing a final objective. To some extent, the objective function in MPC and reward function in RL are similar to each other, and we want to borrow the experience of reward function design in RL and apply it in the design of the additional stage cost for MPC. For instance, we can take advantage of the methods that are introduced in Section 2 to transform the design goal into a stage costs formulation.

References

[1] A. D. Laud, "Theory and Application of Reward Shaping in Reinforcement Learning", PhD thesis, University of Illinois at Urbana-Champaign, the USA, 2004.

[2] M. J. Mataric, "Reward functions for accelerated learning." *Machine Learning Proceedings 1994*. Morgan Kaufmann, 1994. 181-189.

Comparison of deep learning methods for system identification

Gerben Beintema, Roland Tóth, Maarten Schouken
Control Systems Group, Electrical Engineering, Eindhoven University of Technology
Email: g.i.beintema@tue.nl

1 Introduction

There has been a recent interest in using deep learning techniques for data-driven modeling of dynamical systems in engineering and control due to the apparent function approximation capabilities of deep neural network models and due to the powerful computational methods developed within the deep learning framework. The introduction of these methods to data-driven modeling of engineering systems has been relatively ad hoc [1] and thus a more structured in-depth comparison study including the well-established methods [2] need to be performed. To this end, a unified framework should be established, including the newly developed deep learning approaches, to understand the practical and theoretical implications of choosing a particular model structure and an associated learning approach in the context of data-driven modelling.

2 Problem Statement

Developing such a unified framework can be split up in a theoretical and a practical part.

The theoretical part entails the analysis of these newly introduced methods using the already well-established frameworks known in system identification. This analysis should, for instance, consider the structure of these new models, discussing the noise model, model class generality, and dynamics representation. Furthermore, an analysis of the impact of the widely used regularization, normalization, and training techniques in machine learning would also be necessary.

The practical part of the framework would entail a direct comparison of the most impactful classical methods and the most newly introduced methods evaluated on many kinds of practical (non-linear) system identification problems to determine the problem-dependent performance. Furthermore, the comparison would need to consider a large set of performance measures derived from: one-step-ahead prediction, simulation evaluation, extrapolation performance, computational cost, and problem-specific hyperparameter sensitivity i.e. ease of use.

3 Approach

Our first step in realizing this unified framework is providing a platform for the practical part as represented in Figure 1. We are developing an open-source python-based programming environment (i.e. module) which allows for the
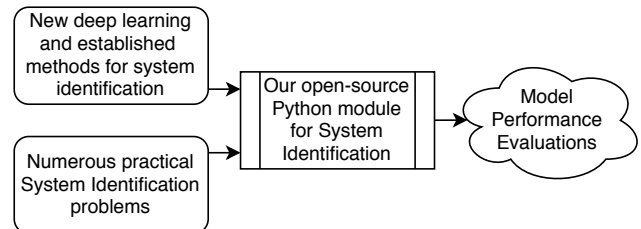
Figure 1: Our first step in creating a unified framework is the realization of a platform for evaluating system identification methods.

implementation of system identification methods with relative ease. Currently, we have implemented many well-established methods such as ARX, OE, linear state-space models, and feed-forward neural networks [2] and newly introduced methods such as LSTM, TCN (Temporal CNN), NL-LFR and auto-encoder based state-space methods [3]. Furthermore, our python module has incorporated a diverse set of system identification problems derived from real data sets (currently over 10) [4] and popular toy systems (currently over 20).

4 Conclusion

The development of a practical comparison framework is not only the first step towards a unified framework, for the analysis and comparison of (non-linear) system identification methods, but can also be seen as a tool for future system identification research as it provides an easy tool for comparing with known methods on numerous system identification problems.

References

[1] Y. Wang, "A new concept using LSTM neural networks for dynamic system identification," in *2017 American Control Conference (ACC)*, pp. 5324–5329, Seattle, 2017.

[2] J. Sjöberg *et al.*, "Nonlinear black-box modeling in system identification: a unified overview," *Automatica*, vol. 31, no. 12, pp. 1691–1724, 1995.

[3] I. Goodfellow, Y. Bengio, and A. Courville, *Deep Learning*. MIT Press, 2016.

[4] M. Schoukens, "Nonlinear System Identification Benchmarks." http://www.nonlinearbenchmark.org/. Date Accessed: 2020-01-09.

Analysis and control of interconnected systems: definition of agents

Ayoub Ben Ayed and Denis Dochain
ICTEAM, INMA
Université catholique de Louvain
B-1348 Louvain-la-Neuve, Belgium
ayoub.benayed, denis.dochain@uclouvain.be

Ionela Prodan
Univ. Grenoble Alpes, Grenoble INP*, LCIS
F-26000 Valence, France
ionela.prodan@lcis.grenoble-inp.fr
*Institute of Engineering Univ. Grenoble Alpes

Carlos Eduardo Robles Rodriguez
Dept. Electrical Engineering
Eindhoven University of Technology
Eindhoven, The Netherlands
c.e.robles.rodriguez@tue.nl

Interconnected systems are a class of systems which governs many aspects of our lives. Among technical examples, we find irrigation [1] and wastewater treatment networks [2], transportation infrastructures, power and multi-robot systems, and even biological, economical systems or social networks [3].

The use of classical centralised control for large dimension systems presents several drawbacks, including the inability to handle huge number of input, state and output variables. Moreover, the design of optimal control laws for those systems with strong connectivity results in huge computational burden [3]. For the past 20 years, decentralised control has been designed to benefit from inherent properties of subsystems. However this approach is less robust and suboptimal in comparison with the centralised approach [4]. At halfway between the two approaches, distributed control, has raised much interest recently. In this framework, the subsystems are able to exchange information while keeping individual control [4].

Distributed control exhibits improved performance and greater flexibility but still remain less perfomant than the centralised approach [1]. One important issue of working with interconnected system regards the definition of subsystems which is mostly based on its physical structure or, more and more, on heuristic criteria inspired from multi-agent programming [5].

In this context, we present a first approach for agent decomposition based on rigorous mathematical reasoning and criteria. This definition allows also to determine the minimum information required for each agents and communication structure.

The case study concerns the management of a wastewater treatment network in collaboration with the SIAAP[1].

This syndicate is in charge of collecting and treating the wastewater of the city of Paris and its suburbs. It covers the Seine river and two of its tributaries, the Marne and Oise rivers, for an area of 79000 km^2 (i.e. approximately 13% of the French territory and about 30% of the French population). The SIAAP is managing 6 major wastewater treatment plants (Seine-Aval being by far the largest one) and 440 km of collecting pipes.

The main objective is here to meet the requirements of the European framework directive on water which request that the management should be realised on the whole river bassin to address good chemical and ecological state of its water [2].

Further work will focus on how local objectives and protocol communication should be defined to achieve global objective. The link between local and global properties of multi-agent systems , as robustness and stability, will also be studied.

References

[1] Thang Pham V., Raïevsky C., Jamont J.P., A Multiagent Approach Using Model-Based Predictive Control for an Irrigation Canal, Advances in Intelligent Systems and Computing, vol 293. Springer, 2014
[2] A. Ben Ayed, Real-time optimisation of a wastewater treatment network, Master dissertation, UCL, 2018
[3] F. Deroo, Control of interconnected systems with distributed model knowledge, PhD dissertation, TUM, 2016
[4] M. Mansouri, Observation et commande des systèmes de grande dimension, PhD dissertation, UL - ENIM, 2012
[5] J.-P. Jamont, Démarche, modèles et outils multi-agents pour l'ingénierie des collectifs cyberphysiques, Informatique, PhD dissertation, Université Grenoble Alpes, 2016

[1]Syndicat Interdépartemental pour l'Assainissement de l'Agglomération Parisienne

On Path-Complete Lyapunov Functions : comparison between a graph and its expansion

Virginie DEBAUCHE
Université catholique de Louvain, Belgium
virginie.debauche@uclouvain.be

Raphaël JUNGERS
Université catholique de Louvain, Belgium
raphael.jungers@uclouvain.be

Abstract

We study the stability of switching dynamical systems with the following dynamics:

$$x(t+1) = f_{\sigma(t)} x(t),$$

where $\sigma(t) \in \{1, \ldots, M\} := \langle M \rangle$ is the mode of the system, with an integer $M > 0$. We use the *multiple path-complete Lyapunov function* approach introduced in [1] that provides sufficient conditions for the asymptotic stability of switching systems. This method is characterized by both algebraic and combinatorial components, namely a set $\mathscr{V}$ of candidate Lyapunov functions called a *template*, and a labeled directed graph $G = (S, E)$ with $E \subseteq S \times S \times \langle M \rangle$ that captures all the possible switching sequences, respectively. Figure 1a provides an example of a graph which captures all the switching sequences with two modes. According to the definition [2, Definition 2.4], a *Path-Complete Lyapunov function* is a pair $(G = (S, E), \{V_s \mid s \in S\})$ where the candidate Lyapunov functions $\{V_s \mid s \in S\}$ satisfy the following Lyapunov inequalities:

$$\forall (s, d, \sigma) \in E, \forall x \in \mathbb{R}^n : V_d(f_\sigma(x)) \leq V_s(x).$$

It turns out that different methods (i.e., different graphs) may result in more or less conservative conditions [2, 3] and it is still an open question to compare this conservativeness, for two given different graphs. Under the assumption that the template is closed under linear combination, a Linear Programming-based method has been developed in [3] to order two different graphs. This method only provides a sufficient condition to compare two graphs. The example [2, Example 3.9] also suggests checking compositional relations where the new candidate Lyapunov functions are defined as
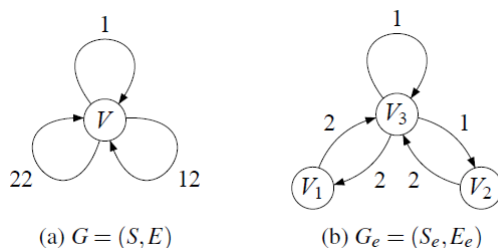
the composition between the old ones and the dynamics. All these order relations are defined for graphs whose edges admit label of length one. However, it has been known since [1, Definition 2.1] that any labeled directed graph $G(S, E)$ can be reduced to a graph with labels of length one thanks to its *expanded graph* denoted by $G_e(S_e, E_e)$. This graph is the outcome of a procedure whose purpose is to split each edge with a label of length larger than one in k new edges linking $k - 1$ new nodes. An example of an expanded graph is provided in Figure 1. We generalize the technique [2, Example 3.9] by showing that any graph is equivalent to its expansion for any template closed under composition.

Theorem 1 *Let $G(S, E)$ be a labeled directed graph, and $G_e(S_e, N_e)$ its expansion. Then, $G_e \leq G$ and $G \leq G_e$ for any template closed under composition.*

For the first inequality, one only has to keep the candidate Lyapunov function for each common node $s \in S \cap S_e$. For the second inequality, one just needs to define

$$V_{s_q} = V_j \circ f_{i_1} \circ \cdots \circ f_{i_{q-1}}$$

for each node s_q added from the expansion of the edge (i, j) with a label $i_1 i_2 \ldots i_k$ of the initial graph. To the best of our knowledge, this result has not appeared in the literature before, as for instance [1] only mention the second inequality. We believe that this simple result is key for developing a decision algorithm allowing to compare two given path-complete Lyapunov function.

Acknowledgements

References

[1]   A. A. Ahmadi, R. M. Jungers, P. A. Parrilo and M. Roozbehani. Joint spectral radius and path-complete graph Lyapunov functions. *SIAM Journal on Control and Optimization*, 52(1):687-717, 2014.

[2]   M. Philippe and R. M. Jungers. A complete characterization of the ordering of Path-Complete methods. *Proc. of IEEE/ACM HSCC*, 2019.

[3]   M. Philippe, N. Athanasopoulos, D. Angeli and R. M. Jungers. On Path-Complete Lyapunov Functions: Geometry and Comparison. *IEEE Transactions on Automatic Control*, 64(5):1947-1957, 2019.

(a) $G = (S, E)$ (b) $G_e = (S_e, E_e)$

Figure 1: Example of a labeled directed graph that captures all the switching sequences of two modes, and its expansion.

Limit Cycles in Replicator-Mutator Dynamics with Game-Environment Feedback

Lulu Gong, Ming Cao

Discrete Technology & Production Automation, University of Groningen

Nijenborgh 4, 9747 AG, Groningen, The Netherlands

Email: {l.gong@rug.nl, m.cao@rug.nl}

1 Introduction

In the classic evolutionary game setting, the payoffs in each pairwise-interaction game are usually predetermined and given in the form of constant payoff matrices. However, in many applications, especially in the context of shared resources, it is recognized that the payoffs for individuals can change over time or be affected directly by the external environment. Thus game-playing individuals' decisions can influence the surrounding environment, and the environment also acts back on the payoff distributions. This mechanism, which is termed *game-environment feedback*, has been studied in biological and sociological models [1, 2].

Interesting system behaviors, such as periodic orbits and heteroclinic cycles, have been revealed by many researchers with the usage of *replicator dynamics*. The replicator dynamics usually do not take the mutation into account, which is a key component of natural selection theory. By allowing individuals to spontaneously change from one strategy to another in small probability, one can involve the mutation and obtain the so-called *replicator-mutator dynamics*, which also have played a prominent role in evolutionary game theory and appeared in a variety of contexts in biology and sociology.

2 Mathematical Model

2.1 Replicator-Mutator equations

Consider a well-mixed infinite population where the individuals play the *Cooperation-Defection* (C-D) game with the environment-dependent payoff matrix $A(r)$. We denote the proportion of individuals choosing C by a variable x. Since there are only two strategies and $x \in [0,1]$, the population state can be represented by the vector $\mathbf{x} = [x \quad 1-x]^T$. Assume the strategies can mutate into each other with the same probability $\mu \in [0,1]$. Thus, the dynamics of x are governed by the following replicator-mutator equation

$$\dot{x} = x[(A(r)\mathbf{x})_1 - \mathbf{x}^T A(r)\mathbf{x}] - \mu x + \mu(1-x), \quad (1)$$

where $(A(r)\mathbf{x})_1$ is the first entry of $A(r)\mathbf{x}$ and represents the fitness of choosing strategy C, and $\mathbf{x}^T A(r)\mathbf{x}$ is the average fitness at the population state $\mathbf{x}$.

2.2 Mathematical model with game-environment feedback

We use the standard logistic model for the environment change which is given by

$$\dot{r} = r(1-r)[\theta x - (1-x)], \quad (2)$$

where $\theta > 0$ represents the ratio between the enhancement effect due to cooperation and degradation effect due to defection. Combining (1) and (2), we obtain a closed-loop planar system describing the population dynamics under the game-enviroment feedback

$$\begin{cases} \dot{x} = x[(A(r)\mathbf{x})_1 - \mathbf{x}^T A(r)\mathbf{x}] + \mu(1-2x) \\ \dot{r} = r(1-r)[\theta x - (1-x)] \end{cases}. \quad (3)$$

3 Hopf Bifurcation and Limit cycles

Taking μ as the bifurcation parameter, it is recognized that the system (3) at the interior equilibrium undergoes a *supercritical Hopf bifurcation* which generates a stable limit cycle.
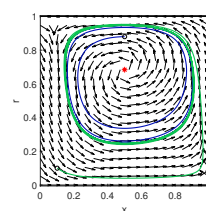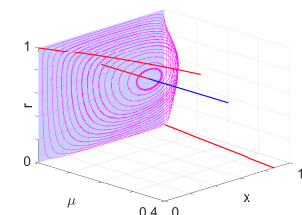
(a) A stable limit cycle   (b) Bifurcation plot

References

[1]   J. S. Weitz, C. Eksin, K. Paarporn, S. P. Brown and W. C. Ratcliff. An oscillating tragedy of the commons in replicator dynamics with game-environment feedback. *PNAS*. 2016.

[2]   J. Lee, Y. Iwasa, U. Dieckmann, and K. Sigmund. Social evolution leads to persistent corruption. *PNAS*. 2019.

Energy efficiency of flow-mediated flocking

Mingming Shi

ICTEAM Institute, UCLouvain, Louvain-la-Neuve 1348, Belgium

m.shi@rug.nl

Julien Hendrickx

ICTEAM Institute, UCLouvain, Louvain-la-Neuve 1348, Belgium

julien.hendrickx@uclouvain.be

1 Abstract

Birds flocking where a group of birds take flight in a certain formation configuration during their migration has been well observed in the nature. Even though researchers have realized that the benefit of airflow from other birds in the flocking may be the reason of birds cooperation, sophisticated mechanisms explaining why birds collaborate with others and fly in a specific flocking configuration, and how do they achieve the configuration remain open questions.

We will report progress on simulation-guided analysis of flow-mediated interaction in a flock of birds, aiming at fully understanding and regenerating the birds flocking behavior from the first principles. As a first step, we consider a simplified additive model of airflow-related benefit of flocking behavior on the bio-mechanical energy consumption of a single bird. We then investigate the long-term energy efficiency of various flocking configurations, also taking into account possible fatigue effects. We also investigate how formations can emerge from different model of bird behavior.

Crucially, the bird behavior and interactions must be consistent with an animal behavior and evolutionary biology. This means that every agent is to some degree selfish, and its actions must be dictated by some form of actual personal gain (e.g. in terms of energy spent). Collaborations are possible only if they benefit to all those involved. Besides, there are strong limitations on the control "algorithms" and on communications that can be considered, typically forbidding methods relying on abstract computations.

Hence, we consider a spectrum of behavior between purely selfish situations and an (unrealistic) centralized control. We focus in particular on pairwise reciprocal collaboration, and on the use of a notion of empathy (a bird suffers from seeing its neighbors suffering), allowing for situations where birds would "selfishly" help each other.

Acknowledgement

References

[1] R. E. Gill et al.,"Extreme endurance flights by landbirds crossing the Pacific Ocean: ecological corridor rather than barrier?, Proc. Biol. Sci., vol. 276, no. 1656, pp. 447457, 2009.

[2] H. Weimerskirch, J. Martin, Y. Clerquin, P. Alexandre, and S. Jiraskova, "Energy saving in flight formation, Nature, vol. 413, no. 6857, pp. 697698, 2001.

[3] B. Voelkl et al., "Matching times of leading and following suggest cooperation through direct reciprocity during V-formation flight in ibis, Proc. Natl. Acad. Sci. U.S.A., vol. 112, no. 7, pp. 21152120, 2015.

[4] K.-K. Oh et al., "A survey of multi-agent formation control, Automatica , vol. 53, pp. 424440, 2015.

[5] B. D. O. Anderson, C. Yu, B. Fidan, J. M. Hendrickx, "Rigid graph control architectures for autonomous formations, IEEE Control Syst., vol. 28, no. 6, pp. 4863, 2008.

[6] S. Coogan and M. Arcak, "Scaling the size of a formation using relative position feedback, Automatica , vol. 48, no. 10, pp. 26772685, 2012.

[7] H. Oh, A. R. Shirazi, C. Sun, and Y. Jin, "Bio-inspired self-organising multi-robot pattern formation: A review, Rob. Auton. Syst., vol. 91, pp. 83100, 2017.

[8] J. A. Carrillo, S. Martin, and V. Panferov, "A new interaction potential for swarming models, Physica D, vol. 260, pp. 112126, 2013.

[9] A. J. Ijspeert, "Central pattern generators for locomotion control in animals and robots: a review, Neural Netw., vol. 21, no. 4, pp. 642653, May 2008.

Bringing intuitive weighting filters into $\mathscr{H}_\infty$ control design practice

Laurens Jacobs, Jan Swevers and Goele Pipeleers

MECO Research Team, Dept. of Mechanical Engineering, KU Leuven, BE-3001 Heverlee

DMMS lab, Flanders Make, BE-3001 Heverlee

`laurens.jacobs@kuleuven.be`

1 Introduction

As part of modern linear feedback control, the synthesis of control filters based on specifications expressed as constraints on $\mathscr{H}_\infty$ norms on closed-loop transfers has gained a lot of attention over the past decades. A deep theoretical understanding as well as computational algorithms have been developed, and have proven to be succesfully applicable to a wide variety of applications. Moreover, closed-loop shaping has some important advantages as compared to classical open-loop shaping, especially for MIMO systems with complex dynamics. In fact, many control problems share very similar specifications with a clear interpretation if they are formulated as a closed-loop shaping problem. This observation was already made in the early eighties (see, e.g., [1]) and was later termed *mixed sensitivity design*.

2 Mixed sensitivity design

In this work, we consider two particular specification types. First, to achieve a decent tracking performance and/or a satisfactory disturbance rejection, one often desires low-frequency roll-off from so-called *sensitivity* transfers of interest. Second, accounting for noise attenuation and limited actuator effort is possible by imposing high-frequency roll-off on so-called *complementary sensitivity* and *input sensitivity* transfers respectively. As the design parameters in a closed-loop shaping approach are the weighting filters, their shape is chosen to be the inverse of the desired transfer shape. Thus, low-frequency roll-off requires unstable weighting filters, whereas high-frequency roll-off involves improper weighting filters. As a well-known and unfortunate fact, unstable and impulsive modes in weighting filters cause difficulties, since their dynamics are either not stabilizable or not detectable by the control filter. Closed-loop admissibility therefore requires exact cancellation of these modes in the closed loop; a situation that is impossible to achieve with numerical algorithms. A common workaround in control engineering practice is the following perturbation of the weighting filters. Instead of choosing unstable weighting filters with poles in 0, one chooses weighting filters with nonzero poles that are sufficiently far below the frequency range containing relevant plant dynamics. Similarly, instead of designing improper weighting filters, one opts for approximate proper weighting filters with large finite poles instead of poles at ∞. This procedure is illustrated for a random SISO plant by the black dashed line in Fig. 1. This figure also demonstrates that postprocessing of the corresponding controller
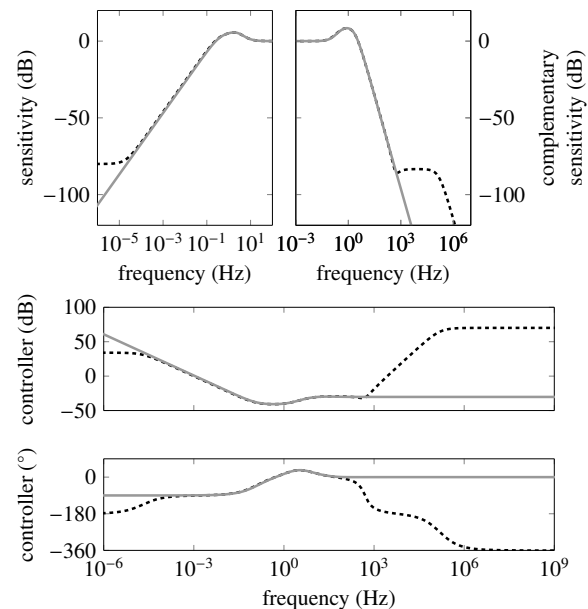
Figure 1: Closed-loop sensitivity and complementary sensitivity transfers obtained by solving a problem with unstable and improper weighting filters.

is still desired to obtain the targeted shapes of the sensitivity and complementary sensitivity transfers, drawn in grey.

3 Unstable and improper weighting filters

To avoid manual postprocessing of the controller, which becomes particularly difficult for MIMO cases, a direct synthesis method based on the construction of a structured controller has been elaborated by [2] for unstable weighting filters, and has later been (partially) extended for improper weighting filters by [3]. The contribution that we will present is the combination of the latter procedure with an LMI-based synthesis method for descriptor systems that is numerically robust for use in industrial control engineering practice. This proposed method is capable of directly returning the controller and the corresponding closed-loop transfers that correspond to the grey lines in Fig. 1.

References

[1] J.C. Doyle and G. Stein. "Multivariable Feedback Design: Concepts for a Classical/Modern Synthesis". *IEEE Transactions on Automatic Control*, vol. 26, no. 1, February 1981.

[2] H. Koroglu. "$\mathscr{H}_\infty$ synthesis with unstable weighting filters: An LMI solution". 52nd IEEE Conference on Decision and Control, December 2013, Florence, Italy.

[3] Y. Feng and M. Yagoubi. "Comprehensive admissibility for descriptor systems". *Automatica*, vol. 66, April 2016.

Extended model order reduction for linear time delay systems

Sajad Naderi Lordejani[1], Bart Besselink[2], Nathan van de Wouw[1,3]

[1]Department of Mechanical Engineering, Eindhoven University of Technology, Eindhoven, The Netherlands
[2]Bernoulli Institute for Mathematics, Computer Science and Artificial Intelligence, University of Groningen, Groningen, The Netherlands
[3]Department of Civil, Environmental & Geo-Engineering, University of Minnesota, Minneapolis, USA
Emails: {s.naderilordejani,n.v.d.wouw}@tue.nl, b.besselink@rug.nl

1 Introduction

We present an extended model order reduction technique for linear time delay systems. This technique preserves the delay-structure and asymptotic stability and provides an a priori error bound.

2 Approach

Extended model order reduction for delay-free systems not only improves the overall quality of model approximation but also facilitates structured/parametrized model reduction. Instead of using observability and controllability matrices directly, extended reduction procedures rely on the use of slack matrices in the balancing procedure. We have developed this concept also for linear time delay systems in [1]. Namely, we define observability and controllability energy functionals that conceptually characterize controllability and observability properties of time delay systems. Those functionals cannot directly be used for the purpose of balanced truncation, as those cannot be computed for given initial/final conditions. Nonetheless, we have shown that there are computable Lyapunov-Krasovskii functionals, described by quadratic terms, that can bound and approximate the observability and controllability energy functionals. Those approximate functionals are characterized by positive (semi-)definite matrices which are solutions to a set of matrix inequalities. Since they capture approximate observability and controllability properties of the delay system, these matrices are treated as gramians in conventional model order reduction and used for the purpose of balanced truncations. Structured/parametrized model order reduction for delay systems can be achieved by enforcing certain structure on these matrices. This, however, compromises the tightness of the bounds and, consequently, degrades the quality of model approximation. Contrary to the conventional method in [2], the proposed extended model reduction technique uses slack matrices for balancing. In this technique, the slack variables are enforced in the matrix inequalities in a way that those do not appear in the approximate functionals. As a crucial property, it allows for structured/parametrized model reduction without imposing any structure on the matrices characterizing the approximate functionals. This in turn improves the feasibility and quality of reduction. The
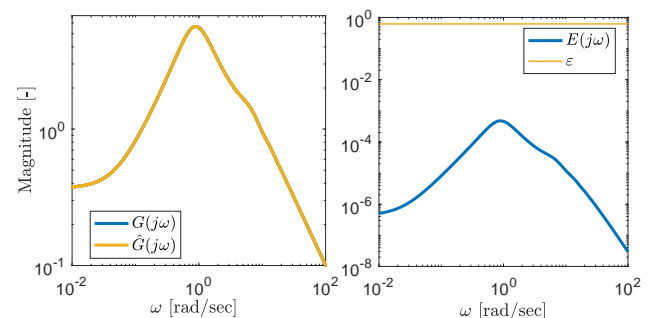
Figure 1: Frequency response functions and error bound.

extended model reduction technique recovers the conventional approach in [2] as a special case. It also preserves stability properties of the original model and provides an error bound.

3 Illustrative example

We consider the structured model reduction of a feedback control system $G(j\omega)$ with an actuation and measurement delay of $\tau = 0.45$ s. While the model reduction method in [2] is not feasible for the considered example, the structured singular values obtained from the proposed method are $\Sigma_p = \text{diag}\{19.12, 18.61\}$ and $\Sigma_c = \text{diag}\{17.97, 0.31\}$, corresponding to the plant and controller, respectively. There is a large difference between the singular values of the controller. Therefore, we truncate the state of the transformed model of the controller that corresponds to the smallest singular value in Σ_c. The frequency response function of the original closed-loop system is compared to that of the reduced-order system, indicated by $\hat{G}(j\omega)$, in Fig. 1. Clearly, the approximation is highly accurate in terms of the $\mathscr{H}_\infty$-norm of the error system $E(j\omega) = G(j\omega) - \hat{G}(j\omega)$.

References

[1] S. Naderi Lordejani, B. Besselink, and N. van de Wouw, "An extended model order reduction technique for linear delay systems," in *Proceeding of the 58th IEEE Conference on Decision and Control*, Nice, France, Dec 2019.

[2] S. Naderi Lordejani, B. Besselink, A. Chaillet, and N. van de Wouw, "Model order reduction for linear time delay systems: A delay-dependent approach based on energy functionals," *Automatica*, vol. 112, p. 108701, Feb. 2020.

A discussion on the canonical decomposition of two dimensional descriptor systems

Bob Vergauwen   Bart De Moor

KU Leuven, Department of Electrical Engineering (ESAT), Stadius Center for Dynamical Systems,
Signal Processing and Data Analytics.
bob.vergauwen@esat.kuleuven.be; bart.demoor@esat.kuleuven.be
Bart De Moor is an IEEE and SIAM Fellow.

1 Introduction

The linear autonomous descriptor systems[2][3] in two dimensions that we will consider are described by

$$
\begin{aligned}
Ex[k+1,l] &= Ax[k,l] \\
Fx[k,l+1] &= Bx[k,l] \\
y[k,l] &= Cx[k,l],
\end{aligned}
\tag{1}
$$

where $y[k,l] \in \mathbb{R}^p$ and $x[k,l] \in \mathbb{R}^n$, the output and the state vector of the system respectively. The system equations are characterized by four square matrices A, B, E and F. A natural question to ask is, *under what conditions is this model well-posed and does there exist a canonical form*? One dimensional descriptor systems have been analyzed in [4][1].

2 Two dimensional descriptor systems

We propose the following: The two-dimensional system described in Eqn. (1), with (E,A) and (F,B), two regular pencils, is well-posed if and only if there exist square matrices P, Q, and U of full rank, such that the equivalent model

$$
\begin{aligned}
PEQx[k+1,l] &= PAQx[k,l] \\
UFQx[k,l+1] &= UBQx[k,l] \\
y[k,l] &= CQx[k,l],
\end{aligned}
$$

exists with

$$
PEQ = \begin{bmatrix} \mathbb{1} & & & \\ & \mathbb{1} & & \\ & & E_1 & \\ & & & E_2 \end{bmatrix}, PAQ = \begin{bmatrix} A_1 & & & \\ & A_2 & & \\ & & \mathbb{1} & \\ & & & \mathbb{1} \end{bmatrix},
$$

$$
UFQ = \begin{bmatrix} \mathbb{1} & & & \\ & F_1 & & \\ & & \mathbb{1} & \\ & & & F_2 \end{bmatrix}, UBQ = \begin{bmatrix} B_1 & & & \\ & \mathbb{1} & & \\ & & B_2 & \\ & & & \mathbb{1} \end{bmatrix},
$$

and

$$
CQ = \begin{bmatrix} C_{RR} & C_{RS} & C_{SR} & C_{SS} \end{bmatrix},
$$

where the matrices E_1, E_2, F_1, and F_2 are nilpotent. In this basis, the state vector has the form

$$
x[k,l] = \begin{bmatrix} x^{RR}[k,l]^T & x^{RS}[k,l]^T & x^{SR}[k,l]^T & x^{SS}[k,l]^T \end{bmatrix}^T
$$

and the following additional equations must hold

$$
A_1B_1 = B_1A_1, A_2F_1 = F_1A_2, E_1B_2 = B_2E_1, E_2F_2 = F_2E_2.
$$

When the two dimensional descriptor system is transformed to this form, all four system matrices E, A, F, B commute. As a consequence, the state sequence $x[k,l]$ satisfies

$$
E^n F^m x[n,m] = A^n B^m x[0,0].
$$

3 Conclusion

In this presentation, some necessary conditions for the existence of a non-trivial state sequence $x[k,l]$ of a two-dimensional descriptor system has been derived. As a consequence of this it is shown that a well-posed descriptor system can always be transformed to a form where the system matrices commute.

References

[1] R. E. Kalman. Canonical structure of linear dynamical systems. *Proceedings of the National Academy of Sciences of the United States of America*, 48(4):596, 1962.

[2] P. Kunkel and V. Mehrmann. *Differential-algebraic equations: analysis and numerical solution*, volume 2. European Mathematical Society, 2006.

[3] F. L. Lewis. A survey of linear singular systems. *Circuits, Systems and Signal Processing*, 5(1):3–36, 1986.

[4] M. Moonen, B. De Moor, J. Ramos, and S. Tan. A subspace identification algorithm for descriptor systems. *Systems & control letters*, 19(1):47–52, 1992.

Sliding mode observer based hysteresis compensation control for piezoelectric stacks

Jiaming Hu, Stephan Trenn

Bernoulli Institute, University of Groningen, 9747 AG, Groningen, The Netherlands

Jiaming.hu@rug.nl

1 Abstract

The piezoelectric stacks (PS) are widely used in high-precision control system due to their pushing force capabilities, fast responses and high positioning accuracies. In this study, we establish a Luenberger-wise observer for compensating the hysteresis effect in PS actuator, and an observer-based robust controller.

2 Problem statements

Strong hysteresis nonlinearity which carried by piezoelectric materials inevitably compromises the performance of the PS. Specifically, hysteretic effect may induce 10%∼15% positioning error at low frequency for open-looped systems, and error is even larger at high frequency.

For depicting the characters of PS system, many mathematic models have been made. The classical Bouc-Wen hysteresis model was modified by[Wen (1976)]. The model contains two sets of differential equation to describe the relationship between input driving voltage $u(t)$ and displacement $x(t)$ of the actuator, it can be stated as follows

$$m\ddot{x}(t) + b\dot{x}(t) + kx = k[du(t) - h(t)] \quad (1)$$

$$\dot{h}(t) = \alpha d\dot{u}(t) - \beta|\dot{u}(t)|h(t) - \gamma\dot{u}(t)|h(t)| \quad (2)$$

The block diagram of the observer-based compensation system is shown in Figure 1. Within this framework, the
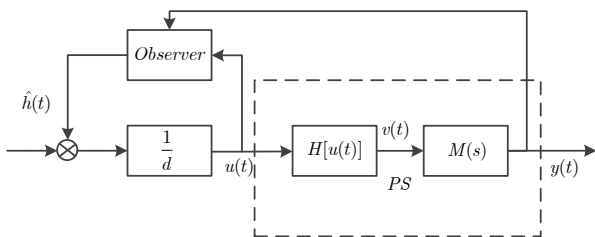
Figure 1: The Framework of the observer-based compensation system

hysteresis observer proposed is given by

$$\begin{cases} \dot{\xi}(t) = T\tilde{A}\tilde{X}(t) + T\tilde{B}\bar{u}(t) + |u_2(t)|TM_1\tilde{X}(t) \\ \qquad + u_2(t)T\Gamma|\tilde{X}(t)| + L[y(t) - \hat{\tilde{C}}X(t)] \\ \hat{X}(t) = \xi(t) + Ny(t) \end{cases} \quad (3)$$

and the robust controller is given by

$$\begin{aligned} u(t) =& k^{-1}\{-k_1[z_2(t) - k_3 z_1(t)] - A_1[z_1(t) + r(t)] \\ & - A_2[z_2(t) + \dot{r}(t) - k_3 z_1(t)] - \check{\phi}\text{sgn}[\sigma(t)] + \ddot{r}(t) \\ & - k_3\dot{z}_1(t) - k_2[\sigma(t) + k_4\text{sgn}(\sigma(t))]\}. \end{aligned} \quad (4)$$

The experiment platform and the control performance are shown in Figure 2 and Figure 3.
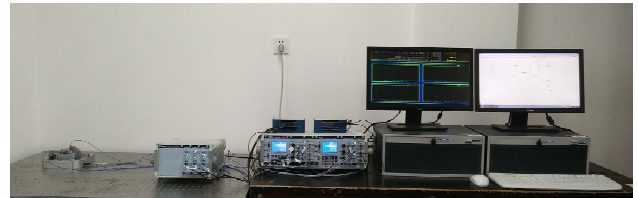
Figure 2: Experimental platform
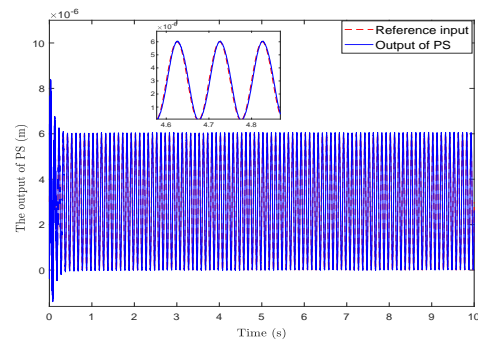
Figure 3: The output of the PS actuator

References

[Wen (1976)] Wen YK (1976) Method for random vibration of hysteresis systems. *Journal of the Engineering Mechanics Division 102(2): 249-263.*

Impulsive control of precision motion system

Reza Behinfaraz
Faculty 3mE
Dep. Precision and Microsystems Engineering
Delft University
Mekelweg 2
2628 CD Delft
The Netherlands
Email: r.behinfaraz@tudelft.nl

S. Hassan HosseinNia
Faculty 3mE
Dep. Precision and Microsystems Engineering
Delft University
Mekelweg 2
2628 CD Delft
The Netherlands
Email: s.h.hosseinniakani@tudelft.nl

1 Abstract

In this paper, the stability of a class of precision motion control systems is discussed. The precision motion control design is highly competitive and challenging due to the ever-increasing demands on speed and precision. It has vast applications in atomic force microscopes, photo-lithography systems, and nano-positioning systems [1]. General equations of a precision motion system can be simplified to a double mass-spring system shown in Fig.1. These equations can be written as:

$$m_1 \frac{d^2 x_1}{dt^2} + (k_1 + k_2)x_1 - k_2 x_2 = F \qquad (1)$$

$$m_2 \frac{d^2 x_2}{dt^2} + k_2 x_2 - k_2 x_1 = 0 \qquad (2)$$
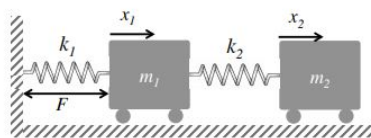
Figure 1: Double mass spring system

Today over 90 percent of industry uses a PID controller with their gold standards[2]. But designing a controller with better transient behavior than PID controllers is an important challenge to overcome the limitations of linear control. In this regard, impulsive feedback control is designed in combination with PID control. The controller is designed to reduce the settling time and transient behavior compared to its linear counterpart.

The basic idea behind impulsive control is the introduction of controlled impulsive forces in specified times to get the zero steady-state error[3]. Resuming, the main contributions of the current paper are as follows. Firstly, we propose an impulsive feedback control design for a precision motion control system. Then we focus on controller parameters to improve the performance. The result of simulation in these conditions is shown in Fig.2. Also, a comparison with linear PID is shown in this figure.
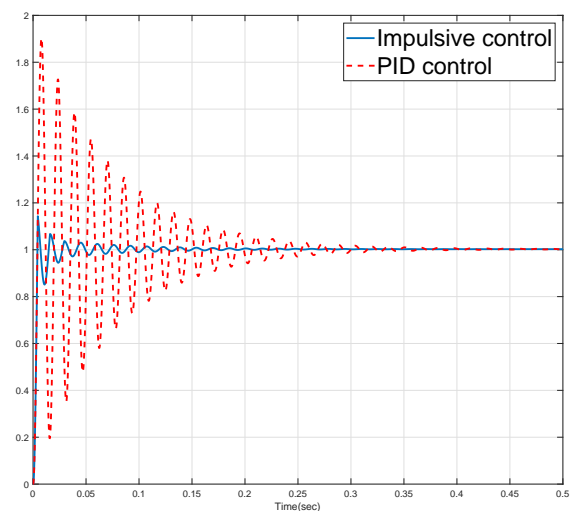
Figure 2: Precision motion system control ; Impulsive control & PID control

In addition, robustness of our method is analyzed against the uncertainty of the plant. The proposed method is implemented to the experimental nano-positioning system and its performance is validated.

References

[1] HosseinNia SH, Saikumar N. Fractional-order Precision Motion Control for Mechatronic Applications.

[2] IFAC newsletter April 2019. Ifac industry committee update: Initiative to increase industrial participation in the control community.

[3] Orlov, Y. Santiesteban, R., and Aguilar, L. T. Impulsive control of a mechanical oscillator with friction. In Proceedings of the 2009 IEEE American Control Conference, St. Louis, U.S.A. (June 2009), pp. 34943499.

Cylinder-individual charge mass estimation by time-frequency analysis of in-cylinder pressure measurements

Prasoon Garg*   Paul Mentink**   Xander Seykens*,**   Frank Willems*,**

*Dept. Mechanical Eng., Eindhoven University of Technology (TU/e), Netherlands

**TNO Automotive, Helmond, Netherlands

(prasoon.garg08@gmail.com, paul.mentink@tno.nl, x.l.j.seykens@tue.nl, f.p.t.willems@tue.nl)

1 Introduction

Real-time information on emissions will be instrumental in meeting the stringent future pollutants regulations for the transportation sector powered by heavy duty (HD) diesel combustion engines. In particular, a virtual NOx sensor would be functional for multiple purposes such as: cost reduction, on-board diagnostics (OBD), faster emissions control at transients and cold start conditions for improved emissions performance [1]. High cylinder-to-cylinder variations in trapped charge states: mass, temperature and composition exists at the intake valve closing (IVC) in multi-cylinder engines. The NOx emissions estimation accuracy with an assumption of equal cylinder behavior is lower than production physical NOx sensors [1]. Therefore, an accurate estimation of these states is essential in the development of a virtual NOx sensor to estimate emissions accurately.

2 Approach

The focus of this work is to estimate cylinder-individual trapped charge mass by performing the time-frequency analysis, also called as spectral analysis of the cylinder pressure signal. In [2], the in-cylinder pressure waves that accompany ignition are modeled to determine the charge mass during the expansion phase. The wave theory relates the mass in the cylindrical chamber with pressure, geometry, resonance frequencies, Bessel Coefficient and speed of sound as,

$$m_{cyl}(\alpha) = \left(\frac{B_{1,0}(\alpha)\sqrt{\gamma(\alpha)\, p_{cyl}(\alpha)V(\alpha)}}{\pi f_{cyl}(\alpha)D} \right)^2 \qquad (1)$$

Here, α is the crank angle, γ is the isentropic coefficient of the charge, p_{cyl} is the measured in-cylinder pressure, f_{cyl} and $B_{1,0}$ are resonance frequencies and the Bessel Coefficient for the first unsymmetrical transverse mode of vibrations, V is the cylinder volume and D is the cylinder bore. In this work, this method is further investigated and a modified approach is proposed to determine the trapped charge mass on engine cycle basis for stationary operating points. The resonance frequencies are identified from the Short Time Fourier Transform (STFT) of the unfiltered pegged pressure signal, see Figure 1. Here, windowing is used to reduce the spectral leakages associated with Discrete Fourier Transform (DFT). Finally, blow-by losses and injected fuel mass

are compensated to estimate trapped charge mass at IVC per engine cycle. An uncertainty analysis is performed to determine the prediction accuracy.
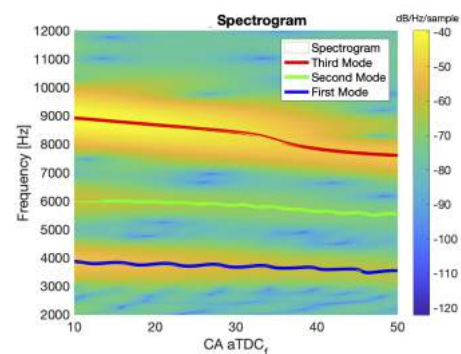
Figure 1: Spectrogram of cylinder pressure

3 Results

This method is applied over wide range of engine speed and load on state-of-the-art 6 cylinder 12.9L Euro-VI Heavy-duty (HD) diesel engine. The in-cylinder pressure is measured using six water cooled piezoelectric transducers at a crank angle resolution of $0.1°$. It is determined that minimum sampling frequency of 10 kHz is required for pressure transducers to identify the first mode frequencies for this engine. Cylinder-individual trapped charge mass is determined on engine cycle basis. Uncertainty analysis shows a maximum uncertainty of 2.5% in charge mass at IVC. Cylinder-individual NOx emissions can be estimated and results show significant cylinder-to-cylinder variations. Based on the results, further analysis on the method is required for real-time implementation, transient operation and for operating conditions with low signal-to-noise ratio and high dampening rate of first mode frequencies.

References

[1]   P. Mentink, X. Seykens, and D. E. Valdivieso, "Development and application of a virtual nox sensor for robust heavy duty diesel engine emission control," *SAE Int. J. Engines*, vol. 10, 2017.

[2]   P. Bares Moreno, "In-cylinder pressure resonance analysis for trapped mass estimation in automotive engines," Ph.D. dissertation, 2017.

User-friendly Nonparametric Framework for Vibro-acoustic Industrial Measurements with Multiple Inputs

Péter Zoltán Csurcsia[1], Bart Peeters[2]
1) Vrije Universiteit Brussel, Pleinlaan 2, 1050 Elsene, Belgium
2) Siemens Industry Software NV., Interleuvenlaan 68, 3001 Leuven, Belgium
Email: `peter.zoltan.csurcsia@vub.ac.be`

1 Introduction

This paper introduces a user-friendly toolbox for industrial measurements of nonlinear vibro-acoustic systems with multiple inputs and it addresses the questions related (semi)-automatic measurement processing. The toolbox is illustrated on various real-life measurements [1][2].

2 The toolbox

The key idea in the proposed framework is to split up the classical coherence function of the FRF measurement into noise and nonlinearity information. The (non)linearity assessment is based on the semi-automatic analysis of the FRF, noise and nonlinearity estimates and it provides a user-friendly interpretation of the nonlinear MIMO measurement data. An overview of the estimation framework can be seen in Fig 2. The proposed framework consists of four interrelated steps:

- Step 1: The Design of experiment and measurement blocks address the issues related to signal design, choice of measurement parameters, instrumentation and execution of the measurement.

- Step 2: The Pre-processing block considers a check-up of the input (reference) channels and provides an early warning to the user when the inputs are correlated. Furthermore, it segments the measurement data and sets up the processing parameters for the BLA transfer function estimation.

- Step 3: The BLA estimation block provides the BLA FRF estimation, calculates advanced statistics of the noise and nonlinearity, and when it applies estimates the transient term.

- Step 4: The Post-processing block makes the estimation results and warnings accessible in a condensed form. It provides users with the FRF, noise and nonlinearity estimates. It is possible to automatically highlight the FRF (or input, output, reference) channels that have significant nonlinearity or noise levels.

3 Summary

The proposed estimation framework is a result of an industrial research program and at its present state it has been implemented as a combination of Simcenter Testlab [3] and Matlab components. Due to the general nature of the analysis and it can be implemented platform independently. The
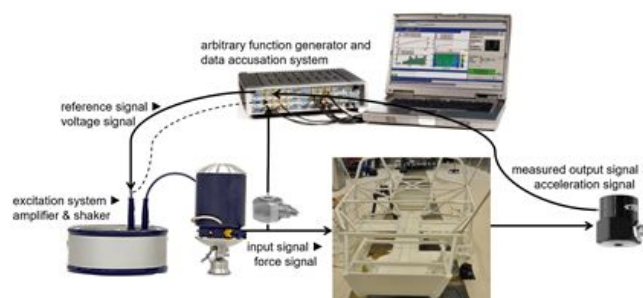
Figure 1: An illustration of the measurement-instrumentation setup used for vibration testing of the Siemens Simrod vehicle.
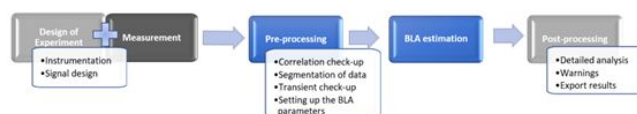
Figure 2: Overview of the proposed estimation framework. Blue blocks require – in normal circumstances – no user interactions. Light gray blocks require moderate user interaction. Dark gray block requires experienced user interaction.

work has been tested with simulations and real-life industrial measurements. The warning-notification system is developed by experiences learned from typical mistakes which popped up during the measurement campaigns.

4 Acknowledgements

References

[1] Csurcsia, P. Z., Di Lorenzo, E., Musella, U., Hallez, R., Debille, J., Peeters, B. (2019). Structural dynamics assessment on a full-electric aircraft: ground vibration testing and in-flight measurements. IFASD, USA

[2] Csurcsia, P. Z., Peeters, B., Schoukens, J. (2019). The Best Linear Approximation of MIMO Systems: First Results on Simplified Nonlinearity Assessment. IMAC, USA

[3] Siemens, Simcenter Testlab, www.plm.automation.siemens.com/global/en/products/simcenter

Extending the method of images to thermomechanical systems

D.W.M. Veldman[*,1], R.H.B. Fey[1], H.J. Zwart[1,2],

M.M.J. van de Wal[3], J.D.B.J. van den Boom[3], H. Nijmeijer[1]

[*]e-mail: d.w.m.veldman@tue.nl [1]Department of Mechanical Engineering, Eindhoven University of Technology, The Netherlands

[2]Faculty of Electrical Engineering, Mathematics and Computer Science, Hybrid Systems Group, University of Twente, The Netherlands

[3]ASML, Veldhoven, The Netherlands

1 Introduction

The method of images has been used since the 19th century to obtain analytic expressions for the temperature field on certain bounded domains $\Omega \subset \mathbb{R}^2$, with zero Dirichlet, Neumann, or Robin boundary conditions, based on the temperature field on $\mathbb{R}^2$, see e.g. [1]. The method of images also enables the efficient computation of the temperature field resulting from repetitive scanning patterns, see [2, Section 4], which appear in many applications such as the scanning of a silicon wafer by a moving heat source as shown in Fig. 1. Motivated by this application, the method of images is extended such that 1) it can be applied to thermomechanical systems, and 2) it can be applied to circular domains to which, to the best of our knowledge, the method has not been applied before.

2 Problem formulation

Consider the following planar thermomechanical system on a spatial domain $\mathbf{x} \in \Omega \subseteq \mathbb{R}^2$

$$\frac{\partial T_\Omega}{\partial t} = D\nabla^2 T_\Omega - \tilde{h}T_\Omega + \frac{1}{c}Q_\Omega, \tag{1}$$

$$\frac{1-\nu}{1+\nu}\nabla^2 \mathbf{d}_\Omega + \nabla\left(\nabla \cdot \mathbf{d}_\Omega\right) - 2\tilde{k}_\mathbf{s}\mathbf{d}_\Omega = 2\alpha\nabla T_\Omega, \tag{2}$$

where $T_\Omega(\mathbf{x},t)$ and $\mathbf{d}_\Omega(\mathbf{x},t)$ denote the temperature and displacement fields, $Q_\Omega(\mathbf{x},t)$ is the applied heat load, ∇, ∇^2, and $\nabla\cdot$ denote the gradient, Laplacian, and divergence operators, D, c, ν, and α, denote the thermal diffusivity, heat capacity per unit area, Poisson's ratio, and coefficient of thermal expansion, $\tilde{h}$ is the cooling rate to the environment, and $\tilde{k}_\mathrm{s}$ models the stiffness of the connection to the environment. The solution $\mathbf{d}_\Omega$ of (2) can be written as [3]

$$\mathbf{d}_\Omega = \nabla\Phi_\Omega + \mathbf{d}_\Omega^{\mathrm{bc}}, \tag{3}$$

where Φ_Ω is the (scalar) displacement potential satisfying

$$\nabla^2\Phi_\Omega - (1+\nu)\tilde{k}_\mathrm{s}\Phi_\Omega = (1+\nu)\alpha T_\Omega, \tag{4}$$

and $\mathbf{d}_\Omega^{\mathrm{bc}}$ is a homogeneous solution of (2) with $T_\Omega \equiv 0$ which is used the satisfy the mechanical boundary conditions.

The extension $Q_{\Omega,\infty} : \mathbb{R}^2 \times \mathbb{R}_+ \to \mathbb{R}$ of $Q_\Omega : \Omega \times \mathbb{R}_+ \to \mathbb{R}$ is defined by setting $Q_{\Omega,\infty}$ to zero outside Ω. The temperature and displacement field potential resulting from $Q_{\Omega,\infty}$ are $T_{\Omega,\infty}$ and $\Phi_{\Omega,\infty}$. Note that $T_{\Omega,\infty}$ and $\Phi_{\Omega,\infty}$ can be obtained efficiently for repetitive scanning patterns, see [2, Section 4].
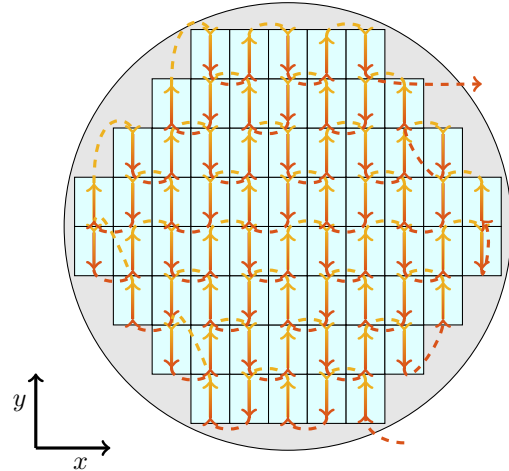
Figure 1: The exposure of a silicon wafer to the projection light is an application with a repetitive heat source

3 Results

The method of images is extended by showing that T_Ω and Φ_Ω can be expressed in terms of $T_{\Omega,\infty}$ and $\Phi_{\Omega,\infty}$ and a kernel $W_\Omega : \Omega \times \Omega' \to \mathbb{R}$ with $\Omega' := \mathbb{R}^2\backslash\Omega$ as

$$T_\Omega(\mathbf{x},t) = T_{\Omega,\infty}(\mathbf{x},t) + \iint_{\Omega'} W_\Omega(\mathbf{x},\mathbf{x}')T_{\Omega,\infty}(\mathbf{x}',t)\,\mathrm{d}\mathbf{x}', \tag{5}$$

$$\Phi_\Omega(\mathbf{x},t) = \Phi_{\Omega,\infty}(\mathbf{x},t) + \iint_{\Omega'} W_\Omega(\mathbf{x},\mathbf{x}')\Phi_{\Omega,\infty}(\mathbf{x}',t)\,\mathrm{d}\mathbf{x}'. \tag{6}$$

The kernel W_Ω needs to satisfy certain conditions and is known for several spatial domains Ω and thermal boundary conditions. For a circular domain, W_Ω can be determined by solving a PDE resembling a two-dimensional wave equation. Note that $\mathbf{d}_\Omega$ now follows from (3) with Φ_Ω as in (6) and $\mathbf{d}_\Omega^{\mathrm{bc}}$ as the solution of an elasticity problem. This extension of the method of images is applied to the wafer heating problem of Fig. 1. Compared to a standard finite element simulation, this results in a significant reduction in computational cost, especially on fine meshes.

References

[1]   G.H. Bryan, "An application of the method of images to the conduction of heat". *Proc. of the London Mathematical Society* 1(1), pp. 424–430, 1890.

[2]   D.W.M. Veldman, R.H.B. Fey, H.J. Zwart, M.M.J. van de Wal, J.D.B.J. van den Boom and H. Nijmeijer. "Semi-analytic approximation of the temperature field resulting from moving heat loads". *Int. J. of Heat and Mass Transfer* 122, pp. 128–137, 2018.

[3]   A.D. Kovalenko. *Thermoelasticity: Basic Theory and Applications.* Wolters-Noordhoff, 1969.

Boundary control of counter-current heat exchanger

Jacques Kadima kazaku, Denis Dochain
ICTEAM, Université Catholique de Louvain
B-1348 Louvain-La-Neuve
Belgium
{jacques.kadima,denis.dochain}@uclouvain.be

Joseph Winkin
Departement of mathematics
Université de Namur, Namur
Belgium
joseph.winkin@unamur.be

Moïse Mukepe Kahilu, Jimmy Kalenga Kaunde Kasongo
Rue Kassapa 1825, Laboratoire de régulation de systèmes
Université de Lubumbashi, Lubumbashi, RD Congo
{jacqueskazaku,moisemukepe,kalenga.kaunde}@polytechunilu.ac.cd

1 Introduction

In this paper we present the boundary control for distributer parameter counter-current heat exchanger, in a context where the output is distributed. The dynamics of this system are described by two linear partial differential equations [2] wich rewrite as a Fattorini model of boundary control as follows:

$$\begin{cases} \partial_t x_1(z,t) = -v_1 \partial_z x_1(z,t) + \alpha_1(x_2(z,t)-x_1(z,t)) \\ \partial_t x_2(z,t) = v_2 \partial_z x_2(z,t) + \alpha_2(x_1(z,t)-x_2(z,t)) + v_2 \delta(z)u(t) \end{cases}$$
(1)

where x_1 and x_2 represent temperature of internal and external fluids respectively, $u(t) = x_{2,in}(L,t)$ manipulated variable applied in $z = L$, α_1 and α_2 global coefficients of heat exchange, v_1 and v_2 represent transport velocities fluid; $\delta(z)$ denote an approximate Dirac delta distribution of finished width $[L,w]$.

2 Control strategy

The main our goal is to control output temperature x_1 by manipulation of $u(t)$ which is boundary condition of x_2.

The strategy developed by [2] consists in deriving the system output $y_m(t) = x_1(L,t)$ until the control quantity $u(t)$ appears. We can verify that $u(t)$ appears in the expression of the first derivative of $y_m(t)$; in this way a dynamic of a first order linear system can be imposed between the desired output $\eta(t)$ and the measured output. In order to guarantee a null asymptotic error, a PI controller is proposed.

The main disadvantage of this control strategy is that it does not use all the information contained in the distributed parameter model. To remedy this, we propose to consider that the output of the system is distributed, which allows us to define the observation equation as follows [1]:

$$y_m(t) = (c(z)x_1)(t) = \int_0^L \Delta_w(L-z)x_1(z,t)dz$$
(2)

where $\Delta_w(\cdot)$ represents a finite pulse of width w defined such that $\Delta_w(z) = w^{-1}$ for $z \in [0,w)$ and $\Delta_w(z) = 0$ elsewhere.

By adopting the above strategy, we can see $u(t)$ appear in

the expression of the second derivative of equation (2); thus a second order dynamic can be imposed between the distributed output y_m and the desired output $\eta(t)$. We then arrive at the expression of the following control law:

$$u(t) = \int_0^L c(z) \frac{1}{\tau_1 \alpha_1 v_2 \delta(z)} \left\{ \eta(t) - \tau_2 \frac{dy_m}{dt} - y_m(t) \right. $$
$$ - \tau_1 v_1^2 \frac{\partial^2 x_1}{\partial z^2} - 2\tau_1 \alpha_1 v_1 \frac{\partial x_1}{\partial z} + \tau_1 \alpha_1 (v_1 - v_2) \frac{\partial x_2}{\partial z} $$
$$ \left. + \tau_1 \alpha_1 (\alpha_1 + \alpha_2)(x_2 - x_1)x_2 \right\} dz $$
(3)

where τ_1 and τ_2 represent the time constants of the closed loop system.

3 Observer results
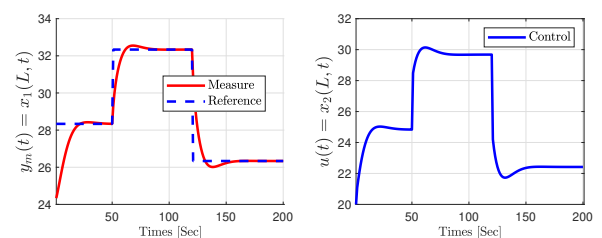
Figure 1: State trajectorie of the closed-loop system

This figure shows a good match between the $x_1(L,t)$ output and the setpoint. In terms of perspective, it is necessary in this context to consider control laws based on an observer so as to give an estimate of the complete state which falls within the control law.

References

[1] J. Winkin, and D. Dochain and P. Ligarius. (2000) *Dynamical analysis of distributed parameter tubular reactors,* Automatica, vol.36, pp:349-361.

[2] A. Maidi, and M. Diaf and J.P. Corriou. (2009) *Boundary geometric control of a counter-current heat exchanger*, Journal of process control, vol.19, pp:297-313.

Optimal control and approximations

Hans Zwart
Department of Applied Mathematics
University of Twente
P.O. Box 217, 7500 AE Enschede
and
Department of Mechanical Engineering
Eindhoven University of Technology
P.O. Box 513, 5600 MB Eindhoven
The Netherlands.
h.j.zwart@utwente.nl, H.J.Zwart@tue.nl

Kirsten Morris
Department of Applied Mathematics
University of Waterloo, Canada
kmorris@uwaterloo.ca

Orest Iftime
Department of Econometrics, Economics and Finance
University of Groningen
Nettelbosje 2, 9747 AE
Groningen, The Netherlands
o.v.iftime@rug.nl

1 Abstract

The Linear Quadratic (LQ) optimal control problem is one of the oldest control problems studied for state space linear system, and so its solution can be found in many text books. For instance, also in [1], where the problem is studied for a system on an infinite-dimensional state space. So the system is given by

$$\dot{x}(t) = Ax(t) + Bu(t), \quad x(0) = x_0$$

and the corresponding cost criteria is given by

$$J(x_0; u) = \int_0^\infty \|Cx(t)\|^2 + \|u(t)\|^2 dt.$$

The solution of this infinite-horizon linear quadratic optimal control problem is given by the state feedback $u(t) = -B^*Px(t)$, where P is the minimal non-negative solution of Algebraic Riccati Equation (ARE),

$$A^*P + PA - PBB^*P + C^*C = 0.$$

Although the solution of this problem is very similar to the finite-dimensional case, the calculation of the corresponding optimal feedback or solution to the Algebraic Riccati Equation (ARE), can almost never be done exactly. Hence approximations are needed. So A, B, and C are replaced by (matrices) A_n, B_n and C_n, respectively. In [2] approximations are studied under weak assumptions. They show that the optimal cost of the approximate system converge to the true optimal cost, i.e., $P_n \to P$, and that the optimal approximate control converges to the true optimal feedback., i.e., $B_n^*P_n \to -B^*P$. However, no result is shown regarding the question what happens when the approximate optimal feedback is applied to the original system. The authors of [2] conjecture that this might not give close to optimal cost, but an example or proof are missing. This means that no guarantee on success is given when stopping the approximation algorithm, and applying the feedback $-B^*P_nx(t)$ for some fix n.

In this paper we take this as our first question. First we show that their conjecture holds, and secondly we show that if a sequence of feedbacks converge to the optimal feedback and if these feedbacks give uniform finite cost, then applying these feedbacks will give cost arbitrarily close to the optimal cost. Finally, we comment on the question of how to construct such an approximation sequence of feedbacks.

References

[1] R.F. Curtain and H.J. Zwart. *An Introduction to Infinite-Dimensional Linear Systems Theory*. Springer Verlag, New-York, 1995.

[2] J.C. Oostveen, R.F. Curtain, and K. Ito. An approximation theory for strongly stabilizing solutions to the operator LQ Riccati equation. *SIAM J. Control Optim.*, 38(6):1909–1937, 2000.

A Convex Formulation of a Bilevel Optimization Problem for Energy Markets

K. Shomalzadeh, J. M. A. Scherpen, and M. K. Camlibel
Jan C. Willems Center for Systems and Control, University of Groningen, The Netherlands
Email: {k.shomalzadeh, j.m.a.scherpen, m.k.camlibel}@rug.nl

1 Introduction

Communication infrastructure in the new paradigm of smart grid facilitates the participation of the prosumers with controllable active demand and supply units in a real-time balancing market. To prevent direct interaction of the prosumers with higher level agents in the market and aggregate them, a market participant, the aggregator, has been introduced. The aggregator needs to minimize the cost for imbalance satisfaction in real-time by proposing a set of optimal incentivizing prices for the prosumers. On the other hand, the prosumers, as price taker and self-interest agents, want to maximize their profit by changing their supplies or demands and providing flexibility based on the proposed incentivizing prices. This problem can be modeled as a bilevel optimization problem. The state-of-the-art approach to solve a bilevel optimization problem is to reformulate it as a Mixed-Integer Programming (MIP) problem. Despite recent developments in the solvers for MIP problems, the computation time for a problem with a large number of decision variables may not be appropriate for real-time applications. New approaches are needed to be developed for this purpose.

2 The aggregator-prosumer model

We consider the static economic optimization problem of a system with a single aggregator and multiple prosumers associated with the aggregator in the real-time balancing market. The aggregator tries to minimize its cost to settle the imbalance and the prosumer's goal is to maximize its revenue and minimize its cost and discomfort by altering its demand or supply given the personalized price proposed by the aggregator. Suppose an aggregator detects a requested flexibility f in real-time. Therefore, the aggregator's responsibility is to incentivize each prosumer $i \in N = \{1, \ldots, n\}$ under its contract by proposing a personalized price x_i to change its generation or consumption. The prosumer i flexibility response y_i given the price x_i can be modeled using the following optimization problem:

$$\max_{y_i} \quad x_i y_i - \left(\frac{1}{2} a_i y_i^2 + b_i y_i\right) \tag{1a}$$

$$\text{subject to} \quad 0 \leq y_i \leq m_i. \tag{1b}$$

In (1a), the first term corresponds to the received payment by the prosumer from the aggregator. The second term models the discomfort of the prosumer for providing flexibility

y_i where $\frac{1}{2} a_i \geq 0$. Finally, the last term shows the payment the prosumer should receive or the cost it should pay with respect to the intraday market plannings for providing flexibility y_i. Moreover, in (1b), $m_i \geq 0$ models the maximum available flexibility of the prosumer i.

The aggregator as the agent responsible for supply and demand balancing in the real-time balancing market has two options to accomplish its goal, namely, to incentivize the prosumers for flexibility provision with the associated cost of $x_i y_i$ or to buy flexibility from the transmission system operator (TSO) with the price $p \geq 0$. The aggregator's problem is to find the best strategy given these two options. Considering the above models, x_i being positive and the prosumers' optimality conditions, we obtain the bilevel optimization problem (2) which has the problem (1) as a constraint for each prosumer.

$$\min_{x,y} \quad \sum_i x_i y_i + p\left(f - \sum_i y_i\right) \tag{2a}$$

$$\text{subject to} \quad x_i \geq 0, \qquad \forall i \in N, \tag{2b}$$

$$\sum_i y_i \leq f, \tag{2c}$$

$$\begin{cases} \max_{y_i} & x_i y_i - \frac{1}{2} a_i y_i^2 - b_i y_i \\ \text{subject to} & 0 \leq y_i \leq m_i, \end{cases} \quad \forall i \in N, \tag{2d}$$

where x and y are vectors with components x_i and y_i, respectively.

3 Results

Bilevel optimization problems are very difficult to solve. The most simple case of a bilevel optimization problem is when both the upper and lower level problems are linear. Even in this case, [1] has shown that the problem is NP-hard. We will show that it suffices to solve a specific convex optimization problem to find the global optimum of the original bilevel optimization problem (2).

References

[1] P. Hansen, B. Jaumard, and G. Savard, "New branch-and-bound rules for linear bilevel programming," SIAM Journal on Scientific and Statistical Computing, 13(5):1194-1217, 1992.

A Microscopic Energy Consumption Prediction Tool

Camiel Beckers* (c.j.j.beckers@tue.nl)[1], Igo Besselink[1], and Henk Nijmeijer[1]

[1]Dynamics & Control, Dept. of Mechanical Engineering, Eindhoven University of Technology, The Netherlands

1 Introduction

For the optimal utilization of battery electric delivery vans, energy consumption prediction is important. Accurate predictions enable efficient vehicle scheduling and charging, and early operational cost assessment. While the physics governing the energy consumption of electric vehicles are well known, the challenge lies in determining the model parameters accurately.

This abstract presents a microscopic energy consumption tool that requires only an intended route as user input. Relevant route parameters are automatically obtained from up-to-date weather, road, and height databases, such as OpenStreetMap[©] and OpenWeatherMap[©]. The tool consists of a velocity profile prediction algorithm and an energy consumption prediction model. Both parts follow a physics-based approach to provide decent extrapolability to unknown geographic regions and operating conditions.

2 Velocity Profile Prediction

The vehicle velocity profile is predicted based on three aspects of available route information: local speed legislation, traffic sign locations, and road curvature. Information about these three effects is obtained from online databases and is used to determine velocity limiting locations along the route, resulting in a maximum velocity as function of travelled distance. A driver model limits the maximum vehicle acceleration. The resulting velocity profile v, in Figure 1, shows a fair correspondence with a measured velocity profile.

3 Energy Consumption Model

The battery power P_{bat} is given by [1]

$$P_{bat} = v\left[m_{eff}\frac{dv}{dt} + f_r mg\cos(\alpha) + \frac{1}{2}\rho C_d A_f (v - v_{wind})^2 \right. $$
$$\left. + mg\sin(\alpha)\right] + P_{loss}(\omega_{wheel}, T_{wheel}) + P_{aux}. \quad (1)$$

This expression depends first of all on the vehicle velocity $v(t)$ as function of time t. Secondly, there are several vehicle parameters, such as vehicle mass m, effective mass m_{eff}, rolling resistance coefficient f_r, aerodynamic drag coefficient C_d, frontal area A_f, and powertrain losses P_{loss} as function of wheel speed ω_{wheel} and wheel torque T_{wheel}. These vehicle parameters are determined though dedicated vehicle tests. Also several environmental conditions are required, such as the gravitational acceleration g, the air density ρ,
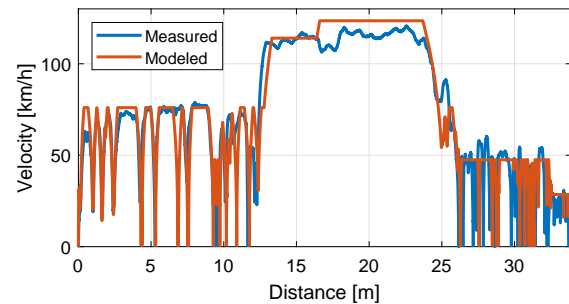
Figure 1: Generated velocity profile compared to a measurement.

the local road slope α, and the effective wind velocity v_{wind}. The latter three of these parameters are obtained from online databases, and are considered route and/or time dependent. The auxiliary power P_{aux}, due to light electric loads and air-conditioning, is assumed constant.

4 Combined Results

The velocity profiles calculated for 5 different routes are used as input for the energy consumption model. The results from these simulations are compared to the measured energy consumption of the battery electric delivery van in Table 1. While results vary, the tool is fairly accurate and has an average deviation of 6 % in terms of energy consumption.

Table 1: The relative error between predicted and measured energy consumption at the end of various routes.

Route	1	2	3	4	5	mean
Error [%]	-1.53	-6.93	8.11	4.48	9.42	6.1

5 Conclusions

The energy consumption prediction tool has been analysed for various routes and has a relative error below 10%. Model validation using a more diverse and larger set of routes is considered future work. The complete results of this model are presented in [2], where also the MATLAB-code of the tool will be published.

References

[1] J. Wang, I.J.M. Besselink, and H. Nijmeijer. Battery electric vehicle energy consumption prediction for a trip based on route information. *Proc. Inst. Mech. Eng. Part D J. Automob. Eng.*, 232(11):1528-1542, Sept. 2018.

[2] C.J.J. Beckers, M. Paroha, I.J.M. Besselink, and H. Nijmeijer, "A Microscopic Energy Consumption Prediction Tool for Fully Electric Delivery Vans," (in press) in EVS33 Int. Batter. Hybrid Fuel Cell Electr. Veh. Symp., Jun. 2020.

Local voltage control of an inverter-based power distribution network with a class of slope-restricted droop controllers

Michelle S. Chong
Department of Mechanical Engineering
Eindhoven University of Technology
m.s.t.chong@tue.nl

David Umsonst, Henrik Sandberg
Division of Decision and Control Systems
KTH Royal Institute of Technology
{umsonst,hsan}@kth.se

1 Motivation and Problem Setup

Motivated by environmental and sustainability concerns, the integration of renewable energy sources such as photovoltaic units in the distribution grid introduces new concerns in the functionality of power distribution systems. In this case, the customer is no longer just a consumer, but also a producer of power, which may cause the received voltages of each customer to fall outside of the desired safety margin.

We address the voltage regulation problem of an inverter-based power distribution in a line configuration (see Figure 1) using local controllers. The substation is at the head of the line, which sends a reference voltage $\bar{v}$ to each customer. The voltage received by each customer $i \in \{1,\ldots,N\}$ is $v_i \in \mathbb{R}$ and the voltage at the connection point to the distribution line is $v_i' \in \mathbb{R}$. The line impedance between each physical point on the distribution line is $Z_i' = R_i' + jX_i'$ and between the customer and the connection point is $Z_i = R_i + jX_i$, where $R_i', R_i \geq 0$ is the resistance and $X_i', X_i \geq 0$ is the reactance. Each customer has a load which can consume reactive $q_{c,i}$ and active powers $\rho_{c,i}$, independently of the generated reactive $q_{g,i}$ and active powers $\rho_{g,i}$. The power flow in the distribution line is modelled as

$$
\begin{aligned}
P_{i+1} &= P_i + \rho_{i+1}, & v_{i+1}'^2 &= v_i'^2 - 2\beta_i(P_i, Q_i), \\
Q_{i+1} &= Q_i + q_{i+1}, & v_i'^2 &= v_i^2 - 2\beta_{i-1}'(\rho_i, q_i),
\end{aligned}
\tag{1}
$$

where P_i and Q_i are the respective total active and reactive powers flowing from customer i to customer $i+1$; $\rho_i := \rho_{g,i} - \rho_{c,i}$ and $q_i := q_{g,i} - q_{c,i}$ are the net injection of the respective active and reactive power into the distribution line from customer i; $\beta_i(r,s) := R_i r + X_i s$ and $\beta_i'(r,s) := R_i' r + X_i' s$ with $\beta_{-1}'(r,s) = 0$ for all $r,s \in \mathbb{R}$.

The aim is to design the inverters Σ_i which has the ability to generate reactive power $q_{g,i}$, given that it has access to the local voltage v_i and the reference voltage $\bar{v}$, such that the received voltage v_i lies within a desired margin $\delta \geq 0$ of the reference voltage $\bar{v}$, i.e. given $\delta \geq 0$, all v_i satisfies

$$
\bar{v} - \delta \leq v_i(t) \leq \bar{v} + \delta, \qquad \forall t \geq 0.
\tag{2}
$$

2 Main result

We show that objective (2) is met with the proposed local controller Σ_i generates reactive power $q_{g,i}$ as follows

$$
\dot{q}_{g,i} = -\frac{1}{\tau_i} q_{g,i} + \frac{1}{\tau_i} K_i(\bar{v}^2 - v_i^2),
\tag{3}
$$
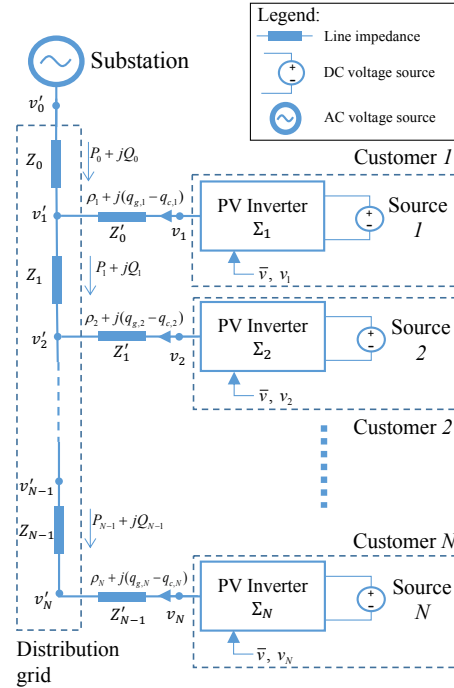
Figure 1: Infrastructure of the low-voltage distribution grid.

where $\tau_i \in \mathbb{R}_{>0}$ is the time-constant of the inverter's response, $\bar{v} \in \mathbb{R}$ is the reference voltage communicated to each customer i and the droop function $K_i(w)$ is a static mapping from the difference of the squared voltages w to the set-point for the reactive power. Differing from the droop control considered in the literature [1], the droop function uses the difference of the squared voltages as a result of the power flow model (1) and we show that this is amenable to our voltage regulation objective. Moreover, we show that the droop function K_i only needs to satisfy the sector bound condition, i.e the droop function K_i in (3) satisfies

$$
0 \leq \frac{K_i(v) - K_i(w)}{v - w} \leq d_i, \qquad \forall v,w \in \mathbb{R}, \ v \neq w,
\tag{4}
$$

and $|K_i(v)| \leq \bar{K}_i$, for all $v \in \mathbb{R}$, where $d_i \geq 0$ and $\bar{K}_i \geq 0$.

References

[1]   F. Andrén, B. Bletterie, S. Kadam, P. Kotsampopoulos, and C. Bucher, "On the stability of local voltage control in distribution networks with a high penetration of inverter-based generation," *IEEE Transactions on Industrial Electronics*, vol. 62, no. 4, pp. 2519–2529, 2015.

Active Damping of a DC Network: An Adaptive Scheme[⋆]

Juan E. Machado
University of Groningen
9747 AG Groningen - The Netherlands
j.e.machado.martinez@rug.nl

Romeo Ortega
CNRS-SUPELEC
91192 Gif-Sur-Yvette - France
romeo.ortega@supelec.fr

Alessandro Astolfi
Imperial College of London
SW7 2AZ London - United Kingdom
a.astolfi@imperial.ac.uk

[⋆] *For the full list of authors please see [1].*

Summary: We explore a nonlinear, adaptive controller aimed at increasing the stability margin of a direct-current (DC), small-scale, electrical network containing an *unknown* constant power load. This type of load reduces the effective damping of the network, leading to voltage oscillations and even to network collapse. The latter is overcome by interconnecting a controlled DC-DC switched power converter in parallel with the constant power load. The design of the control law for the converter is particularly challenging due to the existence of unmeasured states and unknown parameters. We propose a standard input-output linearization stage, to which a suitably tailored adaptive observer is added. The good performance of the controller is validated through experiments on a small-scale network.

1 Problem Statement

Fig. 1 shows an schematic diagram of the network under study. On top we distinguish the network to be stabilized whereas the added circuitry on the bottom represents the switched power converter. The averaged dynamic model of the overall network is given by

$$L_1 \dot{x}_1 = -r_1 x_1 - x_2 + E,$$
$$C_1 \dot{x}_2 = x_1 - \frac{P}{x_2} - x_3,$$
$$L_2 \dot{x}_3 = -r_2 x_3 + x_2 - x_4 u,$$
$$C_2 \dot{x}_4 = -\frac{1}{r_3} x_4 + x_3 u,$$

(1)

where $x = (x_1, ..., x_4)$ is the state vector, L_i, C_i, r_i and E are known parameters, and P is the CPL's power.[1] Then, the control objective is stated next.
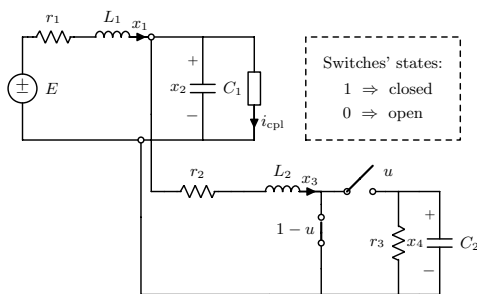
Figure 1: Schematic diagram of the network under consideration.

---

[1]The meaning of these variables can be inferred from Fig. 1.

Objective: *Stabilize the load voltage x_2 around a constant value without measuring the source current x_1 nor knowing the CPL's power P.*

2 Main Results

Proposition 1 *Fix a constant desired voltage $\bar{x}_2 > 0$ and define the output $y = x_2 - \bar{x}_2$. Then, there exists a static-feedback $u = \frac{1}{x_4} \Gamma(x, P, \lambda)$ s.t., along trajectories of* (1)*, the output verifies*

$$\ddot{y} + \lambda_1 \dot{y} + \lambda_2 y = 0, \tag{2}$$

ensuring $\lim_{t \to \infty} y(t) = 0$, exp., if $\lambda_1, \lambda_2 > 0$. Moreover, the equilibrium point $\bar{x}$ is locally exponentially stable.

The above control law, which is obtained from an input-output linearization scheme, depends on the full state vector x—particularly of the immeasurable state x_1—and on the unknown parameter P. To comply with the control objective, we propose next an observer/estimator for x_1 and P.

Proposition 2 *Let $z := (\hat{x}_1(t), \hat{P}(t))$ denote the estimate of the pair (x_1, P) and assume that $x_2^{\min} \leq x_2(t) \leq x_2^{\max} \ \forall t \geq 0$. Then, there exist mappings $\rho : \mathbb{R}^4 \to \mathbb{R}^2$, $\mathscr{F} : \mathbb{R}^4 \times \mathbb{R}^2 \to \mathbb{R}^2$ for which the dynamics*

$$\dot{z} = (\nabla \rho(x))^\top [f(x) + g(x)u] + \mathscr{F}(x, z) \tag{3}$$

is linear in z, independent of u, x_1 and P, and attains $\lim_{t \to \infty} z = (x_1, P)$.[2]

The construction of the mappings ρ and $\mathscr{F}$ is based on the theory of Immersion and Invariance [2]. By plugging the observer/estimate z into the control law (2)—rendering the latter, adaptive—then asymptotic stability can be concluded for the overall network, in satisfaction of the stated objective.

References

[1] J. E. Machado, R. Ortega, A. Astolfi, J. Arocas-Pérez, A. Pyrkin, A. Bobtsov, and R. Griñó, "Active Damping of a DC Network with a Constant Power Load: An Adaptive Observer-based Design," *Proceedings of the European Control Conference (ECC'19)*, Naples, Italy, June 25-28, 2019.

[2] A. Astolfi, D. Karagiannis, and R. Ortega, *Nonlinear and adaptive control with applications*, Springer Science & Business Media, 2007.

---

[2]We use $\dot{x} = f(x) + g(x)u$ to represent the dynamics (1).

Real-Time Inverse Dynamics Learning for Feedforward Control using Gaussian Process Regression

W. van Dijk, W.B.J. Hakvoort, B. Rosic

Department of Mechanics of Solids, Surfaces, and Systems (MS3), University of Twente

P.O. Box 217, 7500 AE Enschede, The Netherlands

{w.vandijk/w.b.j.hakvoort/b.rosic}@utwente.nl

1 Introduction

In the last decade, Gaussian process (GP) regression has found its way into the system identification of non-linear robot dynamics [1]. One particularly interesting variation of GP regression is the incremental sparse spectrum Gaussian process (I-SSGP) [2]. This fully data-driven, non-parametric regression method allows for a straightforward trade-off between computational speed and fitting performance. In this work, the I-SSGP algorithm is used for real-time inverse dynamics learning of a 1 degree-of-freedom (DoF) manipulator while simultaneously making predictions for feedforward control at a sample rate of 1 kHz.

2 I-SSGP

I-SSGP attempts to find a (non-linear) map between an input $\mathbf{x}$ and an output y. To this end, I-SSGP uses a low-rank approximation of the covariance function $K(\mathbf{x}_i, \mathbf{x}_j)$ using a spectral feature mapping $\phi(\mathbf{x})$ truncated at D features. This number of features allows for the trade-off between computational speed and fitting performance. Furthermore, incremental updates are used to obtain a fast algorithm that works well for sequentially arriving observations with sample rates beyond 1 kHz.

The data points $\{\mathbf{x}, y\}$ used for training the non-parametric model are the measured plant output θ (rad) and its time derivatives, and the plant input u (mA), such that $\{\mathbf{x}, y\} = \{[\theta, \dot{\theta}, \ddot{\theta}], u\}$.

The hyperparameters of this method consist of the signal variance σ_s^2, the noise variance σ_n^2, and the characteristic lengthscale of the squared exponential covariance function l. These hyperparameters are learned offline by optimizing the negative log marginal likelihood on a dataset containing measurements of the 1-DoF manipulator. D is selected based on the maximum allowed update time. The rest of the model is learned online while simultaneously making predictions.

3 Results

The I-SSGP model is capable of capturing the linear time-invariant plant dynamics and the non-linear cogging and gravity effects. Figure 1b shows a time plot of the tracking
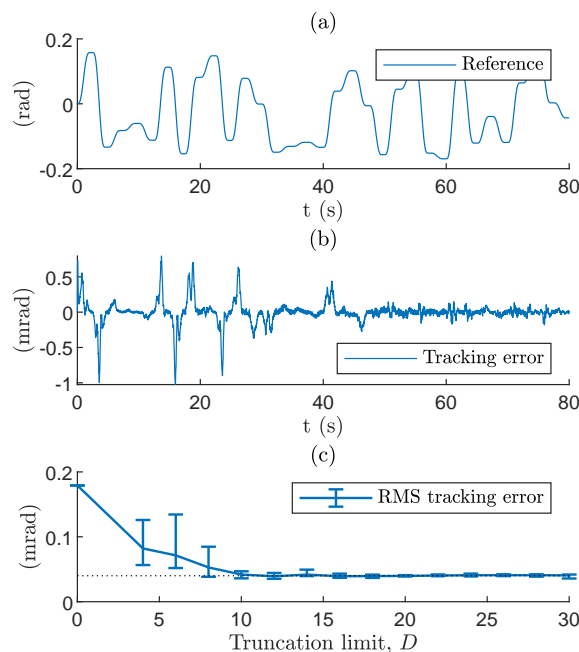
Figure 1: (a): Reference trajectory. (b): Tracking error; Feedforward ($D = 21$) is activated after 40 seconds. (c): Mean RMS tracking error as a function of D. The bars indicate the max. and min. values over 3 realisations of the feature mapping. $D = 0$ indicates no active feedforward.

error. After 40 seconds, the I-SSGP starts learning and predicting the feedforward signal. Within 10 seconds the tracking error is reduced. The remaining error is due to the actuator dynamics that cannot be described using a static map between the input $\mathbf{x}$ and output y. With as little as $D = 11$ spectral points, the I-SSGP feedforward is able to reduce the root mean square (RMS) tracking error with 74.7% (Figure 1c) and the maximum tracking error with 69.0% at sample rate of 1 kHz.

References

[1] C.K. Williams, C.E. Rasmussen, 2006. "Gaussian processes for machine learning", Cambridge, MIT press.

[2] A. Gijsberts, G. Metta, 2013. "Real-time model learning using incremental sparse spectrum gaussian process regression", Neural Networks, 41, (59-69).

Data-driven set invariance verification for black-box nonlinear systems

Zheming Wang[*]   Raphaël M. Jungers[*1]

zheming.wang@uclouvain.be   raphael.jungers@uclouvain.be

[*]ICTEAM Institute, UCLouvain, Louvain-la-Neuve, Belgium

Introduction

An invariant set of a dynamical system refers to a region where the trajectory will never leave once it enters. It is widely used in systems and control for stability analysis and control design. This work proposes a data-driven framework for computing invariant sets of black-box nonlinear systems without analytic dynamical models.

1 Preliminaries and Problem Formulation

We consider discrete-time dynamical systems of the form: $x(t+1) = f(x(t))$, $t \geq 0$, where $x(t) \in \mathbb{R}^n$ is the state vector. The system is subject to safety constraints: $x(t) \in X$, $t \geq 0$. Let us denote by $\phi(t, x_0)$ the solution of the system above with the initial condition x_0 at time $t = 0$. In this paper, we consider the case where we do not have access to the model, i.e., to f and we use the term *black-box* to refer to such systems. The definition of invariant sets for the nonlinear system is given as follows: a nonempty set $Z \subseteq X$ is a (positively) invariant set if and only if $x \in Z$ implies $f(x) \in Z$. The maximal invariant set can be constructed recursively by the following iteration: $O_0 := X, O_{k+1} := O_k \bigcap \{x \in \mathbb{R}^n : f(x) \in O_k\}, k \geq 0$. With these iterates, it can be verified that $X = O_0 \supseteq O_1 \supseteq \cdots \supseteq O_k \supseteq O_{k+1} \supseteq \cdots \supseteq O_\infty$. When an analytic model f is available, many algorithms have been proposed for computing invariant sets or their approximations. However, in black-box systems, these computations are no longer feasible, since the function f is unknown. In this paper, we provide a probabilistic verification for set invariance by observing trajectories of the system.

2 Data-driven set invariance verification

Without any dynamical model, we attempt to verify set invariance by observing N trajectories that are generated from N different initial conditions in X. Consider a probability measure $\mathbb{P}$ over X, these initial conditions, denoted by $\omega_N = \{x_1, x_2, \cdots, x_N\}$, are sampled randomly from the set X according to $\mathbb{P}$. For each initial condition $x \in \omega_N$, we will generate a trajectory $\{x, \phi(1, x), \cdots, \phi(T, x)\}$ by letting the system propagate for a sufficiently long time T. With only a finite set of observations, it is unrealistic to pursue an exact invariant set. Instead, we will discuss sets that are almost invariant except on an arbitrarily small subset. We refer to such a set as an almost-invariant set, which is defined as follows: for any $\varepsilon \in [0,1]$, the set $Z \in \mathscr{F}$ is an ε almost-invariant set if $\mathbb{P}(\{x \in Z : f(x) \notin Z\}) \leq \varepsilon$. Given the initial states ω_N, the following problem is defined

$$\mathscr{P}^*(\omega_N): \quad t^*(\omega_N) := \max_{x \in \omega_N} t^*(x) \tag{1}$$

where $t^*(x) := \min_{t \in \mathbb{Z}^+} t : \phi(t, x) \notin X$, and $t^*(x) = 0$ when $\phi(t, x) \in X$ for all $t \geq 0$. The following result can be derived: for a given $\varepsilon \in (0, 1]$,

$$\mathbb{P}^N(\mathbb{P}(O_{t^*(\omega_N)} \setminus O_{t^*(\omega_N)+1}) \geq \varepsilon) \leq \frac{1}{\varepsilon}\frac{1}{N+1}. \tag{2}$$

This result suggests that $O_{t^*(\omega_N)}$ is an ε almost-invariant set with probability no smaller than $1 - \frac{1}{\varepsilon}\frac{1}{N+1}$.

3 Numerical experiment

We consider a 2-dimensional nonlinear system with the state constraint set is given by $X := \{x : |x_1| \leq 1, |x_2| \leq 1\}$. Let the confidence level to be 0.05 and $\varepsilon = 10^{-3}$. The number of sampled initial states can be obtained from the bound above and it is 2×10^4 for the given tolerance and confidence level. The solution of $\mathscr{P}^*(\omega_N)$ is $t^*(\omega_N) = 3$. The value of $t^*(x)$ for $x \in \omega_N$ is shown in Figure 1.
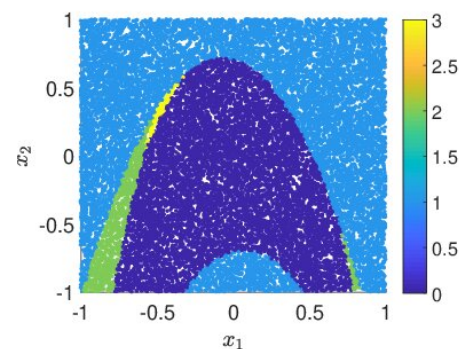
Figure 1: The plot of $t^*(x)$ for the sampled initial states.

References

[1] Z. Wang and R. M. Jungers. Data-driven computation of invariant sets of discrete time-invariant black-box systems. *arXiv preprint arXiv:1907.12075*, 2019.

Tensor-based methods for large-scale sensor fusion and Gaussian process regression

Clara Menzen
DCSC - TU Delft
c.m.menzen@tudelft.nl

dr. Manon Kok
DCSC - TU Delft
m.kok-1@tudelft.nl

dr.ir. Kim Batselier
DCSC - TU Delft
k.batselier@tudelft.nl

1 Introduction

The vast amounts of data that is nowadays available open up for exciting applications but also result in challenges concerning the computational complexity for processing this data. Two promising fields or methods for the modeling of dynamical systems from data are sensor fusion and Gaussian process regression. In sensor fusion, sensory data from distinct sources can be used for inference in dynamical systems and Gaussian process regression is a method to learn models from data. Applications of these fields are system identification, indoor localization, human motion estimation, just to name a few. However, these methods are limited by computational complexity and therefore cannot be performed with truly large-scale datasets. To tackle this problem, tensor methods shall be used to cope with the curse of dimensionality in large-scale.

2 Computational complexity in sensor fusion and Gaussian process regression

Gaussian processes are stochastic processes, meaning a generalization of a probability distribution, that are used for classification and regression of data [2]. A Gaussian process is fully defined by a mean $m(\mathbf{x})$ and a covariance function $k(\mathbf{x}, \mathbf{x}')$:

$$f(\mathbf{x}) \sim \mathscr{GP}\left(m(\mathbf{x}), k\left(\mathbf{x}, \mathbf{x}'\right)\right) \tag{1}$$

The covariance function computes a covariance matrix K which is the size of the number of data points. Part of computing the key predictive equations for Gaussian process regression, is inverting matrix K as shown in the equation below.

$$cov(\mathbf{f}_*) = K(X_*, X_*) - K(X_*, X)\left[K(X, X) + \sigma_n^2 I\right]^{-1} K(X, X_*) \tag{2}$$

Since the inverse scales cubically with the number of data points, the computational complexity increases considerably with the number of data points.

A similar problem is encountered in sensor fusion. In order to retrieve the information from the sensors, a nonlinear least squares problem needs to be solved. This requires again the computation of the inverse of a matrix which can become very large and thus requires a lot of computational complexity. It becomes clear that the size of the data set needs to have an upper bound. However, in many cases the amount of the data that is desired to be analysed, is higher than this upper bound. That is the reason why an approach to handle large data sets without making the computational effort unfeasible is needed.

3 Tensor-based methods

Tensors are multidimensional arrays or a generalization of matrices to order N. They allow to store and organize a large amount of data. Figure 1 shows a representation of tensors of different orders. A tensor of order 0 is a scalar, a tensor of order 1 is a vector and a tensor of order 2 is a matrix. The total number of 'legs' under the circles represent the order of the tensor.
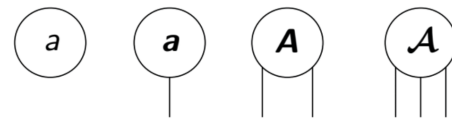
Figure 1: Tensor representation of order 0,1,2 and 3

A way to make it more efficient to work with tensors is by using tensor decompositions. The idea is to approximate the original tensor as a sequence of simpler tensors that are interconnected between each other. Like this tensor decompositions make it possible to considerably reduce the storage and therefore the computational complexity [1]. With the use of tensor decompositions in sensor fusion and Gaussian process regression, a large amount of data can be handled.

As a result, this new approach allows to develop approximation methods for large data sets without the need for supercomputers and without compromising the precision of the results.

References

[1]   Tamara G. Kolda and Brett W. Bader. Tensor decompositions and applications. *SIAM REVIEW*, 51(3):455–500, 2009.

[2]   Carl Edward Rasmussen. Gaussian processes for machine learning. MIT Press, 2006.

Imitation Learning for Autonomous Vehicle Driving using Constrained Policy Networks and B-Spline Parametrization

Flavia Sofia Acerbo, Herman Van der Auweraer, Tong Duy Son
Siemens Digital Industries Software, 3001 Leuven, Belgium
Email: flavia.acerbo@siemens.com

1 Introduction

Autonomous vehicle driving systems face the challenge of providing safe, feasible and human-like driving policy quickly and efficiently. This work presents a combined approach of machine learning-based and model-based control into an imitation learning framework that mimic expert driving behavior while obtaining safe and smooth driving. In this sense, the inputs to the proposed policy network are representative features coming from processed sensor data and the outputs are the reference trajectories, which are tracked by traditional feedback control.

2 Spline-Constrained Policy Network

The novelty of the policy network lies in the combination of constraints in its training loss and parametrization of the predicted trajectory.

2.1 Constrained Training Loss
The pure imitation loss does not incorporate any information about safety, and in case the vehicle is near the boundaries of the constraints, the policy network may violate them. To overcome this issue, we add constraints in the form of barrier functions to the training loss function of the network.

2.2 B-spline parametrization
To be comparable with expert performance, the output trajectory of the policy network should be guaranteed to be smooth and safe. For this reason, the outputs of the policy network have been chosen to be the coefficients of a spline written in B-form, instead of just waypoints.

Combining B-splines and constrained loss, we can obtain a policy network providing safe and smooth trajectories with computational efficiency both in training and deployment. The barrier functions limit the output values, i.e. the spline coefficients, and, thanks to the convex hull property, the overall trajectory will be contained inside the safe area.

3 Lane Keeping Simulation

In order to test the validity of the spline-constrained policy network, we implemented a lane keeping scenario in a simulated environment. In this scenario, we performed the DAgger algorithm [1] using a a 15DOF high-fidelity model implemented in Simcenter Amesim, realistic sensor data modelled in Simcenter Prescan, a NMPC expert implemented in CasADi and a simple PID decoupled control.

The planner can be a shallow fully-connected network. The parametrization of the planned trajectory improve the prediction characteristics in terms of smoothness and scalability for longer horizons. This choice may show more improvements on the computational efficiency of the training phase for larger datasets. The results also show that the convergence speed of the learner during online training can be enhanced by the use of constraints in the training loss, incorporating the task objectives in advance.
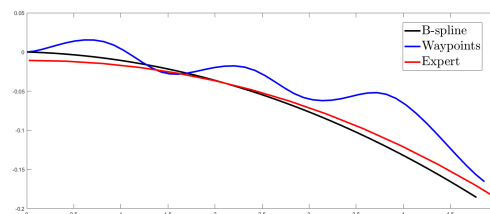
Figure 1: Comparison between different choices of the policy outputs: the parametrization of the trajectory guarantees a behaviour closer to the expert one.
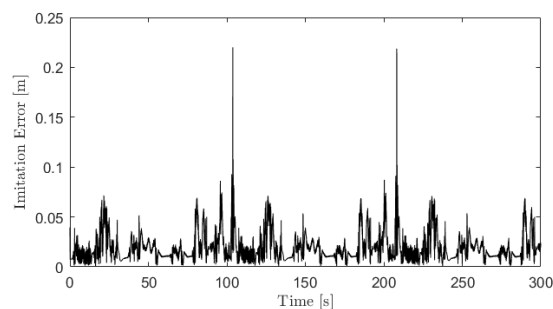
Figure 2: Euclidian distance between expert (NMPC) and policy network planned trajectories at the 2nd DAgger rollout. The car never violates the road boundaries constraints and the imitation error is almost always under 10 cm.

References

[1] Ross S. and Gordon G. and Bagnell D., 'A reduction of imitation learning and structured prediction to no-regret online learning'

Part 3

Plenary Lectures

Learning nonlinear dynamics using sequential Monte Carlo

Part 1 – Background and SMC introduction

Thomas Schön, Uppsala University

2020-03-10

Aim of this mini-course

Aim: To provide an introduction to sequential Monte Carlo (SMC) methods and their use in nonlinear system identification.

After the mini-course you should be able to derive your own SMC-based algorithms allowing you to do inference in nonlinear models.

Ex) Indoor positioning (engineering)

Aim: Compute the **position** of a person moving around indoors using variations in the ambient magnetic field and the motion of the person (acceleration and angular velocities). All of this observed using sensors in a standard smartphone.

Ex) Indoor positioning (engineering)

Key ingredients of the solution:

1. The **particle filter** for computing the position

2. The **Gaussian process** for building and representing the map of the ambient magnetic field

3. **Inertial sensor** signal processing

Movie – map making: www.youtube.com/watch?v=enlMiUqPVJo

Movie – indoor positioning result

Arno Solin, Simo Särkkä, Juho Kannala and Esa Rahtu. **Terrain navigation in the magnetic landscape: Particle filtering for indoor positioning**. *Proc. of the European Navigation Conf. (ENC)*, Helsinki, Finland, June, 2016.

Arno Solin, Manon Kok, Niklas Wahlström, TS and Simo Särkkä. **Modeling and interpolation of the ambient magnetic field by Gaussian processes**. *IEEE Trans. on Robotics* 34(4):1112–1127, 2018

Carl Jidling, Niklas Wahlström, Adrian Wills and TS. **Linearly constrained Gaussian processes**. *Advances in Neural Information Processing Systems (NIPS)*, Long Beach, CA, USA, December, 2017.

Ex) Epidemiological modelling (statistics)

Aim: To learn a model explaining the seasonal influenza epidemics and then make use of this model to compute predictions.

Susceptible/infected/recovered (SIR) model:

$$S_{t+dt} = S_t + \mu \mathcal{P} dt - \mu S_t dt - (1 + F v_t)\beta_t S_t \mathcal{P}^{-1} I_t dt,$$
$$I_{t+dt} = I_t - (\gamma + \mu) I_t dt + (1 + F v_t)\beta_t S_t \mathcal{P}^{-1} I_t dt,$$
$$R_{t+dt} = R_t + \gamma I_t dt - \mu R_t dt,$$
$$\beta_t = R_0(\gamma + \mu)(1 + \alpha \sin(2\pi t/12)),$$

Measurements:

$$y_k = \rho \mathrm{logit}(\bar{I}_k/\mathcal{P}) + e_k, \qquad e_k \sim \mathcal{N}(0, \sigma^2).$$

Information about the unknown parameters $\theta = (\gamma, R_0, \alpha, F, \rho, \sigma)$ and states $x_t = (S_t, I_t, R_t)$ has to be learned from measurements.

4/49

Ex) Epidemiological modelling (statistics)

Compute $p(\theta, x_{1:T} \mid y_{1:T})$, where $y_{1:T} = (y_1, y_2, \ldots, y_T)$ and use it to compute the predictive distribution.
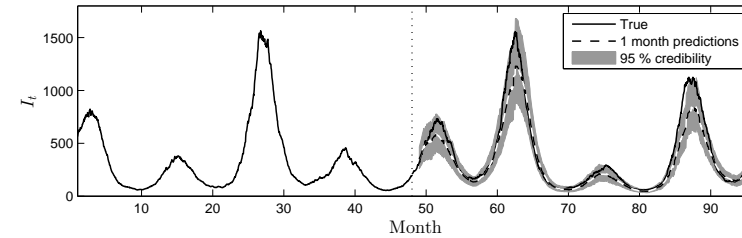
Disease activity (number of infected individuals I_t) over an eight year period.

Fredrik Lindsten, Michael I. Jordan and TS. **Particle Gibbs with ancestor sampling**. *Journal of Machine Learning Research (JMLR)*, 15:2145-2184, June 2014.

5/49

Ex) Probabilistic programming (machine learning)

A **probabilistic programming language (PPL)** provides:

- support for declaring random variables,
- support for conditioning on the observed data,
- and automatic inference.

The memory state of a running probabilistic program evolves dynamically and stochastically in time and so is a **stochastic process**.

SMC is a common inference method for programmatic model.

Creates a clear **separation** between the model and the inference methods. Opens up for the automation of inference!

New conference: **ProbProg**.

```
x ~ Bernoulli(p);    assume(x)
if (x) {             value(x)
    y ~ N(0,1);      assume(y)
} else {
    y <- 0;
```

Lawrence Murray and Thomas B. Schön. **Automated learning with a probabilistic programming language: Birch**. *Annual Reviews in Control*, 46:29-43, 2018.

6/49

Mini-course structure

- **Part 1 – Probabilistic modelling and SMC derivation**
  - Probabilistic modelling and Monte Carlo introduction
  - Derive a first basic particle filter
- **Part 2 – Maximum likelihood system identification**
  - The particle filter as likelihood estimator
  - A new stochastic optimizer
- **Part 3 – Bayesian system identification**
  - Intuition behind MCMC
  - Using unbiased likelihood estimates within Metropolis Hastings

> The only way to really learn something is by **implementing it on your own**.

7/49

Outline – Part 1

> **Aim:** Introductory background on probabilistic modelling and deriving Sequential Monte Carlo (SMC).

Outline:

1. Course introduction
2. **Probabilistic modelling**
3. Nonlinear state space model (SSM)
4. Nonlinear filtering problem and its conceptual solution
5. Importance sampling
6. Bootstrap particle filter

Probabilistic modelling

Modelling

Mathematical model: A compact representation—set of assumptions—of the data that in precise mathematical form captures the key properties of the underlying situation.

This mini-course is concerned with dynamical phenomena. The methods are more general than that and I will hint at this since we can broaden the scope significantly.

Dynamical phenomena produce temporal measurements (data) arriving as a **sequence**

$$y_{1:t} = (y_1, y_2, \ldots, y_t).$$

Nice introduction to probabilistic modelling in Machine Learning

Ghahramani, Z. **Probabilistic machine learning and artificial intelligence**. *Nature* 521:452-459, 2015.

Representing and modifying uncertainty

It is important to maintain a solid representation of uncertainty in all mathematical objects and throughout all calculations.
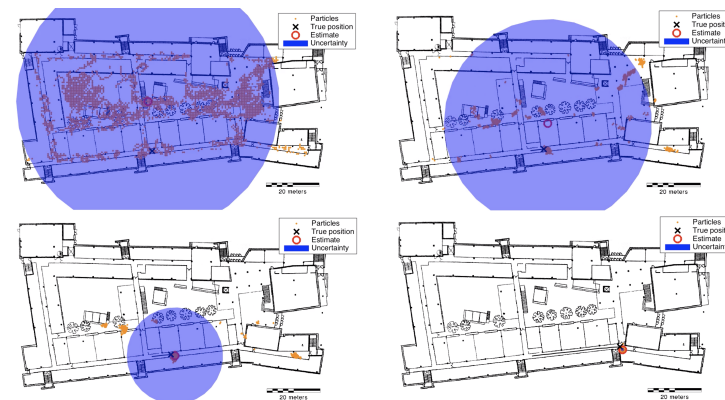
The two basic rules from probability theory

Let x and y be continuous random variables Let $p(\cdot)$ denote a general probability density function.

1. Marginalization (integrate out a variable): $p(x) = \int p(x, y) \mathrm{d}y$.

2. Conditional probability: $p(x, y) = p(x \mid y) p(y)$.

Combine them into Bayes' rule:

$$p(x \mid y) = \frac{p(y \mid x) p(x)}{p(y)} = \frac{p(y \mid x) p(x)}{\int p(y \mid x) p(x) \mathrm{d}x}.$$

Basic variables classes

Measurements $y_{1:T} = (y_1, y_2, \ldots, y_T)$: The measured data somehow obtained from the phenomenon we are interested in.

Unknown (static) model parameters θ: Describes the model, but unknown (or not known well enough) to the user.

Unknown model variables x_t (changing over time): Describes the state of the phenomenon at time t (in the indoor positioning example above x_t includes the unknown position).

Explanatory variables u: Known variables that we do not bother to model as stochastic.

A key task is often to learn θ and/or x_t based on the available measurements $y_{1:T}$.

Computational problems

The problem of learning a model based on data leads to computational challenges, both

- **Integration:** e.g. the high-dimensional integrals arising during marg. (averaging over all possible parameter values θ):

$$p(y_{1:T}) = \int p(y_{1:T} \mid \theta) p(\theta) \mathrm{d}\theta.$$

- **Optimization:** e.g. when extracting point estimates, for example by maximizing the posterior or the likelihood

$$\widehat{\theta} = \arg\max_{\theta} p(y_{1:T} \mid \theta)$$

Typically impossible to compute exactly, use approximate methods
- Monte Carlo (MC), Markov chain MC (MCMC), and sequential Monte Carlo (SMC).
- Variational inference (VI).

Latent variable model

Model variables that are not observed are called **latent** (a.k.a. hidden, missing and unobserved) variables.

The idea of introducing latent variables into models is probably one of the most **powerful concepts** in probabilistic modelling.

Latent variables provide **more expressive** models that can capture **hidden structures** in data that would otherwise not be possible.

Cost: Learning the model becomes (significantly) harder.

Markov chain

The Markov chain is a probabilistic model that is used for modelling a sequence of states $(x_0, x_1, \ldots, x_T)$.

Definition (Markov chain)

A stochastic process $\{x_t\}_{t \geq 0}$ is referred to as a Markov chain if, for every $k > 0$ and t,

$$p(x_{t+k} \mid x_0, x_1, \ldots, x_t) = p(x_{t+k} \mid x_t).$$

A **Markov chain** is completely specified by:

1. An initial value x_0 and
2. a transition model (kernel) $\kappa(x_{t+1} \mid x_t)$ describing the transition from state x_t to state x_{t+1}, according to $x_{t+1} \mid x_t \sim \kappa(x_{t+1} \mid x_t)$.

The **state** acts as a **memory** containing all information there is to know about the phenomenon at this point in time.

Markov chain

Our two most important applications of Markov chains in this course are:

1. The Markov model is used in the **state space model (SSM)** where we can only observe the state indirectly via a measurement that is related to the state.

2. The Markov chain constitutes the basic ingredient in the Markov chain Monte Carlo (MCMC) methods.

Nonlinear state space model

Nonlinear state space model (SSM)

The state space model (SSM) is a **Markov** chain that makes use of a **latent** variable representation to describe dynamical phenomena.

It consists of two stochastic processes:

1. unobserved (state) process $\{x_t\}_{t \geq 0}$ modelling the dynamics,
2. observed process $\{y_t\}_{t \geq 1}$ modelling the measurements and their relationship to the unobserved state process.

$$x_t = f(x_{t-1}, \theta) + v_t,$$
$$y_t = g(x_t, \theta) + e_t,$$

where $\theta \in \mathbb{R}^{n_\theta}$ denotes static model parameters.

Ex) "what are x_t, θ and y_t"?

Aim (motion capture): Compute x_t (position and orientation of the different body segments) of a person (θ describes the body shape) moving around indoors using measurements y_t (accelerometers, gyroscopes and ultrawideband).

Show movie!

Manon Kok, Jeroen D. Hol and TS. **Using inertial sensors for position and orientation estimation**, *Foundations and Trends of Signal Processing* 11(1-2):1-153, 2017.

18/49

Representing the SSM using distributions

Representation using probability distributions

$$x_t \mid x_{t-1}, \theta \sim p(x_t \mid x_{t-1}, \theta),$$
$$y_t \mid x_t, \theta \sim p(y_t \mid x_t, \theta),$$
$$x_0 \sim p(x_0 \mid \theta).$$

The unknown parameters can be modelled as either
1. deterministic but unknown (maximum likelihood) or
2. random variables (Bayesian), $\theta \sim p(\theta)$.

State inference: Learn the state from the observations.

Parameter inference: Learn the (static) parameters from the observations.

Notation: We will use $p(\cdot)$ to denote a probability density function of variables that in some way describes the model or can be induced from the model.

19/49

The nonlinear SSM is just a special case...

A **graphical model** is a probabilistic model where a graph $\mathcal{G} = (\mathcal{V}, \mathcal{E})$ represents the conditional independency structure between random variables,

1. a set of **vertices** $\mathcal{V}$ (nodes) represents the random variables
2. a set of **edges** $\mathcal{E}$ containing elements $(i, j) \in \mathcal{E}$ connecting a pair of nodes $(i, j) \in \mathcal{V}$
3. The arrows pointing to a certain node encodes which variables the corresponding node are conditioned upon.
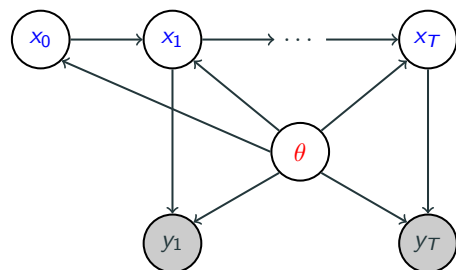
20/49

The nonlinear SSM is just a special case...

Representation using probabilistic program

```
x[1] ~ Gaussian(0.0, 1.0);              p(x₁)
y[1] ~ Gaussian(x[1], 1.0);            p(y₁ | x₁)
for (t in 2..T) {
    x[t] ~ Gaussian(a*x[t - 1], 1.0);   p(xₜ | xₜ₋₁)
    y[t] ~ Gaussian(x[t], 1.0);         p(yₜ | xₜ)
}
```

A **probabilistic program** encodes a **probabilistic model** (here an LG-SSM) according to the semantics of a particular probabilistic programming language (here Birch).

Lawrence Murray and TS. **Automated learning with a probabilistic programming language: Birch**, *Annual Reviews in Control*, 46:29-43, 2018.

21/49

SSM – full probabilistic model

The **full probabilistic model** is given by

$$p(x_{0:T}, \theta, y_{1:T}) = \underbrace{p(y_{1:T} \mid x_{0:T}, \theta)}_{\text{likelihood}} \underbrace{p(x_{0:T}, \theta)}_{\text{prior}}$$

Distribution describing a parametric nonlinear SSM

$$p(x_{0:T}, \theta, y_{1:T}) = \underbrace{\prod_{t=1}^{T} \underbrace{p(y_t \mid x_t, \theta)}_{\text{observation}}}_{\text{likelihood}} \underbrace{\prod_{t=1}^{T} \underbrace{p(x_t \mid x_{t-1}, \theta)}_{\text{dynamics}} \underbrace{p(x_0 \mid \theta)}_{\text{state}} \underbrace{p(\theta)}_{\text{param.}}}_{\text{prior}}$$

Model = probability distribution!

Nonlinear filtering problem

State inference

State inference refers to the problem of learning about the state $x_{k:l}$ based on the available measurements $y_{1:t} = y_{1:t}$.

We will represent this information using **PDFs**.

Name	Probability density function
Filtering	$\mathbf{p(x_t \mid y_{1:t})}$
Joint filtering	$p(x_{0:t} \mid y_{1:t}), t = 1, 2, \ldots$
Prediction	$p(x_{t+1} \mid y_{1:t})$
Joint smoothing	$p(x_{1:T} \mid y_{1:T})$
Marginal smoothing	$p(x_t \mid y_{1:T}),\ t \leq T$

The nonlinear filtering problem

State filtering problem: Learn about the current state x_t based on the available measurements $y_{1:t} = y_{1:t}$ when

$$x_t \mid x_{t-1} \sim p(x_t \mid x_{t-1}), \qquad x_t = f(x_{t-1}) + v_t,$$
$$y_t \mid x_t \sim p(y_t \mid x_t), \qquad y_t = g(x_t) + e_t,$$
$$x_0 \sim p(x_0). \qquad x_0 \sim p(x_0).$$

Strategy: Compute the filter PDF $p(x_t \mid y_{1:t})$ as accurately as possible.

Filtering problem – conceptual solution

The **measurement update**

$$p(x_t \mid y_{1:t}) = \frac{\overbrace{p(y_t \mid x_t)}^{\text{measurement}} \overbrace{p(x_t \mid y_{1:t-1})}^{\text{prediction pdf}}}{p(y_t \mid y_{1:t-1})},$$

and the **time update**

$$p(x_t \mid y_{1:t-1}) = \int \underbrace{p(x_t \mid x_{t-1})}_{\text{dynamics}} \underbrace{p(x_{t-1} \mid y_{1:t-1})}_{\text{filtering pdf}} dx_{t-1}.$$

Alternatively we can of course combine the two

$$p(x_t \mid y_{1:t}) = \frac{p(y_t \mid x_t) \int p(x_t \mid x_{t-1}) p(x_{t-1} \mid y_{1:t-1}) dx_{t-1}}{p(y_t \mid y_{1:t-1})}.$$

No closed-form solutions available except for a few special cases.

Importance sampling

The Monte Carlo idea (I/II)

Let $x \sim \pi(x)$, where we refer to $\pi(x)$ as the **target density**.

(Very) restrictive assumption: Assume that we have N samples $\{x^i\}_{i=1}^N$ from the target density $\pi(x)$, making up an **empirical approximation**

$$\widehat{\pi}^N(x) = \sum_{i=1}^N \frac{1}{N} \delta_{x^i}(x).$$

Allows for the following approximation of the integral,

$$\mathbb{E}_\pi[\varphi(x)] = \int \varphi(x)\pi(x)dx \approx \int \varphi(x) \sum_{i=1}^N \frac{1}{N} \delta_{x^i}(x)dx = \frac{1}{N}\sum_{i=1}^N \varphi(x^i)$$

$$ "\int + \delta \to \sum" $$

The Monte Carlo idea (II/II)

The integral

$$I(\varphi) = \mathbb{E}_\pi[\varphi(x)] = \int \varphi(x)\pi(x)dx$$

is approximated by

$$\widehat{I}_N(\varphi) = \frac{1}{N}\sum_{i=1}^N \varphi(x^i).$$

The strong law of large numbers tells us that

$$\widehat{I}_N(\varphi) \xrightarrow{\text{a.s.}} I(\varphi), \qquad N \to \infty,$$

and the central limit theorem states that

$$\frac{\sqrt{N}\left(\widehat{I}_N(\varphi) - I(\varphi)\right)}{\sigma_\varphi} \xrightarrow{\text{d}} \mathcal{N}(0,1), \qquad N \to \infty.$$

The Monte Carlo idea – toy illustration

$$\pi(x) = 0.3\mathcal{N}(x \,|\, 2, 2) + 0.7\mathcal{N}(x \,|\, 9, 19)$$

5 000 samples

50 000 samples
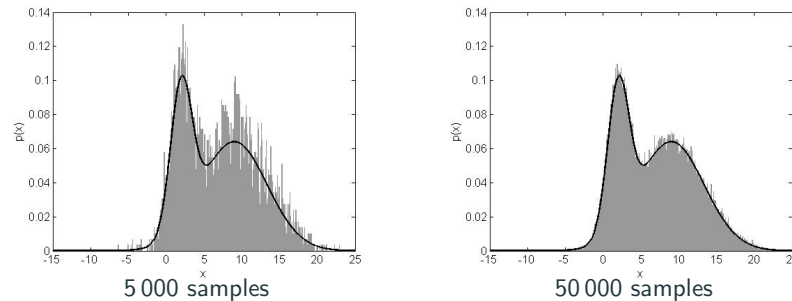
Obvious problem: In general we are **not** able to directly sample from the density we are interested in.

Importance sampling – basic idea

Importance sampling can be used to evaluate integrals of the form

$$I(\varphi) = \mathbb{E}_\pi[\varphi(x)] = \int \varphi(x)\pi(x)\mathrm{d}x$$

without requiring exact samples from the target.

We start by noting that

$$\int \varphi(x)\pi(x)\mathrm{d}x = \int \varphi(x)\underbrace{\frac{\pi(x)}{q(x)}}_{=w(x)}q(x)\mathrm{d}x,$$

where $q(x)$ is referred to as the **proposal distribution** and $w(x) = \pi(x)/q(x)$ is the **weight function**.

Hence, we can write

$$\int \varphi(x)\pi(x)\mathrm{d}x = \int \varphi(x)w(x)q(x)\mathrm{d}x.$$

Importance sampling – proposal distribution

The **proposal distribution** is chosen by the user:

1. It should be simple to sample from and
2. we require $q(x) > 0$ for all x where $\pi(x) > 0$

Idea: Chose the **proposal** density $q(x)$ such that it is easy to generate samples from it and somehow **compensate** for the mismatch between the target and the proposal.

Importance sampling – proposal distribution

By construction it is easy to sample from the proposal distribution $q(x)$ and an MC estimator of $\mathbb{E}_\pi[\varphi(x)]$ is:

1. Sample $x^i \sim q(x)$ for $i = 1, \ldots, N$.
2. Compute $w(x^i) = w^i = \pi(x^i)/q(x^i)$ for $i = 1, \ldots, N$.

The resulting estimator is

$$\widehat{I}^N(\varphi) = \frac{1}{N}\sum_{i=1}^{N} w^i \varphi(x^i),$$

where the importance weights properly accounts for the discrepancy between the proposal and the target.

Point-wise evaluation of the target

It is often the case that the target density $\pi(x)$ can only be evaluated up to an unknown normalization constant Z,

$$\pi(x) = \frac{\widetilde{\pi}(x)}{Z}$$

where $\widetilde{\pi}(x)$ can be evaluated for any x, but the constant Z is unknown.

Ex. (**nonlinear joint filtering problem**) The target density is given by $\pi(x) = p(x_{0:t} \,|\, y_{1:t})$ and we have

$$\underbrace{p(x_{0:t} \,|\, y_{1:t})}_{\pi(x)} = \frac{\overbrace{p(x_{0:t}, y_{1:t})}^{\widetilde{\pi}(x)}}{\underbrace{p(y_{1:t})}_{Z}},$$

where we can evaluate $\widetilde{\pi}(x) = p(x_{0:t}, y_{1:t})$ point-wise, but $Z = p(y_{1:t})$ is intractable in general.

Self-normalized importance sampling

Self-normalized importance sampling

Inserting

$$\pi(x) = \frac{\widetilde{\pi}(x)}{Z}$$

into the importance sampling integral results in

$$I(\varphi) = \mathbb{E}[\varphi(x)] = \int \varphi(x) \frac{\widetilde{\pi}(x)}{Z q(x)} q(x) \mathrm{d}x = \frac{1}{Z} \int \varphi(z) \underbrace{\frac{\widetilde{\pi}(x)}{q(x)}}_{=\omega(x)} q(x) \mathrm{d}x$$

Hence, the importance sampling estimator is

$$\widetilde{I}^N(\varphi) = \frac{1}{NZ} \sum_{i=1}^{N} \widetilde{w}^i \varphi(x^i),$$

where $\widetilde{w}^i = \omega(x^i)$.

> The normalization constant Z is still problematic.

Self-normalized importance sampling

The normalization constant is given by the following integral

$$Z = \int \widetilde{\pi}(x) \mathrm{d}x,$$

which we can approximate using our samples $\{x^i\}_{i=1}^{N}$ from $q(x)$. The result is

$$Z = \int \frac{\widetilde{\pi}(x)}{q(x)} q(x) \mathrm{d}x \approx \frac{1}{N} \sum_{i=1}^{N} \widetilde{w}^i.$$

The **self-normalized** importance sampling estimate is obtained by inserting this into $\widetilde{I}^N(\varphi)$,

$$\widetilde{I}^N(\varphi) = \sum_{i=1}^{N} w^i \varphi(x^i), \qquad w^i = \frac{\widetilde{w}^i}{\sum_{j=1}^{N} \widetilde{w}^j}$$

Self-normalized importance sampling

Algorithm 1 Importance sampler
---
1. Sample $x^i \sim q(x)$.
2. Compute the weights $\widetilde{w}^i = \widetilde{\pi}(x^i)/q(x^i)$.
3. Normalize the weights $w^i = \widetilde{w}^i / \sum_{j=1}^{N} \widetilde{w}^j$.

Each step is carried out for $i = 1, \ldots, N$.

The convergence of the resulting approximation $\widehat{\pi}^N(x) = \sum_{i=1}^{N} w^i \delta_{x^i}(x)$ is since long well established.

> The fact that we are sampling from a user-chosen proposal distribution $q(x)$ is corrected for by the weights, which **accounts for the discrepancy** between the proposal $q(x)$ and the target $\pi(x)$.

Bootstrap particle filter

The importance of a good proposal density
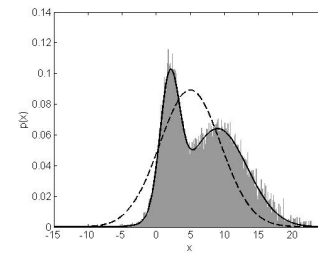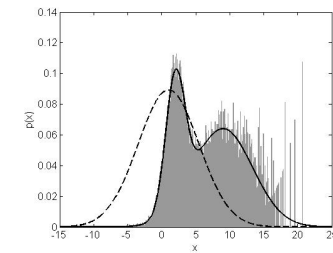
$q_1(x) = \mathcal{N}(x \mid 5, 20)$ (dashed) $q_2(x) = \mathcal{N}(x \mid 1, 20)$ (dashed)

50 000 samples were used in both simulations.

Lesson learned: It is important to be careful in selecting the proposal distribution.

Recall the nonlinear filtering problem

Recall that the nonlinear filtering problem amounts to computing the filter PDF $p(x_t \mid y_{1:t})$ when the model is given by

$$x_{t+1} \mid x_t \sim p(x_{t+1} \mid x_t),$$
$$y_t \mid x_t \sim p(y_t \mid x_t),$$
$$x_0 \sim p(x_0).$$

We have shown that the solution is

$$p(x_t \mid y_{1:t}) = \frac{p(y_t \mid x_t)p(x_t \mid y_{1:t-1})}{p(y_t \mid y_{1:t-1})},$$

$$p(x_t \mid y_{1:t-1}) = \int p(x_t \mid x_{t-1})p(x_{t-1} \mid y_{1:t-1}) \mathrm{d}x_{t-1}.$$

> **Basic idea:** Try to approximate $p(x_t \mid y_{1:t})$ sequentially in time $t = 0, 1, \ldots$ using importance sampling!

Particle filter – representation

The need for approximate methods (such as SMC) is tightly coupled to the intractability of the integrals above.

> SMC provide approximate solutions to **integration** problems where there is a **sequential structure** present.

The **particle filter** approximates $p(x_t \mid y_{1:t})$ by maintaining an **empirical distribution** made up of N samples (particles) $\{x_t^i\}_{i=1}^N$ and the corresponding weights $\{w_t^i\}_{i=1}^N$

$$\underbrace{\widehat{p}(x_t \mid y_{1:t})}_{\widehat{\pi}(x_t)} = \sum_{i=1}^N \frac{w_t^i}{\sum_{l=1}^N w_t^l} \delta_{x_t^i}(x_t).$$

Particle filter – derivation

Assume in an induction-like fashion that we at time $t-1$ have

$$\widehat{p}(x_{t-1} \mid y_{1:t-1}) = \sum_{i=1}^N w_{t-1}^i \delta_{x_{t-1}^i}(x_{t-1}).$$

Insert this approximation into the time-update integral

$$\widehat{p}(x_t \mid y_{1:t-1}) = \int p(x_t \mid x_{t-1}) \sum_{i=1}^N w_{t-1}^i \delta_{x_{t-1}^i}(x_{t-1}) dx_{t-1}$$

$$= \sum_{i=1}^N w_{t-1}^i p(x_t \mid x_{t-1}^i).$$

This is a mixture distribution with one mixture component for each of the N particles.

Particle filter – derivation

The measurement update results in

$$p(x_t \mid y_{1:t}) \approx \frac{p(y_t \mid x_t)}{p(y_t \mid y_{1:t-1})} \sum_{i=1}^N w_{t-1}^i p(x_t \mid x_{t-1}^i)$$

This suggests that we can target $p(x_t \mid y_{1:t})$ using an importance sampler!

Guided by the above expression we choose a mixture as proposal

$$q(x_t \mid y_{1:t}) = \sum_{i=1}^N \nu_{t-1}^i q(x_t \mid x_{t-1}^i, y_t),$$

where the weights ν_{t-1}^i and the mixture components $q(x_t \mid x_{t-1}^i, y_t)$ are both user design choices.

Sampling from the proposal

We sample from the proposal

$$q(x_t \mid y_{1:t}) = \sum_{i=1}^N \nu_{t-1}^i q(x_t \mid x_{t-1}^i, y_t)$$

using a two step procedure:

1. Select one of the components

$$a_t^i \sim \mathcal{C}(\{\nu_{t-1}^j\}_{j=1}^N) \qquad \text{(categorical distribution)}$$

2. Generate a sample from the selected component,

$$x_t^i \sim q(x_t \mid x_{t-1}^{a_t^i}, y_t)$$

Repeat this N times, for $i = 1, \ldots, N$.

Selecting the mixture components – resampling

The particle $\bar{x}^i_{t-1} = x^{a^i_t}_{t-1}$ is referred to as the **ancestor** of x^i_t, since x^i_t is generated conditionally on $\bar{x}^i_{t-1}$.

The variable $a^i_t \in \{1, \ldots, N\}$ is referred to as the **ancestor index**, since it indexes the ancestor of particle x^i_t at time $t-1$.

Sampling the N ancestor indices

$$a^i_t \sim \mathcal{C}(\{\nu^j_{t-1}\}^N_{j=1}), \qquad i = 1, \ldots, N$$

is referred to as **resampling**.

Resampling generates a new set of particles $\{\bar{x}^i_{t-1}\}^N_{i=1}$ by **sampling with replacement** from among $\{x^j_{t-1}\}^N_{j=1}$, according to some weights $\{\nu^j_{t-1}\}^N_{j=1}$.

Next step – computing the weights

Algorithm 2 Importance sampler

1. Sample $x^i \sim q(x)$.
2. **Compute the weights** $\widetilde{w}^i = \widetilde{\pi}(x^i)/q(x^i)$.
3. Normalize the weights $w^i = \widetilde{w}^i / \sum^N_{j=1} \widetilde{w}^j$.

Each step is carried out for $i = 1, \ldots, N$.

Compute the weights

$$\widetilde{w}^i_t = \widetilde{w}_t(x^i_t) = \frac{\widetilde{\pi}(x^i_t)}{q(x^i_t)} = \frac{p(y_t \mid x^i_t) \sum^N_{j=1} w^j_{t-1} p(x^i_t \mid x^j_{t-1})}{\sum^N_{j=1} \nu^j_{t-1} q(x^i_t \mid x^j_{t-1}, y_t)}$$

> Problem: The computational complexity is $\mathcal{O}(N^2)$!

A first pragmatic solution

By using the following proposal distribution

$$q(x_t \mid y_{1:t}) = \widehat{p}(x_t \mid y_{1:t-1}) = \sum^N_{j=1} w^j_{t-1} p(x_t \mid x^j_{t-1}),$$

the resulting weight computation becomes

$$\widetilde{w}^i_t = p(y_t \mid x^i_t),$$

resulting in a linear computational complexity!

Result – A first particle filter

Algorithm 3 Bootstrap particle filter (for $i = 1, \ldots, N$)

1. **Initialization ($t = 0$):**
   (a) Sample $x^i_0 \sim p(x_0)$.
   (b) Set initial weights: $w^i_0 = 1/N$.
2. **for $t = 1$ to T do**
   (a) **Resample:** sample ancestor indices $a^i_t \sim \mathcal{C}(\{w^j_{t-1}\}^N_{j=1})$.
   (b) **Propagate:** sample $x^i_t \sim p(x_t \mid x^{a^i_t}_{t-1})$.
   (c) **Weight:** compute $\widetilde{w}^i_t = p(y_t \mid x^i_t)$ and normalize $w^i_t = \widetilde{w}^i_t / \sum^N_{j=1} \widetilde{w}^j_t$.

SMC structure

Same structure for all SMC algorithms.

For the bootstrap PF, given $\{x_{t-1}^i, w_{t-1}^i\}_{i=1}^N$:

Resampling: $a_t^i \sim \mathcal{C}(\{w_{t-1}^j\}_{j=1}^N)$.

Propagation: $x_t^i \sim p(x_t \mid x_{t-1}^{a_t^i})$.

Weighting: $\widetilde{w}_t^i = p(y_t \mid x_t^i)$ and normalize.

The result is a new weighted set of particles $\{x_t^i, w_t^i\}_{i=1}^N$.

Use of random numbers in the particle filter

Random numbers are used to

1. **initialize**
2. **resample** and
3. **propagate**

the particles.

The weighting step does not require any new random numbers, it is just a function of already existing random numbers.

> We can reason about and make use of the **joint probability distribution of these random variables**, from which the particle filter **generates one realization each time it is executed**.

SMC convergence in one slide...

Let $\varphi : \mathcal{X} \mapsto \mathbb{R}$ be some test function of interest. The expectation

$$\mathbb{E}[\varphi(x_t) \mid y_{1:t}] = \int \varphi(x_t) p(x_t \mid y_{1:t}) \, dx_t,$$

can be estimated by the particle filter

$$\widehat{\varphi}_t^N \triangleq \sum_{i=1}^N w_t^i \varphi(x_t^i).$$

The **CLT** governing the convergence of this estimator states

$$\sqrt{N} \left(\widehat{\varphi}_t^N - \mathbb{E}[\varphi(x_t) \mid y_{1:t}] \right) \xrightarrow{\mathrm{d}} \mathcal{N}(0, \sigma_t^2(\varphi)).$$

The **likelihood estimate** $\widehat{p}_\theta(y_{1:t}) = \prod_{s=1}^t \left\{ \frac{1}{N} \sum_{i=1}^N \widetilde{w}_s^i \right\}$ from the PF is **unbiased**, $\mathbb{E}_{\psi_\theta}[\widehat{p}_\theta(y_{1:t})] = p_\theta(y_{1:t})$ for any value of N and there are **CLTs available** as well.

Short history of SMC

- Bootstrap particle filter invented around 1992–1993
- Auxiliary particle filter, 1999
- Convergence theory: many results in the early 2000 but still an active research area
- SMC Samplers, 2006 (similar ideas going back to at least 2002)
- Particle Markov chain Monte Carlo, around 2010
- SMC for PPL, graphical models, etc. 2010–present

UPPSALA
UNIVERSITET

Learning nonlinear dynamics using sequential Monte Carlo

Part 2 – Maximum likelihood system identification

Thomas Schön, Uppsala University

2020-03-10

Outline – Part 2

Aim: Show how SMC can be used in identifying nonlinear SSMs using maximum likelihood.

Outline:

1. The particle filter as likelihood estimator
2. Maximum likelihood estimation of state-space models
   a. Direct optimization
   b. Expectation maximization

Learning the states and the parameters

Based on our generative model, compute the **posterior distribution**

$$p(x_{0:T}, \theta \mid y_{1:T}) = \underbrace{p(x_{0:T} \mid \theta, y_{1:T})}_{\text{state inf.}} \underbrace{p(\theta \mid y_{1:T})}_{\text{param. inf.}}.$$

Bayesian formulation – model the unknown parameters as a random variable $\theta \sim p(\theta)$ and compute

$$p(\theta \mid y_{1:T}) = \frac{p(y_{1:T} \mid \theta)p(\theta)}{p(y_{1:T})}$$

Maximum likelihood formulation – model the unknown parameters as a deterministic variable and solve

$$\widehat{\theta} = \arg\max_{\theta \in \Theta} p(y_{1:T} \mid \theta).$$

Central object – the likelihood

The likelihood is computed by marginalizing

$$p(x_{0:T}, y_{1:T} \mid \theta) = p(x_0 \mid \theta) \prod_{t=1}^{T} p(y_t \mid x_t, \theta) \prod_{t=1}^{T} p(x_t \mid x_{t-1}, \theta),$$

w.r.t the state sequence $x_{0:T}$,

$$p(y_{1:T} \mid \theta) = \int p(x_{0:T}, y_{1:T} \mid \theta) dx_{0:T}.$$

(We are averaging $p(x_{0:T}, y_{1:T} \mid \theta)$ over all possible state sequences.)

Equivalently we have

$$p(y_{1:T} \mid \theta) = \prod_{t=1}^{T} p(y_t \mid y_{1:t-1}, \theta) = \prod_{t=1}^{T} \int p(y_t \mid x_t, \theta) \underbrace{p(x_t \mid y_{1:t-1}, \theta)}_{\text{key challenge}} dx_t.$$

TS, Fredrik Lindsten, Johan Dahlin, Johan Wagberg, Christian A. Naesseth, Andreas Svensson and Liang Dai. **Sequential Monte Carlo methods for system identification.** In *Proceedings of the 17th IFAC Symposium on System Identification (SYSID)*, Beijing, China, October 2015.

The particle filter as a likelihood estimator

$$p(y_{1:T} \mid \theta) = \prod_{t=1}^{T} p(y_t \mid y_{1:t-1}, \theta) = \prod_{t=1}^{T} \int p(y_t \mid x_t, \theta) \underbrace{p(x_t \mid y_{1:t-1}, \theta)}_{\overset{\text{bPF}}{\approx} \sum_{i=1}^{N} \frac{1}{N} \delta_{x_t^i}(x_t)} dx_t$$

$$\approx \prod_{t=1}^{T} \left(\frac{1}{N} \sum_{i=1}^{N} p(y_t \mid x_t^i, \theta) \right) = \prod_{t=1}^{T} \left(\frac{1}{N} \sum_{i=1}^{N} \widetilde{w}_t^i \right).$$

Hence, we have shown that

$$p(y_{1:T} \mid \theta) \approx \prod_{t=1}^{T} \left(\frac{1}{N} \sum_{i=1}^{N} \widetilde{w}_t^i \right)$$

($\widetilde{w}_t^i$ are the *unnormalized* weights)

It can also be shown (non-trivial) that this estimate is **unbiased**!

4/30

Reminder: The bootstrap particle filter

Algorithm 1 Bootstrap particle filter (for $i = 1, \ldots, N$)

---

1. **Initialization ($t = 0$):**
   (a) Sample $x_0^i \sim p(x_0 \mid \theta)$.
   (b) Set initial weights: $w_0^i = 1/N$.
2. **for $t = 1$ to T do**
   (a) Resample: sample ancestor indices $a_t^i \sim \mathcal{C}(\{w_{t-1}^j\}_{j=1}^N)$.
   (b) Propagate: sample $x_t^i \sim p(x_t \mid x_{t-1}^{a_t^i}, \theta)$.
   (c) Weight: compute $\widetilde{w}_t^i = p(y_t \mid x_t^i, \theta)$ and normalize $w_t^i = \widetilde{w}_t^i / \sum_{j=1}^N \widetilde{w}_t^j$.

$$p(y_{1:T} \mid \theta) \approx \prod_{t=1}^{T} \left(\frac{1}{N} \sum_{i=1}^{N} \widetilde{w}_t^i \right)$$

5/30

Log-weights: an important practical aspect

For realistic problems, $\widetilde{w}_t^i$ might be smaller than machine precision $\rightarrow \widetilde{w}_t^i = 0$ on your computer.

Use **shifted log-weights** v_t^i!

$$v_t^i = \log \widetilde{w}_t^i - c_t, \quad c_t = \max\{\log \widetilde{w}_t^1, \ldots, \log \widetilde{w}_t^N\}$$

Implement your particle filter using shifted log-weights! Store $\{v_t^i\}_{i=1}^N$ and c_t.

From this, the likelihood estimate is obtained

$$\prod_{t=1}^{T} \left(\frac{1}{N} \sum_{i=1}^{N} \widetilde{w}_t^i \right) = \prod_{t=1}^{T} \exp \left(c_t + \log \sum_{i=1}^{N} e^{v_t^i} - \log N \right)$$

Also the normalized weights $\{w_t^i\}_{i=1}^N$ can be computed from $\{v_t^i\}_{i=1}^N$,

$$w_t^i = \frac{\widetilde{w}_t^i}{\sum_{j=1}^N \widetilde{w}_t^j} = \frac{e^{v_t^i + c_t}}{\sum_{j=1}^N e^{v_t^j + c_t}} = \frac{e^{v_t^i}}{\sum_{j=1}^N e^{v_t^j}}$$

6/30

ex) Numerical illustration

Simple LG-SSM,

$$x_t = \theta x_{t-1} + v_t, \qquad v_t \sim \mathcal{N}(0, 1),$$
$$y_t = x_t + e_t, \qquad e_t \sim \mathcal{N}(0, 1).$$

Task: estimate $p(y_{1:100} \mid \theta)$ for a simulated data set. True $\theta^\star = 0.9$.
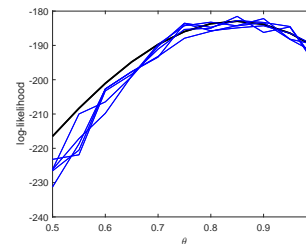
Black line – true likelihood computed using the Kalman filter.

Blue thin lines – 5 different likelihood estimates $\widehat{p}^N(y_{1:100} \mid \theta)$ computed using a bootstrap particle filter with $N = 100$ particles.

7/30

The particle filter as likelihood estimator

- **Good news:** Each run of the particle filter returns an estimate of $p(y_{1:T} \mid \theta)$ in addition to the state estimates!

- **Challenge:** The particle filter contains randomness $\rightarrow$ the estimate of $p(y_{1:T} \mid \theta)$ contains randomness or 'noise'.

Two approaches to maximum likelihood identification:

1. Direct optimization using stochastic optimizers

   Adrian Wills and TS. **Stochastic quasi-Newton with line-search regularization**. *arXiv:1909.01238*, 2019.

2. Expectation maximization formulation

   TS, Adrian Wills and Brett Ninness. **System identification of nonlinear state-space models**. *Automatica*, 47(1):39-49, 2011.
   Andreas Lindholm and Fredrik Lindsten. **Learning dynamical systems with particle stochastic approximation EM**. *arXiv:1806.09548*, 2018

Stochastic optimization

Direct optimization

$$\widehat{\theta} = \arg\max_{\theta} p(y_{1:T} \mid \theta)$$

Can we use standard optimization routines?

Say, `scipy.optimize.minimize(fun=-my_BPF_function,x0 = .2)`

No. The evaluation of the cost function is 'noisy'.

Solution: Use (or design) **stochastic optimization** methods that can work with noisy cost functions.

Problem formulation

What? Solve the non-convex stochastic optimization problem

$$\min_{\theta} f(\theta)$$

when we only have access to **noisy** evaluations of $f(\theta)$ and its derivatives.

Why? These stochastic optimization problems are common:

- When the cost function cannot be evaluated on the entire dataset.
- When numerical methods approximate $f(\theta)$ and $\nabla^i f(\theta)$.
- ...

How?

> **How?** Learn a probabilistic nonlinear model of the Hessian.

Provides a local approximation of the cost function $f(\theta)$.

Use this local model to compute a search direction.

Stochastic line search via a stochastic version of the Wolfe/Armijo condition.

Captures second-order information (curvature) which opens up for better performance compared to a pure gradient-based method.

Intuitive preview example – Rosenbrock's banana function

Let $f(\theta) = (1 - \theta_1)^2 + 100(\theta_2 - \theta_1^2)^2$.

Deterministic problem

$$\min_\theta f(\theta)$$
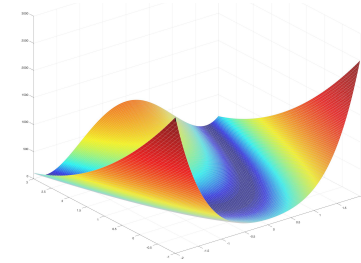
Stochastic problem

$$\min_\theta f(\theta)$$

when we only have access to noisy versions of the cost function
$(\widetilde{f}(\theta) = f(\theta) + e,\ e = \mathcal{N}(0, 30^2))$
and its noisy gradients.
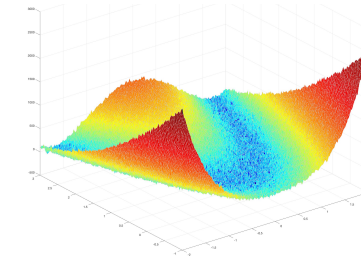
Quasi-Newton – A non-standard take

Our problem is of the form

$$\min_\theta f(\theta)$$

> **Idea underlying (quasi-)Newton methods:** Learn a local quadratic model $q(\theta_k, \delta)$ of the cost function $f(\theta)$ around the current iterate θ_k
>
> $$q(\theta_k, \delta) = f(\theta_k) + g(\theta_k)^\mathsf{T}\delta + \frac{1}{2}\delta^\mathsf{T} H(\theta_k)\delta$$

$$g(\theta_k) = \nabla f(\theta)\big|_{\theta=\theta_k}, \qquad H(\theta_k) = \nabla^2 f(\theta)\big|_{\theta=\theta_k}, \qquad \delta = \theta - \theta_k.$$

We have measurements of
- the cost function $f_k = f(\theta_k)$,
- and its gradient $g_k = g(\theta_k)$.

Question: How do we update the Hessian model?

Useful basic facts

Line segment connecting two adjacent iterates θ_k and θ_{k+1}:

$$r_k(\tau) = \theta_k + \tau(\theta_{k+1} - \theta_k), \qquad \tau \in [0, 1].$$

---

1. The **fundamental theorem of calculus** states that

$$\int_0^1 \frac{\partial}{\partial \tau}\nabla f(r_k(\tau))\mathrm{d}\tau = \nabla f(r_k(1)) - \nabla f(r_k(0)) = \underbrace{\nabla f(\theta_{k+1})}_{g_{k+1}} - \underbrace{\nabla f(\theta_k)}_{g_k}.$$

2. The **chain rule** tells us that

$$\frac{\partial}{\partial \tau}\nabla f(r_k(\tau)) = \nabla^2 f(r_k(\tau))\frac{\partial r_k(\tau)}{\partial \tau} = \nabla^2 f(r_k(\tau))(\theta_{k+1} - \theta_k).$$

> $$\underbrace{g_{k+1} - g_k}_{=y_k} = \int_0^1 \frac{\partial}{\partial \tau}\nabla f(r_k(\tau))\mathrm{d}\tau = \int_0^1 \nabla^2 f(r_k(\tau))\mathrm{d}\tau \underbrace{(\theta_{k+1} - \theta_k)}_{s_k}.$$

Result – the quasi-Newton integral

With the definitions $y_k \triangleq g_{k+1} - g_k$ and $s_k \triangleq \theta_{k+1} - \theta_k$ we have

$$y_k = \int_0^1 \nabla^2 f(r_k(\tau)) \mathrm{d}\tau s_k.$$

Interpretation: The difference between two consecutive gradients (y_k) constitute a **line integral observation of the Hessian**.

Problem: Since the Hessian is unknown there is no functional form available for it.

Solution 1 – recovering existing quasi-Newton algorithms

Existing quasi-Newton algorithms (e.g. BFGS, DFP, Broyden's method) assume the Hessian to be constant

$$\nabla^2 f(r_k(\tau)) \approx H_{k+1}, \qquad \tau \in [0, 1],$$

implying the following approximation of the integral (**secant condition**)

$$y_k = H_{k+1} s_k.$$

Find H_{k+1} by **regularizing** H:

$$H_{k+1} = \min_H \quad \|H - H_k\|_W^2,$$
$$\text{s.t.} \quad H = H^\mathsf{T}, \quad H s_k = y_k,$$

Equivalently, the existing quasi-Newton methods can be interpreted as **particular instances of Bayesian linear regression**.

Philipp Hennig. **Probabilistic interpretation of linear solvers**, *SIAM Journal on Optimization*, 25(1):234–260, 2015.

Solution 2 – use a flexible nonlinear model

The approach used here is fundamentally different.

Recall that the problem is **stochastic** and **nonlinear**.

Hence, we need a model that can deal with such a problem.

Idea: Represent the Hessian using a **Gaussian process** learnt from data.

GP prior for the Hessian

Stochastic quasi-Newton integral

$$y_k = \int_0^1 \underbrace{B(r_k(\tau))}_{=\nabla^2 f(r_k(\tau))} s_k \mathrm{d}\tau + e_k,$$

corresponds to noisy (e_k) gradient observations.

Since $B(x)s_k$ is a column vector, the integrand is given by

$$\mathrm{vec}(B(x)s_k) = (s_k^\mathsf{T} \otimes I)\mathrm{vec}(B(x)) = (s_k^\mathsf{T} \otimes I)\mathrm{vec}(B(x)),$$

where $\mathrm{vec}(B(x)) = D\underbrace{\mathrm{vech}(B(x))}_{\widetilde{B}(x)}$.

Let us use a GP model for the unique elements of the Hessian

$$\widetilde{B}(x) \sim \mathcal{GP}(\mu(x), \kappa(x, x')).$$

Resulting stochastic qN integral and Hessian model

Summary: resulting stochastic quasi-Newton integral:

$$y_k = D_k \int_0^1 \widetilde{B}(r_k(\tau)) \mathrm{d}\tau + e_k,$$

with the following model for the Hessian

$$\widetilde{B}(\theta) \sim \mathcal{GP}(\mu(\theta), \kappa(\theta, \theta')).$$

The Hessian can now be estimated using tailored GP regression.

Linear operators (such as a line integral or a derivative) acting on a GP results in a another GP.

Resulting stochastic optimization algorithm

Standard numerical optimization loop with **non-standard components**.

Algorithm 2 Stochastic optimization

1. **Initialization ($k = 1$)**

2. **while** *not terminated* **do**

   (a) Compute a **search direction** p_k using the current approximation of the gradient g_k and Hessian B_k.

   (b) **Stochastic line search** to find a step length α_k and set
   $$\theta_{k+1} = \theta_k + \alpha_k p_k.$$

   (c) **Update the Hessian model** (tailored GP regression).

   (d) Set $k := k + 1$.

3. **end while**

Derived a stochastic Armijo condition enabling stochastic line search.

Adrian Wills and TS. **Stochastic quasi-Newton with line-search regularization**. arXiv:1909.01238, 2019.

ex) Simple linear toy problem

Identify the parameters $\theta = (a, c, q, r)^\mathsf{T}$ in

$$x_{t+1} = ax_t + w_t, \qquad w_t \sim \mathcal{N}(0, q^2),$$
$$y_t = cx_t + e_t, \qquad e_t \sim \mathcal{N}(0, r^2).$$

Observations:

- The likelihood $L(\theta) = p(y_{1:T} \mid \theta)$ and its gradient $\nabla_\theta L(\theta)$ are available in closed form via standard Kalman filter equations.
- Standard gradient-based search algorithms applies.
- Deterministic optimization problem ($L(\theta), \nabla_\theta L(\theta)$ noise-free).

ex) Simple linear toy problem
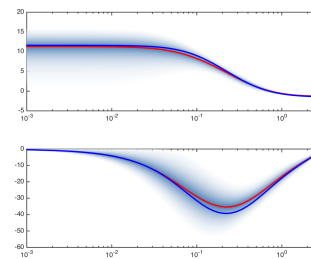
Both alg. in the noise-free case.

100 independent datasets.

Clear blue – True system
Red – Mean value of estimate
Shaded blue – individual results
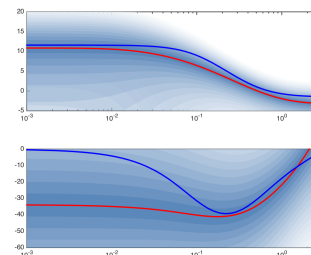
Classical BFGS alg. for noisy observations of $L(\theta)$ and $\nabla L(\theta)$.
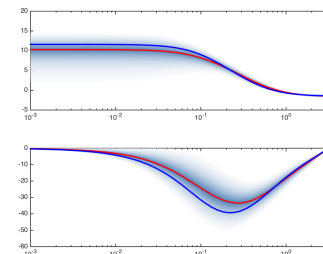
GP-based BFGS alg. with noisy observations of $L(\theta)$ and $\nabla L(\theta)$.

ex) Nonlinear system

Identify the parameters $\theta = (a, c, d, q, r)^{\mathsf{T}}$ in

$$x_{t+1} = ax_t + b\frac{x_t}{1 + x_t^2} + c\cos(1.2t) + w_t, \qquad w_t \sim \mathcal{N}(0, q^2),$$

$$y_t = dx_t^2 + e_t, \qquad\qquad\qquad\qquad e_t \sim \mathcal{N}(0, r^2).$$
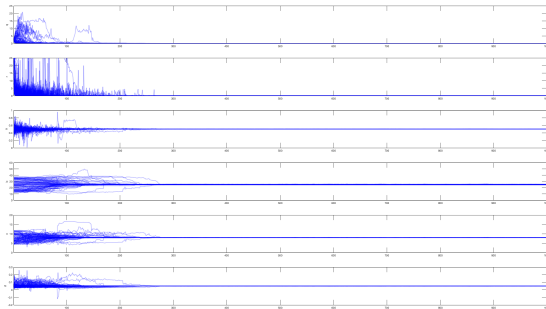
Scaling up to large(r) problems

What is the key limitation of our GP-based optimization algorithm?

It **does not** scale to large-scale problems!

Still highly useful and competitive for **small to medium** sized problems.

We have developed a **new** technique that scales to **large(r)** problems.

Scaling up to large(r) problems

Key innovations:

- Replace the GP with a matrix updated using fast Cholesky routines.
- Exploit a receding history of iterates and gradients akin to L-BFGS.
- Same stochastic line search applicable.
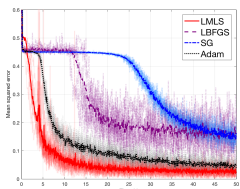
Training a deep CNN for MNIST data.
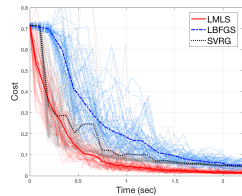
Logistic loss function with an L2 regularizer, gisette, 6 000 observations and 5 000 unknown variables.
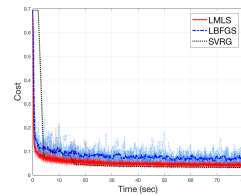
Logistic loss function with an L2 regularizer, URL, 2 396 130 observations and 3 231 961 unknown variables.

Adrian Wills and TS and Carl Jidling. **A fast quasi-Newton-type method for large-scale stochastic optimisation**. In *Proceedings of the IFAC World Congress*, Berlin, Germany, July, 2020.

Estimating likelihood gradients

We can also get noisy approximations for the gradient of the likelihood.

Fisher's identity $\nabla_\theta \log p(y_{1:T} \,|\, \theta) = \mathbb{E}_\theta[\nabla_\theta \log p(x_{1:T}, y_{1:T} \,|\, \theta) \,|\, y_{1:T}],$

where

$$\nabla_\theta \log p(x_{1:T}, y_{1:T} \,|\, \theta) = \sum_{t=1}^{T} \nabla_\theta \log p(x_t \,|\, x_{t-1}, \theta) + \nabla_\theta \log p(y_t \,|\, x_t, \theta),$$

$$\Rightarrow \nabla_\theta \log p(y_{1:T} \,|\, \theta) =$$

$$\sum_{t=1}^{T} \int [\nabla_\theta \log p(x_t \,|\, x_{t-1}, \theta) + \nabla_\theta \log p(y_t \,|\, x_t, \theta)]\, p(x_{t-1:t} \,|\, y_{1:T}, \theta) \mathrm{d}x_{t-1:t}.$$

Here, $p(x_{t-1:t} \,|\, y_{1:T}, \theta)$ requires a particle **smoother**. Several SMC-based alternative exists, but this is not discussed in the mini-course.

Expectation Maximization

Expectation Maximization

As an alternative to direct optimization of $p(y_{1:T} \mid \theta)$, we can use the **Expectation Maximization** (EM) method.

Dempster, Arthur P., Nan M. Laird, and Donald B. Rubin. **Maximum likelihood from incomplete data via the EM algorithm**. *Journal of the Royal Statistical Society: Series B (Methodological)*, 39(1):1–22, 1977.

Idea:

(E) Let $\mathcal{Q}(\theta, \theta_{k-1}) = \int \log p(y_{1:T}, x_{0:T} \mid \theta) p(x_{0:T} \mid y_{1:T}, \theta_{k-1}) dx_{0:T}$

(M) Solve $\theta_k \leftarrow \mathrm{argmax}_\theta \ \mathcal{Q}_k(\theta, \theta_{k-1})$

Iterate until convergence.

Note: Does not make use of the particle filter as a likelihood estimator, but uses a particle smoother.

Computing the intermediate quantity $\mathcal{Q}$

Inserting

$$\log p(x_{0:T}, y_{1:T} \mid \theta) = \log \left(\prod_{t=1}^{T} p(y_t \mid x_t, \theta) \prod_{t=1}^{T} p(x_t \mid x_{t-1}, \theta) p(x_0 \mid \theta) \right)$$

$$= \sum_{t=1}^{T} \log p(y_t \mid x_t, \theta) + \sum_{t=1}^{T} \log p(x_t \mid x_{t-1}, \theta) + \log p(x_0 \mid \theta)$$

into the expression for $\mathcal{Q}(\theta, \theta_k)$ results in

$$\mathcal{Q}(\theta, \theta_k) = \int \sum_{t=1}^{T} \log p(y_t \mid x_t, \theta) p(x_t \mid y_{1:T}, \theta_k) dx_t$$

$$+ \int \sum_{t=1}^{T} \log p(x_t \mid x_{t-1}, \theta) p(x_{t-1:t} \mid y_{1:T}, \theta_k) dx_{t-1:t}$$

$$+ \int \log p(x_0 \mid \theta) p(x_0 \mid y_{1:T}, \theta_k) dx_0.$$

Final EM algorithm

Inserting particle smoothing approximations now allows for straightforward approximation of $\mathcal{Q}(\theta, \theta_k)$,

$$\widehat{\mathcal{Q}}(\theta, \theta_k) = \sum_{t=1}^{T} \sum_{i=1}^{N} \log p(y_t \mid x_{t\mid T}^i, \theta) + \sum_{t=1}^{T} \sum_{i=1}^{N} \log p(x_{t\mid T}^i \mid x_{t-1\mid T}^i, \theta)$$

$$+ \log \sum_{i=1}^{N} p(x_{0\mid T}^i \mid \theta).$$

1. Initialize θ_0 and run a particle smoother conditional on θ_0.

2. Use the result from previous step to compute $\widehat{\mathcal{Q}}(\theta, \theta_0)$.

3. Solve $\theta_1 = \arg\max_\theta \widehat{\mathcal{Q}}(\theta, \theta_0)$.

4. Run a particle smoother conditional on θ_1.

5. ....

Requires $N \to \infty$ **and** infinitely many iterations. There are more intricate solutions.

Further reading

Survey/tutorial papers

Nikolas Kantas, Arnaud Doucet, Sumeetpal S. Singh, Jan Maciejowski and Nicolas Chopin. **On particle methods for parameter estimation in general state-space models**. *Statistical Science*, 30(3):328-351, 2015.

TS, Fredrik Lindsten, Johan Dahlin, Johan Wagberg, Christian A. Naesseth, Andreas Svensson and Liang Dai. **Sequential Monte Carlo methods for system identification**. *Proceedings of the 17th IFAC Symposium on System Identification (SYSID)*, Beijing, China, 2015.

Maximum likelihood using stochastic optimization

Adrian G. Wills and TS. **Stochastic quasi-Newton with line-search regularization**. *arXiv:1909.01238*, 2019.

Maximum likelihood using EM

TS, Adrian Wills and Brett Ninness. **System identification of nonlinear state-space models**. *Automatica*, 47(1):39-49, 2011.

Andreas Lindholm and Fredrik Lindsten. **Learning dynamical systems with particle stochastic approximation EM**. *arXiv:1806.09548*, 2018

30/30

Learning nonlinear dynamics using sequential Monte Carlo

Part 3 – Bayesian system identification

Thomas Schön, Uppsala University

2020-03-11

Outline – Part 3

Aim: Show how SMC can be used in identifying nonlinear SSMs using Bayesian approach.

Outline:

1. Bayesian inference and the MCMC idea
2. The Metropolis Hastings algorithm
3. Background on Bayesian system identification
4. Using unbiased estimates within Metropolis Hastings
5. Exact approximation – Particle Metropolis Hastings (PMH)
6. Outlook (if there is time)

Bayesian inference – setup for now

Bayesian inference comes down to computing the target distribution $\pi(x)$.

More commonly our interest lies in some integral of the form:

$$\mathbb{E}_\pi[\varphi(x)\,|\,y_{1:T}] = \int \varphi(x)p(x\,|\,y_{1:T})\mathrm{d}x.$$

Ex. (nonlinear dynamical systems)

Here our interest is often $x = \theta$ and $\pi(\theta) = p(\theta\,|\,y_{1:T})$

or $x = (x_{1:T}, \theta)$ and $\pi(x_{1:T}, \theta) = p(x_{1:T}, \theta\,|\,y_{1:T})$.

We keep the development general for now and specialize later.

How?

The two main strategies for the Bayesian inference problem:

1. **Variational methods** provides an approximation by assuming a certain functional form containing unknown parameters, which are found using optimization, where some distance measure is minimized.
2. **Markov chain Monte Carlo (MCMC)** works by simulating a Markov chain which is designed in such a way that its stationary distribution coincides with the target distribution.

MCMC and Metropolis Hastings

Toy illustration – AR(1)

Let us play the game where you are asked to generate samples from

$$\pi(x) = \mathcal{N}\big(x \,|\, 0, 1/(1 - 0.8^2)\big).$$

One realisation from $x[t+1] = 0.8x[t] + v[t]$ where $v[t] \sim \mathcal{N}(0,1)$. Initialise in $x[0] = -40$.
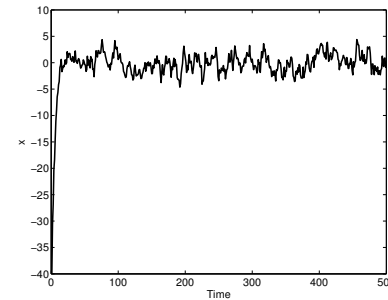
This will eventually generate samples from the following **stationary distribution**:

$$p^{\mathrm{s}}(x) = \mathcal{N}\big(x \,|\, 0, 1/(1 - 0.8^2)\big)$$

as $t \to \infty$.

Toy illustration – AR(1)

1 000 samples
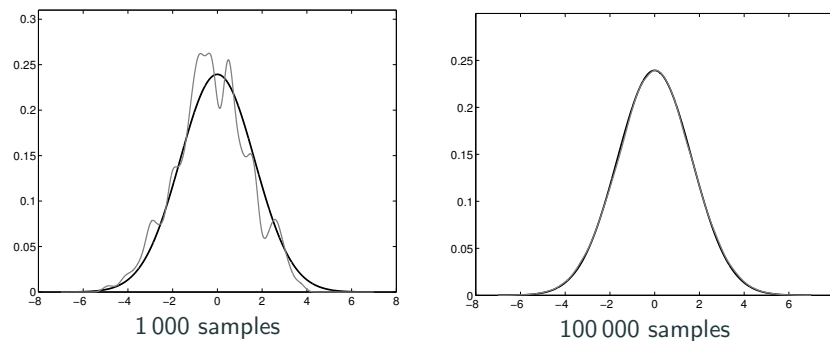
100 000 samples

The true stationary distribution is shown in black and the empirical histogram obtained by simulating the Markov chain $x[t+1] = 0.8x[t] + v[t]$ is plotted in gray.

The initial 1 000 samples are discarded (burn-in).

Metropolis Hastings algorithm

A systematic method for constructing such Markov chains is provided by:

1. Sample a candidate x' from a proposal (akin to what we did in importance sampling)

$$x' \sim q(x \,|\, x[m])$$

2. Choose the candidate sample x' as the next state of the Markov chain with probability (for intuition: think about the importance weights)

$$\alpha = \min\left(1, \frac{\pi(x')}{\pi(x[m])} \frac{q(x[m] \,|\, x')}{q(x' \,|\, x[m])}\right)$$

Select the new state of the Markov chain according to

$$x[m+1] = \begin{cases} x' & \text{w.p.}\,\alpha \\ x[m] & \text{w.p.}\,1-\alpha \end{cases}$$

Metropolis, N., Rosenbluth, A.W., Rosenbluth, M.N., Teller, A.H. and Teller, E. **Equations of state calculations by fast computing machine**, *J. Chem. Phys.* 21(6): 1087–1092, 1953.

Hastings, W.K. **Monte Carlo Sampling Methods Using Markov Chains and Their Applications**. *Biometrika*. 57(1): 97–109, 1970.

Metropolis Hastings algorithm

Algorithm 1 Metropolis Hastings (MH)

1. **Initialize:** Set the initial state of the Markov chain $x[1]$.
2. **For** $m = 1$ **to** M, **iterate:**

    a. Sample $x' \sim q(x \mid x[m])$.

    b. Sample $u \sim \mathcal{U}[0, 1]$.

    c. Compute the acceptance probability
    $$\alpha = \min\left(1, \frac{\pi(x')}{\pi(x[m])} \frac{q(x[m] \mid x')}{q(x' \mid x[m])}\right)$$

    d. Set the next state $x[m+1]$ of the Markov chain according to
    $$x[m+1] = \begin{cases} x' & u \leq \alpha \\ x[m] & \text{otherwise} \end{cases}$$

Resulting empirical approx. of the posterior: $\widehat{\pi}(x) = \frac{1}{M} \sum_{m=1}^{M} \delta_{x[m]}(x)$.

7/43

Using MH for Bayesian inference in dynamical systems

Statistical properties of MCMC

The MCMC estimator
$$\widehat{I}[\varphi] = \frac{1}{M} \sum_{m=0}^{M} \varphi(x[m])$$

is by the **ergodic theorem** known to be strongly consistent, i.e.

$$\underbrace{\frac{1}{M} \sum_{m=0}^{M} \varphi(x[m])}_{\widehat{I}[\varphi]} \xrightarrow{a.s.} \underbrace{\int \varphi(x) p(x \mid y_{1:T})}_{I[\varphi]}$$

when $M \to \infty$.

Central limit theorem (CLT) stating that
$$\sqrt{M}\left(\widehat{I}[\varphi] - I[\varphi]\right) \xrightarrow{d} \mathcal{N}(0, \sigma^2_{\text{MCMC}})$$

when $M \to \infty$.

8/43

Recall the Bayesian problem formulation

Bayesian SSM representation using probability distributions
$$x_t \mid x_{t-1}, \theta \sim p(x_t \mid x_{t-1}, \theta),$$
$$y_t \mid x_t, \theta \sim p(y_t \mid x_t, \theta),$$
$$x_0 \sim p(x_0 \mid \theta),$$
$$\theta \sim p(\theta).$$

Based on our generative model, compute the **posterior distribution**
$$p(x_{0:T}, \theta \mid y_{1:T}) = \underbrace{p(x_{0:T} \mid \theta, y_{1:T})}_{\text{state inf.}} \underbrace{p(\theta \mid y_{1:T})}_{\text{param. inf.}}.$$

> **Bayesian** formulation – model the unknown parameters as a random variable $\theta \sim p(\theta)$ and compute
> $$p(\theta \mid y_{1:T}) = \frac{p(y_{1:T} \mid \theta) p(\theta)}{p(y_{1:T})} = \frac{p(y_{1:T} \mid \theta) p(\theta)}{\int p(y_{1:T} \mid \theta) p(\theta) \mathrm{d}\theta}$$

9/43

Using MH for parameter inference in a dynamical system

Algorithm 2 Metropolis Hastings (MH)

---

1. **Initialize:** Set the initial state of the Markov chain $\theta[1]$.

2. **For** $m = 1$ **to** M, **iterate:**

   a. Sample $\theta' \sim q(\theta \,|\, \theta[m])$.

   b. Sample $u \sim \mathcal{U}[0, 1]$.

   c. Compute the acceptance probability
   $$\alpha = \min\left(1, \frac{p(y_{1:T} \,|\, \theta')p(\theta')}{p(y_{1:T} \,|\, \theta[m])p(\theta[m])} \frac{q(\theta[m] \,|\, \theta')}{q(\theta' \,|\, \theta[m])} \right)$$

   d. Set the next state $\theta[m+1]$ of the Markov chain according to
   $$\theta[m+1] = \begin{cases} \theta' & u \leq \alpha \\ \theta[m] & \text{otherwise} \end{cases}$$

Setting up an MH algorithm

To be able to use MH we need to

1. decide on a proposal q to use and

2. compute the acceptance probability α.

Important question

> **Problem:** We cannot evaluate the acceptance probability α since the likelihood $p(y_{1:T} \,|\, \theta)$ is intractable.

We know that SMC provides an estimate of the likelihood.

> **Important question:** Is it possible to use an estimate of the likelihood in computing the acceptance probability and still end up with a valid algorithm?

Valid here means that the method converges in the sense of

$$\frac{1}{M} \sum_{m=1}^{M} \varphi(\theta[m]) \xrightarrow{a.s.} \int \varphi(\theta)p(\theta \,|\, y_{1:T}), \quad \text{when } M \to \infty.$$

Particle Metropolis Hastings

The particle filter as a likelihood estimator

Fact: The particle filter provides a

- non-negative
- and unbiased

estimate $\widehat{z}$ of the likelihood $p(y_{1:T} \mid \theta)$.

This likelihood estimator $\widehat{z}$ is itself a random variable distributed according to

$$\widehat{z} \sim \psi(z \mid \theta, y_{1:T}).$$

This is a very complicated distribution, but importantly we will (as we will see) never be required to evaluate it, only sample from it.

Auxiliary variables – very useful construction

Target distribution: $\pi(x)$, difficult to sample from

Idea: Introduce another variable u with conditional distribution $\pi(u \mid x)$

The joint distribution $\pi(x, u) = \pi(u \mid x)\pi(x)$ admits $\pi(x)$ as a marginal by construction, i.e., $\int \pi(x, u)\mathrm{d}u = \pi(x)$.

Sampling from the joint $\pi(x, u)$ may be easier than directly sampling from the marginal $\pi(x)$!

The variable u is an **auxiliary variable**. It may have some "physical" interpretation (an unobserved measurement, unknown temperature, . . .) but this is not necessary.

What about introducing $\widehat{z}$ as an auxiliary variable?

Consider an extended model where $\widehat{z}$ is included as an auxiliary variable

$$(\theta, \widehat{z}) \sim \psi(\theta, z \mid y_{1:T}) = \psi(z \mid \theta, y_{1:T})p(\theta \mid y_{1:T})$$
$$= \frac{p(y_{1:T} \mid \theta)p(\theta)\psi(z \mid \theta, y_{1:T})}{p(y_{1:T})}$$

Importantly we note that the original target distribution $p(\theta \mid y_{1:T})$ is by construction obtained my marginalizing $\psi(\theta, z \mid y_{1:T})$ w.r.t. z.

Key question: If we now were to construct a Metropolis Hastings algorithm for θ and z, have we solved the problem?

Trick – defining a new extended target distribution

Enabling trick: Define a new joint target distribution over $(\theta, \widehat{z})$ by simply replacing $p(y_{1:T} \mid \theta)$ with its estimator $\widehat{z}$.

Hence, our new target distribution is given by

$$\pi(\theta, z \mid y_{1:T}) = \frac{zp(\theta)\psi(z \mid \theta, y_{1:T})}{p(y_{1:T})}$$

Key question: Is this ok?

Verifying that our new extended target is indeed ok

Requirements on π:

1. Non-negative.
2. Integrate to 1.
3. Correct marginal distribution: $\int \pi(\theta, z \mid y_{1:T}) dz = p(\theta \mid y_{1:T})$.

Requirement 1 follows from the non-negativity of $\hat{z}$.

What about requirement 2 and 3?

Let us start by noting that

$$\int \pi(\theta, z \mid y_{1:T}) dz = \frac{p(\theta)}{p(y_{1:T})} \int z\psi(z \mid \theta, y_{1:T}) dz.$$

What can we say about this integral?

The fact that the likelihood estimate from the particle filter is unbiased means that

$$\int z\psi(z \mid \theta, y_{1:T}) dz = p(y_{1:T} \mid \theta)!!$$

Hence, we have shown that

$$\int \pi(\theta, z \mid y_{1:T}) dz = \frac{p(\theta)}{p(y_{1:T})} p(y_{1:T} \mid \theta) = p(\theta \mid y_{1:T}),$$

which means that 3 is ok and also 2.

Particle Metropolis Hastings

The use of a non-negative and unbiased likelihood estimate within Metropolis Hastings is called the **pseudo-marginal approach**.

Algorithm 3 Particle Metropolis Hastings
1. **Initialize ($m = 1$):** Set $\theta[1]$ and run a particle filter for $\hat{z}[1]$.
2. **For $m = 2$ to M, iterate:**
   a. Sample $\theta' \sim q(\theta \mid \theta[m-1])$.
   b. Sample $\hat{z}' \sim \psi(z \mid \theta', y_{1:T})$ (i.e. run a particle filter).
   c. With probability
   $$\alpha = \min \left(1, \frac{\hat{z}' p(\theta')}{\hat{z}[m-1] p(\theta[m-1])} \frac{q(\theta[m-1] \mid \theta')}{q(\theta' \mid \theta[m-1])} \right)$$
   set $\{\theta[m], \hat{z}[m]\} \leftarrow \{\theta', \hat{z}'\}$ (accept candidate sample) and with prob. $1 - \alpha$ set $\{\theta[m], \hat{z}[m]\} \leftarrow \{\theta[m-1], \hat{z}[m-1]\}$ (reject candidate sample).

Exact approximation

The pseudo-marginal Metropolis Hastings algorithm is one member of the family of so-called **exact approximation** algorithms.

Explanation for this slightly awkward name:

- It is an **exact** Metropolis Hastings algorithm in the sense that the target distribution of interest is the stationary distribution of the Markov chain,
- despite the fact that it makes use of an **approximation** of the likelihood in evaluating the acceptance probability.

The variance of the estimator $\hat{z}$ will significantly impact the convergence speed.

Two reflections on the PMH algorithm

1. PMH is a **standard MH algorithm** sampling from the joint target $\pi(\theta, z)$, rather than the original target $\pi(\theta)$. We have used the auxiliary variables trick, where the marginal of the joint target $\pi(\theta, z)$ w.r.t. z is by construction the original target $\pi(\theta)$.

2. Using a likelihood estimator $\widehat{z}$ means that the marginal of

$$\pi(\theta, z \mid y_{1:T}) = \frac{z p(\theta) \psi(z \mid \theta, y_{1:T})}{p(y_{1:T})}$$

w.r.t. $\widehat{z}$ will **not equal** the marginal of

$$\psi(\theta, z \mid y_{1:T}) = \frac{p(y_{1:T} \mid \theta) p(\theta) \psi(z \mid \theta, y_{1:T})}{p(y_{1:T})}$$

w.r.t. $\widehat{z}$. This is ok, since we are only interested in the marginal w.r.t. θ, which remains the same for both π and ψ, namely $p(\theta \mid y_{1:T})$.

Using the PMH for smoothing

A possibly under-appreciated fact is that the PMH algorithm provides a **solution to the smoothing problem as well**!

In step 2b, when we run the PF, select one of the state trajectories according to its weights and store that together with the unbiased likelihood estimate.

We then accept or reject the new parameter, the likelihood estimate and the state trajectory is step 2c.

ex) The pseudo-marginal idea is general

CG example (rendering images in heterogeneous media): An MH algorithm producing samples of the light paths connecting the sensor with light sources in the scene.

Results using equal time rendering

Our method that builds on MLT

Metropolis light transport (MLT)

Joel Kronander, TS and Jonas Unger. **Pseudo-marginal Metropolis light transport**. *Proceedings of SIGGRAPH ASIA Technical Briefs.* Kobe, Japan, November, 2015.

Particle MCMC = SMC + MCMC

A systematic and correct way of combining SMC and MCMC.

Builds on an extended target construction.

Intuitively: SMC is used as a high-dimensional proposal mechanism on the space of state trajectories $\mathcal{X}^T$.

A bit more precise: Construct a Markov chain with $p(\theta, x_{1:T} \mid y_{1:T})$ (or one of its marginals) as its stationary distribution.

Very useful both for parameter and state learning.

Exact approximations

Further reading

Introducing PMCMC:

Christophe Andrieu, Arnaud Doucet and Roman Holenstein. **Particle Markov chain Monte Carlo methods**. *Journal of the Royal Statistical Society: Series B* 72:269–342, 2010.

A (hopefully) pedagogical tutorial on PMH:

TS, Andreas Svensson, Lawrence Murray and Fredrik Lindsten. **Probabilistic learning of nonlinear dynamical systems using sequential Monte Carlo**. *Mechanical Systems and Signal Processing (MSSP)* 104:866–883, 2018.

Introducing the pseudo-marginal idea in a general setting:

Christophe Andrieu and Gareth O. Roberts. **The pseudo-marginal approach for efficient Monte Carlo computations**. *The Annals of Statistics* 37(2):697–725, 2009.

Concrete simple pedagogical LG-SSM examples of Bayesian inference:

TS, Fredrik Lindsten, Johan Dahlin, Johan Wagberg, Christian A. Naesseth, Andreas Svensson and Liang Dai. **Sequential Monte Carlo methods for system identification**. *Proceedings of the 17th IFAC Symposium on System Identification (SYSID)*, Beijing, China, 2015.

Adrian Wills, TS, Fredrik Lindsten and Brett Ninness, **Estimation of linear systems using a Gibbs sampler**, in *Proceedings of the 16th IFAC Symposium on System Identification (SYSID)*, Brussels, Belgium, July 2012.

Outlook

Outlook – Gaussian process SSM

The Gaussian process (GP) is a **non-parametric** and **probabilistic** model for nonlinear functions.

Non-parametric means that it does not rely on any particular parametric functional form to be postulated.

$$x_t = f(x_{t-1}) + v_t, \qquad \text{s.t.} \quad f(x) \sim \mathcal{GP}(0, \kappa_{\eta,f}(x, x')),$$
$$y_t = g(x_t) + e_t, \qquad \text{s.t.} \quad g(x) \sim \mathcal{GP}(0, \kappa_{\eta,g}(x, x')).$$

The model functions f and g are assumed to be realizations from Gaussian process priors and $v_t \sim \mathcal{N}(0, Q)$, $e_t \sim \mathcal{N}(0, R)$.

Task: Compute the posterior $p(f, g, Q, R, \eta, x_{0:T} \mid y_{1:T})$.

Roger Frigola, Fredrik Lindsten, TS, and Carl Rasmussen. **Bayesian inference and learning in Gaussian process state-space models with particle MCMC.** *Neural Information Processing Systems (NIPS)*, 2013.

Andreas Svensson and TS. **A flexible state space model for learning nonlinear dynamical systems.** *Automatica*, 80:189-199, June, 2017.

Sequential Monte Carlo (SMC) – abstract

The distribution of interest $\pi(x)$ is called the **target distribution**.

(Abstract) problem formulation: **Sample from a sequence** of probability distributions $\{\pi_t(x_{0:t})\}_{t \geq 1}$ defined on a sequence of spaces of increasing dimension, where

$$\pi_t(x_{0:t}) = \frac{\widetilde{\pi}_t(x_{0:t})}{Z_t},$$

such that $\widetilde{\pi}_t(x_t) : \mathcal{X}^t \to \mathbb{R}^+$ is known point-wise and $Z_t = \int \pi(x_{0:t}) \mathrm{d}x_{0:t}$ is often computationally challenging.

SMC methods are a class of sampling-based algorithms capable of:

1. Approximating $\pi(x)$ and compute integrals $\int \varphi(x)\pi(x)\mathrm{d}x$.
2. Approximating the normalizing constant Z (unbiased).

Important question: How general is this formulation?

SMC is actually more general than we first thought

The sequence of target distributions $\{\pi_t(x_{1:t})\}_{t=1}^n$ can be constructed in **many** different ways.

The most basic construction arises from **chain-structured graphs**, such as the state space model.
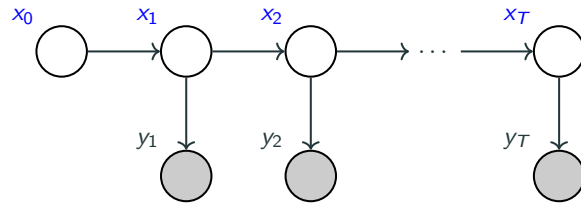
$$\overbrace{p(x_{1:t} \mid y_{1:t})}^{\pi_t(x_{1:t})} = \frac{\overbrace{p(x_{1:t}, y_{1:t})}^{\widetilde{\pi}_t(x_{1:t})}}{\underbrace{p(y_{1:t})}_{Z_t}}$$

28/43

SMC can be used for general graphical models

SMC methods are used to approximate a **sequence of probability distributions** on a sequence of spaces of increasing dimension.

Key idea:
1. Introduce a **sequential decomposition** of any probabilistic graphical model.
2. Each **subgraph** induces an intermediate target dist.
3. Apply SMC to the sequence of intermediate target dist.

SMC also provides an unbiased estimate of the **normalization constant**!

Christian A. Naesseth, Fredrik Lindsten and TS. **Sequential Monte Carlo methods for graphical models**. In *Advances in Neural Information Processing Systems (NIPS)* 27, Montreal, Canada, December, 2014.

29/43

Going from classical SMC fo D&C-SMC

The **computational graph** of classic SMC is a sequence (chain)
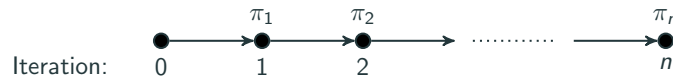
D&C-SMC generalize the classical SMC framework **from sequences to trees**.
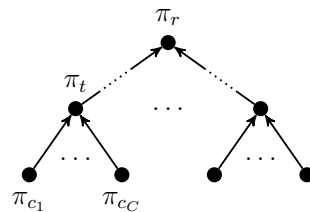
Fredrik Lindsten, Adam M. Johansen, Christian A. Naesseth, Bonnie Kirkpatrick, TS, John Aston and Alexandre Bouchard-Côté. **Divide-and-Conquer with Sequential Monte Carlo**. *Journal of Computational and Graphical Statistics (JCGS)*, 26(2):445-458, 2017.

30/43

Approximate Bayesian inference – blending
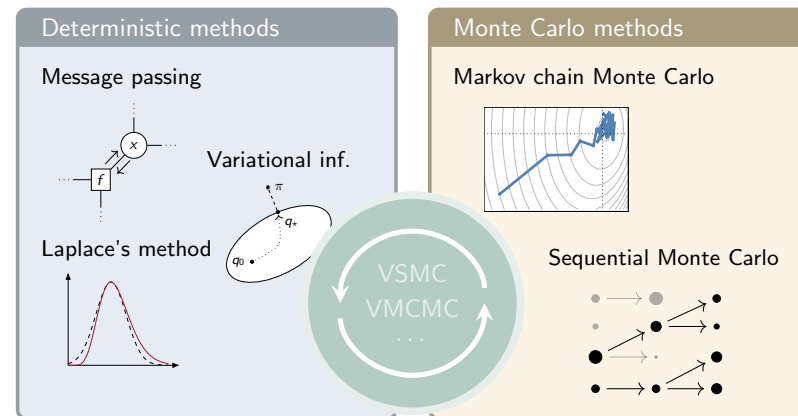
31/43

Blending deterministic and Monte Carlo methods

Deterministic methods:
  Good: Accurate and rapid inference
  Bad: Results in biases that are hard to quantify

Monte Carlo methods:
  Good: Asymptotic consistency, lots of theory available
  Bad: Can suffer from a high computational cost

Examples of freedom in the SMC algorithm that opens up for **blending**:

  The **proposal** distributions can be defined in many ways.

  The **intermediate target** distributions can be defined in many ways.

Leads to very interesting and useful algorithms, **many of them still remain to be discovered and explored**.

32/43

Deep probabilistic regression (if we for some reason still have some time left...)

Background: regression using deep neural networks

Supervised regression: learn to predict a continuous output (target) value $y^\star \in \mathcal{Y} = \mathbb{R}^K$ from a corresponding input $x^\star \in \mathcal{X}$, given a training set $\mathcal{D}$ of i.i.d. input-output data

$$\mathcal{D} = \{(x_n, y_n)\}_{n=1}^N, \qquad (x_n, y_n) \sim p(x, y).$$

Deep neural network (DNN): a function $f_\theta : \mathcal{X} \to \mathcal{Y}$, parameterized by $\theta \in \mathbb{R}^P$, that maps an input $x \in \mathcal{X}$ to an output $f_\theta(x) \in \mathcal{Y}$.

33/43

Our ongoing work on deep regression

Deep learning for classification is handled using standard losses and output representations.

This is **not** the case when it comes to regression.

Train a model $p(y \mid x; \theta)$ of the conditional target density using a DNN to predict the un-normalized density **directly** from input-output pair (x, y).
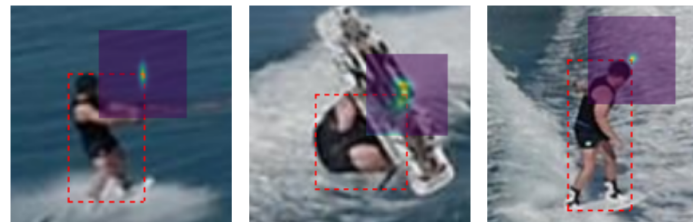
34/43

Four existing approaches: 1. Direct regression

Train a DNN $f_\theta : \mathcal{X} \to \mathcal{Y}$ to directly predict the target $y^\star = f_\theta(x^\star)$.

Learn the parameters θ by minimizing a loss function $\ell(f_\theta(x_n), y_n)$, penalizing discrepancy between prediction $f_\theta(x_n)$ and ground truth y_n

$$J(\theta) = \frac{1}{N} \sum_{n=1}^{N} \ell(f_\theta(x_n), y_n), \qquad \theta = \arg\min_{\theta'} J(\theta').$$

Common choices for ℓ are the L^2 loss, $\ell(\hat{y}, y) = \|\hat{y} - y\|_2^2$, and the L^1 loss.

Minimizing $J(\theta)$ then corresponds to minimizing the negative log-likelihood $\sum_{n=1}^{N} -\log p(y_n \mid x_n; \theta)$, **for a specific model** $p(y \mid x; \theta)$ of the conditional target density.

Ex: The L^2 loss corresponds to a fixed-variance Gaussian model:
$$p(y \mid x; \theta) = \mathcal{N}(y; f_\theta(x), \sigma^2).$$

Four existing approaches: 2. Probabilistic regression

Why not explicitly employ this probabilistic perspective and try to create more **flexible** models $p(y \mid x; \theta)$ of the conditional target density $p(y \mid x)$?

Probabilistic regression: train a DNN $f_\theta : \mathcal{X} \to \mathcal{Y}$ to predict the parameters ϕ of a certain family of probability distributions $p(y; \phi)$, then model $p(y \mid x)$ with
$$p(y \mid x; \theta) = p(y; \phi(x)), \qquad \phi(x) = f_\theta(x).$$

The parameters θ are learned by minimizing $\sum_{n=1}^{N} -\log p(y_n \mid x_n; \theta)$.

Ex: A general 1D Gaussian model can be realized as:

$$p(y \mid x; \theta) = \mathcal{N}\big(y; \mu_\theta(x), \sigma_\theta^2(x)\big), \qquad f_\theta(x) = \big(\mu_\theta(x) \quad \log \sigma_\theta^2(x)\big)^\mathsf{T} \in \mathbb{R}^2.$$

Four existing approaches: 3. Confidence-based regression

The quest for improved regression accuracy has also led to the development of more specialized methods.

Confidence-based regression: train a DNN $f_\theta : \mathcal{X} \times \mathcal{Y} \to \mathbb{R}$ to predict a scalar confidence value $f_\theta(x, y)$, and maximize this quantity over y to predict the target
$$y^\star = \arg\max_y f_\theta(x^\star, y)$$

The parameters θ are learned by generating **pseudo** ground truth confidence values $c(x_n, y_n, y)$, and minimizing a loss function $\ell\big(f_\theta(x_n, y), c(x_n, y_n, y)\big)$.

4. Regression-by-classification: Discretize the output space $\mathcal{Y}$ into a finite set of C classes and use standard classification techniques...

Our (simple and very general) construction

A general regression method with a **clear probabilistic interpretation** in the sense that we learn a model $p(y \mid x, \theta)$ **without** requiring $p(y \mid x, \theta)$ to belong to a particular family of distributions.

Let the DNN be a function $f_\theta : \mathcal{X} \times \mathcal{Y} \to \mathbb{R}$ that maps an input-output pair $\{x_n, y_n\}$ to a scalar value $f_\theta(x_n, y_n) \in \mathbb{R}$.

Define the resulting (flexible) probabilistic model as

$$p(y \mid x, \theta) = \frac{e^{f_\theta(x,y)}}{Z(x, \theta)}, \qquad Z(x, \theta) = \int e^{f_\theta(x,y)} dy$$

Learning flexible deep conditional target densities

1D toy illustration showing that we can learn multi-modal and asymmetric distributions, i.e. our model is **flexible**.

Ground truth   Gaussian   **Ours**
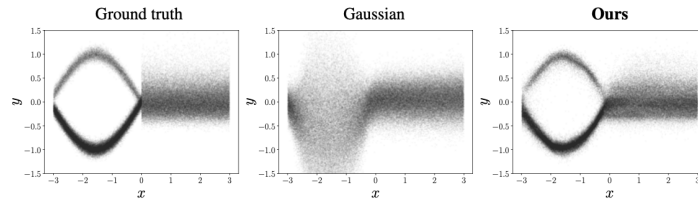
We train by maximizing the log-likelihood:

$$\max_\theta \sum_{n=1}^N \log p(y_n \mid x_n, \theta) = \max_\theta \sum_{n=1}^N - \log \underbrace{\left(\int e^{f_\theta(x,y)} dy \right)}_{Z(x_n, \theta)} + f_\theta(x_n, y_n)$$

Challenge: Requires the normalization constant to be evaluated...

Solution: Monte Carlo! (via a simple importance sampling construction)

39/43

Training the model

$$p(y \mid x, \theta) = \frac{e^{f_\theta(x,y)}}{Z(x,\theta)}, \qquad Z(x,\theta) = \int e^{f_\theta(x,y)} dy$$

The parameters θ are learned by minimizing $\sum_{n=1}^N - \log p(y_n \mid x_n; \theta)$.

Use importance sampling to evaluate $Z(x, \theta)$:

$$- \log p(y_n \mid x_n; \theta) = \log \left(\int e^{f_\theta(x_n, y)} dy \right) - f_\theta(x_n, y_n)$$

$$= \log \left(\int \frac{e^{f_\theta(x_n, y)}}{q(y)} q(y) dy \right) - f_\theta(x_n, y_n)$$

$$\approx \log \left(\frac{1}{M} \sum_{k=1}^M \frac{e^{f_\theta(x_n, y^{(k)})}}{q(y^{(k)})} \right) - f_\theta(x_n, y_n), \quad y^{(k)} \sim q(y).$$

Use a Gaussian mixture as proposal.

40/43

Experiments

Good results on four different computer vision (regression) problems:
1. Object detection, 2. Age estimation, 3. Head-pose estimation and
4. **Visual tracking**.

Task (visual tracking): Estimate a bounding box of a target object in every frame of a video. The target object is defined by a given box in the first video frame.

Show Movie!

Fredrik K. Gustafsson, Martin Danelljan, Goutam Bhat and TS. **Learning deep conditional target densities for accurate regression.** Submitted, March, 2020.

41/43

Advertisement – New course and book on ML

Over the past 4 years we have developed a **Machine Learning course for engineering students**.

We found no appropriate textbook, so we ended up writing our own. It will be published by Cambridge University Press in 2021.

All the material is freely available online.

Book website:

smlbook.org/

Course website:

www.it.uu.se/edu/course/homepage/sml/

You are most welcome to use the material.

42/43

Conclusion

> SMC provide approximate solutions to **integration** problems where there is a **sequential structure** present.

- SMC can deal with the computational challenges in solving many nonlinear system identification problems.
- SMC is **more general** than we first though.
- SMC can indeed be **computationally expensive**, but it comes with rather well-developed analysis and guarantees.
- There is still a lot of freedom **waiting to be exploited**.

TU/e EINDHOVEN UNIVERSITY OF TECHNOLOGY

Data-driven model learning in linear dynamic networks

Paul Van den Hof

39th Benelux Meeting on Systems and Control
Elspeet, the Netherlands, 11 March 2020

www.sysdynet.eu
www.pvandenhof.nl
p.m.j.vandenhof@tue.nl

erc
European Research Council

Introduction – dynamic networks

Decentralized process control

Smart power grid

Pierre et al. (2012)

Autonomous driving

www.envidia.com

Brain network

P. Hagmann et al. (2008)
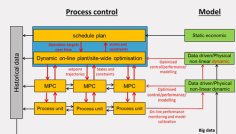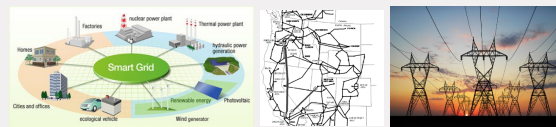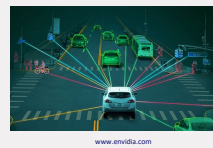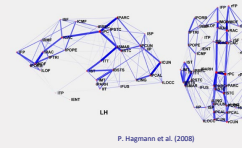
Hydrocarbon reservoirs

Mansoori (2014)

TU/e

2

Introduction

Overall trend:

- (Large-scale) interconnected systems
- With hybrid dynamics
- Distributed / multi-agent type monitoring, control and optimization problems
- Data is "everywhere", big data era
- Model-based operations require accurate/relevant models
- → **Learning models from data** (including physical insights when available)

TU/e

3
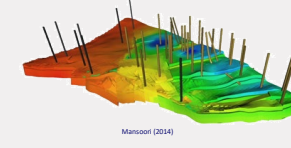
Introduction

Distributed / multi-agent control:
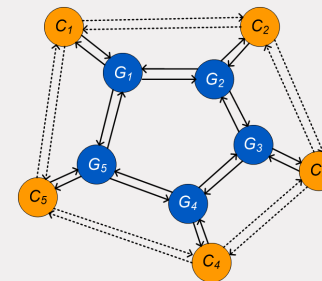
With both physical and communication links between systems G_i and controllers C_i

How to address data-driven modelling problems in such a setting?

TU/e

4

Introduction

The classical (multivariable) identification problems[1]:

open loop   closed loop
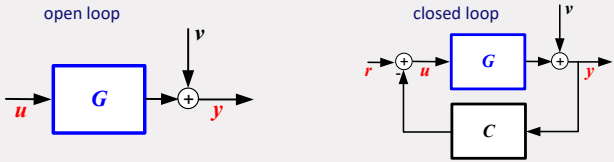
Identify a model of G on the basis of measured signals u, y (and possibly r), focusing on *continuous LTI dynamics*.

> We have to move from a simple and fixed configuration to deal with **structure** in the problem.

[1] Ljung (1999), Söderström and Stoica (1989), Pintelon and Schoukens (2012)

TU/e

5

Early contributors

Topology detection: Materassi, Innocenti, Salapaka, Yuan, Stan, Warnick, Goncalves, Sanandaji, Vincent, Wakin, Chiuso, Pillonetto
exploring Granger causality, Bayesian networks, Wiener filters

Subspace algorithms for **spatially distributed systems** with identical modules (Fraanje, Verhaegen, Werner), or non-identical ones (Torres, van Wingerden, Verhaegen, Sarwar, Salapaka, Haber)

Here: focus on **structural aspects** in identification setups.

TU/e

6

TU/e EINDHOVEN UNIVERSITY OF TECHNOLOGY

Contents

- Introduction and motivation
- How to model a dynamic network?
- Single module identification
- Global network identification
- Physical networks
- Extensions - Discussion

Dynamic networks for data-driven modeling

Network models
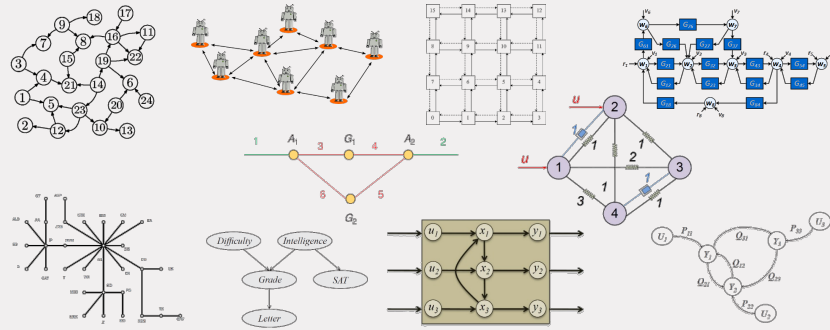
D. Materassi and M.V. Salapaka (2012)
R.N. Mantegna (1999)

www.momo.cs.okayama-u.ac.jp
J.C. Willems (2007)
D. Koller and N. Friedman (2009)

E.A. Carara and F.G. Moraes (2008)
P.E. Paré et al (2013)

P.M.J. Van den Hof et al (2013)
X.Cheng (2019)
E. Yeung et al (2010)

TU/e

9

Network models
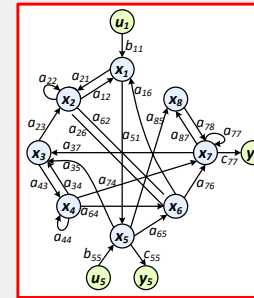
State space representation [1]

Module representation [2]

[1] Goncalves, Warnick, Sandberg, Yeung, Yuan, Scherpen,…
[2] VdH, Dankers, Goncalves, Warnick, Gevers, Bazanella, Hendrickx, Materassi, Weerts,…
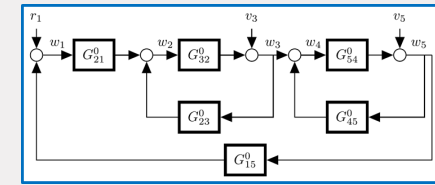
TU/e
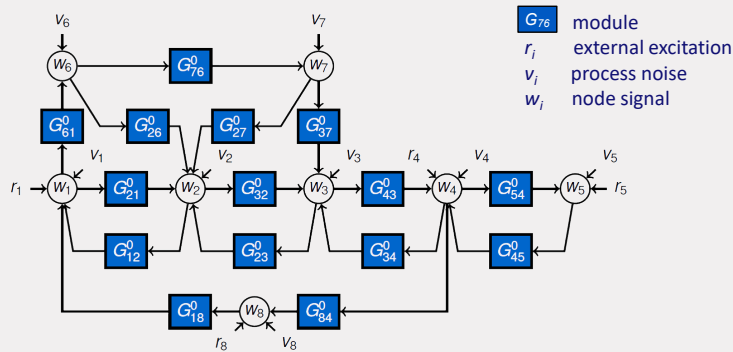
10

Dynamic network setup

G_{76} module
r_i external excitation
v_i process noise
w_i node signal

TU/e

11

Dynamic network setup

G_{76} module
r_i external excitation
v_i process noise
w_i node signal

TU/e

12

Dynamic network setup

G_{76} module
r_i external excitation
v_i process noise
w_i node signal

13

Dynamic network setup

G_{76} module
r_i external excitation
v_i process noise
w_i node signal

14

Dynamic network setup

G_{76} module
r_i external excitation
v_i process noise
w_i node signal

15
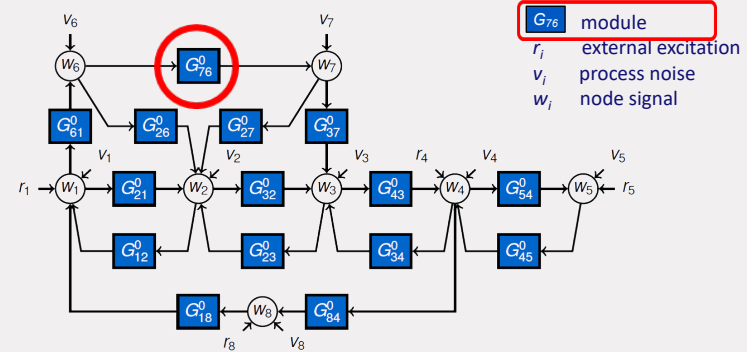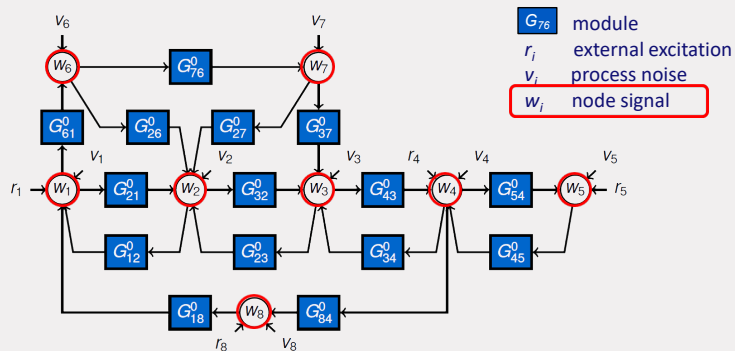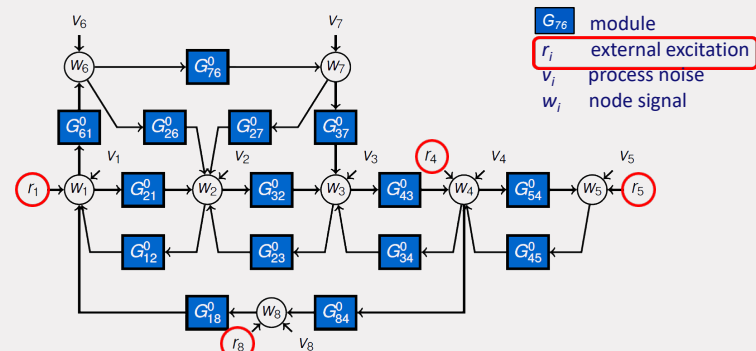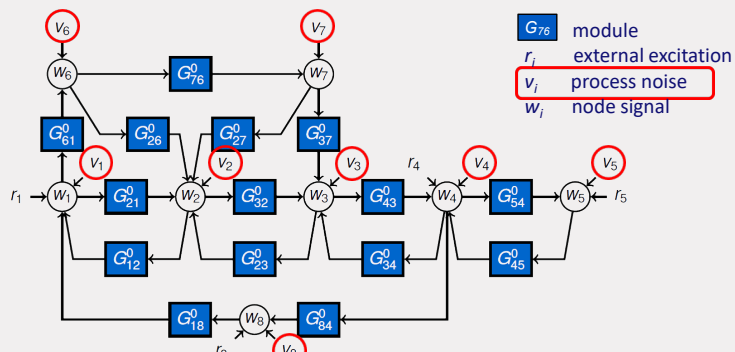
Dynamic network setup
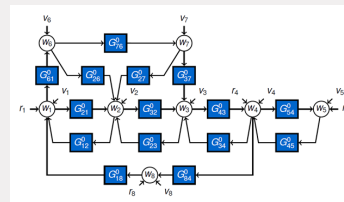
Assumptions:
- Total of L nodes
- Network is well-posed and stable
- Modules are dynamic LTI, may be unstable
- Disturbances are stationary stochastic and can be correlated

$$\begin{bmatrix} w_1 \\ w_2 \\ \vdots \\ w_L \end{bmatrix} = \underbrace{\begin{bmatrix} 0 & G_{12}^0 & \cdots & G_{1L}^0 \\ G_{21}^0 & 0 & \cdots & G_{2L}^0 \\ \vdots & \ddots & \ddots & \vdots \\ G_{L1}^0 & G_{L2}^0 & \cdots & 0 \end{bmatrix}}_{G^0(q)} \begin{bmatrix} w_1 \\ w_2 \\ \vdots \\ w_L \end{bmatrix} + R^0 \begin{bmatrix} r_1 \\ r_2 \\ \vdots \\ r_K \end{bmatrix} + \begin{bmatrix} v_1 \\ v_2 \\ \vdots \\ v_L \end{bmatrix}$$

$$w(t) = G^0(q)w(t) + R^0(q)r(t) + v(t)$$

J. Gonçalves and S. Warnick, IEEE TAC, 2008.
PVdH et al., Automatica, 2013.

16

Dynamic network setup

Setup covers the situation of bilaterally coupled (physical) systems:
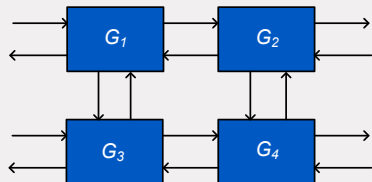
Dynamic network setup
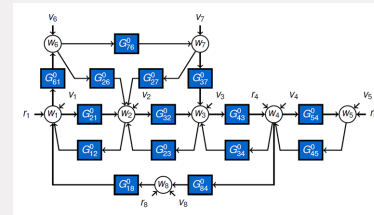
Many new data-driven modeling questions can be formulated

Measured time series:
$$\{w_i(t)\}_{i=1,\dots L}; \ \{r_j(t)\}_{j=1,\dots K}$$
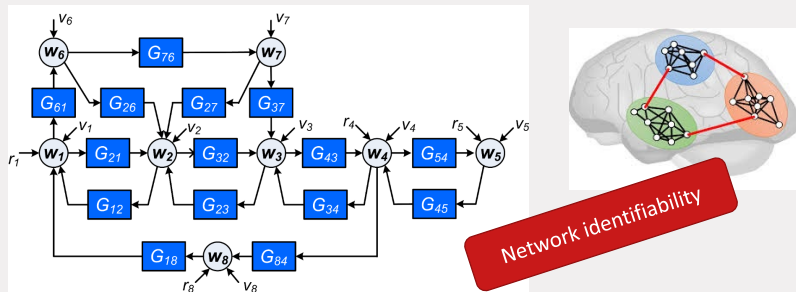
Model learning problems

Network identifiability

Under which conditions can we estimate the topology and/or dynamics of the full network?

Model learning problems
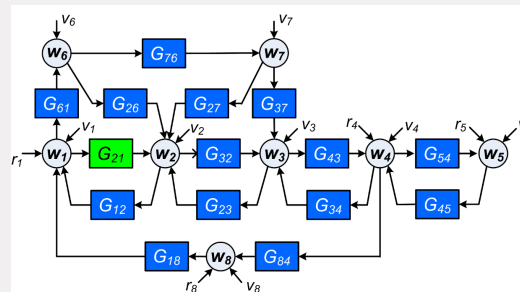
How/when can we learn a local module from data (with known/unkown network topology) ?   Which signals to measure?

Model learning problems
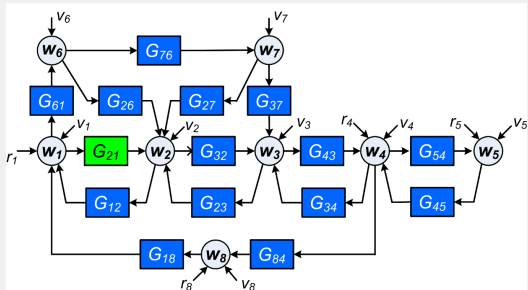
Where to optimally locate sensors and actuators?

21

Model learning problems
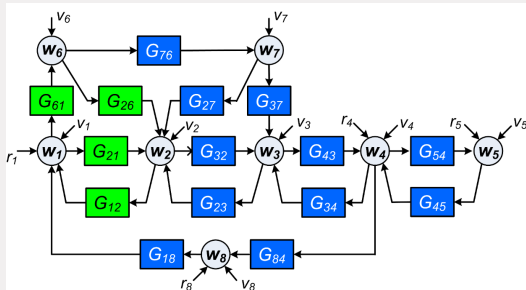
Same questions for a subnetwork

22

Model learning problems
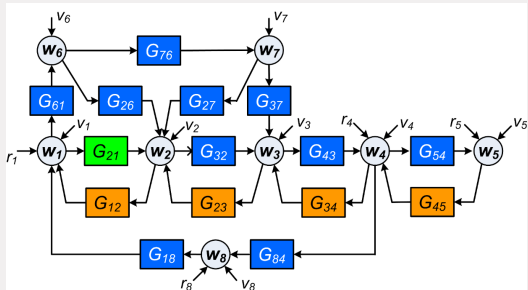
How can we benefit from known modules?

23

Model learning problems
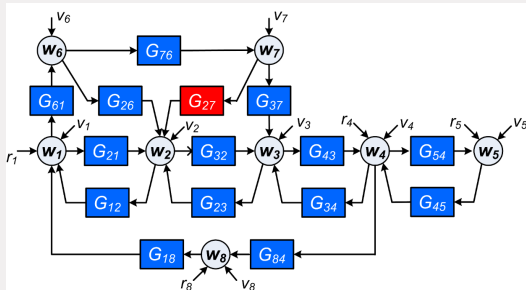
Fault detection and diagnosis; detect/handle nonlinear elements

24

Model learning problems
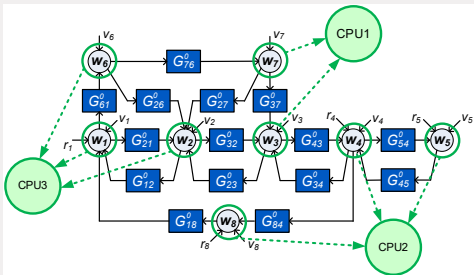
Can we distribute the computations?

25

Dynamic network setup
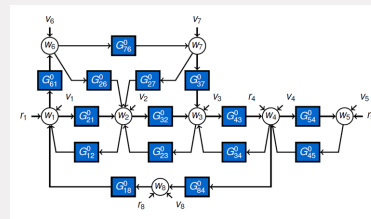
Measured time series:
$$\{w_i(t)\}_{i=1,\cdots L}; \quad \{r_j(t)\}_{j=1,\cdots K}$$

Many new data-driven modeling questions can be formulated

- Identification of a local module (known topology)
- Identification of the full network
- Topology estimation
- Identifiability
- Sensor and excitation allocation
- Fault detection
- User prior knowledge of modules
- Distributed identification
- **Scalable algorithms**

26

Dynamic network setup - graph
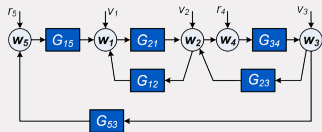
Nodes are vertices; modules/links are edges
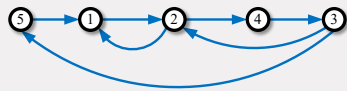
Extended graph:
including the external signals
and disturbance correlations

27
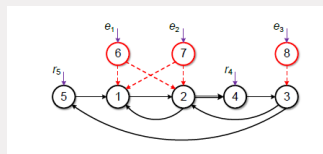
Application: Networks of (damped) oscillators
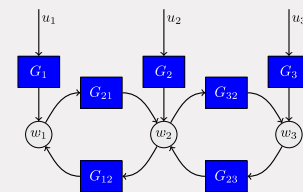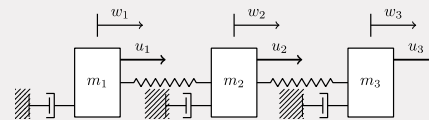
- Power systems, vehicle platoons, thermal building dynamics, …

- Spatially distributed

- Bilaterally coupled

- No central coordination $\Rightarrow$ local identification problems

28

Single module identification - Example
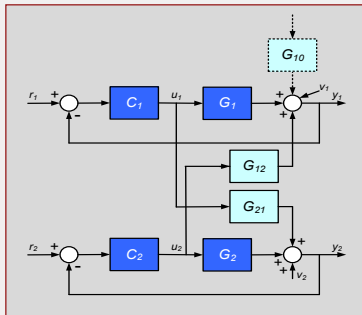
Decentralized MPC
2 interconnected MPC loops

Target:
Identify interaction dynamics
$$G_{21}, G_{12}$$

Addressed by Gudi & Rawlings (2006)
for the situation $G_{12} = 0$ (no cycles)

Gudi, R. D. and Rawlings, J. B. (2006). Identification for decentralized model predictive control. AIChE Journal, 52(6):2198-2210.

TU/e

29

Single module identification

TU/e EINDHOVEN UNIVERSITY OF TECHNOLOGY

Contents

- Introduction and motivation
- How to model a dynamic network?
- Single module identification
- Global network identification
- Physical networks
- Extensions - Discussion

Single module identification
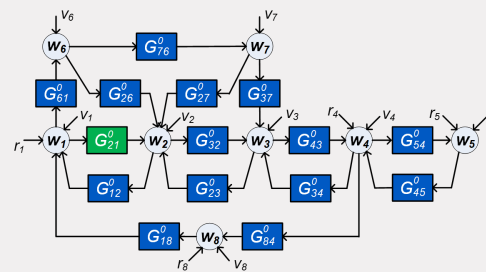
For a network with known topology:

- Identify G_{21}^0 on the basis of measured signals
- Which signals to measure? Preference for local measurements
- When is there enough excitation / data informativity?

TU/e

32

Single module identification
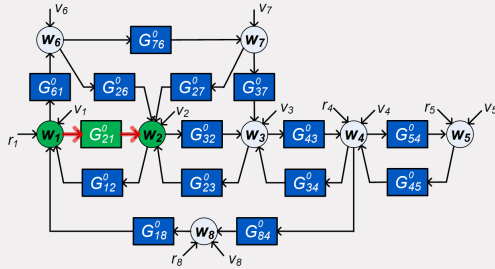
Naïve approach: identify based on w_1 and w_2 : in general does not work.

Single module identification
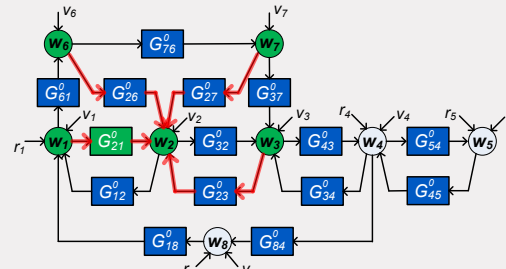
If noises v_k are correlated it may even be part of a MIMO problem

Identifiying G_{21}^0 is part of a 4-input, 1-output problem
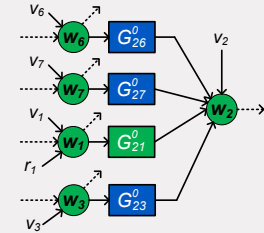
Single module identification

Input signals will be correlated:
similar as in a closed-loop situation

What is required for **identifiability / data informativity**?

Ability to distinguish between models
independent of id-method

Information content of signals
dependent on id-method

Identifiying G_{21}^0 is part of a 4-input, 1-output problem
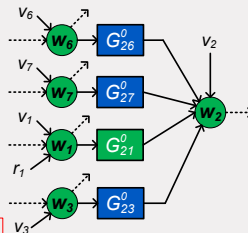
Single module identification
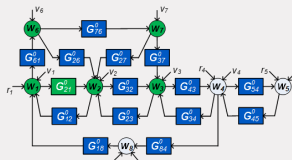
Generic identifiability:
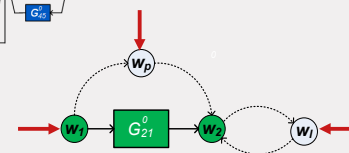
All parallel paths, and loops around the output, plus input w_1 should have an independent external signal r or v

Identifiying G_{21}^0 is part of a 4-input, 1-output problem
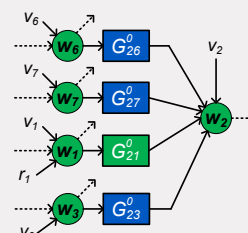
[1] Weerts et al., Automatica 2018, CDC 2018
[2] Bazanella et al. CDC2017; Hendrickx et al., IEEE-TAC, 2019.
[3] Dankers et al., TAC 2016
[4] Shi et al., IFAC 2020 submitted.

Single module identification
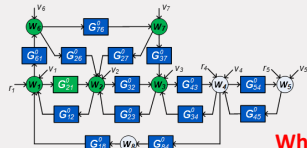
Which node signals to measure?

Dependent on
- v signals uncorrelated or not
- Excitation conditions satisfied through r- and/or v-signals

Typical solution:
- One additional measured signal for each parallel path/loop
- Additional signals if excitation is through v signals
- Variation in available algorithms / options
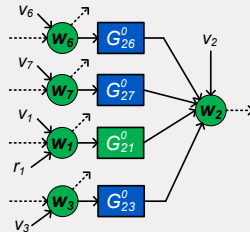
[1] Dankers et al., TAC 2016
[2] Hendrickx et al., IEEE-TAC, 2019.
[3] Gevers et al. SYSID 2018
[4] Bazanella et al., CDC2019
[5] PVdH, Ramaswamy, CDC2019
[6] Shi et al., IFAC 2020 submitted.

TU/e

37

Single module identification

one signal per parallel path/loop:

With a 3-input, 1 output model we can consistently identify G_{21}^0
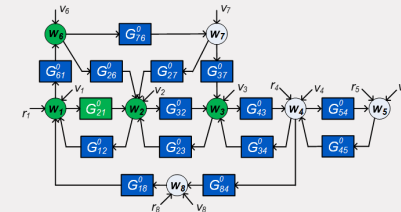
When excitation is through disturbance signals v:

- dealing with **confounding variables,** [1][2] i.e. correlated disturbances on inputs and outputs
- can be addressed by adding inputs/outputs to the estimation problem [3]
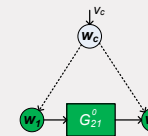
[1] J. Pearl, *Stat. Surveys, 3*, 96-146, 2009
[2] A.G. Dankers et al., *Proc. IFAC World Congress*, 2017.
[3] PVdH et al, CDC 2019

TU/e

38

Single module identification

Typical solution:
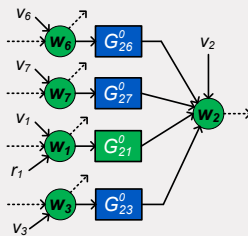
- MISO (sometimes MIMO) estimation problem
- to be solved by any (closed-loop) identification algorithm, e.g. direct/indirect method

TU/e

39

Machine learning in local module identification

- MISO identification with all modules parameterized
- Brings in two major problems :
  - Large number of parameters to estimate
  - Model order selection step for each module (CV, AIC, BIC)

- For 5 modules, combinations = 244,140,625

⚠ Increases variance
Computationally challenging
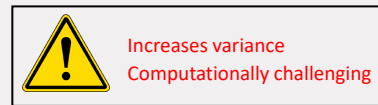
- We need only the target module. No NUISANCE!

TU/e

40

Machine learning in local module identification

Impulse response		Strategy	Model

G_{ji} → g_{ji} → Parametric model $G_{ji}(\theta)$ → $g_{ji}(\theta)$

S_j → s_j → Gaussian process + TC Kernel → $s_j \sim \mathcal{N}(0, \lambda_j K_{\beta j})$

S_{jk_1} → s_{k_1} → Gaussian process + TC Kernel → $s_{k_1} \sim \mathcal{N}(0, \lambda_{k1} K_{\beta k1})$

S_{jk_p} → s_{k_p} → Gaussian process + TC Kernel → $s_{k_p} \sim \mathcal{N}(0, \lambda_{kp} K_{\beta kp})$

- smaller no. of parameters
- simpler model order selection step
- scalable to large dynamic networks
- simpler optimization problems to estimate parameters ✅

Maximize marginal likelihood of output data: $\hat{\eta} = \arg\max_{\eta} p(w_j; \eta)$

$$\eta := \begin{bmatrix} \theta & \lambda_j & \lambda_{k_1} & \dots & \lambda_{k_p} & \beta_j & \beta_{k_1} & \dots & \beta_{k_p} & \sigma_j^2 \end{bmatrix}^\top$$

[1] Everitt et al., Automatica 2017.
[2] K.R. Ramaswamy et al., CDC 2018.

TU/e

41

Numerical simulation

- Identify G_{31} given data
- 50 independent MC simulation
- Data = 500

FIT for estimated model in dynamic network

FIT for impulse response

TS+TO DM+TO DM+MOS EBDM

b_1, b_2, a_1, a_2: DM+TO DM+MOS EBDM

TU/e

Summary single module identification

- Path-based conditions for **network identifiability** (where to excite?)

- Graph tools for checking conditions

- Degrees of freedom in selection of measured signals – sensor selection

- Methods for **consistent** and **minimum variance** module estimation, and effective (scalable) algorithms

- A priori known modules can be accounted for

TU/e

43

TU/e EINDHOVEN UNIVERSITY OF TECHNOLOGY

Contents

- Introduction and motivation
- How to model a dynamic network?
- Single module identification
- Global network identification
- Diffusively coupled physical networks
- Extensions - Discussion

Full network identification
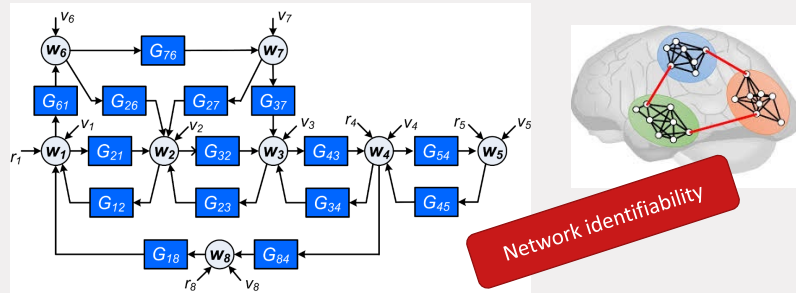
Under which conditions can we estimate the topology and/or dynamics of the full network?

45

Network identifiability

blue = unknown
red = known
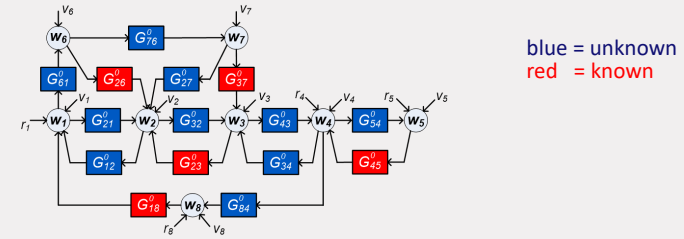
Question: Can different dynamic networks be *distinguished* from each other from measured signals w, r?

46

Network identifiability

The identifiability problem:

The network **model**:

$$w(t) = G(q)w(t) + R(q)r(t) + \underbrace{H(q)e(t)}_{v(t)}$$

can be transformed with any rational $P(q)$:

$$P(q)w(t) = P(q)\{G(q)w(t)+R(q)r(t)+H(q)e(t)\}$$

to an **equivalent model**:

$$w(t) = \tilde{G}(q)w(t) + \tilde{R}(q)r(t) + \tilde{H}(q)e(t)$$

⟹ **Nonuniqueness,** unless there are structural constraints on G, R, H.
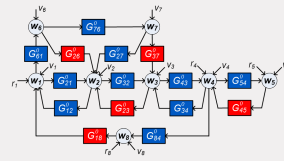
[1] Weerts, Linder et al., Automatica, 2020, to appear.
[2] Bottegal et al., SYSID 2017

47

Network identifiability

Consider a **network model set**:

$$\mathcal{M} = \{(G(\theta), R(\theta), H(\theta))\}_{\theta \in \Theta}$$

representing structural constraints on the considered models:
- modules that are fixed and/or zero (topology)
- locations of excitation signals
- disturbance correlation

Generic identifiability of $\mathcal{M}$:

    - There do not exist distinct equivalent models
    - for almost all models in the set.

[1] Weerts et al., SYSID2015; Weerts et al., Automatica, March 2018;
[2] Bazanella, CDC2017; Hendrickx et al., IEEE-TAC, 2019.

48

Example 5-node network

Conditions for identifiability ➡ rank conditions on transfer function
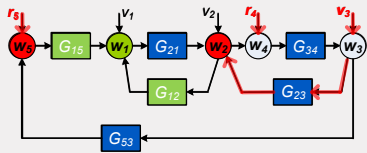
Full row rank of

$$\begin{bmatrix} v_3 \\ r_4 \\ r_5 \end{bmatrix} \rightarrow \begin{bmatrix} w_2 \\ w_5 \end{bmatrix}$$

For the **generic case**, the rank can be calculated by a graph-based condition[1],[2],[3] :

Generic rank = number of vertex-disjoint paths

2 vertex-disjoint paths → full row rank 2 ✅
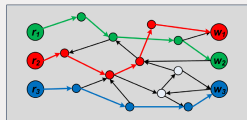
The rank condition has to be checked for all nodes.

[1] Van der Woude, 1991
[2] Hendrickx, Gevers & Bazanella, CDC 2017, TAC 2019
[3] van Waarde et al., ArXiv, 2018.

49

TU/e

Synthesis solution for network identifiability

Allocating external signals for generic identifiability:

1. Cover the graph of the network model set by a set of **disjoint pseudo-trees**

   Pseudo-trees:

   Tree with root in green
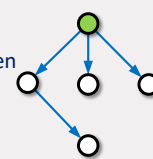
   Cycle with outgoing trees;
   Any node in cycle is root
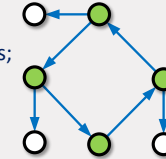
   Edges are **disjoint** and all out-neighbours of a node are in the same pseudo-tree

2. Assign an independent external signal (r or e) at a root of each pseudo-tree.

   This guarantees generic identifiability of the model set.

[1] X. Cheng, S. Shi and PVdH, CDC 2019.

50

TU/e

Where to allocate external excitations for network identifiability?
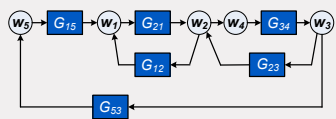
All indicated modules are parametrized

Two disjoint pseudo-trees

51

TU/e
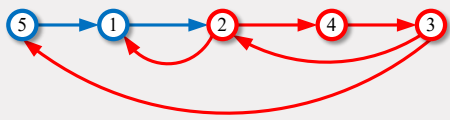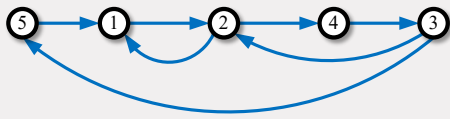
Where to allocate external excitations for network identifiability?
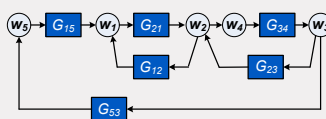
Two independent excitations
guarantee
generic network identifiability
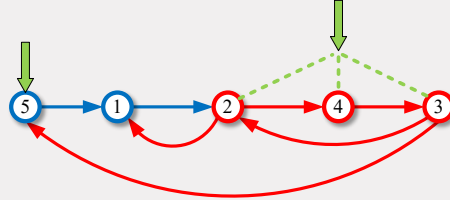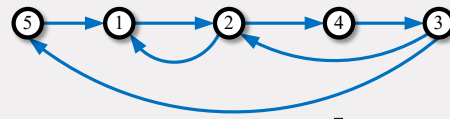
[1] X. Cheng, S. Shi and PVdH, CDC 2019.

52

TU/e

Where to allocate external excitations for network identifiability?

Pseudo-tree merging algorithm [1]
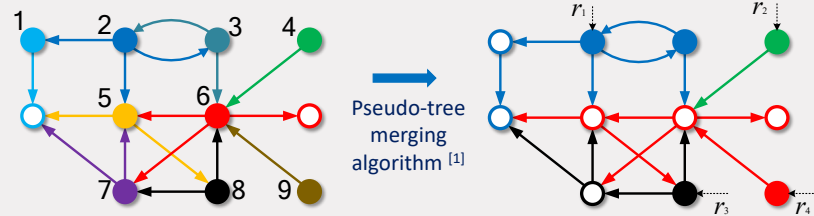
- Nodes are signals w and external signals (r, e) that are input to parametrized link

- Known (nonparametrized) links do not need to be covered

[1] X. Cheng, S. Shi and PVdH, CDC 2019.

53

TU/e

Summary identifiability of full network

Identifiability of network model sets is determined by

- Presence and location of external signals, and
- Correlation of disturbances
- Topology of parametrized modules

- Graphic-based tool for synthesizing allocation of external signals

Extensions:
- Situations where not all node signals are measured [1]

[1] Bazanella, CDC 2019.

54

TU/e

Algorithms for identification of full network

(Prediction error) identification methods will typically lead to large-scale **non-convex** optimization problems

Convex relaxation algorithms are being developed[1] as well as machine learning tools

[1] Weerts, Galrinho et al., SYSID 2018

55

TU/e

Topology identification

- Topology resulting from full dynamic model

- Alternative: non-parametric models (Wiener filters [1]) or kernel-based approaches [2][3]
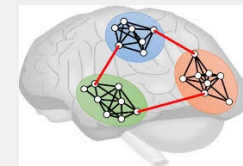
- modeling module dynamics by Gaussian processes,

    kernel with 2 parameters for each dynamic module

- Optimizing likelihood of the data as function of parameters and topology:

$$p(\{w(t)\}_{t=1}^{N} | \theta, \mathcal{G})$$

- Forward-backward search over topologies + empirical Bayes (EM) for parameters

[1] Materassi & Innocenti, TAC 2010.   [3] Shi, Bottegal, PVdH, ECC 2019
[2] Chiuso & Pillonetto, Automatica, 2012.

56

TU/e

Topology identification
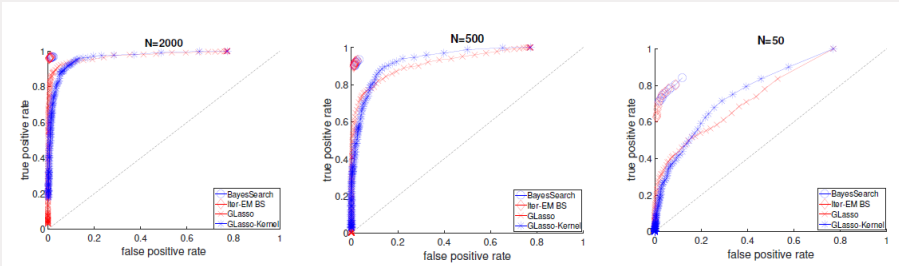
50 MC realizations of network with 6 nodes.

[1] Shi, Bottegal, PVdH, ECC 2019

57

Neurodynamic effect of listening to Mozart music

Identifying changes in network connections in the brain, after intensely listening for one week

(a) Connection from the posterior default mode network to the fronto-parietal right network.

(b) Connection from the sensori-motor superior network to the fronto-parietal right network.

(c) Connection from the central executive network to the sensori-motor superior network.

(d) Connection from the lateral sensori-motor network to the superior temporal gyrus.

(e) Connection from the dorsal attention network to the angular gyrus.

(f) Connection from the anterior default mode network to the dorsal attention network.

Figure 3: Spatial maps of the 20 active brain networks found through the ICA decomposition. Each image consists of 3 relevant horizontal slices of the brain, where the spatial map is indicated by the red color scale.

[1] R. van Esch, S. Shi, A. Bernas, S. Zinger, A. Aldenkamp, PVdH, 2019

58

Algorithms for identification of full network

Particular feature for larger networks:

Modeling disturbances as a **reduced rank process**:
(cf dynamic factor analysis[1])

e

H

v

$\dim(e) < \dim(v)$

Consequences for **estimation**[3]:

- Optimization becomes a constrained quadratic problem with ML properties for Gaussian noise
- Reworked Cramer Rao lower bound
- Some parameters can be estimated variance free → regularization effect
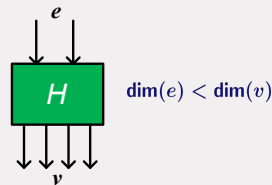
[1] Deistler et al., EJC, 2010.
[2] Zorzi and Chiuso, Automatica 2017.
[3] Weerts et al., Automatica dec 2018.

59

TU/e EINDHOVEN UNIVERSITY OF TECHNOLOGY

Contents

- Introduction and motivation
- How to model a dynamic network?
- Single module identification
- Global network identification
- Physical networks
- Extensions - Discussion

TU/e EINDHOVEN UNIVERSITY OF TECHNOLOGY

Physical networks

Back to the basics of physical interconnections

In connecting physical systems, there is often no predetermined direction of information [1]
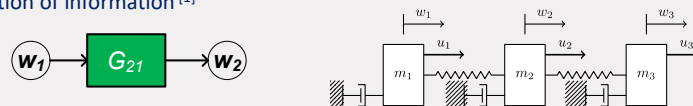
Example: resistor / spring connection in electrical / mechanical system:

Resistor

$$I = \frac{1}{R}(V_1 - V_2)$$

Spring

$$F = K(x_1 - x_2)$$
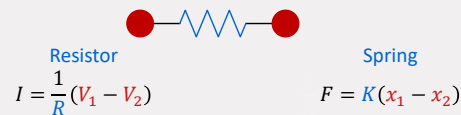
Difference of node signals drives the interaction: **diffusive coupling**

[1] J.C. Willems (1997,2010)

TU/e

62

Diffusively coupled physical network

Equation for node j:

$$M_j \ddot{w}_j(t) + D_{j0}\dot{w}_j(t) + \sum_{k \neq j} D_{jk}(\dot{w}_j(t) - \dot{w}_k(t)) + K_{j0}w_j(t) + \sum_{k \neq j} K_{jk}(w_j(t) - w_k(t)) = u_j(t),$$

TU/e

63

Mass-spring-damper system

- Masses M_j
- Springs K_{jk}
- Dampers D_{jk}
- Input u_j
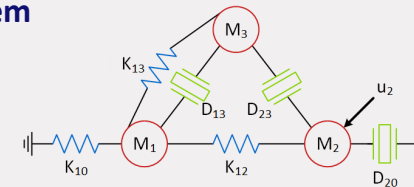
$$\begin{bmatrix} M_1 & & \\ & M_2 & \\ & & M_3 \end{bmatrix}\begin{bmatrix} \ddot{w}_1 \\ \ddot{w}_2 \\ \ddot{w}_3 \end{bmatrix} + \begin{bmatrix} 0 & & \\ & D_{20} & \\ & & 0 \end{bmatrix}\begin{bmatrix} \dot{w}_1 \\ \dot{w}_2 \\ \dot{w}_3 \end{bmatrix} + \begin{bmatrix} K_{10} & 0 & \\ 0 & 0 & \\ & & 0 \end{bmatrix}\begin{bmatrix} w_1 \\ w_2 \\ w_3 \end{bmatrix}$$

$$+ \begin{bmatrix} D_{13} & 0 & -D_{13} \\ 0 & D_{23} & -D_{23} \\ -D_{13} & -D_{23} & D_{13}+D_{23} \end{bmatrix}\begin{bmatrix} \dot{w}_1 \\ \dot{w}_2 \\ \dot{w}_3 \end{bmatrix} + \begin{bmatrix} K_{12}+K_{13} & -K_{12} & -K_{13} \\ -K_{12} & K_{12} & 0 \\ -K_{13} & 0 & K_{13} \end{bmatrix}\begin{bmatrix} w_1 \\ w_2 \\ w_3 \end{bmatrix} = \begin{bmatrix} 0 \\ u_2 \\ 0 \end{bmatrix}$$

$$[\ \underbrace{A(p)}_{diagonal}\ +\ \underbrace{B(p)}_{Laplacian}\ ]\ w(t) = u(t) \qquad A(p), B(p)\ \text{polynomial} \qquad p = \frac{d}{dt}$$

TU/e

64

Mass-spring-damper system

$$\big[\ \underbrace{A(p)}_{diagonal}\ +\ \underbrace{B(p)}_{Laplacian}\ \big]\ w(t) = u(t) \qquad A(p), B(p)\ \text{polynomial}$$

$$\big[\ \underbrace{Q(p)}_{diagonal}\ -\ \underbrace{P(p)}_{hollow\&symmetric}\ \big]\ w(t) = u(t)$$

This fully fits in the earlier module representation:

$$w(t) = Gw(t) + \underbrace{Rr(t) + He(t)}_{Q^{-1}(p)u(t)}$$

with the additional condition that:

$$G(p) = Q(p)^{-1}P(p) \qquad Q(p), P(p)\ \text{polynomial}$$

$P(p)$ symmetric, $Q(p)$ diagonal

65

Module representation

Consequences for node interactions:
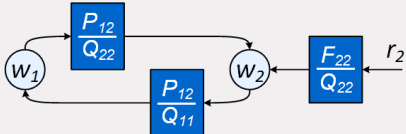
- Node interactions come in pairs of modules
- Where numerators are the same

Framework for network identification remains the same

- Symmetry can simply be incorporated in identification

66

Local network identification

Identification of **one** physical interconnection

Identification of **two** modules G_{jk} and G_{kj}

67
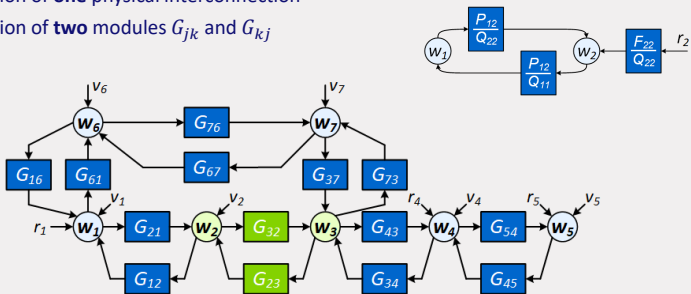
Immersion conditions

For simultaneously identifying two modules in one interconnection:
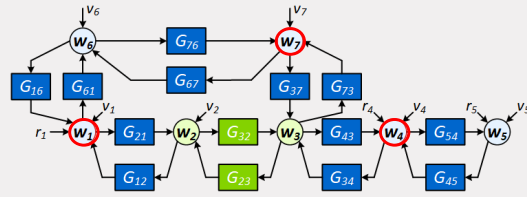
The parallel path and loops-around-the-output condition, now simplifies to:

Measuring/exciting all neighbouring nodes of w_2 and w_3 leads to a solution

E.E.M. Kivits et al., CDC 2019.

68

Summary physical networks

- Physical networks fit within the module framework (special case)

  - no restriction to second order equations

- Earlier identification framework can be utilized

- Local identification is well-addressed (and stays really local)

- Framework is fit for representing **cyber-physical systems**
  (combining physical bi-directional links, and cyber uni-directional links).

TU/e

69

Extensions - Discussion

Extensions - Discussion

- **Including sensor noise** [1]

  - Errors-in-variabels problems can be more easily handled in a network setting

- **Distributed estimation (MISO models)** [2]
  - Communication constraints between different agents
  - Recursive (distributed) estimator converges to global optimizer (more slowly)

- **Experiment design** [3],[4]
  - design of least costly experiments

[1] Dankers et al., Automatica, 2015.
[2] Steentjes et al., IFAC-NECSYS, 2018.
[3] Gevers and Bazanella, CDC 2015.
[4] Morelli, Bombois et al., ECC 2019;

TU/e

71

Summary

- **Dynamic network modeling:**

  intriguing research topic with many open questions

- The (centralized) LTI framework is only just the beginning

- Further move towards data-aspects related to distributed control

- and large-scale aspects

- and bring it to real-life applications

TU/e

72

Acknowledgements

Co-authors, contributors and discussion partners:

Arne Dankers   Harm Weerts

Xavier Bombois
Peter Heuberger
Donatelllo Materassi
Manfred Deistler
Michel Gevers
Jonas Linder
Sean Warnick
Alessandro Chiuso
Hakan Hjalmarsson
Miguel Galrinho
Martin Enqvist

Lizan Kivits, Shengling Shi, Karthik Ramaswamy,
Tom Steentjes, Mircea Lazar, Jobert Ludlage, Mannes Dreef,
Tijs Donkers, Giulio Bottegal, Maarten Schoukens, Xiaodong Cheng

erc
European Research Council

TU/e

73

Further reading

- P.M.J. Van den Hof, A. Dankers, P. Heuberger and X. Bombois (2013). Identification of dynamic models in complex networks with prediction error methods - basic methods for consistent module estimates. *Automatica*, Vol. 49, no. 10, pp. 2994-3006.
- A. Dankers, P.M.J. Van den Hof, X. Bombois and P.S.C. Heuberger (2015). Errors-in-variables identification in dynamic networks - consistency results for an instrumental variable approach. *Automatica*, Vol. 62, pp. 39-50, December 2015.
- A. Dankers, P.M.J. Van den Hof, P.S.C. Heuberger and X. Bombois (2016). Identification of dynamic models in complex networks with predictior error methods - predictor input selection. *IEEE Trans. Autom. Contr.*, *61 (4)*, pp. 937-952, 2016.
- H.H.M. Weerts, P.M.J. Van den Hof and A.G. Dankers (2018). Identifiability of linear dynamic networks. *Automatica*, 89, pp. 247-258, March 2018.
- H.H.M. Weerts, P.M.J. Van den Hof and A.G. Dankers (2018). Prediction error identification of linear dynamic networks with rank-reduced noise. *Automatica*, *98*, pp. 256-268, December 2018.
- H.H.M. Weerts, P.M.J. Van den Hof and A.G. Dankers (2018). Single module identifiability in linear dynamic networks. Proc. 57th IEEE CDC 2018.
- K.R. Ramaswamy, G. Bottegal and P.M.J. Van den Hof (2018). Local module identification in dynamic networks using regularized kernel-based methods. Proc. 57th CDC, 2018.
- H.H.M. Weerts, J. Linder, M. Enqvist and P.M.J. Van den Hof (2019). Abstractions of linear dynamic networks for input selection in local module identification. To appear in Automatica, 2020. ArXiv 1901.00348.
- P.M.J. Van den Hof, K.R. Ramaswamy, A.G. Dankers and G. Bottegal. Local module identification in dynamic networks with correlated noise: the full input case. Proc. 2019 CDC.
- K.R. Ramaswamy and P.M.J. Van den Hof (2019). A local direct method for module identification in dynamic networks with correlated noise. Provisionally accepted by IEEE Trans. Automatic Control. ArXiv:1908.00976.
- X. Cheng, S. Shi and P.M.J. Van den Hof (2019). Allocation of excitation signals for generic identifiability of linear dynamic networks. Proc. 2019 CDC. ArXiv 1910.04525.
- K.R. Ramaswamy, P.M.J. Van den Hof and A.G. Dankers (2019). Generalized sensing and actuation schemes for local module identification in dynamic networks. Proc. 2019 CDC.
- E.M.M. Kivits and P.M.J. Van den Hof (2019). A dynamic network approach to identification of physical systems. Proc. 2019 CDC.
- S. Shi, G. Bottegal and P.M.J. Van den Hof (2019). Bayesian topology identification of linear dynamic networks. Proc. 2019 ECC, Napels, Italy, pp. 2814-2819.

Papers available at www.pvandenhof.nl

TU/e

74

TU/e EINDHOVEN UNIVERSITY OF TECHNOLOGY

The end

Cooperative and/or Autonomous driving

Henk Nijmeijer
Dynamics & Control

11 March 2020

TU/e Technische Universiteit
Eindhoven
University of Technology

Where innovation starts

Symposium AcTI en KNAW: Autonoom vervoer

Hoewel autonoom vervoer steeds dichterbij komt, rijden er nog geen zelfrijdende auto's door onze straten. Hoe kan dat? Sprekers belichten de uitdagingen in het realiseren ervan vanuit verschillende invalshoeken.

Terwijl meerdere grote bedrijven er al geruime tijd op volle kracht aan werken, bijten ingenieurs, juristen, verkeerskundigen en ethici hun tanden erop stuk, en bereiden overheden en verzekeringsmaatschappijen zich voor op deze nieuwe technologie. Blijkbaar is het zowel technologisch als maatschappelijk een flinke uitdaging om autonoom vervoer te realiseren.

TU/e Technische Universiteit
Eindhoven
University of Technology

The near future of automated driving

2
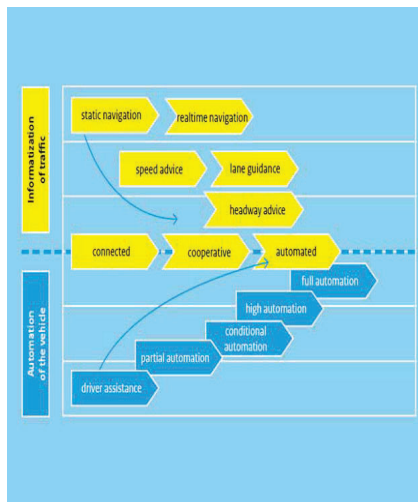
The full potential of automated driving can only be reached by combining cooperative driving (V2x enabled) and automated driving to improve:

- Vehicle and traffic efficiency
- Safety
- Comfort

TU/e Technische Universiteit
Eindhoven
University of Technology

Contents

3

- What is an autonomous vehicle?
  - Levels of automation
  - Autonomous vs cooperative automated

- Cooperative adaptive cruise control – so far no steering!

- Autonomous versus Cooperative

- Path-planning and Camera-vision (detection)

- Future

TU/e Technische Universiteit
Eindhoven
University of Technology

Levels of automation

4

Level	Name	Narrative definition	Execution of steering and acceleration/deceleration	Monitoring of driving environment	Fallback performance of *dynamic driving task*	System capability *(driving modes)*
Human driver monitors the driving environment						
0	No Automation	the full-time performance by the *human driver* of all aspects of the *dynamic driving task*, even when enhanced by warning or intervention systems	Human driver	Human driver	Human driver	n/a
1	Driver Assistance	the *driving mode*-specific execution by a driver assistance system of either steering or acceleration/deceleration using information about the driving environment and with the expectation that the *human driver* perform all remaining aspects of the *dynamic driving task*	Human driver and system	Human driver	Human driver	Some driving modes
2	Partial Automation	the *driving mode*-specific execution by one or more driver assistance systems of both steering and acceleration/deceleration using information about the driving environment and with the expectation that the *human driver* perform all remaining aspects of the *dynamic driving task*	System	Human driver	Human driver	Some driving modes
Automated driving system ("system") monitors the driving environment						
3	Conditional Automation	the *driving mode*-specific performance by an *automated driving system* of all aspects of the *dynamic driving task* with the expectation that the *human driver* will respond appropriately to a *request to intervene*	System	System	Human driver	Some driving modes
4	High Automation	the *driving mode*-specific performance by an *automated driving system* of all aspects of the *dynamic driving task*, even if a *human driver* does not respond appropriately to a *request to intervene*	System	System	System	Some driving modes
5	Full Automation	the full-time performance by an *automated driving system* of all aspects of the *dynamic driving task* under all roadway and environmental conditions that can be managed by a human driver	System	System	System	All driving modes

TU/e Technische Universiteit Eindhoven University of Technology

Levels of automation

5

- Starting at level 4 automation the driver can be taken out in well-defined situations.
- At level 3 automation the driver is used as a fall-back mechanism, but what does this mean?

- What time does the driver have to perform the take-over?
  - What kind of situations should the driver expect?
  - In aviation pilots are already struggling when having to intervene.

  Level 3 is not full autonomy and can be dangerous when implemented in every day traffic!
- Safe operation mainly relies on the safety margins maintained by the vehicle (in combination with human 'comfort' levels).
- **How do we guarantee efficient traffic in that way?**

-

TU/e Technische Universiteit Eindhoven University of Technology

Autonomous vs cooperative automated

6

Autonomous

Cooperative

Action → Reaction   vs   Intention → *Coordinated* reaction

Conclusion:

Autonomous vehicle priority on interacting with the environment (reactive). Cooperative vehicle priority on understanding traffic behavior, taking coordinated action (pro-active).

TU/e Technische Universiteit Eindhoven University of Technology

Autonomous vs cooperative automated

7

- Action → reaction, creates over-reaction! (traffic jams, emergency braking)
  - Humans create traffic jams (time-delay, distraction, drowsiness, ignorance, misunderstanding etc.) but, …
  - At the same time we humans have an extremely good capability to *anticipate* and *interact* on sudden situations
- Automated vehicles have limited capability of anticipation and interaction
  - Extreme perception and intelligence needed for prediction of behavior

TU/e Technische Universiteit Eindhoven University of Technology

Autonomous?
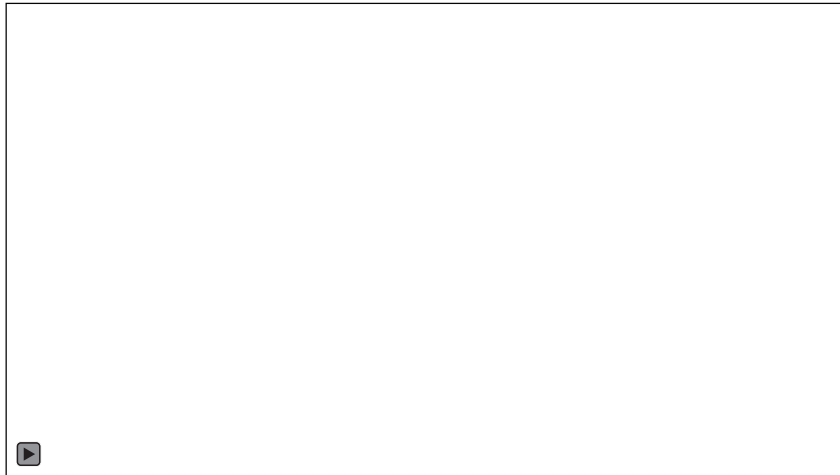
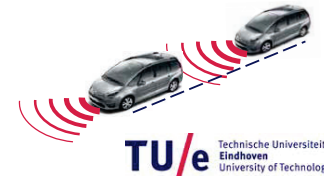## Cooperative Adaptive Cruise Control

- Cooperative Adaptive Cruise Control (CACC)
  - Vehicle-following control system (longitudinal vehicle automation)
  - Employs wireless inter-vehicle communication (future 5G)
    - beyond line-of-sight of onboard sensors
    - more information than possible with onboard sensors

- CACC benefits: Increase road capacity and fuel efficiency by decreasing time gap between vehicles (≤ 0.3 s), compared to ACC
- Main CACC vulnerability:
  - Dependency on wireless link
  - Packet loss over extended time period
  - Non-equipped vehicles

Cooperative Adaptive Cruise Control

Vehicle-following objective

- Spacing policy $d_{r,i} = r +$

C - ACC (2)
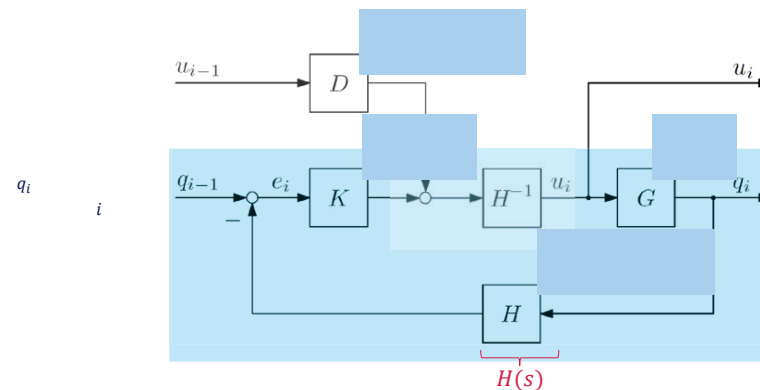
- Laplace domain: $e_i(s) = q_{i-1}(s) \quad (1 + hs)q_i(s)$

C - ACC (2)

- Distance error
- $e_i(t) = d_i(t) \quad d_{r,i}(t) = \begin{pmatrix} q_{i-1}(t) & q_i^i(t) \end{pmatrix} \quad q_i(t)$

- ($r = 0$, vehicle length is 0)

Cooperative Adaptive Cruise Control

String stability
- Attenuation of the effects of disturbances along the vehicle string
- Condition (strict $_2$ string stability):
  $\|\ _i(s)\|_\infty \quad 1$
- In words: No overshoot of the velocity of the following vehicle along the string of vehicles.
- Dependent on numerous parameters:
  - Quality of communication
  - Vehicle parameters
  - Controller implementation
- Without communication there are ways of maintaining part of the vehicle performance (dCACC)

CACC results

- CACC $0.3s = 8.3m$ at 100 km/h

- ACC $3.2s = 88.9m$ at 100 km/h

- dCACC $1.2s = 33.3m$ at 100 km/h

- Humans typically drive at +/- 1.3s

$\|\ (s)\|_\infty = 1.2$
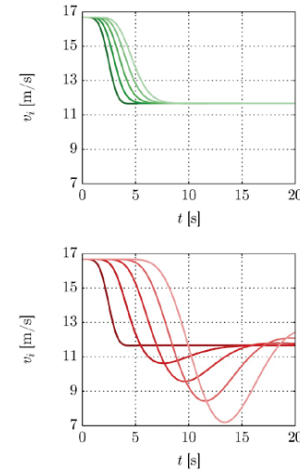
Experimental validation: test vehicles

- Collaboration TNO-TU/e
- Implementation in 3 cars (Toyota Prius III Executive)
- Forward-looking radar
- ITS G5 (IEEE 802.11p) wireless communication

Experimental validation

Measured vehicle response with an inter vehicle distance of only 0.6s.

CACC ACC dCACC
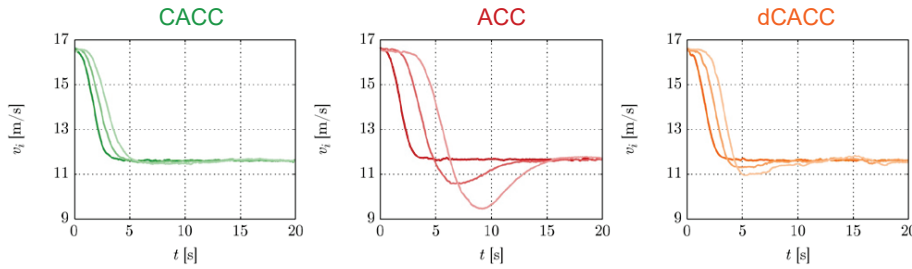
CACC and dCACC ('ideal settings')

- CACC allows for short-distance vehicle following
  - Improves road throughput
  - Decreases fuel consumption (for commercial vehicles)

- Fail-safe mechanism essential for practical implementation
  - Employs acceleration estimation using radar measurements only, counteracting:
    - Communication loss for an extended period of time,
    - Non-communicating preceding vehicle
  - Limited increase of time headway necessary to regain string stability   graceful degradation

Next step: Cooperative steering!?

Autonomous vehicles versus cooperative
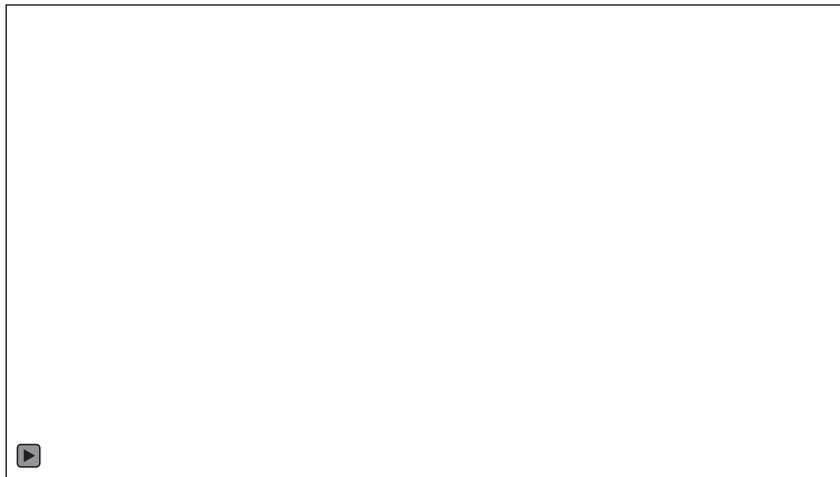
i-cave programme

Pathplanner+controller

20
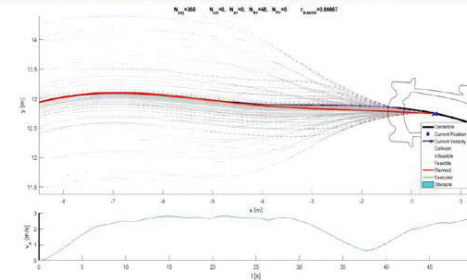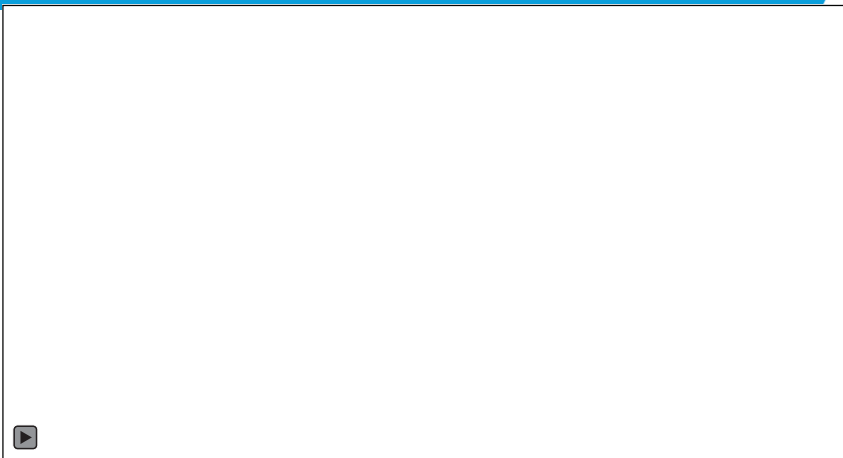
Camera-vision + reconstruction

8   DE VOLKSKRANT
VRIJDAG 29 NOVEMBER 2019

Ten eerste

Met zelfrijdende auto gaat het nog te vaak mis

21

22

23

Strategic Decision-Making and Learning for Autonomous Agents

Ming Cao

Engineering and Technology Institute
University of Groningen
The Netherlands

1

An evolutionary approach to coordination of self-interested agents

Advances in
- mobile sensor platforms
- intelligent autonomous robots

"selfishness": individuals maximize their own payoffs, might leading to a great cost to the group

Challenges
- local information vs. global team goal
- unknown, changing environment

Special issues on robotics
Science Magazine
October 2014 and November 2007

2

An evolutionary approach to coordination of self-interested agents

3

An evolutionary approach to coordination of self-interested agents

Key difference from the existing control of complex systems
- incentive-based mechanisms
- co-evolves with changing environment

Sociology: social dilemma in modern society   Biology: understanding cooperating behavior in social animals

4

An evolutionary approach to coordination of self-interested agents

5

Outline

- Paradox of cooperation

- Repeated games and zero-determinant strategies

- Nash equilibrium matters

- Continuous-time replicator dynamics

- Various extensions

7

An **evolutionary** approach to coordination of self-interested agents
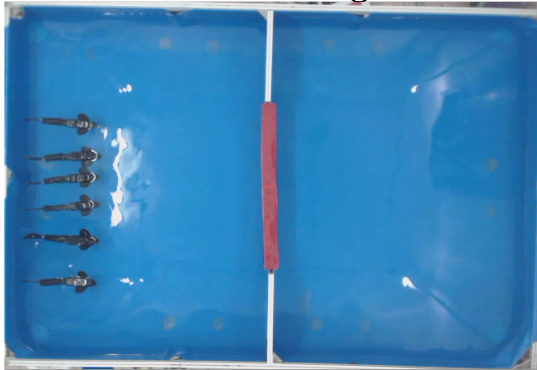
Carry out the task repeatedly; adjust strategies over time
- each time the task is taken as a group game
- new insight into how cooperation emerges as an evolutionary outcome

The paradox of cooperation

Natural selection is based on competition. How can it lead to cooperation?

Cooperation is often costly for the individual, while benefits are distributed over a collective

Cooperation (altruism) is an evolutionary puzzle!
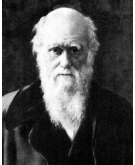
Charles Darwin (1809-1882)

8

Mechanism for evolution of cooperation is a central topic

9

REVIEW

Five Rules for the Evolution of Cooperation

Martin A. Nowak

Cooperation is needed for evolution to construct new levels of organization. Genomes, cells, multicellular organisms, social insects, and human society are all based on cooperation. Cooperation means that selfish replicators forgo some of their reproductive potential to help one another. But natural selection implies competition and therefore opposes cooperation unless a specific mechanism is at work. Here I discuss five mechanisms for the evolution of cooperation: kin selection, direct reciprocity, indirect reciprocity, network reciprocity, and group selection. For each mechanism, a simple rule is derived that specifies whether natural selection can lead to cooperation.

M. A. Nowak,
Science,
V314,
1560-1563,
2006

- Kin selection
- Direct reciprocity ("tit-for-tat")
- Indirect reciprocity
- Network reciprocity
- Group selection

rich theory – limited predictive power…

10

Free-rider problem: the prisoner's dilemma

	cooperate	defect
cooperate	$b-c$	$-c$
defect	b	0

$$b > c > 0$$

Mutual cooperation more profitable than mutual defection

But: under all circumstances to defect is the dominant strategy

11

Will players change strategies if the game is repeated ?

BBC 1986 documentary by Richard Dawkins, author of "The Selfish Gene" (1976)

Tit for Tat: starts off by cooperating, then copies the opponent's last move;
Win-stay lose-shift: repeats when rewarded and changes otherwise.

12

Revisit the prisoner's dilemma

	Cooperate (C)	Defect (D)
Cooperate (C)	R	S
Defect (D)	T	P

R: reward (good)
S: sucker's payoff (very bad)
T: temptation (very good)
P: punishment (bad)

$S < P < R < T$

Define the player's strategy to be her probabilities to cooperate in view of the two players' strategies in the last round:
If both cooperative (C,C) $\rightarrow p_1$; if (C,D)$\rightarrow p_2$; if (D,C) $\rightarrow p_3$; if (D,D) $\rightarrow p_4$.

Use $p = [p_1, p_2, p_3, p_4]^{\mathsf{T}}$ and $q = [q_1, q_2, q_3, q_4]^{\mathsf{T}}$ to denote the two players' strategies.

13
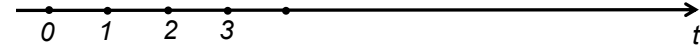
(C,C)
(C,D)
(D,C)
(D,D)

A player's strategy is her probabilities to cooperate in view of the two players' strategies in the last round:
Player 1: (C,C) $\rightarrow p_1$; if (C,D)$\rightarrow p_2$; if (D,C) $\rightarrow p_3$; if (D,D) $\rightarrow p_4$.

Player 2: (C,C) $\rightarrow q_1$; if (C,D)$\rightarrow q_2$; if (D,C) $\rightarrow q_3$; if (D,D) $\rightarrow q_4$.

14
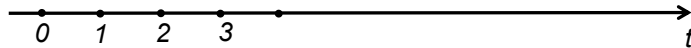
(C,C) $\quad v_1$
(C,D) $\quad v_2$
(D,C) $\quad v_3$
(D,D) $\quad v_4$

$$M = \begin{bmatrix} p_1 q_1 & p_1(1-q_1) & (1-p_1)q_1 & (1-p_1)(1-q_1) \\ p_2 q_3 & p_2(1-q_3) & (1-p_2)q_3 & (1-p_2)(1-q_3) \\ p_2 q_2 & p_3(1-q_2) & (1-p_3)q_2 & (1-p_3)(1-q_2) \\ p_4 q_4 & p_4(1-q_4) & (1-p_4)q_4 & (1-p_4)(1-q_4) \end{bmatrix}$$

$v = \begin{bmatrix} v_1 & v_2 & v_3 & v_4 \end{bmatrix}$ $\qquad vM = v$ $\qquad \Longrightarrow \qquad v(M-I) = 0$

A player's strategy is her probabilities to cooperate in view of the two players' strategies in the last round:
Player 1: (C,C) $\rightarrow p_1$; if (C,D)$\rightarrow p_2$; if (D,C) $\rightarrow p_3$; if (D,D) $\rightarrow p_4$.

Player 2: (C,C) $\rightarrow q_1$; if (C,D)$\rightarrow q_2$; if (D,C) $\rightarrow q_3$; if (D,D) $\rightarrow q_4$.

15
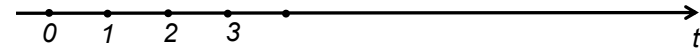
(C,C) $\quad v_1$
(C,D) $\quad v_2$
(D,C) $\quad v_3$
(D,D) $\quad v_4$

$$M = \begin{bmatrix} p_1 q_1 & p_1(1-q_1) & (1-p_1)q_1 & (1-p_1)(1-q_1) \\ p_2 q_3 & p_2(1-q_3) & (1-p_2)q_3 & (1-p_2)(1-q_3) \\ p_2 q_2 & p_3(1-q_2) & (1-p_3)q_2 & (1-p_3)(1-q_2) \\ p_4 q_4 & p_4(1-q_4) & (1-p_4)q_4 & (1-p_4)(1-q_4) \end{bmatrix}$$

$v = \begin{bmatrix} v_1 & v_2 & v_3 & v_4 \end{bmatrix}$ $\qquad vM = v$ $\qquad \Longrightarrow \qquad v(M-I) = 0$

Once v is computed, then the first player's expected payoff can be computed by

$$s_1 = \begin{vmatrix} -1 + p_1 q_1 & -1 + p_1 & -1 + q_1 & R \\ p_2 q_3 & -1 + p_2 & q_3 & S \\ p_3 q_2 & p_3 & -1 + q_2 & T \\ p_4 q_4 & p_4 & q_4 & P \end{vmatrix}$$

Similarly, the second player's expected payoff s_2 can be computed.

16

In fact, the two players' expected payoffs s_1 and s_2 have to satisfy some linear relationship, namely for some constants α, β and γ, it holds

$$\alpha s_1 + \beta s_2 + \gamma = \begin{vmatrix} -1+p_1q_1 & -1+p_1 & -1+q_1 & (\alpha+\beta)R+\gamma \\ p_2q_3 & -1+p_2 & q_3 & \alpha S+\beta T+\gamma \\ p_3q_2 & p_3 & -1+q_2 & \alpha T+\beta S+\gamma \\ p_4q_4 & p_4 & q_4 & (\alpha+\beta)P+\gamma \end{vmatrix}$$

Once v is computed, then the first player's expected payoff can be computed by

$$s_1 = \begin{vmatrix} -1+p_1q_1 & -1+p_1 & -1+q_1 & R \\ p_2q_3 & -1+p_2 & q_3 & S \\ p_3q_2 & p_3 & -1+q_2 & T \\ p_4q_4 & p_4 & q_4 & P \end{vmatrix}$$

Similarly, the second player's expected payoff s_2 can be computed.

17

In fact, the two players' expected payoffs s_1 and s_2 are coupled. To see this, for some constants α, β and γ, it holds

$$\alpha s_1 + \beta s_2 + \gamma = \begin{vmatrix} -1+p_1q_1 & \boxed{-1+p_1} & \boxed{-1+q_1} & (\alpha+\beta)R+\gamma \\ p_2q_3 & -1+p_2 & q_3 & \alpha S+\beta T+\gamma \\ p_3q_2 & p_3 & -1+q_2 & \alpha T+\beta S+\gamma \\ p_4q_4 & p_4 & q_4 & (\alpha+\beta)P+\gamma \end{vmatrix}$$

If player 1 chooses its strategy in order to make the second column *equal* the fourth column, then the determinant becomes zero (this becomes the so-called *zero-determinant strategy*), then s_1 and s_2 satisfy the *linear* relationship:

$$\alpha s_1 + \beta s_2 + \gamma = 0$$

In the special case setting α =0, one has $\quad s_2 = -\frac{\gamma}{\beta}$

In fact, player 1 can *unilaterally* force the relationship

$$s_1 - P = k(s_2 - P), \qquad k > 0$$

18

Zero-determinant strategies and "theory of mind"

The presumption that others have a mind is termed a "theory of mind".

"Iterated Prisoner's Dilemma contains strategies that dominate any evolutionary opponent", W.H. Press, F.J. Dyson, PNAS 2012

If player 1 chooses its strategy in order to make the second column *equal* the fourth column, then the determinant becomes zero (this becomes the so-called *zero-determinant strategy*), then s_1 and s_2 satisfy the *linear* relationship:

$$\alpha s_1 + \beta s_2 + \gamma = 0$$

In the special case setting α=0, one has $\quad s_2 = -\frac{\gamma}{\beta}$

In fact, player 1 can *unilaterally* force the relationship

$$s_1 - P = k(s_2 - P), \qquad k > 0$$

19

Outline

- Paradox of cooperation

- Repeated games and zero-determinant strategies

- Nash equilibrium matters

- Continuous-time replicator dynamics

- Various extensions

20

There is more to cooperation than the prisoner's dilemma

The Snowdrift game:

	cooperate	defect
cooperate	$b - \frac{1}{2}c$	$b - c$
defect	b	0

$$b > c > 0$$

mixed-strategy Nash equilibrium: $\hat{p}_c = \dfrac{b - c}{b - \frac{1}{2}c}$

21

There is more to cooperation than the prisoner's dilemma

The Stag hunt game:

	cooperate	hunt alone
cooperate	B	0
hunt alone	b	b

$$B > b > 0$$

two pure-strategy Nash equilibria: coordination game

22

Evolutionary game theory: History and motivation

John Maynard Smith was interested in why so many animals engage in ritualized fighting ("The logic of animal conflict", *Nature*, 1973)

Evolutionary game theory refers to the study of large populations of interacting agents, and how various behaviors and traits might evolve.

Differences from classical game theory
- Players   = sub-populations, employing a common strategy
- Strategies = behaviors or traits encoded in genes
- Payoffs   = fitness, which determines reproductive rates

Key concept: The fitness of an individual must be evaluated in the context of the population in which it lives and interacts

23

Dynamical system description for evolutionary games

Matrix game (symmetric two-player normal form with finitely many strategies)

Pure strategies: $e_1, e_2, \ldots, e_m$ unit vectors in $\mathbb{R}^m$
Mixed strategies: $p = (p_1, \ldots, p_m) \in \Delta^m$

where $\Delta^m = \{p \mid \sum_{i=1}^{m} p_i = 1\}$
$p_i \geq 0$
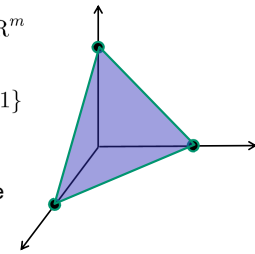
- Payoff: Individuals interact in a two-player game

- Let $\pi(e_i, e_j)$ be the payoff of e_i against e_j,
  then the m-by-m payoff matrix A has entries $A_{ij} = \pi(e_i, e_j)$

- The payoff of p against q is $\pi(p, q) = \displaystyle\sum_{i,j=1}^{m} p_i \pi(e_i, e_j) q_j = p^T A q$

24

Dynamical system description for evolutionary games

Matrix game (symmetric two-player normal form with finitely many strategies)

Assumptions:

- Well-mixed large population (all-to-all network)
- Random pairwise interaction per unit time
- Payoff translate directly into fitness that determines reproductive rate
- Individuals use pure strategies

Key concept: The fitness of an individual must be evaluated in the context of the population in which it lives and interacts

Let $x_i(t)$ denote the share of those individuals using strategy e_i at time t, and $x = [x_1, x_2, \ldots, x_m]$ be the population vector. Then

- The payoff of p against q is $\quad \pi(p,q) = \displaystyle\sum_{i,j=1}^{m} p_i \pi(e_i, e_j) q_j = p^T A q$

Replicator dynamics: $\dot{x}_i = x_i(\pi(e_i, x) - \pi(x, x))$

25

Tempting claims for evolutionary game dynamics

Replicator dynamics: $\dot{x}_i = x_i(\pi(e_i, x) - \pi(x, x))$

26

Tempting claims for evolutionary game dynamics

Replicator dynamics: $\dot{x}_i = x_i(\pi(e_i, x) - \pi(x, x))$

Tempting claim: For the replicator dynamics of a matrix game, it holds that
(a) Any trajectory in the interior of $\triangle^m$ evolves to a Nash equilibrium

x^* is a Nash equilibrium if for all x, $\quad \pi(x, x^*) \leq \pi(x^*, x^*)$

Appealing: Nash equilibria are for individuals as rational decision makers, but replicator dynamics do not assume rationality of the individuals

27

Tempting claims for evolutionary game dynamics

Replicator dynamics: $\dot{x}_i = x_i(\pi(e_i, x) - \pi(x, x))$

Tempting claim: For the replicator dynamics of a matrix game, it holds that
(a) Any trajectory in the interior of $\triangle^m$ evolves to a Nash equilibrium

x^* is a Nash equilibrium if for all x, $\quad \pi(x, x^*) \leq \pi(x^*, x^*)$

Evolutionarily stable strategy (ESS): x^* is ESS if for all other x, we have
(i) The Nash equilibrium condition: $\pi(x, x^*) \leq \pi(x^*, x^*)$
(ii) The stability condition: $\pi(x^*, x) > \pi(x, x)$ if $\pi(x, x^*) = \pi(x^*, x^*)$

Further tempting statement:
(b) A converging trajectory in the interior evolves to an ESS equilibrium

28

Generalized rock-scissors-paper game

Consider the three-strategy matrix game with the payoff matrix

$$A = \begin{array}{c} \\ R \\ S \\ P \end{array} \begin{array}{ccc} R & S & P \\ \begin{pmatrix} 0 & 6 & -4 \\ -4 & 0 & 4 \\ 2 & -2 & 0 \end{pmatrix} \end{array}$$

Cyclic dominance: R beats S, S beats P and P beats R.
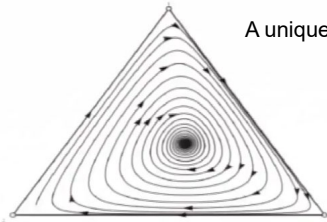
A unique Nash equilibrium: $x^* = (10/29, 8/29, 11/29)$

Almost globally asymptotically stable

But not ESS since

$$\pi(e_1, x^*) = \pi(x^*, x^*) = \tfrac{4}{29}$$
$$\pi(x^*, e_1) = -\tfrac{10}{29} < 0 = \pi(e_1, e_1)$$

The game with the payoff matrix –A reverses the trajectories. The interior trajectories do not converge to a Nash equilibrium, but a heteroclinic cycle

29

Remark on convergence for 4th- or higher-order replicator dynamics

Global analysis in general relies on the construction of Lyapunov functions, which is in general difficult
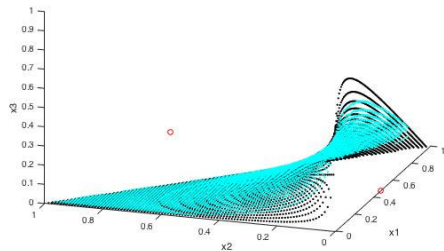
Chaotic behavior can appear.

31

Theorem on ESS for replicator dynamics of a matrix game

(a) x^* is an ESS iff $\pi(x^*, x) > \pi(x, x)$ for all x near x^*

(b) An ESS x^* is a locally asymptotically stable equilibrium

(c) An interior ESS x^* is an almost globally asymptotically stable equilibrium

(a) "locally superior", check (Weibull 1995, Cressman 2010)

(b)(c) (Hofbauer et al, 1979) $V(x) = \Pi_i x_i^{x_i^*}$

is a strict local Lyapunov function.

30

Outline

- Paradox of cooperation

- Repeated games and zero-determinant strategies

- Nash equilibrium matters

- Continuous-time replicator dynamics

- Various extensions

32

Extension 1: Two-population replicator dynamics

- Replicator dynamics for the matrix game with strategies $\{e_1, ..., e_m\}$

$$\dot{x}_i = x_i(\pi(e_i, x) - \pi(x, x)),$$

- Two-population replicator dynamics

$$\dot{p}_i^k = p_i^k[U_i^k(\mathbf{p}) - \bar{U}^k(\mathbf{p})], \qquad k = 1, 2$$

where p_i^k is the proportion of individuals in population k using s_i.

- We use x and y to denote the states of the two populations.

Extension 1 : Payoff matrices with environmental feedback

Individuals from population 1 interact with individuals from population 2, and vise versa.

Dynamic payoff matrices

$$A(r)^{12} = \begin{bmatrix} a_{11}r + b_{11} & \dots & a_{1m}r + b_{1m} \\ \vdots & \ddots & \vdots \\ a_{m1}r + b_{m1} & \dots & a_{mm}r + b_{mm} \end{bmatrix}$$

$$A(r)^{21} = \begin{bmatrix} c_{11}r + d_{11} & \dots & c_{1m}r + d_{1m} \\ \vdots & \ddots & \vdots \\ c_{m1}r + d_{m1} & \dots & c_{mm}r + d_{mm} \end{bmatrix}$$

Dynamics of the environment

$$\dot{r} = r(1 - r)h(x, y)$$

where $h(x, y)$ denotes the impact of population states on the environment, which may enhance or reduce resources.

34

Extension 1 : Specific payoff matrices

Consider the following asymmetric payoff matrices

$$A(r) = (1 - r)\begin{bmatrix} T_1 & P_1 \\ R_1 & S_1 \end{bmatrix} + r\begin{bmatrix} R_1 & S_1 \\ T_1 & P_1 \end{bmatrix}$$

$$B(r) = (1 - r)\begin{bmatrix} T_2 & P_2 \\ R_2 & S_2 \end{bmatrix} + r\begin{bmatrix} R_2 & S_2 \\ T_2 & P_2 \end{bmatrix}$$

with $P_1 > S_1$, $T_1 > R_1$; $P_2 > S_2$, $T_2 > R_2$.

Each matrix has an embedded symmetry to ensure that mutual cooperation is a Nash equilibrium when *r* = 0 and mutual defection is a Nash equilibrium when *r* = 1.

Then the dynamics become

$$\Sigma_1 : \begin{cases} \dot{x} = x(1 - x)[\delta_{PS_1} + (\delta_{TR_1} - \delta_{PS_1})y](1 - 2r) \\ \dot{y} = y(1 - y)[\delta_{PS_2} + (\delta_{TR_2} - \delta_{PS_2})x](1 - 2r) \\ \dot{r} = r(1 - r)[(1 + \theta_1)x + (1 + \theta_2)y - 2] \end{cases}$$

with $\delta_{PS_i} = P_i - S_i > 0$, $\delta_{TR_i} = T_i - R_i > 0$ and θ_k is the enhancement to degradation ratio in population *k*.

Extension 1 : Main result to prove

Theorem

The two-population co-evolutionary game dynamics have infinitely many periodic orbits in the interior of $I_{[0,1]}^3 = [0, 1]^3$.

36

Extension 1 : Reversible system

- Reversible system

  A dynamical system is said to be *reversible* if there is an involution G in its phase space which reverses the direction of time, i.e. the dynamics are invariant under a change in the sign of time.

- Periodic Orbits

  An orbit (not a fixed point) is *periodic and symmetric* with respect to G if and only if the orbit intersects $\mathrm{Fix}(G)$ at precisely two points.

For system Σ_1, one can find

$$G : x \to x, y \to y, r \to 1 - r$$

$$Fix(G) : \quad \{r = 1/2\}$$

such that

$$\Sigma_1 \overset{G}{\Rightarrow} \tilde{\Sigma}_1 \overset{G}{\Rightarrow} \Sigma_1$$

37

Extension 1 : Reversible system

Divide $I_{(0,1)}^3 = (0,1)^3$ into four regions by the two planes

$$\{r = 1/2\}$$

$$\{(1 + \theta_1)x + (1 + \theta_2)y = 2\}$$

$\Omega_1 : \{\frac{1}{2} < r < 1, (1 + \theta_1)x + (1 + \theta_2)y > 2\}$

$\Omega_2 : \{\frac{1}{2} < r < 1, (1 + \theta_1)x + (1 + \theta_2)y < 2\}$

$\Omega_3 : \{0 < r < \frac{1}{2}, (1 + \theta_1)x + (1 + \theta_2)y < 2\}$

$\Omega_4 : \{0 < r < \frac{1}{2}, (1 + \theta_1)x + (1 + \theta_2)y > 2\}$
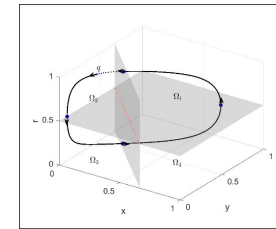
A typical trajectory
Consider an arbitrary trajectory starting from point q;
it goes across the plane $\{r = 1/2\}$ and into Ω_3;
crosses plane $\{(1 + \theta_1)x + (1 + \theta_2)y = 2\}$
and enters Ω_4;
then crosses plane $\{r = 1/2\}$ again;
returns to the starting point and forms a periodic orbit.

38

Extension 2 : A discrete-time stochastic model

Switching probability

$$u_{A \to B} = \frac{1}{1 + e^{-\beta(\pi_B - \pi_A)}}$$

- Individuals' bounded rationality implies their limited cognition and decision-making capabilities

- Computations might be cognitively expensive and thus unfavorable

- False information, error, noise …

$$p_i(t+1) = p_i(t)[1 - U_{A \to B}^i(t)] + [1 - p_i(t)]U_{B \to A}^i(t)$$

where p_i is agent i's probability to employ strategy A at time t

39

Extension 2 : A discrete-time stochastic model

Switching probability
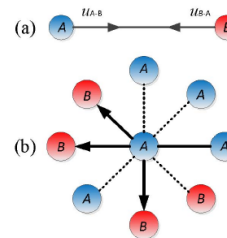
$$\begin{cases} U_{A \to B}^i = 1 - [1 - u_{A \to B}(1 - p_{\Omega_i})]^m \\ U_{B \to A}^i = 1 - (1 - u_{B \to A} p_{\Omega_i})^m \end{cases}$$
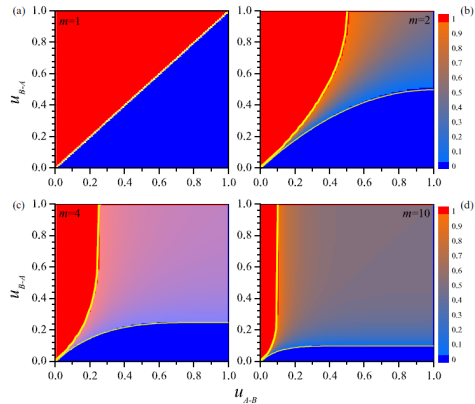
At equilibrium,

$$\hat{p}_i \cdot \hat{U}_{A \to B}^i = (1 - \hat{p}_i) \cdot \hat{U}_{B \to A}^i$$

40

Extension 2 : results
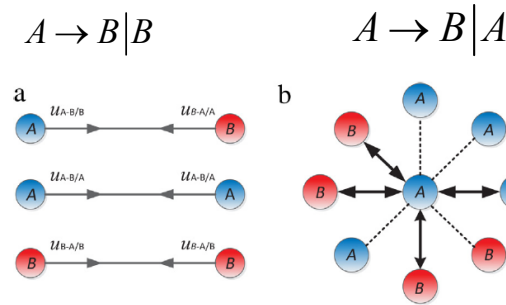
Coexistence of strategies for regular graphs:

A *persists* if $u_{B\to A} > \dfrac{1-\left(1-u_{A\to B}\right)^m}{m}$; B persists if $u_{A\to B} > \dfrac{1-\left(1-u_{B\to A}\right)^m}{m}$

41

Extension 2 : More sophisticated model

Strategy revisions:

$$A \to B\,\big|\,B \qquad\qquad A \to B\,\big|\,A$$

$$P_i\left(t+1\right) = P_i\left(t\right)\left[1 - U^i_{A\to B}\left(t\right)\right] + \left(1 - P_i\left(t\right)\right)U^i_{B\to A}\left(t\right)$$

42

Extension 3: ZD strategies in multi-player finitely repeated games

For an *n*-player repeated game, the strategy profile is $\sigma \in \{C, D\}^n$.

The vector of the outcome probabilities at round *t* is $v(t) = (v_\sigma(t))_{\sigma \in \{C,D\}^n}$

In any given round the probability that the next round takes place is determined by a discount factor $\delta \in (0,1)$

Then the expected number of the rounds of the repeated game is $\dfrac{1}{1-\delta}$

43

Extension 3: ZD strategies in multi-player finitely repeated games

Let the expected payoff of the ZD-player be denoted by π^i, and the expected payoff of the remaining players be π^{-i}

Then the ZD-player can unilaterally enforce a linear payoff relation

$$\pi_{-i} = s\pi_i + (1-s)\bar{\pi}, \qquad 0 \le s \le 1$$

In particular, one may have the following categories

44

Extension 3:ZD strategies in multi-player finitely repeated games

Let the expected payoff of the ZD-player be denoted by π^i, and the expected payoff of the remaining players be π^{-i}

Then the ZD-player can unilaterally enforce a linear payoff relation

$$\pi_{-i} = s\pi_i + (1-s)\bar{\pi}, \qquad 0 \leq s \leq 1$$

In particular, one may have the following categories

ZD-strategy	Parameter values	Enforced relation
Fair	s=1	$\pi^{-i} = \pi^i$
Generous	0<s<1, $\bar{\pi} = \pi_{max}$	$\pi^{-i} \geq \pi^i$
Extortionate	0<s<1, $\bar{\pi} = \pi_{min}$	$\pi^{-i} \leq \pi^i$
Equalizer	s=0	$\pi^{-i} = \bar{\pi}$

Note: one needs to check the conditions to see whether the relations are enforceable

45

Research supported by

Support from all my collaborators
especially colleagues at the Jan C. Willems Center for Systems and Control
research group of Discrete Technology and Production Automation (DTPA)

Franjo Weissing   James Riehl   Pouria Ramazi   Chen Wang   Jianlei Zhang
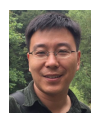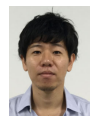
Yu Kawano   Luke Gong   Alain Govaert

47

Outline

- Paradox of cooperation

- Repeated games and zero-determinant strategies

- Nash equilibrium matters

- Continuous-time replicator dynamics

- Various extensions
  - Multi-population with environmental feedback
  - Stochastic models
  - ZD strategy in multi-player finitely repeated games

46

Some selected recent publications from my group on related topics

"Incentive-based control of asynchronous best-response dynamics on binary decision networks," J. R. Riehl, P. Ramazi, and M. Cao. *IEEE Trans. on Control of Network Systems*, 2019

"Evolutionary dynamics of two communities under environmental feedback," Y. Kawano, L. Gong, B. D. O. Anderson, and M. Cao. *IEEE Control Systems Letters*, special issue on Control and Network Theory for Biological Systems, 2019

"A survey on the analysis and control of evolutionary matrix games," J. R. Riehl, P. Ramazi and M. Cao. *Annual Reviews in Control*, 45(6), 87-106, 2018

"Asynchronous decision-making dynamics under best-response update rule in finite heterogeneous populations," P. Ramazi and M. Cao. *IEEE Transactions on Automatic Control*, 63(3), 742-751, 2018.

"Networks of conforming or nonconforming individuals tend to reach satisfactory decisions," P. Ramazi, J. R. Riehl, and M. Cao. *Proceedings of the National Academy of Science of USA (PNAS)*, 113(46), pp12985-12990, 2016

"Crucial role of strategy updating for coexistence of strategies in interaction networks," J. Zhang, C. Zhang, M. Cao and F. J. Weissing. *Phsical Review E*, 042101, 2015

--- The end ---

Hybrid Integrator-Gain Systems:
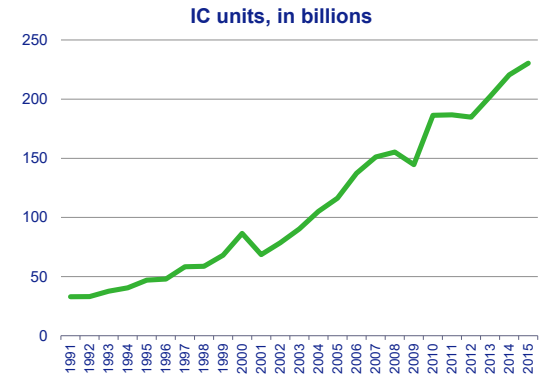How to use them in motion control of wafer scanners

Marcel Heertjes[1], Sebastiaan van den Eijnden[2], Bardia Sharif[3]

[1]D&E, Mechatronics, Wafer Stage Control
[2]D&C group, Mechanical Engineering, TU/e
[3]CST group, Mechanical Engineering, TU/e

10/04/2019
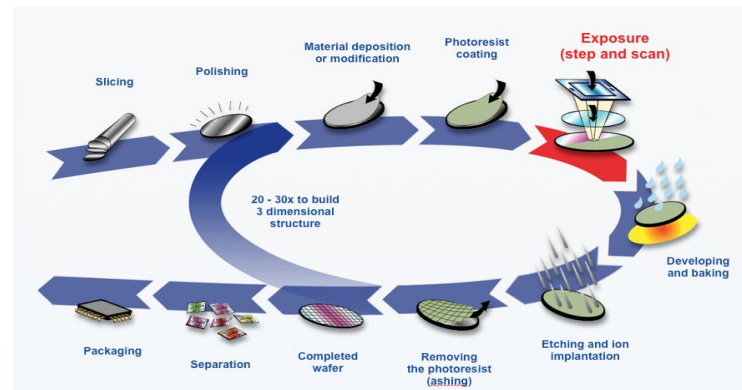
Public

Wafer scanner are used to produce microchips

Slide 2
3/12/2020

IC units, in billions

Public

Semiconductor industry: revenues in M$

Slide 3
3/12/2020

© 2019 IHS Markit

Public

Photolithography: one step in making microchips

Slide 4
3/12/2020

Public

Modern wafer scanners
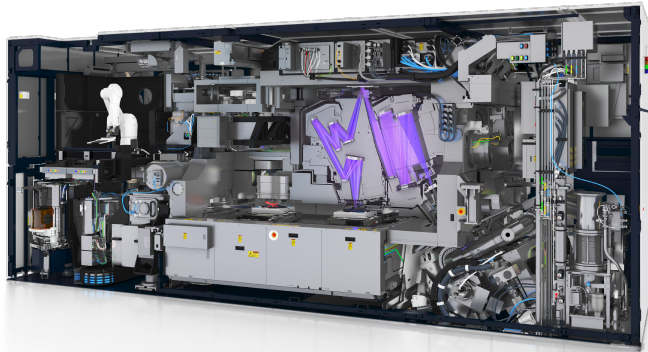
- ❑ Key performance indicators: overlay, focus & imaging, throughput

Modern wafer scanners: high-precision mechatronics
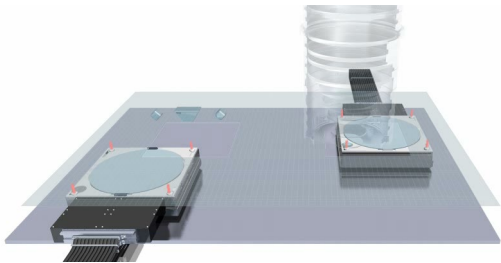
Wafer scanning

- ❑ Fast motion ($50\ m/s^2$), accurate tracking ($10\ nm$) while scanning ($\approx 1\ m/s$)
- ❑ Drive $100\ km/s$, keep wheels within $1\ mm$ of broken white line
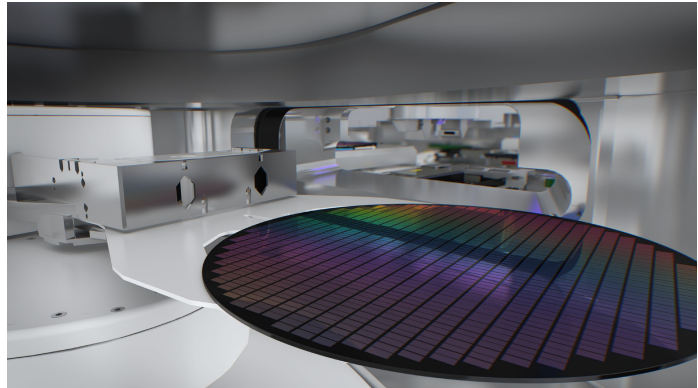
Motion control design
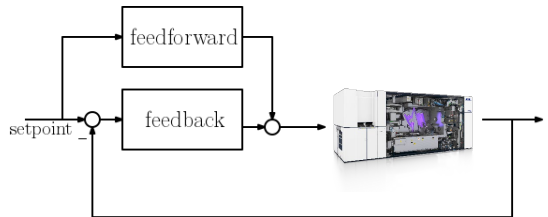
- ❑ Feedforward control for servo/tracking problem
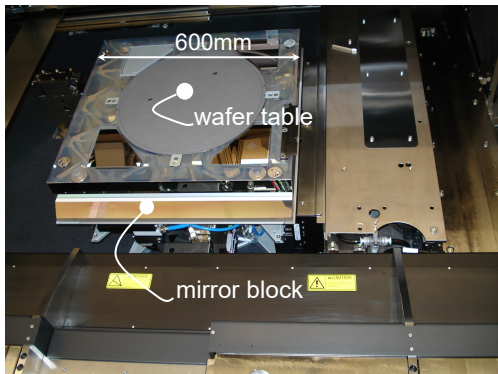- ❑ Feedback control for regulator (disturbance rejection) problem (this talk)

Bosgra, Kwakernaak, Meinsma (2007) Design methods for control systems, DISC lecture notes
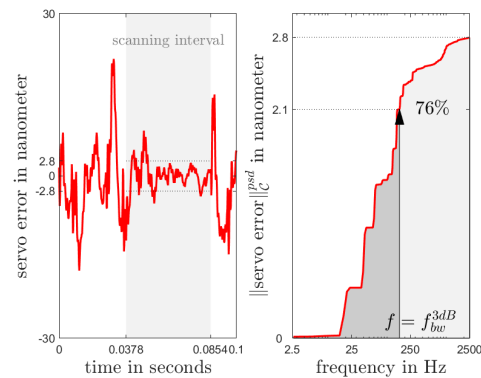
Short-stroke wafer stage mirror block

600mm

wafer table

mirror block

Bakshi, editor (2018) EUV Lithography, Second Edition. SPIE Press, ISBN 9781510616783

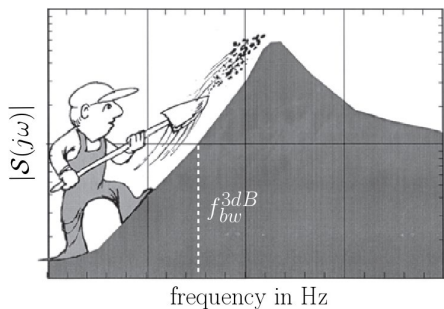Public

Wafer stage (non)reproducible servo error

Public

Nonlinear feedback control: fighting against nature?
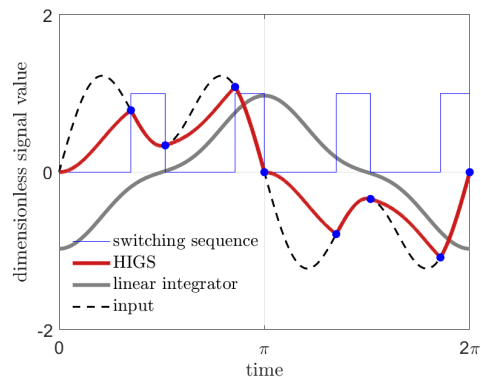
$|S(j\omega)|$

f_{bw}^{3dB}

frequency in Hz

Stein (2003) Respect the unstable, IEEE Control Systems Magazine, 23(4), pp. 12-25

Public

Phase lag and losing sign: all about not being too late

switching sequence
HIGS
linear integrator
input
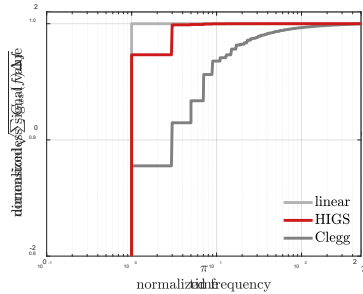
dimensionless signal value

time

Prieur, Queinnec, Tarbouriech, Zaccarian (2018). Analysis and Synthesis of Reset Control Systems, Foundations and Trends in Systems and Control, 6(2-3), pp. 117-338 Public

Reset control: Clegg integrator

ASML
Slide 13
3/12/2020

Clegg integrator ('58)

$$\mathcal{R}(e) = \begin{cases} \dot{x} = \omega_c e, & when \ e \neq 0 \\ x(t^+) = 0, & when \ e = 0 \\ u = x, & x(0) = 0 \end{cases}$$

❏ generalizations: FORE/SORE
Horowitz & Rosenbaum, 1975
❏ closed-loop stability: $\mathcal{H}_\beta$ condition
Beker, Hollot, Chait, Han, 2001/2004
❏ hybrid control framework:
Zaccarian, Nešić, Teel, 2005/2008
❏ passivity approaches: Carrasco, Baños,
Van der Schaft, 2008
❏ $\mathcal{L}_2$-performance: Aangenent, Witvoet, Heemels,
Van de Molengraft, Steinbuch, 2009
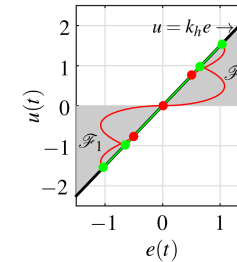❏ … many more e.g. CLOC, HosseinNia, Saikumar

Baños & Barreiro (2012) Reset control systems, In Advances in Industrial Control, Springer, New York

Public

HIGS description: differential algebraic equations

ASML
Slide 14
3/12/2020

Hybrid integrator-gain system (HIGS)

❏ $\mathcal{H}(e, \dot{e}, u) = \begin{cases} \dot{x} = \omega_h e, & if \ (e, \dot{e}, u) \in \mathcal{F}_1 \\ x = k_h e, & if \ (e, \dot{e}, u) \in \mathcal{F}_2 \\ u = x \end{cases}$

Modes of operation

❏ $\mathcal{F} = \mathcal{F}_1 \cup \mathcal{F}_2 = \{(e, \dot{e}, u) \in \mathbb{R}^2 | k_h e u \geq u^2\}$
$\mathcal{F}_1 = \mathcal{F} \setminus \mathcal{F}_2$
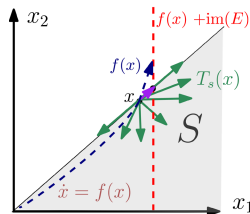$\mathcal{F}_2 = \{(e, \dot{e}, u) \in \mathcal{F} | u = k_h e \wedge \omega_h e^2 > k_h \dot{e} e\}$

Deenen, Heertjes, Heemels, Nijmeijer (2017) Hybrid integrator design for enhanced tracking in motion control, ACC, pp.2863-2868

Public

HIGS description: and now a bit more formal

ASML
Slide 15
3/12/2020

❏ Extended projected dynamical system (ePDS):

$$\dot{x} = \Pi_{S,E}(x, A_i x) = argmin_{w \in T_S(x), w - A_i x \in imE} \|w - A_i x\|$$

Tangent cone of permissible partial projections

❏ HIGS control systems are well-posed → global existence of solutions

Sharif, Heertjes, Heemels (2019) Extended projected dynamical systems with applications to hybrid integrator-gain systems, CDC, pp.5773-5778

Public

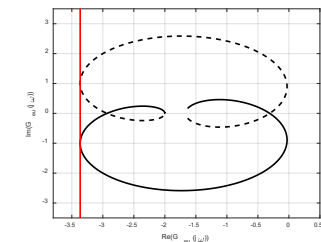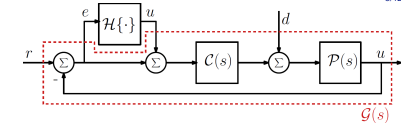## Stability: common quadratic Lyapunov function

ASML
Slide 16
3/12/2020

(Modified) circle criterion

❏ $\mathcal{G}(s)$ Hurwitz
❏ $\mathcal{G}(s)$ satisfying
$\frac{1}{k_h} + Re(\mathcal{G}(j\omega)) > 0, \forall \omega \in \mathbb{R}$
❏ HIGS $\mathcal{H}$ is strictly passive

Properties

❏ input-to-state stability (ISS)
❏ graphical tool in frequency domain
❏ possibly conservative

Heertjes, Irigoyen, Deenen (2018) Robust control and data-driven tuning of a hybrid integrator-gain system with applications to wafer scanners, IJACSP, pp.1-17

Public

Stability: piecewise quadratic Lyapunov functions

ASML

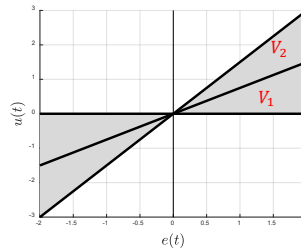**PWQLP** of the form $V_i = x^T P_i x, P_i > 0$

- ❑ 2D sector partitioning
- ❑ solve set of linear matrix inequalities (LMIs)

$$P_i - S_i^T W_i S_i > 0$$
$$A_1^T P_i + P_i A_1 + S_i^T U_i S_i \prec 0$$
$$A_2^T P_i + P_i A_2 + T_i^T V_i T_i \prec 0$$
$$P_i - F_i^T T_i F_i = 0$$

Properties

- ❑ input-to-state stability (ISS)
- ❑ numerical tool (need parametric model)
- ❑ possibly less conservative

Aangenent, Witvoet, Heemels, Van de Molengraft, Steinbuch (2009) Performance analysis of reset control systems, IJRNC, pp.1213-1233

Public

Stability: piecewise quadratic Lyapunov functions

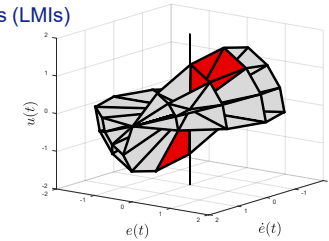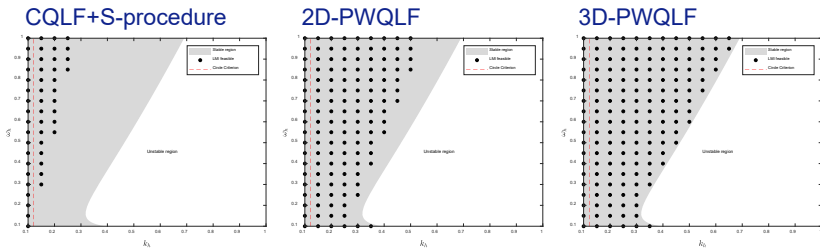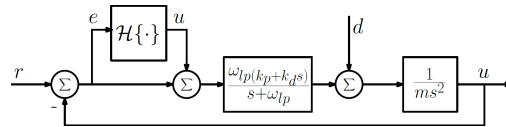**ASML**

PWQLP of the form $V_i = x^T P_i x, P_i > 0$

- ❑ 3D sector partitioning
- ❑ solve set of linear matrix inequalities (LMIs)
- ❑ example for cell

$$P_i - S_i^T W_i S_i > 0$$
$$A_1^T P_i + P_i A_1 + S_i^T U_i S_i \prec 0$$
$$A_2^T P_i + P_i A_2 + T_i^T V_i T_i \prec 0$$
$$Z_{ij}^T (P_i - P_j) Z_{ij} = 0$$

Deenen, Sharif, Van den Eijnden, Nijmeijer, Heemels, Heertjes (2019) From reset to projection-based integrators, Automatica, submitted for publication

Public

Stability: comparison studies

ASML

Example

- ❑ simple motion system:

- ❑ techniques compared:

CQLF+S-procedure   2D-PWQLF   3D-PWQLF

Public

Frequency-domain design: HIGS integrator

ASML

Properties

- ❑ schematics:
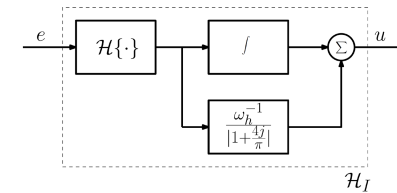
- ❑ need extra state for $\lim_{t \to \infty} e(t) = 0$
- ❑ describing function with $\gamma = 2\tan^{-1}(\omega/\omega_h)$:

$$\mathcal{H}\{\cdot\} \approx \mathcal{D}(j\omega) = \frac{\omega_h}{j\omega}\left(\frac{\gamma}{\pi} + j\frac{e^{-2j\gamma}-1}{2\pi} - 4j\frac{e^{-j\gamma}-1}{2\pi}\right) + \left(\frac{\pi-\gamma}{\pi} + j\frac{e^{-2j\gamma}-1}{2\pi}\right)$$

- ❑ for $\gamma \to \pi$, $\mathcal{D}(j\omega) \to \frac{\omega_h}{j\omega}\left(1 + \frac{4j}{\pi}\right)$ similar to Clegg integrator

Eijnden, Heertjes, Nijmeijer (2020) Experimental demonstration of a nonlinear PID-based control design using multiple hybrid integrator-gain elements, ACC, to appear

Public

Frequency-domain design: design freedom

$\omega_h = 0.25\pi$

Frequency-domain design: fundamental limitations

Closed-loop system

- ❏ schematics:

$\mathcal{H}_I$

- ❏ $P(s)$ having real unstable pole
- ❏ step input $r(t)$
- ❏ overshoot for **all** internally stabilizing LTI controllers
- ❏ changed ordering $\mathcal{H}_I$ crucial

HIGS integrator
linear integrator

Public

Frequency-domain design: HIGS lowpass filter

$2\beta\omega_{lp}$ $\omega_{lp}^2\mathcal{H}_I$ ω_{lp}^2

Eijnden, Knops, Heertjes (2018) A hybrid integrator-gain based low-pass filter for nonlinear motion control, CCTA, pp.1108-1113

Frequency-domain design: less phase lag, extra gain

$\omega_h = 0.25\pi$

Public

Frequency-domain design: HIGS-PID+LP filter

magnitude in dB
- HIGS-PID
- PID

phase in degrees
- phase benefit
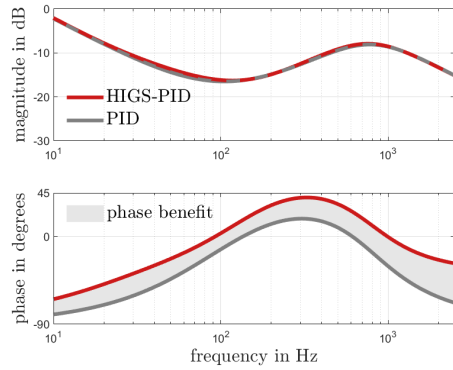
frequency in Hz

Eijnden, Francke, Nijmeijer, Heertjes (2020) Improving wafer stage performance with multiple hybrid integrator-gain systems, IFAC-WC, to appear

Public

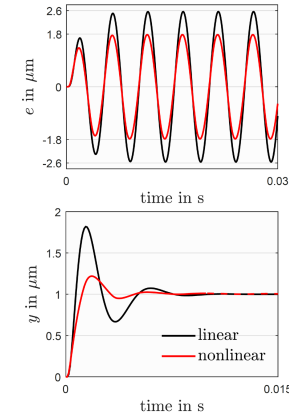## Frequency-domain design: stage tuning guidelines

Controlled double-integrator system
- ❑ $m = 20\ kg,\ \omega_{bw} = 2\pi \times 300\ rad/s$
- ❑ PID+LP controller

Tuning guidelines
- ❑ $k_p = 0.52 m\omega_{bw}^2$
- ❑ $\omega_i = 0.35\omega_{bw}$
- ❑ $\omega_d = 0.55\omega_{bw}$
- ❑ $\omega_{lp} = 6.4\omega_{bw}$
- ❑ $\beta_{lp} = 0.83$
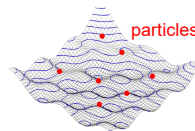- ❑ $\omega_h^i = \omega_i/8$
- ❑ $\omega_h^{lp} = \omega_{lp}/3$

e in μm — time in s

y in μm
- linear
- nonlinear

time in s

Public

Frequency-domain design: autotuner `fba.m`

- ❑ four-block optimal control problem:

$$\arg\sup_{\rho}\ \gamma_i(\rho_i) = \left\| \begin{matrix} \{W_S(\omega)T_S(\omega,\rho_i)\}_{\mathcal{P}} \\ \{W_T(\omega)T_T(\omega,\rho_i)\}_{\mathcal{P}} \\ \{W_{PS}(\omega)T_{PS}(\omega,\rho_i)\}_{\mathcal{P}} \\ \{W_{CS}(\omega)T_{CS}(\omega,\rho_i)\}_{\mathcal{P}} \end{matrix} \right\|_{\infty} < 1, \mathcal{P} = \{\mathcal{P}_1 \dots \mathcal{P}_n\}$$

particles

- ❑ HIGS control elements via describing functions
- ❑ non-convexity: global (PSO) + local (Nelder-Mead simplex) search
- ❑ cascaded optimization:
  - i. inner loop minimizes γ_i
  - ii. outer loop maximizes ω_{bw}
- ❑ no guarantees on global optimality/performance … but
- ❑ useful starting point for fine-tuning regarding time-domain measures

Public

Frequency-domain design: robust control in practice

magnitude in dB
- HIGS-PID
- PID

cPSD(error) in nm

57%

$f = f_{bw}^{3dB}$

frequency in Hz
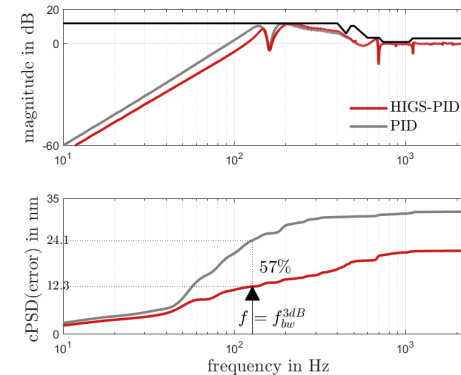
Public

Applications: stage control performance

Moving average (MA)
- overlay (MMO, DCO…)
- layer-to-layer positioning accuracy
- LP: $MA\big(e(t)\big) = \frac{1}{T}\int_{t-T/2}^{t+T/2} e(\tau)d\tau$

ASML
Slide 29
3/12/2020

$1\,\mu m$
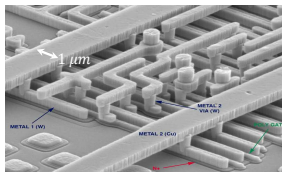
Moving standard deviation (MSD)
- critical dimension uniformity (CD,CDU)
- image 'blur'
- HP: $MSD\big(e(t)\big) =$
  $\sqrt{\frac{1}{T}\int_{t-T/2}^{t+T/2}\big(e(\tau) - MA(e(t))\big)^2 d\tau}$

$14\,nm$ node
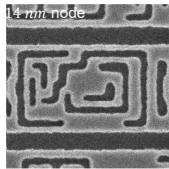
Public

Applications: HIGS motion control
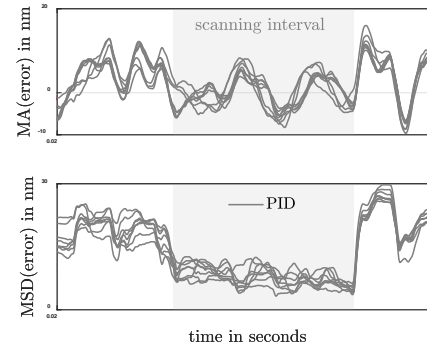
ASML
Slide 30
3/12/2020

Public

Applications: active vibration isolation systems

ASML
Slide 31
3/12/2020

Public

Applications: vibration isolation problem

ASML
Slide 32
3/12/2020

close-up of an isolation module (IM)
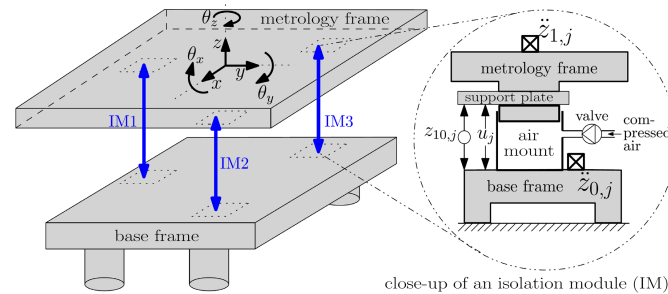
Beijen, Heertjes, Butler, Steinbuch (2019) Mixed feedback and feedforward control design for multi-axis vibration isolation systems, Mechatronics, 61, pp. 106-116

Public

Applications: AVIS HIGS skyhook damping

Heertjes, Eijnden, Sharif, Heemels, Nijmeijer (2019) Hybrid integrator-gain system for active vibration isolation with improved transient response, Mechatronics 2019

Public

Applications: HIGS bandpass filter

Properties

❑ schematics:

❑ Bode plot (describing functions)
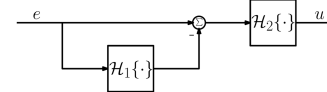
❑ parameters

sensing: $\omega_{hp} = 2\pi \times 0.1$

actuation: $\omega_{lp} = 2\pi \times 10$

HIGS: $\omega_{h,1} = \frac{\omega_{hp}}{2\alpha}, \omega_{h,2} = \frac{\omega_{lp}}{\alpha}$

$\alpha = |1 + 4j/\pi|, \ k_{h,1} = k_{h,2} = 1$

❑ HIGS BP sector-bounded: $u^2 \leq eu$
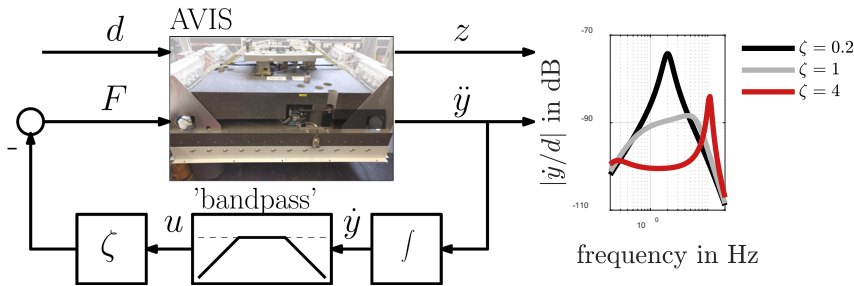
❑ closed-loop stability from circle criterion

Public

Applications: vibration isolation performance

Compliance - force disturbances

❑ non-stationary (transient) effects

overshoot & settling times
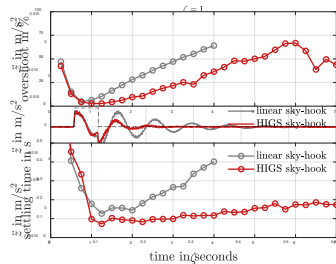
Transmissibility – 'floor' disturbances

❑ steady-state properties

(extra) skyhook gain

❑ stationary disturbances

no substantial effect higher harmonics

Public
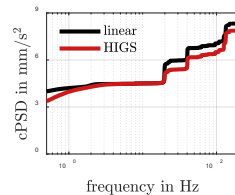
HIGS in feedback control: are we done?

HIGS control design

❑ enabler for improved error response

❑ more freedom regarding design trade-offs

❑ paves the way for future nonlinear plant design

Need for

❑ robust control design with time-domain relevance

❑ simple tools for rigorous stability and performance guarantees

❑ tools for nonlinear controller synthesis

Public

Acknowledgements

ASML

Slide 37
3/12/2020

ASML

Public

Public

Part 4

List of Participants

Leontine Aarnoudse
Eindhoven University of Technology
The Netherlands
l.i.m.aarnoudse@tue.nl

Flavia Sofia Acerbo
Siemens Industry Software
Belgium
flavia.acerbo@siemens.com

Muhammad Zaki Almuzakki
University of Groningen
The Netherlands
m.z.almuzakki@rug.nl

Javier Alonso-Mora
Delft University of Technology
The Netherlands
j.alonsomora@tudelft.nl

Michele Ambrosino
Université Libre de Bruxelles
Belgium
michele.ambrosino@ulb.ac.be

Pieter Appeltans
Katholieke Universiteit Leuven
Belgium
pieter.appeltans@cs.kuleuven.be

Ömür Arslan
Eindhoven University of Technology
The Netherlands
o.arslan@tue.nl

Alejandro Astudillo Vigoya
Katholieke Universiteit Leuven
Belgium
alejandro.astudillovigoya@kuleuven.be

Kim Batselier
Delft University of Technology
The Netherlands
k.batselier@tudelft.nl

Camiel Beckers
Eindhoven University of Technology
The Netherlands
c.j.j.beckers@tue.nl

Reza Behinfaraz
Delft University of Technology
The Netherlands
r.behinfaraz@tudelt.nl

Gerben Beintema
Eindhoven University of Technology
The Netherlands
g.i.beintema@tue.nl

Ayoub Ben Ayed
Université Catholique de Louvain
Belgium
ayoub.benayed@uclouvain.be

Bart Besselink
University of Groningen
The Netherlands
b.besselink@rug.nl

Mattia Bianchi
Delft University of Technology
The Netherlands
m.bianchi@tudelft.nl

Georgios Birpoutsoukis
Université Catholique de Louvain
Belgium
georgios.birpoutsoukis@uclouvain.be

Tom Bloemers
Eindhoven University of Technology
The Netherlands
t.a.h.bloemers@tue.nl

Nicolas Bono Rossello
Université Libre de Bruxelles
Belgium
nicolas.bono.rossello@ulb.ac.be

Pablo Borja
University of Groningen
The Netherlands
l.p.borja.rosales@rug.nl

Mathias Bos
Katholieke Universiteit Leuven
Belgium
mathias.bos@kuleuven.be

Clarisse Petua Bosman Barros
Eindhoven University of Technology
The Netherlands
c.p.bosman.barros@tue.nl

Azka Muji Burohman
University of Groningen
The Netherlands
a.m.burohman@rug.nl

Brandon Caasenbrood
Eindhoven University of Technology
The Netherlands
b.j.caasenbrood@tue.nl

Ming Cao
University of Groningen
The Netherlands
m.cao@rug.nl

Raffaella Carloni
University of Groningen
The Netherlands
r.carloni@rug.nl

Carlo Cenedese
University of Groningen
The Netherlands
c.cenedese@rug.nl

Carmen Chan
University of Groningen
The Netherlands
c.chan.zheng@rug.nl

Yahao Chen
University of Groningen
The Netherlands
yahao.chen@rug.nl

Zhenyu Chen
Delft University of Technology
The Netherlands
czy_ac@outlook.com

Xiaodong Cheng
Eindhoven University of Technology
The Netherlands
x.cheng@tue.nl

Ashish Cherukuri
University of Groningen
The Netherlands
a.k.cherukuri@rug.nl

Michelle Chong
Eindhoven University of Technology
The Netherlands
mstchong@gmail.com

Koen Classens
Eindhoven University of Technology
The Netherlands
k.h.j.classens@tue.nl

Roy Cobbenhagen
Eindhoven University of Technology
The Netherlands
a.t.j.r.cobbenhagen@tue.nl

Peter Coppens
Katholieke Universiteit Leuven
Belgium
peter.coppens@kuleuven.be

Andrés Cotorruelo Jimenez
Université Libre de Bruxelles
Belgium
andres.cotorruelo.jimenez@ulb.ac.be

Peter Zoltan Csurcsia
Vrije Universiteit Brussel
Belgium
pcsurcsi@vub.ac.be

Michele Cucuzzella
University of Groningen
The Netherlands
m.cucuzzella@rug.nl

Rafael Cunha
University of Groningen
The Netherlands
r.f.cunha@rug.nl

Riccardo D'Anniballe
University of Groningen
The Netherlands
r.danniballe@rug.nl

Kobe De Becker
Katholieke Universiteit Leuven
Belgium
kobe.debecker@kuleuven.be

Oscar de Groot
Delft University of Technology
The Netherlands
groot.oscar.de@gmail.com

Bram de Jager
Eindhoven University of Technology
The Netherlands
A.G.de.Jager@tue.nl

Bayu Jayawardhana
University of Groningen
The Netherlands
b.jayawardhana@rug.nl

Massimo De Mauri
Katholieke Universiteit Leuven
Belgium
massimo.demauri@kuleuven.be

Silvane de Melo Schons
Université Libre de Bruxelles
Belgium
silvane.de.melo.schons@ulb.ac.be

Leonardo de Paula Carvalho
University of Groningen
The Netherlands
eng.leonardocarvalho@gmail.com

Bart De Schutter
Delft University of Technology
The Netherlands
b.deschutter@tudelft.nl

Virginie Debauche
Université Catholique de Louvain
Belgium
virginie.debauche@uclouvain.be

Wilm Decré
Katholieke Universiteit Leuven
Belgium
wilm.decre@kuleuven.be

Jan Decuyper
Vrije Universiteit Brussel
Belgium
jan.decuyper@vub.be

Ousmane Diao
Université Catholique de Louvain
Belgium
ousmane.diao@uclouvain.be

Nic Dirkx
ASML
The Netherlands
nic.dirkx@asml.com

Mannes Dreef
Eindhoven University of Technology
The Netherlands
h.j.dreef@tue.nl

Jaap Eising
University of Groningen
The Netherlands
j.eising@rug.nl

Chyannie Fahdzyana
Eindhoven University of Technology
The Netherlands
chyannieamarillio@gmail.com

Le Fan
Katholieke Universiteit Leuven
Belgium
le.fan@student.kuleuven.be

Mihai Florea
Université Catholique de Louvain
Belgium
mihai.florea@uclouvain.be

Stefanie Fonken
Eindhoven University of Technology
The Netherlands
s.j.m.fonken@student.tue.nl

Karlijn Fransen
Vanderlande Industries B.V.
The Netherlands
karlijn.fransen@vanderlande.com

Jeroen Fransman
Delft University of Technology
The Netherlands
j.e.fransman@tudelft.nl

Jianfeng Fu
Delft University of Technology
The Netherlands
J.Fu-1@tudelft.nl

Camilo Garcia-Tenorio
Mons University
Belgium
camilo.garciatenorio@umons.ac.be

Prasoon Garg
Eindhoven University of Technology
The Netherlands
prasoon.garg08@gmail.com

Bram Geelen
Katholieke Universiteit Leuven
Belgium
bram.geelen@esat.kuleuven.be

Joris Gillis
Katholieke Universiteit Leuven
Belgium
joris.gillis@kuleuven.be

Alejandro Goldar Davila
Université Libre de Bruxelles
Belgium
alejandro.goldar.davila@ulb.ac.be

Lulu Gong
University of Groningen
The Netherlands
l.gong@rug.nl

Marvyn Gulina
University of Namur
Belgium
marvyn.gulina@unamur.be

Miao Guo
University of Groningen
The Netherlands
m.guo@rug.nl

Wouter Hakvoort
University of Twente
The Netherlands
w.b.j.hakvoort@utwente.nl

Noël Hallemans
Vrije Universiteit Brussel
Belgium
noel.hallemans@vub.be

Anthony Hastir
University of Namur
Belgium
anthony.hastir@unamur.be

Marcel Heertjes
Eindhoven University of Technology
The Netherlands
m.f.heertjes@tue.nl

Julien Hendrickx
Université Catholique de Louvain
Belgium
julien.hendrickx@uclouvain.be

Ben Hermans
Katholieke Universiteit Leuven
Belgium
ben.hermans2@kuleuven.be

Feye Hoekstra
Eindhoven University of Technology
The Netherlands
f.s.j.hoekstra@tue.nl

Md Sumon Hossain
University of Groningen
The Netherlands
s.hossain@rug.nl

Runsheng Hu
Delft University of Technology
The Netherlands
R.Hu-2@tudelft.nl

Jiaming Hu
University of Groningen
The Netherlands
Jiaming.hu@rug.nl

Feng Huang
University of Groningen
The Netherlands
feng.huang@rug.nl

Anne-Men Huijzer
University of Groningen
The Netherlands
m.a.huijzer@rug.nl

Lucian Cristian Iacob
Eindhoven University of Technology
The Netherlands
l.c.iacob@tue.nl

Laurens Jacobs
Katholieke Universiteit Leuven
Belgium
laurens.jacobs@kuleuven.be

Daniel Jarne Ornia
Delft University of Technology
The Netherlands
d.jarneornia@tudelft.nl

Mark Jeeninga
University of Groningen
The Netherlands
m.jeeninga@rug.nl

Jiajia Jia
University of Groningen
The Netherlands
j.jia@rug.nl

Junjie Jiao
University of Groningen
The Netherlands
j.jiao@rug.nl

Bo Jin
University of Groningen
The Netherlands
b.jin@rug.nl

Raphael Jungers
Université Catholique de Louvain
Belgium
raphael.jungers@uclouvain.be

Jacques Kadima Kazaku
Université Catholique de Louvain
Belgium
jacqueskazaku@gmail.com

Nima Karbasizadeh
Delft University of Technology
The Netherlands
n.karbasizadehesfahani@tudelft.nl

Karel Keesman
Wageningen University & Research
The Netherlands
karel.keesman@wur.nl

Twan Keijzer
Delft University of Technology
The Netherlands
t.keijzer@tudelft.nl

Zuan Khalik
Eindhoven University of Technology
The Netherlands
z.khalik@tue.nl

Lizan Kivits
Eindhoven University of Technology
The Netherlands
e.m.m.kivits@tue.nl

Patrick Koelewijn
Eindhoven University of Technology
The Netherlands
p.j.w.koelewijn@tue.nl

Manon Kok
Delft University of Technology
The Netherlands
m.kok-1@tudelft.nl

Armin Küper
Katholieke Universiteit Leuven
Belgium
armin.kuper@kuleuven.be

Francois Lamoline
University of Luxembourg
Luxembourg
francois.lamoline@uni.lu

Rie B. Larsen
Delft University of Technology
The Netherlands
R.B.Larsen@tudelft.nl

John Lataire
Vrije Universiteit Brussel
Belgium
jlataire@vub.ac.be

Oliver Lauwers
Katholieke Universiteit Leuven
Belgium
oliverlauwers@gmail.com

Erjen Lefeber
Eindhoven University of Technology
The Netherlands
A.A.J.Lefeber@tue.nl

Antoine Legat
Université Catholique de Louvain
Belgium
antoine.legat@uclouvain.be

Benoit Legat
Université Catholique de Louvain
Belgium
benoit.legat@uclouvain.be

Ningbo Li
University of Groningen
The Netherlands
ningbo.li@rug.nl

Di Liu
University of Groningen
The Netherlands
di.liu@rug.nl

Jorge Lopez-Jimenez
Mons University
Belgium
jorgealfredo.lopezjimenez@umons.ac.be

Juan Eduardo Machado Martinez
University of Groningen
The Netherlands
j.e.machado.martinez@rug.nl

Mir Mamunuzzaman
University of Twente
The Netherlands
m.mamunuzzaman@utwente.nl

Emin Martirosyan
University of Groningen
The Netherlands
e.n.martirosyan@rug.nl

Alexandre Mauroy
University of Namur
Belgium
alexandre.mauroy@unamur.be

Veronika Mazulina
Eindhoven University of Technology
The Netherlands
v.mazulina@tue.nl

Farhad Mehdifar
Université Catholique de Louvain
Belgium
farhad.mehdifar@uclouvain.be

Tomas Meijer
Eindhoven University of Technology
The Netherlands
t.j.meijer@tue.nl

Carlos Samuel Mendez Blanco
Eindhoven University of Technology
The Netherlands
c.s.mendez.blanco@tue.nl

Clara Menzen
Delft University of Technology
The Netherlands
c.m.menzen@tudelft.nl

Rishi Mohan
Eindhoven University of Technology
The Netherlands
r.mohan@tue.nl

Charles Monnoyer de Galland
Université Catholique de Louvain
Belgium
charles.monnoyer@uclouvain.be

Nima Monshizadeh
University of Groningen
The Netherlands
n.monshizadeh@rug.nl

Noud Mooren
Eindhoven University of Technology
The Netherlands
n.f.m.mooren@tue.nl

Lars Moormann
Eindhoven University of Technology
The Netherlands
l.moormann@tue.nl

Christian Mugisho Zagabe
University of Namur
Belgium
christian.mugisho@unamur.be

Carlos Gerardo Murguía Rendón
Eindhoven University of Technology
The Netherlands
c.g.murguia@tue.nl

Sajad Naderi Lordejani
Eindhoven University of Technology
The Netherlands
s.naderilordejani@tue.nl

Henk Nijmeijer
Eindhoven University of Technology
The Netherlands
h.nijmeijer@tue.nl

Brice Njinwoua
Mons University
Belgium
Brice.Njinwoua@umons.ac.be

Jean-Philippe Noel
Eindhoven University of Technology
The Netherlands
j.m.m.g.noel@tue.nl

Wataru Ohnishi
Eindhoven University of Technology
The Netherlands
w.ohnishi@tue.nl

Tom Oomen
Eindhoven University of Technology
The Netherlands
t.a.e.oomen@tue.nl

Nick Paape
Eindhoven University of Technology
The Netherlands
n.paape@tue.nl

Giovanny Paul Padilla
Eindhoven University of Technology
The Netherlands
g.p.padilla.cazar@gmail.com

Ralf Peeters
Maastricht University
The Netherlands
ralf.peeters@maastrichtuniversity.nl

Kristin Y. Pettersen
Norwegian University of Science and Technology
Norway
kristin.y.pettersen@ntnu.no

Matthias Pezzuto
Université Libre de Bruxelles
Belgium
matthias.pezzuto@ulb.ac.be

Alexander Pogromsky
Eindhoven University of Technology
The Netherlands
a.pogromsky@tue.nl

Maurice Poot
Eindhoven University of Technology
The Netherlands
m.m.poot@tue.nl

Mohamad Agung Prawira Negara
University of Groningen
The Netherlands
m.a.prawira.negara@rug.nl

Karthik Raghavan Ramaswamy
Eindhoven University of Technology
The Netherlands
k.r.ramaswamy@tue.nl

Timo Ravensbergen
DIFFER
The Netherlands
T.Ravensbergen@differ.nl

Ferdie Reijnen
Eindhoven University of Technology
The Netherlands
f.f.h.reijnen@tue.nl

Joey Reinders
Eindhoven University of Technology
The Netherlands
j.m.f.reinders@tue.nl

András Retzler
Katholieke Universiteit Leuven
Belgium
andras.retzler@kuleuven.be

Kirill Rogov
Eindhoven University of Technology
Belgium
k.rogov@tue.nl

Daniele Ronzani
Katholieke Universiteit Leuven
Belgium
daniele.ronzani@kuleuven.be

Tabitha Rosa
University of Groningen
The Netherlands
t.esteves.rosa@rug.nl

Alessandro Saccon
Eindhoven University of Technology
The Netherlands
a.saccon@tue.nl

Arash Sadeghzadeh
Eindhoven University of Technology
The Netherlands
a.sadeghzadeh@tue.nl

Tommaso Sartor
Katholieke Universiteit Leuven
Belgium
jan.swevers@kuleuven.be

Ajay Suresha Sathya
Katholieke Universiteit Leuven
Belgium
ajay.sathya@kuleuven.be

Jacquelien Scherpen
University of Groningen
The Netherlands
j.m.a.scherpen@rug.nl

Anja Eva Maria Schmerbauch
University of Groningen
The Netherlands
a.e.m.schmerbauch@rug.nl

Wouter Scholte
Eindhoven University of Technology
The Netherlands
w.j.scholte@tue.nl

Johan Schoukens
Vrije Universiteit Brussel
Belgium
johan.schoukens@vub.be

Maarten Schoukens
Eindhoven University of Technology
Belgium
maarten.schoukens@gmail.com

Thomas Schön
Uppsala University
Sweden
thomas.schon@it.uu.se

Mathijs Schuurmans
Katholieke Universiteit Leuven
Belgium
mathijs.schuurmans@kuleuven.be

Fahim Shakib
Eindhoven University of Technology
The Netherlands
m.f.shakib@tue.nl

Brayan Shali
University of Groningen
The Netherlands
b.m.shali@rug.nl

Mehrad Sharabiany
Vrije Universiteit Brussel
Belgium
mehrad.sharabiany@gmail.com

Bardia Sharif
Eindhoven University of Technology
The Netherlands
b.sharif@tue.nl

Shengling Shi
Eindhoven University of Technology
The Netherlands
s.shi@tue.nl

Mingming Shi
Université Catholique de Louvain
The Netherlands
mingming.shi@uclouvain.be

Koorosh Shomalzadeh
University of Groningen
The Netherlands
k.shomalzadeh@rug.nl

Amirreza Silani
University of Groningen
The Netherlands
A.Silani@rug.nl

Taranjitsingh Singh
Katholieke Universiteit Leuven
Belgium
taranjitsingh.singh@kuleuven.be

Candy Sonveaux
University of Namur
Belgium
candy.sonveaux@unamur.be

Tom Steentjes
Eindhoven University of Technology
The Netherlands
t.r.v.steentjes@tue.nl

Maarten Steinbuch
Eindhoven University of Technology
The Netherlands
m.steinbuch@tue.nl

Armin Steinhauser
Katholieke Universiteit Leuven
Belgium
armin.steinhauser@kuleuven.be

Nard Strijbosch
Eindhoven University of Technology
The Netherlands
n.strijbosch@gmail.com

Dingshan Sun
Delft University of Technology
The Netherlands
D.Sun-1@tudelft.nl

Zhiyong Sun
Eindhoven University of Technology
The Netherlands
z.sun@tue.nl

Sutrisno Sutrisno
University of Groningen
The Netherlands
s.sutrisno@rug.nl

Jan Swevers
Katholieke Universiteit Leuven
Belgium
jan.swevers@kuleuven.be

Paul Tacx
Eindhoven University of Technology
The Netherlands
pjmmt63@gmail.com

Xuegang Tan
University of Groningen
The Netherlands
redloner_tan@hotmail.com

Pauline Thémans
University of Namur
Belgium
pauline.themans@unamur.be

Sander Thuijsman
Eindhoven University of Technology
The Netherlands
s.b.thuijsman@tue.nl

Koen Tiels
Eindhoven University of Technology
The Netherlands
k.tiels@tue.nl

Roland Toth
Eindhoven University of Technology
The Netherlands
r.toth@tue.nl

Stephan Trenn
University of Groningen
The Netherlands
s.trenn@rug.nl

Ronald van 't Veld
University of Twente
The Netherlands
r.c.vantveld@utwente.nl

Ton van den Boom
Delft University of Technology
The Netherlands
a.j.j.vandenboom@tudelft.nl

Paul Van den Hof
Eindhoven University of Technology
The Netherlands
p.m.j.vandenhof@tue.nl

Wouter van Dijk
University of Twente
The Netherlands
w.vandijk@utwente.nl

Joost van Eekelen
Eindhoven University of Technology
The Netherlands
j.a.w.m.v.eekelen@tue.nl

Birgit van Huijgevoort
Eindhoven University of Technology
The Netherlands
b.c.v.huijgevoort@tue.nl

Ricky van Kampen
DIFFER
The Netherlands
R.J.R.vanKampen@differ.nl

Simon van Mourik
Wageningen University & Research
The Netherlands
simon.vanmourik@wur.nl

Henk van Waarde
University of Groningen
The Netherlands
h.j.van.waarde@rug.nl

Bastiaan Vandewal
Katholieke Universiteit Leuven
Belgium
bastiaan.vandewal@kuleuven.be

Marco Augusto Vasquez Beltran
University of Groningen
The Netherlands
m.a.vasquez.beltran@rug.nl

Daniel Veldman
Eindhoven University of Technology
The Netherlands
d.w.m.veldman@tue.nl

Julio Cezar Vendrichoski
Université Libre de Bruxelles
Belgium
pascale.lathouwers@ulb.ac.be

Jeroen Verbakel
Eindhoven University of Technology
The Netherlands
j.j.verbakel@tue.nl

Jasper Verbree
University of Groningen
The Netherlands
j.verbree@rug.nl

Bob Vergauwen
Katholieke Universiteit Leuven
Belgium
bob.vergauwen@esat.kuleuven.be

Chris Verhoek
Eindhoven University of Technology
The Netherlands
c.verhoek@student.tue.nl

Christof Vermeersch
Katholieke Universiteit Leuven
Belgium
christof.vermeersch@esat.kuleuven.be

Quentin Voortman
Eindhoven University of Technology
The Netherlands
q.j.t.voortman@tue.nl

Steffen Waldherr
Katholieke Universiteit Leuven
Belgium
steffen.waldherr@kuleuven.be

Zheming Wang
Université Catholique de Louvain
Belgium
zheming.wang@uclouvain.be

Benjamin Wauthion
Université Libre de Bruxelles
Belgium
benjamin.wauthion@ulb.ac.be

Paul Wijnbergen
University of Groningen
The Netherlands
p.wijnbergen@rug.nl

Van Roy Wim
Katholieke Universiteit Leuven
Belgium
wim.vanroy@kuleuven.be

Joseph Winkin
University of Namur
Belgium
joseph.winkin@unamur.be

Gert Witvoet
Eindhoven University of Technology
The Netherlands
g.witvoet@tue.nl

Nathan Wouw van de
Eindhoven University of Technology
The Netherlands
n.v.d.wouw@tue.nl

Haiwen Wu
University of Groningen
The Netherlands
haiwen.wu@rug.nl

Teke Xu
University of Groningen
The Netherlands
t.xu@rug.nl

Weijia Yao
University of Groningen
The Netherlands
w.yao@rug.nl

Dongdong Yue
Delft University of Technology
The Netherlands
d.yue@tudelft.nl

Ivan Francisco Yupanqui Tello
Mons University
Belgium
ivan.uni.fim@gmail.com

Lorenzo Zino
University of Groningen
The Netherlands
lorenzo.zino@rug.nl

Hans Zwart
University of Twente
The Netherlands
h.j.zwart@utwente.nl

Part 5

Organizational Comments

Welcome

The Organizing Committee has the pleasure of welcoming you to the *39th Benelux Meeting on Systems and Control*, at the Hotel Mennorode in Elspeet, The Netherlands.

Aim

The aim of the Benelux Meeting is to promote research activities and to enhance cooperation between researchers in Systems and Control. This is the thirty-ninth in a series of annual conferences that are held alternately in Belgium and The Netherlands.

Scientific Program Overview

1. Mini course by *Thomas Schön* (Uppsala University, Uppsala, Sweden) on **Learning nonlinear dynamics using sequential Monte Carlo**.

2. Plenary lecture by *Paul Van den Hof* (Eindhoven University of Technology, The Netherlands) on **Data-driven model learning in linear dynamic networks**.

3. Plenary lecture by *Henk Nijmeijer* (Eindhoven University of Technology, The Netherlands) on **Cooperative and/or Autonomous driving: where are we going?**.

4. Plenary lecture by *Ming Cao* (University of Groningen, The Netherlands) on: **Strategic decision-making and learning for autonomous agents**.

5. Plenary lecture by *Marcel Heertjes* (Eindhoven University of Technology, The Netherlands) on: **Hybrid integrator-gain systems: How to use them in motion control of wafer scanners?**

6. Contributed short lectures. See the list of sessions for the titles and authors of these lectures.

Directions for speakers

For a contributed lecture, the available time is 25 minutes. Please leave a few minutes for discussion and room changes, and adhere to the indicated schedule. In each room LCD projectors are available, as well as VGA and HDMI cables. *When using a projector, you have to provide a notebook yourself.*

Registration

The Benelux Meeting registration desk, located in the foyer, will be open on Tuesday, March 10, from 10:00 to 14:00. Late registrations can be made at the Benelux Meeting registration desk, when space is still available. The on-site fee schedule is:

Arrangement	Price
single room	€575
shared room	€475
only meals (no dinners)	€375
one day (no dinner)	€275

The registration fee includes:

- Admission to all sessions.

- Coffee and tea during the breaks.

- In the case of *accommodation* arrangement: lunch and dinner on Tuesday; breakfast, lunch, dinner on Wednesday; breakfast and lunch on Thursday.

- In the case of *only meals (no dinner)* arrangement: lunch on Tuesday, Wednesday, Thursday.

- In the case of *one day (no dinner)* arrangement: lunch on Tuesday, or Wednesday, or Thursday.

- Free use of a wireless Internet connection (no password required).

Organization

The meeting has been organized by Raffaella Carloni (University of Groningen), Bayu Jayawardhana (University of Groningen), and Erjen Lefeber (Eindhoven University of Technology).

The Organizing Committee of the 39th Benelux Meeting consists of

Robert Babuska
Delft University of Technology
E-mail: r.babuska@tudelft.nl

Raffaella Carloni
University of Groningen
E-mail: r.carloni@rug.nl

Bart de Moor
Katholieke Universiteit Leuven
E-mail: bart.demoor@esat.kuleuven.be

Dennis Dochain
Universite Catholique de Louvain
E-mail: denis.dochain@uclouvain.be

Jorge Goncalves
University of Luxembourg
E-mail: jorge.goncalves@uni.lu

Maurice Heemels
Eindhoven University of Technology
E-mail: m.heemels@tue.nl

Bayu Jayawardhana
University of Groningen
E-mail: b.jayawardhana@rug.nl

Mircea Lazar
Eindhoven University of Technology
E-mail: m.lazar@tue.nl

Erjen Lefeber
Eindhoven University of Technology
E-mail: a.a.j.lefeber@tue.nl

Sarthak Misra
University of Twente
E-mail: s.misra@utwente.nl

Henk Nijmeijer
Eindhoven University of Technology
E-mail: h.nijmeijer@tue.nl

Panagiotis Patrinos
Katholieke Universiteit Leuven
E-mail: panos.patrinos@esat.kuleuven.be

Arjan J. van der Schaft
University of Groningen
E-mail: a.j.van.der.schaft@math.rug.nl

Bart de Schutter
Delft University of Technology
E-mail: b.deschutter@tudelft.nl

Hans Stigter
University of Wageningen
E-mail: hans.stigter@wur.nl

Paul M.J. Van den Hof
Eindhoven University of Technology
E-mail: p.m.j.vandenhof@tue.nl

Steffen Waldherr
Katholieke Universiteit Leuven
E-mail: steffen.waldherr@kuleuven.be

Nathan van de Wouw
Eindhoven University of Technology
E-mail: n.v.d.wouw@tue.nl

Hans J. Zwart
University of Twente

E-mail: h.j.zwart@utwente.nl

Sponsor

The meeting is supported by the following organizations:

- Dutch Institute for Systems and Control (DISC).

- Netherlands Organization for Scientific Research (NWO).

Conference location

The lecture rooms of the Hotel Mennorode are situated on the ground and first floors. Consult the map at the end of this booklet to locate rooms. Breakfast will be served between 7:30 and 10:00 AM. Room keys can be picked up at the reception from Tuesday at 15:00, and need to be returned before 10:00 on the day of departure. Parking is free of charge.

The address of the Hotel Mennorode is

> Apeldoornseweg 185
> 8075 RJ Elspeet
> The Netherlands

Best junior presentation award

Continuing a tradition that started in 1996, the 39th Benelux Meeting will close with the announcement of the winner of the Best Junior Presentation Award. This award is given for the best presentation, given by a junior researcher, and it consists of a trophy that may be kept for one year and a certificate. The award is specifically given for quality of presentation rather than quality of research, which is judged in a different way. At the meeting, the chairs of sessions will ask three volunteers in the audience to fill out an evaluation form. After the session, the evaluation forms will be collected by the Prize Commissioners who will then compute a ranking. The winner will be announced on Thursday, March 12, in room **De Grote Zael**, 12:30-12:45. The evaluation forms of each presentation will be returned to the junior researcher who gave the presentation. The Prize Commissioners are Julien Hendrickx (Université Catholique de Louvain), Sergio Grammatico (Delft University of Technology), and Bart Besselink (University of Groningen). The organizing committee counts on the cooperation of the participants to make this contest a success.

Website

An *electronic version* of the Book of Abstracts can be downloaded from the Benelux Meeting web site.

Meeting

The following meeting is scheduled: Management Team DISC on Tuesday, March 10, room Lucasgat A, 20:00 – 22:00.

DISC certificates and best thesis award

The ceremony for the distribution of the DISC certificates and for the Best Thesis Award will be held on Wednesday, March 11, room **De Grote Zael**, 18:30–18:45. The jury of the Best Thesis Award is formed by Karel Keesman (Wageningen University), Jens Kober (Delft University of Technology), and Tom Oomen (Eindhoven University of Technology).

Tuesday March 10, 2020

11:25 – 11:30	P0 – De Grote Zael *Welcome and Opening*
11:30 – 12:30	P1 – De Grote Zael Thomas Schön – *Learning nonlinear dynamics using sequential Monte Carlo - Part I*
12:30 – 13:40	Lunch
13:40 – 14:40	P2 – De Grote Zael Thomas Schön – *Learning nonlinear dynamics using sequential Monte Carlo - Part II*
14:40 – 15:00	Coffee Break

Room TuA	Lucasgat A TuA01 *Drones, Autonomous Vehicle & Logistics I*	Lucasgat B TuA02 *Mobile Robots & Robotics I*	Lucasgat C TuA03 *Nonlinear & Hybrid Control Systems I*	Lucasgat D TuA04 *Distributed Parameter Systems I*	Lucasgat E TuA05 *Energy Systems I*	Solsegat TuA06 *Optimal Control I*	Hooge Duvel TuA07 *Systems Identification I*	Groenendal TuA08 *State Observer, Fault Detection and Isolation*
15:00 – 15:25	Bono Rossello	Yao	v/d Eijnden	Hastir	Hoekstra	Arslan	Dreef	Jia
15:25 – 15:50	Mazulina	Sathya	Chen	Tello	Silani	Larsen	Shi	Schons
15:50 – 16:15	Pelosi	Langius	Rogov	van Kampen	Jeeninga	Cotorruelo	Hallemans	Rosa
16:15 – 16:40	Liu	Astudillo	Sharif	Mamunuzzaman	Goldar	Declercq	Legat	Voortman
16:40 – 17:05	Schuurmans	Caasenbrood	Vasquez	Xu	Fu	Ambrosino	Shakib	Keijzer
17:05 – 17:30	Scholte	-	Karbasizadeh	-	-	-	Blanco	Wauthion

17:30 – 18:15	Reception
18:15 – 20:00	Dinner
20:00 – 22:00	Management Team DISC (room Lucasgat A)

Wednesday March 11, 2020

8:30 – 9:30	P3 – De Grote Zael Thomas Schön – *Learning nonlinear dynamics using sequential Monte Carlo - Part III*							
9:30 – 9:45	Coffee break							
Room WeM	Lucasgat A WeM01 *Drones, Autonomous Vehicle & Logistics II*	Lucasgat B WeM02 *Mobile Robots & Robotics II*	Lucasgat C WeM03 *Nonlinear & Hybrid Control Systems II*	Lucasgat D WeM04 *Discrete-event & Embedded Control Systems*	Lucasgat E WeM05 *Medicine and Systems Biology*	Solsegat WeM06 *Optimal Control II*	Hooge Duvel WeM07 *Systems Identification II*	Groenendal WeM08 *Learning in Control I*
9:45 – 10:10	Bos	Mehdifar	Verhoek	Reijnen	Thémans	Jin	Dirkx	Reinders
10:10 – 10:35	Verbakel	Chan	Hendrickx	Moormann	Sonveaux	De Mauri	Sharabiany	Willems
10:35 – 11:00	Fransman	Guo	Koelewijn	Thuijsman	De Becker	Debrouwere	Noël	Mooren
11:00 – 11:25	Vendrichoski	de Groot	Chan-Zheng	v. Huijgevoort	Lopez	Meijer	Fonken	Ohnishi
11:25 – 11:50	Nijnwoua	Li	Sadeghzadeh	Paape	Negara	Legat	Kivits	Ronzani
11:50 – 12:15	Liu	Yue	Almuzakki	-	Diao	Cobbenhagen	Geelen	Strijbosch
12:15 – 13:30	Lunch							
13:30 – 14:30	P4 – De Grote Zael Paul Van den Hof – *Data-driven model learning in linear dynamic networks*							
14:30 – 14:45	Break							
Room WeA	Lucasgat A WeA01 *Games and Multi-Agent Systems I*	Lucasgat B WeA02 *System Theory I*	Lucasgat C WeA03 *Electromech. Systems I*	Lucasgat D WeA04 *Gaussian Processes*	Lucasgat E WeA05 *Optimization*	Solsegat WeA06 *Data-driven Control I*	Hooge Duvel WeA07 *System Identification III*	Groenendal WeA08 *Learning in Control II*
14:45 – 15:10	Cenedese	Huijzer	Singh	Garcia	Florea	Coppens	Ramaswamy	Aarnoudse
15:10 – 15:35	de Galland	Wijnbergen	Schmerbauch	Gulina	Hermans	Eising	Cheng	Steinhauser
15:35 – 16:00	Zino	Pezzutto	Khalik	Zagabe	Fahdzyana	van Waarde	Tacx	Beck
16:00 – 16:25	Bianchi	Appeltans	Bosman	Küper	Van Roy	Burohman	van 't Veld	Poot
16:25 – 16:50	Jiao	Shali	Driesen	Birpoutsoukis	Gillis	Bloemers	Vermeersch	Sun
16:50 – 17:15	Martirosyan	Hossain	Classen	Iacob	Vandewal	Steentjes	Lauwers	Beintema
17:30 – 18:30	P5 – De Grote Zael Henk Nijmeijer – *Cooperative and/or Autonomous driving: where are we going?*							
18:30 – 18:45	E1 – Best Thesis Award Ceremony							
19:00 – 21:00	Dinner							

Thursday March 12, 2020

8:30 − 9:30	P6 – De Grote Zael Ming Cao – *Strategic decision-making and learning for autonomous agents*							
9:30 − 9:45	Coffee break							
9:45 − 10:45	P7 – De Grote Zael Marcel Heertjes – *Hybrid integrator-gain systems: How to use them in motion control of wafer scanners?*							
Room ThM	Lucasgat A ThM01 *Games &* *Multi-Agent* *Systems II*	Lucasgat B ThM02 *System* *Theory II*	Lucasgat C ThM03 *Electromech.* *Systems II*	Lucasgat D ThM04 *Distributed* *Parameter* *Systems II*	Lucasgat E ThM05 *Energy* *Systems II*	Solsegat ThM06 *Data-driven* *Control II*	Hooge Duvel	Groenendal
10:45 − 11:10	Ben Ayed	Jacobs	Hu	Veldman	Shomalzadeh	van Dijk	-	-
11:10 − 11:35	Debauche	Lordejani	Behinfaraz	Kazaku	Beckers	Wang	-	-
11:35 − 12:00	Gong	Vergauwen	Garg	Zwart	Chong	Menzen	-	-
12:00 − 12:25	Shi	-	Csurcsia	-	Machado	Acerbo	-	-
12:30 − 12:50	E2 – De Grote Zael *DISC certificates & Best Junior Presentation Award Ceremony*							
12:50 − 13:00	P8 – De Grote Zael *Closure of the 39th Benelux Meeting*							
13:00 − 14:00	*Lunch*							

HOTEL MENNORODE

Vergaderzalen b.g. Meeting rooms

Hotelkamers Hotel rooms

Openbare ruimten Public areas

Bars & restaurants

Lift / Elevator

Ingang / Entrance

Trap / Stairs

Hotel

51 - 61 begane grond / ground floor
100, 300, 500 - serie 1ᵉ verdieping / 1st floor
200, 400 - serie begane grond / ground floor

Zalen / Meeting rooms

K	Kleine Zaal	GZ	Grote Zaal
S	Solse Gat	LE	't Leesten
H	Hooge Duvel *	HI	Hindeloopen
R	Roode Heggen	LU	De Luwte
B	Broodberg *	AM	Amfitheater
L	Lucasgat	KD	Kroondomein
G	Groenendaal	FI	Fietsverhuur & E-bikes
V	Voorplein		
	* 1ᵉ verdieping / 1st floor		

Algemene ruimten / Public areas

Receptie / Front desk

Ontbijt restaurant

Grand Café De Schaapskooi

Terras / Terrace

Vergaderfoyer

Tennis

Fietsenstalling / Bicycle storage

Fitness & Recreatie

Minder valide parkeerplaats

Oplaadpaal